

AD-A147 163

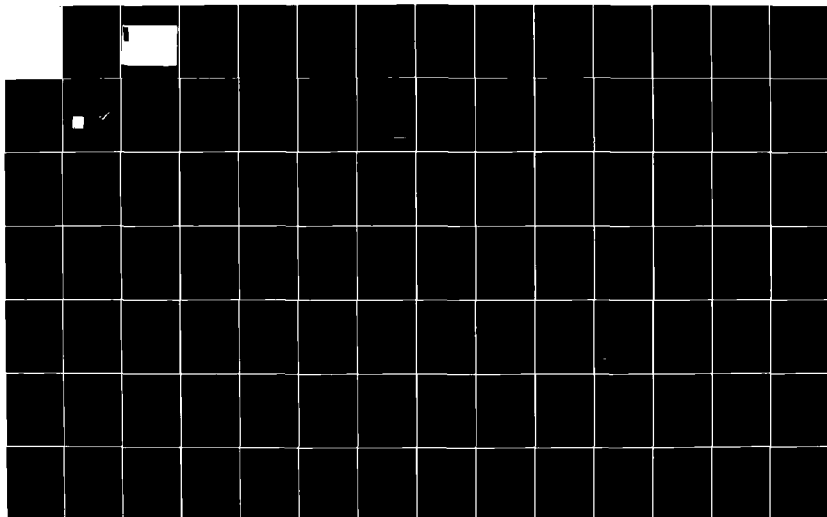
INTERNATIONAL CONFERENCE ON ELECTRONIC PROPERTIES OF  
TWO DIMENSIONAL SYSTEMS (5TH) HELD AT OXFORD ENGLAND ON  
5-9 SEPTEMBER 1983(U) OXFORD UNIV (ENGLAND) 1983

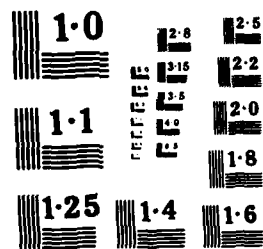
1/4

UNCLASSIFIED

F/G 9/3

NL





AD-A147 163

THE PREPARATION OF THIS WORKBOOK  
HAS BEEN MADE POSSIBLE BY THE  
SUBSTANTIAL SUPPORT OF GEC THROUGH  
A GRANT FROM THE GEC RESEARCH  
LABORATORIES

**S&C**

Approved For	
Mr. J. Kelly	<input checked="" type="checkbox"/>
Mr. J. Nicholas	<input checked="" type="checkbox"/>
Mr. J. Portal	<input checked="" type="checkbox"/>
Mr. G. Roberts	<input checked="" type="checkbox"/>
Mr. A. Stradling	<input checked="" type="checkbox"/>
Date	
by	
Dist. Special	
A-1	



# PREFACE

This Volume contains refereed manuscripts scheduled for presentation at the Fifth International Conference on Electronic Properties of Two-Dimensional Systems to be held at Oxford, UK, 5-9 September 1983. In some cases abstracts or extended abstracts have been inserted for manuscripts not ready in time for the preparation of this volume. Refereed manuscripts are to be published in a special issue of Surface Science scheduled for Spring 1984. The Proceedings of earlier conferences in this series have appeared in Volumes 58, 73, 98 and 113 of Surface Science.

We are grateful for the direct financial support of the sponsors listed on the adjoining page, and for the indirect support of several institutions, especially those with which the Organising Committee Members are affiliated, and the UK Department of Industry for sponsoring the attendance of young UK industrial scientists.

We thank all our colleagues whose work makes this field stimulating and repeat the regret of the Programme Committee that it was able to include only just over half the papers submitted for the Conference.

## Organising Committee

M J Kelly  
R J Nicholas (Chairman)  
J C Portal  
G G Roberts  
R A Stradling

July 1983

- i -



CONFERENCE SPONSORS

The General Electric Company, p.l.c.  
British Telecom  
Hughes Microelectronics Limited  
I C I  
National Semiconductor (UK) Limited  
ISA Riber  
Standard Telecommunication Laboratories Ltd  
Thompson - CSF  
European Research Office, United States Army  
European Office of Aerospace Research and Development,  
United States Air Force  
U S Office of Naval Research - London Branch

INTERNATIONAL ADVISORY COMMITTEE

T Ando, Tsukuba  
G Dorda, Munich  
L Esaki, Yorktown Heights  
H Fukuyama, Tokyo  
C C Grimes, Bell Lab  
S Kawasaki, Tokyo  
J F Koch, Munich  
G Landwehr, Grenoble  
N T Linh, Paris  
M Pepper, Cambridge  
J J Quinn, Brown Univ  
F Stern, Yorktown Heights  
R H Tredgold, Lancaster  
D C Tsui, Princeton  
R G Wheeler, Yale

PROGRAMME COMMITTEE

E Gornik, Innsbruck  
K von Klitzing, Munich  
G G Roberts, Durham  
R A Stradling, St Andrews  
B Vinter, Paris  
M Voos, Paris  
F I B Williams, Saclay

# CONTENTS

## Preface

## Conference Sponsors

## Committee Members

A Hartstein, R A Webb, A B Fowler and J J Walner

1

### One-Dimensional Conductance in Silicon MOSFET's

W J Skocpol, L D Jackel, R E Howard, H G Craighead, L A Fetter,  
P M Mankiewicz, P Grabe and D M Tennant

17

### Magnetoconductance and Quantized Confinement in Narrow Silicon Inversion Layers

R G Wheeler, K K Choi and R Wisniew

23

### Quasi-One Dimensional Effects in Submicron Width Silicon Inversion Layers

R A Davies, C C Dean and M Pepper

29

### Weak Localisation and Interaction Effects in Two Dimensions

M A Paalanen, D C Tsui, B J Lin and A C Gossard

37

### Localization of 2D Electrons in GaAs-Al<sub>x</sub>Ga<sub>1-x</sub>As Heterostructures

J C Hensel, R T Tung, J M Poate and F C Unterwald

43

### Transport Studies in Single-Crystal Films of CoSi<sub>2</sub> and NiSi<sub>2</sub>: A New Class of Two-Dimensional Metals

G Remenyi, S Uchida, G Landwehr, A Briggs and E Bengert

49

### Anomalous Magneto-Transport Properties of p-Type Germanium Inversion Layers at Very Low Temperatures

G M Kramer and R F Wallis

55

### Theory of Impurity Band Conductivity in Inversion Layers in Magnetic Fields

K Kajita

61

### A New Two-Dimensional Electron System on the Surface of Solid Neon

V B Shikin

80

### Critical Electron Density at the Liquid Helium

D B Mast, C J Guo, M A Stan, R Mehrotra, Y Z Ruan and A J Dahm

85

### Dynamics of Dislocation Mediated Melting of a Two-Dimensional Electron Lattice

E Andrei

91

### Localisation of Electrons Above a He Film

M Hansen, U Merkt and J P Kotthaus

92

### Localization of Inversion Electrons on InP

R J Markiewicz, C J Rollins and J S Brooks

98

### Dimensional Crossover of Spin-Orbit Scattering Observed in 2-D Localisation

F Komori, S Kobayashi and M Sasaki

99

### Weak Localization in Metallic Thin Films

Th Englert, J C Maan, G Remenyi, H Kinzel, K Ploog, A Fischer and A Briggs

106

### Weak Localisation Effects in GaAs Doping Superlattices

A Mackinnon, L Schweitzer and B Kramer

112

### Magneto-Transport in 2d: Some Numerical Results

G M Gusev, Z D Kvon, I G Neizvestnyi and V N Ovsyuk

120

### Logarithmic Corrections to the Conductivity of a Two-Dimensional Hole Gas

Yoichi Kawaguchi and Shinji Kawaji

126

### Negative and Positive Magnetoresistance in Cs Adsorbed Si (111) N-Inversion Layers

H Reisinger, A B Fowler and A Hartstein

132

### Magnetic Field Dependence of 2D Sodium Impurity Band Conduction in Activated Regions

F Green, D Neilson and J Szymanski

137

### Bound Electron States of Coulombic Impurities and Their Effect on Mobility in Inversion Layers

Marcos H Degani and Oscar Hipólito

143

### Two-Dimensional Electrons Trapped on a Helium Surface

*iii*

Motohiko Saitoh	149	R B Laughlin	246
Strongly-Coupled Ripplonic Polarons in High Magnetic Fields		Anomalous Quantum Hall Effect	
P Vashishta, R K Kalia and J J Quinn	155	M Pomerantz	247
Topological Defects and Melting of Wigner Solid on Corrugated Surfaces		Two-Dimensional Magnetism	
S A Jackson	162	L Friedman	248
The Effect of Interactions on the Polaronic State of Two Dimensional Electrons on the Surface of Liquid Helium		Thermoelectric Power of Superlattices	
Wlodek Zawadzki and Rudolf Lassnig	163	R P Smith, H Closs and P J Stiles	254
Magnetization, Specific Heat, Magneto-Thermal Effect and Thermo-Electric Power of Two-Dimensional Electron Gas in a Quantising Magnetic Field		Thermoelectric Effects in Silicon MOSFETs in High Magnetic Fields	
H Obloh, K v Klitzing and K Ploog	179	B Tausendfreund and K v Klitzing	260
Thermopower Measurements on the Two-Dimensional Electron Gas of GaAs-Al <sub>x</sub> Ga <sub>1-x</sub> As Heterostructures		Analysis of Quantized Hall Resistance at Finite Temperatures	
J C Hensel, R C Dynes, B I Halperin and D C Tsui	185	Y Guldner, J P Hirtz, A Briggs, J P Vieren, M Voos and M Razeghi	266
Scattering and Absorption of Ballistic Phonons by the Electron Inversion Layer of Si: Theory and Experiment		Quantum Hall Effect and Hopping Conduction in In <sub>x</sub> Ga <sub>1-x</sub> As-InP Heterojunctions at Low Temperature	
A M Chang, M A Paalanen, H L Störmer, J C M Hwang and D C Tsui	191	J T Chalker	272
Fractional Quantum Hall Effect at Low Temperatures		The Quantum Hall Effect: A Sum Rule	
D A Syphers, F F Fang and P J Stiles	197	J E Furneaux and T L Reinecke	278
Multiply Connected Quantized Resistance Regions		The Effect of Interface Charge on the Quantum Hall Effect	
E E Mendez, L L Chang, C A Chang, L F Alexander and L Esaki	204	T L Reinecke	283
Quantized Hall Effect in Single Quantum Wells of InAs		Plateaus in the Quantized Hall Resistance Without Localized States	
H L Störmer	210	U Gummich and J Hajdu	287
Novel Physics in Two-Dimensions with Modulation-Doped Heterostructures		On the Quantum Hall Effect	
D J Thouless	224	F Kuchar, G Bauer, G Weimann and H Burkhard	288
Theory of the Quantized Hall Effect		Non-Equilibrium Behaviour of the Two-Dimensional Electron Gas in the Quantized Hall Resistance Regime of GaAs/Al <sub>0.3</sub> Ga <sub>0.7</sub> As	
D Yoshioka, B I Halperin and P A Lee	232	Y Gefen, J Imry and M Ya Azbel	294
The Ground State of the 2-d Electrons in a Strong Magnetic Field and the Anomalous Quantized Hall Effect		Quantum Oscillations in Small Rings at Low Temperatures	
		L C Zhao, B B Goldberg, D A Syphers and P J Stiles	303
		The Complex Capacitance of Si Inversion Layers in the Quantized Resistance Regime	

R K Goodall, R J Higgins and J P Harring	309	J Scholz, F Koch, J Ziegler and H Maier	402
Use of Capacitance Technique in the Study of Two-Dimensional Layers in Silicon MOSFETs.		Electric Subbands in the Limit $E_g \rightarrow 0$	
P K Basu and B R Nag	310	A D Wieck, E Batke, D Heitmann and J P Kotthaus	408
Alloy Scattering Limited Mobility of Two Dimensional Electron Gas Formed in $\text{In}_{0.53}\text{Ga}_{0.47}\text{As}$		Intersubband Resonance of Holes and Interaction with 2D-Plasmons on Si	
F A Riddoch and B K Ridley	316	D Stein, G Ebert, K v Klitzing and G Weimann	414
Phonon Scattering of Electrons in Quasi-One-Dimensional and Quasi-Two-Dimensional Quantum Wells		Photoconductivity on $\text{GaAs-Al}_x\text{Ga}_{1-x}\text{As}$ Heterostructures	
M Toan Thang and G Fishman	322	G H Döhler and P Ruden	420
Interband Scattering in Mobility in $\text{GaAs-GaAlAs}$ Heterostructures		Properties of n-i-p-i Doping Superlattices in III-V and IV-VI Semiconductors	
R A Höpfel and E Gornik	328	J M Morlock, A C Maciel, A Petrou, C H Perry, R L Aggarwal, M Smith, A C Gossard and W Wiegmann	436
Two-Dimensional Plasmons and Far Infrared Emission		Magneto-Optical Studies of Two-Dimensional Electronics in MQW Heterostructures	
M Baumgartner and G Abstreiter	343	A Pinczuk and J Shah	442
Interaction Between Electronic and Phonon Raman Scattering in Hole Space Charge Layers on Silicon		Investigation of Optical Processes in a Semiconductor 2D Electron Plasma	
R Lassnig and W Zawadzki	349	K Muro, S Mori, S Narita, S Miyamizu and K Nanbu	448
Interface Optic Phonons and Magneto-Phonon Effect in Polar Double-Heterostructures		Cyclotron Resonance of Two-Dimensional Electrons in $\text{AlGaAs/GaAs}$ Heterojunction	
M Seidenbusch, G Lindemann, R Lassnig, J Edlinger and E Gornik	356	M Zhao, C Mazuré, F Koch, J Ziegler and H Maier	454
Cyclotron Resonance Studies of Screening and Polaron Effects in $\text{GaAs-AlGaAs}$ Heterostructures		Surface Cyclotron Resonance in a Strong $B_{  }$	
M A Brummell, R J Nicholas, L C Brunel, S Huant, M Baj, J C Portal, M Razeghi, M A di Forte-Poisson, K Y Cheng and A Y Cho	362	B Vinter	461
Cyclotron Resonance and Polaron Effects in a 2DEG in $\text{GaInAs}$		Subbands in Back-Gated Heterojunctions	
K E Ambrosch, H Clemens, E J Fantner, G Bauer, M Kriechbaum, P Kocevar and R J Nicholas	368	W L Bloss	467
Structural and Electronic Properties of $\text{PbTe/Pb}_{1-x}\text{Sn}_x\text{Te}$ Superlattices		Plasmon and Intersubband Modes of a Superlattice -Classical Versus Quantum Limits	
S Das Sarma	374	R Lassnig and W Zawadzki	473
Electron-Phonon Interaction and Screening Effects in Quasi-Two Dimensional Electron Systems		Theory of Resonant Polarons in Barrow Gap Semiconductors	
Z Schlesinger, J C M Huang, S J Allen, Jr, H L Stormer and M Le	396	G F Giuliani, G Qin and J J Quinn	479
Infrared Studies of the $\text{GaAs}/(\text{GaAl})\text{As}$ 2DEG		Intrasubband Plasma Modes of a Semi-Infinite Superlattice: A New Type of Surface Wave	

J C Portal, G Gregoris, M A Brummell, R J Nicholas, M Razeghi, M A di Forte-Poisson, K Y Cheng and A Y Cho	485
Two Dimensional Magnetophonon Resonance in GaInAs-InP and GaInAs-AlInAs Heterojunctions and Superlattices	
C Zeller, G Abstreiter and K Ploog	491
Resonant Tunneling in Doping Quantum Well Structures	
A Tselis, G Gonzalez de la Cruz and J J Quinn	497
Collective Modes of Type II Semiconductor Superlattices	
H Fujiyasa, A Ishida, H Kuwabara, S Shimomura, S Takaoka and K Murase	503
Optical and Electrical Properties of PbTe-Pb <sub>1-x</sub> Sn <sub>x</sub> Te Superlattices Prepared on KCl by a MBE	
C Delalande, U O Ziemelis, G Bastard, M Voos, A C Gossard and W Wegmann	509
Photoluminescence and Excitation Spectroscopy in Coupled GaAs-Ga(Al)As Quantum Wells	
H Sakaki, K Hirakawa, J Yoshino, S P Svensson, Y Sekiguchi, T Hotta, S Nishi and N Miura	515
Effects of Electron Heating on the Two-Dimensional Magnetotransport in GaAlAs/GaAs Heterostructures	
W Hönlein and G Landwehr	517
Negative Magnetoresistance of (100) n-Si-MOSFETs under Substrate Bias	
R L Greene and K K Bajaj	523
Effect of Magnetic Field on the Binding Energy of a Hydrogenic Impurity Centre in Quantum Well Structures	
P Voisin	524
Optical Studies of Semiconductor Superlattices	
A Fasolino and M Altarelli	540
Landau Levels and Magneto-Optics of Semiconductor Superlattices	
G Bastard	546
Self Consistent Variational Calculations and Alloy Scattering in Semiconductor Heterojunctions	
B V Shanabrook and J Comes	552
Photoluminescence from "Spike Doped" Hydrogenic Donors in Al <sub>0.3</sub> Ga <sub>0.7</sub> As-GaAs Quantum Wells	

J Yoshino, H Sakaki and T Hotta	558
Magnetic Breakdown in GaAlAs/GaAs Quantum Well Structures	
F F Fang and P J Stiles	564
deHaas-van Alphen Effect in Silicon Inversion Layers	
T Haavasoja, H J Störmer, D J Bishop, V Narayanamurti, A C Gossard and W Wegmann	571
Magnetization Measurements on a Two Dimensional Electron System	
J M Mercy, C Bousquet, J L Robert, A Raymond, G Gregoris, J Beerens, J C Portal, P M Frijlink, P Delecluse, J Chevrier and T Linh	577
Hydrostatic Pressure Control of the Carrier Density in GaAs/GaAlAs Heterostructures: Influence of the Metastable Deep Levels	
G F Giuliani and J J Quinn	584
Coulomb Inelastic Lifetime of a Quasi-Particle in a Two Dimensional Electron Gas	
U Kunze and G Lautz	590
Tunneling Spectroscopy of Landau-Levels in Electron Inversion Layers on (100)-Si Surfaces	
F Capasso	596
Multilayer Semiconductor Optoelectronic Devices	
T P Pearsall	597
High Speed Heterostructure Devices	
P O Mahn, S Yokohama and M Henzler	598
Dependence of Interface State Density on the Atomic Roughness at the Si-SiO <sub>2</sub> Interface	
J-Y Marzin, M Quillec, E Y K Rao, G Leroux and L Goldstein	604
Optical Properties of Strained In <sub>x</sub> Ga <sub>1-x</sub> As Multi Quantum Well Structures	
W Thoren, G Heiland, D Kohl, M V Löbneyesen, W Platen and H-J Schink	610
New Experimental Results for Electron Transport in Weak Accumulation Layers on ZnO Crystals	

G Grabecki, T Dietl, J Kossut and W Zawadzki	612
Quantum Transport in Semimagnetic HgMnTe Inversion Layers-Experiment and Theory	
Y Guldner, G Bastard, J P Vieren, M Voos, J P Faurie and A Million	618
Magneto-Optics in a II-VI Superlattice: HgTe-CdTe	
C A Chang, E E Mendez, L L Chang and L Esaki	624
Quantum Wells of InAs Between AlSb	
M Pomerantz	630
Experiments on Literally Two-Dimensional Magnets	
T P Pearsall	646
Two-Dimensional Electronic Systems For High-Speed Device Applications	
H Sakaki, K Hirakawa, J Yoshino, S P Svensson, Y Sekiguchi, T Hotta, S Nishi and N Miura	666
Effects of Electron Heating On The Two-Dimensional Magnetotransport in AsGaAs/GaAs Heterostructures	
P S Markiewicz, C J Rollins and J S Brooks	675
Dimensionality Cross-over of Spin-Orbit Scattering Observed via Localisation Effects	

- vii -

## ONE-DIMENSIONAL CONDUCTANCE IN SILICON MOSFET'S

A. Hartstein, R. A. Webb, A. B. Fowler and J. J. Wainer

IBM - Thomas J. Watson Research Center  
Yorktown Heights, New York

A review is given of experiments on the conductance of 1-D MOSFET's. The types of samples studied, the phenomena observed and our theoretical understanding of these phenomena are discussed. Particular attention is given to the strong localization regime and the structure in the conductance as a function of gate voltage.

Over the last several years there has been considerable interest in the conductance of 1-D systems. This has been prompted at least in part by the growing body of novel theoretical predictions, as well as the recent possibility of making such systems. The range of phenomena which can be studied in 1-D systems is quite large. It is possible to study both strong and weak localization. It is conceptually possible to study 1-D subband structure arising from size quantization in an elementary particle-in-a-box picture. It is also possible to explore the occurrence of resonant tunneling phenomena (1,2) in the 1-D system.

The first 1-D MOSFET's reported showed strong localization behavior (3,4). The dominant conduction mechanism was by variable range hopping, and a transition was observed between 1-D and 2-D behavior. This work was done on pinched accumulation layer samples. Other workers (5-7) have explored the weak localization regime, looking at both conductance and magnetoconductance to elucidate the physics. This work was done using both narrow gate (5,6) and pinched type (7) samples. In the pinched accumulation layer type samples the experiments suggest a departure from lowest order weak localization behavior. A notable feature of all of these experiments is the occurrence of structure in the conductance as a function of gate voltage. The structure was particularly large in the first pinched accumulation layer samples. In the main body of this paper we will present detailed data on this structure, and try to understand its origin.

The use of inversion layer and accumulation layer MOSFET's to study the physics of a 2-D electron gas has been extremely important (8). Probably the single most important feature of these systems is the ability to vary the Fermi energy in the system simply by controlling the gate voltage. This can be used as a powerful tool. In the MOSFET system an electric field perpendicular to the interface between silicon and silicon dioxide produces an interface charge sufficiently narrow to quantize the electron or hole wave functions perpendicular to the surface. The carriers are still free to move parallel to the surface and thus form a 2-D electron gas as long as the temperature is small compared to the energy level spacing for motion perpendicular to the surface.

In recent years 1-D MOSFET samples have been produced by a variety of techniques in order to exploit the ability to vary the Fermi level position to study the physics of conduction in a 1-D system. The most obvious technique for obtaining a 1-D MOSFET is to use a narrow gate. Optical lithography (6) has been used to produce gates as narrow as 400 nm. Electron beam lithography (5) has been used to produce gates as narrow as 100 nm. These techniques suffer from the drawback that width variations of 5 - 10% are typically obtained. Shadowing techniques (9) can result in gates as narrow as 10 - 20 nm. However, results obtained on samples produced by this method have not yet been published. All of these samples suffer from a common problem that the conductance curves exhibit a rather large hysteresis as a function of gate voltage and irreproducibility after thermal cycling. This probably results from charge collecting on the surface of the device adjacent to the narrow gate changing the effective width of the inversion layer channel. The problem is of course most important for the narrowest devices. An attempt to overcome this problem by defining a mesa structure for the device (5) by reactive ion etching leaves the sides of the device open to similar problems. This type of structure, however, has one big advantage. It is readily amenable to modelling of the potentials, energy levels, and electron distributions. Only the boundary conditions at the edges remain ill-defined.

1-D MOSFET's can also be obtained by a technique of electric field pinching of the 2-D electron gas in an accumulation layer MOSFET (3,4,7). This technique has both advantages and disadvantages. It requires no special lithography so that samples can be processed by fairly standard and well characterized techniques. No free surface area is located adjacent to the conducting channel, so that no hysteresis is observed in these devices. The effective width of the 1-D channel can be altered by voltages applied to the device. The major drawback to the technique is that the resulting devices cannot be readily modelled, so that the effective channel width must be inferred from rather indirect experimental measurements. The effective width of the conducting channel is believed to have been varied between 20 nm. and 1  $\mu$ m. in our previous measurements (3,4), and from 100 nm. to 2  $\mu$ m. by Dean and Pepper (7).

The range of 1-D phenomena which can occur impose different restrictions on the width of the samples necessary to observe each phenomenon. In order to observe a 1-D variable range hopping, it is necessary for the sample to be narrower than the average hopping length for the electrons. This was found to be on the order of 30 nm. On the other hand weak localization behavior can be observed when the sample width is less than the inelastic scattering length. This can be greater than 1  $\mu$ m in these systems (5). Particle in a box type behavior will be easiest to obtain in the narrowest samples. In order to observe this type of behavior it is important that the width of the channel be very uniform. At the present time no one has presented convincing evidence for particle-in-a-box type behavior.

Fig. 1 shows idealized top and cross section views of our pinched accumulation layer samples. The substrate is 10 ohm-cm n-type <100> silicon. Two n<sup>+</sup> diffusions are used as the source and drain contacts to the accumulation layer. The two lateral p<sup>+</sup> diffusions are used to control the width of the accumulation layer. The electrons at the surface are in effect pinched into a narrow region because of the electric field applied from these control electrodes and arising from the built-in potential between the p<sup>+</sup> regions and the n-type substrate. The separation between the control elec-

trodes is about 1  $\mu$ m, and the length of the narrow conducting region is about 10  $\mu$ m. The gate oxide is 30 nm. thick, and the gate is made of aluminum.

In the actual device, shown in Fig. 2, the dimensions are seen to be not nearly as ideal as indicated in Fig. 1. In fact we have no way of ascertaining the effective width variations in this type of device. Actually, we don't even know the width of the conducting channel, except from our analysis of the experimental data. The effect of an applied gate voltage is two-fold in samples of this geometry. A positive gate voltage will induce electrons at the surface, thereby changing the carrier density and Fermi energy. Moreover, it will tend to broaden the width of the accumulation layer channel. A negative bias applied to the control electrodes will pinch the channel down to narrower widths, but will also tend to change the threshold voltage and thereby reduce the accumulation layer carrier density.

Our devices were measured using an AC modulation of the source-drain voltage. To avoid hot electron effects the source-drain field was generally kept below 2 mV/cm. The samples were measured in a dilution refrigerator. Great care was taken to eliminate extraneous noise signals. In our original experiments noise heating made any measurements below about 100 mK questionable. In our more recent set of measurements this limit was extended to about 50 mK. The bulk of the data in our original measurements were taken by setting a gate voltage and varying the temperature. In our latest measurements we measured conductance as a function of gate voltage for fixed temperature. Therefore, the derived temperature dependent curves from the recent data show somewhat more scatter.

The mass of data needed to explore fully the nature of the structure in the conductance curves necessitated the use of an elaborate data acquisition system. In order to obtain these data it was necessary to build a noise free voltage ramp and to carefully interface the equipment to a data acquisition system. The experiment and the computer system were decoupled by use of active filters on all interconnecting lines. These measures were necessary to avoid noise heating of the electrons.



Typical data obtained in this way are shown in Fig. 3. The notable feature of these data is the large structure in the conductance as a function of gate voltage observed in this system. This structure is reproducible in a given sample, but varies from sample to sample. This structure was not observed to change over a period of more than six months and numerous temperature cyclings up to 300 K. The relative amplitudes of the peaks can be seen to decrease at higher gate voltages. The widths of the peaks are observed to increase with increasing gate voltage. As the temperature is raised, the peaks broaden and the smaller ones gradually disappear.

These data look qualitatively like peaks superimposed on a baseline when viewed on a linear scale. For this reason we will first try to understand the overall gate voltage and temperature dependences of the conductance before concentrating on the peak structures themselves. Fig. 4 shows the temperature dependence of representative conductance minima. These data were obtained in the original experiment by selecting a gate voltage and varying the temperature. As we have discussed before (3,4), the temperature dependence at low gate voltages is  $\ln G \sim T^{-1/2}$ , and for higher gate voltages goes over to  $\ln G \sim T^{-1/3}$ .

A least squared fit to the data was made to the form  $\ln G/G_0 = -(T_0/T)^n$ . The best fit exponents are shown in Fig. 5. It is clear from this figure that the exponent has a value near 1/2 for low gate voltages and shows a transition to a value of 1/3 at higher gate voltages. We have interpreted this result as a transition from 1-D variable range hopping to 2-D variable range hopping in this system. This has been discussed in considerable detail in our previous publications (3,4) and will not be treated in detail here.

If the gate voltage is increased still further, the conductance enters a weak localization regime. We have obtained data covering the entire range from strong localization, through a transition region and into the weak localization regime. Because the width of the accumulation layer is smaller than the inelastic scattering

length, 1-D weak localization behavior is observed. These data will be discussed elsewhere.

One can also obtain values for the parameter  $T_0$  as a function of gate voltage from the data in Fig. 4. To reduce experimental fluctuations, we assumed  $n$  to be the exponents of either 1/2 or 1/3 depending on the gate voltage and then obtained least squared fits to the remaining parameters in order to determine  $T_0$ . Values of  $T_0$  show considerable fluctuations as a function of gate voltage in much the same way that the conductance does. In order to obtain averaged values for  $T_0$ , we averaged over a range of gate voltages to effectively average out the peak structure. The gate voltage range employed was  $\pm 0.5$  V. These averaged conductance values show the same temperature dependence as shown in Fig. 4 for conductance minima. The values of  $T_0$  were then extracted from these averaged plots using a least squared fitting routine. The results of this analysis are shown in Fig. 6 for both the 1-D and 2-D regimes. Essentially the same results can be obtained by analysing the conductance minima. The procedure used gives slightly higher values for  $T_0$  than using the conductance minima, and emphasizes the fact that the behavior is the average behavior of the data.

These results are surprising. In the 1-D regime variable range hopping theory gives  $T_0 = 4\pi/N_1 k$ , where  $1/\pi$  is the decay length of the localized wave functions,  $N_1$  is the 1-D density of states, and  $k$  is Boltzmann's constant. In the 2-D regime  $T_0' = 27\pi^2/wN_2 k$ , where  $N_2$  is the 2-D density of states at the Fermi energy. Here  $N_1$  is approximately equal to  $N_2 w$ , where  $w$  is the effective channel width. All of the quantities which determine  $T_0$  were believed to be slowly varying functions of gate voltage. However, Fig. 6 clearly demonstrates that  $T_0$  is an exponential function of gate voltage.

From the curves one obtains  $\ln T_0/T_{0,0} = -aV_g$ , where  $T_{0,0}$  and  $a$  are fitting parameters and  $V_g$  is the gate voltage. In the 1-D regime  $a = 0.8 \text{ V}^{-1}$  and  $T_{0,0} = 610 \text{ K}$ . In the 2-D regime  $a' = 1.5 \text{ V}^{-1}$  and  $T_{0,0}' = 5.4 \times 10^3 \text{ K}$ . It is interesting to

note that  $a'/a \sim 2$ . This could be understood if one assumed that  $a$  varied exponentially with gate voltage. This is contrary to the 2-D result obtained on wide samples (10), but these narrow samples appear to behave differently.

Let us now turn our attention to the peaked structure shown in Fig. 3. Let us first consider the possibility that buried beneath the mass of peaks is some systematic structure arising from a particle-in-a-box quantization in our sample. In order to evaluate this possibility, we first obtained averaged conductance values by averaging  $\ln G$  as discussed above. This was then subtracted from the conductance curves, leaving the structure on a zero baseline,  $G'$ . The correlation function  $\int G'(V_g)G'(V_g + \Delta V_g) dV_g$  was formed, as well as the correlation functions for other powers of  $V_g$ . If any systematic structure had been evident in the conductance curves, it would have showed up as peaks in the correlation functions. No such structure was observed. The correlation functions show only smooth featureless behavior, except in the region,  $\Delta V_g \sim 0$ , which corresponds to the width of the individual peaks.

To better understand the origin of the peaks, let us look at the temperature dependence of the conductance on a peak. These data are shown in Fig. 7. It is clear that the conductance shows two separate regions of temperature dependence. These curves can be characterized by essentially three parameters:  $T_0$ , the slope for the upper temperature region,  $T^*$ , the slope for the lower temperature region, and a temperature,  $T_1$ , where the transition occurs. We use the notation  $T_0$  for the upper temperature region because in this region the peaks have disappeared and the slopes for peaks and valleys are essentially the same. It is also clear from the figure that all three parameters decrease with increasing gate voltage.

It is instructive to plot the ratios  $T_1/T_0$  and  $T^*/T_0$  as a function of gate voltage. This is shown in Figs. 8 and 9. Since  $T_0$  varies exponentially with gate voltage, it is clear that  $T_1$  and  $T^*$  both scale with  $T_0$  to first order. There is some small systematic dependence on gate voltage that remains as well as fluctuations. The full significance

of these results is not yet clear, but these dependences should be instructive in arriving at a theoretical understanding of these experiments.

Fig. 10 shows the widths of the peaks plotted as a function of gate voltage. These data show a general trend of increasing width with increasing gate voltage. If the average density of states at these gate voltages is essentially constant, as one might well expect at these high carrier densities, then this shows that the energy width of the peaks increases with increasing gate voltage. In our earlier publications (3,4), we argued that the peaked structure might arise from fluctuations in the density of states. Within this model, one would expect that the transition temperature,  $T_1$ , would be given by  $\Delta E/k$ , the width of the density of states peaks. Therefore,  $T_1$  would be expected to increase with gate voltage in a somewhat random way as shown in Fig. 10. However, we have noted in Figs. 7 and 8 that  $T_1$  actually decreases with increasing gate voltage. We have no explanation for this apparent contradiction.

There is another quantitative reason to question the density of states model for the structure. Fig. 9 shows that  $T^*/T_0$  may obtain values as small as 0.2. The density of states model would therefore require that the peak density of states be 5 times larger than the background for these large peaks. It is hard to see how such a large variation in the density of states could arise from random fluctuations in this system.

Azbel (2) has suggested that the structure in the conductance curves might arise from a resonant tunneling of electrons in this 1-D system. The theory shows that electrons can tunnel through the entire sample if the Fermi energy has a few very select values determined from the microscopic structure of the random system. At these particular values of gate voltage the electrons could be expected to tunnel through the sample with a high probability, via resonant states near the center of the sample. This is a zero temperature theory, but in a very natural way can account for the large differences in conductance. When finite temperature effects are incorporated into the theory, the highest peaks are found to decrease with increasing tempera-

ture because of thermal broadening of the incident electron distribution. We have looked carefully in all of our low temperature data for this effect. No peaks were found that behave in this manner.

One might also consider whether or not it would be possible to have resonant tunneling in parallel with a variable range hopping conductance. This might give resonance peaks on top of a variable range hopping background with the familiar  $\ln G \sim -(T_0/T)^{1/2}$  dependence. When the data were analysed to allow for this possibility, the experimental results were found to be incompatible with this suggestion. In effect what we have shown is that inelastic processes, as incorporated in the variable range hopping theory, are important in this system. The theories of resonant tunneling, which we have analysed, have not included these processes.

A modified resonant tunneling theory, which adequately accounted for the inelastic processes, might explain our measurements. We are currently working on such a theory in collaboration with M. Ya. Azbel, and the results look very encouraging.

In this paper we have presented the results of a comprehensive experiment aimed at understanding the origin of the peaked structure observed in all small 1-D MOS-FET samples. We have examined the characteristic features of the peaks and the temperature dependence of the conductance associated with the peaks. In discussing these results, it has been possible to eliminate several candidate theories as possible explanations. However, it has not yet been possible to establish a complete theory which can explain all of our observations.

We thank M. Ya. Azbel for many valuable discussions on his resonant tunneling theory. We also acknowledge the able technical assistance of J. Tornello.

#### REFERENCES

- (1) M. Ya. Azbel and Paul Soven, *Phys. Rev. B* **27**, 831 (1983).

- (2) M. Ya. Azbel, *Solid State Commun.* **45**, 527 (1983).
- (3) A. B. Fowler, A. Hartstein and R. A. Webb, *Phys. Rev. Lett.* **48**, 196 (1982).
- (4) A. B. Fowler, A. Hartstein and R. A. Webb, *Physica* **117B & 118B**, 661 (1983).
- (5) W. J. Skocpol, L. D. Jackel, E. L. Hu, R. E. Howard and L. A. Fetter, *Phys. Rev. Lett.* **49**, 951 (1982).
- (6) R. G. Wheeler, K. K. Choi, A. Goel, R. Winieff and D. E. Prober, *Phys. Rev. Lett.* **49**, 1674 (1982).
- (7) C. C. Dean and M. Pepper, *J. Phys. C* **15**, L1287 (1982).
- (8) T. Ando, A. B. Fowler and F. Stern, *Rev. Mod. Phys.* **54**, 437 (1982).
- (9) N. Giordano, W. Gilson and D. E. Prober, *Phys. Rev. Lett.* **43**, 725 (1979).
- (10) M. Pepper, S. Pollitt and C. J. Adkins, *J. Phys. C* **7**, L273 (1974).

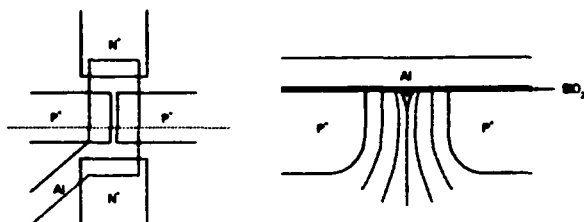


Fig 1 - The upper part shows an idealized top view of a sample. The two  $n^+$  regions are the source and drain. The  $p^+$  regions are the control electrodes. The width between the controls is  $1-2 \mu\text{m}$ , and the length of the controls is  $14 \mu\text{m}$ . The lower part shows a cross section along the dotted line. The diffusions are about  $1 \mu\text{m}$  deep, and the oxide thickness is  $30 \text{ nm}$ . Potential lines are sketched for a positive gate voltage, indicating the narrow conducting channel.



Fig 2 - A micrograph of the device corresponding to the idealized sketch of Fig. 1. The effective channel length is about  $10 \mu\text{m}$ .

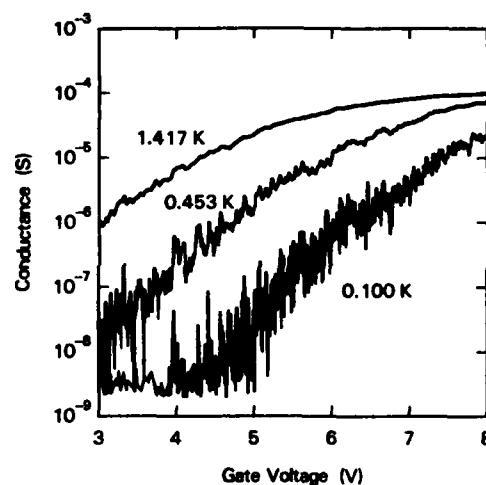


Fig. 3 - Conductance is shown as a function of gate voltage for three temperatures. The structure in the figure is real and not noise. In fact the resolution of the figure is insufficient to resolve the sharpest structures.

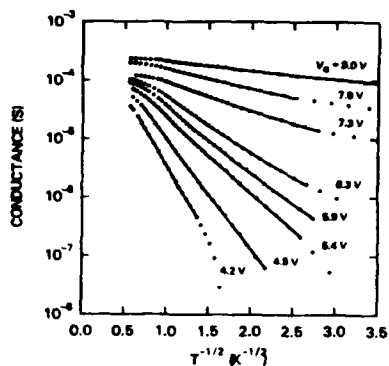


Fig 4 - Temperature dependence of the conductance is shown for several gate voltages. The data were obtained with source, substrate and control electrodes grounded. The solid lines are best least squared fits.

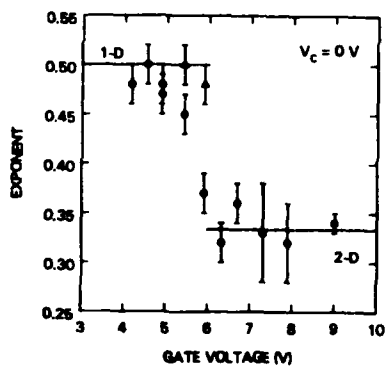


Fig 5 - The exponents that best fit the data in Fig. 4 are shown as a function of gate voltage. The dots are from fits to the entire temperature range, while the open triangles are fits to a restricted low temperature range.

13

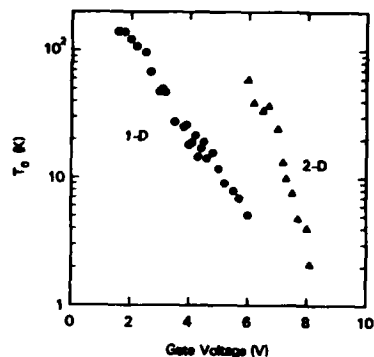


Fig 6 - The variable range hopping parameter,  $T_0$ , is plotted as a function of gate voltage for both the 1-D and 2-D regimes. It is surprising that  $T_0$  varies exponentially with gate voltage, and that the slopes of this dependence vary by a factor of 2 between the 1-D and 2-D regimes.

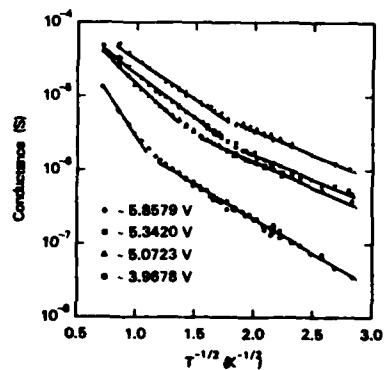


Fig 7 - The temperature dependence of representative conductance maxima is shown for the indicated gate voltages. Each curve shows a break between two different temperature dependences. The slopes and transition temperatures vary systematically with gate voltage.

14

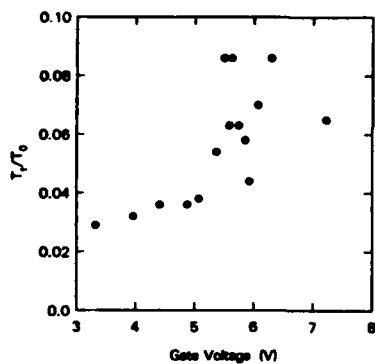


Fig. 8 - The ratio  $T_1/T_0$  is plotted as a function of gate voltage for numerous peaks. The data show a great deal of scatter and some systematic behavior. Both  $T_0$  and  $T_1$  decrease rapidly with increasing gate voltage.

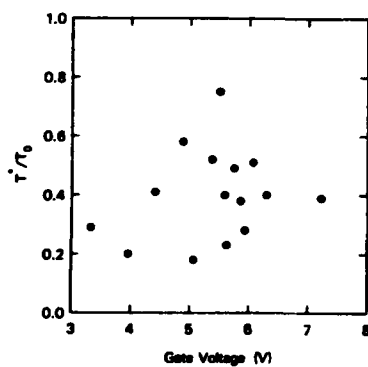


Fig. 9 - The ratio  $T'/T_0$  is shown as a function of gate voltage. No systematic behavior is evident.

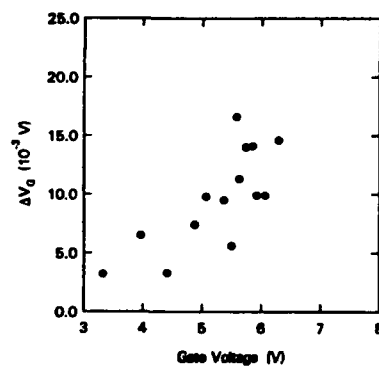


Fig. 10 - The full width at half maximum for several peaks is shown as a function of gate voltage. The width increases systematically with increasing gate voltage.

Magnetoconductance and Quantized Confinement  
in Narrow Silicon Inversion Layers

W.J. Skocpol, L.D. Jackel, R.E. Howard, H.G. Craighead,  
L.A. Fetter, P.M. Mankiewich, P. Grabbe, and D.M. Tennant

Bell Laboratories, Holmdel NJ 07733, USA

We report conductance and magnetoconductance measurements on narrow silicon inversion layers 40-200 nm wide, with mobilities of 1000-5000  $\text{cm}^2/\text{V}\cdot\text{sec}$  at 2 K. At high magnetic fields Shubnikov-de Haas oscillations are observed, but at zero field there still is pronounced structure in the conductance versus electron density, with irregular spacings roughly that expected from quantum confinement ("particle in a box") associated with the lithographically defined width.

1. Narrow Inversion Layers

We are interested in the transition from two-dimensional to one-dimensional conduction in the narrow silicon inversion layers of special MOS-FETs that contain segments of gate and channel as narrow as 40 nm. The gate pattern is formed by electron-beam lithography and transferred to the channel by reactive-ion etching, using the gate metal as a self-aligning mask. The narrow segment is sufficiently long to dominate the resistance (conductance) of the device. The fabrication is similar to that described previously [1], except that each device contains only a single narrow segment about 1  $\mu\text{m}$  long. Also the optically patterned metallization level is tungsten, which allows higher-temperature annealing of the devices. The lithography on chips with devices narrower than 100 nm was written using a Phillips 400T Scanning (Transmission) Electron Microscope with 2 nm diameter spot and 120 keV beam

energy; in that case the liftoff stencil was a single well-baked layer of polymethylmethacrylate (PMMA) 100 nm thick. [2] This gave highly uniform widths, even in the smallest devices.

2. Shubnikov-de Haas Measurements

That such narrow channels conduct at all is perhaps surprising. In fact the mobility of narrow channels inferred from the conductance measurements is generally comparable to that of wider devices subjected to the same processing, i.e., the conductance scales approximately with the width. Devices annealed at 450  $^{\circ}\text{C}$  can have mobilities at liquid helium temperatures greater than 5000  $\text{cm}^2/\text{V}\cdot\text{sec}$ . Figure 1a shows the Shubnikov-de Haas magnetoconductance oscillations observed for such a device, approximately 140 nm wide. The observability of oscillations at 20 kG is a clearcut indication of excellent device quality. The spacing in gate voltage of the peaks (corresponding to the Landau level structure of the density of states) confirms that the electron density in the narrow channel can be calculated with approximately 10% accuracy from the usual simple capacitance formula, using the measured oxide thickness of 65 nm. Devices annealed at lower temperatures, such as 250  $^{\circ}\text{C}$ , have lower mobilities in the range 1000-2000  $\text{cm}^2/\text{V}\cdot\text{sec}$ . Figure 1b shows Shubnikov-de Haas measurements on such a device, 110 nm wide with a 50 nm oxide. The Landau level structure at high fields is less pronounced, as expected, but still observable.

3. One-Dimensional "Particle in a Box" Density of States?

Even in zero magnetic field, the device in Figure 1b shows considerable quasiregular structure of the conductance versus gate voltage. Such structure tends to be more pronounced in narrow, low conductance samples. By analogy to

the Shubnikov-de Haas effect, one expects that we are seeing structure in the density of states. The density of states could affect the conductance either by direct modulation of the scattering rates, or by indirect modification of the nonmetallic localization and interaction effects observed in narrow samples. [1] The magnitude and temperature dependence of the observed structure is somewhat suggestive of the latter interpretation.

The question then becomes whether the structure is statistical fluctuations caused by the influence of inhomogeneities on the several thousand electron eigenstates in such a device, or whether it reflects a regular organization of eigenstates caused by quantization of the transverse electron wavefunctions. In the simplest version of the latter explanation, the energy of the "particle in a box" eigenstates is given by

$$E = E_0 + \frac{\hbar^2}{2m^*} \left( \frac{\pi p}{W} \right)^2 + \frac{\hbar^2}{2m^*} K^2$$

where  $E_0$  depends on the shape of the potential well binding the inversion layer to the interface,  $p$  enumerates the transverse quantization, and  $K$  is a more closely spaced longitudinal momentum variable. Clearly there will be a peak in the density of states whenever the Fermi level reaches the bottom of another parabolic subband. We can estimate the electron density at which this occurs for each integer  $p$  by summing the number of states below the bottom of each subband, which closely corresponds to the number determined from the usual 2D density of states. Thus, peaks occur when

$$n = \pi^2 W^2$$

This predicts that about a dozen bumps should be observed in Figure 1b, quadratically spaced.

Clearcut proof of "particle in a box" behavior requires observing sufficiently regular structure that the spacing can be seen to have the magnitude

and width dependence predicted by the simple theory. Like numerous other devices of order 100 nm wide that we have investigated, the structure shown in Figure 1b is sufficiently irregular that the agreement with theory is tantalizing, but inconclusive. Devices up to a factor of two wider still show some structure, but a characteristic spacing for quantitative comparison is difficult to identify. Recently we have begun to make devices up to a factor of two narrower, and preliminary results are more promising, but still inconclusive.

Figure 2 shows a comprehensive data set from four devices varying in width from 55 to 120 nm, all on the same chip annealed at 250 °C. The conductance (measured two-terminal) scales approximately with width. The numbers indicate the positions of structure predicted by the simple theory based on the width observed in electron micrographs. Despite the irregularities, one could argue that the data shows the expected trend, since the numbers serve as a powerful guide to the mind and eye. Close examination reveals, however, that short range structure and longer-range fluctuations are present in all of the curves, and the differences are at best a subtle difference in emphasis. Moreover, data taken on a subsequent day in the same devices over a narrower range of gate voltages shows different, and less convincing, variation of the structure. After prolonged stress at high gate voltages our devices have lower mobilities and more positive thresholds, which could account for greater disorganization of the eigenstates. Nevertheless, at the time that this is being written, we consider the case for "particle in a box" behavior unproved.

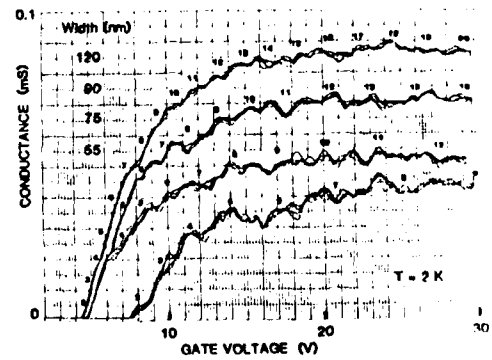
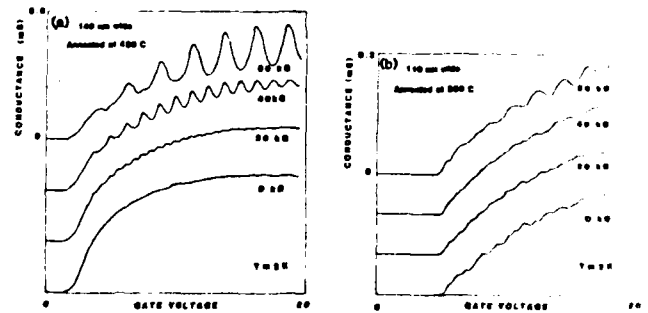
- [1] W.J. Skocpol, L.D. Jackel, E.L. Hu, R.E. Howard, and L.A. Pettey, Phys. Rev. Letters **42**, 951 (1982).
- [2] H.G. Craighead, R.E. Howard, L.D. Jackel, and P.M. Mankiewich, Appl. Phys. Letters **42**, 38 (1983).



# Figure Captions

Figure 1. Shubnikov-de Haas oscillations in narrow devices. (a) High mobility device. (b) Low mobility device. Also note zero-field structure, particularly in (b).

Figure 2. Zero-field structure in four devices of different widths on the same chip. The small numbers indicate the pattern of structure expected from simple "particle in a box" quantization, based on the measured device widths.



Quasi One Dimensional Effects in Submicron Width  
Silicon Inversion Layers

R. G. Wheeler, K. K. Choi and R. Misra  
Yale University  
New Haven, Conn.

Abstract

Evidence of spatial quantization is observed in narrow inversion layers when the electron inelastic length is greater than the channel width. The quasi one dimensional density of states is detected by variations in the localization resistance as a function of electron density.

When the inelastic electron mean free path  $l_{in}$  in a silicon inversion layer is greater than  $W/p_1$ , where  $W$  is the width of the channel, the small changes in conductance with temperature and magnetic field are characteristic of a one dimensional system.<sup>1</sup> These results suggest that spatial quantization in the conduction properties will be observable if one can construct a uniform channel width such that  $W < l_{in}$ .

For noninteracting electrons, the "particle in a box" quantization restricts the value of  $Kx$  to values  $p(p_1/W)$ , where  $p$  is an integer > 1 such that a "saw tooth" like density of states arises.

$$N(E) = N_0(E) \left( \frac{2}{\pi} \right) \sum_{n=1}^p \left[ (p-\gamma)^2 - n^2 \right]^{-1/2} \quad (1)$$

where  $N_0(E)$  is the usual two-dimensional density of states and  $p + \gamma$  is defined from the Fermi energy,

$$E_F = \hbar^2 / 2m^* (p + \gamma)^2 (\pi/W)^2 \quad (2)$$

where  $0 < \gamma < 1$  expresses the quasicontinuous nature of the motion parallel to the boundaries. Channel conductance is given in terms of  $N(E)$

$$G = e^2 N(E) D \quad (3)$$

where  $D$  is the electron diffusivity. Since  $D \sim 1/N(E)$ , this "sawtooth" density can be observed only through second order effects. Considering the change in conductance due to localization<sup>2</sup>,

$$\Delta G = (-e^2/\pi\hbar) l_{in} = (-e^2/\pi\hbar) (D \tau_{in})^{1/2} \quad (4)$$

where the inelastic scattering time

$$\tau_{in} \sim N(E) [D/kT]^{1/2} \quad (5)$$

for impurity mitigated scattering.<sup>3</sup> With the dependence of diffusivity upon density one finds that  $\Delta G \sim [N(E)]^{-1/4}$ . Similarly the conductance change due to electron-electron interaction<sup>4</sup> is proportional to  $\sim [N(E)]^{-1/4}$ .

Thus a minima in the localization resistance occurs when the Fermi energy is coincident with the bottom of a subband. The relative magnitudes of  $l_{in}$  between local extrema are determined by comparison with a magnetic length in magnetoconduction. As can be seen in figure 1 the density of states peaks are asymmetric which implies that  $kT$  need be much less than the level spacing in order to observe resistance oscillations.

For high mobility samples the inelastic length is about  $1 \times 10^{-6}$  m at 1 K. In order to fabricate gate widths less than this value we have used a combination of optical macro- and micro- photolithographic techniques on an initially wide gate structure. <sup>3</sup> The design creates both a narrow and a two dimensional channel in series, where each segment is probed potentiometrically. The distance between probes on the narrow section is  $25 \times 10^{-6}$  m. The devices have an oxide thickness of about  $3.5 \times 10^{-6}$  m with maximum mobilities between 17,000 and 20,000  $\text{cm}^2/\text{V}\cdot\text{sec}$ . After all electrical measurements were completed the width of the narrow section was measured by scanning electron microscopy. In order to associate a local minima in resistance with a density of state peak, figure 2 shows the result of magnetoconductance measurements on a device of width  $0.8 \times 10^{-6}$  m at  $n_s \sim 5 \times 10^{16}$  per  $\text{m}^2$  and at 0.47 K. We conclude that the resistance minima corresponds to a minima in  $\ln$ , thus the position in  $E_F$  of such minima are chosen to be the energies of the subbands at  $K_y = 0$ . We fit these minima to

$$E_F = \frac{\hbar^2}{2m^*} p^2 \left( \frac{\pi}{W} \right)^2; \text{ or } n_s = p^2 \pi / W^2 \quad (6)$$

for the [100] surface of silicon. Width variations on  $0.8 \times 10^{-6}$  m devices cause differing regions of the channel to experience density of state peaks labelled by  $p$  to occur at different electron densities. Thus variations in the resistance of the channel will be the result of a superposition of resistance oscillations associated with each elemental width, weighted by the distribution of widths down the channel length. Reduction in the width helps resolve this problem by increasing the level spacing. We report here the results on our narrowest devices to date.  $W \sim 0.3 \times 10^{-6}$  m. Figure 3 displays the small resistance oscil-

lations as a function of electron density at 0.5 K. At 4 K no oscillations are apparent; in the wide channel such oscillations are absent at all temperatures. For  $W \sim 0.3 \times 10^{-6}$  m,  $n_s \sim 2.75 \times 10^{16}$  per  $\text{m}^2$  the level spacing from equation 6 is  $\Delta n_s \sim 0.2 \times 10^{16}$  per  $\text{m}^2$ . The mean spacing in the data is too small by a factor of two. We have then fitted the data with two overlapping sets of state densities corresponding to two widths. Figure 4 shows the results of the fit and the deduced widths. Figure 5 shows the width distribution deduced from measurements made with the scanning electron microscope. The mean width of the device is  $0.33 \pm 0.03 \times 10^{-6}$  m. The fact that the deduced width is smaller than the measured width may reside in our simple assumption of non-interacting electrons, implied in equation 6, or due to fringing fields at the edge of the gate modifying the shape of the quantizing potential. This work has been supported in part by the National Science Foundation under grant no. DMR - 82130809.

#### REFERENCES

1. R.G. Wheeler, K.K. Choi, A. Goel, R. Wisniewski and D.E. Prober, Phys. Rev. Lett. 49, 1674 (1982)
2. B.L. Al'tshuler and A.G. Aronov, Pis'ma Zh. Eksp. Teor. Fiz. 33, 515 (1981). [JETP Lett. 33 499 (1981)].
3. M.D. Feuer and D.E. Prober, IEEE Trans. Electron Devices 28, 1375 (1981)

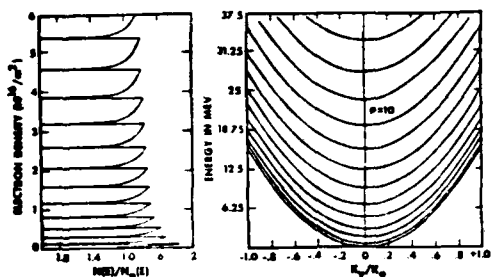


Fig. 1. Subbands and density of states as a function of Fermi Energy, for a channel width =  $0.1 \times 10^{-6}$  m

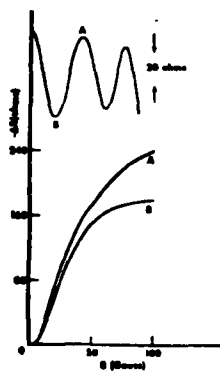


Fig. 2. Magnetoconductance observed on device AU33 at a resistance maxima (A) and at a minima (B) at 0.47 K. The resistance oscillations corresponding to these extrema are shown on the upper curve.

27

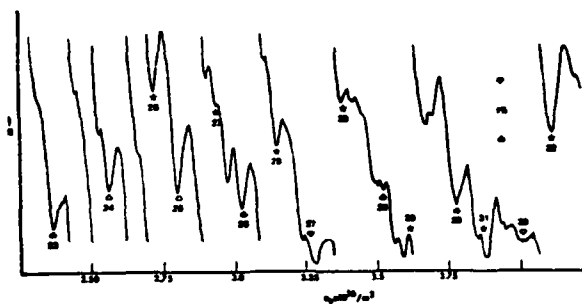


Fig. 3. Resistance oscillations as a function of electron density at 0.5 K for device AU317. The star labels and arrow labels are the positions of the fits to the equation for two widths.

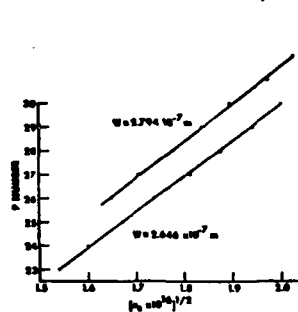


Fig. 4. Data fits to equation 6.

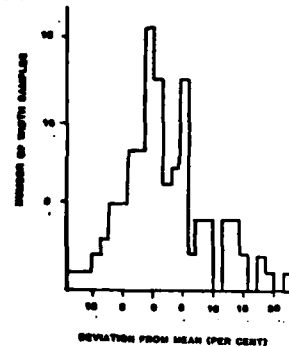


Fig. 5. Measured width distribution.

28

# WEAK LOCALIZATION AND INTERACTION EFFECTS IN TWO DIMENSIONS

R.A. Davies<sup>1</sup>, C.C. Dean and M. Pepper<sup>2</sup>  
Cavendish Laboratory, Cambridge

1. Now at G.E.C. Research Laboratories, Hirst Research Centre, Wembley, Middlesex
2. G.E.C. Research Laboratories, Hirst Research Centre, Wembley, Middlesex and Cavendish Laboratory, Cambridge

## Extended Abstract

In this article a brief summary is given of our work on weak localization and interaction effects in 2D. For small changes in conductivity, the correction  $\delta\sigma$  due to the weak localization of all states is

$$\delta\sigma = -\frac{e^2}{\pi^2 h} \ln(L_{IH}/\ell)$$

as the inelastic diffusion length  $L_{IH}$  varies as  $T^{-1/2}$  this becomes

$$\delta\sigma = -\frac{e^2}{2\pi^2 h} \ln(L_{IH}/\ell),$$

where  $\ell$  is a constant near unity and  $\ell$  is the elastic mean free path.

The interaction correction is

$$\delta\sigma = -\frac{g^2}{2\pi^2 h} \ln(T/T_1),$$

$T_1$  is a constant and the coupling constant  $g \ll 1$  in Si inversion layers due to screening.

These mechanisms are most conveniently separated by a magnetic field<sup>3,4,5,6</sup>, which has the following effects.

1. The effective length scale in the localization correction is reduced by the introduction of the cyclotron length  $L_C$ . To a good approximation the new length  $L'$  is given by

$$L' = (L_{IH}^{-4} + L_C^{-4})^{-1/4}$$

The result is a negative magneto-resistance which is an orbital effect and hence dependent on field direction<sup>7,8</sup>. A field parallel to the current direction also produces a negative magneto-resistance<sup>9</sup> but this is much smaller due to the short confinement length perpendicular to the plane of transport<sup>10</sup>.

2. The magnetic field reduces the effects of screening on the electron-electron interaction. The coupling constant  $g$  increasing to near unity so resulting in a large increase in the magnitude of this correction<sup>11</sup>.

The enhancement of the interaction effect is principally a spin effect, although there is some orbital contribution. Thus a transverse magnetic field will separate the two correction terms but a parallel field will add them (to first order), until the field becomes sufficiently great to remove the localisation contribution.

As the interaction contribution in the Si inversion layer is small for  $gH \ll kT$  metallic behaviour down to temperatures of  $\sim 50\text{mK}$  can be obtained provided  $H$  is sufficiently big that  $L_D \ll L_{ij}$  and the temperature dependence is removed. The ability to achieve complete separation consequently depends on the value of mobility and hence  $L_{ij}$ . If this is small then the interaction effects will be found at values of field such that the temperature dependence due to localization is still present.

As the magnetic field induced interaction effect disappears for  $kT \gg gH$ , the positive magneto-resistance disappears to be replaced by negative.

The principal experimental evidence for the existence of interaction effects comes from the Hall effect<sup>4,5,12</sup>. Experiments have confirmed the theoretical prediction that the relationship between the corrections in the Hall constant,  $R_H$ , and resistance,  $R$ , is

$$\frac{\delta R_H}{R_H} = \frac{2\delta R}{R}$$

The initial confirmation of this relation was for "large" magnetic fields where localization effects were suppressed and interaction effects enhanced. Recently we have measured the temperature dependence of  $\delta R_H/R_H$  at magnetic fields down to 0.01 Tesla, which were not sufficient to enhance interaction effects. It was found<sup>13</sup> that the temperature dependence of  $\delta R_H/R_H$  was the same as at higher magnetic fields, a result also apparent in the earlier data of Uren et al<sup>3,5</sup>. The temperature dependence of  $\frac{\delta R_H}{R_H}$  was independent of magnetic field and hence independent of the magnitude of the change of  $\delta R/R$  or the mechanism determining the temperature dependence of the resistance. The explanation may be in the behaviour of the  $g_2$  and  $g_4$  terms (in the notation of Fukuyama) which are suppressed by increasing the

terms (in the notation of Fukuyama) which are suppressed by increasing the magnetic field. It is clear that whereas the effects of screening on the conductivity are understood this is not true of the Hall effect. The results were principally obtained using Si inversion layers but are substantiated by work on GaAs-GaAlAs heterojunctions. We have also investigated the behaviour of the interaction corrections in the conductivity and Hall effect when the magnetic field is sufficiently strong for Landau levels to be formed<sup>14</sup>. As is theoretically predicted we find a sign change in the temperature dependence of resistance but not in the Hall coefficient.

Turning now to the regime of weak localization which in Si inversion layers (unlike GaAs systems) can be investigated without the complication of significant interaction effects. Abrahams et al<sup>1</sup> have suggested that all states in 2D are exponentially localized and a scaling ( $\beta$ ) function exists defined by

$$\beta = \frac{d \ln g}{d \ln L}$$

where  $g$  is the conductance and  $L$  is the length scale. At finite temperatures the length  $L$  is the inelastic diffusion length. We have defined an experimental scaling function  $\beta_E$  defined by

$$\beta_E = \frac{-d \ln g}{d \ln T} \quad \text{and} \quad \beta_E = \gamma \beta \quad \text{where} \quad \gamma = \frac{-d \ln L}{d \ln T}$$

We find<sup>15</sup> that  $\beta_E$  is not uniquely defined by the value of  $g$  but is a function of both  $g$  and the Fermi energy. We have published a detailed analysis of our results and give reasons as to why the relationship between  $\beta$  and  $\beta_E$  does not invalidate the conclusion that a single parameter scaling function does not exist. There are two main objections to this conclusion, the first is the electron-electron interaction and the second is the nature

of inelastic scattering. Measurements of the interaction correction in the range of temperature and carrier concentration used show that its incorporation would have no effect on the obtained values of  $\sigma$ . There is of course the possibility that the interaction enters in a more subtle way. Measurements of the electron-electron scattering rate as a function of temperature support the assumption that  $\gamma = \gamma(q)$ . In order for our results to be consistent with one parameter scaling we would require  $L$  to vary as  $T^{-1/6}$ , a relation not found experimentally. Recently Kaveh<sup>16</sup> suggested that the obtained experimental behaviour of  $\beta_E$  can be explained theoretically on the power law localization model of Kaveh and Mott<sup>17</sup>. In this model a localization edge exists which separates exponentially localized states in the band tail from states which are power law localized. In this model the 2D conductivity as a function of length  $\sigma(L)$  is given by

$$\sigma(L) = \frac{\sigma}{(1 + \frac{\lambda}{2} \ln L/\ell)^2}$$

where  $\sigma_0$  is the Boltzmann conductivity,  $\ell$  is the elastic mean free path and  $\lambda$  is  $2/\pi k_F \ell$ . This formula gives a  $\beta_E$  function in good agreement with experiment. We note that such an experiment could not be performed on GaAs heterojunctions where Poole et al<sup>18</sup> have shown that the interaction effects are always present or in p inversion<sup>20</sup> layers where spin-orbit coupling is present.

We have investigated in detail the rate of electron-electron scattering from analysis of the negative magneto-resistance<sup>21</sup>. We confirm our earlier findings<sup>5,6</sup> that the rate  $(1/\tau_{ee})$  is due to a  $T$  term and a  $T^2$  term.

$$\tau_{ee}^{-1} = A_1 T + A_2 T^2.$$

We find that  $A_1$  is in agreement with the prediction of Uren et al<sup>5,6</sup> based on static screening which gives a value of  $2k/\hbar k_F \ell$ . The dynamic screening formula of Abrahams et al<sup>22</sup> which predicts a temperature dependence of  $T \ln T$  is in serious disagreement with experiment, as we have also found with other systems<sup>19,20</sup>. The  $A_2$  term is found to be in reasonable agreement with theory for Landau-Maker scattering. We have also investigated the electron-phonon coupling<sup>23</sup> and find that the effect of disorder is to introduce a more rapid scattering process in a similar manner to that found in electron-electron scattering.

We have previously reported experiments on the transition between three and two dimensions<sup>24,25</sup> and the associated change in the localization and interaction corrections. In a similar way we have electrically narrowed Si accumulation layers and observe large changes in conductivity and the temperature dependence of the conductivity<sup>26</sup>. These results indicate that when transport is 1D, or intermediate between 2D and 1D the corrections are large and cannot be regarded as a perturbation. The conductance oscillations do not appear to be a consequence of 1D behaviour<sup>27</sup>, but may be related to Coulomb effects in small regions.

This work was supported by the SERC and, in part, by the European Research Office of the U.S. Army.

# REFERENCES

1. Abrahams E, Anderson PW, Licciardello DC, Ramakrishnan TV, Phys. Rev. Lett. 42, 673, 1979.
2. Altshuler BL, Aronov AG and Lee PA, Phys. Rev. Lett. 44, 1268, 1980.
3. Uren MJ, Davies RA and Pepper M, J. Phys. C, 13, 1985, 1980.
4. Davies RA, Uren MJ and Pepper M, J. Phys. C, 15, L371, 1981
5. Uren MJ, Davies RA, Kaveh M and Pepper M, J. Phys. C, 14, 5737, 1981.
6. Dynes RC, Surf. Sci. 113, 510, 1982.
7. Kaveh M, Uren MJ, Davies RA and Pepper M, J. Phys. C, 14, L413, 1981.
8. Uren MJ, Davies RA, Kaveh M and Pepper M, J. Phys. C, 14, L395, 1981.
9. References 3, c. 14.
10. Altshuler BL and Aronov AG, JETP Lett. 33, 499, 1981
11. Kawabata A, Surf. Sci. 113, 510, 1982.
12. Bishop DJ, Tsui DC and Dynes RC, Phys. Rev. Lett. 46, 360, 1981.
13. Davies RA and Pepper M, J. Phys. C, 16, L361, 1983.
14. Davies RA and Pepper M, J. Phys. C, 16, L679, 1983.
15. Davies RA, Pepper M and Kaveh M, J. Phys. C, 16, L285, 1983.
16. Kaveh M, J. Phys. C, in the press.
17. Kaveh M and Mott NP, J. Phys. C, 14, L177, 1981.
18. Kaveh M and Mott NP, J. Phys. C, in the press.
19. Poole DA, Pepper M and Glew RJ, J. Phys. C, 14, L995, 1981.
20. Poole DA, Pepper M and Hughes A, J. Phys. C, 15, L1137, 1982.
21. Davies RA and Pepper M, J. Phys. C, 16, L353, 1983
22. Abrahams E, Anderson PW, Lee PA and Ramakrishnan TV, Phys. Rev. B, 24, 6783, 1981.
23. Payne MC, Davies RA, Inkson JC and Pepper M, J. Phys. C 15, L291, 1983.
24. Poole DA, Pepper M and Myron RW, Physica 117B, 697, 1983.
25. Poole DA, Pepper M, Berggren K-F, Hill G and Myron RW, J. Phys. C, 15, L21, 1982.
26. Dean CC and Pepper M, J. Phys. C, 15, L1287, 1982
27. Pepper M and Uren MJ, J. Phys. C 15, L617, 1982



# **Localization of 2D Electrons in GaAs-Al<sub>0.3</sub>Ga<sub>0.7</sub>As Heterostructures**

M. A. Paalanen\*, D. C. Tsui†, H. J. Van† and A. C. Gossard\*

\*Bell Laboratories, Murray Hill, NJ 07974

†Department of Electrical Engineering and Computer Science  
Princeton University, Princeton, NJ 08544

## **Abstract**

We determined in the weak localization regime the localization parameter  $\alpha$ , the interaction coefficient (1-F), the inelastic scattering time  $\tau_{in}$ , and its temperature coefficient  $p$ . Scattering by the Maki-Thompson process reduces  $\alpha$  to less than 1. In the extreme quantum limit, localization due to disorder, known to give rise to wide integral quantum Hall plateaus, is demonstrated to inhibit the fractional quantum Hall effect.

## **1. Introduction**

Localization is believed to be central to the many physical phenomena observed in two-dimensional (2D) electronic systems [1]. In this paper we report the results from two experiments on the localization of the 2D electrons in GaAs-AlGaAs heterostructures. In the first experiment [2], we investigated the weak localization phenomenon, which is observed experimentally as a logarithmic correction to the Drude conductivity. From detailed measurements on the temperature dependences of the resistance and the low field magnetoresistance, we determined directly the localization parameter,  $\alpha$ , the Coulomb interaction coefficient, (1-F), the inelastic electron scattering time,  $\tau_{in}$ , and its temperature coefficient,  $p$ . The experiment shows unambiguously that both the localization effect and the interaction effects are important in 2D electronic transport. We found that  $\alpha < 1$ . This reduction of  $\alpha$  is explained by the Maki-Thompson process, which is also operative in the case of the repulsive electron-electron interaction in our system. However, several outstanding features of the data remain unexplained. They include (1)  $\tau_{in}$  being ten times larger than theory, (2) (1-F) at a high density being five times its expected value, and (3) a temperature sensitive negative magnetoresistance in parallel B.

In the second experiment, we investigated the magnetotransport in the extreme quantum limit in a sample in which the recently discovered fractional quantum phenomenon [3] was not observed. The temperature dependences of both the diagonal resistivity,  $\rho_{xx}$ , and the Hall resistivity,  $\rho_{xy}$ , were studied as a function of the Landau level filling factor,  $\nu = nh/eB$ . We found that both  $\rho_{xx}$  and  $\rho_{xy}$  show a thermally activated, nonmetal-like behavior for  $\nu < 1/2$ . Our results demonstrate that while localization due to disorder is essential to the observation of the integral quantum Hall effect [4], extremely high electron mobility, indicative of minimal disorder and a high degree of lattice and interfacial perfection, is prerequisite for the fractional quantum Hall effect. The two effects are different in origin and in fact competing with each other.

## **2. Experimental Details**

Our samples were GaAs-AlGaAs heterostructures, consisting of a 1  $\mu$ m thick undoped GaAs layer, an undoped Al<sub>0.3</sub>Ga<sub>0.7</sub>As layer, a Si-doped Al<sub>0.3</sub>Ga<sub>0.7</sub>As layer, and a thin GaAs cap layer, sequentially grown on Cr-doped GaAs substrates by molecular beam epitaxy. The Si-doped Al<sub>0.3</sub>Ga<sub>0.7</sub>As layer was made sufficiently thin that the depletion layer extends throughout the entire Al<sub>0.3</sub>Ga<sub>0.7</sub>As layer. As a result, the doped layers are depleted of free carriers and the electronic conduction is by the 2D electrons in the undoped GaAs layer confined to the GaAs-AlGaAs interface. The electron density was determined from measuring the quantum oscillations of the 2D electrons [5], and from low field Hall measurements. Agreement between the two measurements indicates that no parallel channel conduction existed in our samples. Our transport and low field magnetotransport measurements from 0.05 K to 0.8 K were carried out in a dilution refrigerator with a superconducting solenoid, using standard four terminal arrangements.

## **3. Weak Localization**

Detailed measurements were made in the weak localization regime on three different samples with electron densities  $n = 7.11 \times 10^{11}/\text{cm}^2$ ,  $2.86 \times 10^{11}/\text{cm}^2$ , and  $0.87 \times 10^{11}/\text{cm}^2$  and mobilities  $\mu = 2.99 \times 10^4 \text{ cm}^2/\text{Vsec}$ ,  $0.55 \times 10^4 \text{ cm}^2/\text{Vsec}$ , and  $1.65 \times 10^4 \text{ cm}^2/\text{Vsec}$ , respectively. All samples show logarithmic T dependence in their conductivity in the absence of an external magnetic field, B, and a negative magnetoresistance in a perpendicular B. The results are interpreted in terms of the scaling theory of localization [6] and the theory of Coulomb effects [7] on transport in disordered media. Since details of this work are to be published elsewhere [2], only a brief summary will be given here.

In the absence of B, both the localization and the interaction effects contribute  $\tau_0$  to the observed logarithmic T dependence in conductivity according to [6,7]

$$\Delta\sigma(T) = \alpha p \sigma_N \ln \left[ \frac{T}{T_0} \right] \quad (1a)$$

and

$$\Delta\sigma(T) = (1-F) \sigma_N \ln \left[ \frac{T}{T_0} \right] \quad (1b)$$

respectively. Here  $\sigma_N = e^2/2\pi^2\hbar$  and  $p$  is the temperature exponent of the inelastic scattering time,  $\tau_{in} \propto T^p$ . The localization parameter  $\alpha$  is unity for independent particles and the Hartree parameter  $F$  is defined by

$$F = \int_0^{k_F} \frac{d\theta/2\pi}{(1 + 2k_F/K)\sin\theta} \quad (2)$$

where  $k_F$  is the Fermi-wave vector and  $K = m^*e^2/2\pi\epsilon\hbar$  is the 2D screening constant. In this work,  $\alpha$ ,  $p$ , and (1-F) are regarded as the unknown parameters determined by fitting our experimental data to theory [8]. This is accomplished by applying a perpendicular B, which affects the two effects differently in different ranges of B. More specifically, in the weak B limit ( $B < 0.1$  T), the observed negative magnetoresistance allows a direct determination of  $\alpha$  and  $\tau_{in}$ .

and the  $T$  dependence of  $\tau_{tr}$  yields  $p$  directly [9]. On the other hand, with  $B \sim 0.3$  T, the localization term is quenched entirely and the  $T$  dependence of the conductivity directly determines  $(1-F)$ .

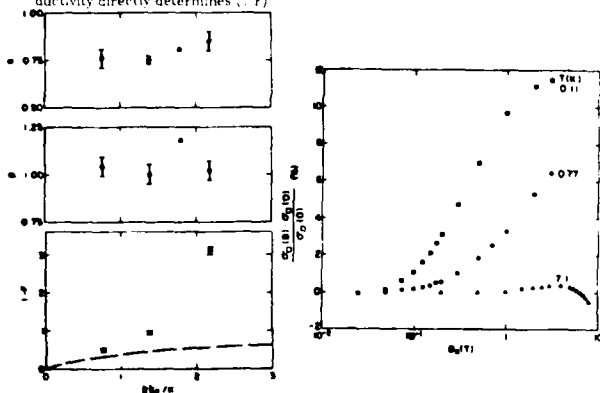


Figure 1.  $\alpha$ ,  $p$  and  $(1-F)$  plotted as a function of  $T$ ,  $K$  from three samples. The triangle is from Ref. [4] and the dashed curve is calculated from Eq. (2).

Figure 2. Percentage change in the conductivity as a function of parallel  $B$  from the sample with  $n_s = 2.86 \times 10^{11}/\text{cm}^2$  and  $\mu = 0.55 \times 10^4 \text{ cm}^2/\text{Vsec}$ .

Figure 1 summarizes our results on  $\alpha$ ,  $p$  and  $(1-F)$ . Several comments are in order. First,  $\alpha < 1$ , and this fact cannot be accounted by the spin-orbit interaction in GaAs [2]. We attribute this reduction of  $\alpha$  to scattering by the Vaxel-Thompson process that gives rise to fluctuations in superconductivity. It was pointed out by Larkin [10] that this process is expected to be also operative in the case of repulsive electron-electron interactions. Second,  $p = 1$ , suggesting electron-electron scattering as the dominant inelastic process. However the magnitude of  $\tau_{tr}$  ( $\sim 5 \times 10^{-11}$  sec at 1 K) is an order of magnitude larger than that from the theory of Abrahams et al. [11]. Third,  $(1-F)$  is considerably larger than that calculated from Eq. (2) (dashed curve in Fig. 1). The difference is especially large at large  $n$ , where saturation is expected. Finally, Fig. 2 shows the percentage change in the conductivity with  $B$  parallel to the plane of the 2D electrons. Instead of the expected positive magneto-resistance [7], a strongly  $T$  dependent negative magneto-resistance was observed. This effect, also seen in the 2D electrons in  $\text{ZnO}$  [12] and in  $\text{InAs}$  [13], remains unexplained.

#### 4. Localization in the Extreme Quantum Limit

Figure 3 shows the high field magnetotransport data taken from a sample with  $n = 8.6 \times 10^{10}/\text{cm}^2$  and  $\mu = 2.1 \times 10^4 \text{ cm}^2/\text{Vsec}$ . The integral quantum Hall plateaus given by  $R_H = \rho_{xy} = h/ie^2$ , with  $i = 2$  and  $1$  are well developed, together with the vanishing of  $\rho_{xx}$  around  $B \sim 2$  T and  $4$  T respectively. However, structures due to the fractional quantum Hall effect around  $\nu = 2/3$  and  $1/3$  is not observable at all with  $T$  down to  $0.05$  K. Our failure to observe any structure attributable to the fractional quantum Hall effect results from the fact that this sample has low  $\mu$ , indicative of strong disorder in the 2D electron system. The presence of such strong disorder inhibits the formation of the new electronic ground state, which gives rise to the fractional quantum phenomenon. Our data can be understood in terms of the localization due to the disorder, which in the current picture for the integral quantum Hall effect are essential to the observability of the Hall plateaus.

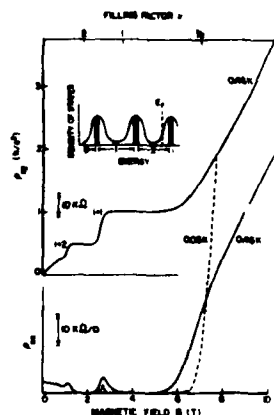


Figure 3.  $\rho_{xx}$  and  $\rho_{xy}$  vs.  $B$  from a sample having  $n_s = 8.6 \times 10^{10}/\text{cm}^2$  and  $\mu = 2.1 \times 10^4 \text{ cm}^2/\text{Vsec}$ . The filling factor is defined by  $\nu = nh/eB$ . Inset illustrates the disorder broadened lowest three Landau levels. The extended states are the shaded regions.

According to Laughlin's argument [4], observation of the integral quantum Hall plateaus necessarily implies the existence of a finite number of extended states in every Landau level beneath  $E_F$  to carry the Hall current. As illustrated in the inset of Fig. 3, each Landau level, broadened by disorder into a band, must contain some extended states (shaded regions in the illustration), separated from the localized states. When  $E_F$  is in the region of the localized states labeled 2, the Hall current is carried by the extended states in the lowest two subbands and the  $i = 2$  plateau is observed. When  $B$  is increased,  $E_F$  moves

into the extended states in the second Landau level between regions 1 and 2 and  $\rho_{xx}$  increases. It reaches the  $\nu = 1$  plateau as  $E_F$  enters the localized region. Unlike the 2D electrons in Si-inversion layers, where the  $\nu = 1$  plateau was not resolved, the  $\nu = 1$  plateau is obvious here and it demonstrates the fact that not all the states in the lowest level are localized. If the broadening is symmetric, the extended states are expected to center at  $\nu = 1/2$ . Under this condition,  $\rho_{xy}$  will remain on the  $\nu = 1$  plateau until  $E_F$  is sufficiently close to the center of the band to allow thermal excitations in the extended states. At sufficiently high B, when  $E_F$  enters the localized region labeled 0, there is no extended states below  $E_F$  to carry the Hall current and  $\rho_{xy}$  should reflect that of the thermally excited states in the center of the band. At  $T = 0$ ,  $\rho_{xy}$  is expected to increase abruptly to infinity from the  $\nu = 1$  plateau and  $\rho_{xx}$  from its vanishing value, at  $\nu = 1/2$ .

Figures 4 and 5 show the temperatures dependences of  $\rho_{xy}$  and  $\rho_{xx}$  near  $\nu = 1/2$ . It is clear that at  $\nu = 0.37$  both  $\rho_{xy}$  and  $\rho_{xx}$  are thermally activated, indicative of an  $E_F$  inside the localized region of the lower part of the band. At  $\nu = 0.58$ ,  $\rho_{xy}$  decreases towards the  $\nu = 1$  plateau (i.e.  $h/e^2$ ) and  $\rho_{xx}$  decreases towards zero with decreasing T. This is the expected behavior when  $E_F$  is located inside the localized region of the upper part of the band (i.e. region 2). The transition from the first to the second behavior occurs at  $\nu \sim 0.5$ , as expected. However, our data are insufficient to determine the number of the extended states or whether sharp mobility edges do exist, separating them from the localized states.

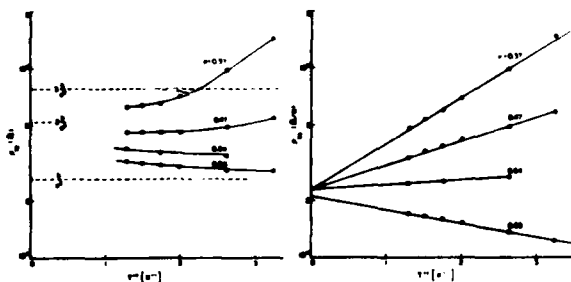


Figure 4.  $\rho_{xy}$  vs.  $1/T$

Figure 5.  $\rho_{xx}$  vs.  $1/T$

The work at Princeton University was supported by the Office of Naval Research through Contract No. N00014-82-K-0450

#### References

1. See for example, T. Ando, A.B. Fowler and F. Stern, *Rev. Mod. Phys.* **54**, 437 (1982).
2. B.J.F. Lin, M.A. Paalanen, D.C. Tsui and A.C. Gossard (to be published).
3. D.C. Tsui, H.L. Stormer and A.C. Gossard, *Phys. Rev. Lett.* **48**, 1559 (1982).
4. R.B. Laughlin, *Phys. Rev. B* **23**, 5632 (1981).
5. D.C. Tsui and R.A. Logan, *Appl. Phys. Lett.* **35**, 99 (1979).
6. E. Abrahams, P.W. Anderson, D.C. Licciardello and T.V. Ramakrishnan, *Phys. Rev. Lett.* **42**, 673 (1979).
7. B.C. Altshuler, A.G. Aronov and P.A. Lee, *Phys. Rev. Lett.* **44**, 1288 (1980).
8. B.L. Altshuler, D. Khmelntzku, A.I. Larkin and P.A. Lee, *Phys. Rev. B* **22**, 5142 (1980).
9. R.G. Wheeler, *Phys. Rev. B* **24**, 4645 (1981).
10. A.I. Larkin, *JETP Letters* **31**, 219 (1980).
11. E. Abrahams, P.W. Anderson, P.A. Lee and T.V. Ramakrishnan, *Phys. Rev. B* **24**, 6783 (1981).
12. Y. Goldstein, Y. Grinshpan and A. Many, *Phys. Rev.* **19**, 2256 (1979).
13. S. Kawaji and Y. Kawaguchi, *Proc. 9th Intl. Conf. Phys. Semiconductors, Moscow (Nanka, Leningrad)*, p. 730, 1968.
14. D.A. Poole, M. Pepper and R.W. Glen, *J. Phys. C* **14**, L995 (1981).

## TRANSPORT STUDIES IN SINGLE-CRYSTAL FILMS OF $\text{CoSi}_2$ AND $\text{NiSi}_2$ : A NEW CLASS OF QUASI TWO-DIMENSIONAL METALS

J. C. Hensel, R. T. Tung, J. M. Pate  
and F. C. Unterwald

Bell Laboratories, Murray Hill, New Jersey 07974, USA

Measurements have been made of electrical transport in single-crystal, thin films of  $\text{CoSi}_2$  and  $\text{NiSi}_2$ . Controlled amounts of defects were introduced into certain films by 2 MeV  $^4\text{He}$  bombardment. These systems possess novel properties favorable for studies of quasi 2-dimensional phenomena in metals such as weak localization

### 1. Introduction

Metal silicide thin films occupy a prominent place in present-day integrated circuit technology, serving as conductors to link circuit elements and as contacts. In this connection, the formation and structure of thin film disilicides have been extensively investigated.<sup>1</sup> Relatively less is known about the electronic properties of these important materials. In particular, apart from the fact that they behave typically as good metals with high conductivities, not much else is available regarding their electrical transport properties and the mechanisms responsible for resistivity — a little surprising in view of their use as conductors. To address this problem we have undertaken transport studies in thin films of  $\text{CoSi}_2$  and  $\text{NiSi}_2$ . Preliminary results suggest that these thin films possess novel features that could be exploited in the study of quasi 2D phenomena, e.g., weak localization.

### 2. Structural Properties of $\text{NiSi}_2$ and $\text{CoSi}_2$ Thin Films

Much of what is distinctive about  $\text{NiSi}_2$  and  $\text{CoSi}_2$  thin films owes to their structural properties which we briefly summarize. Of all the metal silicides  $\text{CoSi}_2$  and  $\text{NiSi}_2$  are unique in that they crystallize in the (cubic) fluorite structure and, moreover, have lattice constants within a percent or two of that of Si. Thus they are particularly good candidates for epitaxial growth on Si substrates; and, indeed, extensive studies<sup>2</sup> have demonstrated that under UHV conditions single crystal epitaxial films of extraordinary perfection can be grown with thicknesses varying from the ultra thin ( $\sim 60$  Å)

up to 1000 Å or more. The continuity and uniformity of these film is excellent as monitored by RBS and TEM. In addition, the interface of these structures is found to be remarkably sharp, in fact under favorable conditions it becomes essentially perfect on an atomic scale.

In the present work the thinner films were single crystal grown by means of the UHV techniques we have described earlier.<sup>3</sup> The thicker films were either single crystal or polycrystalline of grain size  $\sim 1000$  Å, both types exhibit essentially the same resistivity. All films were grown on n-type Si substrates, either (001) or (111) orientations, of 1-10  $\Omega\text{cm}$  resistivity. Controlled levels of defects were introduced into certain films by bombardment at 77K with 2 MeV  $^4\text{He}$  ions.<sup>3</sup>

### 3. Transport Measurements

Measurements of the resistivity of comparatively thick films ( $\sim 1000$  Å) of  $\text{CoSi}_2$  and  $\text{NiSi}_2$  are shown in Fig. 1 as a function of temperature. The measurements were made in a 4 probe configuration on bridge shaped samples patterned by photolithography and etched chemically. The curves are of the usual form having at high temperatures a linear temperature dependence owing to phonon scattering and flattening off at low temperature to a value  $\rho_0$ , the residual resistivity due to defects, impurities, boundary scattering, etc. Assuming Matthiessen's rule to hold we can express the total resistivity as a sum of residual and phonon scattering contributions,  $\rho = \rho_0 + \rho_1(T)$ . If we examine first the data in Fig. 1 labelled "undamaged" we see that the phonon scattering contribution,  $\rho_1(T)$ , is virtually identical for  $\text{CoSi}_2$  and  $\text{NiSi}_2$ , but the residual resistivity for  $\text{NiSi}_2$  ( $\rho_0 = 20 \mu\Omega\text{cm}$ ) is almost an order of magnitude larger than for  $\text{CoSi}_2$  ( $\rho_0 = 2.6 \mu\Omega\text{cm}$ ). (In the former case  $\rho_0$  is to some extent sample dependent, but  $20 \mu\Omega\text{cm}$  is the lowest value observed so far.) The implication is that there is a rather substantial inherent concentration of defect centers in  $\text{NiSi}_2$  not present or present at a much lower concentration in  $\text{CoSi}_2$ , a rather surprising development in view of the similarity of  $\text{CoSi}_2$  and  $\text{NiSi}_2$  in so many other respects.

If defects are indeed the explanation, one should be able to simulate the properties of  $\text{NiSi}_2$  by damaging  $\text{CoSi}_2$  with high energy ion bombardment. The results shown in Fig. 1 by a family of curves each representing a different bombardment dose of 2 MeV  $^4\text{He}$  ions bear out this supposition.

A dose of  $\sim 2.4 \times 10^{16}$  He/cm<sup>2</sup> would render CoSi<sub>2</sub> roughly equivalent to undamaged NiSi<sub>2</sub>. Also included in Fig. 1 is one case of NiSi<sub>2</sub> bombarded with a dose of  $5 \times 10^{16}$  He/cm<sup>2</sup>, more than doubling its  $\rho_0$ . A most remarkable feature of Fig. 1 is that all curves display virtually identical temperature dependences; they differ only in their vertical displacements representing different values of  $\rho_0$  — all in all an impressive testimony to Matthiessen's rule.

Next, by plotting in Fig. 2 the incremental change in  $\rho_0$  for CoSi<sub>2</sub> produced by ion bombardment we observe that there is a linear dependence to the highest level reached,  $\rho_0 \approx 86 \mu\Omega\text{cm}$ . Eventually (perhaps 2 to 3 times higher) saturation would be expected to occur when the material becomes so strongly disordered as to become essentially a metallic glass. The fact that saturation has not yet been reached at  $\approx 86 \mu\Omega\text{cm}$  establishes a lower limit on the elastic scattering length  $l_e$  in undamaged CoSi<sub>2</sub> for which  $\rho_0 = 26 \mu\Omega\text{cm}$ . By invoking the Ioffe-Regel criterion we note that  $l_e > (86/26)a_0$  where  $a_0 = 2.4 \text{ \AA}$  is the atomic spacing in CoSi<sub>2</sub>, resulting in  $l_e > 80 \text{ \AA}$ . Also in Fig. 2 is one datum for NiSi<sub>2</sub> which interestingly enough almost exactly coincides with CoSi<sub>2</sub>. This would tentatively suggest that these two materials are essentially equally susceptible to defect formation by ion bombardment.

The nature of the defects responsible for the large  $\rho_0$  in NiSi<sub>2</sub> is unknown. One is tempted to speculate that there exists in NiSi<sub>2</sub> an intrinsic concentration of natural defects, perhaps antisite defects or possibly a slight unbalance in stoichiometry. The very large changes of  $\rho_0$  with bombardment dose evidences an unusual degree of susceptibility of the CoSi<sub>2</sub> and NiSi<sub>2</sub> lattices to damage, quite reminiscent of a similar behavior seen earlier<sup>1</sup> in the A-15 compounds and associated with the easy breaking of tetrahedral bonds. The same explanation could apply to the fluorite structure of CoSi<sub>2</sub> where the Si's occupy tetrahedral sites.

#### 4. Weak Localization

The scaling theory of weak localization<sup>4</sup> predicts that in 2D no true metallic conduction can occur and as  $T \rightarrow 0$  the resistivity does not approach a constant value, but instead diverges logarithmically.

$$\frac{R(T) - R(T_0)}{R(T_0)} = \frac{\Delta R}{R_0} = \frac{\alpha P}{2\pi^2 \left( \frac{\hbar}{e^2} \right)} R_0 \ln \left( \frac{T}{T_0} \right) \quad (1)$$

Here,  $P$  is an exponent in the temperature dependence of the inelastic scattering time ( $\tau_i \propto T^{-P}$ ) and  $\alpha$  is a constant of order unity. A number of studies of these effects in thin metallic films have been reported.<sup>5</sup>

It is our purpose here to point out that CoSi<sub>2</sub> and NiSi<sub>2</sub>, as the transport measurement demonstrate, can provide a significant feature that has been lacking in most work, namely the ability to control independently the important parameters,  $R_0$  (representing the strength of localization) and film thickness (representing the degree of quasi two dimensionality). This is in addition to the very desirable structural properties mentioned earlier. As an example, some tentative data has been obtained for a 240 Å single crystal film of CoSi<sub>2</sub> grown with a rather high concentration of defects but otherwise of excellent quality as regards to uniformity, structure, etc. The results in Fig. 3 show a logarithmic dependence in sheet resistance below  $\sim 20\text{K}$ , consistent with a localization picture, with  $\alpha P \approx 5$ , somewhat larger than the values in the neighborhood of 2 more typically seen. Simple estimates would indicate that  $k_F l_e \geq 1$  ( $k_F$  is the Fermi wavevector) insuring the validity of (1) for the case under consideration. The extent to which Coulomb interactions and/or Kondo scattering contribute to the logarithmic dependence will become clearer as these studies progress.

#### Acknowledgements

It is a pleasure to thank R. C. Dynes for a number of invaluable discussions and D. C. Jacobson for his contributions to the experimental work.

#### References

- [1] S. P. Murarka, "Silicides for VLSI Applications" (Academic Press, New York, 1983)
- [2] See for example R. T. Tung, J. M. Poate, J. C. Bean, J. M. Gibson and D. C. Jacobson, *Thin Solid Films* 93, (1982) 77; and R. T. Tung, J. M. Gibson and J. M. Poate, *Phys. Rev.*

*Lett.* 50, (1983) 429, and *Appl. Phys. Lett.* 42, (1983) 888

- [3] L. R. Testardi, J. M. Puente and H. J. Levinstein, *Phys. Rev. B* 15 (1977) 2570
- [4] E. Abraham, P. W. Anderson, D. C. Licciardello and T. V. Ramakrishnan, *Phys. Rev. Lett.* 42, (1979) 673
- [5] I. Van den dries, C. van Heesendonck, Y. Bruynseraede and G. Deutscher, *Phys. Rev. Lett.* 46, (1981) 565; R. S. Markiewicz and L. A. Harris, *Phys. Rev. Lett.* 46, (1981) 1149; G. Bergman, *Phys. Rev. Lett.* 48, (1982) 1046, and A. White, R. C. Dynes and J. P. Garno (to be published)

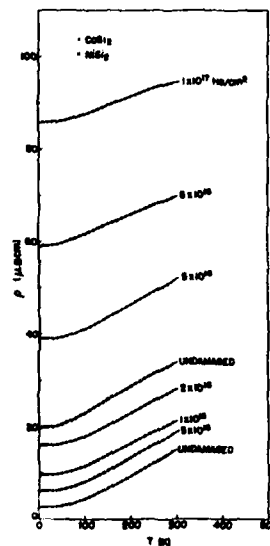


Fig. 1.  
Temperature dependence of resistivity of 1100 Å thick epitaxial films of CoSi<sub>2</sub> and NiSi<sub>2</sub> [Si(001)] damaged by 2 MeV <sup>4</sup>He ion bombardment.

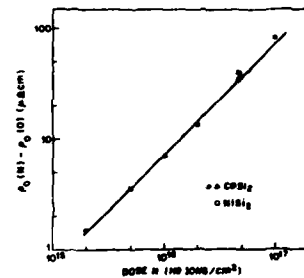


Fig. 2.  
Incremental increase of residual resistivity with 2 MeV <sup>4</sup>He ion bombardment dose N. The datum symbolized by the triangle was obtained by means of bombardment with 2 MeV <sup>3</sup>He ions with a dose (5 × 10<sup>14</sup> He/cm<sup>2</sup>) equivalent to 5 × 10<sup>16</sup> cm<sup>-2</sup> of <sup>4</sup>He ions.

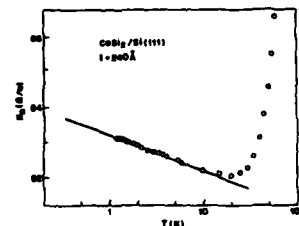


Fig. 3.  
Low temperature logarithmic dependence on T of sheet resistance R<sub>s</sub> for a 240 Å thick epitaxial film of CoSi<sub>2</sub>/Si(111).

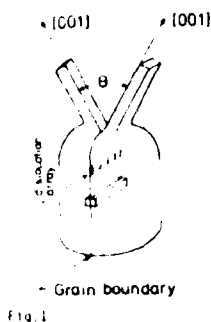
# ANOMALOUS MAGNETO-TRANSPORT PROPERTIES OF p-TYPE GERMANIUM INVERSION LAYERS AT VERY LOW TEMPERATURES

G. Kemenyi, S. Uchida\*, G. Landwehr, Max-Planck-Institut für Festkörperforschung, Hochfeldmagnetlabor Grenoble, F38042 Grenoble, France, A. Briggs, C.R.T.B.T. and S.N.C.I., Centre National de la Recherche Scientifique, Grenoble, and E. Baumert, Physikalisches Institut der Universität Würzburg, Germany.

\*present address : University of Tokyo, Department of Applied Physics

**Abstract :** A logarithmic increase of resistivity of p-type Ge-inversion layers adjacent to a grain boundary in Ge-bicrystals levels off in the mK range, whereas the longitudinal magneto-resistance continues to rise. At very low temperature a negative magnetoresistance is observed which is possibly connected with the Kondo-effect.

Recently we have begun to study the magneto-transport properties of p-type germanium inversion layers present in germanium bicrystals (1). These can be produced in a controlled fashion by pulling crystals in which the 2 halves have been tilted with respect to each other. In our case we investigated bicrystals in which the [001] directions were tilted relative to a [100] axis, the twist angle being negligibly small. This is schematically shown in fig.1.



In this configuration a grain boundary arises which is stabilized by an array of dislocations. For not too large tilt angles a regular sequence of edge dislocations with acceptor character exists (2). The resulting hole concentration is so large that a degenerate p-type layer arises for tilt angles  $\theta > 8^\circ$ . The linear character of the acceptors manifests itself in an anisotropy of the conductivity, depending on whether the current flows parallel or perpendicular with

respect to the dislocations. It became evident already many years ago that the holes adjacent to a grain boundary with a tilt angle of  $20^\circ$  represent a two-dimensional electronic system (3). This was clearly demonstrated recently (4) when the anisotropy of Shubnikov-de Haas oscillations in a bicrystal with a  $15^\circ$  tilt angle was analysed. Self-consistent solutions of Schrödinger's and Poisson's equation indicated that the system is quantized with discrete electrical subbands. For surface carrier concentrations above  $10^{12}/\text{cm}^2$  both the heavy and light hole subband are occupied, with a splitting substantially larger than  $kT$  at helium temperatures. Whereas the heavy hole mass does not differ much from the bulk values, the light hole mass is substantially enhanced, the actual value depending on the carrier concentration.

From the logarithmic increase of resistivity and Hall coefficient with decreasing temperature it was deduced (1) that many-body effects dominate in specimens prepared from bicrystals with  $10^\circ$  and  $15^\circ$  tilt angle. In magnetic fields up to  $B = 10$  T the magneto-resistance increased logarithmically with  $B$ . The existence of a finite longitudinal magneto-resistance indicates that localization effects caused by quantum interference in the 2d-system are of minor importance. This conclusion is corroborated by the absence of a negative transverse magneto-resistance in the low field range.

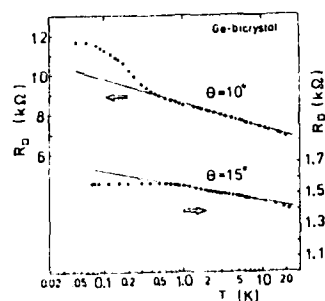


Fig.2.

In the meantime we have extended measurements of resistivity, longitudinal and transverse magneto-resistance of bicrystal specimens with a tilt angle of  $10^\circ$  and  $15^\circ$  to temperatures down to 50 mK. It turned out that the logarithmic increase of resistivity with decreasing temperature does not continue in the mK range. This is

shown in fig. 2 where the resistance per unit area has been plotted as a function of temperature for samples with  $\theta=10^\circ$  and  $15^\circ$ . Whereas for the  $15^\circ$  specimens the resistivity levels off at about 600 mK a larger increase is observed in the  $10^\circ$  specimens below 500 mK before R is getting constant at about 80mK. It was checked that this is not due to noise heating. External high frequency signals were effectively blocked off. The dissipated power due to the sample current was below  $10^{-13}$  W, an increase of the power by about 2 orders of magnitude did not change the resistivity measurably. A temperature independent resistivity in the mK range has also been observed in Si-inversion layers (5).

The longitudinal magneto-resistance for both the  $15^\circ$  and  $10^\circ$  specimens increased logarithmically as a function of B down to about 1.2 K with a scaling behaviour proportional B/T. At  $T = 0.6$  K significant deviations from scaling showed up which became more and more pronounced when the temperature was lowered further. This may be visualized in fig.3 where the negative change of

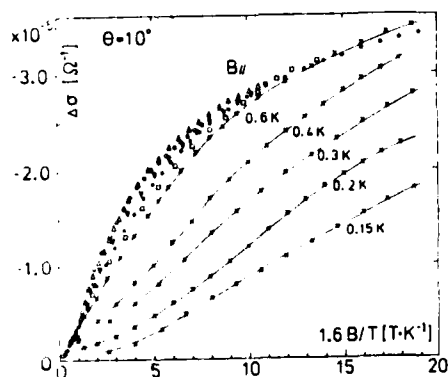


Fig. 3.

conductivity has been plotted against B/T for a  $10^\circ$  specimen. The observed change in resistance in a longitudinal magnetic field increases very strongly with the temperature in the mK range. This can be seen in fig. 4. Whereas the

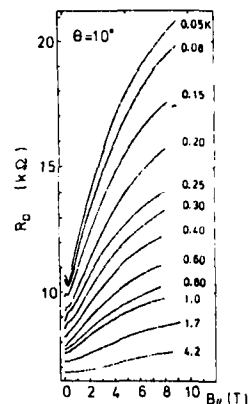


Fig. 4.

lowered. A negative magneto-resistance develops at  $T < 0.3$  K, at a temperature of 0.1 K the magneto-resistance is negative between about 0.5 and 2.5 T. At high magnetic fields the magneto-conductivity shows a linear dependence on the magnetic field. So far a negative magneto-resistance in the mK range has only been observed in specimens in which the dislocations were oriented parallel to the current.

relative change of resistance in a longitudinal field of 8 T is about 10% the changes observed at 50 mT are larger than 100%. In the low temperature range a negative magneto-resistance shows up which becomes positive above  $B = 1$  T. A similar behaviour was found in samples with a tilt angle of  $15^\circ$ . This is demonstrated in fig.5. Because of the presence of high mobility holes in the light hole subband we preferred to plot the negative change of conductivity with magnetic field. One can see that a hump in the  $\Delta\sigma$  vs B curves develops which becomes more and more pronounced when the temperature is

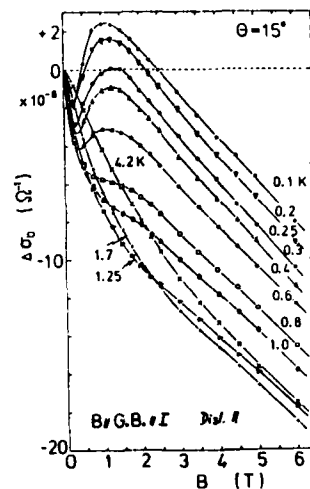


Fig. 5.



The magneto-transport data obtained previously on samples with  $\theta = 10^\circ$  and  $15^\circ$  can be analysed within the framework of a theory by Fukuyama (5) which employs 4 parameters,  $g_1$  to  $g_4$ . The measurement of the magneto-resistance in parallel and transverse magnetic fields allows a complete evaluation of the constants. Deviations from the predictions of the first order theory (5) indicate the necessity to incorporate higher order effects (6). The scaling behaviour as a function of  $B/T$  suggests that the Zeemann splitting of the energy levels is the origin of the relatively large longitudinal magneto-resistance. It should be noted, however, that the magneto-resistance observed in our specimens is very large (up to 100%) so that it is doubtful whether it is allowed to make use of results which have been obtained by perturbation theory. The observed negative magneto-resistance in the mK range at not too high fields suggests that spin dependent scattering could be the origin of the effect. The interplay between the Kondo effect and localization and the many-body effects could be the origin of the observed anomalies. It is not probable that a substantial concentration of magnetic impurities is present at the grain boundary of our bicrystals. One should keep in mind, however, that the dangling bonds of edge dislocations in germanium may have a high concentration. It is probable that only a relatively small percentage of the acceptor states along the dislocation are occupied due to the band bending caused by the Coulomb field.

It seems that it is necessary to take also anisotropy effects into account because the negative magneto-resistance in the mK range has only been observed in samples with parallel dislocations.

**Acknowledgements :** The authors would like to thank Mr. Köhler of the Max-Planck-Institut für Festkörperforschung, Stuttgart for pulling the crystals and Prof. H. Fukuyama, Tokyo for communicating results prior to publication.

#### References :

- (1) S. Uchida and G. Landwehr, in Application of High Magnetic Fields in Semiconductor Physics, Grenoble 1982, G. Landwehr Ed., Springer Verlag, 1983, p. 65
- (2) See, e.g. H. F. Mataré: Defect Electronics in Semiconductors, Wiley Interscience, 1971
- (3) G. Landwehr and P. Handler, J. Phys. Chem. Solids **23**, 891 (1982)
- (4) S. Uchida, G. Landwehr and E. Bangert, Solid State Comm. **45**, 869 (1983)
- (5) M. J. Uren, R. A. Davies, M. Kavch and M. Pepper, J. Phys. C: Solid State Physics **14**, 5737 (1981)
- (6) H. Fukuyama, J. Phys. Soc. Japan **48**, 216 (1980)
- (7) H. Fukuyama, Y. Isawa and H. Yasuhara, to be published.

#### Figure captions :

- Fig. 1 : Schematic drawing of a bicrystal. The {001} seeds are tilted by the angle  $\theta$ .
- Fig. 2 : Resistance per unit area as a function of temperature for 2 bicrystals with different tilt angle.
- Fig. 3 : Change of conductivity (with negative sign) as a function of  $B/T$  for a longitudinal magnetic field.
- Fig. 4 : Resistance per unit area as a function of a longitudinal magnetic field for a  $10^\circ$  bicrystal at various temperatures.
- Fig. 5 : Negative change in conductivity per unit area as a function of a parallel magnetic field with the temperature as parameter.

# Theory of Impurity Band Conductivity in Inversion Layers in Magnetic Fields

G. M. Kramer and R. P. Wallis  
Physics Department

University of California, Irvine, CA 92717, USA

A theoretical investigation has been made of the electrical conductivity of an impurity band in an inversion layer in an external magnetic field. The specific case of an n-type inversion layer on a (100) surface of silicon is considered. A distribution of impurity ions is assumed to exist at the interface between the inversion layer and the oxide. Results are obtained for several values of the electric field in the inversion layer and for the two-dimensional limit corresponding to zero inversion layer thickness. Contact is made with the experimental results of Hartstein, Fowler and Woo.

## 1. Introduction

Over the last few years, Hartstein and Fowler [1] have carried out a series of experiments on the electrical conductivity of silicon inversion layers where  $\text{Na}^+$  have been diffused to the oxide-inversion layer interface. Over a certain temperature range, they found that the data can be understood on the basis of variable range hopping of charge carriers in an impurity band. Recently, Hartstein, Fowler, and Woo [2] found that an external magnetic field significantly decreases the conductivity at fields above 4T and attribute this behavior to the shrinkage of the impurity orbit size by the magnetic field. In the present paper, we develop a theory of variable range hopping conductivity in inversion layers in magnetic fields.

## 2. Theoretical development

The system which we consider is composed of two semi-infinite half-spaces, one of p-type silicon and the other of silicon dioxide with a common boundary parallel to a (100) plane of the silicon. The inversion layer is produced by an electric field normal to the interface which is assumed to be constant over the extent of the inversion layer. A distribution of impurity ions of charge  $+e$  is assumed to be present at the oxide-semiconductor interface. The external magnetic field is taken to be constant and oriented normal to the interface.

The first step in our calculation is to write the Hamiltonian in atomic units [3] in the form

$$H = H_0 + H_1 + H_2, \quad (1)$$

$$H_0 = -\frac{\mu}{2} \frac{\partial^2}{\partial x^2} + \frac{\delta}{x} + \kappa \epsilon z, \quad x > 0, \quad (1a)$$

$$H_1 = -\frac{\delta^2}{\partial x^2} - \frac{\delta^2}{\partial y^2} + i\gamma(y \frac{\partial}{\partial x} - x \frac{\partial}{\partial y}) + \frac{\gamma^2}{4} (x^2 + y^2), \quad (1b)$$

$$H_2 = U(x) = -2/[x^2 + y^2 + z^2]^{1/2}, \quad (1c)$$

where  $\mu = m_e/m_i$ ,  $\delta = (\epsilon_2 - \epsilon_1)/4\epsilon_2$ ,  $\kappa = \hbar^4(\epsilon_1 + \epsilon_2)^3/4m_e^2 e^5$ ,  $\epsilon$  is the electric field in esu,  $m_e$  and  $m_i$  are the transverse and longitudinal effective masses,  $\epsilon_1$  and  $\epsilon_2$  are the dielectric constants of  $\text{SiO}_2$  and Si, respectively,  $\gamma = (a_0^*)^2/(\hbar c/eH)$ ,  $a_0^*$  is the effective Bohr radius [3] and  $H$  is the magnetic field. The quantity  $U(x)$  is the Coulomb interaction of the electron with the impurity ion neglecting screening by the free carriers.

For the ground state wave function, we take the form

$$\psi(x, y, z) = \chi(x, y) f(z). \quad (2)$$

The functions  $\chi(x, y)$  and  $f(z)$  have the variational forms

$$\chi(x, y) = A \exp[-\frac{1}{2} \alpha (x^2 + y^2)^{1/2}] \quad (3)$$

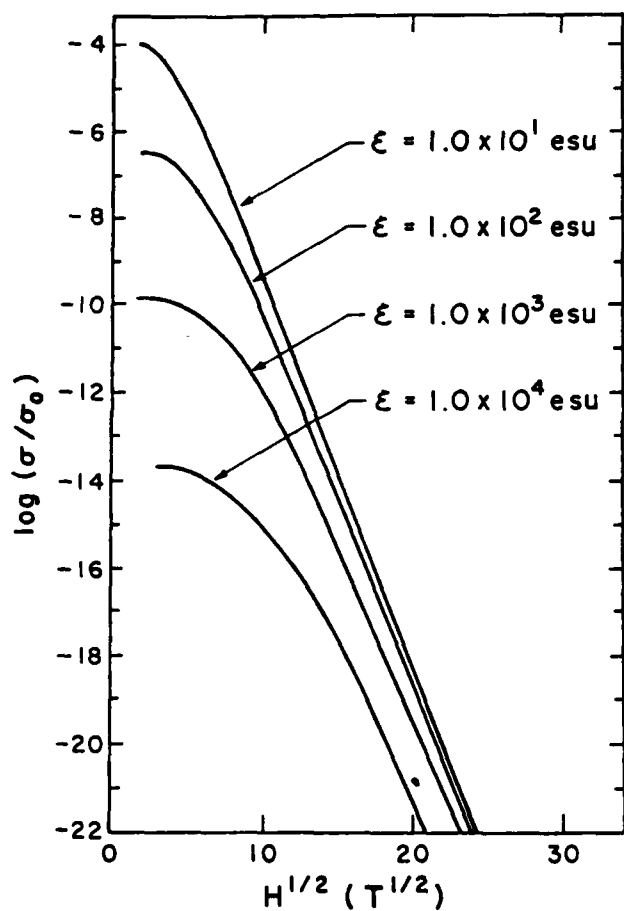


Fig. 1. Magnetic field dependence of impurity band conductivity for several values of electric field.

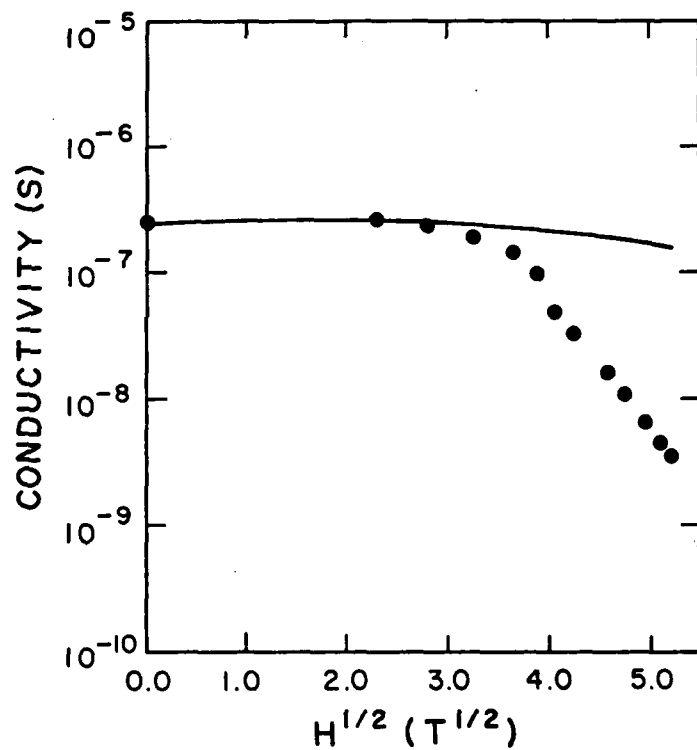


Fig. 2. Magnetic field dependence of impurity band conductivity for the two-dimensional case. The circles are experimental data from ref. [2].

# NEW TWO-DIMENSIONAL ELECTRON SYSTEM ON THE SURFACE OF SOLID NEON

K. KASITA

Department of Physics, Faculty of Science, Toho University,  
 4-5-16, Miyagi, Funabashi, 274, JAPAN

A brief review is given on a new two dimensional electron system with electron density between  $10^9/\text{cm}^2$  and  $3 \times 10^{10}/\text{cm}^2$  formed on the surface of solid neon. Electron conductivity is measured as a function of the electron density, the density of scattering centers, temperature and driving electric field strength. When the electron density is high, the electron correlation was found to play an important role in the transport phenomena. Electrons on the surface of thin helium film adsorbed on solid neon are also mentioned. It is shown that surface electrons with high electron density is stable in the present system.

## 1. Introduction

2DEG (two dimensional electron gas) formed on the liquid helium surface has been intensively studied for this decade as it gives an ideal testing ground for classical 2DEG. One of the most significant discoveries in this system is the electron crystal caused by correlation effect (1).

The phase transition of electrons to the crystal has been found to be characterized by a relation  $r_s(\pi N_e)^{1/2} e^2 / kT \approx 131$  (1), where  $N_e$  is the electron density and  $T$  is the temperature.  $r_s$  gives a measure of the strength of electron correlation for a classical 2DEG. In the high  $N_e$  region, however, a slight deviation of the phase diagram from the  $r_s \approx 131$  relation has been recognized (2), which has been attributed to the change of the electronic state from the classical to the degenerate quantum state. Unfortunately, the quantum effect observed was very weak even at the highest  $N_e = 2 \times 10^9/\text{cm}^2$  (3) which can be sustained on the liquid helium surface. In order to clarify the quantum effect on the electron correlation, a new 2DEG with  $N_e$  above  $2 \times 10^9/\text{cm}^2$  is, thus, required.

It is not easy to find such a new system among 2D electron systems formed inside of solids, because electrons with low  $N_e$  are liable to be localized due to lattice imperfections. Electron systems on the outer surface of dielectric materials, on the other hand, will be candidates for the new system, since electrons on the surface of solids are less affected by imperfections.

In a paper in which Cole et al. (4) predicted the existence of 2D electrons on liquid helium, they also showed that 2D electrons are possible on the surface of solid neon and hydrogen. Priyanovskii et al. (5) were the first to demonstrate that electrons are

are adsorbed on the surface of these materials.

In addition, we give a brief review on the new ZBEG formed on the surface of solid neon. It was found that electrons on the surface are visualized even when  $N_e < 10^{10} \text{ cm}^{-2}$  and that the surface is free of any impurities. This new system is a free electron gas with a wide range of  $N_e$  will open a new window for studying the quantum effects on ZBEG. Table I gives the characteristic features of this system (4).

The motion of electrons is examined as functions of  $N_e$ , temperature, density of scattering centers and the strength of driving electric field. It is shown that electron correlation plays an important role in the high  $N_e$  region.

The electron system trapped on a thin helium film is another topic of this review (5-7). We have found that electrons are stable on helium films adsorbed on solid neon. Moreover, it

was found that electrons with  $N_e$  much higher than that accessible on solid neon can be formed on the surface of helium films.

#### 2. Experimental procedures

The experimental system shown in the inset of Fig. 1 consists of a thin flat plate electrodes and a glass plate. Two electrodes are attached to the bottom of the glass plate. They are separated from each other by a gap of about 20  $\mu\text{m}$ . These electrodes are used mainly to attract electrons and to measure the electron mobility. The third electrode is located a few millimeters above the glass plate, which confirms the electrical ground level.

First, solid neon with a thickness of 10-30  $\mu\text{m}$  is formed in the glass plate. Keeping the bottom electrodes at a positive dc voltage, electrons are fed onto the surface of neon. The electron

density  $N_e$  on the surface is determined by the voltage  $V$  as  $N_e = CV/e$ , where  $C = \epsilon_0(d_g/\epsilon_g + d_n/\epsilon_n)^{-1}$  is the capacitance between the electron sheet and the bottom electrodes for unit area. Here,  $\epsilon_0$  is the permittivity of vacuum,  $d_g$  and  $d_n$  are the thickness of the glass plate and the solid neon, and  $\epsilon_g \approx 5$ ,  $\epsilon_n = 1.24$  are the dielectric constants for the glass and solid neon, respectively. For the present system ( $d_g = 0.10 \text{ mm}$ ,  $d_n = 10 \mu\text{m}$ ), we obtain  $N_e = 1.37 \times 10^{10} \times (V/\text{volt}) \text{ cm}^{-2}$ . (It is noted that when electrons with  $N_e$  are trapped on the surface, they are pressed to the surface by an electric field  $E = 1.8 \times 10^4 \times (N_e/10^{10} \text{ cm}^{-2}) \text{ volt/cm}$ .)

The resistance  $R$  of the electron sheet is determined by applying an rf electric voltage  $V_{\text{eff}}$  on one of the bottom electrodes and measuring the image current signal,  $I$ , which appears on the other electrode. The signal is written as

$$I = A [1/(1 + (\omega C_e R)^2) + i \omega C_e R / (1 + (\omega C_e R)^2)] \cdot V_{\text{eff}},$$

where,  $\omega$  is the angular frequency of the rf field which is about 10 MHz in the present experiments.  $A$  and  $C_e$  are the constants which depend on the electrode arrangement.

When the absolute value of the conductivity  $\sigma$  is needed, we have measured the magnetoresistance  $M = (R(H) - R(0))/R(0)$ . This gives the magnetoresistance mobility  $\mu$  as  $\mu = M/H^2$ . Using the value of  $\mu$  we can calculate the absolute value of  $\sigma$  as  $\sigma = N_e e \mu$ .

#### 3. Electron mobility in the low $N_e$ region

In this section, the conductivity of surface electrons with  $N_e$  low enough so that electron correlation is negligible is discussed. Figure 1 shows the electron mobility at 4.2 K. The mobility is measured as a function of the density  $N_e$  of helium gas atoms which have been intentionally introduced into the

experimental cell. It is one of the important advantage of the present system that we can control the density of the scattering centers with other conditions fixed.

The data in Fig. 1 are explained by considering two scattering mechanisms, the surface roughness scattering and the helium gas atom scattering.

#### 1. Low $N_G$ region

As far as the gas atom density is not so high, the scattering rate, or the inverse of the scattering time  $\tau^{-1}$ , of the electron is expressed as

$$\tau^{-1} = \tau_G^{-1} + \tau_S^{-1}$$

where  $\tau_G^{-1}$  is the scattering rate due to helium gas atoms which is proportional to  $N_G$ , and  $\tau_S^{-1}$  is the scattering rate due to the surface roughness which is independent of  $N_G$  but depends on the character of the surface.

From the data in Fig. 2, we can deduce  $\tau_G$  and  $\tau_S$  separately. We obtain  $\tau_G = 1.4 \times 10^{-12} / (N_G / (10^{20} / \text{cm}^3))$  sec and  $\tau_S = 4.67 \times 10^{-12}$  sec,  $1.91 \times 10^{-12}$  sec for two different neon surfaces.

The theoretical calculation of the scattering time for a classical 2DEG has been performed by Saitoh (9). He has given  $\tau_G = 1.47 \times 10^{-13} \times (b/\text{\AA}) / (N_G / (10^{20} / \text{cm}^3))$  sec. Here,  $b$  gives the extension of the electronic wave function  $\psi = (4/b^3)^{1/2} \exp(-z/b)$  in the direction  $z$  normal to the surface. Since  $b$  for electrons on solid neon is estimated to be  $19\text{\AA}$  (4), we obtain  $\tau_G = 2.79 \times 10^{-12} / (N_G / (10^{20} / \text{cm}^3))$  sec. This value agrees with the experimental results within a factor of 2.

#### 2. High $N_G$ region

The linear relation of  $\tau_G^{-1}$  on  $N_G$  breaks when  $N_G$  is high.

In Fig. 2, we see that  $\tau_G^{-1}$  increases nonlinearly with  $N_G$  in the region  $N_G > 2 \times 10^{20} / \text{cm}^3$ . We have found that the critical  $N_G$  depends on the temperature. For examples, when  $T$  is 13K,  $\tau_G^{-1}$  is proportional to  $N_G$  up to  $N_G = 4 \times 10^{20} / \text{cm}^3$  whereas at  $T = 2.9\text{K}$ , the deviation from  $\tau_G^{-1} \propto N_G$  relation begins at  $N_G = 1.5 \times 10^{20} / \text{cm}^3$ .

At critical densities, the mean free path of an electron is found to be comparable to the wavelength of the electron. This means that in higher  $N_G$  than the critical density, interference of adjacently scattered electron waves is important. The abrupt increase of  $\tau_G^{-1}$  in high  $N_G$  is, thus, to be explained from the point of view of the localization of 2D electrons in a random potential. Similar phenomena have been observed for the 3D electrons in the helium gas space (10) and for the 2D electrons on liquid helium (11).

#### 4. Electron conductivity in the high $N_G$ region

We have succeeded in forming a 2DEG with  $N_G$  up to  $3 \times 10^{10} / \text{cm}^2$ . This value is about one order of magnitude higher than that can be sustained on liquid helium. Here, we discuss anomalous transport phenomena in the high  $N_G$  region.

One of the anomalies is shown in Fig. 3, where the conductivity  $\sigma$  is plotted against the electron density  $N_G$ . In the region  $N_G < 10^9 / \text{cm}^2$ , the conductivity is normal, that is, it is directly proportional to  $N_G$ , while in the higher  $N_G$  region, the value of  $\sigma$  tends to saturate. This implies that in high  $N_G$ , either some part of electrons are localized or the electron mobility decreases. Magnetoresistance measurement has shown that the change in the mobility dominates the phenomenon.

To clarify the nature of the conductivity anomalies,

We have performed the measurements of the conductivity as a function of the helium gas atom density, and have found that the reduction of the electron mobility is affected by the existence of scattering centers such as helium gas atoms.

The results are shown in Fig. 4. The electron density  $N_e = 1.8 \times 10^{10} \text{ cm}^{-2}$  belongs to the region where the electron transport is normal, while  $N_e = 1.8 \times 10^9 \text{ cm}^{-2}$  belongs to the region where the conductivity saturation is observed.

To compare the data of  $\sigma T^{-1}$  for two  $N_e$ , we tentatively assume that the reduction of the mobility in high  $N_e$  is due to the appearance of a new scattering process and that  $\sigma T^{-1}$  is written as  $\sigma T^{-1} = \sigma_0 T^{-1} + \sigma_1 T^{-1} + \sigma_2 T^{-1}$ , where the first two terms correspond to the ionization and surface roughness scattering, and the third term corresponds to the new scattering process. Since  $\sigma_0 T^{-1} = 1.1 \times 10^{-11} \text{ cm}^2/\text{V}$ ,  $\sigma_1 T^{-1} = 1.1 \times 10^{-11} \text{ cm}^2/\text{V}$ ,  $\sigma_2 T^{-1} = 1.1 \times 10^{-11} \text{ cm}^2/\text{V}$ , the solid curve in the figure gives  $\sigma_2 T^{-1}$  for  $N_e = 1.8 \times 10^9 \text{ cm}^{-2}$ . It is noted that  $\sigma_2 T^{-1}$  increases with increasing  $N_e$ . This fact is important since it indicates that the reduction of  $\sigma$  in high  $N_e$  depends on the density of the scattering centers and suggests that the conductivity anomaly is due to the electron correlation.

Electron correlation does not affect the conductivity by itself, because it is an inner force. However, if other scattering mechanisms exist, electron correlation may enhance the scattering and lowers the conductivity as is shown in the experiment in Fig. 4.

The evidence which shows the conductivity anomaly is due to the correlation effect is also obtained from the value of  $\beta$  at the density above which the saturation in  $\sigma$  is observed. For an example,  $N_e = 10^9 \text{ cm}^{-2}$  at 4.2K gives  $\beta = 10$ . It is well known that the

electron correlation effect becomes important when  $\beta$  exceeds this value (12,13).

Another interesting phenomenon is seen in the temperature dependence of conductivity. Figure 5 shows the preliminary data. When  $N_e$  is low,  $\sigma$  is rather independent of  $T$ , while in high  $N_e$ ,  $\sigma$  depends strongly on  $T$ . It seems that there exists a critical temperature  $T_c$  below which the decreasing rate of  $\sigma$  with decreasing  $T$  is very high. This temperature becomes high when  $N_e$  is high. We emphasize that the value of  $\beta$  calculated for each  $T_c$  and  $N_e$  gives  $\beta = 135$  which is the value where the electron crystal is expected to be formed (1). The highest  $T_c$  we obtained is 2.5K for  $N_e = 1.8 \times 10^{10} \text{ cm}^{-2}$ .

Nonlinear transport phenomenon is also a characteristic feature of the present electron system with high  $N_e$ . It seems as if the effect of electron correlation which causes the reduction of  $\sigma$  becomes less effective when the driving electric field is strong.

##### 5. Electrons on thin films of liquid helium

Electrons on thin helium films has been a subject of theoretical investigations (14) because no experimental attempts have succeeded in forming stable electrons on thin helium films. Here, we give an experimental demonstration that electrons are stably trapped on thin helium films which is adsorbed on solid neon.

Figure 6 is the electron conductivity plotted against the gas atom density for  $T = 2.02\text{K}$  (6). In the vicinity of the saturated gas density for 2.02K, we have observed a sudden increase in  $\sigma$ . This increase in  $\sigma$  has been attributed to the electrons floating on the surface of helium film.

Figure 7 gives the conductivity plotted against the helium film thickness,  $d$  (7.8). For a very low pressing electric field  $E$ , a film with  $d = \infty$  is about 3.5 times of that on solid neon. When the pressing field  $E$  is high, the change in  $d$  is less significant.

Throughout the region of  $d$  in Fig. 7, electron scattering is dominated by helium gas atoms with a constant density which is calculated density at the temperature. In such a case, the electron conductivity is proportional to the range of the electron wave function as is shown by Salton (9).

The wave function of electrons is determined by the potential energy of the electrons

$$V = -4\pi\epsilon_0 d \times 10^{-18} \text{ eV} / 2 + 2.0 \times 10^{-2} \text{ eV} / 2 + d \times 10^{-18} \text{ eV} / 2$$

where the first term is the image potential due to the helium film, the second is that from the solid neon and the third term is the electric field potential.

If the pressing field  $E$  is weak, the range of the wave function  $d$  varies from  $19\text{\AA}$  for  $d=0$  to  $75\text{\AA}$  for  $d=\infty$ . The solid line in Fig. 7 gives the value of  $b$  for  $E=0$ . The agreement between experiment and theory is good. When a high pressing field  $E$  is applied, on the other hand, the third term of the above equation becomes important. Since this term is independent of  $d$ , the change in  $d$  with increasing  $d$  is small, which explains the experimental results for  $E=0.2 \times 10^5 \text{ V/cm}$  in Fig. 7.

#### Electron bubble and the surface electrons

It has been pointed out theoretically that electrons with  $N_e$  can be sustained on bulk liquid helium, can be trapped on the helium films (15). This is because a thin film is

stiff due to the van der Waals force from the substrate (16).

For electrons trapped on the helium film adsorbed on solid neon, we can say more, that is, we can show that electrons are stable even if the film is not stiff.

To show this, we compare the energy of surface electrons with that of electronic state in the helium film. In our system, the possible electronic state in the film is an electron bubble (17,8) at the interface of solid neon and liquid helium. In the pressing field  $E$ , the energy of the bubble electron is estimated to be about  $0.2\text{eV} - eEd$  (17), where the first term is the formation energy of the bubble state in the liquid helium and the second term comes from the fact that the bubble is located at a distance  $d$  below the surface of helium film. On the other hand, the energy  $\epsilon$  of the surface electrons is written as  $\epsilon = \epsilon_b + \epsilon_k$ , where  $\epsilon_b$  is the binding energy of the electron and  $\epsilon_k$  is the kinetic energy. Since  $\epsilon_b < 0.2\text{eV}$ , the energy of the surface electron is lower than that of a bubble electron unless  $eEd > 0.2\text{eV}$ . For  $d=100\text{\AA}$ , for an example, this gives  $E > 2 \times 10^5 \text{ V/cm}$ . This value of  $E$  corresponds to  $N_e \approx 10^{11}/\text{cm}^2$  as is shown in section 2. Thus, it is shown that electrons with  $N_e \approx 10^{11}/\text{cm}^2$  are stable on a helium film of  $100\text{\AA}$ .

In such a high  $E$ , however, electrons once jumped into the helium film will stay there for a long time, since it is very difficult for an electron in the bubble to tunnel onto the surface by receiving the surface tension energy from the bubble. On the other hand, if  $N_e < 4 \times 10^{10}/\text{cm}^2$  for  $d=100\text{\AA}$ , it is shown that electrons in the bubble can come onto the film surface in a short time by leaving the bubble as it is. In this sense, we can say that electrons with  $N_e < 4 \times 10^{10}/\text{cm}^2$  on a helium film with  $d=100\text{\AA}$  is



Table 1.

Author's note.

The author would like to express his sincere thanks to Professor V. L. Ginzburg for his encouragement and discussions. This work is supported by the Kutata Research Grant and the Grant-in-Aid for Scientific Research from the Ministry of Education.

Table 1.

Electronic states on liquid helium and solid neon.  $\epsilon_0$  is the ground state energy, and  $\phi$  is the extension of the wave function.  $N_0$  is the electron density which can be sustained. (from reference 14)

	$\epsilon_0$ eV	$\phi$ Å	$N_0$ /cm <sup>2</sup>
liq. He	-0.68	76	$< 2 \times 10^9$
sol. He	-4.7	19	at least up to $5 \times 10^{10}$

# References

1. D.C. Grimes and G. Adams, Phys. Rev. Letters 42 (1979) 795.
2. R. Menon, B.M. Guenin and A.J. Dahm, Phys. Rev. Letters 48 (1982) 641.
3. S.K. Haykal and Yu.Z. Kovdya, Sov. J. Low Temp. Phys. 1 (1975) 474.
4. M.W. Lee and M.H. Cohen, Phys. Rev. Letters 24 (1969) 1236.
5. H. Moriyama, A.P. Zolodin and M.S. Khaikin, JETP Letters 29 (1979) 382.
6. K. Kajita and M. Sasaki, Surface Sci. 113 (1982) 419.
7. K. Kajita, J. Phys. Soc. Jpn. 51 (1982) 3747.
8. K. Kajita, J. Phys. Soc. Jpn. 52 (1983) 372.
9. M. Sasaki, J. Phys. Soc. Jpn. 42 (1977) 201.
10. J. Lee and T.M. Sanders, Jr., Phys. Rev. 154 (1967) 138.
11. W. Lommer and D.J. Tanner, Phys. Rev. Letters 27 (1971) 1349.
12. J. Lee, T.R. Brown and D.C. Grimes, Phys. Rev. Letters 37 (1976) 1760.
13. K. Kajita, K. Kajita, S. Kobayashi and M. Sasaki, Surface Sci. 113 (1982) 436.
14. For example, M. Saito, in this conference.
15. H. Lee and H.M. Whitman, Phys. Rev. B23 (1981) 1145.
16. S. Lee, J. Phys. Soc. Jpn. 47 (1973) 790.
17. W.D. Fowler and D.L. Dexter, Phys. Rev. 176 (1968) 337.

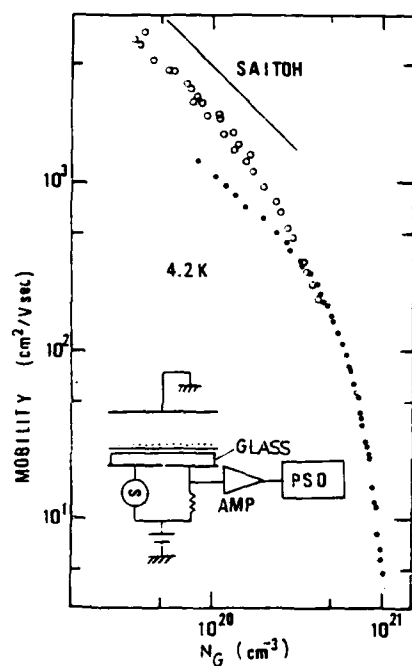


Fig.1 Electron mobility against the helium gas density for two different neon crystals. The solid line gives the theoretical calculation by Saitoh (9). The inset shows the experimental system.

73

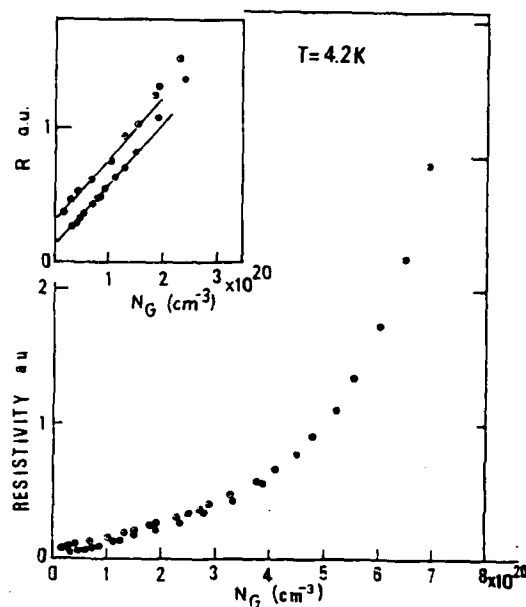


Fig.2 Resistivity ( $\mu^{-1}$ ) of electron sheet against  $N_G$ . The inset is an enlarged figure of the results in low  $N_G$ .

74

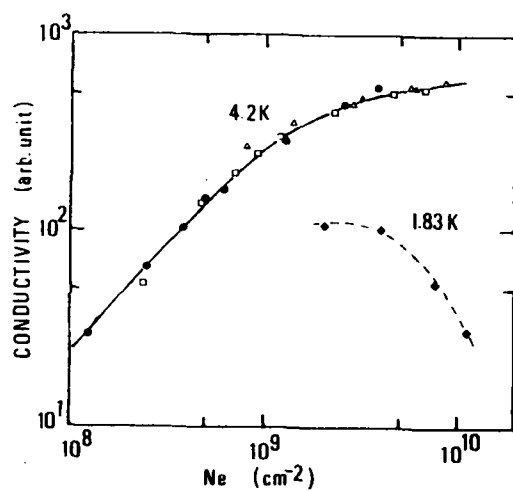


Fig.3 Electron conductivity against the electron density  $N_e$  at  $T=4.2\text{K}$  and  $1.8\text{K}$ .

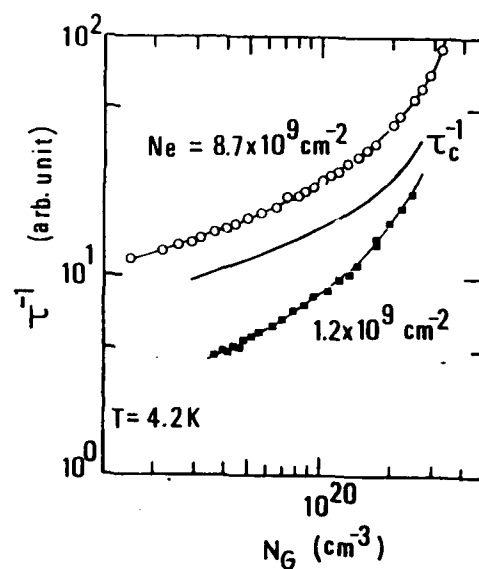


Fig.4  $\tau^{-1}$  against  $N_G$  at  $4.2\text{K}$  for two electron densities.

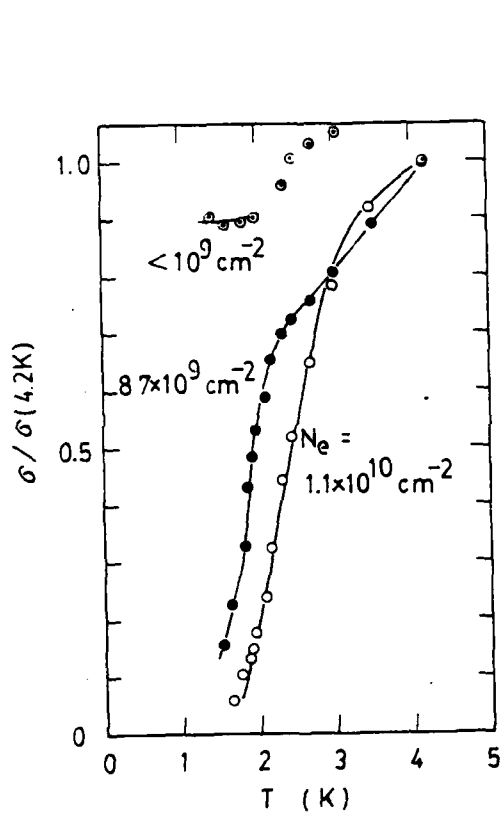


Fig.5 Temperature dependence of electron conductivity for three different electron densities. The vertical axis is normalized to 1.0 at 4.2K.

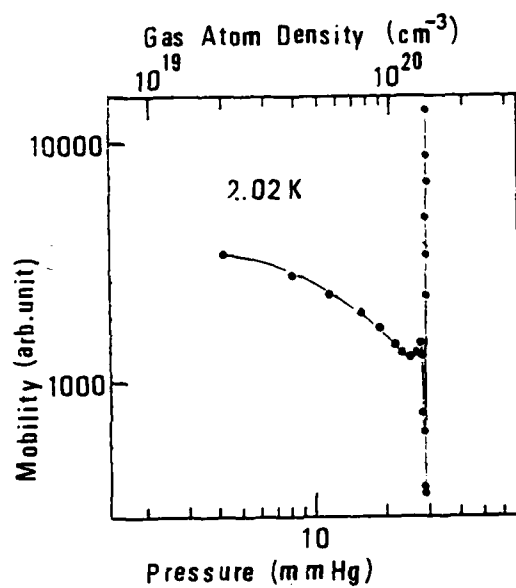


Fig.6 Electron mobility against the helium gas density at 2.02K (6).

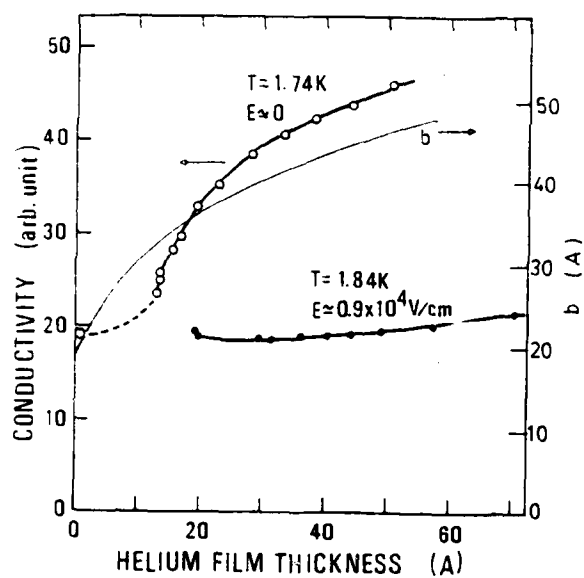


Fig.7 Electron conductivity against the helium film thickness for two pressing electric fields. Thin solid curve shows the range of the electronic wave function  $b$  for  $E \approx 0$  (8).

# CRITICAL ELECTRON DENSITY AT THE LIQUID HELIUM SURFACE

V.B. Shikin

Institute of Solid State Physics, Academy of Sciences  
USSR, Chernogolovka, Moscow district 142432, USSR

Various possibilities are discussed of increasing the critical electron density on the liquid helium surface.

In recent years intense search has been made of various methods to heighten critical electron density at the liquid helium surface. One of these methods suppose to use thin helium films as a substrate for the two-dimensional electron system. In such films existence of the additional van der Waals forces increases considerably the capillary constant  $\alpha$  of helium which leads automatically to increase of the critical density  $n_c$  of the electrons on the film as compared with its bulk value. This idea is supported by quantitative calculations [1-3]. There are also first experimental data which confirm that this idea is reasonable [4-6]. However, in the given case, if one has in mind Wigner's crystallization, the question is that, in fact, it is a new problem since on a thin helium film we deal not with the Coulomb but with the dipole gas (the distance between electrons on a thin film is comparable with the distance between an electron and a hard substrate, so each electron interacts mainly with its image but not with the neighbouring electrons). This problem is being developed successfully (Monarkha [3]) but up to now only theoretically.

One more possibility has been outlined recently in connection

with the experiments by Savignac, Leiderer [7] and Volodin, Edelman [8]. In the first of the works mentioned it was shown that a multielectron dimple on the solid helium surface can exist in the region of electric field exceeding considerably (3-4 times) the field  $E_L^{crit}$  at which such dimple appears. Accounting that the charged core radius  $Q$  of a multielectron dimple is inversely proportional to  $E_L$  squared in the range  $\alpha Q \ll 1$  and the electron density  $n_c$  in the dimple center has the scale  $n_c \sim Q^{-1}$ , it is easy to see that the electron density  $n_c$  (increasing as  $E_L^4$  as the electric field increases) can exceed considerably the critical homogeneous electron density above bulk helium. In other words, a multielectron dimple is a suitable object for creation electron densities on the helium surface higher than the critical homogeneous one.

An independent but ideologically very close to ref. [7] result has been obtained by Volodin and Edelman [8]. The authors [8] showed that using special substrate for a liquid helium film which had the form of a comb with the tooth height  $h$  being of the order of the helium capillary constant and a typical period much less than  $\alpha^{-1}$ , one can sharply increase the critical instability field maintaining the electron mobility on the helium film characteristic for the case of bulk helium. It is worthy to note that the idea about artificial suppression of the capillary instability of the charged surface of bulk helium by boundary conditions hindering development of charged liquid surface vibrations with small wave numbers (of the order of the capillary constant) has been presented in the Williams review article [9]. Thus, it is a useful idea with successful applications. It is evident also that the results though

they seem to differ from each other, present arguments in favor of the advantages of multielectron dimples and, especially, artificial ones as objects with heightened critical value of electron density.

In the given note mechanism of destruction of a multielectron dimple in a strong electric field is discussed and a critical electron density in the dimple is estimated when such destruction occurs.

In order to obtain quantitative information on conditions of the dimple destruction in a strong electric field  $E_L$  we consider the general equation of mechanical equilibrium near the dimple center

$$\frac{\Delta}{2} \left( \frac{1}{R_1} + \frac{1}{R_2} \right) = e E_L n(r), \quad \int n(r) d^2r = N \quad (1)$$

Here  $\Delta$  is the surface tension coefficient,  $R_1$  and  $R_2$  are the main curvature radii of the dimple surface,  $n(r)$  is the electron distribution in the charged dimple core,  $r$  is a two-dimensional radius from the dimple center. The gravitational term in eq. (1) is omitted.

Using the general definition of the mean curvature of the dimple surface and expansion of the shape  $\xi(r)$  of the dimple surface near its center in the form

$$\xi(r) \approx \xi_0 + \frac{1}{2} \xi''_0 r^2, \quad \xi''_0 = \frac{\partial^2 \xi}{\partial r^2} \Big|_{r=0} \quad (2)$$

one may write eq.(1) as follows

$$\Delta \frac{2 \xi''_0 + (\xi''_0)^2 r^2}{2 [1 + (\xi''_0)^2 r^2]^{\frac{3}{2}}} = e E_L n(r) \quad (3)$$

Integrating now both parts of eq.(3) over the area  $\pi a^2$  where  $a$  is the radius of the charged dimple core and accounting

for the normality condition  $\int n(r) d^2r = N$  we find

$$\frac{\xi''_0 a^2}{[1 + (\xi''_0)^2 a^2]^{\frac{3}{2}}} = \frac{E_L Q}{2 \pi \Delta}, \quad Q = e N \quad (4)$$

The eq.(4) gives us relation between  $\xi''_0$  and  $a$ .

The second of the equations describing according to refs. [10], [11] the equilibrium lineshape of the dimple has the form  $e E_L \xi + \varphi = \text{const}$  ( $\varphi(r)$  is the electropotential associated with the electron distribution  $n(r)$  on the dimple surface). This equation is valid in the region of high fields and yields an additional relation between  $\xi''_0$  and  $a$

$$\xi''_0 = 3 \pi Q / 4 a^3 E_L \quad (5)$$

Combining determinations (4) and (5) we have

$$(a_c/a)^2 = (1 - \sqrt{1 - 4 \Lambda^2}) / 2 \Lambda^2 \quad (6)$$

$$\Lambda = E_L^3 Q / 3 \pi^3 \Delta^2, \quad a_c^2 = 3 \pi Q / 4 E_L$$

In the limit  $\Lambda \ll 1$  the value  $a = 3 \pi^{\frac{1}{2}} \Delta / 2 E_L^{\frac{1}{2}}$  following from (6) coincides within a factor accuracy with the definition "a" from refs. [10, 11]. This definition of "a" is independent of  $Q$  and inversely proportional to  $E_L^{\frac{1}{2}}$ . But if  $\Lambda \rightarrow \frac{1}{2}$  the situation changes. It turns out that the definition "a" from (6) is valid only in the region  $\Lambda < \frac{1}{2}$  or which is the same when

$$E_L < E_L^{\text{max}}, \quad E_L^{\text{max}} = (3 \pi^{\frac{1}{2}} \Delta^2 / 2 Q)^{\frac{1}{3}} \quad (7)$$

This inequality defines at a given  $Q$  the value of the critical field  $E_L^{\text{max}}$  destructing the dimple. The corresponding  $a_{\text{min}}$  from (6) becomes a function of  $Q$

$$a_{\text{min}}^2 = 3 \pi Q / 4 E_L^{\text{max}} \quad (8)$$

Dynamics of Dislocation Mediated Melting  
of a Two-Dimensional Electron Lattice

D.B. Mast, C.J. Guo, M.A. Stan, R. Mehrotra, Y.Z. Ruan, and A.J. Dahm  
Case Western Reserve University, Cleveland, Ohio 44118

Abstract

The power absorbed by a two dimensional sheet of electrons when driven in a low frequency compressional mode exhibits a sharp maximum versus temperature just above the melting point. The dependence of this excess power absorption on frequency is explained by the theory of dislocation mediated melting.

Measurements of dynamic properties of a 2D electron lattice supported by a liquid helium surface in the vicinity of the melting point are reported and are interpreted with the theory of melting via the dissociation of dislocation pairs. The data are fit very well by this theory, and we believe that these measurements, combined with the measurements by Gallet *et al.*<sup>1</sup> on the abrupt drop in the shear modulus at the melting point, provide convincing evidence in support of dislocation mediated melting.

A cross-section of our experimental cell is shown in Fig. 1. Our measurements consist of driving a low frequency compressional mode of the lattice (parallel to the liquid surface) by applying an ac voltage at angular frequency  $\omega$  to electrode  $T_1$  near one side of the crystal and sampling the capacitively induced response of the electrons on electrode  $T_2$  located near the opposite side of the lattice.<sup>2</sup> The in phase component of the detected signal can be shown to be proportional to the power absorbed by the lattice.

Superimposed on the background power loss caused by the

scattering of ripples from the crystal is a sharp excess power loss peak that occurs in the vicinity of the melting point. This excess power loss has been measured as a function of temperature in the range 1-55 MHz. The temperature dependence of the excess scattering peaks for two excitation frequencies is shown in Fig. 2. The temperature at which maximum power loss occurs is a monotonically increasing function of the frequency of the excitation voltage. This loss peak is the direct analog of the dissipation peak in the experiment of Bishop and Reppy<sup>3</sup> on a thin liquid helium film, and the explanation of our experiment parallels theirs with dislocations playing the role of vortices in helium films.

Our experimental results are interpreted within the framework of the 2D melting theory of Kosterlitz-Thouless<sup>4</sup>, Halperin-Nelson<sup>5</sup>, and Young.<sup>6</sup> In this theory dislocation pairs exist in thermal equilibrium below the melting temperature  $T_m$ . As  $T_m$  is approached from below the average separation of the two partners of a pair increases with increasing temperature, and at  $T_m$  some pairs separate to become free dislocations. At temperatures above  $T_m$  both pairs and free dislocations exist, and the density of free dislocations increases rapidly with temperature. In the absence of dislocations, the energy of our compressed lattice is stored as elastic energy and is given back to the power supply as the voltage is removed. However, when either free or paired dislocations are present they move in such a way as to relieve the lattice strain caused by the distortion of the lattice and dissipate energy by creating lattice phonons. This leads to the excess power dissipation.

The temperature dependence of the excess dissipation has been worked out by Ambegaokar *et al.*<sup>7</sup> The equations describing the



The critical density in the dimple center  $n_0^{\max} = 1/\pi a_{\min}^2$  with allowance for  $Q_{\min}$  (8) and  $E_1^{\max}$  (7) is as follows

$$n_0^{\max} \approx \frac{4}{3\pi e} \left( \frac{3\alpha^2}{2Q} \right)^{\frac{1}{3}} \quad (9)$$

according to (9)  $n_0^{\max}$  increases as the total charge  $Q$  decreases. This circumstance should be taken into account when looking for possibilities to heighten critical electron density on the helium surface. The numerical value  $n_0^{\max}$  for  $N \sim 10^5$  is of the order  $n_0^{\max} \sim 10^{10} \text{ cm}^{-2}$ .

#### REFERENCES

1. H. Ikezi and P.M. Platzman. Phys. Rev. B23 (1982) 1145.
2. V.V. Tatarskiy, N.I. Shikina, V.B. Shikin. ZhETF (in press).
3. Yu.P. Monarkha. FNT 8 (1982) 1133.
4. A.P. Volodin, M.S. Khaikin, V.S. Edel'man. Pis'ma ZhETF 26 (1976) 524, (JETP Lett. 23 (1976) 478).
5. K. Kajita and W. Sasaki. Surf. Sci., 113 (1982) 419.
6. K. Kajita. Preprint 1982.
7. D. Savignac. Diplom Physik-Department TUM E10, München 1982.
8. A.C. Volodin, V.S. Edel'man. Pis'ma ZhETF 37 (1983) 8.
9. F.I.B. Williams, Surf. Sci., 113 (1982) 371.
10. V. Shikin and P. Leiderer. ZhETF 81 (1981) 184. Sov. Phys. JETP 54 (1981) 92.
11. V.L. Mel'nikov and S.V. Meshkov. ZhETF 81 (1981) 951. Sov. Phys. JETP 54 (1981) 505.

dislocations are analogous to the equations of a charged 2D gas. When a "test" dislocation (charge) is introduced into the lattice, other paired and free dislocations (dipoles and charges) respond to screen the strain created by the "test" dislocation. This screening can be written in terms of a dielectric constant. The difference between the usual dielectric medium and this system is that the dislocation pairs (dipoles) occur with various pair separations  $r$ , and thus with different polarizabilities. The dielectric constant  $\epsilon(r, T)$  is greater for pairs with large  $r$  since these pairs are screened by smaller bound pairs. Because of the enhanced screening of the strain field for larger pairs and the logarithmic interaction between dislocation pairs, large pairs are more weakly bound when compared to smaller pairs.

The power dissipation  $P(T)$  for dislocations can also be written from analogy with a charged system as

$$P(T) = \text{Im}[\epsilon^{-1}(r, T)] = \frac{\epsilon''}{(\epsilon')^2 + (\epsilon'')^2} \quad (1)$$

The real part of  $\epsilon = \epsilon' + i\epsilon''$  is due to the polarization of pairs while the imaginary part is due to the lossy motion of both paired and free dislocations. Since  $\epsilon'$  is nearly temperature independent, a maximum occurs in the power dissipation when  $\epsilon'' = \epsilon'$ . The temperature dependence of  $P(T)$  is obtained by integrating the Kosterlitz-Thouless equations numerically<sup>7</sup> to evaluate  $\epsilon'$  and  $\epsilon''$  at a series of temperatures and then substituting these values into Eq. (1).

The reason for the observed frequency and temperature dependence of this peak dissipation stems from the fact that pairs of different

separation  $r$  are bound with different strengths and relax to equilibrium, when the lattice strain is removed, with different relaxation times,  $\tau$ . This relaxation time is given approximately by

$$\tau^{-1} = 12 D/r^2, \quad (2)$$

where  $D$  is the dislocation diffusion constant. The pairs which dominate the power losses are those pairs for which the dislocation separation is such that  $\omega\tau = 1$ . This means that pairs of different separation are probed at different frequencies  $\omega$ . The dielectric constant  $\epsilon(r, T)$  used in Eq. (1) is thus evaluated for a particular value of  $r$  given by  $r = (12D/\omega)^{1/2}$ . Therefore, it is the temperature dependence of the pair separation that determines the temperature of the maximum of the excess scattering peak for a given frequency.

There are four parameters used in fitting the data;  $T_m$ ,  $D$ , the dislocation core energy  $E_c$  (which enters the expression for  $\epsilon$ ) and an uncertainty factor of approximately 2 in the density of free dislocations. The temperature dependence of the maximum power absorption as a function of excitation frequency is fit very well with  $D = \frac{1}{2} \omega_m a^2$ , where  $\omega_m$  is the maximum transverse phonon frequency and  $a$  is a lattice spacing, and with  $E_c = 5T_m$ .

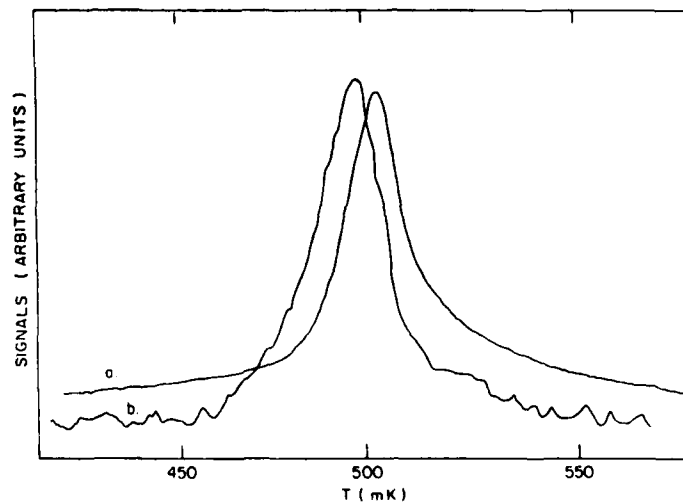
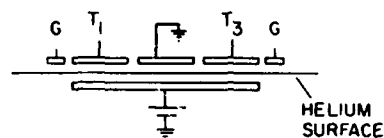
# References

1. F. Gallet, G. Deville, A. Valdes, and F.I.B. Williams, Phys. Rev. Lett. **49**, (1982) 212.
2. This technique is briefly described in R. Mehrotra, B.M. Guenin, and A.J. Dahm, Phys. Rev. Lett. **48**, (1982) 641.
3. D.J. Bishop and J.D. Reppy, Phys. Rev. Lett. **40**, (1978) 1727.
4. J.M. Kosterlitz and D.J. Thouless, J. Phys C **6**, (1973) 1181.
5. D.R. Nelson and B.I. Halperin, Phys. Rev. B **19**, (1979) 2457.
6. A.P. Young, Phys. Rev. B **19**, (1979) 1855.
7. V. Ambegaokar, B.I. Halperin, D.R. Nelson, and E.D. Siggia, Phys. Rev. B. **21**, (1980) 1806.

## Figure Captions

Fig. 1 Cross-section of the rectangular (2.5cm x 1.8cm) experimental cell. A dc voltage applied to the submerged electrode provides the holding voltage for the electrons on the helium surface. The symbol G refers to an outer guard electrode.

Fig. 2 Excess power absorption peaks with the background subtracted near  $T_m$  versus temperature for excitation frequencies: a) 23 MHz and b) 4.0 MHz.



# LOCALIZATION OF ELECTRONS

## ABOVE A He FILM

by

Eva Andrei

Bell Laboratories  
Murray Hill, NJ 07974

The mobility and effective mass of electrons above a liquid He film were measured as a function of film thickness for different temperatures and densities. The film thickness was varied in the range 1nm-700Å and the temperature 1.5-4°K. For films of thickness 1600Å-2000Å (depending on temperature) a sharp 4<sup>th</sup> order of magnitude drop in the mobility was observed. This drop was accompanied by a 8 order of magnitude increase in the electronic effective mass. These observations are strongly suggestive of the localization of the electron in a polaronic state. Theoretical work<sup>1,2</sup> on the single electron polaron predicts this transition to occur for a film thickness of ~100Å. Electron-electron interactions are probably responsible for its occurring on thicker films.

1. S. A. Jackson and P. M. Platzman, Phys. Rev. B24, 499 (1981).
2. G. Hipolito, G. A. Farias, and N. Studart, Surf. Sci. 113, 394 (1982).

# Localization of Inversion Electrons on InP

W. Hansen, U. Merkt, and J. P. Kotthaus  
 Institut für Angewandte Physik, Universität Hamburg  
 Jungiusstraße 11, 2000 Hamburg 36, F. R. Germany

The high-frequency conductivity of inversion electrons on InP is measured by Fourier transform spectroscopy. At sufficiently low temperatures deviations from Drude behaviour are found that reveal localization of part of the carriers. In comparison to electrons on silicon, localization on InP prevails to relatively high carrier densities, frequencies, and temperatures.

Recent cyclotron resonance experiments on two-dimensional (2D) electron space-charge layers on InP have revealed anomalous line shapes that cannot be simply described by cyclotron resonance in an unperturbed 2D electron system /1/. By analogy to earlier cyclotron resonance experiments on silicon /2/ these observations have tentatively been linked to carrier localization. We have studied the frequency and temperature dependence of the conductivity in the absence of magnetic fields to enable quantitative comparison of the results to existing theories and to avoid complications in the interpretation that are caused by the presence of magnetic fields.

The samples are MOS capacitors fabricated on mechanically and chemically polished (0.01% bromine in methanol) p-type (100) InP ( $N_A = 5 \times 10^{15} \text{ cm}^{-3}$ ). The gate insulator is a thin ( $d = 250 \text{ nm}$ ) silicon dioxide film, deposited by a plasma-enhanced CVD process /3/. The gate metal is a semitransparent NiCr film. The induced carrier density  $N_s$  is calculated from the capacitance and threshold voltage  $V_T$ , as determined from the onset of the high-frequency conductivity ( $\bar{\nu} \sim 100 \text{ cm}^{-1}$ ).

The high frequency conductivity at various induced electron densities  $N_s$  is shown in Figs. 1 and 2 for two different samples. Figure 1 depicts spectra of a sample with relatively high conductivities at the temperatures  $T = 15 \text{ K}$  and  $80 \text{ K}$ . The conductivity scale is calculated from the relative change in transmission  $-\Delta T/T = (T(V_T) - T(V_G))/T(V_T) = 2 \text{ Real}(\sigma(\omega)/Y)$ , where  $V_G$  is the applied gate voltage, and  $Y$  the wave admittance /4/. At the lower temperature (Fig. 1a) the conductivity differs drastically from Drude behaviour up to electron densities  $N_s = 2 \times 10^{12} \text{ cm}^{-2}$ , exhibiting a pronounced maximum at finite frequencies. At low densities ( $N_s = 0.2 - 0.8 \times 10^{12} \text{ cm}^{-2}$ ) the maximum is observed at about  $70 \text{ cm}^{-1}$ , shifting to lower frequencies with increasing density. At the higher temperature (Fig. 1b) the spectra approach Drude like behaviour. The sample in Fig. 2 exhibits lower conductivities than the one in Fig. 1. In this case, the maxima are broader and are observed at still higher frequencies ( $\bar{\nu} = 100 \text{ cm}^{-1}$ ).

We have also studied the quasi-static conductivity at radio and microwave frequencies. In the inset of Fig. 2 an example for the gate voltage dependence of the r.f. conductivity is depicted together with the simultaneously measured low-frequency

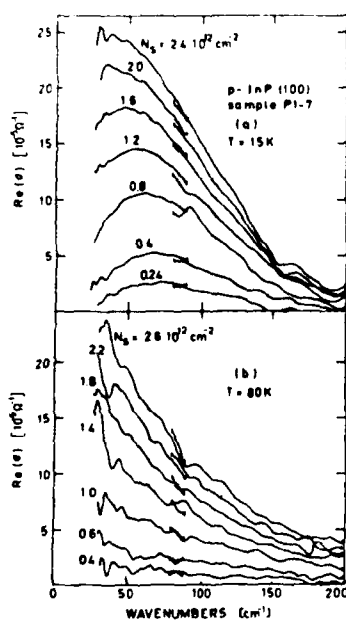


Fig. 1. High-frequency conductivity of inversion electrons on InP at  $T=15 \text{ K}$  (a) and  $T=80 \text{ K}$  (b). At each density the two lines are different pieces of the spectra obtained with different beamsplitters in the Fourier spectrometer.

CV-curve. The quasistatic microwave and r.f. conductivities evidence strong localization in that at low temperatures the conductivity threshold occurs at higher induced electron densities than the CV-inversion threshold ( $N_s = 5 \times 10^{11} \text{ cm}^{-2}$  at  $T=5 \text{ K}$ ). The conductivity threshold approaches the CV-threshold with increasing temperature, and coincides with it at typically  $T=80 \text{ K}$  and above. Also, we observe a negative magnetoresistance that is most pronounced at low densities  $N_s$ . Similar effects in silicon inversion layers have previously been connected with localization

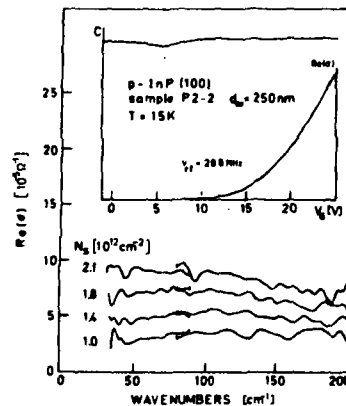


Fig. 2. High-frequency conductivity of inversion electrons on InP at  $T=15 \text{ K}$ . The inset shows the gate voltage dependent r.f. conductivity and the low-frequency CV curve ( $v=8 \text{ Hz}$ ) at the same temperature. Data are taken in the presence of above band gap radiation.

/5/. Because of experimental limitations imposed by using r.f. methods we have not yet been able to study the temperature dependence of the conductivity at low densities  $N_g$  for exponential temperature dependence.

We feel that the strong localization effects we observe are caused by oxide charges and interface impurities that are found in plasma-enhanced CVD oxides. It is well known that such oxides contain impurities like water /3/ that has been found to cause charge trapping centers in silicon dioxide films on silicon that were subjected to water diffusion /6/. In addition non-stoichiometry of the uppermost InP layers may produce even n-type behaviour on nominally p-type substrates /1/ and may contribute to the strong localization potentials that are evidenced by our experiments. Our interpretation that a relatively high density of charged impurities near the oxide-semiconductor interface exists is supported by a recent theoretical study /7/ of the metal-insulator transition in 2D electron systems on Si and InP in the presence of charged impurities. However, we only find qualitative agreement of spectra such as those shown in Fig. 2 with theoretical expectations /7/.

We wish to thank A. Gold for stimulating discussions and acknowledge financial support of the Deutsche Forschungsgemeinschaft.

#### References

1. H. C. Cheng and F. Koch, Phys. Rev. B 26 (1982), 1989.
2. J. P. Kotthaus, G. Abstreiter, F. Koch, and R. Ranvaud, Phys. Rev. Lett. 34 (1975) 151.
3. U. Mackens and U. Merkt, Thin Solid Films 97 (1982) 53.
4. A. Gold, S. J. Allen, B. A. Wilson, and D. C. Tsui, Phys. Rev. B 25, (1982) 3519.
5. D.J.Bishop, R.C.Dynes, and D.C.Tsui, Phys. Rev. B 26 (1982) 773.
6. A. Hartstein and D. R. Young, Appl. Phys. Lett. 38 (1981) 631.
7. A. Gold und W. Götze, preprint and private communications.

Dimensional Crossover of Spin-Orbit Scattering  
Observed in 2-d Localization

R. J. Markiewicz and C. J. Rollins  
Northeastern University, Boston, Mass. U.S.A.

and

Francis Bitter National Magnet Lab,<sup>+</sup>  
Cambridge, Mass. U.S.A.

and

J. S. Brooks  
Boston University, Boston, Mass. U.S.A.

and

Francis Bitter National Magnet Lab,<sup>+</sup>  
Cambridge, Mass. U.S.A.

In the temperature range 4-20K, ultrathin films of  $\text{Pd/Pd}_2\text{Si}$  (6-50Å) show a positive, anisotropic magnetoresistance which is logarithmic in field at high magnetic fields, characteristic of two-dimensional localization with strong (three-dimensional) spin-orbit scattering. At lower temperatures, the magnetoresistance saturates to a field-independent value. We interpret this change as due to a crossover of spin-orbit scattering from its bulk value to a form characteristic of a 2-d film. The resulting magnetoresistance is consistent with the theoretical results of Hikami, Larkin and Nagaoka.

Below ~0.5K, our analysis is complicated by superconducting effects in the  $\text{Pd}_2\text{Si}$ .

<sup>+</sup>Supported at MIT by the National Science Foundation



# Weak Localization in Metallic Thin Films

F. Komori, S. Kobayashi and W. Sasaki

Department of Physics, University of Tokyo  
7-3-1 Hongo, Bunkyo-ku, Tokyo 113, Japan

## Abstracts

Electronic conduction is studied in various metallic thin films and discussed in terms of weak localization. The roles of inelastic scattering time, spin-orbit scattering time and spin scattering time are clarified by analysing the magnetoconductivity of several thin films with different values of the parameters. Also by analysing temperature dependence of the conductivity, the effect of electron-electron interaction in these films is confirmed.

In weak localization there are several important parameters such as inelastic scattering time  $\tau_c$ , spin-orbit scattering time  $\tau_{so}$  and spin scattering time  $\tau_s$ . The roles of these parameters are systematically studied using several kinds of metallic thin films with different values of the parameters. In addition to these in the localization effect, electron-electron interaction causes another important effect on electronic conduction of metallic thin films, and is one of the origins of logarithmic temperature dependence in the conductivity.

In the later analysis of the experimental results of the magnetoconductivity, we make use of general theoretical expressions of conductivity due to only the localization mechanism (1,2,3,4) because in the interaction mechanism the terms insensitive to magnetic field mainly contribute to the conductivity. The expression due to the localization contain diffusion constant  $D$ , carrier  $g$ -factor  $g$ , elastic scattering time  $\tau_0$  and thickness of the film  $t$  as

parameters other than  $\tau_c$ ,  $\tau_{so}$  and  $\tau_s$ . In order to get physical information from the experiments we should be careful to choose principal parameters of each analysis among them because they are not always independent. Here we assume that  $\tau_0$ ,  $\tau_{so}$  and  $D$  are proportional to  $\sigma/t$  to treat several films with different sheet conductivity  $\sigma_0$ , and that  $g = 2$  for simplicity. On the other hand in the analysis of the temperature dependence of the conductivity, theories of both localization and interaction effects (5) are used.

First we demonstrate the effect of spin-orbit scattering in the localization mechanism by showing in Fig.1 the magnetoconductivity of composite films; Cu-Cu, Cu-Ag and Cu-Au films. (6) These films are 30 Å thick and prepared by repeating vacuum deposition and oxidation three times. The former two layers are made of Cu, and the last of Cu, Ag or Au. Because these three elements are isoelectronic, only the strength of spin-orbit interaction is varied.

By adjusting only  $\tau_{so}$  for these three films, the theoretical curves of the localization, which are shown in Fig.1 as solid lines, reproduce well the experimental results in both directions of magnetic field while the other parameters are kept common. Here  $\tau_s$  is neglected for simplicity. The values of the parameters are given in Table 1. The strength of the spin-orbit interaction in heavy elements is generally stronger than that in light ones. This fact reasonably explains the change of  $\tau_{so}$  obtained for these three films from above analysis.

The role of spin scattering in the localization mechanism is studied by analysing magnetoconductivity in Cu-Mn alloy films with various concentrations of Mn. (7) The samples are prepared by the similar method as that for above noble metal films, and Cu-Mn alloy is used for the evaporation source. Figure 2 shows the magnetoconductivity of these films. The Mn concentrations of the films are directly measured by PIXE method (8) after the conductivity measurements, and are given in table 2 together with other parameters.

adjusting only  $\tau_s$  for these films, the theoretical curves of the magnetoresistance, which are shown as solid lines in Fig. 2, reproduce well the experimental results. Here the other parameters are also kept common to all samples. The variety of the magnetoconductivity in Cu-Mn alloy films can be explained in terms of the difference of  $\tau_s$ , which decreases as Mn concentration increases. As a limiting behavior of short spin scattering time, decreasing magnetoconductivity is observed in pure Mn films. (7) In this case spin scattering destroys the localization effect completely.

Systematic studies of inelastic scattering time are performed in Bi films which are prepared by a simple deposition in a vacuum with the thickness varying up to 120 Å. (9) Only by adjusting  $\tau_s$  the variation of the magnetoconductivity curves at different temperatures in these films is well reproduced when the other parameters in the localization theories are kept common. The values of  $\tau_s$  are shown in Fig. 3 as a function of temperature and other parameters are given in table 1. Here  $\tau_s$  is neglected for simplicity.

In all these samples  $\tau_s$  is proportional to  $T^{-1}$  in lower temperature range below 1 K, and is proportional to  $T^{-2}$  at higher temperatures. In recent studies on two-dimensional disordered systems (10,11,12)  $\tau_s$  due to electron-electron interaction is proportional to  $D/T \ln(T_0/T)$  at low temperatures with a constant  $T_0$ . To compare the experimental results with this,  $\tau_s$  is assumed to be given as  $\tau_s = A/T$  and the values of A are given in table 3. These values are proportional to D, being consistent with the theories.

Though the magnetoconductivity depends on temperature also in the noble metal films, the dependence becomes weaker as temperature decreases. (13)

The behavior can be explained by taking impurity spin scattering into account; the localization effect depends little on temperature when  $\tau_s > \tau_{sp}$  as we observed in the magnetic films.

Now we discuss the logarithmic temperature dependence of conductivity in

these films. The origin of this term in magnetic films such as the Cu-Mn alloy films is the interaction mechanism because short spin scattering time suppresses the  $\log T$  term due to the localization mechanism. In the case of the noble metal films the interaction mechanism is also the main origin of the  $\log T$  term because it is observed even in high magnetic field and the coefficient in the field is almost the same as that in zero field. The absence of  $\log T$  term due to the localization is ascribed also to the considerable magnitude of spin scattering in these films. On the other hand in Bi films the temperature dependence of conductivity is described as the sum of two terms due to both the interaction and localization mechanisms though the latter term disappears in high magnetic field.

By comparing the amplitudes of above  $\log T$  dependence with the theories, it is commonly found that the term independent of magnetic field is dominant among the interaction effect. This is consistent with the results that magnetoconductivity is well explained only by the localization mechanism.

Systematic studies described here clarify how the localization and interaction mechanisms cause the various behaviors of electronic conduction in metallic thin films. Most of experimental results in thin films at low temperature can be now well understood as the combinations of the both effects including spin-orbit scattering and spin scattering.

#### References

- (1) S. Hikami, A.I. Larkin and Y. Nagaoka, Prog. Theore. Phys. **63** (1980) 707.
- (2) S. Maekawa and H. Fukuyama, J. Phys. Soc. Japan **50** (1981) 2516.
- (3) B.L. Altshuler and A.G. Aronov, Sov. Phys.-JETP Lett. **33** (1981) 499.
- (4) R.S. Markiewicz and C.J. Mullins, preprint.
- (5) Y. Nagaoka and H. Fukuyama ed., Anderson Localization (Springer Verlag, Berlin, 1982)

- (10) E. Komori, S. Kubayashi and W. Sasaki, J. Phys. Soc. Japan 51 (1982) 3136.
- (11) E. Komori, S. Kubayashi and W. Sasaki, J. Magn. and Magn. Mater. 35 (1983) 1.
- (12) A. Sakell, Annual Review of Nuclear and Particle Science, Ed. J.D. Jackson, Annual Reviews, Palo Alto, California, 1980 ) p.211.
- (13) E. Komori, S. Kubayashi and W. Sasaki, J. Phys. Soc. Japan 52 (1983) 368.
- (14) E. Abrahams, P.W. Anderson, P.A. Lee and T.V. Ramakrishnan, Phys. Rev. B24 (1981) 6738.
- (15) H. Fukuyama and E. Abrahams, preprint.
- (16) B.I. Altshuler and A.G. Aronov, Solid State Commu. 46 (1983) 429.
- (17) E. Komori, S. Kubayashi and W. Sasaki, to be published.

#### Tables

Table 1. List of Cu, Cu-Ag and Cu-Au films. Values of  $\sigma(H=0)$  and other parameters are given.

	$\sigma(H=0)$ ( $\Omega^{-1}$ )	$\sigma(H=0)$ ( $\Omega^{-1}$ )	$\sigma$ ( $\Omega^{-1}$ )	$\tau_0$ ( $\times 10^{-14}$ sec)	$\tau_{\infty}$ ( $\times 10^{-13}$ sec)	$\tau_c$ ( $\times 10^{-12}$ sec)	$\chi^2$ (%)
Cu	1.127	1.121	1.0	9.2	48	5.2	1.7
Cu-Ag	1.127	1.121	1.0	9.2	48	5.2	1.7
Cu-Au	1.127	1.121	1.0	9.2	48	5.2	1.7
Cu	1.127	1.121	1.0	9.2	48	5.2	1.7
Cu-Ag	1.127	1.121	1.0	9.2	48	5.2	1.7
Cu-Au	1.127	1.121	1.0	9.2	48	5.2	1.7

Table 2. List of Cu-Mn alloy films. Mn concentrations and other parameters are given.

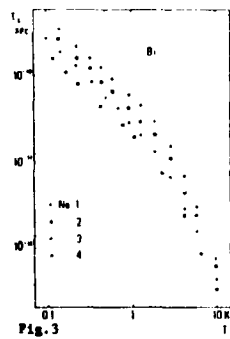
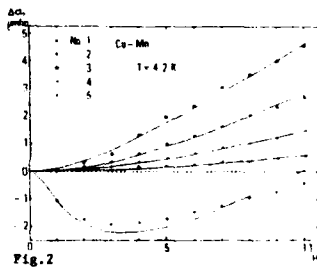
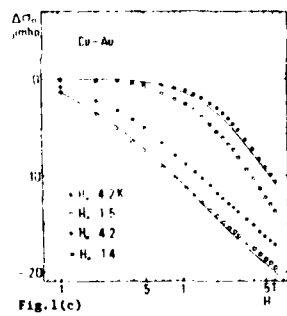
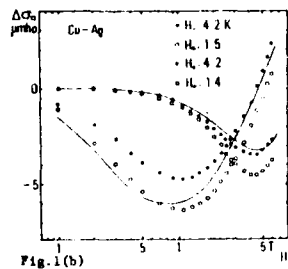
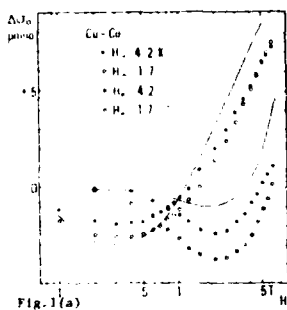
	$\sigma(H=0)$ ( $\Omega^{-1}$ )	$\sigma$ ( $\Omega^{-1}$ )	$\tau_0$ ( $\times 10^{-14}$ sec)	$\tau_{\infty}$ ( $\times 10^{-13}$ sec)	$\tau_c$ ( $\times 10^{-12}$ sec)	Mn concentration (at%)
no. 1	1.127	1.0	9.2	48	5.2	0.1
no. 2	1.127	1.0	9.2	48	5.2	0.2
no. 3	1.127	1.0	9.2	48	5.2	0.3
no. 4	1.127	1.0	9.2	48	5.2	0.4
no. 5	1.127	1.0	9.2	48	5.2	0.5

Table 3. List of Bi films. Thickness and other parameters are given.

Bi film	$\sigma(H=0)$ ( $\Omega^{-1}$ )	$\sigma$ ( $\Omega^{-1}$ )	$\tau_0$ ( $\times 10^{-14}$ sec)	$\tau_{\infty}$ ( $\times 10^{-13}$ sec)	$\tau_c$ ( $\times 10^{-12}$ sec)	$\chi^2$ (%)
no. 1	1.127	1.0	9.2	48	5.2	1.7
no. 2	1.127	1.0	9.2	48	5.2	1.7
no. 3	1.127	1.0	9.2	48	5.2	1.7
no. 4	1.127	1.0	9.2	48	5.2	1.7

#### Figure Captions

- Fig.1 Magnetoconductivity  $\Delta\sigma(H) = \sigma(H) - \sigma(0)$  of Cu-Cu (a), Cu-Ag (b) and Cu-Au (c) films. Values of  $\sigma(0)$  are given in table 1. Magnetic field is perpendicular ( $H_{\perp}$ ) and parallel ( $H_{\parallel}$ ) to the films. Solid lines are theoretical curves with parameters given in table 1.
- Fig.2 Magnetoconductivity of several Cu-Mn alloy films at 4.2K in the field perpendicular to the films. Values of  $\sigma(0)$  and Mn concentrations are given in Table 2. No.1 sample is the Cu-Cu film whose data are the same as those in Fig.1(a). Solid lines are theoretical curves with  $\tau_c = 7 \times 10^{-12}$  sec and other parameters given in table 2.
- Fig.3 Inelastic scattering time  $\tau_c$  of several Bi films as a function of temperature. These values are obtained as a fitting parameters of magnetoconductivity due to the localization mechanism. Other parameters are given in Table 3.



# WEAK LOCALISATION EFFECTS IN GAAS DOPING SUPERLATTICES

Th. Englert, J.C. Maan, G. Remenyi, H. Künzel, K. Ploog, A. Fischer  
Max-Planck-Institut für Festkörperforschung,  
F-38042 Grenoble and D-7000 Stuttgart

A. Briggs  
SNCI, CNRS Grenoble, France

## Abstract

The conductivity of an n-layer in a GaAs doping superlattice decreases logarithmically with temperature between about 25K and 250 mK. The magnetoresistance in low fields is negative and varies logarithmically. The results are explained in terms of the theory of weak localisation in two dimensions. The inelastic scattering time is determined from a fit of the magnetoresistance as a function of temperature and carrier density.

In recent years the concept of weak localisation has proved to be very fruitful for an understanding of the electronic transport in a regime between complete localisation and quasimetallic behaviour, especially in two-dimensional (2D) systems such as Si-MOS, GaAs/AlGaAs heterostructures and in thin metallic films (1). In the present paper we report the observation of weak localisation effects in a new quasi-2D system, the doping superlattice on GaAs. Such a structure consists of alternating periodic thin layers of n- and p-type doping. The electrons from the donors in the n-layer transfer to the acceptors in the p-layers and the resulting space charge leads to potential wells in the n-layers for the electrons and in the p-layers for the holes. Through selective contacting of the n- and p-layers, the potential difference between the layers can be changed externally. In this way the carrier density of the layers can be varied by injection or extraction of carriers. Up to now a number of different experiments (2,3) have confirmed the quasi-2D nature of the system predicted theoretically (4). In many aspects this system seems to be particularly well suited for

studying localisation phenomena, because there is a considerable amount of disorder due to the relatively high doping level and the density of mobile carriers can be changed easily.

Three MBE-grown samples have been used for the present study, two multilayer structures with 10 alternating n- and p-layers (sample A:  $N_D = 7 \times 10^{17} \text{ cm}^{-3}$ ,  $N_A = 7.85 \times 10^{17} \text{ cm}^{-3}$ , doping layer thickness  $d = 90 \text{ nm}$ ; sample B:  $N_D = 5.25 \times 10^{17} \text{ cm}^{-3}$ ,  $N_A = 6.75 \times 10^{17} \text{ cm}^{-3}$ ,  $d = 100 \text{ nm}$ ) and one single layer sample consisting of one n-layer sandwiched between two p-layers ( $N_D = N_A = 7 \times 10^{17} \text{ cm}^{-3}$ ,  $d_n = 90 \text{ nm}$ ,  $d_p = 500 \text{ nm}$ ). For the analysis a multilayer sample is considered as 10 layers electrically connected in parallel. In Fig.1 the sheet conductivity of the n-layer is plotted as a function of temperature between 50 mK and 25K for samples A and B. It shows a logarithmic behaviour over two orders of magnitude in T and saturates below about 150mK. The slope of the straight lines connecting the data is  $dP = 1.0 \pm 0.1$  in agreement with the theory of weak localisation (equ.1). This result indicates that the weak localisation mechanism rather than interaction effects is dominant at these T. The saturation of the conductivity at low temperatures is not an experimental artifact. It has also been observed in Si-MOS, and has been attributed to an "hot electron - finite size effect", which occurs when the energy relaxation length becomes comparable with the sample dimensions (5). The inset in Fig.1 shows the magnetoresistance for two different temperatures in the low T regime. It varies logarithmically in agreement with theory and with experimental results obtained on other 2D systems (5,6). In the following we determine the inelastic scattering time  $\tau_i$  from a fit of the negative magnetoresistance. Theoretically the temperature and magnetic field dependence of the conductivity is given by (5):

$$\sigma(T, H) = \sigma(T_0, 0) + \frac{e^2 P \tau_i^2}{2e^2 h} \ln \frac{T}{T_0} + \frac{e^2}{2e^2 h} \left( \psi\left(\frac{\sigma}{\sigma_0} + \frac{1}{2}\right) - \ln \sigma \right) \quad (1)$$

where  $\sigma = e^2 / 2e^2 h$ ,  $\psi$  is the digamma function. The additional term depending on  $\mu_B h / kT$  can be neglected in the present case, since the g-factor in GaAs is small and in the limit of very low T, where  $\mu_B h / kT$  becomes important the conductivity and the

magnetoresistance were found to saturate. The negative magnetoresistance given by equ. 1 should depend on the perpendicular component of the magnetic field only. This is confirmed by our experiment in the limit of very small magnetic fields. Fig. 2 shows the magnetoresistance for  $B$  perpendicular and parallel to the layer plane for the single layer sample. Also shown is a fit using equ. 1 with  $\tau_i = 4.7 \times 10^{-11}$  sec and  $\beta = 0.9$ . The other sample parameters ( $E_g = 37$  meV,  $\mu = 2350$  cm<sup>2</sup>/Vs) are known from measurements in higher fields (7). A strong anisotropy is observed, however there is also a negative component for  $B \parallel$ , whereas equ. 1 yields a straight line as indicated. This additional magnetoresistance is found to be sample dependent and presumably indicates deviation from a strictly 2D behaviour (8).

From a fit of the negative magnetoresistance we have determined  $\tau_i$  as a function of  $T$  for sample A in a range where the conductivity varies logarithmically and no saturation is observed (Fig. 3). The line connecting the data points corresponds to  $T^{-0.74}$ . This dependence is somewhat weaker than predicted for electron-electron scattering and the experimental values found in the Si MOS system (6).

As already mentioned the carrier density of the system can be changed by applying an  $U_{np}$  bias voltage. The inelastic scattering time as a function of the 2D carrier density is plotted in Fig. 4 for  $T = 4.2$  K, where  $n_s$  is taken from the Hall effect and Shubnikov-de Haas oscillations at high  $B$  (3). The increase of  $\tau_i$  with  $n_s$  may qualitatively be attributed to screening. The variation is much weaker than found in Si MOS. However comparing these two systems one has to consider that here an increase in  $n_s$  is not directly correlated with an increase in the Fermi energy, but with a widening of the space charge potential and thus a reduction of the subband separation, which leads to the occupation of higher subbands. In the limit of high forward bias a transition occurs from 2D to 3D.

In summary we have found that electrons in thin layers of GaAs produced by alternating n- and p-doping are weakly localized at low temperatures. The temperature dependence of the sheet conductivity and the negative magnetoresistance can be understood in terms of the existing theories. The results further substantiate the 2D behaviour of the system in the limit of low carrier density.

#### References

- (1) see e.g., P.W. Anderson, in: Proc. of the 16th Int. Conf. on the Physics of Semiconductors, ed.: M. Averous, (North-Holland Amsterdam, 1983) Part I, p.30 and Ref. therein
- (2) G.H. Döhler, H.Künzel, D.Olego, K.Ploog, P.Ruden, H.J. Stolz, G. Abstreiter, Phys. Rev. Letters 47 (1982) 864
- (3) J.C. Maan, Th. Englert, Ch. Uihlein, H.Künzel, K.Ploog, A. Fischer, J. Vac. Sci. Technol. in press
- (4) G.H. Döhler, phys. stat. sol. (b) (1972) 53 and 533, J. Vac. Sci. Technol. 16 (1979) 851
- (5) D.J. Bishop, R.C. Dynes, D.C. Tsui, Phys. Rev. B26 (1982) 773
- (6) Y. Kawaguchi, S. Kawaji, Surface Sci. 113 (1982) 505
- (7) J.C. Maan, Th. Englert, Ch. Uihlein, H.Künzel, K.Ploog, A. Fischer, Solid State Commun. in press
- (8) Z. Ovadyahu, S. Moehlecke, Y. Imry, Surface Sci. 113 (1982) 544

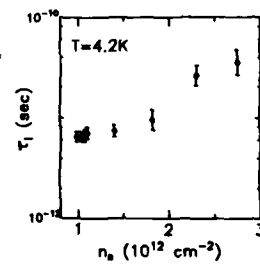
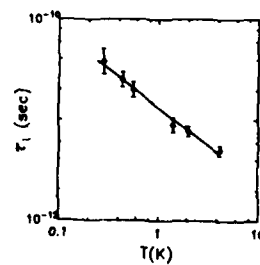
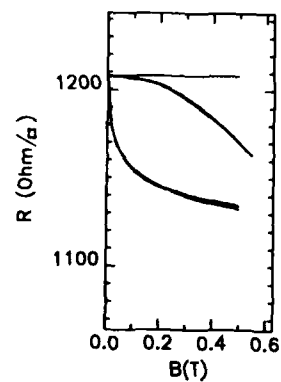
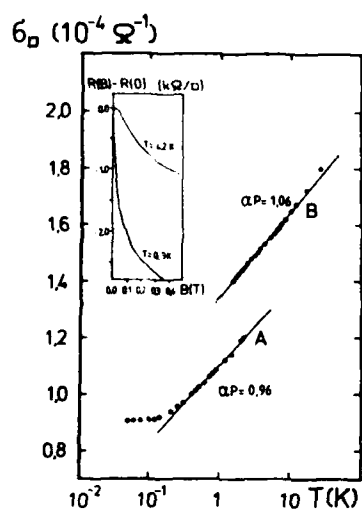
#### Figure captions

Fig. 1: Sheet conductivity vs.  $T$  for two different samples with  $U_{np} = 0$ . The inset shows the magnetoresistance at  $T = 4.2$  K and  $T = 0.3$  K for sample A with  $U_{np} = -5$  Volt. The sheet resistances at  $B = 0$  are 10087 Ohm and 12188 Ohm respectively.

Fig. 2: Magnetoresistance and fit for a single layer with  $B$  perpendicular and parallel to the layer plane. The temperature is  $T = 1.5$  K.

Fig. 3: Inelastic scattering time as determined from a fit of the negative magnetoresistance versus  $T$ .

Fig. 4: Inelastic scattering time versus 2D carrier density at  $T = 4.2$  K.



A. MacKinnon

Blackett Laboratory, Imperial College, London SW7 2BZ, U.K.

L. Schweitzer, B. Kramer

Physikalisch-Technische Bundesanstalt, Bundesallee 100, 3300 Braunschweig, F.R.G.

#### Abstract

We present numerical results on the effect of a stochastic potential and the finite size of a sample on the density of states and the exponential decay length of the transmission coefficient of a two dimensional system. For periodic boundary conditions the data suggest the existence of extended states in the center of the magnetic subbands. For nonperiodic boundary conditions the existence of disorder independent edge states is demonstrated, which extend along the whole length of boundary of the sample. The implications of these data for the explanation of the quantum Hall-effect is discussed.

#### 1. Introduction

The theory of the quantum Hall-effect [1] is still in its infancy, although a number of models have been proposed during recent years, which are capable of explaining various aspects. However, there is no model, which gives a satisfactory explanation of all experimental data presently available.

There are two main streams of arguments starting from more or less complementary points of view. One is based on the localisation of electrons in a random potential [2,3]. Here one deals with a system in its thermodynamic limit such that surface effects are eliminated. The other one, which essentially needs the finiteness of the sample, depends on the existence of edge states and was worked out for special annular geometry [4,5].

The essential question in the localisation theory is whether a magnetic field  $B$  can delocalise one-electron states in the center of the Landau bands

which are localised exponentially for  $B=0$  [2]. There is also no rigorous argument which gives the steps in the Hall conductivity at integer numbers in an infinite system with stochastic potential. The approach using edge states needs detailed information on the influence of sample geometry and disorder. If both models are correct there must be some possibility of joining the two ideas for large sample sizes. In this contribution we want to address the question of (i) the localisation and (ii) the influence of disorder on the edge states.

#### 2. Model and boundary conditions

We consider the tight binding model for an electron in a two dimensional random potential and a magnetic field described by the Hamiltonian [6,7]

$$H = \sum_{j,k} \sum_{j',k'} V_{jk,j'k'} |jk\rangle \langle j'k'| + \sum_{j,k} \epsilon_{jk} |jk\rangle \langle jk| \quad (1)$$

where

$$V_{jk,j'k'} = \begin{cases} 1 & \text{if } k = k' \text{ and } j' = j \pm 1 \\ \exp(\pm i e/h B a^2) & \text{if } j = j' \text{ and } k' = k \pm 1. \end{cases}$$

$\epsilon_{jk}$  is the random potential distributed according to some probability distribution which we take as a rectangular box of width  $W$ . Thus,  $W$  characterises the disorder. For simplicity we consider a square lattice. For  $W=0$  the spectral properties of  $H$  were discussed earlier [8,9]. The result is the so called "self-similar-butterfly". For  $W \neq 0$ , there is no quantitative information about the spectrum. We present results for the density of states and the exponential decay length of the transmission coefficient for systems which are essentially infinitely long in, say, the  $x$ -direction, which is characterised by  $j$  in eq. (1). In the  $y$ -direction the system is of finite width  $M \cdot a$  ( $a$  - lattice spacing). We consider both periodic boundary conditions in the  $y$ -direction ( $P$ -system), which correspond to a cylinder like geometry, as well as nonperiodic boundary conditions ( $N$ -system), which correspond to a strip geometry.



### 3. Method and results

We have evaluated the density of states  $n(E)$ , and the decay length  $\lambda_M(E)$  using the iterative procedure described previously [10]. The respective definitions are

$$n(E) = -1/\pi \lim_{n \rightarrow 0} \text{Im} \left\{ \sum_k G_{jk,jk}(E + i\eta) \right\} \quad (2)$$

and

$$\lambda_M^{-1}(E) = \lim_{N \rightarrow \infty} [2(N-1)]^{-1} \ln \sum_{k,k'} |G_{1k,Nk}| \quad (3)$$

where  $G_{1k,Nk}$  are the matrix elements of the resolvent  $G = (E-H)^{-1}$  between the first and the  $N$ -th slice of the system. We also calculate the local density of states  $n(E,k)$  as a function of the  $y$ -coordinate, i.e.

$$n(E,k) = -1/\pi \lim_{n \rightarrow 0} \text{Im} \left\{ \sum_j G_{jk,jk}(E + i\eta) \right\} \quad (4)$$

The results are shown in figs. 1 to 4. The magnetic field was taken such that

$$L_B = \frac{h}{e} \frac{1}{B a^2} = 8 \quad (5)$$

This corresponds to 1/8 flux quanta per unit cell and splits for  $W=0$  the tight binding band into 8 magnetic subbands, which are symmetric about  $E=0$ . If  $W \neq 0$  these bands will remain well separated as long as  $W$  is small compared with the magnitude of the band gaps. The imaginary part of the energy,  $\eta$ , was taken as 0.02 throughout all density of states calculations.

In fig. 1 we have plotted the total density of states of the lowest magnetic subband for a P-system with  $W=0.5$ . Within the accuracy of our calculation (1%) this had already converged as a function of  $M$ , such that it represents the total density of states of the infinite two dimensional system.

$\lambda_M(E)$  shown in this figure is for the same system. There are characteristic variations with  $M$ . In the tails of the band the ratio  $\lambda_M/M$  decreases with increasing  $M$  such that one may conclude that

$$\lambda_\infty = \lim_{M \rightarrow \infty} \lambda_M \quad (6)$$

stays finite. In the center of the band  $\lambda_M/M$  is found to increase with  $M$ .

It is, however, not yet certain whether  $\lambda_M/M$  increases to infinity if  $M$  is further increased. Nevertheless, one may adopt the interpretation that  $\lambda_M$  tends to infinity in the center of the band at least in proportion to  $M$ . If one could establish a relation between the behaviour of  $\lambda_M$  and the conductivity as for  $B=0$  [11], one would identify the energies where  $\lambda_M/M = \text{const}$  with the mobility edges.

Fig. 2 shows the results for the total density of states for the N-system with  $W=0.5$  again for energies near the lowest band for three different values of  $M$  ( $M=8, 16, 32$ ). It is seen that the data have not yet converged. Increasing  $M$  leads to an increase of  $n(E)$  at energies lower than  $-3.2$  and a decrease in the band tail above this energy. We suspect that the boundary plays an essential role in determining the behaviour of the states. This is verified in fig. 3 where we have plotted  $n(E,k)$  for  $M=16$  at  $E = -3.3$  and  $E = -3.1$  for  $W=0.5$  and  $D=1$ .

The exponential decay length for the N-system behaves differently to that for periodic boundary conditions. At energies below the first magnetic subband  $\lambda_M/M$  is similar to the data shown in fig. 1. At energies above first calculations indicate that  $\lambda_M$  diverges for finite  $M$ . Further calculations have to be performed in order to clarify the behaviour of the states near the center of the magnetic subband.

### 4. Discussion

Our results for the P-system indicate that the magnetic field is able to "delocalise" electronic states. These are the states near the centres of the magnetic subbands. However, the quantitative aspects of this "delocalisation" are not yet quite understood. Although, for instance, it is possible to derive a scaling function for these data similar to the case of vanishing magnetic field [11], it is not yet established whether  $\lambda_M/M$  stays finite for  $M$  or tends to infinity. In addition, at energies near the centre of the tight binding band the behaviour seems to be more complicated [12]. There is not yet any conclusion about the transport properties of such a system.

without periodic boundary conditions, we observe edge states, which are situated energetically between the subbands. These were discussed earlier by Halperin for an annular geometry [5]. They are well localised within about one lattice distance of the edges of the strip, which is what one would expect from the magnitude of the cyclotron radius  $r_c = \sqrt{\hbar/2m} a = 1.13a$  in our case. The result that  $\rho_{xx} \propto 1/M$  with  $N \propto M$  for finite  $M$  indicates that these edge states extend along the whole length of the strip. For  $M=0$  such states were obtained recently [13]. Our data demonstrate that the edge states are essentially independent of the disorder.

##### 5. Towards the explanation of the quantum Hall-effect

The explanation of the quantum Hall-effect needs two ingredients: (i) There must be states between the magnetic subbands, which are able to pin the Fermi energy, and which do not contribute to transport. (ii) There must be some state, which carries the Hall current.

If one accepts that each sample contains a certain amount of disorder the first ingredient is easily provided by the states localised exponentially within the volume of a sample. The data for  $\rho_{xx}$  shown in fig. 1 demonstrate that for energies well between the subbands the exponential decay length is small compared with the strip width. Therefore, the contribution of these states to the transport properties vanishes exponentially, in particular at  $T=0K$   $\rho_{xx} = 0$  within the gaps. We have indications that this is still true for the states within the bulk of a system with nonperiodic boundary conditions. If one admits the fact that each sample is of finite size, the second ingredient may be provided by the edge states, which, according to our data, seem to be decoupled from the bulk properties such as disorder, for instance. As it has been shown earlier [5] that these states can account for the steps in the quantum Hall-effect in an ordered system. This must remain true in the disordered case, since the states are unaffected by a certain amount of disorder.

It is worth noting at this point that this result can be expressed purely in terms of the behaviour of states around the Fermi level, whereas in a system with periodic boundary conditions it is necessary to sum the contributions from all occupied states. Thus we have two methods which give the same results for the macroscopic Hall current in spite of the fact that it arises from completely different microscopic behaviour. A one-electron picture, where the electrons and the electric field are decoupled, is therefore unable to predict the local current distribution.

The situation is more complicated when the Fermi energy lies near the centre of the subbands. Here, for periodic boundary conditions the exponential decay length is of the same order or larger than the strip width. Again, we have preliminary data which indicate that this will remain true for the bulk states when nonperiodic boundary conditions are applied. A further complication arises from the fact that there is no clearcut distinction between edge and bulk states in this regime. However, if we make the assumption (which is well supported by our data) that the states may still be characterized by the exponential decay length and that this appears to obey a scaling function similar to the case of zero magnetic field [11], a region of extended states exists around the centre of the Landau level which will contribute to  $\sigma_{xx}$ .

Our data are for very large magnetic fields, however, so it is by no means certain that such extended states must exist for physically more realistic fields. Our analysis of the quantum Hall-effect in terms of edge states does not depend on the existence of bulk extended states, but only on the existence of some conduction mechanism however weak [4]. This is always available in a finite sample or at finite temperature.

# Acknowledgements

We thank Wolfgang Wöger, Gerd Czycholl and the participants of the symposium on the quantum hall-effect in Schleching, which was sponsored by the Deutsche Forschungsgemeinschaft, for useful discussions. This work was supported by the Bundesministerium für Wirtschaft.

One of us (A. MacKinnon) would like to thank the PTB Braunschweig for their hospitality and B.P. Venture Research for financial support.

# References

- [1] K. v. Klitzing, G. Dorda, and M. Pepper  
Phys. Rev. Letters **45**, 494 (1980)
- [2] H. Aoki and T. Ando, Sol. St. Commun. **38**, 1079 (1981)
- [3] T. Ando, in "Anderson Localisation", Y. Nagaoka and H. Fukuyama, Eds.,  
Springer Series in Solid State Sciences **39**, 196 (Springer 1982)
- [4] R.B. Laughlin, Phys. Rev. B **23**, 5632 (1981)
- [5] B.I. Halperin, Phys. Rev. B **25**, 2185 (1982)
- [6] J.M. Luttinger, Phys. Rev. **84**, 814 (1951)
- [7] P.G. Harper, Proc. Phys. Soc. London A **68**, 874 (1955)
- [8] D.R. Hofstadter, Phys. Rev. B **14**, 2239 (1970)
- [9] G.M. Wannier, G.M. Obermair, and R. Ray,  
phys. stat. sol. (b) **93**, 337 (1979)
- [10] A. MacKinnon, J. Phys. C **13**, L 1031 (1980)
- [11] A. MacKinnon and B. Kramer, preprint (1983)
- [12] A. MacKinnon and B. Kramer, in "The Application of High Magnetic Fields in  
Semiconductor Physics", G. Landwehr Ed.,  
Lecture Notes in Physics **177**, 74 (Springer 1983)
- [13] R. Rammal, G. Toulouse, M.T. Jaekel, and B.I. Halperin,  
Phys. Rev. B **27**, 5142 (1983)

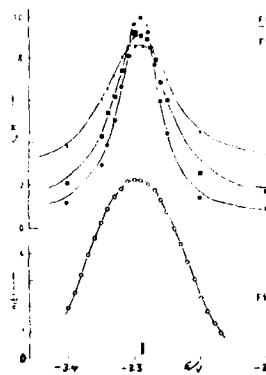


FIG. 1

## Figure captions

Fig. 1 The density of states  $n(E)$  and the exponential decay length  $L(E)$  of the transmission coefficient for a two dimensional disordered system (disorder parameter  $W=0.5$ ) in a magnetic field corresponding to 0.125 flux quanta per unit cell. The position of the magnetic subband for  $W=0$  is at  $-3.285$ , approximately. The system is infinitely long in  $x$ -direction. The width in  $y$ -direction is  $M \cdot a$  ( $a$  - lattice constant). Periodic boundary conditions are applied in  $y$ -direction. Data for  $n(E)$  are for  $M=4$  (x), 8 (square), and 16 (circle). The data for  $n(E)$  are converged already at  $M=16$  within the statistical accuracy of 1%. Phenomenological broadening (imaginary part of energy) is  $\eta = 0.02$ .

Fig. 2 The density of states  $n(E)$  for a system with the same parameters as in Fig. 1 except that nonperiodic boundary conditions are applied in  $y$ -direction. The system width correspond to  $M=8$  (x), 16 (circle), and 32 (square). Arrows indicate energies at which the local density of states plotted in Fig. 3 are calculated.

Fig. 3 The local density of states  $n(E, k)$  at  $y = M \cdot a$  ( $a$  - lattice constant) for a system with the same parameters as in Fig. 2 at  $E = -3.1$  (square) and  $E = -3.3$  (circle). System width is  $M=16$ . Disorder parameters are  $W=0.5$  (open symbols) and  $W=0.1$  (closed symbols). Within the statistical accuracy (1%)  $n(E, k)$  at  $E = -3.1$  is the same for both values of the disorder parameter.

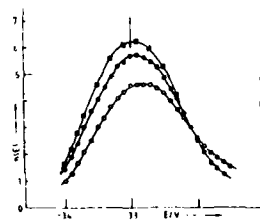


FIG. 2

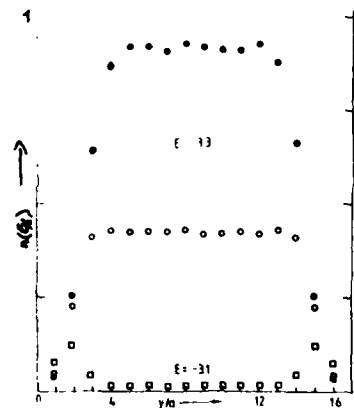


FIG. 3

# LOGARITHMIC CORRECTIONS TO THE CONDUCTIVITY OF A TWO-DIMENSIONAL HOLE GAS.

G.M. Gusev, L.D. Rykov, I.G. Reizvestnyi, V.M. Lvskyuk  
Institut of Semiconductor Physics Academy of Sciences  
of the USSR Siberian Branch, Novosibirsk, USSR.

In this work logarithmic corrections to the conductivity of a two-dimensional hole gas near (111) Si surface have been observed and studied over the temperature range 0.3 - 5 K in the absence and in the presence of the magnetic field. The value of logarithmic prefactor  $A$  was found to be 0.3 ( $\ln e^2/2\pi^2\hbar$ ). In magnetic field increasing of  $A$  to 0.9 was observed because of the suppression of the contributions to the conductivity of effects in the Cooper channel. In this case logarithmic corrections are determined by only exchange effects, because Hartree-like term cancelled by spin-orbit scattering of holes.

In the work [1] the anomalous magnetoresistance (AMR) in two-dimensional (2D) hole gas with a positive sign has been found to be due to the influence of the magnetic field on the scattering of holes by superconducting fluctuations [2].

Absence of a negative AMR in this work have been assumed because of the suppression of localization correction by the strong spin-orbit scattering of holes by impurities. This feature in behaviour of 2D hole gas should lead to the differences between temperature dependence of logarithmic corrections of hole and electron gas.

In this work we report our observation of logarithmic corrections to the conductivity of 2D hole gas near (111) Si surface over the temperature range 0.3-5 K in the absence and in the presence of the magnetic field. The behaviour of these corrections was found to be completely determined by the effects of hole interaction, when the strong spin-orbit scattering was taken into account.

Experimental devices were p-channel Si MOS transistors as were used in [1].

Fig. 1 shows channel conductivity of one of these samples as a function of the temperature for the different hole concentration. One sees that the conductivity at  $p_g = 2.7 \cdot 10^{12} \text{ cm}^{-2}$  is decreased following to the slow logarithmic law over the temperature range 5.2 - 1 K. At  $T < 1 \text{ K}$  the sharp drop of  $T$ -dependence of the conductivity is observed. At slightly high hole concentration the inclination of  $T$ -dependence of  $G$  from  $\ln T$  was not observed, and conductivity was decreased logarithmically to 0.3 K.

As it follows from the theory [3-5], the change of the conductivity with the temperature is:

$$G(T) = \frac{e^2}{2\pi^2\hbar} A \ln T/\hbar \quad (1)$$

where  $A = -d\rho + (p-1)\beta(\cdot) - 4 + 3 \frac{2+F}{2} \ln(1+F/2)$

The first term is due to the Anderson localization

[3,4]. Three cases should be considered:

- a)  $d = 1$ , spin-orbit interaction is negligible;
- b)  $d = -1/2$ , relaxation process of the spin parallel to 2D plane (for example, elastic scattering between subband of heavy

and light holes) are taken into account;

c)  $\lambda = 0$ , relaxation process of the spin perpendicular to 2D plane (spin-orbit scattering of holes by impurities), are taken into account.

The second term in expression (1) is the contribution to the conductivity of carriers scattering by superconducting fluctuations [7],  $\beta$  is the coefficient, depending on the constant of the mutual hole-hole interaction in Cooper channel.

$4 - 3 \frac{2 + F}{F} \ln(1 + F/2)$  is due to hole-hole mutual interaction in diffusion channel [5,6], where  $F$  describes the contribution to the conductivity of Hartree-like term. In (1) the contribution due to interaction with the small differences of energy and momenta (Cooper channel) is absent we neglect this term, because it was not found in ABR measurements.

Before our experiments only 2D electron gas have been studied. Logarithmic corrections to the conductivity of 2D electron gas is surely provided to be first of all due to the localization, i.e. first term in expression (1), and logarithmic prefactor  $\lambda$  is equal to 1 [8,9]. It can be seen in fig. 1 that the slope of curves gives  $\lambda = 0.3-0.4$ , i.e. 3 times lower than for 2D electrons. It can be explained by the fact of the existence in 2D hole gas of the strong spin-orbit scattering and the case c) must be taken into account.

In this case, for 2D hole gas interaction effects and spin-orbit interaction play the important role in conductivity rather than for 2D electron gas. This suggestion is

confirmed by our measurements of  $G(T)$  in  $H$ . The magnetic field as it follows from [1], gives a rise to the positive ABR, i.e. suppresses corrections which increase the conductivity with decreasing of the temperature and connecting with the first and the second term in the expression (1). It is clear, that the magnetic field leads to increasing of the value of the logarithmic prefactor  $\lambda$ , as is really observed in experiments. Fig. 2 shows  $H$ -dependence of  $\lambda$ . One sees, that  $\lambda$  is increased to the value 0.9 and after becomes a constant. It shows, that at  $H > 1.5$  kG in the terms in expression (1) connecting with the electron-electron interaction remains only, and corrections to the conductivity due to effects in Cooper channel are suppressed.

In 2D hole gas the ratio  $\lambda/p_F$  (where  $\lambda$  is the inverse screening length in 2D) is not small, therefore  $F$  and consequent term in (1) are large enough to contribute to the  $T$ -dependence of conductivity. But the experiment gives  $\lambda = 0.9$ , i.e. Hartree-like term is negligible. Therefore, the existence of the strong spin-orbit scattering in 2D hole gas, as it has been assumed in [1], is emphasized here. The theoretical works [10,11] have shown, that in the presence of the spin relaxation process Hartree-like term becomes independent on  $\ln T$ . Consequently, in magnetic field the correction to the conductivity due only to the exchange effects is observed. The small difference  $\lambda$  from 1 can be explained by the existence of the rest of the contribution of Hartree-like term.

It should be noted that the influence of the strong spin-orbit scattering is a main difference in this case between hole and electron gas, where Hartree-like term contributes to  $G$ , but it is completely compensated by the exchange term, and

interaction effects in 2D electron gas is not occur [9].

ACKNOWLEDGEMENT: We should like to thank N.V. Zavaritsky for assistance in low-temperature measurements, B.L. Al'tshuler and A.Yu. Zuzin for stimulating discussions.

#### REFERENCES:

1. G.M. Gusev, Z.D. Kvon, I.G. Neizvestnyi, V.N. Ovsyuk & A.M. Palkin, Sov. Phys., JETP Lett., 35, 256, 1982.
2. A.I. Larkin, Sov. Phys., JETP Lett., 31, 219, 1980.
3. E. Abrahams, P. Anderson, D.C. Liccardello, T.V. Ramakrishnan, Phys. Rev. Lett., 42, 673, 1979.
4. B.L. Al'tshuler, A.G. Aronov, A.I. Larkin, D.E. Khmel'nitskii, Sov. Phys., 54, 411, 1981.
5. A.M. Finkel'shtein, Zh. Eksp. Teor. Fiz., 84, 168, 1983.
6. B.L. Al'tshuler, A.G. Aronov & P.A. Lee, Phys. Rev. Lett., 44, 1288, 1980.
7. B.L. Al'tshuler et al, Zh. Eksp. Teor. Fiz., 6, 1983.
8. D.J. Bishop, D.C. Tsui, R.C. Dynes, Phys. Rev. Lett., 44, 1153, 1980.
9. M.J. Uren, R.E. Davies, M. Pepper, J. Phys. C, Solid, State Physics, 1985, 1980.
10. B.L. Al'tshuler, A.G. Aronov, A.Yu. Zuzin, Sol. St. Comm., 44, 137, 1982.
11. B.L. Al'tshuler, A.G. Aronov, Sol. St. Comm., 46, 429, 1983.

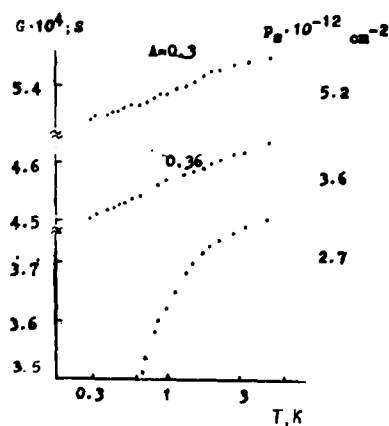


Fig. 1 Channel conductivity  $G$  as a function  $\ln T$

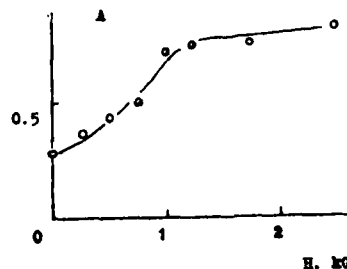


Fig. 2 H-dependence of logarithmic prefactor  $A$  at hole concentration  $p_h = 3.6 \cdot 10^{12} \text{ cm}^{-2}$

NEGATIVE AND POSITIVE MAGNETORESISTANCE IN Cs ADSORBED  
Si (111) N-INVERSION LAYERS

Yoichi KAWAGUCHI

Gakushuin Women's Junior College, Toyama, Shinjuku-ku, Tokyo 162, JAPAN  
Shinji KAWAJI

Department of Physics, Gakushuin University, Mejiro, Toshima-ku, Tokyo 171

In n-channel inversion layers on Cs adsorbed Si (111) surfaces, the range of electron-electron interaction constants  $g_i$ 's are determined by magnetoresistance experiments (the positive magnetoresistance in the field parallel to the surface and the negative magnetoresistance in the field perpendicular to the surface) and the  $\log T$  dependence of the conductivity. The results are  $0.95 \leq g_4 \leq 1.52$ ,  $0.36 \leq g_1 \leq 0.55$ ,  $0 \leq g_2 \leq 1.14$  and  $0 \leq g_3 \leq 0.57$  for  $n_V=6$ . For  $n_V=2$  the value of  $g_1$  is the same as the previous one and the values of other  $g_i$ 's are one third of  $g_i$ 's for  $n_V=6$ .

§1. Introduction

The recent development of the theoretical and experimental studies on the electrical conduction of two dimensional electrons in metallic region has shown that the Coulomb interaction effect (1) and the spin-zeeman effect (2) contribute to the conduction as well as the localization effect (3). The Coulomb and the localization effects come from the orbital motion of electrons and are sensitive to only the magnetic field component perpendicular to the surface. Both of them contribute to the  $\log T$  dependence of conductivity. The Coulomb interaction gives rise to the positive magnetoresistance and on the other hand the localization effect contributes to the negative magnetoresistance. On the contrary, the spin-zeeman effect contribute to the positive magnetoresistance in the field parallel to the surface. Therefore, it is possible through the analysis of the magnetoresistance in both of the fields parallel and perpendicular to the surface and the  $\log T$  dependence of conductivity to estimate

the interaction constants in these process. However, it is difficult to observe these three effects experimentally in usual silicon MOSFETs.

The positive magnetoresistance in the perpendicular field and the  $\log T$  dependence of conductivity have been observed simultaneously in the conduction in n-inversion layers on highly cesium adsorbed p-Si (111) surfaces at temperatures lower than 20K (4). The electron concentration is estimated at  $8 \times 10^{16} \text{ cm}^{-2}$  from the Corbino magnetoresistance at 40K. Though the conductivity of  $150 \mu\text{ho}$  at temperatures around 4K gives  $k_F L = 0.5$ , the temperature dependence of conductivity is still metallic or not an activation type. Electrons in the inversion layers show the clear two dimensional behavior at temperatures lower than 200K. The angular dependence and the field dependence of the magnetoresistance are well explained by the combination of three effects; the Coulomb interaction, the spin-zeeman effect and the localization effect. In the present paper we will estimate the interaction constants through the analysis of 1) the positive magnetoresistance in the field parallel to the surface using the Kawabata's formula (2) due to the spin-zeeman effect, 2) the negative magnetoresistance in the field perpendicular to the surface and 3) the  $\log T$  dependence of conductivity using the Fukuyama's formula (1) including the localization term and the Coulomb interaction term, and discuss the value of the interaction constants. In the following discussion, we use the formula in the limit that the intervalley scattering happens very frequently in comparison with the inelastic scattering as shown later.

§2. Positive Magnetoresistance in the Field Parallel to the Surface

Positive magnetoresistance increases with lowering the temperature and is proportional to the square of field at high fields as shown in Fig. 1. Excluding the negative magnetoresistance part observed at lower fields, the magnetoresistance is well explained by Kawabata's formula (2) divided by valley degeneracy factor 6 (5) as

$$\Delta\sigma_{ZH} = 12.32 (g_3 + g_4) G(b) (\mu\text{ho}),$$

where  $g_3$  and  $g_4$  are the electron-electron interaction constants associated

with the Hartree type correction,  $b = \hbar \omega_c / 2\pi kT = 0.214 B(T)/T(K)$  for electrons in silicon and the function  $G(b)$  is  $G(b) = -\pi b^2 (b^2 + 3n^2) / (n^2 + b^2)^2$ . For  $b \ll 1$ ,  $G(b) \approx -3.16 b^2$ . In the present case,  $b \approx 0.2$ . The  $B^2$  dependence of the magnetoresistance is well described by

$$\Delta \sigma_{2H} = 2.04 (g_3 + g_4) B^2(T) / T^2(K) \text{ } [\mu\text{mho}].$$

In Fig. 2, the slope of the  $\Delta \sigma_{2H}$  versus  $B^2$  curves are plotted as a function of  $T^{-2}$ . The result gives the mean value of  $(1/6) (g_3 + g_4) = 1.52$ .

### 3.3. Negative Magnetoresistance in the Field Perpendicular to the Surface

The negative magnetoresistance observed in the field perpendicular to the surface cannot be explained by only the localization effect over the whole range of field observed as shown in Fig. 3. The critical field  $B_c$  at which the cyclotron radius is comparable to the mean free path is given by

$$B_c = 31,000 n_V N_S (10^{16} \text{ cm}^{-2}) / \sigma^2 (\mu\text{mho}) \text{ } [T]$$

and  $B_c \approx 50 T$  in the present system. The magnetoresistance data are fairly well reproduced by only the localization term up to the characteristic strength of the field to observe the interaction term  $B_0$ , which is given by

$$B_0 = 440 r_m n_V / \sigma (\mu\text{mho}) \tau_e (\text{ps}) \text{ } [T],$$

where  $r_m$  is the ratio of effective mass to electron mass. In the present system, we have  $B_0 \approx 0.5 T$ . To get a perfect fit between the theory and experimental data, one should take the interaction term into account. The formula for the magnetoresistance in the field perpendicular to the surface is given by the combination of the localization (3), Coulomb interaction (1) and spin-zeeman (2) terms,  $\Delta \sigma_\perp = \Delta \sigma_L + \Delta \sigma_1 + \Delta \sigma_2$ , and each of them is given by

$$\Delta \sigma_L = 12.32 \left( \psi(1/2 + 1/h) - \psi(1/2 + \tau_e/h) + \ln(\tau_e/h) \right) \text{ } [\mu\text{mho}],$$

$$\Delta \sigma_1 = 12.32 (g_2 - 2g_4) E E' \left[ \psi''(1/2 + (E+h)/\gamma h) / (\gamma h)^2 + 1/(\gamma + h)^2 \right] \text{ } [\mu\text{mho}],$$

$$\Delta \sigma_2 = 12.32 g_3 G(b) \text{ } [\mu\text{mho}],$$

where  $\psi$  and  $\psi''$  are the Psi- and Tetra-gamma function, respectively and  $h = a \tau_e = 0.00423 \sigma (\mu\text{mho}) \cdot B(T) \cdot \tau_e (\text{ps})$ .

The procedure of fitting for data in the whole range in the field is as

follows. 1) The interaction constant  $g_3$  in the spin-zeeman term is assumed to be the half of  $(g_3 + g_4)$  value estimated from the magnetoresistance in the field parallel to the surface. 2) At low field limit the data is reproduced by the localization term only by adjusting the single parameter  $\tau_e$ . 3) Finally, the whole experimental data are fitted to the total magnetoresistance formula by adjusting the value of  $(g_2 - 2g_4)$ .

The inelastic scattering time  $\tau_e$  extracted by the preceding procedure is fairly well expressed by  $\tau_e = (18 \pm 1)/T$  [ps]. The temperature dependence of  $\tau_e$  is qualitatively explained by the inelastic scattering time due to the electron-electron interaction at dirty limit discussed by Abraham et al. (6). However, their theory gives the inelastic scattering time of 0.04 ps at 4K which is the one hundredth of the observed value in the present system.

It is expected that the intervalley scattering time  $\tau'$  is a several times of  $\tau$  as for the electrons in Si (100) channels (7). The elastic scattering time  $\tau$  is equal to 0.002 ps at 4K and has not considerable change with temperature. As  $\tau'/\tau \ll 1$ , the intervalley scattering happens many times in the interval between the inelastic scattering. Therefore, one is allowed to use the localization formula for the single valley case.

### 5.4. Results and Discussion

The interaction constant extracted from the data in the field perpendicular to the surface  $-(g_2 - 2g_4)$  decreases with decreasing temperature and at low temperatures the value of  $-(g_2 - 2g_4)$  tends to 1.9 as shown in Fig. 4. The increase of  $-(g_2 - 2g_4)$  with increasing temperature arises from the increase of  $\tau'/\tau_e$  with increasing temperature since  $\tau_e \propto 1/T$  and  $\tau'$  is almost independent of temperature.

The temperature dependence of conductivity is well described by  $\sigma = 15.6 \ln T(K) + 124.1$  [ $\mu\text{mho}$ ]. The temperature dependence of the quantum correction term in the conductivity is given by Fukuyama (1) as

$$\sigma'_1 = 12.32 [p + (6g_1 + g_2 - 2(g_3 + g_4))] \ln T \text{ } [\mu\text{mho}],$$

where  $p$  is the power in the expression of  $\tau_e = T^{-p}$ . From the comparison between



the theory and the experiment.  $6g_1 + g_2 - 2(g_3 + g_4) = 0.26$  by giving  $p=1$  in the present system.

From the positive magnetoresistance in the field parallel to the surface, the negative magnetoresistance in the field perpendicular to the surface and the temperature dependence of conductivity, three relations between the interaction constants  $g_i$ 's are extracted as 1)  $g_3 + g_4 = 1.52$ , 2)  $g_2 - 2g_4 = -1.9$  and 3)  $6g_1 + g_2 - 2(g_3 + g_4) = 0.26$ . If dynamically screened Coulomb interaction is assumed and give  $1/6$  to the value of  $g_1$ , the value of  $g_3$  becomes to be  $-0.58$ . To get a positive value for  $g_3$ , one should give the value larger than  $0.36$  to  $g_1$ . And  $g_1$  value larger than  $0.55$  gives a negative value to  $g_2$ . So as to keep all interaction constants  $g_i$ 's positive, each  $g_i$  should be in the following ranges:  $0.36 \leq g_1 \leq 0.55$ ,  $0 \leq g_2 \leq 1.14$ ,  $0 \leq g_3 \leq 0.57$  and  $0.95 \leq g_4 \leq 1.52$ .

In conclusions, 1) the Coulomb interaction correction plays an important role in the quantum correction of conductivity. The magnetoresistance in the field perpendicular to the surface cannot be reproduced by the localization theory only except the lowest field region in the experiments. 2) The range of the electron-electron interaction constants  $g_i$ 's were given by three independent measurements, positive magnetoresistance in the field parallel to the surface, negative magnetoresistance in the field perpendicular to the surface and  $\ln T$  dependence of the conductivity. In the analysis we have assumed the valley degeneracy  $n_v$  of 6. If  $n_v=2$ , then  $g_2$ ,  $g_3$  and  $g_4$  are reduced to one third of the values for  $n_v=6$ , however  $g_1$  does not change.

#### References

- (1) H. Fukuyama, J. Phys. Soc. Jpn. 50 (1981) 3407
- (2) A. Kawabata, Surface Sci. 113 (1982) 527
- (3) S. Hikami, A. I. Larkin and Y. Nagaoka, Prog. Theor. Phys. 63 (1980) 607
- (4) Y. Kawaguchi, H. Kitahara and S. Kawaji, Surface Sci. 73 (1978) 520
- (5) H. Fukuyama, J. Phys. Soc. Jpn. 50 (1981) 3562
- (6) E. Abrahams, P. M. Anderson, P. A. Lee and T. V. Ramakrishnan, Phys. Rev. 24 (1981) 6783
- (7) Y. Kawaguchi and S. Kawaji, Surface Sci. 113 (1982) 505

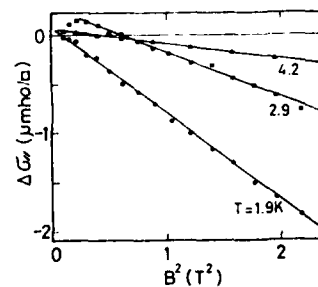


Fig. 1. Magnetic field dependence of positive magnetoresistance in the field parallel to the surface.

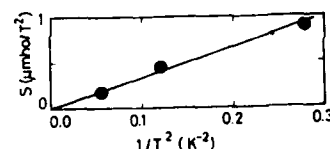


Fig. 2. Temperature dependence of the slope of  $\Delta G$  versus  $B^2$ ,  $S = d(\Delta G)/d(B^2)$ .

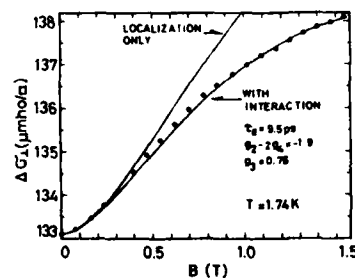


Fig. 3. Magnetic field dependence of negative magnetoresistance in the field perpendicular to the surface. Experimental data cannot be explained by the localization theory only.

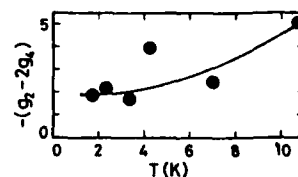


Fig. 4. Temperature dependence of the interaction constants,  $-(g_2 - 2g_4)$  estimated from the negative magnetoresistance in the field perpendicular to the surface.

# MAGNETIC FIELD DEPENDENCE OF 2D SODIUM IMPURITY BAND CONDUCTION IN ACTIVATED REGIONS

H. Reisinger, A. B. Fowler and A. Hartstein

I.B.M. Thomas J. Watson Research Center  
Yorktown Heights, New York 10598

## ABSTRACT

We have measured the temperature dependence of conductance of electrons in 2D sodium induced impurity bands in silicon inversion layers from 4.2K to 80K observing both activation of electrons to a mobility edge,  $E_1$ , and nearest neighbor hopping,  $E_3$  in magnetic fields up to 25T. The results are that  $E_1$  decreases slightly between 0 and about 20T and then increases slightly. The prefactor decreases by about a factor of four.  $E_3$  increases monotonically. None of these results was expected.

Impurity levels in Si inversion layers may be created by drifting  $\text{Na}^+$  ions in the  $\text{SiO}_2$  close to the Si-SiO<sub>2</sub> interface. The temperature dependence of conductance due to these impurity levels shows three ranges. The one highest in temperature (40-80K) corresponds to activation to the mobility edge ( $E_1$ ), the middle one (30-10K) to nearest-neighbor hopping, ( $E_3$ ) and the lowest one to variable range hopping. Temperature dependence as a function of  $\text{Na}^+$  concentration and filling-factor of the impurity band has been studied in previous experiments<sup>1</sup>. The effect of magnetic field on variable range hopping has also been studied<sup>2,3</sup>. In this paper we present the effect of a magnetic field perpendicular to the surface on the conductance in the two higher temperature ranges.

The samples used for this study were MOSFET devices with a circular gate of 80 microns diameter, and with  $L$ , the gate length, equal to 10 microns. The  $\text{Na}^+$  concentration was set to  $4 \times 10^{11} \text{ cm}^{-2}$ . Conductance was measured as a function of temperature. The temperature was determined from the resistance of a carbon glass thermometer using a correction for the magnetic field dependence of this resistance<sup>4</sup>. Conductance measurements were made at the peak of conductance which has been assumed to correspond to the peak in the density of states. The conductance peak did not change in gate voltage with the magnetic field or temperature.

Fig. 1 shows the log of conductivity vs. inverse temperature for some representative magnetic fields. The solid lines in Fig. 1 are from least-square fits of the experimental data (dots) to the equation

$$\sigma = \sigma_1 \exp - \frac{E_1}{k_B T} + \sigma_3 \exp - \frac{E_3}{k_B T}$$

From these least square fits the energies  $E_1$  and  $E_3$  as well as the prefactors  $\sigma_1$  and  $\sigma_3$  were determined for each value of magnetic field. When  $\sigma_1$  was taken as proportional to  $T$  similar fits were obtained.

It can be clearly seen in Fig. 1, that the conductivity decreases monotonically with magnetic field at all temperatures. In Fig. 2 the parameters  $E_1$  and  $E_3$  are shown as functions of magnetic field.  $E_3$  increases linearly with magnetic field by about a factor of two between 0 and 25 T. As can be seen also in Fig. 1, the magnetic field has only a small influence on  $E_1$ . The decrease between 0 and 20 Tesla is nevertheless an effect which is far above the error due to the fitting of the data. The estimated fitting errors are indicated in Fig. 2.

In Fig. 3 the prefactors,  $\sigma_1$  and  $\sigma_3$ , are plotted against magnetic field. The magnetic field dependence of  $\sigma_1$  in the given geometry might be expected in the simple case to be given by  $\sigma = \sigma_{\text{min}} (1 + \omega_c \tau)^{-1}$ . The solid line in Fig. 3 is  $\sigma$  fitted to the above formula and shows that  $\sigma$  basically behaves as expected.  $\tau$  is about  $6 \times 10^{-14}$  sec for the fit.

As shown in Fig. 2,  $E_1$  decreases from a maximum value of 17.5 meV at zero field to about 15.5 meV at 20 T and then increases again to about 15.8 meV at 25T. It was expected that the magnetic field should have increased the binding energy of electrons in isolated states. Half of the Landau energy is about 6.2 meV at 20T so that it is significant in magnitude compared to the binding energy of an electron band to an isolated sodium ion of 20-30 meV<sup>1,2</sup>. The only calculations of this effect are due to Kramer and Wallis<sup>5</sup>. These calculations are for fields much higher than the range covered by our experiments. The surface field in these experiments was about  $4 \times 10^4 \text{ V/cm}$  or  $1.3 \times 10^2 \text{ esu}$ . Since the experiment supposedly measures activation to a mobility edge the unexpected decrease in  $E_1$  may be the result of a decrease in the position of the mobility edge in the band tail. This decrease in  $E_1$  is against experience, which tends to show increased localization in a magnetic field. We have no explanation for this result.

$E_3$  is presumably a measure of the band width<sup>6,7</sup>. It may be seen to increase from about 2.7 meV to about 4.5 meV. If it is a measure of the band width, one may infer that the

density of states at the Fermi level at the band center must decrease by about a factor of two. If the effect of the magnetic field were to increase the binding the electron might screen more poorly so that the effects of fluctuations in surface field might be greater which would lead to a broader band. However, this argument doesn't seem to be consistent with the observed decrease in  $E_1$ , which might be expected to increase if the screening decreases.

The prefactor  $\sigma_1$  decreases from about 600  $\mu\text{S}$  to 120  $\mu\text{S}$ . According to Hayden and Butcher<sup>7</sup>,  $\sigma_1$  is proportional to  $\exp\{-2.39a / N_{\text{os}}\}$  where  $a$  is the decay constant for the Bohr orbit. Earlier estimates were that  $a \sim 1.4 \times 10^6 \text{ cm}^{-1}$ . A very crude estimate would be that  $a$  is increased by about 30% at 25T. Again this would be expected to correspond to a significant increase in binding energy and  $E_1$ .

In summary we have found a totally unexpected and unexplained result.  $E_1$ , the activation energy to the mobility edge, decreases as the magnetic field increases. On the other hand,  $\sigma_1$ ,  $\sigma_3$  and  $E_3$  behave qualitatively as one might have intuitively expected. Because we have no theory, no quantitative analysis is possible.

We would like to thank F. Stern and S. Das Sarma for helpful discussions, and J. Tornello for technical assistance.

This work was partially performed at the Francis Bitter National Magnet Laboratory at MIT which is supported in part by the National Science Foundation and the cooperation and hospitality of the Magnet Lab is gratefully acknowledged.

#### References

1. Ando, T., Fowler, A.B. and Stern, F., *Rev. Mod. Phys.*, **54**, 437 (1982). See Sec. VC.
2. Hartstein, A., Fowler, A.B., and Woo, K.C., *Physica* 117B and 118B, 655 (1983).
3. Hartstein, A., Fowler, A.B. and Woo, K.C., *Proceedings of the Int. Conf. on the Application of High magnetic Fields in Semiconductor Physics, Grenoble, Sept. 13-17, 1982*, to be published.
4. Sample, H.H., B.L. Brandt and Rubin, L.G., *Rev. Sci. Instrum.*, **53**(8), Aug. 1982.
5. Kramer, G.M. and Wallis, R.F., *Surf. Sci.* **113**, 148 (1982).
6. Hayden, K.J. and Butcher, P.N., *Philos. Mag.* **B38**, 603 (1979).

7. Al-Sadee, S.R., Butcher, P.N., and Hayden, K.J., *Philos. Mag.* **B43**, 173 (1981).

#### FIGURE CAPTIONS

Fig. 1

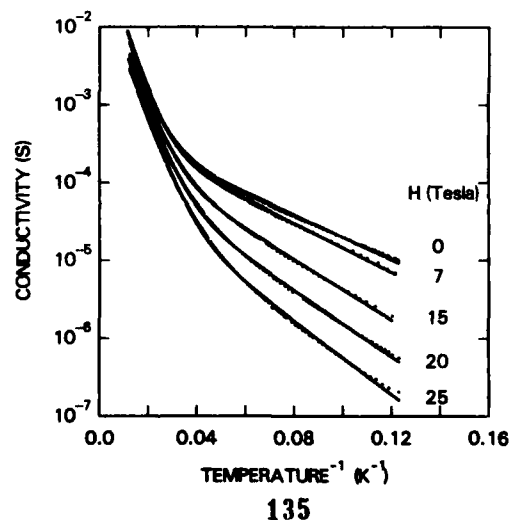
The log of the conductivity at an impurity band peak ( $N_{\text{os}} \approx 4 \times 10^{11} \text{ cm}^{-2}$ ,  $N_{\text{S}} \approx 2 \times 10^{11} \text{ cm}^{-2}$ ) as a function of reciprocal temperature. The data are shown as a function of magnetic field perpendicular to the surface. The lines are least-square fits to the data assuming two activated processes.

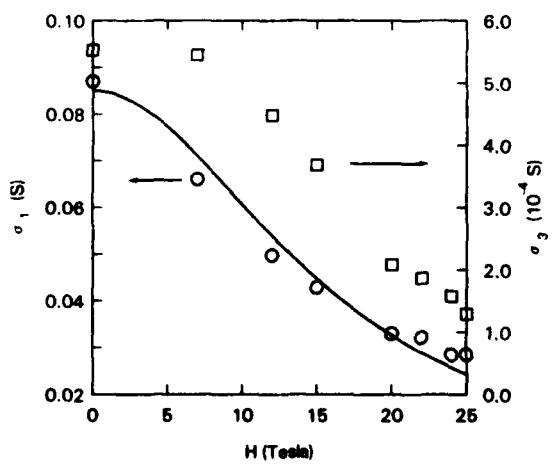
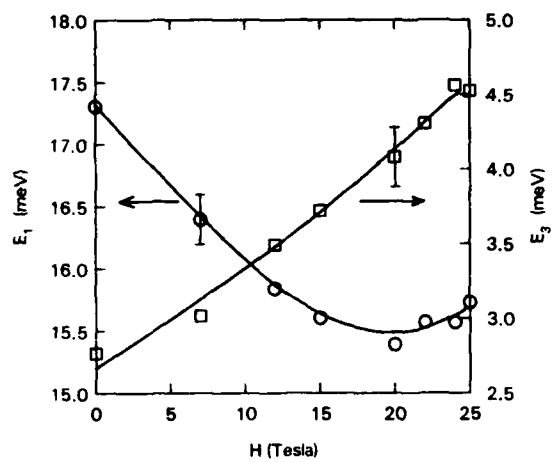
Fig. 2

The activation energies  $E_1$  and  $E_3$  taken from the least-square fits to the data in Fig. 1. The data for  $E_1$  are circles and the scale is the lefthand one. The error bars are the same for all data. The lines drawn through the data are only meant to guide the eye.

Fig. 3

The prefactors,  $\sigma_1$  and  $\sigma_3$ , from the least-square fit. The solid line is a fit to  $\sigma = \sigma_{\text{min}} (1 + \omega_c^2 \tau^2)^{-1}$ .





# BOUND ELECTRON STATES OF COULOMBIC IMPURITIES AND THEIR EFFECT ON MOBILITY IN INVERSION LAYERS

F. Green, D. Neilson\* and J. Szymanski†  
School of Physics, University of New South Wales,  
Kensington - Sydney, Australia 2033.

Bound state energies and wave functions have been calculated for a charged impurity in an inversion layer. We apply a Lippmann - Schwinger scattering approach which permits an unambiguous interpretation of the bound state properties. The effect neutralised impurity scattering has on electron mobilities is discussed.

## 1. INTRODUCTION

The present level of refinement of conductivity measurements in Si/SiO<sub>2</sub> inversion layers with ionized impurities introduced into the oxide (See [1,2]) requires precise theoretical information on impurity bound states and scattering rates. The theory must take into account the screening by free electrons, which is crucial in the experimental range at electron densities.

In previous calculations of bound states the screening has either been treated in a Thomas-Fermi-like fashion [3,4,5] or neglected entirely [6,7]. In an attempt to take into account the influence of the bound electron on screening Takada [8] added to the energy of the bound electron the electrostatic energy due to bound-screening electron interaction. The most consistent approach via the density functional formalism [9] still leaves the question of the bound state energy not clearly answered.

Our approach to the calculation of bound state energies and wave functions is based on multiple scattering theory using the Lippmann - Schwinger equation. In the case of an occupied bound state the screening electron wave function is also given by the Lippmann - Schwinger equation

with the potential including the electrostatic field of the bound electron. The calculation is carried out in a self-consistent manner.

## 2. THEORY

The hamiltonian for electrons in the Si(100)/SiO<sub>2</sub> inversion layer in the presence of a Coulombic impurity can be written as

$$H = H_0 + V_{ie} + V_{ee} \quad (1)$$

where  $H_0$  is the self-consistent hamiltonian for the inversion layer electrons in the absence of impurities,  $V_{ie}$  is the bare impurity - electron interaction and  $V_{ee}$  the bare electron - electron interaction.

In order to determine bound states of this hamiltonian some approximation must be introduced. The simplest is the linearised Random Phase Approximation (RPA) in which  $V_{ee}$  is omitted and the bare impurity-electron matrix element  $v_{ie}(q)$  is replaced by its linearly screened counterpart

$$\bar{v}_{ie}(q) = \frac{v_{ie}(q)}{1 - v_{ee}(q)\Pi_0(q)} \quad (2)$$

where  $\Pi_0(q)$  is the Lindhard function for two-dimensions [10] and  $v_{ee}(q)$  is the bare electron - electron matrix element.

A serious drawback of this simple scheme is the overestimation of screening. This is due to the neglect of correlations, particularly between the bound electron and the screening electron.

In our approach we add to the impurity - electron potential (2) a non-linear term which takes into account the non-linear screening effects due to a single electron. (This includes the electrostatic effects considered by Takada [8].) We use this effective potential to calculate the bound state energy and wave function, and the scattering rates off the neutralised impurity. Because the impurity is massive the non-linear term can be replaced by an equivalent two-body scattering term in the presence of an external potential, and this can be solved without approximation.

Our procedure gives the dominant non-linear corrections to the RPA for

this particular problem. It approximately takes into account the simultaneous non-linear interaction of the screening electron cloud with the impurity - bound electron system. It reproduces the known bound state properties as the electron concentration tends to zero. Further arguments about using only one screening electron to approximate non-linear effects may be found in ref. 11.

Accordingly, we replace (2) by the expression

$$v_{ie}(q) = \frac{v_{ie}(q)}{1 - \Pi_0(q)} + v_{ie}(q) \left[ \sum_{e'} A_{e'}(q) - \Pi_0(q) \right] v_{ee}(q), \quad (3)$$

where  $v_{e'e}(q)$  includes both nonlinear polarisability and electrostatic effects from the electron  $e'$  (fig. 1).

We follow a self-consistent iterative procedure [11]. On the first iteration  $t_{ie}$  and  $t_{ie}$ , in fig. 1 are the bare Coulomb interactions. The electron - electron interaction  $t_{e'e}$  is taken to be the solution of the Bethe - Goldstone equation for electron - electron scattering with a bare Coulomb interaction [11].  $t_{e'e}$  is not modified upon iteration. The Lippmann - Schwinger equation can now be solved with the interaction  $v_{ie}(q)$  from (3) for the conduction band electrons (S) in the presence of the screened impurity, and also for the bound electron (B). The solutions  $t_{is}$  and  $t_{ib}$  are then used as the appropriate  $t_{ie}$  and  $t_{ie}$ , amplitudes for the next iteration. The iterations continue until  $t_{is}$  and  $t_{ib}$  are consistent after successive iterations.

### 3. RESULTS

In this preliminary application of the theory we approximate  $A_{e'}(q)$  for scattering electrons (S) by a simple local construction using the correlated wave-function  $\psi_S$  from the previous iteration,

$$A_S(q) = \langle \psi_S^{-1} | \psi_S \rangle_{\text{local}} \Pi_0(q), \quad (4)$$

where  $\psi$  is the unperturbed electron wave-function, and  $\psi_S$  is given by

$$t_{is} \psi = \bar{v}_{is} \psi_S \quad (5)$$

For the bound electron (B) we approximate  $A_B(q)$  by its leading term, the electrostatic field of the bound electron.

Finally, we assume that electrons in the first subband are described by the variational wave function [3],

$$\psi_K(\vec{r}, z) = N e^{i\vec{k}\vec{r}} z e^{-bz/2} \quad (6)$$

Appropriate  $v_{ie}(q)$  and  $v_{ee}(q)$  can be found in [12].

In table 1 we present our results for the bound state energy and the mobility at various electron densities. Scattering rates used in the calculation are for a neutral centre. In all cases the density of the depletion layer is  $3.6 \times 10^{11} \text{ cm}^{-2}$  and the ions are located at the interface in the oxide. The experimental results for mobilities are taken from [1].

It should be noted that the bound state energy  $E_B$  exhibits a maximum around  $N_S = 4 \times 10^{12} \text{ cm}^{-2}$ , while the mobility flattens out at the same electron concentration. Both effects seem to be due to the interplay between the change of the screening and the change of layer thickness as functions of  $N_S$ .

These preliminary numerical estimates are somewhat crude, and we shall report elsewhere on a more complete calculation of  $A_{e'}(q)$ . The formalism is not restricted to the simple wave-functions (6), nor to the single subband approximation. Being a microscopic scattering theory, the approach provides scope for the unambiguous treatment of bound state properties.

### REFERENCES

- \* Formerly D.M. Lowy
- + Also at Department of Physics, University of Wollongong, Wollongong 2500.
- (1) A. Hartstein, A.B. Fowler, and M. Albert, Surf. Sci. 98 (1980) 181.
- (2) A.B. Fowler and A. Hartstein, Phil. Mag. 8 (1980) 949.
- (3) F. Stern and W.E. Howard, Phys. Rev. 163 (1967) 816.
- (4) F. Stern, Surf. Sci. 58 (1976) 162.

- (5) O. Hipólito and W.B. Campos, Phys. Rev. B 19 (1979) 3083.  
 (6) B.G. Martin and R.F. Wallis, Phys. Rev. B 18 (1978) 5644.  
 (7) N.O. Lipari, J. Vac. Sci. Technol. 15 (1978) 1412.  
 (8) Y. Takada, J. Phys. Soc. Japan 46 (1979) 114.  
 (9) B. Vinter, Solid State Comm. 28 (1978) 861.  
 (10) F. Stern, Phys. Rev. Lett. 18 (1967) 546.  
 (11) D.N. Lowy and A.D. Jackson, Phys. Rev. B12 (1975) 1689.  
 D.N. Lowy and G.E. Brown, Phys. Rev. (1975) 2138.  
 (12) T. Ando, A.B. Fowler and F. Stern, Rev. Mod. Phys. 54 (1982) 437.

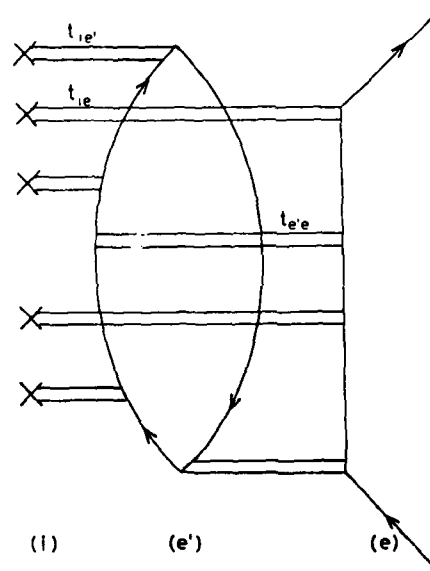


TABLE 1.

$N_S (10^{12} \text{ cm}^{-2})$	2	4	6	8	10
$\epsilon_B (P_{\gamma})$	-0.09	-0.02	-0.03	-0.09	-0.14
$\nu_{ox} N_{ox}$ ( $10^{15} \text{ V}^{-1} \text{ s}^{-1}$ )	theory 2.7	2.8	4.3	4.6	5.8
	experim 1.6	1.5	1.8	2.2	2.5

FIGURE 1.

A typical contribution to the term  $[v_{ie}(q) \sum_{e'} A_{e'}(q) v_{ee}(q)]$  appearing in (3). The corresponding exchange terms are also present. (i) is the charged impurity and (e) and (e') are interchangeable labels for the conduction band electrons or the bound electron. The scattering amplitudes  $t_{ie}$ ,  $t_{ie'}$  and  $t_{e'e}$  are discussed in the text.

# TWO-DIMENSIONAL ELECTRONS TRAPPED ON A HELIUM SURFACE

Marcos H. Degani and Oscar Hipólito  
Departamento de Física e Ciência dos Materiais  
Instituto de Física e Química de São Carlos, USP  
13560, São Carlos, SP, Brasil

*A simple unitary-transformation formalism is used in order to investigate the ground-state properties of an electron bounded on a liquid-helium surface and interacting with the surface modes of oscillation (ripples). A first-order phase-transition-like behavior from the quasifree to the self trapping electron state as the lamina external electric field exceeds a certain critical value is observed. The results are presented for both cases, electrons on films of helium adsorbed on solid neon and electrons at the interface of phase separated  $\text{He}^3\text{-He}^4$  mixtures.*

Recently Farias [1], Hipólito et al [2] and Jackson and Platzman [3] have worked out the path-integral formalism as introduced by Feynman for the polaron problem to compute the ground-state energy and effective mass of a two-dimensional electron on the surface of films of liquid helium. In references [1] and [2] the problem was treated strictly in the range of large pressing field corresponding to a strong-coupling limit. In ref. [3] on the other hand, the calculation was performed for all values of the coupling constant but only for one particular thickness of the film. The purpose of this paper is twofold: (a) to show that all the results of [1-3] can be obtained within a canonical-transformation method, in a much simpler manner, and

(b) to apply the formalism for electrons on films of helium adsorbed on solid neon and electrons at the interface of phase-separated  $\text{He}^3\text{-He}^4$  mixtures.

The electron motion parallel to the interface and interacting with ripples of frequency  $\omega_k$  is

$$H = \frac{p^2}{2m} + \sum_k \hbar \omega_k a_k^\dagger a_k + A^{-1/2} \sum_k V_k \exp(i\mathbf{k} \cdot \mathbf{r}) (a_k^\dagger - a_k), \quad (1)$$

where  $\mathbf{p}$ ,  $\mathbf{r}$  are the 2D momentum and coordinate of the electron,  $m$  is the free mass,  $a_k^\dagger (a_k)$  is the creation (annihilation) operator of a ripplon with wave number  $\mathbf{k}$ ,  $A$  is the surface area and  $V_k$  is the Fourier coefficient of the interaction potential.

For the electron-ripplon ground-state, the variational wave function  $|\psi\rangle$  will be postulated to be a product of an electron wave function and a coherent ripplon state. Then, this surface state is not an eigenstate of the total parallel momentum operator  $\mathbf{p}_t$ ,

$$\mathbf{p}_t = \mathbf{p} + \sum_k \hbar \mathbf{k} a_k^\dagger a_k \quad (2)$$

and the minimization of the energy should be performed by constraining the operator  $\mathbf{p}_t$  as

$$\delta \langle \psi | (H - \mathbf{p}_t \cdot \mathbf{p}_0) | \psi \rangle = 0, \quad (3)$$

where  $\mathbf{p}_0$  is the Lagrange multiplier, introduced to keep the expected value of the total momentum a constant.

The canonical-transformation technique [4,5] consists first in subjecting the Hamiltonian  $\mathcal{H} = H - \mathbf{p}_0 \cdot \mathbf{p}_t$  to a unitary transformation  $S = \exp(-i\eta \sum_k \mathbf{k} \cdot \mathbf{r} a_k^\dagger a_k)$ , where  $\eta$  is a variational parameter, recovering the weak-coupling approximation in the case  $\eta = 1$  and the strong-coupling theory in the limit  $\eta \rightarrow 0$ .

Next the expectation value of the resulting Hamiltonian



is evaluated for a trial wave function given by

$$|\Psi\rangle = \left(\frac{m\lambda}{\pi\hbar}\right)^{1/2} \exp(-m\lambda r^2/2\hbar) \exp(-i\vec{p}_0 \cdot \vec{r}) S_2 |0\rangle, \quad (4)$$

where  $|0\rangle$  is the ripplon ground state wave function, obtained from  $a_k |0\rangle = 0$  and  $\langle 0|0\rangle = 1$ .  $\lambda$  and  $\vec{p}_0$  are variational parameters and  $S_2$  is the second Lee-Low-Pines canonical transformation,  $S_2 = \exp\left[\sum_k \left(\frac{1}{\hbar} a_k^\dagger - \frac{1}{\hbar} a_k\right) \epsilon_k\right]$  with the function  $\epsilon_k$  to be determined variationally. Minimization of the energy with respect to those variational parameters, and up to second order in the velocity  $\vec{u}$ , we obtain for the ground-state energy and effective mass the following expressions

$$E_0 = \frac{\hbar\lambda}{2} - \sum_k \frac{|V_k|^2 \exp(-(1-\eta)^2 \hbar k^2/2m\lambda)}{\hbar\omega_k + \eta^2 \hbar^2 k^2/2m} \quad (5)$$

$$m^* = m + \hbar^2 \sum_k \frac{k^2 |V_k|^2 \exp(-(1-\eta)^2 \hbar k^2/2m\lambda)}{(\hbar\omega_k + \eta^2 \hbar^2 k^2/2m)^3} \quad (6)$$

We shall now apply this formalism for electrons on films of helium adsorbed on solid neon and electrons at the interface  $\text{He}^3\text{-He}^4$  mixtures.

#### 1. Electrons on films of helium

The electron-ripplon interaction potential, in this case, is given by [6-8]

$$V_k = (\hbar k \tanh kd/2\rho\omega_k)^{1/2} (eE + \Lambda/d^2) \quad (7)$$

The ripplon eigenfrequency  $\omega_k$  is well described by

$$\omega_k^2 = (g'k + (\sigma/\rho)k^3) \tanh kd, \quad (8)$$

where  $\rho$ ,  $\sigma$ ,  $g'$  and  $d$  are the density, surface tension, Van der

Waals acceleration and thickness of the liquid helium layer.  $e$  is the clamping external electric field and  $\Lambda$  is related to  $\epsilon_1$ ,  $\epsilon_2$  and  $\epsilon_3$  the dielectric constants of the vapor, liquid and substrate respectively, as  $\Lambda = e^2 \epsilon_2 (\epsilon_1 - \epsilon_2) / (\epsilon_1 + \epsilon_2)^2 (\epsilon_2 + \epsilon_3)$ .

We have carried out the numerical minimization of the ground-state energy eq.(5), with respect to the parameters  $\lambda$  and  $\eta$ . Hence, with the best-fit values of these parameters we have finally obtained the energy and effective mass. In figs.(1) and (2) the results are plotted against the external electric field for various values of the helium layer thickness, in the case where the substrate is solid neon ( $\epsilon_3 = 1.24$  and  $k_c = 1.45 \cdot 10^9/d^2$ ). As we can see from fig.(1), the energy has two distinct branches. The first branch corresponds to the weak-coupling regime and the second one corresponds to the strong-coupling limit. At the crossing point of the two branches there is a discontinuous change in the slope of the energy characterizing a first order phase-transition behavior in which the polaron state transforms from a nearly-free to a localized state type. The extremely rapid variation at the critical electric field  $E_c$  is most clear seen in fig.(2) which shows the effective mass changing by several orders of magnitude of the free electron mass. The transition referred here as localization is not to be taken so literally but in the same spirit of Toyozawa's work [9], i.e., in terms of the magnitude and rapidity of the change of the effective mass of this system.

We finally note that for very thin helium films, the contribution to the substrate becomes important and totally dominates the external electric field.

## 2. Electrons at the interface of $\text{He}^3$ - $\text{He}^4$

The Fourier coefficient of the electron-ripplon interaction potential  $V_k$  is given by [8]

$$V_k = \left( \hbar k / 2 (\rho_4 + \rho_3) \omega_k \right)^{1/2} e E \quad (9)$$

with  $\omega_k$  described by

$$(\rho_4 + \rho_3) \omega_k^2 = (\rho_4 - \rho_3) g k + \sigma' k^3, \quad (10)$$

where  $\rho_4$  and  $\rho_3$  are the densities of  $\text{He}^4$  and  $\text{He}^3$ ,  $g$  the acceleration of gravity and  $\sigma'$  the interfacial tension. The results we have obtained are plotted in figs. (2-4) as function of the external electric field. The present results are in perfect agreement with those earlier obtained in the high electric field limit by Farias [1] and Hipólito et al. [2] who used Feynman's path integral method for the polaron problem.

By comparing these results with those of the previous section we can note that the electron localization at the surface of very thin films of helium, then forming a two-dimensional Coulomb system, is easier to be observable than the similar system on the interface of phase separated  $\text{He}^3$ - $\text{He}^4$  mixtures.

We can also observe that the value of the critical external electric field  $E_c = 0.65$  v/cm, where the transition occurs is in a region physically unaccessible (with an extremely small binding energy  $E_0 \approx 10^{-10}$  meV).

### REFERENCES

1. G.A. Farias, PhD Thesis, USP, São Carlos, Brasil (1980) (unpublished)
2. C. Hipólito, G.A. Farias and N. Studart, *Surface Sci.* 113 (1982) 394
3. S.A. Jackson and P.M. Platzman, *Phys. Rev. B* 24 (1981) 499
4. W.J. Huybrechts, *J. Phys. C: Solid State Phys.* 9 (1976) L 211; *J. Phys. C: Solid State Phys.* 10 (1977) 3761
5. E.L. Bodas and C. Hipólito, *Phys. Rev. B* 27 (1983) 1110
6. V.B. Shikin and Yu.P. Monarkha, *Soviet Phys. - JETP* 38 (1974) 373

7. Yu. P. Monarkha, *Soviet J. Low Temp. Phys.* 1 (1975) 258
8. V.B. Shikin and Yu.P. Monarkha, *Soviet J. Low Temp. Phys.* 1 (1975) 459
9. V. Toyozawa, *Prog. Theor. Phys.* 26, (1961) 29

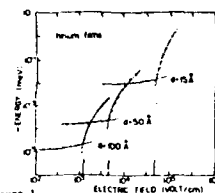


Figure 1  
Ground-state energy as function of the clamping external field for three values of the film thickness. Points are numerical results. The lines are only guides to the eye.

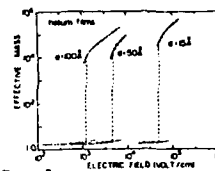


Figure 2  
Effective mass in units of the free electron mass as function of the external electric field for three values of the film thickness. Points are numerical results and the lines are only guides to the eye.

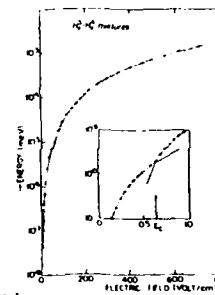


Figure 3  
Ground-state energy as function of the external electric field. Points are the numerical results and lines are only guides to the eye.

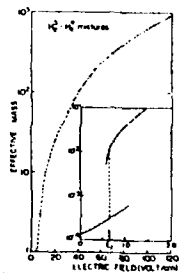


Figure 4  
Effective mass in units of the atomic helium mass against the external electric field. Points are numerical results and lines are only guides to the eye.

# STRONGLY-COUPLED RIPPLONIC POLARONS IN HIGH MAGNETIC FIELDS

Motohiko SAITOH

I.C.M., Cavendish Laboratory, Madingley Rd., Cambridge CB4 0HE, U.K.\*

The quasi-two dimensional system of electrons on a thin liquid He film, which are strongly coupled to the gravity-capillary waves (ripplonic polarons), is investigated theoretically when a high magnetic field is applied perpendicularly to the surface. The free energy and the absorption line-shape of the cyclotron resonance are calculated with the use of the path-integral method. The expression for the cyclotron mass has the same form as the one for the weak coupling case, and is always smaller than the electron vacuum mass. The line-width is of activation type with the activation energy proportional to the coupling constant, and is very narrow. The pre-factor of the line-width is dependent both on the coupling constant and the magnetic field, and is different from that of the inverse dc collision time.

## 1. Introduction

The system of electrons on the bulk liquid helium is now well-established as one of the most ideal physical realizations of quasi-two-dimensional systems. For details readers are referred to the review articles which appeared in the series of the proceedings of this conference [1]. Recently considerable attention has been focused on the system of electrons on the thin film (typically the thickness of 100 Å) of liquid helium which is substrated on dielectric materials such as solid neon [2,3]. In particular the possibility is pointed out [4,5] of having ripplonic polarons strongly coupled to the surface roughness created by the thermal fluctuations of the gravity-capillary waves of the thin film, their quantized versions being called ripples. The ground-state energy of ripplonic polarons, the free energy, the effective mass and the dc mobility have been studied theoretically [4,6-10].

The purpose of this report, as a series with [10,11], is to investigate such a strongly-coupled system in a high magnetic field. The free energy, the mass-shift and the line-width of the cyclotron resonance will be computed with the use of the path-integral method which was developed by the author [12-14]. Section 2 presents the solutions to the

coupled equations which are set up by the variational principle to the free energy and the expression of the free energy is obtained. Section 3 deals with the calculation of the cyclotron mass and the line-width.

## 2. The solution to the coupled equations and the free energy

The coupling function  $\int_q$  between electrons on a thin liquid He film and ripples is described by [10]

$$\int_q^2 / \hbar \Omega_q = 2\pi\alpha / (q^2 + k_c^2) S, \quad (2.1)$$

where  $\Omega_q$  is the ripplon angular frequency with the two-dimensional wave vector  $q$ ,  $\alpha$  the coupling constant,  $k_c^{-1}$  the capillary length and  $S$  the area of the system. The coupling constant  $\alpha$  is related to the appropriate holding field  $F_z$  normal to the surface through

$$\alpha = (eF_z)^2 / 4\pi\sigma, \quad (2.2)$$

where  $\sigma$  is the surface tension of liquid He. The ripplon angular frequency  $\Omega_q$  is given by

$$\Omega_q = sq(1 + q^2/k_c^2)^{1/2}, \quad (2.3)$$

where  $s$  is the sound velocity equal to the geometric mean of the effective gravitational acceleration  $g'$  and the film thickness  $d$ . In our path-integral formalism [12-14] physical quantities such as the free energy and the conductivity are expressed in terms of the variational functions. These variational functions are determined by the coupled integral equations which are set up by the minimization principle to the free energy. The coupled equations which we have to solve are exactly the same as the set of equations (2.11), (2.12) and (2.13) of reference [10], except that (2.12) is replaced by

$$\Lambda(\tau) = \frac{4}{\beta} \sum_{\nu \neq 0} \frac{g_\nu}{1 + \hbar^2 \omega_c^2 \nu^2 g_\nu^2} (1 - \cos \nu \tau), \quad (2.4)$$

because of the presence of the magnetic field, where  $\nu = 2\pi n/\beta$  with  $n$  being an integer and  $\beta$  the inverse temperature and  $\omega_c$  is the bare cyclotron frequency. The technique of solving the coupled equations is exactly the same as before [10] and similar to the spirit of the adiabatic approximation. We list here only the result

$$u_L = (\nu^2 + u^2) / \nu^2 (\nu^2 + v^2), \quad (2.5)$$

where

$$v^2 = \alpha (\sqrt{H^2 \omega_c^2 + \alpha^2} + \alpha) / 2, \quad (2.6)$$

$$u^2 = m^2 (\sqrt{H^2 \omega_c^2 + \alpha^2} + \alpha), \quad (2.7)$$

and  $m$  is the electron vacuum mass. With this solution we have

$$\Lambda(\tau) = \frac{1}{\sqrt{H^2 \omega_c^2 + \alpha^2} + \alpha} \left[ \coth \frac{\delta \beta}{2} - \frac{\cosh(\delta(\tau - \beta/2))}{\sinh(\delta \beta/2)} \right] + \coth \frac{\delta \beta}{2} - \frac{\cosh(\delta(\tau - \beta/2))}{\sinh(\delta \beta/2)} + \frac{2m^2}{\alpha} \left[ 1 - \frac{\tau}{\beta} \right], \quad (2.8)$$

where

$$\delta = \sqrt{H^2 \omega_c^2 + \alpha^2} + \alpha + H \omega_c / 2, \quad (2.9)$$

$$\delta = \sqrt{H^2 \omega_c^2 + \alpha^2} + \alpha - H \omega_c / 2. \quad (2.10)$$

The solutions above are valid under the conditions

$$H \omega_c \gg \alpha \gg 1/\beta, \quad 2m^2 H \omega_c \beta, \quad (2m^2 H \omega_c)^{1/2} \text{ and } H^2 \omega_c^2 / 2m \approx E_c. \quad (2.11)$$

The physical interpretation of (2.8) is that the internal excited state with energy  $\alpha$  of a ripplonic polaron at zero magnetic field is split into two branches with energies  $\delta'$  and  $\delta$ , with the  $\delta'$ -branch being of the character of the first Landau level, and that the center of gravity of the cyclotron orbit drifts freely with the effective mass  $\alpha/2m^2$ .

The free energy can be calculated from the formula [12]

$$F = -\frac{1}{\beta} \sum_{\nu > 0} \ln \frac{\nu^2 (\nu^2 + H^2 \omega_c^2) u_\nu^2}{1 + H^2 \omega_c^2 \nu^2 u_\nu^2} - \frac{2}{\beta} \sum_{\nu > 0} \frac{1 - \nu^2 u_\nu}{1 + H^2 \omega_c^2 \nu^2 u_\nu^2} - \frac{1}{2} \sum_q \Gamma_q^2 \int_0^\beta d\tau \frac{\cosh(H \Omega_q (\tau - \beta/2))}{\sinh(H \Omega_q \beta/2)} e^{-H^2 q^2 \Lambda(\tau)/2m}. \quad (2.12)$$

Note that the free energies of free Landau electrons and free ripples are not included in the above expression. The final result is obtained by approximating  $\Lambda$  in the last integral by a constant

$$\Lambda_0 = 2/(\sqrt{H^2 \omega_c^2 + \alpha^2} + \alpha) \text{ yielding}$$

$$F = -(\alpha/2) \ln[(\sqrt{H^2 \omega_c^2 + \alpha^2} + \alpha)/2e^{1/2} E_c] + (\sqrt{H^2 \omega_c^2 + \alpha^2} - H \omega_c)/2, \quad (2.13)$$

where  $\delta' = 0.5772...$  is the Euler constant. The dominant first term comes from the last term of (2.12). Note that when  $\omega_c = 0$ , we recover exactly the same result as the zero-field free energy which was obtained before [10]. This result is, therefore, the natural extension to the case of finite magnetic fields. The factor in the logarithm indicates that the electron wavefunction in the adiabatic approximation has the Gaussian form with the decay length  $[H^2/2m(\sqrt{H^2 \omega_c^2 + \alpha^2} + \alpha)]^{1/2}$ .

### 3. The cyclotron mass and the line-width of the absorption line-shape

The mass-shift and the line-width of the absorption line-shape of the cyclotron resonance are related to the following memory function [13,14]

$$M(\omega) = \frac{21}{\omega} \sum_q \frac{q^2}{2m \sinh(H \Omega_q \beta/2)} \times \left[ \int_0^{\beta \hbar} d\tau (\cosh H \omega \tau - 1) \cosh(H \Omega_q (\tau - \beta/2)) e^{-H^2 q^2 \Lambda(\tau)/2m} - 1 \sinh(H \omega \beta/2) \int_0^\infty dt e^{-i H \omega t} \cos(H \Omega_q t) e^{-H^2 q^2 \Lambda(1t + \beta/2)/2m} \right]. \quad (3.1)$$

The resonance point of the cyclotron resonance is determined from

$$\omega - (\omega_c + \text{Im } M(\omega)) = 0. \quad (3.2)$$

For the calculation of  $\text{Im } M(\omega)$ , it is safe to treat  $\Lambda$  as constant  $\Lambda_0$ . After some algebra we have

$$\text{Im } M(\omega) = -\alpha(\sqrt{\hbar^2 \omega_c^2 + \alpha^2} + \alpha) / 2\hbar^2 \omega. \quad (3.3)$$

Putting this back into (3.2), we obtain  $\omega = \gamma/\hbar$  as expected, and therefore we reach the expression for the cyclotron mass  $m_c$ :

$$m_c = \hbar \omega_c / \gamma \approx (1 + \alpha/2\hbar \omega_c)^{-1}. \quad (3.4)$$

Since the separation of the first Landau level is widened because of the electron-ripplon coupling, the cyclotron mass is smaller than the electron mass. This mass formula in the strong coupling case persists also in the weak coupling case [11]. In both cases the ripplon frequency is very small compared with the cyclotron frequency, and the polarization field caused by ripples is almost static, and so the adiabatic approximation employed here is accurate [15]. The widening of the Landau level separation or the reduction of the cyclotron mass occurs as long as  $\omega_c \gg \Omega_q \sim \omega/\hbar$ .

For the evaluation of the line-width  $\Gamma$  we only need to evaluate  $\text{Re } M$  at  $\omega = \gamma/\hbar$ . In this case the full  $t$ -dependence of  $\Lambda$  should be retained, otherwise no line-width is obtainable since the magnetic field quantizes all the electronic levels into discrete Landau states. The last term of (2.8) represents the free drift motion of the cyclotron orbit center and is the main source of blurring of the Landau levels. This motion is so slow because of the large effective mass  $\alpha/2\hbar^2$  that the inelasticity due to ripples (the  $\cos \hbar \Omega_q t$ -term in the second integrand of (3.1)) must also be taken into account. The second oscillatory factor in  $\Lambda$  which is due to the internal excited state with energy  $\delta$  is much slower than the first term and so we can safely neglect it. If we perform the  $t$ -integration, the first oscillating factor introduces another reduction factor  $\alpha \hbar^2 q^2 / 8m v^2$  to the current vertex, and we finally obtain

$$\Gamma = \hbar \text{Re } M(\gamma/\hbar) = (8\pi E_c / \hbar^3 \omega_c^2 \alpha \beta^2) (2E_c / \hbar v^2)^{1/2} e^{-\alpha \beta / 4}. \quad (3.5)$$

The dominant contribution comes from the intra-Landau state scattering. It is seen that the line-width is of activation type with the activation energy equal to a quarter of the coupling energy  $\alpha$ . This is common in the

dc collision time [10]. However the pre-factor of  $\Gamma$  is dependent on the coupling constant, the magnetic field and temperature and appreciably different from the inverse dc collision time.

The conditions of the feasibility of the strong coupling system were discussed fully in [10], and need not be repeated here. It is only emphasized that the present system of electrons on a thin film of liquid He holds a unique status since the strong coupling conditions will be achieved by a careful arrangement of the experimental conditions, while no other systems have fulfilled the strong coupling conditions so far.

#### Acknowledgements

The author would be grateful to Professor S.F. Edwards for providing him the opportunity to stay at the Cavendish Laboratory and for the hospitality extended to him. He is much obliged to Dr. R. Joynt for the critical reading of the manuscript. This work is performed with the partial financial support from the Science and Engineering Research Council.

#### References

- \* Permanent address: the Institute of Physics, College of General Education, University of Tokyo, Komaba, Meguroku, Tokyo 153, Japan.
- [1] Surface Sci. 58(1976); 73(1978); 98(1980); 113(1982).
- [2] K. Kajita and W. Saaki, Surface Sci. 113(1982)419.
- [3] K. Kajita, to be published.
- [4] L.M. Sander, Phys. Rev. B11(1975)4350.
- [5] H. Ikezi and P.M. Platzman, Phys. Rev. B23(1981)1145.
- [6] S.A. Jackson and P.M. Platzman, Phys. Rev. B24(1981)499.
- [7] S.A. Jackson and P.M. Platzman, Phys. Rev. B25(1982)4886.
- [8] O. Hipulito, C.A. Ferias and N. Studart, Surface Sci. 113(1982)394.
- [9] N. Tokuda and H. Kato, J. Phys. C(1983) in press.
- [10] M. Saitoh, J. Phys. C submitted.
- [11] M. Saitoh, J. Phys. C submitted.
- [12] M. Saitoh, J. Phys. Soc. Japan 50(1981)2295.
- [13] M. Saitoh, J. Phys. C15(1982)6981.
- [14] M. Saitoh, J. Phys. A16(1983) in press.
- [15] A. Cheng and P.M. Platzman, Solid State Comm. 25(1978)813.

# TOPOLOGICAL DEFECTS AND MELTING OF WIGNER SOLID ON CORRUGATED SURFACES\*

P. Vashishta, R. K. Kalia

Materials Science and Technology Division  
Argonne National Laboratory, Argonne, Illinois 60439, U.S.A.

and

J. J. Quinn

Department of Physics  
Brown University, Providence, Rhode Island 02912, U.S.A.

## Abstract

Melting of electrons on sinusoidally corrugated surfaces  $S_2$  and  $S_4$  (of wave lengths  $\lambda = \sqrt{3}a$  and  $\sqrt{3}a$ ,  $a$  = lattice spacing), is investigated using the method of molecular dynamics. Both continuous and discontinuous melting transitions are observed: Melting on  $S_2$  is found to be discontinuous if  $U_0$  is less than the critical value  $U_c$  whereas for  $U_0 > U_c$  the transition is continuous. On  $S_4$  the transition is always discontinuous. Upon melting, grain-boundary loops are observed in systems which undergo discontinuous melting transitions whereas continuous melting transitions are accompanied by a small density of defects.

\*Work supported by the U.S. Department of Energy.

Electrons on the surface of liquid helium form a classical two-dimensional system whose properties are completely determined by the dimensionless variable,  $r = e^2(\pi \rho_s)^{1/2}/k_B T$ , where  $\rho_s$  is the surface electron density. Experimental (1) and computer simulation (2) studies reveal that the electrons form a triangular Wigner solid at large values of  $r$  and that the solid melts around  $r \sim 130$ . However, many of the experimental 2D systems, e.g., rare gases adsorbed on substrates, are different in that they are formed on periodic substrates. These systems exhibit a rich variety of commensurate and incommensurate phases and melting from these solids have been the focus of several recent investigations (3-5).

In this paper, it is shown that the underlying substrate can alter the nature of the melting transition. A system of electrons on periodic corrugations  $S_2$  and  $S_4$  (see Fig. 1) is investigated as a function of height of the corrugation  $U_0$ , using the molecular dynamics (MD) method. The MD calculations are performed for a system of  $N = 256$  electrons with a neutralizing, uniform, positive background. The density of electrons is kept fixed at  $\rho_s = 1.477 \times 10^8 \text{ cm}^{-2}$  and periodic boundary conditions are used. The long range nature of the electron-electron interaction is properly taken into account by the Ewald summation.

For  $U_0 = 0$ , it was previously found that the melting transition is first order (2). The temperature variations of the internal energy and the constant of self-diffusion showed hysteresis, supercooling, and release of latent heat on melting. The entropy change on melting was found to be  $0.3 k_B$  and the melting transition was observed between  $r = 118-132$ , in excellent agreement with experiments (1).

On  $S_2$ , the effect of  $U_0$  on the melting transition is shown in Fig. 2. For  $U_0 = 0.125, 0.25$  and  $1.0$  K, there is no evidence of hysteresis or release of latent heat on melting and so the melting transition is continuous for  $U_0 > 0.125$  K, whereas for smaller  $U_0$  the transition is first order. This conclusion is also supported by the MD results on crystallization. A liquid slightly above the melting temperature is cooled suddenly and then the system is allowed to run uninterruptedly for several thousand time steps. The time development of the instantaneous temperature  $T(t) \propto \frac{1}{2} \overline{mv_i^2(t)}$  is shown in Fig. 3. The values of  $T(t)$  rise sharply in the first 200 molecular dynamics time steps and then the temperatures oscillate around the mean values; the systems lack diffusivity and are in the ordered state. This behavior is very different from what is observed for  $U_0 = 0$  where the transition is first order (2): At  $U_0 = 0$ , the system first goes into a metastable phase and remains there for several thousand time steps after which  $T(t)$  changes abruptly and the system goes into an ordered state. Thus, the MD results show that the nature of the melting transition changes from discontinuous to continuous around  $U_0 \sim 0.06$  K. In other words, there is a tricritical melting point on  $S_2$ .

On  $S_4$ , the melting transition is investigated at  $U_0 = 1$  K. The internal energy and the constants of self-diffusion show discontinuous jumps around the melting temperature and the transition is accompanied by an abrupt change in entropy which suggests that the melting transition is first order.

Study of defects upon melting reveals grain-boundary loops on  $S_4$  and also on  $S_2$  if  $U_0 < U_c$ . However, for  $U_0 > U_c$  the density of defects on  $S_2$  is much smaller. Thus, the corrugation height appears to enhance the dislocation core energy, thereby reducing the density of defects and changing discontinuous melting into continuous melting.

#### References

- (1) C. C. Grimes and G. Adams, Phys. Rev. Lett. 42 (1979)795; R. Mehrotra, B. M. Guenin and A. J. Dahm, 48 (1982)641.
- (2) P. Vashishta and R. K. Kalia in: Melting, Localization and Chaos, Eds. R. K. Kalia and P. Vashishta (North-Holland, New York, 1982)p. 43; see references therein.
- (3) J. M. Kosterlitz and D. J. Thouless, J. Phys. C 5 (1973)L124; D. R. Nelson and B. I. Halperin, Phys. Rev. B 19 (1979)2457; A. P. Young, Phys. Rev. B 19 (1979)1855; S.-T. Chui, in: Melting, Localization and Chaos, Eds. R. K. Kalia and P. Vashishta (North-Holland, New York, 1982)p. 29; T.V. Ramakrishnan, Phys. Rev. Lett. 48 (1982)541.
- (4) P. A. Heiney, R. J. Birgeneau, G. S. Brown, P. H. Horn, D. E. Moncton and P. W. Stephens, Phys. Rev. Lett. 48 (1982)104.
- (5) F. F. Abraham, Phys. Rev. Lett. 50 (1983)978.

# Figure Captions

Figure 1: Triangular electron solid of spacing  $a$  in the presence of corrugations  $S_1$ ,  $S_2$ ,  $S_3$  and  $S_4$  with wave vectors  $K = 1, 2, 3$ , and  $4$ , respectively. Here  $K$  is measured in units of  $G_x (= \pi(2\rho_s/\sqrt{3})^{1/2})$ , i.e., the x-component of the smallest reciprocal lattice vector of the triangular lattice.

Figure 2: Total internal energy per particle,  $E$ , as a function of temperature for three values of the corrugation height  $U_0$ .  $S$  and  $L$  denote the solid and liquid phases. The melting temperature changes from 0.3 K to 0.6 K as  $U_0$  is increased from 0 to 1 K.

Figure 3: Time dependence of instantaneous temperatures,  $T(t) \propto \sum_i m_i v_i^2(t)/2$ , for three values of  $U_0$  after the systems have been cooled from the liquid phase. First  $T(t)$  rise sharply and then oscillate around the mean temperature corresponding to stable solid phases.

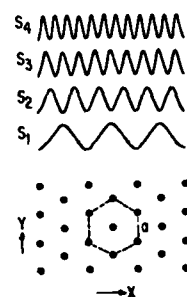


Figure 1



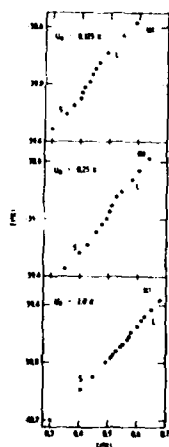


Figure 2

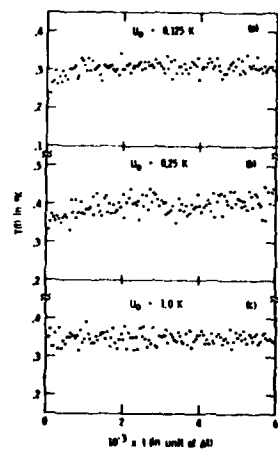


Figure 3

The Effect of Interactions on the Polaronic  
State of Two Dimensional Electrons on the  
Surface of Liquid Helium

S. A. Jackson  
Bell Laboratories, Murray Hill, NJ

ABSTRACT

In earlier work<sup>(1)</sup>, we predicted that two-dimensional electrons on the surface of a liquid helium thin film would form a polaronic state with a mass enhancement of at least five orders of magnitude. We have recently done a more general calculation of the threshold holding field where the polaronic state forms as a function of film thickness and areal density of electrons on the surface of the liquid helium, in particular, the contribution of interactions between electrons to the localization of a given electron and to its mass enhancement. We relate these results to recent measurements of E. Andrei<sup>(2)</sup> on the mass enhancement and mobility decrease of electrons on liquid helium films.

Refs:

- <sup>1</sup>S. A. Jackson and P. M. Platzman, Phys. Rev. B24, 499 (1981);  
Phys. Rev. B25, 4886 (1982); Surface Science 113, 401 (1982).  
<sup>2</sup>E. Andrei, to be published.

Magnetization, Specific Heat, Magneto-Thermal Effect and  
Thermoelectric Power of Two-dimensional Electron Gas in  
a Quantizing Magnetic Field

Wlodek Zawadzki

Institute of Physics, Polish Academy of Sciences  
00-688 Warsaw, Poland

Institute for Experimental Physics, University of Innsbruck  
Innsbruck, Austria

and

Rudolf Lassnig

Institute for Experimental Physics, University of Innsbruck  
Innsbruck, Austria

Abstract

Oscillatory magnetization, specific heat, magneto-thermal effect and thermoelectric power of the two-dimensional gas of noninteracting electrons in the presence of a quantizing magnetic field and a finite temperature are considered theoretically. The magnetization due to Landau quantisation oscillates around the zero value as a function of magnetic field and vanishes in the zero-field limit. The specific heat consists of an intralevel and an interlevel contributions, both strongly oscillating. Magneto-thermal oscillations of a thermally isolated superlattice are shown to be of the order of 1K at low temperatures, which is  $10^3$  times larger than in 3D semimetals. The thermoelectric power at high magnetic fields does not depend on electron scattering and it is directly proportional to the entropy. Its oscillations in a magnetic field as well as its dependence on the temperature and the level broadening are discussed.

Two-dimensional electron gas in the presence of a quantizing magnetic field is known to possess strongly variable properties depending on the relative position of the Fermi level with respect to the Landau levels. In the transport effects the subband edges are of crucial meaning, whereas in the equilibrium phenomena the extended and the localised states play comparable roles. The purpose of this paper is to consider equilibrium thermodynamics of the 2D electron gas in strong magnetic fields, when the electron scattering is of secondary importance, in order to provide an independent information on the density of states, a pinning of the Fermi energy and related problems.

1. Electron Density, Fermi Energy, Magnetization.

We consider thermodynamic properties of 2D gas of noninteracting electrons in a parabolic, spherical energy band at finite temperature  $T$  in the presence of a quantizing magnetic field  $H$ . We include the spin degeneracy but assume the spin-splitting factor  $g^* = 0$ . Inversion layers and superlattices based on GaAs satisfy quite well these assumptions, if the  $g^*$ -value enhancement is neglected. An incorporation of the spin splitting into the theory is straightforward. We assume further that only one electric subband is populated. The energetic density of states is taken in the form of a sum of Gaussian peaks

$$\rho(\epsilon) = \frac{2}{2\pi L^2} \sum_n \frac{1}{\Gamma} \exp -2\left(\frac{\epsilon - \lambda_n}{\Gamma}\right)^2 \quad (1)$$

where  $L = (\hbar c / eH)^{1/2}$ ;  $\lambda_n = \hbar \omega_c (n + \frac{1}{2})$  and  $\Gamma$  is the broadening parameter (the level width  $\Delta\epsilon = 2\Gamma$ ). A dependence of broadening on the magnetic field is neglected, cf. [1]. The electron density in  $1 \text{ cm}^2$  is

$$N = A \sum_n \frac{1}{\Gamma} \int_0^\infty \frac{1}{1 + e^{-z - \eta}} e^{-2y_n^2} dz \quad (2)$$

where  $A = (1/\pi)(eH/\hbar c)$ ,  $y_n = (z - \theta_n)/\gamma$  and  $z = \epsilon/kT$ ,  $\eta = \epsilon/kT$ ,  $\theta_n = \lambda_n/kT$ ,  $\gamma = \Gamma/kT$  are the reduced quantities. The filling factor of the system is defined as  $\nu = N/A$ , denoting the number of occupied Landau levels. The condition of a constant electron density in the sample leads to an integral equation for the Fermi energy  $\epsilon(H)$ . Fig. 1 shows this dependence calculated for  $m^* = 0.0665 m_0$ ,  $N_0 = 8 \times 10^{11} \text{ cm}^{-2}$ ,  $\Gamma = 0.5 \text{ meV}$  and  $T = 6 \text{ K}$ .

The free energy of the system is

$$F = N\epsilon - kT \int \rho(\epsilon) \ln [1 + \exp(\frac{\epsilon - \epsilon_F}{kT})] d\epsilon \quad (3)$$

It is convenient to write  $\rho(\epsilon)$  in the form

$$\rho(\epsilon, H) = a \cdot H \cdot R(\epsilon, H) \quad (4)$$

where  $a = (1/\pi)(e/\hbar c)$ . The magnetization of the system is  $M = -dF/dH$ . After some manipulation one obtains

$$M = kT a \sum_n \frac{1}{\Gamma} \int_0^\infty \ln(1 + e^{-z - \eta}) e^{-2y_n^2} (1 + \frac{\theta_n}{\gamma} y_n) dz \quad (5)$$

In order to calculate a contribution to magnetisation from one

completely filled Landau level one should put  $n \rightarrow \infty$  and the integration limits  $\pm \infty$ . The integral can then be calculated to give  $M_p = kT\alpha(n-2\theta_p)$ . Figure 2 shows the magnetization calculated according to Eq.(5) for the above  $m^*$ ,  $N_0$ ,  $\Gamma$  and  $T = 4.2K$ . It can be seen that the diamagnetism of the 2D electron gas oscillates symmetrically around the zero value, vanishing in the limit of  $H \rightarrow 0$ . This is in contrast to the 3D situation, where, apart from the deHaas - van Alphen oscillatory component, one has also a monotonic contribution to magnetization, which at low fields represents the Landau diamagnetism, cf. [2]. The inclusion of the spin splitting does not change the situation - it simply doubles the number of levels. Thus, we conclude that also the paramagnetism of the 2D electron gas vanishes in the low-field limit. As follows from Figs. 1 and 2 the magnetization oscillations follow quite closely those of the Fermi level. On the other hand the Shubnikov-deHaas oscillations of magnetoresistance have maxima when the Landau levels cross the Fermi energy. It follows then that there should be a phase shift between the magnetization and the magneto-resistance oscillations. In fact, this has been observed recently in the magnetization measurements on GaAs - GaAlAs superlattice [3].

The first theory of magnetization for the 2D electron gas has been carried out using the delta-like density of states, with the results quite similar to those presented in Fig.2. [2]. It is also of interest to note that in the first explanation of the dHvA effect in 3D metals Peierls used a two-dimensional model of a metal at  $T=0$ . Already this early consideration exhibited certain features presented above (cf. [4]).

#### 1. Specific Heat, Magneto-thermal Effect.

The specific heat is given in general as

$$C_V = \int_0^\infty \frac{d\epsilon}{dT} (\epsilon - \epsilon_0) \rho(\epsilon) d\epsilon \quad (6)$$

in which

$$\frac{d\epsilon}{dT} = - \frac{\partial \epsilon}{\partial T} \left( \frac{\epsilon - \epsilon_0}{T} + \frac{\partial \epsilon_0}{\partial T} \right) \quad (7)$$

The dependence  $\partial \epsilon / \partial T$  at a constant concentration is determined by differentiating Eq.(2) with respect to  $T$  and using Eq.(7). This leads to

$$\frac{\partial \epsilon}{\partial T} = - \frac{L_1}{T_0} \quad (8)$$

and

$$C_V = kA(L_2 - \frac{L_1^2}{T_0}) \quad (9)$$

where

$$L_1 = \sum_n \int_0^\infty \frac{1}{y} \int_0^\infty \frac{e^x}{(1+e^x)^2} x^r e^{-2y^2} dz \quad (10)$$

in which  $x = z - n$  and the other quantities are defined above. The Fermi energy is first calculated from the condition  $N = \text{const.}$  and then all the integrals computed as functions of the magnetic field for the corresponding  $\epsilon$  values. Fig. 3 shows the specific heat calculated for the above parameters at  $T=6K$ .

The specific heat of 2D electron gas is seen to consist of two contributions. At high magnetic fields, where  $\hbar\omega_c \gg kT$ , only the intralevel thermal excitations contribute to  $C_V$ . When the Fermi energy is between two Landau levels, the lower levels are completely filled, the upper ones completely empty, and  $C_V$  vanishes. At such a magnetic field the system can not absorb low energy excitations. At weaker magnetic fields the interlevel excitations begin to come into play if the temperature is not too low. They are of importance when the Fermi energy lies between two Landau levels. The interlevel contribution to  $C_V$  is seen in Fig. 3 in the form of sharp spikes since, as follows from Fig. 1, the Fermi energy "jumps" between two Landau levels within a narrow range of magnetic field strength. The rise of this contribution with decreasing magnetic field follows the general behavior of  $C_V$  for two-level systems [4]. Thus, Fig. 3 illustrates a continuous transition of the specific heat from the intralevel to the interlevel behavior, which is characterized, among other, by a change of phase of the magneto-oscillations.

At very high magnetic fields the Fermi energy is forced below the lowest Landau level and the electron statistics becomes non-degenerate. In this limit only the lowest level is occupied and the specific heat as well as the electron concentration can be calculated analytically, to give at a finite temperature

$$C_V = \frac{1}{4} \gamma^2 kN \quad (11)$$

It can be seen that the intralevel part of  $C_v$  depends crucially on the level broadening, going to zero at vanishing  $\Gamma$ .

Fig. 4 shows the peak value of  $C_v$  for the filling factor  $\nu=2.5$  ( $a^*H = 56$  kG) as a function of  $kT/\Gamma$ . Consider the regime  $\hbar\omega_c \gg kT$  and  $\hbar\omega_c \gg \Gamma$ , and the Fermi energy in the vicinity of the  $n$ -th Landau level. The completely filled levels contain  $A \cdot n$  electrons, which do not contribute to the specific heat. One can show both analytically and numerically that in this situation at a fixed magnetic field the contribution of the  $n$ -th level to  $C_v$  is determined only by  $kT/\Gamma$ . This means that the dependence shown in Fig. 4 is universal in the sense that it can be used for any given  $\Gamma$  in order to determine the behavior of  $C_v$  with temperature.

It is of interest to examine validity of the general formula for the specific heat of a strongly degenerate electron gas:  $C_v = (\pi^2/3) k^2 T_0(\zeta)$ . It can be easily seen that this formula does not account for the interlevel contribution to  $C_v$ , describing only the linear range of the intralevel part, as seen in Fig. 4. The above expression is usually derived using the Sommerfeld expansion of the statistical integrals with respect to the small parameter  $(kT/\zeta)^2$ , in which the Fermi energy  $\zeta$  is counted from the band edge [5]. In our case, however, the completely filled Landau levels below the Fermi energy are statistically inactive and within one partly occupied level the expansion parameter becomes  $(kT/\Gamma)^2$ . In good samples this parameter is small with respect to one only at very low temperatures (below 1K). Thus, for the 2D electron gas in a magnetic field the whole concept of strong degeneracy and the validity of corresponding approximations is limited to the very narrow range of lowest temperatures.

If the above effects are to be observable, the specific heat of the electron gas should be comparable to that of the lattice. A typical period of a superlattice is 200 Å. For this value we calculate, using the coefficient  $A$  in Eq. (2), the electronic specific heat  $C_v/k = 2.42 \times 10^{15} [\dots] (\text{cm}^{-3})$ , where the values in brackets are plotted in Figs 3 and 4. At low temperatures the specific heat of the lattice, due to three acoustic phonon branches, is  $C_v^1 = 234k(N_A/2)(T/\theta_D)^3$ , where  $N_A$  is the number of atoms and  $\theta_D$  is the Debye temperature [4]. The factor 1/2 accounts for two atoms per unit cell in GaAs-type materials. Taking for GaAs  $N_A = 2.21 \times 10^{22} \text{ cm}^{-3}$  and  $\theta_D = 426\text{K}$  we obtain  $C_v^1/k =$

$= 3.34 \times 10^{16} \text{ T}^3 (\text{cm}^{-3})$ , so that at  $T = 1\text{K}$  the electronic and the lattice specific heats are, in fact, well comparable.

Next we consider magnetothermal oscillations, which denote temperature variations of a thermally isolated system as a function of a magnetic field. This effect has been measured in three-dimensional semimetals [6], where the temperature changes are of the order of  $10^{-3}\text{K}$ . In a thermally isolated sample the processes occur adiabatically, i.e. the entropy must remain constant. Since the entropy is an oscillatory function of a magnetic field and an increasing function of temperature, the latter must oscillate in order to keep the entropy constant. The same principle is used in the magnetic cooling. The entropy is  $S_{e1} = -(\partial F/\partial T)_v$ , which becomes in the previous notation

$$S_{e1} = k \cdot A \sum_n \frac{1}{\sqrt{\pi}} \int_0^\infty \left[ \ln(1 + e^{-x}) + \frac{x}{1 + e^{-x}} \right] e^{-2y_n^2} dz \quad (12)$$

It can be easily seen from the above expression that the completely filled levels ( $x = z - n \ll 0$ ) give vanishing contribution to the entropy. Together with the condition of a constant electron concentration, cf. Eq. (2), we have two integral equations for two unknowns  $\zeta(H)$  and  $T(H)$ , the second being of experimental interest.

Fig. 5 shows the temperature of the two-dimensional electron gas as a function of magnetic field calculated for a GaAs sample, as characterized above. The constant value of entropy is chosen to be  $S_0 = 9.68 \times 10^{16} \text{ k}$  (corresponding to  $T = 1.25\text{K}$  at  $H = 100\text{kG}$ ). The very strong oscillations of temperature result from vanishing values of the intralevel specific heat at the minima (cf. Fig. 3). On the other hand, the phallic shapes of peaks and the strong damping at lower magnetic fields are due to the fact that, as the temperature rises, the interlevel contribution to  $C_v$  comes into play hampering further temperature increase.

The magnetothermal oscillations can be calculated for the realistic case, including the entropy of the lattice. In the low temperature region, where  $C_v^1 = A T^3$ , the entropy of the lattice is simply  $S_1 = C_v^1/3$ . This can be included in the constant-entropy condition:  $S_{e1} + S_1 = \text{const}$ .

The result is shown in Fig. 6, with  $S_{e1} + S_1 = 9.68 \times 10^{16} \text{ k}$ . Since the lattice prevents strong temperature rise, the interlevel

contribution to electronic specific heat is negligible and the magneto-thermal oscillations have spike-like behavior. This should allow one to use the effect as a spectroscopy tool in 2D systems. At low temperatures the amplitude of oscillations is of the order of 1K, which is  $10^3$  times larger than in the three-dimensional case. The effect is so large that it can be used for magnetic cooling.

### 3. Thermoelectric Power

A quantum theory of thermo-magnetic transport phenomena offers some serious difficulties, since in the presence of a temperature gradient the system is not homogeneous. As a consequence, the automatic application of the Kubo method led in the past to results, which did not satisfy the Onsager symmetry relations, violated the third law of thermodynamics, etc. [7,8,9]. These paradoxes and puzzles were resolved by Obratsov [10,11], who showed that, in order to obtain a correct description of the off-diagonal components of thermo-magnetic tensors, one should explicitly include in the theory a contribution of the magnetization. This is related to the fact that the microscopic surface currents, which determine the Landau magnetization of conduction electrons, make a significant contribution to the macroscopic current density when a temperature gradient is present. At high magnetic fields, i.e. for  $\omega_c \tau \gg 1$ , the diagonal components of the transport tensor may be neglected with respect to the off-diagonal ones. The latter do not depend on electron scattering in the high-field limit. Taking into account the contribution of magnetization  $M$  one obtains for the off-diagonal component of the macroscopic thermoelectric tensor

$$\beta_{xy} = \beta_{xy}^0 + c \frac{dM}{dT} = \frac{c}{N} S \quad (13)$$

where  $\beta_{xy}^0$  determines the microscopic current density. When  $\beta_{xy}^0$  is calculated using the standard methods of the density matrix, the equality (13) is obtained, in which  $S$  is the entropy of the electron gas. The thermoelectric power becomes

$$\alpha(H) = \frac{\beta_{xy}}{\beta_{xx}} = - \frac{S}{cN} \quad (14)$$

$N$  is given in Eq. (2) and  $S$  in Eq. (12), so that  $\alpha(H)$  can be readily calculated in the no-scattering limit. By measuring  $\alpha$

at a constant electron concentration one determines directly the entropy of the electron gas.

Fig. 7 shows the thermo-power of the 2D gas in a strong transverse magnetic field calculated for the above parameters and  $T = 6K$ . At high fields, as long as the interlevel contribution to  $C_v$  is negligible (cf. Fig. 3), the entropy (and consequently  $\alpha$ ) vanishes when the Fermi energy is between two Landau levels. At lower fields the interlevel contribution to  $C_v$  becomes of importance and the entropy, as well as  $\alpha$ , does not reach the zero values. These general predictions agree quite well with the first experimental observations of the thermo-power oscillations in GaAs-GaAlAs heterostructures [12]. In Fig. 8 we show the maximal values of  $\alpha(H)$  calculated from Eqs (2) and (12) as functions of  $kT/\Gamma$  in the limit of  $\hbar\omega_c \gg kT$  and  $\hbar\omega_c \gg \Gamma$ . This dependence is universal in the same sense as the one presented in Fig. 4.

It is of interest to compare the above results with the published calculations of magneto-thermo-power in 2D systems [13, 14, 15]. All above authors used the delta-like density of states, which is equivalent to taking  $\Gamma = 0$ . In this limit there is  $1/2\pi(1/\gamma)\exp(-2y_n^2) + \delta(z - \theta_n)$ . The integrals in Eqs (2) and (12) are then equal to their integrands with  $z$  replaced by  $\theta_n$ . A maximum of the  $n$ -th peak occurs for  $n = \theta_n$ , i.e. for  $x=0$ , at which the filling factor is  $\nu = n + \frac{1}{2}$ . Hence, we have  $N = A(n + \frac{1}{2})$  and the thermo-power at the maximum becomes

$$\alpha_n = - \frac{k}{e} \frac{\ln 2}{n + \frac{1}{2}} \quad (15)$$

This is the result quoted in [14, 15] (the authors of [13] erroneously estimated  $\nu = n$ ). It should be borne in mind that the assumptions  $\Gamma = 0$  and  $T \neq 0$  correspond to the limit  $kT/\Gamma = \infty$ . It can be seen from Fig. 8 that, in fact, we obtain the above value of  $\alpha$  in the limit of  $kT/\Gamma = \infty$ . However, the experiments are usually performed in the range of  $kT/\Gamma < 0.5$ , where the maximal values of  $\alpha$  are distinctly lower, as seen from Fig. 8. We conclude: 1/ The "universal values" of thermopower, as claimed in the quoted papers, are not really universal; 2/ These values are not likely to be reached experimentally.

AD-A147 163

INTERNATIONAL CONFERENCE ON ELECTRONIC PROPERTIES OF  
TWO DIMENSIONAL SYSTEMS (5TH) HELD AT OXFORD ENGLAND ON  
5-9 SEPTEMBER 1983(11) OXFORD UNIV (ENGLAND) 1983

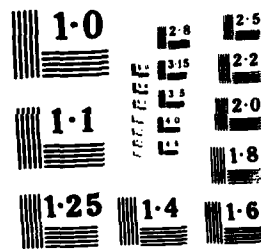
2/4

UNCLASSIFIED

F/G 9/3

NL







#### 4. Summary

The magnetization, the specific heat, the magneto-thermal effect and the thermoelectric power of the two-dimensional electron gas have been calculated as functions of a magnetic field. An oscillatory character of these effects is much more dramatic than that for the three dimensional system, due to more pronounced oscillations of the energetic density of states. A concept of strong degeneracy of the 2D gas in a magnetic field is limited to very low temperatures (below 1K). A broadening of the Landau levels  $\Gamma$  is not essential for the behavior of magnetization but it is of great importance for the thermal effects, as it allows for the intralevel, low-energy excitations. At high fields, when the interlevel thermal excitations are negligible, the thermodynamic properties become universal functions of  $kT/\Gamma$ . These theoretical predictions are in good agreement with preliminary observations of the magnetization and of the thermoelectric power in GaAs-GaAlAs heterostructures.

#### Acknowledgments

We are grateful to Dr. H.L. Stormer and to Prof. K. von Klitzing for information on their experimental results prior to publication. One of us (W.Z.) acknowledges the generous hospitality of Prof. Erich Gornik and of the University of Innsbruck during his stay in Austria, where most of this work has been done.

#### References

1. T.Ando, A.B.Fowler and F.Stern, *Rev.Mod.Phys.* **54** (1982) 537.
2. W.Zawadzki, *Solid State Commun.* (in print).
3. H.L.Stormer et al. (to be published).
4. C.Kittel, "Introduction to Solid State Physics", 3<sup>d</sup> Edition (John Wiley).
5. A.H.Wilson, "The Theory of Metals" (Cambridge Univ.Press 1965) p.144.
6. J.E.Kunzler, F.S.L. Hsu and W.S.Boyle, *Phys.Rev.* **128** (1962) 1084.
7. A.I.Anselm and B.M.Askerov, *Sov.Phys.Sol.State* **3** (1961).
8. M.I.Klinger, *Sov.Phys.Sol.State* **2** (1961) 974.
9. L.E.Gurevich and G.Nedlin, *Sov.Phys.Sol.State* **3** (1961) 2029.
10. Yu.N.Obratsov, *Sov.Phys.Sol.State* **6** (1964) 331.
11. Yu.N.Obratsov, *Sov.Phys.Sol.State* **7** (1965) 455.
12. K.von Klitzing, private communication.
13. S.P.Zelenin, A.S.Kondrat'ev and A.E.Kuchma, *Sov.Phys.Semicond.* **16** (1982) 355.
14. S.M.Girvin and M.Jonson, *J.Phys.C:Sol.St.Phys.* **15** (1982) L1147.
15. P.Streda, *J.Phys.C: Sol.St.Phys.* **16** (1983) L369.

# Figure Captions

Fig.1 The Fermi energy versus magnetic field calculated for the 2D electron gas in GaAs at a constant electron density and the temperature of 6K. The Landau levels are also indicated.

Fig.2 Magnetization of the 2D electron gas versus magnetic field calculated for the same conditions as in Fig.1 and  $T = 4.0K$ ,  $M_0 = kT(2e/hc)$ .

Fig.3 Specific heat of the 2D electron gas versus magnetic field calculated for the same conditions as in Fig.1. A transition from the intralevel regime to the interlevel regime of thermal excitations is clearly seen.  $A_1 = (1/\pi) \cdot (eH/hc)$  for  $H = 1kG$ .

Fig.4 Intralevel contribution to the specific heat calculated for the filling factor  $\nu = 2.5$  as a function of  $kT/\Gamma$ .

Fig.5 Magneto-thermal oscillations of the 2D electron gas in GaAs versus the filling factor calculated for a constant electron concentration and a constant entropy. The entropy of the lattice is not included.

Fig.6 Magneto-thermal oscillations versus the filling factor calculated for a GaAs-GaAlAs superlattice including the entropy of the lattice.

Fig.7 The thermoelectric power of the 2D electron gas versus magnetic field calculated for GaAs parameters and  $T = 6K$ . The dashed line indicates values of  $(-e/k)(\ln 2)/\nu$ .

Fig.8 The thermoelectric power at the filling factor  $\nu = n + \frac{1}{2}$  calculated as a function of  $kT/\Gamma$  in the range  $\hbar\omega_c \gg kT$  and  $\hbar\omega_c \ll kT$ . We denote  $S_0 = \alpha(-e/k) \cdot (n + \frac{1}{2})/\ln 2$ .

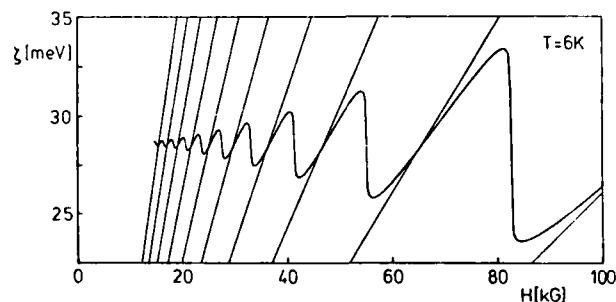


FIGURE 1

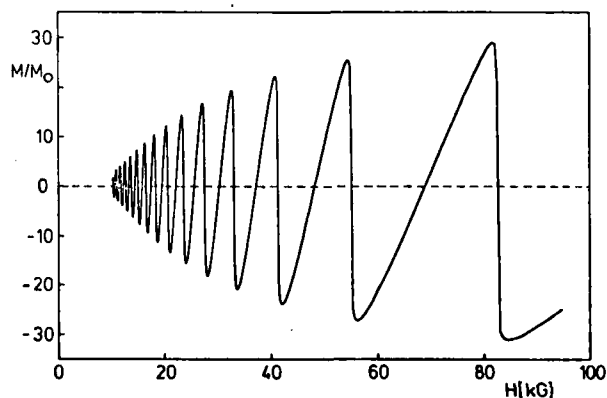


FIGURE 2

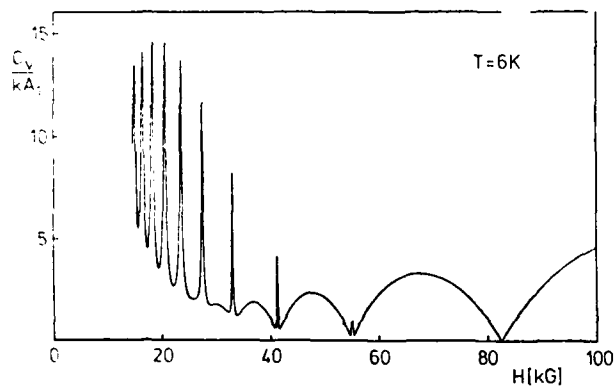


FIGURE 3

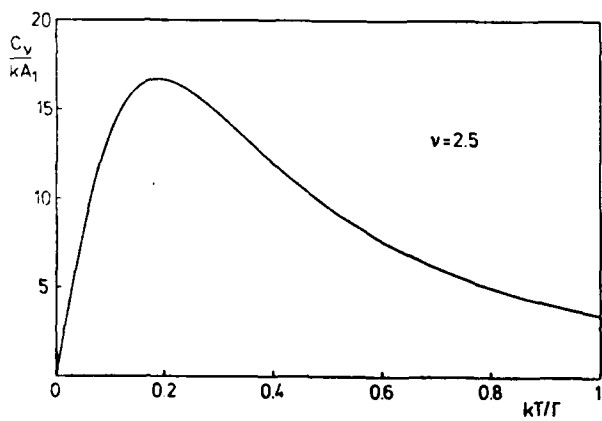


FIGURE 4

175

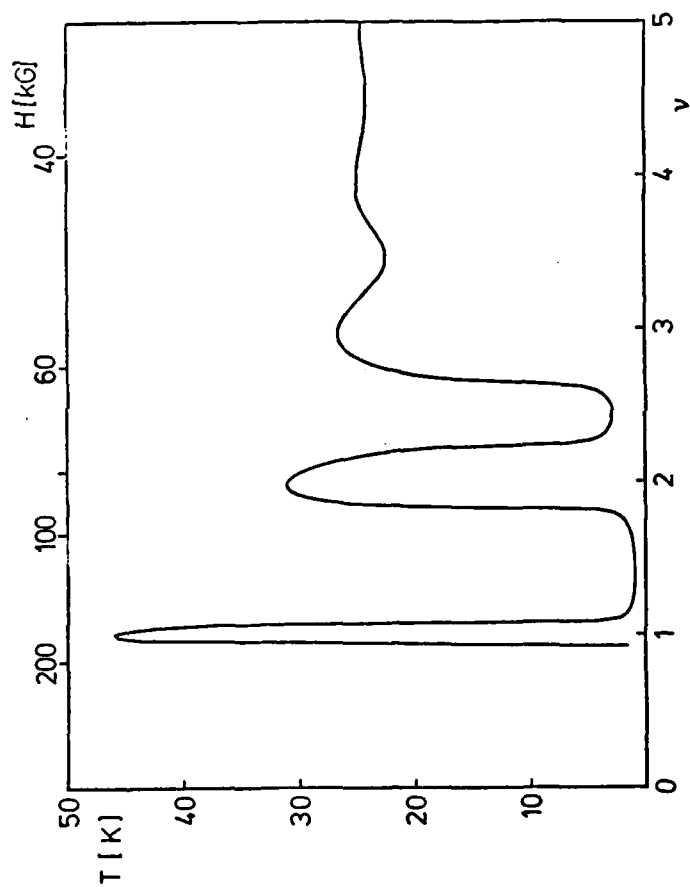
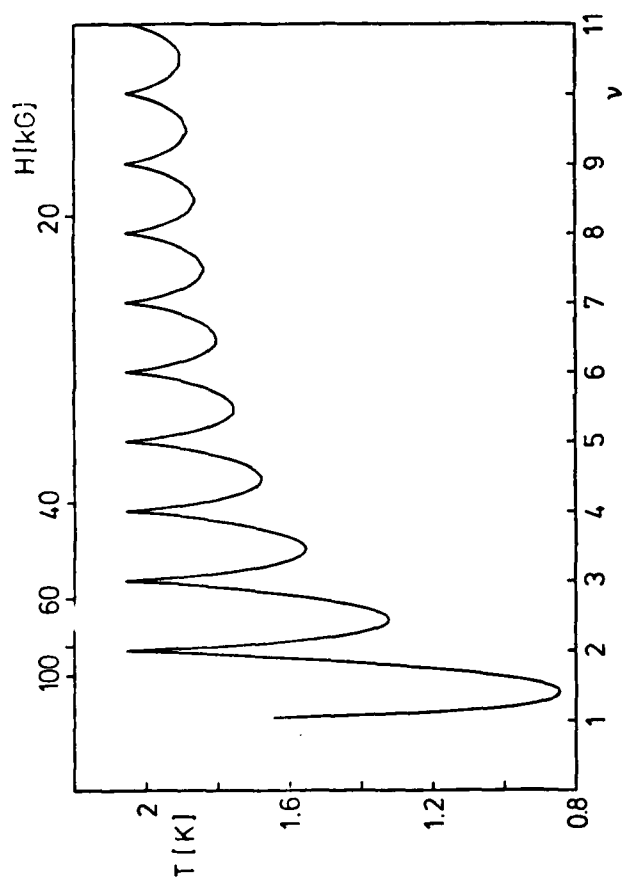


FIGURE 5

176



177

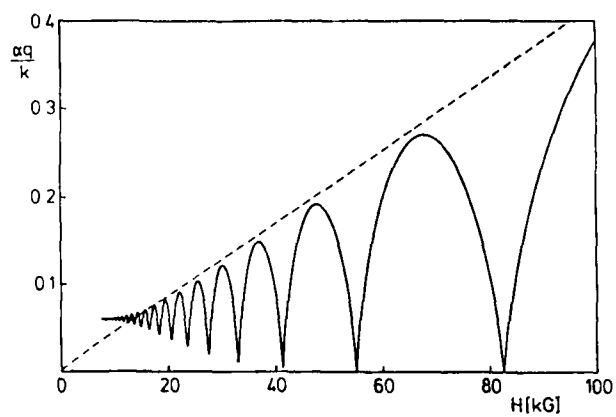


FIGURE 7

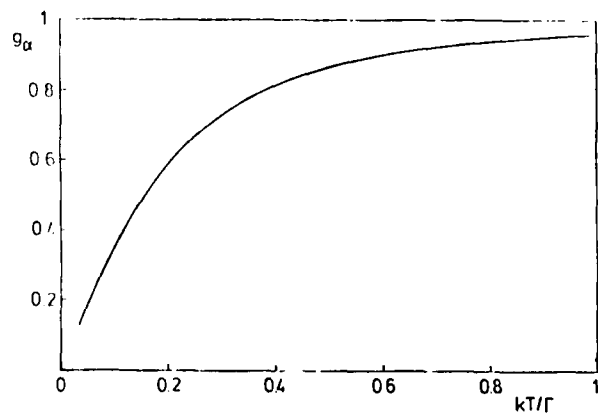


FIGURE 8

178

THERMOPOWER MEASUREMENTS ON THE TWO-DIMENSIONAL  
ELECTRON GAS OF  $\text{GaAs-Al}_x\text{Ga}_{1-x}\text{As}$  HETEROSTRUCTURES

H. Obloh and K. v. Klitzing  
Physik-Department, Technische Universität München  
8046 Garching, Fed. Rep. of Germany  
and  
K. Ploog  
Max-Planck-Institut für Festkörperforschung  
7000 Stuttgart, Fed. Rep. of Germany

Abstract

Thermopower measurements on  $\text{GaAs-Al}_x\text{Ga}_{1-x}\text{As}$  heterostructures show that the Seebeck coefficient  $\alpha_{xx}$  oscillates as a function of magnetic field with peak values  $\alpha_{xx}^{\text{max}}$  at half filled Landau levels. On devices with mobilities higher than  $\mu = 41 \times 10^3 \text{ cm}^2/\text{Vs}$  a temperature-independent value of  $\alpha_{xx}^{\text{max}} \approx 40 \text{ } \mu\text{V/K}$  is found at helium temperatures ( $2 \text{ K} < T < 5 \text{ K}$ ) for the Landau quantum number  $M_L = 1$ . However, on a sample with lower mobility ( $\mu = 24 \times 10^3 \text{ cm}^2/\text{Vs}$ )  $\alpha_{xx}^{\text{max}}$  decreases with decreasing temperature and reaches a value of about  $31 \text{ } \mu\text{V/K}$  at  $T = 2.8 \text{ K}$ . The  $\alpha_{xy}$ -component shows a complicated oscillating behavior and changes within the experimental range  $\nu > 2$  ( $\nu$  = filling factor) its sign at magnetic fields close to the filling factor  $\nu = 3$ . In the plateau region of the quantized Hall resistance both  $\alpha_{xx}$  and  $\alpha_{xy}$  tend to zero.

Thermomagnetic coefficients of a two-dimensional system in strong magnetic fields have been calculated by different authors<sup>1,2/</sup>, but experimental data are not published. In this paper we present preliminary data of thermopower measurements on  $\text{GaAs-Al}_x\text{Ga}_{1-x}\text{As}$  heterostructures in high magnetic fields.

The experimental set-up used for our thermopower measurements is shown in Fig. 1. The  $\text{GaAs-Al}_x\text{Ga}_{1-x}\text{As}$  heterostructures with standard Hall geometry and a typical overall length of  $7 \text{ mm}$  are located within an evacuated sample holder in the center of a superconducting coil. A temperature gradient in the direction of the long axis of the device is obtained by connecting the device to an electric heater and to a heat sink (bath temperature  $T_B$ ) as shown in Fig. 1. The temperature difference  $\Delta T$  between the potential probes is measured with AuFe-chromel thermocouples, and values up to  $\Delta T = 0.2 \text{ K}$  are realized. The estimated uncertainty in  $\Delta T$  is about  $0.01 \text{ K}$ . The thermal voltages parallel and perpendicular to the temperature gradient are measured with a resolution of  $\pm 20 \text{ nV}$ .

Three different devices were investigated with the following carrier densities  $n_s$  and mobilities  $\mu$ :

Sample 5185 A:  $n_s = 6.6 \times 10^{11} \text{ cm}^{-2}$ ;  $\mu = 107000 \text{ cm}^2/\text{Vs}$ .

Sample 4084 E:  $n_s = 3.7 \times 10^{11} \text{ cm}^{-2}$ ;  $\mu = 41000 \text{ cm}^2/\text{Vs}$ .

Sample 5170 A:  $n_s = 2.4 \times 10^{11} \text{ cm}^{-2}$ ;  $\mu = 24000 \text{ cm}^2/\text{Vs}$ .

In Fig. 2 the thermal voltage  $V_{pp}^{\text{th}}$  as a function of magnetic field is plotted for different temperature gradients at a bath temperature  $T_B = 4.2 \text{ K}$ . The mean temperature  $T_M$  of the sample varies with  $\Delta T$  and increases approximately up to  $6\Delta T$  above  $T_B$  depending on the length of the device. Within the experimental accuracy  $V_{pp}^{\text{th}}$  varies linearly with the temperature gradient  $\Delta T$ , indicating that  $V_{pp}^{\text{th}}/\Delta T = \alpha_{xx}$  is not strongly influenced by a small variation of the mean temperature. The vanishing of  $\alpha_{xx}$  between  $3.1 \text{ T}$  and  $3.4 \text{ T}$  (corresponding to the plateau region of the quantized Hall resistance) demonstrates

that contributions from the substrate material can be neglected. The measured  $\alpha_{xx}$  is always negative (as expected for electrons) and shows maxima and minima at the same magnetic field positions as observed in SdH-experiments (see Fig. 3).

The peak value  $\alpha_{xx}^{\max}$  increases with decreasing Landau quantum number and approaches a value of about 40  $\mu\text{V/K}$  for the Landau quantum number  $N_L = 1$ . As shown in Fig. 4 this value seems to be constant within the investigated temperature region (2 K - 5 K) for high-quality devices ( $\mu \gtrsim 41 \times 10^3 \text{ cm}^2/\text{Vs}$ ). This result agrees with calculations<sup>/1-3/</sup> predicting a value  $\alpha_{xx}^{\max} = - (k \ln 2 / (e(N_L + 1/2)))$  ( $N_L$ : Landau quantum number). However, W. Zawadzki<sup>/4/</sup> has pointed out that this equation is correct only in the limit  $kT/\Gamma \gg 1$  ( $\Gamma$  = collision broadening). Therefore, with decreasing temperature  $\alpha_{xx}^{\max}$  should be reduced. Our experiments at  $T > 2$  K show that this deviation is small for samples with mobilities above  $\mu \gtrsim 41 \times 10^3 \text{ cm}^2/\text{Vs}$  but seems to be visible below  $T \approx 7$  K on our device with  $\mu = 24 \times 10^3 \text{ cm}^2/\text{Vs}$ .

A comparison between  $\alpha_{xx}$  and  $\alpha_{xy} = E_y/V_x T$  as a function of the magnetic field is shown in Fig. 5. The off-diagonal element  $\alpha_{xy}$  oscillates in a different manner than found for  $\alpha_{xx}$  and changes its sign at a magnetic field close to the filling factor  $\nu = 3$ . This behavior has been observed for different devices. A theoretical discussion of the measured  $\alpha_{xy}$ -component is complicated because  $\alpha_{xy}$  consists of a sum of different contributions which may explain the observed change in sign. However, in the plateau region of the quantized Hall resistance all contributions to the thermal voltage disappear and both  $\alpha_{xx}$  and  $\alpha_{xy}$  tend to zero at these magnetic fields.

#### Acknowledgements

The authors would like to thank W. Zawadzki and R. Lessnik for valuable discussions. This work has been supported by the Deutsche Forschungsgemeinschaft.

#### References:

- 1) S.M. Girvin and M. Jonson, J. Phys. C **15**, L 1147 (1982)
- 2) S.P. Zelenin, A.S. Kondrat'ev, A.E. Kuchma, Sov. Phys. Semicond. **16**, 355 (1982)
- 3) P. Streda, J. Phys. C **16**, L 369 (1983)
- 4) W. Zawadzki, this conference.

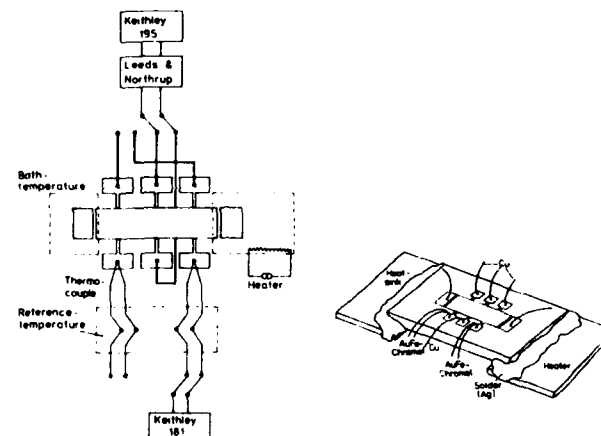


Fig. 1: Experimental set-up used for our thermopower measurements.

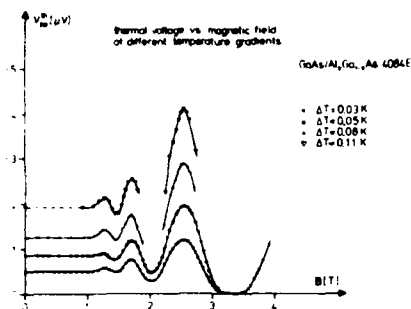


Fig. 2: Thermal voltage  $V_{pp}^{th}$  as a function of magnetic field at different temperature gradients  $\Delta T$ . The bath temperature  $T_B$  is 4.2 K.

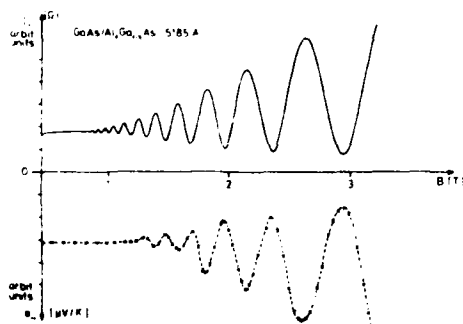


Fig. 3: Comparison between  $\alpha_{xx}$  and  $\rho_{xx}$  for magnetic fields up to 3 Tesla for device 5185 A.

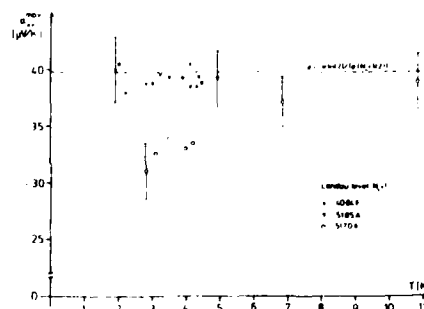


Fig. 4: Temperature dependence of  $\alpha_{xx}^{max}$  for 3 different samples at Landau quantum number  $N_L = 1$ .

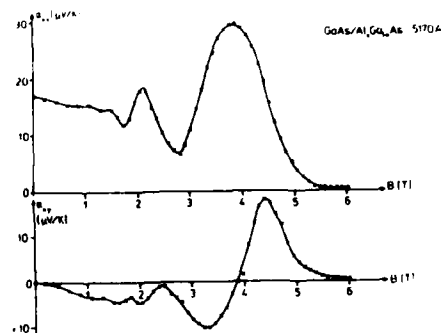


Fig. 5: Comparison between  $\alpha_{xx}$  and  $\alpha_{xy}$  measured at  $T_B = 4.2$  K as a function of magnetic field.

# Scattering and Absorption of Ballistic Phonons by the Electron Inversion Layer in Silicon: Theory and Experiment

J. C. Henkel,<sup>a</sup> R. C. Dynes,<sup>a</sup> B. I. Halperin<sup>b</sup> and D. C. Tsui<sup>a</sup>

<sup>a</sup>Bell Laboratories, Murray Hill, New Jersey 07974, USA

<sup>b</sup>Department of Physics, Harvard University, Cambridge, Massachusetts 02138 USA

We report experiments on the propagation of ballistic phonons through the (001) inversion layer of Si. An attenuation is observed which is an order of magnitude larger than can be accounted for by absorption alone. A new, dynamical phonon scattering theory is presented which provides an explanation.

## 1. Introduction

The two-dimensional electron gas (2DEG) has been investigated extensively,<sup>1</sup> but the experimental probes which have been brought to bear on this problem are mainly of two kinds, optical and electrical transport (or some combination thereof). In our work we introduce a new probe based on the absorption and scattering of high frequency ballistic phonons by the 2DEG. Substantial ranges of energy  $\hbar\omega$  and momentum transfers  $\hbar\vec{q}$  in the plane can be accessed in this manner.

Previously we reported<sup>2,3</sup> an experiment employing the propagation the transmission of ballistic phonons through the (001) inversion layer of Si which showed attenuation an order of magnitude too large to be explained by absorption via the 3D (bulk) electron-phonon interaction. This was particularly intriguing in light of earlier suspicions (stemming mostly from electrical transport) that the electron-phonon interaction for a 2DEG might be anomalously large.<sup>4</sup> In the present work measurements have been extended and a new, dynamical theory has been developed which successfully accounts for the observations, a compelling argument against the occurrence of anything anomalous in the electron-phonon coupling in a 2DEG.

## 2. Experiments

The experiments were performed as shown in Fig. 1. Ballistic propagation from source (foc. od, pulsed laser spot) to detector (superconducting film) is confined by a collimating slot to those

phonons which specularly reflect from the Si-SiO<sub>2</sub> interface of the MOSFET device on the (001) basal plane and thereby pass twice through the inversion layer. The inset in Fig. 1 displays a typical detected spectrum time resolved into longitudinal (LA), mode converted (MC) and transverse acoustic (TA) phonons. A square-wave potential (from threshold voltage  $V_T$  to some specified voltage  $V_g$ ) applied to the gate modulates the electron (areal) density from zero to a value  $n_s = \frac{C}{e} (V_g - V_T)$  where  $C$  is the oxide capacitance per unit area. The concomitant change  $\Delta I$  of the phonon intensity  $I$  is synchronously detected. Figure 2 shows  $\Delta I/I$  for LA modes plotted versus  $(V_g - V_T)^{1/2}$ , which is directly proportional to the Fermi wave vector  $k_F = \sqrt{\pi n_s}$  (note upper scale). Thus the experiment in effect provides a measurement of  $\Delta I/I$  as the Fermi surface (a circle of diameter  $2k_F$ ) is expanded in size. Four profiles of  $\Delta I/I$  are shown, each corresponding to a selected phonon source temperature  $T_s$  defined by the optical excitation power density  $P/A$  according to a black-body radiation law<sup>5</sup>  $P/A = \sigma(T_s^4 - T_0^4)$ , where  $T_0$  is the ambient temperature and  $\sigma$  is a Stefan-Boltzmann constant for phonons. The emitted phonons have a Planckian spectrum, but a high frequency cutoff develops in propagation owing to a Rayleigh-like scattering of the phonons by the mixture of Si isotopes. The profiles in Fig. 2 represent convolutions of this phonon distribution function,  $U(q, T_s)$  with some structure function  $\Delta I(q)/I$  which we shall consider next.

## 3. Theory and Discussion

An earlier theory<sup>2,3</sup> revealed that  $\Delta I(q)/I$  given by absorption alone fails to account for the data in Fig. 2. (The calculated convolution  $\Delta I/I$  is, for example, an order of magnitude too weak). If the reflection were total, an absorption model might not be a bad approximation. But in fact we are dealing with an interface with small reflectance ( $r \sim 4\%$ ) inasmuch as the angle of incidence  $\theta \sim 54^\circ$  is not far from the Brewster angle. Therefore, contributions from other sources cannot be ignored, in particular phonons backscattered from the inversion layer itself. These backscattered amplitudes can interfere with the amplitudes specularly reflected from the interface and because the latter are relatively quite weak, the interference effect is correspondingly enhanced (by roughly a factor of  $r^{-1/2} \sim 5$ ).



In our new approach<sup>3</sup> we calculate the linear response of the 2DEG to perturbations by the phonons. The radiation fields thus set up are contributed by both the real and imaginary parts of the complex linear response function  $\chi(\vec{q}, \omega)$  at wavevector  $\vec{q}$  in the plane and frequency  $\omega$ . This is a dynamical theory whereas the earlier one was "static" in the sense that it dealt exclusively with  $\text{Im}\chi(\vec{q}, \omega)$  as an absorption mechanism. To facilitate calculations we approximate the probability density  $f(z)$  of the inversion layer normal to the plane by a rectangular profile of thickness  $s$  spaced a distance  $h$  from the interface located at  $z = 0$ ; i.e.,  $f(z) = s^{-1}[\theta(z-h+s) - \theta(z-h)]$  where  $\theta(z)$  is the unit step function. By making this simplification and taking advantage of the fact that the perturbations are weak (they are only a few percent in the present case) we are able to obtain an essentially "exact" analytical expression to first order in  $\chi(\vec{q}, \omega)$  for the total, far-field LA amplitude in reflection from which follows our final results (quoted for brevity's sake in the limit  $s \rightarrow 0$ ).

$$\frac{\Delta I(q)}{I} = -\frac{1}{R_{\text{eff}}} \frac{B^2}{\rho c_f \cos \theta} [q \text{Im}\chi \cos 2k_f h - q \text{Re}\chi \sin 2k_f h] \\ - \frac{2B^2}{\rho c_f \cos \theta \sin \theta} q \text{Im}\chi \\ + 6 \text{ more terms} \quad (1)$$

Here  $R_{\text{eff}}$  is a reflection coefficient, i.e., ratio of reflected to incident LA amplitudes,  $\rho$  is the crystal density,  $c_f$  is the LA phonon velocity and  $k_f = q \cos \theta$  is the LA phonon wavevector normal to the plane. The electron-phonon coupling is represented by  $B = a \sin^2 \theta + b \cos^2 \theta$  where  $a$  and  $b$  are deformation potential constants.<sup>4</sup> A plot of (1) (in its entirety) is shown in Fig. 3(a) for  $\chi(\vec{q}, \omega)$  calculated for a noninteracting electron gas<sup>5</sup> at zero Kelvin [Fig. 3(b)].

A striking feature of Eq. (1) is the oscillatory nature of  $\Delta I(q)/I$  evidencing the interference between amplitudes scattered from the 2DEG and reflected from the interface, the phase difference being essentially the ratio of path difference  $2h$  to phonon wavelength,  $2\pi k^{-1}$  (In the experiment  $k$ 's are limited to values  $\leq 2\pi/2h$ , so the oscillation is less than one cycle). Both  $\text{Re}\chi$  and  $\text{Im}\chi$  appear in (1) in a mix depending upon the phase difference. The leading term in (1), enhanced by  $R_{\text{eff}}^{-1}$  ( $\approx -5.0$ ), arises from direct radiation (wave 1 in Fig. 4) excited by the incident LA wave. The

second term (roughly  $10\times$  smaller) represents bona-fide absorption suffered by incident and reflected primary waves in passing through the electron layer (represented in Fig. 4 by destructively interfering forward scattered waves 2 and 2'). Waves 3 and 4 in Fig. 4 represent 2 of the 6 contributions omitted from Eq. (1).

The convolution  $\Delta I/I$  of Eq. (1) (all 8 terms) with appropriate phonon distributions  $U(q, T_p)$  is shown in Fig. 5. We see that there is rather good agreement with the data in Fig. 2 in the main areas where accord was formerly lacking: the overall magnitudes are now accounted for and the shapes of the profiles, particularly the sustained tails, are rather better represented. The only serious discrepancy is that the curves are shifted to larger  $2k_f$ . For the moment this remains unexplained; it may be that our characterization of the phonon spectrum bears closer scrutiny. It should be emphasized that there are no free parameters in the theory except  $s$  and  $h$ . But these must roughly conform to the actual density profile  $f(z)$  of the inversion layer; and, indeed, the best fit is obtained when the profile midpoint position,  $z = h - s/2$ , is chosen to fall at  $\sim 3.5 a_0$  (where  $a_0$  is the variational thickness parameter of the lowest subband given by Eq. (3.30) of ref. 1) — very close to the variational first moment of  $z$  for the charge density,  $z_c = 3a_0$ .

#### 4. Conclusion

Theory and experiment are now in accord on the strong attenuation observed in the propagation of ballistic phonons through a 2DEG, giving convincing testimony that the electron-phonon interaction is basically no different in 2D than in 3D. Interestingly, the work reveals that phonon scattering may permit direct spectroscopy on the linear response function via the function  $\Delta I(q)/I$ , something that is quite inaccessible otherwise. This could be particularly interesting in the presence of quantizing magnetic fields.

#### Acknowledgments

The contributions of G. Kaminsky and J. P. Garso in sample preparation are gratefully acknowledged. Special thanks go to F. C. Usterwald for his crucial role in the execution of the experiments. One of the authors (BIH) is grateful to the hospitality of the National Institute of

Theoretical Physics, Santa Barbara and for support by the NSF through Grant DMR 82-07431.

# References

- [1] T. Ando, A. B. Fowler, and F. Stern, *Rev. Mod. Phys.* **54**, (1982) 437.
- [2] J. C. Hensel, R. C. Dynes and D. C. Tsui, *Surface Science* **113**, (1982) 249 and *J. Physique* **42**, (1981) C6-308.
- [3] J. C. Hensel, R. C. Dynes and D. C. Tsui, *Phys. Rev.* (to be published).
- [4] For a more complete discussion see ref. 2.
- [5] J. C. Hensel, B. I. Halperin and R. C. Dynes (to be published).
- [6] In the more familiar notation of Herring,  $a = E_d$  and  $b = E_d + E_g$ . For Si  $E_d = -6.0$  eV and  $E_g = +9.0$  eV.
- [7] F. Stern, *Phys. Rev. Lett.* **18**, (1967) 546.

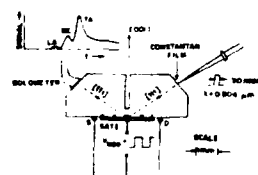


Fig. 1  
Physical layout of prism sample.  
Inset: a time-resolved ballistic phonon spectrum.

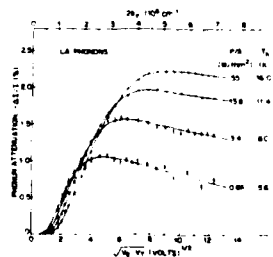


Fig. 2  
Profiles of the attenuation of LA phonons by the (001) Si inversion layer measured in reflection at  $\theta = 54^\circ$  ( $T_g = 2.15K$ ).

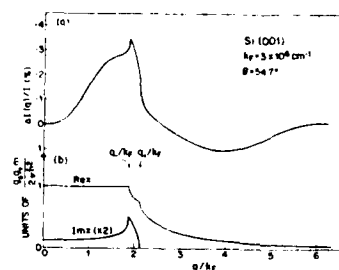


Fig. 3  
(a) Fractional change in reflected intensity  $\Delta I(q)/I$  for LA phonons of wavevector  $q$  in the plane calculated for conditions corresponding to Fig. 2. Designated  $q$ 's are  $q_x = 2k_F \pm 2 mc/h$  where  $c = c_F/hm$ . (b)  $\chi(q, \omega)$  for noninteracting electrons of valley degeneracy  $g_v = 2$ , spin degeneracy  $g_s = 2$ , and effective mass  $m = 0.19 m_0$ .



Fig. 4  
Identification of individual contributions to  $\Delta I(q)/I$  [cf. Eq. (1) in text].

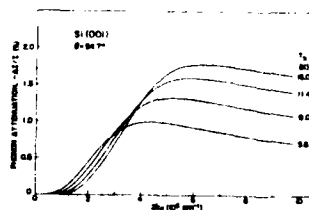


Fig. 5  
Profiles of  $\Delta I/I$  for LA phonons calculated by convolving  $\Delta I(q)/I$  [e.g. Fig. 3(a)] with phonon distribution functions for the heater temperatures  $T_g$  specified.

# Fractional Quantum Hall Effect at Low Temperatures

A M Chang\*, M A Paalanen<sup>†</sup>, H L Stormer<sup>‡</sup>,  
J C M Hwang<sup>§</sup> and D C Tsui\*

\*Department of Electrical Engineering and Computer Science  
Princeton University, Princeton, NJ 08544

<sup>†</sup>Bell Laboratories  
Murray Hill, NJ 07974

## Abstract

We report results of low temperature (85 mK to 770 mK) magneto-transport measurements of the  $2/3$  quantum Hall plateau in an  $n$ -type  $\text{GaAs-Al}_x\text{Ga}_{1-x}\text{As}$  heterostructure. Both the diagonal resistivity  $\rho_{xx}$  and the Hall resistivity  $\rho_{xy}$  show thermally activated behavior. The thermal activation energy was measured as a function of the Landau level filling factor,  $\nu$ , at fixed magnetic fields,  $B$ , by varying the density of the two-dimensional electrons with a back-gate bias. The activation energy  $\Delta$  of  $\rho_{xx}$  is maximum at the center of the Hall plateau, when  $\nu = 2/3$ , and decreases on either side of it, as  $\nu$  moves away from  $2/3$ . This resonance-like dependence on  $\nu$  is characterized by a maximum activation energy  $\Delta_{\text{max}} = 830$  mK and  $\Delta\nu/\nu = 8\%$  at  $B = 92.5$  kG. In addition, we have verified that the Hall conductance is quantized to  $(2/3)e^2/h$  to an accuracy of 3 parts in  $10^4$ , and that the  $I$ - $V$  relation is linear down to an electric field of less than  $10^{-5}$  V/cm, showing no evidence for pinning.

The recent discovery by Tsui, Stormer and Gossard [1] of a fractionally quantized Hall plateau at the value of  $1/3$  has generated a great deal of interest. Further experimentation [2] has shown the existence of an additional plateau at  $2/3$ . These plateaus are observed at low temperatures in a high mobility two-dimensional electron gas system in  $\text{GaAs-Al}_x\text{Ga}_{1-x}\text{As}$  heterostructures when placed in a strong perpendicular magnetic field. They occur when the lowest Landau level is fractionally occupied - the  $1/3$  and  $2/3$  plateaus at  $1/3$  and  $2/3$  fillings respectively. At the same time the diagonal resistivity ( $\rho_{xx}$ ) develops a minimum which becomes more pronounced at lower temperatures. More recent experiments [3] reveal that the  $1/3$  plateau is quantized to an accuracy of better than one part in  $10^4$  and that  $\rho_{xx}$  is activated near both  $1/3$  and  $2/3$  fillings over a limited dynamic range. Current theoretical results [4,5] indicate that these unusual phenomena are associated with the formation of an

incompressible electron fluid arising from the strong electron-electron Coulomb interaction. A theory due to Laughlin [4] predicts the existence of  $1/3$  charge excitations at  $1/3$  filling of the lowest Landau level and a gap in the excitation spectrum.

In this paper, we report a detailed, low temperature (85 mK) study of the  $2/3$  quantum Hall effect in a  $\text{GaAs-AlGaAs}$  sample of extremely high mobility ( $\sim 10^6$  cm<sup>2</sup>/V-sec), in magnetic fields between 68 and 106 T. We verify that the Hall plateau is accurately quantized to 3 parts in  $10^4$ . The curve is linear at low electric fields ( $< 10^{-5}$  V/cm). We investigate the temperature dependence of  $\rho_{xx}$  and  $\rho_{xy}$  (the Hall resistivity). We find that at each filling factor  $\nu = nh/eB$ , where  $n$  is the electron density,  $B$  the magnetic field strength, and  $h/e$  the flux quantum,  $\rho_{xx}$  and  $\Delta\rho_{xy} = \rho_{xy} - (3/2)h/e^2$  are activated with the same activation energy. The activation energy has a maximum value at  $\nu = 2/3$  and decreases to each side. Other than the  $2/3$  quantum Hall effect, we have observed structures in  $\rho_{xx}$  near  $\nu = 5/3, 4/3, 4/5$ , and  $3/5$ , consistent with a recent report [6] of extra structures close to these values. Only  $5/3$  and  $4/3$  show plateau development in  $\rho_{xy}$ . The  $5/3$  plateau is accurately quantized to 1.1 part in  $10^3$ .

Our sample is a modulation doped  $\text{GaAs-Al}_x\text{Ga}_{1-x}\text{As}$  heterostructure grown by molecular beam epitaxy. The layered structure consists of  $1 \mu\text{m}$  undoped  $\text{GaAs}$ ,  $300 \text{ \AA}$  of undoped  $\text{AlGaAs}$ , and  $400 \text{ \AA}$  of Si doped ( $2 \times 10^{18} \text{ cm}^{-3}$ )  $\text{AlGaAs}$ . Electrons ionized from the Si donors are trapped at the  $\text{GaAs-AlGaAs}$  interface and form the 2-dimensional gas. The region of undoped  $\text{AlGaAs}$  separates the electrons from the donors and reduces impurity scattering. Our sample has a mobility around  $10^6 \text{ cm}^2/\text{V-sec}$  at 112 mK. By using a back-gate bias [7], we are able to vary the electron density continuously between  $1$  and  $2.1 \times 10^{11} \text{ cm}^{-2}$ .

Figure 1 shows typical traces of  $\rho_{xx}$  and  $\rho_{xy}$  as a function of gate voltage at

several temperatures. The filling factor  $\nu$  is plotted at the top. The various  $\rho_{xx}$  traces correspond to different contact pairs in our Hall bar of a geometry depicted in the inset. The traces are taken at  $B = 94.5$  kG. The  $\rho_{xx}$  minimum and Hall plateau at  $\nu = 2/3$  are evident. At low temperatures,  $\rho_{xx}$  approaches zero over a finite range in  $\nu$ . Figure 2a shows raw data for the temperature dependence of  $\rho_{xx}$  around  $\nu = 2/3$  at several fixed gate voltages ( $V_g$ ). It is held constant at 92.5 kG. At each  $V_g$  corresponding to a certain  $\nu$ ,  $\rho_{xx}$  is activated. The best data at  $V_g = 40$  volts covers a dynamic range of 2 orders of magnitude in  $\rho_{xx}$  and a factor of 6 in temperature. In Fig. 2b, we plot the activation energy as a function of  $V_g$  and  $\nu$  for both  $\rho_{xx}$  and  $\Delta\rho_{xy}$ . The resulting resonance-like curve is characterized by a full width at half maximum of  $\Delta\nu \approx 0.05$ . The maximum energy occurs at  $\nu = 2/3$  with a value of  $830 \text{ mK} \pm 50 \text{ mK}$ . Unlike a usual resonance, however, the activation energy must go to zero at a certain point to each side corresponding to a mobility edge. The number of localized states which fall between the mobility edges is approximately 0.1 in terms of filling factor.

In addition to the  $2/3$  quantum Hall effect, Fig. 1 shows other prominent structures near  $\nu = 4/5$ ,  $3/5$ , and  $3/4$ . However, the lack of consistency between different contact pairs and temperatures and the absence of corroborating plateau development in  $\rho_{xy}$  preclude any definitive statements concerning their exact quantum numbers. The possibility of  $3/4$  is particularly intriguing, since the even denominator indicates the presence of electron pairing, as suggested by Halperin [8].

In Fig. 3 we show magnetic field traces of  $\rho_{xy}$  and  $\rho_{xx}$  with the gate voltage held at 700 volts. A flat  $5/3$  plateau is observed at a temperature of 65 mK along with a deep minimum in  $\rho_{xx}$ . A rough measurement of the temperature of  $\rho_{xx}$  gives an activation energy of 200 mK. Plateau development is also observed at  $4/3$ . However, it is less flat than the  $5/3$  at nearly identical magnetic fields.

This is a surprising result since the  $1/3$  plateau develops much more readily than the  $2/3$  plateau at similar fields.

In conclusion, several interesting results have emerged from our study of the fractional quantum Hall effect in the high mobility, low temperature regime. First, the  $2/3$  and  $5/3$  states are found to be accurately quantized, the former to 3 parts in  $10^4$  and the latter 1:1 part in  $10^5$ . The I-V characteristic is linear at low electric fields indicating that the ground state at  $\nu = 2/3$  is not a pinned charge density wave state. Other structures are seen near  $4/5$ ,  $3/5$ , and  $3/4$ , but their quantum numbers are not precisely determined from the data. Both  $\rho_{xx}$  and  $\Delta\rho_{xy}$  show thermally activated behavior around  $\nu = 2/3$  over a fairly large dynamic range. This activated behavior demonstrates the existence of an energy gap in the excitation spectrum above the ground state at  $\nu = 2/3$ .

The work at Princeton University was supported by the Office of Naval Research and the National Science Foundation.

<sup>(a)</sup>G. E. Electronics Laboratory, P.O. Box 488, Syracuse, NY 13221.

#### References

1. D.C. Tsui, H.L. Stormer, and A.C. Gossard, Phys. Rev. Lett. **48**, 1559 (1982).
2. H.L. Stormer, D.C. Tsui, A.C. Gossard, and J.C.M. Hwang, Physica **117B & 118A**, 688 (1983).
3. D.C. Tsui, H.L. Stormer, J.C.M. Hwang, J.S. Brooks, and M.J. Naughton, Phys. Rev. B (to be published).
4. R.B. Laughlin, Phys. Rev. Lett. **50**, 1395 (1983).
5. D. Yoshioka, B.I. Halperin, and P.A. Lee, Phys. Rev. Lett. **50**, 1219 (1983).
6. H.L. Stormer, A.M. Chang, D.C. Tsui, J.C.M. Hwang, A.C. Gossard, and W. Wiegmann, Phys. Rev. Lett. **50**, 1953 (1983).

7. H. Stormer, A.C. Gossard, and W. Wiegmann, Appl. Phys. Lett. **39**, 493 (1981).
8. B. Halperin, invited talk presented at the Conference of the Condensed Matter Division of the European Physical Society, Lausanne, 28-30 March, 1983. Proceedings to appear in Helvetica Physica Acta.

#### Figure Captions

1.  $\rho_{xx}$  and  $\rho_{xy}$  versus back-gate voltage ( $V_g$ ) and filling factor ( $\nu$ ) at  $B = 94.5$  kG and various temperatures. a) Hall bar contact pair 5-6, b) 4-5, c) 1-2, and d) 2-5.  $\nu$  ranges between 0.5 and 0.9. Inset in d), Hall bar geometry.
2. a)  $\rho_{xx}$  versus  $T^{-1}$  at  $B = 92.5$  at various  $V_g$  for  $\nu$  around  $2/3$ . b) Activation energy of  $\rho_{xx}$  and  $\Delta\rho_{xy} = 3/2 \hbar/e^2$  versus  $V_g$  and  $\nu$ . Solid circles:  $\rho_{xx}$ . Squares:  $\Delta\rho_{xy}$ .
3. Magnetic field traces of  $\rho_{xx}$  and  $\rho_{xy}$  at  $V_g = 700$  volts and  $T = 65$  mK. The  $5/3$  plateau appears very flat. A corresponding minimum occurs in  $\rho_{xx}$ .  $4/3$  also shows plateau development.

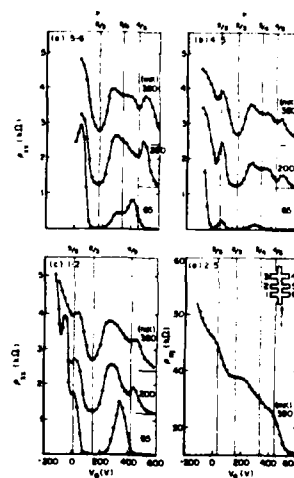


Fig. 1

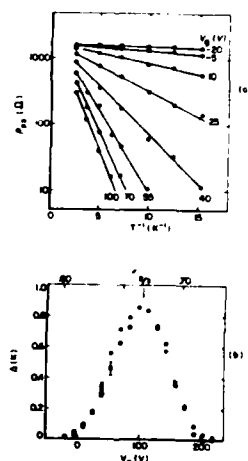


Fig. 2

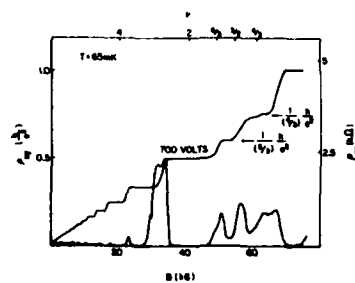


Fig. 3

#### Multiply Connected Quantized Resistance Regions

D. A. Syphers\*, F. F. Fang<sup>†</sup> and P. J. Stiles\*

\* Physics Dept., Brown University, Providence RI 02912  
IBM Thomas J. Watson Research Center, Yorktown Heights NY 10598

#### Abstract

We have examined the results of multiple connections on a single quantized resistance region and inter-connected quantized resistance regions. The experiments were done in magnetic fields up to 15 Tesla at low temperatures in Si MOSFETs. Interconnected regions are connected in two different configurations: (1) isolated regions connected by some region of low resistance, and (2) contiguous quantized regions. Both single quantized resistance regions and connected regions of type 1 separately allow the tailoring of resistances to any desired rational fraction of the quantized resistance. These measured resistances are easily accurate to better than a few parts in  $10^6$  of the idealized resistance. Connected regions of type 2 do not act as separate and distinct regions. These regions behave as if they interact via the  $\mu_{xy}$  term which is dominated by the region characterized by the lowest Landau level index.

#### Single Regions

There has been much interest in the quantized Hall effect [1-5] since its discovery in 1980 [6]. The Hall resistance has been shown to be equal to  $h/ie^2$  to within a part in  $10^7$  [7] for filled Landau levels where  $i$  is an integer representing the Landau level index. It is expected that studies of multiply connected quantized resistance regions will shed some light on this unique two-dimensional state.

A single quantized resistance (QR) region characterized by Landau level index  $i$  can be multiply connected between terminals on the perimeter such that the "source-drain" resistance of the region can be any rational fraction of the quantized resistance. An arbitrary single QR region with multiple connections can be evaluated by two equivalent methods:

- (1) By using Kirchhoff's laws where an arbitrary QR region can be represented by a collection of resistances and voltages as shown in Fig. 1.
- (2) By describing the region with currents leaving terminals and voltages on the perimeter which are constant between current-carrying terminals as outlined in Fig. 1.

The second method shows that the only discontinuity in potential along the perimeter occurs at the points where current leaves the sample.

The second method is also perhaps the easiest method to use for analyzing a single multiply connected QR region. Examples of some interesting multiple connections of a single region are shown in Fig. 2. Plots of resistance versus gate voltage for these configurations are also shown in Fig. 2. The accuracy of the values is the same as any source-drain resistance of a QR region which has been shown to be equal to the Hall resistance to within a few parts in  $10^5$  [8]. It is also observed that reversing the magnetic field can change the current path, in some cases becoming radically different. However, the change in current path has no effect whatsoever on the resistance value of the configuration. More work has been done on multiply connected single regions and will be published elsewhere [9].

#### Multiply Regions

Isolated quantized resistance regions can be interconnected by regions of low resistance (such as  $n$  contacts) to attain any desired rational fraction of the quantized resistance. The accuracy of the value attained is also limited by the relative accuracy of the source-drain resistance of a single sample as compared to the Hall resistance as above. An arbitrary set of inter-connected QR regions can be evaluated by the same methods described above for a multiply connected single QR region. Using either of those methods, the voltage between any two probes divided by the total current can be easily calculated. The resulting resistance can be made to be virtually any rational fraction of the quantized resistance. Some simple examples and the resultant resistances are shown in Table 1. An accompanying experimental example is shown in Fig. 3.

All voltage differences are measured from points on the sample perimeter through which no current passes. As a result, the deviation from the calculated resistance is due only to differences between the actual current and the calculated current. These differences originate from the differences in the resistance of individual contacts connecting the

quantized regions. Thus the measured resistances can easily be accurate to better than a few parts in  $10^6$  of the idealized resistance.

#### Contiguous Regions

Contiguous QR regions have regions of differing densities characterized by different Landau level indices. These regions exhibit entirely different properties. Such properties require an entirely different perspective to understand the interaction between contiguous regions. They do not behave as separate and distinct regions. We have performed preliminary experiments on devices which have a uniform oxide thickness and the gate is composed of a region of fixed voltage contiguous with a standard gate electrode. These experiments indicate that these regions "communicate" via the  $\rho_{xy}$  term.

A conductance device (open geometry with large  $w/l$ ) was modified in this way with each region connecting the source and drain (see Fig. 4a.). We studied the fixed density region of the sample in isolation to characterize it. We observed Shubnikov-de Haas oscillations, but they were not as distinct as those resulting from a voltage only on the gate electrode.

At constant magnetic field we varied the voltage on the gate electrode and plotted the sample resistance versus gate voltage. The results are shown in Fig. 4a. They show that there is a strong interaction between the regions. The resistances at the  $i=2$  and  $i=4$  levels are far above the values expected for non-interacting regions. When the density due to the gate electrode is at a filled Landau level, the resistance of the sample tends toward the resistance of whichever region has the higher Landau level index. We do not have enough data to unambiguously state what exact interaction causes this other than that it occurs via the  $\rho_{xy}$  term. We suggest a model in which the sample behaves like one overall region characterized by the smaller Landau level index in parallel with a smaller region characterized by the difference between the Landau level indices. This suggests a picture in which the electrons in each filled Landau level interact only

with electrons within that level.

We also observed the effects of similar modifications on devices of closed geometry (see Fig. 4b.). A corbino disk was modified to have two contiguous regions with each region connecting the source and drain of the device. The SdH oscillations of the fixed density part of the sample were not as strong as in the previous sample, and the results are not as pronounced. In spite of this they still show that the two regions are not acting as independent regions. Typical results at 8 Tesla are shown in Fig. 4b. When the region of variable density is at Landau level index  $i=4$  the resistance becomes even larger than the resistance of the fixed density region alone. Two independent regions would combine in parallel and give a lower resistance. These results suggest that this type of device may act like a Corbino disk characterized by the smaller Landau level index in parallel with a conductance region characterized by the difference between the Landau level indices, although better devices are needed to determine this unambiguously. However, both the open and closed geometry devices show that the contiguous regions communicate via the  $\rho_{xy}$  parameter.

We have also investigated devices with periodic "islands" of differing oxide thickness. The resistance of this device as a function of gate voltage is shown in Fig. 5 along with an outline of the device. Analyzing this plot shows that the islands do not affect the resistance of the overall region when the latter is strongly quantized between Landau levels (note  $i=2$  and  $i=4$ ). The value of the sample resistance at the  $i=1$  level is most likely due to a non-zero value of  $\rho_{xx}$  such that there is coupling between the bulk region and the islands. The basic difference between these devices and the contiguous region devices described previously is the topology of the contiguous regions. If the islands had spanned the width of this device, then there would be coupling between regions via the  $\rho_{xy}$  term as with the other samples and not just via the  $\rho_{xx}$  term. Put in simple terms, the electronic state at filled Landau levels does not inter-

act with other states unless it is forced to do so. More work on better samples of contiguous quantized regions is underway to determine completely the dynamics of contiguous regions and the effect that topology has on them.

We would like to thank M. Thomas for his technical assistance with some of the experiments. This work was supported in part by the National Science Foundation.

#### References

- [1] M. A. Paalanen, D. C. Tsui and A.C. Gossard, *Physical Review B* 25, (1982)5566.
- [2] K. Yoshinori, J. Kinoshita, K. Inagaki, C. Yamanouchi, J. Moriyama and S. Kawaji, *Journal of Physical Society of Japan* 51, (1982)5.
- [3] D.C. Tsui and A. C. Gossard, *Applied Physics Letters* 38, (1981)550.
- [4] R. E. Prange, *Physical Review B* 23, (1981)4802.
- [5] R.B. Laughlin, *Physical Review B* 23, (1981)5632.
- [6] K. von Klitzing, G. Dorde and M. Pepper, *Physical Review Letters* 45, (1980)494.
- [7] D. C. Tsui, A. C. Gossard, B. F. Field, M. E. Cage and R. F. Dziuba, *Physical Review Letters* 48, (1982)3.
- [8] F. F. Fang and P. J. Stiles, *Physical Review B* 27, (1983)6487.
- [9] F. F. Fang, P. J. Stiles, To be published.

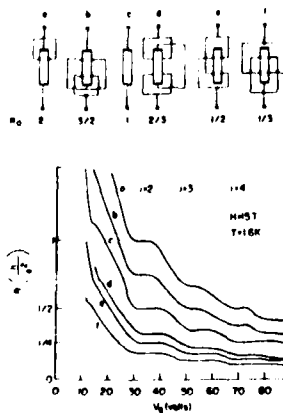


Fig. 2. Some multiple connection configurations and their related plots of gate voltage vs. sample resistance.

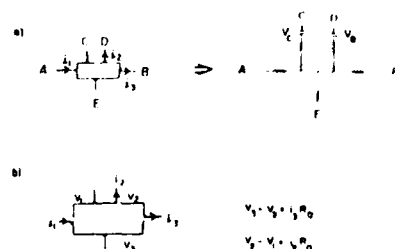


Fig. 3. In case (a) the "voltage sources" are equal to the quantized resistance multiplied by the net current passing between a terminal and some arbitrary reference terminal (chosen as F). In case (b) the "voltage sources" are equal to the quantized resistance multiplied by the net current passing between a terminal and some arbitrary reference terminal (chosen as F). In case (c) the "voltage sources" are equal to the quantized resistance multiplied by the net current passing between a terminal and some arbitrary reference terminal (chosen as F). The discontinuity in potential across a terminal is determined by  $R_0$  as shown.

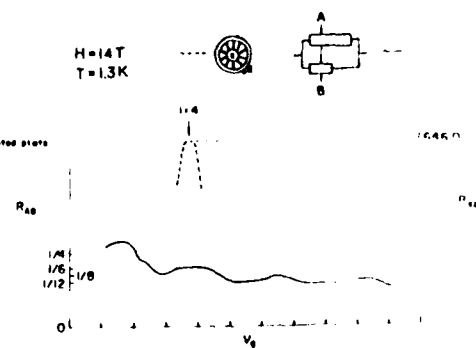


Fig. 4. Resistance vs. gate voltage for two multiple connection configurations. The resistance of the 10 ohm sample is parallel to  $1/2$  is shown to be within  $\pm 5$  of the idealized value and is fitted to the experimental accuracy. The resistance of the second configuration should be  $2/3$  of  $R_0$  of filled Landau levels and is seen to be just that.



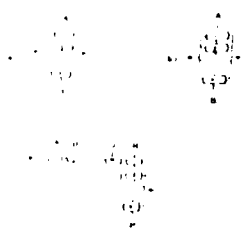


Table 1

a) $V_{AB}$	$= \frac{R}{n+1}$
b) $V_{AB}$	$= \frac{R}{n+1} R_0$
c) $V_{AB}$	$= \frac{R}{n+1} R_0$
d) $V_{AB}$	$= \frac{R}{n+1} R_0$

$n = 2$

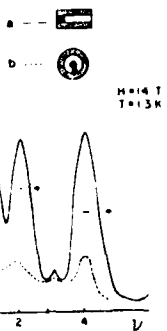


Fig. 4. Resistance vs. voltage for both open and closed geometry configurations. The error is 10% for the resistance values reported for the non-interacting regions. In (b) the resistance is higher at  $V=4.5$  than at  $V=2.5$ .

SCW II<sub>9</sub>  
 1000A  
 200A  
 167K  
 15T  
 1μA

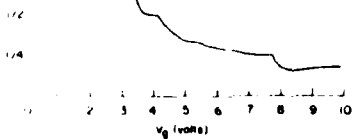


Fig. 5. Resistance vs. gate voltage for a device with "islands" of alternating low resistance.

## QUANTIZED HALL EFFECT IN SINGLE QUANTUM WELLS OF InAs\*

E. E. Mendez†, L. L. Chang†, C.-A. Chang, L. F. Alexander, and L. Esaki

IBM Thomas J. Watson Research Center  
P. O. Box 218, Yorktown Heights, N. Y. 10598

We report magnetotransport measurements, down to 0.55 K and up to 28 T, on GaSb-InAs-GaSb heterostructures. At moderate and high fields, the magnetoresistance vanishes and the Hall resistance shows plateaus at values of  $h/ie^2$  when  $i$  ( $i = 1, 2, 3, \dots$ ) magnetic levels are fully occupied. In addition, in high mobility samples, new features appear, the most prominent being a plateau at  $i = 5/2$ . The characteristics of these features are different from those observed in GaAs-GaAlAs at fractional occupation numbers, suggesting that they are likely related to the presence of holes in this system.

The study of two-dimensional (2D) carriers confined at the interface between two semiconductors has attracted great attention especially in connection with the Quantized Hall Effect (QHE). So far the only system studied in detail has been GaAs-GaAlAs,<sup>1-4</sup> and to a much less extent InGaAs-InP.<sup>5,6</sup> Recently an anomalous QHE has been observed in the former system<sup>7-9</sup>; Hall plateaus develop at magnetic fields above the quantum limit for fractional Landau-level occupation numbers  $i = 1/3$  and  $2/3$ . Additional features have been resolved for  $i = 4/3, 5/3, 2/5, 3/5, 4/5$  and  $2/7$ . No structures however have been detected for any series corresponding to even inverse filling factors like  $1/2$  or  $1/4$ , although the possibility of a charge density wave with a square density pattern at  $i = 1/2$  has been suggested.<sup>10</sup>

InAs-GaSb constitutes a system qualitatively different from GaAs-GaAlAs in that electrons and holes coexist. Because of the relative energy position of the valence and conduction bands of bulk InAs and GaSb, in a heterojunction of the two materials a 2D electron gas is formed in InAs, and a 2D hole gas, of the same density, is formed on the GaSb side of the heterostructure. The intrinsic nature of the process determines the density of the 2D gases and prevents the possibility of varying the carrier concentration in an InAs-GaSb heterojunction. This limitation can be overcome in a GaSb-InAs-GaSb double heterostructure (see Fig. 1), in which the semimetallic nature of the system is preserved but the number of transferred electrons into the InAs layer depends on its thickness  $L$ . Above a critical thickness ( $\approx 60 \text{ \AA}$ ), below which no transfer occurs, the number of carriers increases monotonically and tends to saturate for  $L \geq 300 \text{ \AA}$ , when more than one electron subband is occupied<sup>11</sup>.

In this paper we report a study of the QHE in GaSb-InAs-GaSb Quantum Wells (QW) with  $L$  ranging from 70  $\text{\AA}$  to 200  $\text{\AA}$ . The structures were grown by molecular beam epitaxy on semi-insulating GaAs substrates. The thin InAs layer was deposited on a thick (3000  $\text{\AA}$ ) GaSb buffer, and finally 200  $\text{\AA}$  of GaSb were evaporated on top. Six-arm Hall bars, 2 mm. long and 0.1 mm wide, were prepared using photolithographic techniques and ohmic contacts to the 2D carriers were made. The electron concentration and mobility, as determined from low-field Hall measurements at 4.2 K, increased with  $L$  from  $5 \times 10^{11} \text{ cm}^{-2}$  to  $8.5 \times 10^{11} \text{ cm}^{-2}$ , and from  $4 \times 10^4 \text{ cm}^2/\text{Vsec}$  to

$2.1 \times 10^5 \text{ cm}^2/\text{Vsec}$ , respectively. Background doping levels for bulk InAs (n type) and GaSb (p type) grown under similar conditions were in the low  $10^{16} \text{ cm}^{-3}$  range. The magnetotransport experiments were performed at the National Magnet Laboratory, with fields up to 22 T with a Bitter coil alone, or up to 28 T by placing a Bitter coil inside a superconducting magnet. Sample temperatures down to 0.55 K were reached using pumped liquid He<sup>3</sup>.

Figure 2 shows the magneto and Hall resistance, at 1.6 K, for a QW with  $L = 100 \text{ \AA}$ . The magnetoresistance exhibits a typical oscillatory behavior, corresponding to the crossing of the electron Landau levels ( $N = 1, 2, \dots$ ) through the Fermi level. At moderate fields,  $\approx 8 \text{ T}$ , the levels are spin-split, as indicated by the  $\pm$  signs. A zero-resistance state, already hinted at 1.6 K in Fig. 2, is reached at temperatures lower than 1 K. The Hall resistance shows well defined plateaus for fields as low as 2.5 T, and a good agreement was found (better than 1 %) between the experimental and the theoretical values ( $h/e^2$ ). A similar behavior was observed in other moderate-mobility samples, up to the extreme quantum limit, which for a sample with  $L = 70 \text{ \AA}$  was reached at  $\approx 22 \text{ T}$ .

On the other hand, samples with mobilities  $\geq 1.5 \times 10^5 \text{ cm}^2/\text{Vsec}$  presented a different behavior. In addition to the regular Hall plateaus they exhibited extra Hall structures, like the ones shown in Fig. 3. There, three extra features are revealed in  $\rho_{xy}$ , at fields of 5.3, 12 and 23.5 T. The most prominent is a plateau, that, if described by a fractional filling factor, corresponds to  $i = 5/2$  (within 1%). In all cases corresponding structures were

observed in  $\rho_{xx}$ . Several aspects of these results are noteworthy: (1) The suggestion of quantization of the Hall effect for fractional filling factors  $i > 5$ . (2) A better-defined fractional quantization for  $i = 2.5$  than for  $i < 2$ . (3) The existence of a Hall-quantized region (at 12 T) without a clear indication of a corresponding zero-resistance region. All these characteristics are remarkably different from those of GaAs-GaAAs, where (a) fractional quantization has been observed only up to  $5/3$ , (b) the structures are always better resolved at higher fields and (c) no evidence of inverse even fractions is found. Moreover, for the sample of Fig. 3 the plateau at 12 T was clearly distinguishable at 4.2 K, a temperature at which the fractional structures are unobservable in GaAs-GaAlAs. At this temperature the broad peak in  $\rho_{xx}$ , centered at 12 T, was clearly resolved into two, and, as it was lowered to 0.55 K, the high-field peak decreased in intensity and moved to lower fields. Preliminary data at much lower temperatures also indicate a very different behavior between the two peaks of the doublet in  $\rho_{xx}$  at 5.3 T.

These facts suggest that the origin of the extra structures is different from the regular Hall plateaus. The presence of electrons and holes in the system makes the analysis much more difficult. In a truly metallic structure ( $n = p$ ) the crossing of the electron and hole Landau levels through the Fermi level should be simultaneous, and thus no new features, due directly to holes, would be expected. The observed new structures could result then from an electron-hole interaction in a way not known at the present time. It is also possible that they arise from a deviation from complete balance between the

two types of carriers, so that the field-induced emptying of the Landau levels is not concurrent. The additional structures would then be due to holes, which would explain the different temperature dependence found. This interpretation is also consistent with the fact that none of the additional features is observed in low-mobility samples, in which the hole mobility, always much lower than the electron mobility, is expected to scale down accordingly.

We are indebted to P. Tedrow for his cooperation in the low temperature measurements.

#### REFERENCES

- \* Sponsored in part by the US Army Research Office.
- † Visiting scientist at the National Magnet Laboratory, Cambridge, MA.
1. D. C. Tsui and A. C. Gossard, *Appl. Phys. Lett.* **38**, 550 (1981).
2. M. A. Paalanen, D. C. Tsui, and A. C. Gossard, *Phys. Rev. B* **25**, 5566 (1982).
3. G. Ebert, K. v. Klitzing, C. Probst, and K. Ploog, *Solid State Commun.* **44**, 95 (1982).
4. G. Ebert, K. v. Klitzing, C. Probst, E. Schubert, K. Ploog, and G. Weimann, *Solid State Commun.* **45**, 625 (1983).
5. Y. Guldner, J. P. Hirtz, J. P. Vieren, P. Voisin, M. Voos, and M. Razeghi, *J. Physique* **42**, L-613 (1982).
6. R. J. Nicholas, M. A. Brummel, J. C. Portal, M. Razeghi, and M. A. Poisson, *Solid State Commun.* **43**, 825 (1982).
7. D. C. Tsui, H. I. Stormer, and A. C. Gossard, *Phys. Rev. Lett.* **48**, 1559 (1982).
8. H. I. Stormer, A. Chang, D. C. Tsui, J. C. M. Hwang, A. C. Gossard, and W. Wiegmann, *Phys. Rev. Lett.* **50**, 1953 (1983).
9. F. E. Mendez, M. Heiblum, L. L. Chang, and L. Esaki, (submitted for publication).
10. Y. Kuramoto, *Phys. Rev. Lett.* **50**, 866 (1983).
11. G. Bastard, F. E. Mendez, L. L. Chang, and L. Esaki, *J. Vac. Sci. Technol.* **21**, 531 (1982).

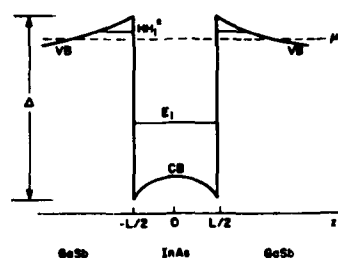


Fig. 1 Band structure, in the electric quantum limit, for a GaSb-InAs-GaSb double heterostructure. The valence band (VB) of GaSb lies higher in energy, by an amount  $\Delta$  ( $\approx 0.15$  eV), than the conduction band (CB) of InAs, which is the origin of the electron transfer. The electron and heavy hole levels are indicated by  $E_1$  and  $HH_1$ . The Fermi energy is represented by  $\mu$ .

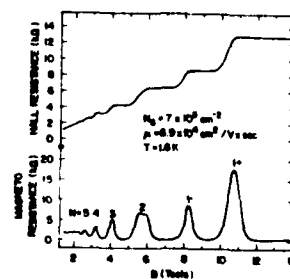


Fig. 2 Magneto (bottom) and Hall (top) resistance for a quantum well with  $L = 100 \text{ \AA}$ . The length to width ratio for the magnetoresistance data was 10.

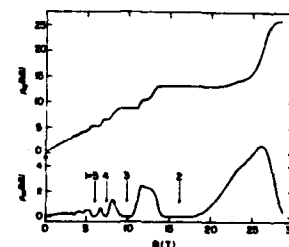


Fig. 3 Magnetoresistance,  $\rho_{xx}$ , in  $k\Omega/\square$ , and Hall resistance,  $\rho_{xy}$ , at 0.55 K, for a sample with  $L = 150 \text{ \AA}$  and a mobility of  $2.1 \times 10^5 \text{ cm}^2/\text{Vsec}$ . The arrows indicate a full Landau-level occupation corresponding to  $i$  levels.

# Novel Physics in Two-Dimensions With Modulation-Doped Heterostructures

R. L. Störmer  
Bell Laboratories  
Murray Hill, New Jersey 07974

Recent progress with modulation-doped two-dimensional carrier systems is reviewed with emphasis on the observation of new phenomena like: deHaas-van Alphen effect in two dimensions, quantized Hall effect, zero-resistance state, fractional quantization and two-dimensional hole subband structure.

A two-dimensional (2D) electron system is a theoretical concept. Translational invariance in the x-y plane and no degree of freedom in the z-direction are its predominant ingredients.<sup>1</sup> These ideal conditions can be approached experimentally in a number of different media. Electrons on the surface of liquid He<sup>2</sup> and at the semiconductor/oxide interface of a Si-MOSFET<sup>3</sup> are the classical examples of such systems. The success to which the intrinsic properties of a 2D system can be determined experimentally depends largely on the degree to which the physical structure reflects the ideal 2D concept. This requires minimization of undesired interaction of the 2D system with the host. Modifications due to the periodic potential of the host are easily worked into the theory and of little concern. The prime concern must be random fluctuations in the carrier confining potential which leads to scattering of the 2D electrons and thus a finite scattering time  $\tau$  (conveniently determined by the mobility  $\mu = e\tau/m^*$ ). The persistent striving to improve the scattering time in real 2D systems is led by the aim to approach the ideal 2D system and hence to be able to examine its intrinsic properties.

Enormous improvements in  $\tau$  have been achieved during the past 5 years. A novel doping technique, dubbed modulation-doping (MD), allows generation of 2D electron systems at the hetero-junction between two III-V semiconductor materials.<sup>3</sup> Different from the traditional Si-MOSFET where the electrons reside at

the interface between a crystalline semiconductor and a glassy oxide, in modulation-doped (MD) heterojunctions the carriers are bound to a lattice-matched interface between two crystalline materials.<sup>4</sup> A variety of III-V materials including their ternary and quaternary alloys which allow for a vast number of lattice-matched material combinations. Many high-quality 2D electron systems can now be created in a whole class of materials incompatible with the standard MOS technique. The high quality of the crystalline interface and the high degree of control of the MBE (molecular beam epitaxy) growth process<sup>5</sup> allowed increase of low-temperature electron mobilities in MD GaAs-(AlGa)As interfaces to values well beyond  $10^6 \text{ cm}^2/\text{Vsec}$ .<sup>6,7</sup> These mobilities translate into scattering times of  $\sim 5 \times 10^{-11} \text{ sec}$  and a mean free path of  $\lambda \sim 5 \mu\text{m}$  for an elastic event to occur. MD-materials had considerable impact not only on experimental 2D physics but also on today's transistor technology.<sup>8-10</sup>

In the following, I will briefly review modulation-doping, focusing on recent progress in electron mobilities. The second part of this review describes recent experiments on 2D systems in MD GaAs-(AlGa)As with emphasis on the observation of fractional quantization of the Hall effect. This observation is now believed to be evidence for the existence of a novel correlated electronic state.

## MODULATION DOPING: MATERIALS AND MOBILITIES

In modulation-doped heterostructures, the 2D electron system is created via MBE at a semiconductor interface by doping exclusively the wide-gap material while the neighboring narrow-gap material is kept free from dopant, (Fig.1) At the junction, carriers from the impurities transfer across the interface, thus populating the low-lying band edge states of the narrow-gap semiconductor. These carriers form a 2D electron system kept at the interface by the band-edge discontinuity at the heterojunction and by the Coulomb forces of their ionized parent impurities across the interface. The heterojunction separates mobile carriers from the strong part of the scattering potential of the ionized donors.

reducing considerably the scattering rate.

Though MD has now been demonstrated in a variety of III-V materials,<sup>3,10-12</sup> most of the data have been accumulated in the GaAs-(AlGa)As system on which we will concentrate from now on. In MD GaAs-(AlGa)As, Si is the preferred n-type dopant. Areal densities are fixed and established during growth. They are determined by the doping concentration, the distribution of dopant over the structure, the donor binding energy, the discontinuity between bands (Al-concentration  $x$ ) and the proximity of the surface. Electron densities range up to  $2 \cdot 10^{12} \text{ cm}^{-2}$  limited by the maximum density of electrically active Si achievable in (AlGa)As and its  $x$ -dependent binding energy. Typical structures contain 30% Al ( $x=0.3$ ) and  $1 \cdot 10^{18} \text{ cm}^{-3}$  Si resulting in the population of generally only one subband with  $T$ -independent 2D densities around  $3 \cdot 10^{11} \text{ cm}^{-2}$  and low- $T$  mobilities of  $2 \cdot 5 \cdot 10^5 \text{ cm}^2/\text{Vsec}$ . Mobilities drop to  $8 \cdot 10^3/\text{Vsec}$  when raising  $T$  to 300K.

Fig. 2. shows, as an example, experimental results of the low-field mobility ( $\mu$ ) of one of the best quality GaAs-(AlGa)As heterojunctions<sup>6</sup> and compares it with the mobility of high-purity bulk GaAs ( $4 \cdot 10^{13} \text{ cm}^{-3}$ ).<sup>13</sup> Above 750K  $\mu$  of both samples is limited by optical phonon scattering. Below this temperature,  $\mu$  of the bulk sample decays rapidly due to ionized-impurity scattering while  $\mu$  of the MD material keeps increasing reaching a maximum of  $1.6 \cdot 10^6 \text{ cm}^2/\text{Vsec}$  at 1.2K. Between 10K and 50K, the  $T$ -dependence of the MD sample is very closely described by a  $T^{-1/2}$  law suggesting scattering by piezo-electric coupling to acoustic phonons<sup>14</sup> to be the dominating scattering process. Below 10K,  $\mu$  is flat and most likely limited by impurity or interface roughness scattering. It is interesting to point out that MD material with a density equivalent to a 3D density of  $1 \cdot 10^{17} \text{ cm}^{-3}$  exceeds the low- $T$  mobility of the  $4 \cdot 10^{13} \text{ cm}^{-3}$  bulk material by orders of magnitude. Mobilities of  $10^{17} \text{ cm}^{-3}$  bulk GaAs hardly exceeds  $10^4 \text{ cm}^2/\text{Vsec}$  at any  $T$ . The enhancement results from the fact that MD allows one to create a degenerate electron system corresponding to an enormous

reduction in phase-space for scattering to occur without having to increase simultaneously the number of scatterers in the form of impurities. The same phase-space reduction is responsible for the density dependence of the low- $T$  mobility.<sup>15,16</sup> With increasing density an increasing Fermi-wavevector  $k_F$  decreases the effectiveness of a scattering process of given wavevector  $q$ . This is the origin of the density dependence of  $\mu$ . Enhanced screening of the ionized impurity potential due to increased electron density, an often quoted source for this dependence, is of much less importance.

The enormous improvements in mobility that have been achieved during the past years are mostly due to two facts: 1) Improved cleanliness in the MBE growth process. 2) The introduction of an undoped spacer layer between dopant and the 2D system, see Fig. 3.<sup>17,18</sup> This spacer layer further reduced the strength of the Coulomb potential of the ionized impurities in the (AlGa)As at the site of mobile carriers. Undoped spacer layers were already incorporated in the first MD-samples.<sup>3</sup> Systematic studies of the mobility dependence on spacer layer thickness seemed to reveal an unexpected optimum spacer layer thickness.<sup>19,20</sup> The existence of an optimum is now understood to result from a competition between mobility enhancement due to an increased distance between carriers and scatterers and mobility reduction due to a decrease in carrier density for the thick spacer layers.

In concluding the first part of this review, we would like to summarize that modulation-doping of semiconductor heterostructures has supplied a new set of versatile 2D electron systems with such reduced low- $T$  scattering rates well suited to further investigate the fundamental properties of 2D electrons.

#### NOVEL PHYSICS WITH MD MATERIAL

The low carrier scattering rate in MD material and the possibility to stack a large number of such 2D systems during the growth process (multilayers) allowed for a number of novel experiments and observation. The multilayer-

advantage as well as the material combination GaAs-(AlGa)As was instrumental for a whole set of light scattering experiments which allowed probing the properties of 2D systems optically within a wavelength regime conveniently accessible to dye-lasers techniques.<sup>21</sup> Subband-level schemes,<sup>22,23</sup> the depolarization field effect,<sup>24</sup> 2D plasmons<sup>25</sup> and Landau level transitions<sup>26</sup> can now be studied by optical means. This field has recently been reviewed.<sup>21</sup>

#### deHaas-van Alphen Effect

The capability of stacking many identical layers and using them to enhance an otherwise vanishing signal has been employed to observe the deHaas-van Alphen (dHvA) effect in a 2D system<sup>27,28</sup> which so far has only been a theoretical textbook example, see Fig. 4. 4000 layers of 2D electrons equivalent to an area of  $240 \text{ cm}^2$  have been stacked to provide a magnetic moment sufficiently large to be detected by a commercial SQUID-system. The experimental results show unambiguously the oscillatory variation of the magnetic moment with varying magnetic field. The oscillations which are due to quantization into discrete Landau levels have the same period in  $1/B$  as the well known Shubnikov-deHaas (SdH) oscillations taken on the same sample. The amplitude of the oscillations is considerably less than expected on theoretical grounds. Inhomogeneities in carrier density among the layers which constitute the specimen are a likely source of amplitude reduction. With the advance of MBE and by improving the experimental technique to probe the magnetization of a smaller specimen it should be possible to suppress this artifact in future measurements.

The importance of the observation of the dHvA-effect in 2D systems lies in the fact that it provides a unique tool to determine the shape of the 2D-density of states (DOS) in a magnetic field. While magneto-transport is a convolution of DOS and carrier scattering processes, the dHvA-effect at low-T is solely dependent on the DOS. Hence, under favorable circumstances, the DOS can be determined directly from the experimental data. Measurements of the magnetic moment with a SQUID-system are of particular interest since such d.o.

214

experiments cannot be perturbed by long lasting eddy-currents which are unavoidable in 2D systems in the regime of the zero-resistance state.

#### Quantized Hall Effect

Shortly after the observation of the quantized Hall effect (QHE) in a Si-MOSFET<sup>29</sup> the same quantization was observed in the 2D electron system of a MD GaAs-(AlGa)As heterostructure,<sup>30</sup> (see Fig. 5). By now at least two other MD-systems showed this quantum effect.<sup>11,12</sup> GaAs-(AlGa)As heterojunctions remain the preferred material combination for studies of these kind. The small cyclotron mass of electrons in GaAs ( $m^*=0.066m$ ) assures a large Landau level splitting at technologically easy attainable magnetic fields (80kG). A small carrier mass is advantageous in optimizing  $\hbar\omega_c/kT$  in particular since there exists a lower limit on the electron temperature which is achievable in practice in transport-measurements on 2D systems. Yet unclear is the benefit of the long scattering time  $\tau$  to the width of the Hall plateaus. Since small scattering rates indicate small amounts of potential fluctuations and since the occurrence of the QHE is intimately connected with the existence of states localized due to potential fluctuations, one might argue that large scattering rates would be beneficial to the width of the plateau. Such a correlation between  $\tau$  and the plateau width actually has been found in Si-MOSFET's<sup>31,32</sup> but has not yet been examined in MD material. This lack of data is mostly due to the fact that the  $n$ -density in MD-material is difficult to control and hence comparison between different samples is unreliable since an  $n$ -dependence can obscure a  $\tau$ -dependence.

#### Zero Resistance State

At the field position where the Hall resistance assumes its quantized value ( $\rho_{xy} = \frac{h}{e^2} i, i=1,2,\dots$ ) the diagonal resistivity  $\rho_{xx}$  vanishes as  $T \rightarrow 0$ . Resistivities as small as  $\rho_{xx} = 5 \cdot 10^{-7} \Omega/\square$  (and indirectly  $10^{10} \Omega/\square$ )<sup>28</sup> have been measured at 1.2K<sup>33</sup> (see Fig. 6). Finite conductivity  $\sigma_{xx}$  has been attri-

215

puted to 2D variable range hopping via the localized states in the tails of the Landau levels. Temperature dependences of  $\sigma_{xx}$  of  $\exp(-T_0/T)^{1/3}$ <sup>33</sup> characteristic for 2D variable range hopping in the absence of a magnetic field as well as  $\sigma_{xx}$  of  $\exp(-T_0/T)^{1/2}$ <sup>34,35</sup> (in agreement with a recent theory assuming Gaussian localization of the states induced by the magnetic field) have been found experimentally in MD GaAs-(AlGa)As heterostructures. The experiments indicating a  $T^{-1/2}$  dependence also produce the correct exponent for the temperature dependent prefactor. However, the density of localized states at  $E_c$  derived from its magnitude is unphysically large.<sup>34</sup> The discrepancies between the different experimental results as well as those between experiments and theory are yet to be resolved.

#### Fractional Quantization of the Hall Effect

A recent observation of plateaus in the Hall resistance  $\rho_{xy}$  and simultaneously vanishing resistivity  $\rho_{xx}$  at fractional occupation of the lower spin-state of the lowest Landau-level (see Fig. 7)<sup>36</sup> has induced a considerable amount of speculation about the origin of this phenomena. While quantization of  $\rho_{xy}$  and simultaneously vanishing of  $\rho_{xx}$  are expected to occur only at integral values of filling factor<sup>37</sup>,  $\nu = \frac{n\Phi_0}{4\pi e^2}$  where the Fermi energy  $E_F$  resides within the region of localized states between Landau or spin levels, both phenomena have now been observed at fractional values of  $\nu$ . This quantization occurs at characteristic temperatures much lower than the temperatures necessary for the observation of quantization at integral values of  $\nu$ . In low-density, high-mobility ( $>10^5$  cm<sup>2</sup>/Vsec) GaAs-(AlGa)As heterostructures minima in  $\rho_{xx}$  have been observed at values close to  $\nu=1/3$ ,  $2/3$ ,  $4/3$  and  $5/3$ ,  $\nu=2/5$ ,  $3/5$  and  $4/5$  and  $\nu=2/7$ , and plateaus were clearly identified in the vicinity of  $\nu=1/3$ ,  $2/3$  and  $3/5$ <sup>38</sup> (see Fig. 8). The relative strength of structure in  $\rho_{xx}$  and  $\rho_{xy}$  is analogous to their relative strength in the normal quantized Hall effect. At the position of the plateaus around  $\nu=1/3$  and  $2/3$  the Hall resistance was found to be quantized to  $\rho_{xy} = \frac{h}{4\pi^2 e^2}$  to better than 1 part in  $10^4$ <sup>39</sup>

and  $\rho_{xy} = \frac{h}{2/3\pi^2}$  to better than 3 parts in  $10^4$ <sup>40</sup>, respectively. At other values of  $\nu$  where minima are observed in  $\rho_{xx}$ ,  $\rho_{xy}$  starts to develop plateaus.

Generalizing the experimental results, one can speculate that fractional quantization exists for  $\nu = 1/q$  ( $q = 3, 5, 7, \dots$ ) and all their multiples  $\nu = p/q$ . Its strength increases with increasing  $B$  and decreases as  $q$  increases. At fixed  $B$ , the strength is independent of  $p$ . Fractional quantization at even inverse filling factors is either completely absent or occurs at  $T$  lower than of their odd counterparts. Experiments at still lower  $T$  are in preparation to examine these speculations.

While the existence of the normal quantized Hall effect is a result of the gaps in the single particle density of states of a 2D system in a high magnetic field and the existence of localized states within those gap regions<sup>37</sup>, fractional quantization of the Hall effect cannot be understood on this basis. The existence of a new kind of gaps at fractional values of  $\nu$  caused by the condensation of the 2D carriers into a coherent many particle state with a finite gap in its excitation spectrum has been postulated to be the origin of the experimental observation. Recent analytical calculations<sup>41,42</sup> and numerical simulations<sup>43</sup> indicate that the many particle ground state responsible for fractional quantization of the Hall effect is an incompressible electron liquid which exists exclusively at rational fractions of  $\nu$ . Initial theoretical work concluded the state exists only at  $\nu = \frac{1}{q}$ ,  $q = 3, 5, 7, \dots$  and with the presence of electron-hole symmetry also at  $\nu = 1 - \frac{1}{q}$ .<sup>41</sup> More recent studies, motivated by the observation of a much wider variety of rational fractions, seem to be able to account for all fraction with odd integers or even all integers as the denominator.<sup>44-47</sup> At this time the experimental data are not yet sufficient to be compared with any of the predictions based on one or the other theoretical model.

Finally, we call attention to the fact that all the data on fractional quantization were taken from samples with high mobilities, indicating a low



degree of potential fluctuation at the position of the 2D system. Samples of lower mobilities show no indications of fractional quantization at any noninteger value of  $\nu$ . Instead, such samples develop extremely wide plateaus in  $\rho_{xx}$  and wide zero-resistance minima in  $\rho_{xy}$  at integral  $\nu$ , suppressing any additional structure. We conclude from this observation that the integral quantum Hall effect and the fractional quantum Hall effect are very different in origin and actually are competing with one another.

#### 2D Hole Systems

In the final section, I would like to present a new 2D system with large potential for interesting future investigations. It consists of a modulation-doped 2D hole gas generated in complete analogy to the 2D electron gas at the interface of a GaAs-(AlGa)As heterostructure. Though this system has been introduced earlier<sup>48</sup>, only recently could its carrier mobilities be improved to be equivalent to those of similar 2D electron system.<sup>6</sup> Mobilities of more than  $50,000 \text{ cm}^2/\text{Vsec}$  have been demonstrated by now. Considering the difference in carrier mass between electrons and holes (roughly a factor of 8), scattering times in 2D holes are now equal to scattering times of the best MD 2D electron systems. Fig. 9 shows the  $T$ -dependence of  $\mu$  of a 2D hole system<sup>49</sup> combined with data on the  $T$ -dependence of the best high-purity  $p$ -type bulk GaAs published in the literature.<sup>50</sup> Again, as in the case of the 2D electrons,  $\mu$  of the 2D holes follows the data of the high-purity bulk material down to  $\sim 40\text{K}$  and finally exceeds its values for the lowest  $T$  measured. Comparison with Fig. 2 suggests that the quality of the 2D hole system can be further improved. The characteristics of the  $T$ -dependence of  $\mu$  in 2D holes are similar to those of 2D electrons. However, in the intermediate  $T$ -region the influence of scattering via acoustic phonon seems to be much more pronounced than in 2D electrons. At the lowest temperatures,  $\mu$  of both systems becomes  $T$ -independent, indicating similar  $p$ -limiting processes to be present.

While the mobility behavior is rather similar for 2D electrons and 2D holes, their subband structure is very different from one another due to the existence of light and heavy masses in the valence band and due to the strong anisotropies of their dispersion relation. In spite of all these complication, the quantized Hall effect<sup>51</sup> and even fractional quantization<sup>38</sup> has been observed in such a system (see Fig. 10), indicating convincingly that the existence of the phenomena is independent of the details of the band structure. The observation of fractional quantization in a hole samples with mobilities as low as  $20,000 \text{ cm}^2/\text{Vsec}$  shows clearly that the scattering time  $\tau$  and not the mobility  $\mu$  is the important parameter deciding if this phenomenon can be observed in a given material.

Of particular interest is the effect of the interface on the electric subband structure of the 2D holes. It has been postulated that the lack of inversion symmetry due to the existence of strong interfacial electric fields would lift the spin degeneracy of the bound states.<sup>52,53</sup> Such a lifting of the degeneracy has recently been observed in 2D holes<sup>51</sup> and also in 2D electrons.<sup>54</sup> In the case of 2D holes, its effect on the subband structure is considerable. The splitting of the degeneracy actually leads to the observation of two different hole masses which both seem to derive from the heavy hole band, though a simple model would lead to a light in-plane mass of the lowest bound state. As expected from theory, both subbands are found to be degenerate at  $k=0$ . With the possibility of tuning the interfacial electric field by a gate this splitting will allow to vary the carrier mass of a 2D system by simple external means. At this time detailed theoretical calculations on the subband structure, dispersion and anisotropies of 2D holes are very desirable to understand the spectrum of new results.

#### ACKNOWLEDGMENTS

Most of the reviewed work results from a very fruitful collaboration with several colleagues from Bell Labs and Princeton University to whom I am

grateful for creating such a stimulating ambience. Those colleagues are

D. C. Tsui, Z. Schlesinger, A. M. Chang, A. Pinczuk, T. Haavasoja, A. C. Gossard, S. J. Allen, M. A. Paalanen and J. C. M. Hwang. K. Baldwin and W. Wiegmann I would like to thank for excellent technical support. Much of the work in high magnetic fields was performed at the National Magnet Lab in Cambridge, Massachusetts.

#### References

1. Review T. Ando, A. B. Fowler and F. Stern, *Rev. Mod. Phys.* **54**, 437 (1982).
2. C. C. Grimes, *Surf. Sci.* **73**, 379 (1978).
3. H. L. Störmer, R. Dingle, A. C. Gossard and W. Wiegmann, *Conf. Series* **43**, 557 (1978). B. C. H. Wilson ed. *Inst. of Physics, Bristol, London*; R. Dingle, H. L. Störmer, A. C. Gossard and W. Wiegmann, *Appl. Phys. Lett.* **33**, 665 (1978).
4. H. L. Störmer, R. Dingle, A. C. Gossard, W. Wiegmann and M. D. Sturge, *Solid State Commun.* **29**, 705 (1979).
5. A. Y. Cho and J. R. Arthur, *Prog. in Sol. State Chem.* **10**, 147 (1975).
6. J. C. M. Hwang, A. Kastalsky, H. L. Störmer and V. G. Keramidas, 2nd Intl. Symp. on Molecular Beam Epitaxy, Tokyo, Japan, 1982 (unpublished).
7. S. Hivamizu, K. Nanbu, J. Saito, T. Ishikawa and Hashimoto, 2nd Intl. Symp. on Molecular Beam Epitaxy, Tokyo, Japan 1982 (unpublished).
8. T. Mimura, S. Hivamizu, T. Fujii and K. Nanbu, *Jap. J. Appl. Phys.* **19**, L225 (1980).
9. D. Delagebeaudeuf, P. Delecluse, P. Etienne, M. Laviro, J. Chaplart and N. T. Linh, *Electron Lett.* **16**, 667 (1980).
10. R. A. Kiehl, M. D. Feuer, R. H. Hendel, J. C. M. Hwang, V. G. Keramidas, C. I. Allyn and K. Dingle, 41 Ann. Device Research Conf. Burlington, Vt. (1983) (unpub.).
11. Y. Guldner, J. P. Hirtz, J. P. Vieren, P. Voisin, M. Voos and M. Razeghi, *J. Phys. Lett.* **43**, L613 (1982).
12. A. Kastalsky, R. Dingle, K. Y. Cheng and A. Y. Cho, *Appl. Phys. Lett.* **41**, 274 (1982).
13. C. M. Wolfe, G. E. Stillmann and W. T. Lindley, *J. Appl. Phys.* **41**, 3088 (1970).
14. P. J. Price, *Surf. Science* **113**, 199 (1982).
15. D. C. Tsui, A. C. Gossard, G. Kaminsky and W. Wiegmann, *Appl. Phys. Lett.* **39**, 712 (1981).
16. H. L. Störmer, A. C. Gossard, W. Wiegmann and K. Baldwin, *Appl. Phys. Lett.* **39**, 912 (1981).
17. L. C. Witkowski, T. J. Drummond, C. M. Stanchak and H. Morkoc, *Appl. Phys. Lett.* **37**, 1033 (1980).
18. H. L. Störmer, A. Pinczuk, A. C. Gossard and W. Wiegmann, *Appl. Phys. Lett.* **38**, 691 (1981).
19. T. J. Drummond, H. Morkoc and A. Y. Cho, *J. Appl. Phys.* **52**, 1380 (1981).
20. P. Delecluse, M. Laviro, J. Chaplart, D. Delagebeaudeuf and N. T. Linh, *Electronic Lett.* **17**, 344 (1981).
21. A. Pinczuk and J. M. Worlock, *Surf. Sci.* **113**, 69 (1982).
22. G. Abstreiter and K. Ploog, *Phys. Rev. Lett.* **42**, 1308 (1979).
23. A. Pinczuk, H. L. Störmer, R. Dingle, J. M. Worlock, W. Wiegmann and A. C. Gossard, *Solid State Commun.* **32**, 1001 (1979).
24. A. Pinczuk, J. M. Worlock, H. L. Störmer, R. Dingle, W. Wiegmann and A. C. Gossard, *Solid State Commun.* **36**, 43 (1980).
25. A. Pinczuk, I. Shah, A. C. Gossard and W. Wiegmann, *Phys. Rev. Lett.* **46**, 1307 (1981).
26. J. M. Worlock, A. Pinczuk, Z. J. Tian, C. H. Perry, H. L. Störmer, R. Dingle, A. C. Gossard, W. Wiegmann and R. L. Aggarwal, *Solid State Commun.* **40**, 876 (1981).
27. H. L. Störmer, T. Haavasoja, V. Narayanamurti, A. C. Gossard and W. Wiegmann, *J. Vac. Sci. and Technol.* **B1**, 423 (1981).
28. T. Haavasoja, H. L. Störmer, D. Bishop, V. Narayanamurti, A. C. Gossard and W. Wiegmann, this volume.
29. K. v. Klitzing, G. Dorda and H. Pepper, *Phys. Rev. Lett.* **45**, 494 (1980).
30. D. C. Tsui and A. C. Gossard, *Appl. Phys. Lett.* **37**, 550 (1981).
31. H. L. Störmer, D. C. Tsui and A. C. Gossard, *Surf. Science* **113**, 32 (1982).
32. J. E. Furneaux and T. L. Reinecke (this volume).
33. D. C. Tsui, H. L. Störmer, A. C. Gossard, *Phys. Rev. B* **25**, 1405 (1982).
34. G. Ebert, K. v. Klitzing, C. Probst and K. Ploog, *Solid State Commun.* **45**, 625 (1983).
35. A. Briggs, Y. Guldner, J. P. Hirtz, J. P. Vieren, M. Voos and M. Razeghi, *Phys. Rev. B* **27**, 6549 (1983).
36. D. C. Tsui, H. L. Störmer, A. C. Gossard, *Phys. Rev. Lett.* **48**, 1559 (1982).
37. R. B. Laughlin, *Phys. Rev. B* **23**, 5632 (1981).
38. H. L. Störmer, A. M. Chang, D. C. Tsui, J. C. M. Hwang, A. C. Gossard and W. Wiegmann, *Phys. Rev. Lett.* **50**, 1953 (1983).
39. D. C. Tsui, H. L. Störmer, J. Brooks and J. C. M. Hwang, *Phys. Rev. B* (July 1983).
40. A. M. Chang, M. A. Paalanen, H. L. Störmer, J. C. M. Hwang and D. C. Tsui (this volume).
41. R. B. Laughlin, *Phys. Rev. Lett.* **50**, 1395 (1983).
42. R. Tao and P. J. Thouless (preprint).
43. D. Yoshioka, B. I. Halperin and P. A. Lee, *Phys. Rev. Lett.* **50**, 1219 (1983).
44. P. W. Anderson (preprint).
45. B. I. Halperin, *Proceeding of the Conf. of the Condensed Matter Division of the European Physical Society* (preprint).
46. R. Tao (preprint).
47. F. D. M. Haldane (preprint).
48. H. L. Störmer and W. T. Tsang, *Appl. Phys. Lett.* **36**, 685 (1980).
49. H. L. Störmer, A. C. Gossard and W. Wiegmann (to be published).
50. J. D. Wiley in *Semicond. and Semimetals* **10**, 91 (1975) Academic Press, New York.
51. H. L. Störmer, A. M. Chang, Z. Schlesinger, D. C. Tsui, A. C. Gossard and W. Wiegmann, *Phys. Rev. Lett.* (July 1983).
52. F. J. Ohkawa and Y. Demura, *Suppl. Prog. of Theoret. Physics* **57**, 164 (1975).
53. E. Bangert and G. Landwehr, *Surf. Science*, **58**, 138 (1976).
54. D. Stein, K. v. Klitzing and G. Weinmann (preprint).

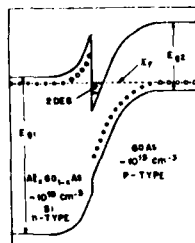


Fig. 1. Band bending in the vicinity of a modulation-doped GaAs-(AlGa)As heterojunction,  $E_F$  is the Fermi energy,  $E_{G1}$  and  $E_{G2}$  are the bandgap energies.

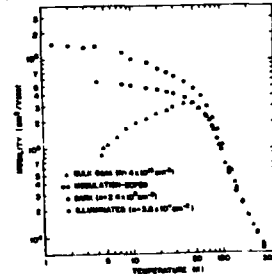


Fig. 2. Comparison of the T-dependence of the mobility between a modulation-doped GaAs-(AlGa)As heterostructure (ref. 13) and high-purity bulk GaAs (ref. 6).

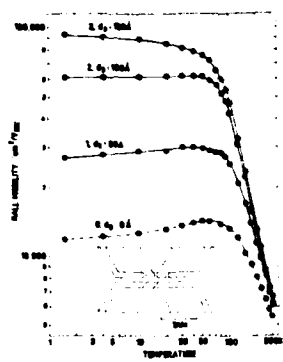


Fig. 3. T-dependence of the mobility of 3 modulation-doped samples with different width ( $d_3$ ) of the undoped (AlGa)As spacer layer. The mobility improves with increasing separation of carrier from ionized impurities. Inset shows the shape of the Hall bridge(ref.18).

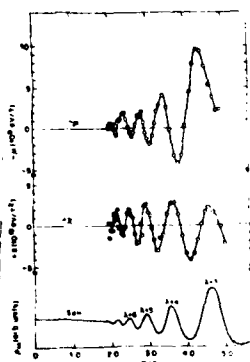


Fig. 4. Experimental result on the dHvA-effect in a 2D electron system of 4,000 stacked layers.  $\mu$  is the magnetic moment and  $\chi$  is the susceptibility. SdH denotes Shubnikov-deHaas data(ref.27).

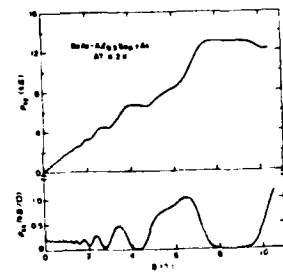


Fig. 5. The quantized Hall effect in a MD GaAs-(AlGa)As heterojunction (ref.30).

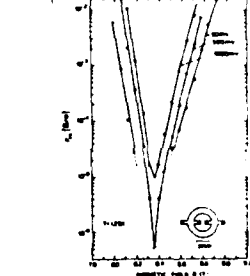


Fig. 6. Diagonal resistivity  $\rho_{xx}$  in the vicinity of 8.4T of Fig.9 at  $T=1.23K$ . Nonlinearities cause slightly different results for 3 different applied voltages.(ref.31).

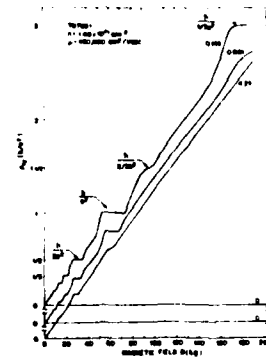


Fig. 7.  $\rho_{xy}$  as a function of magnetic field at 3 different temperatures. A plateau with  $\rho_{xy} = 17.5k\Omega$  at  $\nu = \frac{1}{2}$  is clearly developed. At  $\nu = \frac{2}{3}$  a second plateau appears.(ref.39).

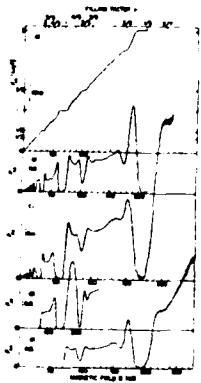


Fig. 8.  $\rho_{xx}$  and  $\rho_{xy}$  data on four different samples at  $T=0.5K$ . Magnetic fields have been scaled to fit a common filling factor scale(top). Minima and plateaus are developed close to a number of rational fractions of  $\nu$ .(ref.38).

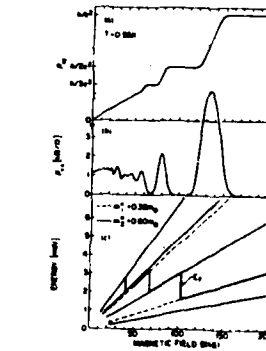


Fig. 9. Quantized Hall effect in a 2D hole system at  $T=0.5K$ . Lower part shows a Landau fan and the Fermi level position using the experimental cyclotron masses. (ref.51)

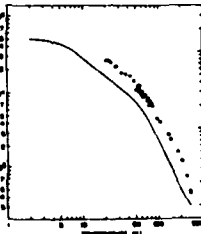


Fig. 10. T-dependence of the mobility of a 2D hole system. Open symbols are bulk data from ref. 49.

## THEORY OF THE QUANTIZED HALL EFFECT

D.J. Thouless

Dept. of Physics FM-15, Univ. of Washington,  
Seattle, WA 98195, USA

**Abstract** A review is given of the current state of the theory of the quantum Hall effect. The integer values of the Hall conductance seen in systems with moderate disorder and predicted for systems with periodic modulation are fairly well understood. Charge density wave and Fermi liquid theories of the fractional quantization observed in systems with low disorder are briefly described.

### 1. Integer Quantization

The discovery by von Klitzing, Dorda and Pepper[1] that the Hall conductance of a two-dimensional electron system can be, with very high precision, an integer multiple of  $e^2/h$  was a triumph of experimental physics. In most comparable cases, such as the quantization of flux in superconductivity or the quantization of circulation for superfluid helium, there have been previous theoretical suggestions of the existence of the effect, even if there were unexpected features in the experimental result. In this case there was no more than approximate quantization suggested[2], and so there was no reason for the experimentalists to examine the transverse voltage in their device with the precision which they used.

Once the discovery had been made we theorists rushed in to show why the result had been obvious all the time. There were a large number of papers, of which I list only a few [3-6], which used bulk perturbative arguments to show that the disorder in the substrate potential gave no correction to the simple quantized result which can be obtained from full Landau levels in an ideal two-dimensional system with no disorder. These arguments are sufficient to show that corrections due to disorder or electron-electron interactions vanish to all orders in perturbation theory. One such argument says that the Lorentz transformation allows us to move to a frame of reference moving with velocity  $-E/B$ , in which there is no electric field, and in this frame the substrate potential makes a local perturbation of the electron density, but does not carry any electron charge with it when the Fermi energy lies in a gap because the perturbation of the electron density falls off exponentially with distance from the perturbing potential. In this frame the current is entirely carried by the positively charged substrate (in an n type layer) moving with velocity  $E/B$ . These arguments also show that localized states, even if they are shifted from the unperturbed Landau level enough to pass through the Fermi surface, do not affect the quantization and do not change the value of the quantized current.

A more profound approach to the problem was introduced by Laughlin[7]. He used gauge invariance to show that, for a system with the topology of an annulus, a change in the flux threading the annulus by an integer amount would lead to the transfer of an integer number of electrons from one edge to the other. Since the change in flux, by Faraday's law, is given by the time integral of the EMF, and the transfer of charge is given by the time integral of the current, it follows that the ratio of current in one direction to voltage in the perpendicular direction is an integer multiple of  $e$  divided by the quantum of flux. This powerful argument has the great advantage that it can be applied in circumstances in which the perturbative arguments are not applicable, such as, for example, when a Landau level is split into sub-bands by a periodic potential; in this case, as I shall discuss in the next section, each sub-band must carry a multiple of the quantized current carried by the entire level. It has the disadvantage that it makes the Hall current appear to be an edge effect, and therefore possibly sensitive to boundary conditions, while the perturbative arguments make it clear

that it is a bulk effect. One knows, however, that two-dimensional bulk effects and edge effects can be related by some version of Stokes' theorem.

All these arguments assume that the electric field is weak. In the perturbative arguments the response linear in the electric field is calculated, while in Laughlin's argument it is assumed that the rate of change of the vector potential is slow enough that the electrons can follow it adiabatically. In a strong field we can be sure that the quantization is not exact, since there will be a tunnelling current parallel to the electric field due to electrons tunnelling from a full Landau level to an empty one, and this longitudinal current must in turn affect the transverse current. Such corrections must depend exponentially on the inverse of the field strength, so it is reasonable to ask if there are any corrections which are algebraic in the field strength. It seems likely, both from the precision of the experimental results and on theoretical grounds, that there are no such algebraic terms, but I do not know of any general proof of this result.

It is generally thought that in the absence of a magnetic field all states in a two-dimensional disordered system are localized [8-10]. The existence of the quantum Hall effect shows that this is not the case in the presence of a magnetic field, since some nonlocalized states are needed to carry the Hall current. The question naturally arises whether in the presence of disorder the Landau level is broadened into a band whose tail states are localized but whose central region consists of extended states, as some numerical calculations have suggested [11], or if all the current is carried at some singular energy, as a simple semiclassical argument suggests [12,13]. If the potential varies slowly over a magnetic length, the electrons should be confined to constant energy curves on the potential surface. For a random potential these curves will either be electron-like, surrounding a minimum, or hole-like, surrounding a maximum. It is only at the singular energy dividing the two that there can be an open orbit capable of carrying a current. In the presence of an electric field this open orbit is broadened into a band of open orbits whose width depends on the field strength. In this model, which seems to give a fairly good account of the experimental situation, the steps between Hall plateaus, and the corresponding regions of nonzero longitudinal resistance, should get sharper and sharper as the electric field strength is reduced. The problem of the existence of extended states in the presence of a magnetic field has recently been discussed on the basis of the nonlinear sigma model [14], but the question of whether the extended states form a broad band or lie at a singular energy is still open.

## 2. Periodic Potentials

It has already been mentioned that a periodic modulation of the substrate breaks the degeneracy of the Landau level in the ideal system and breaks it up into a set of sub-bands separated by gaps. The number of sub-bands produced is  $p$ , where the number of flux quanta per unit cell is  $p/q$ , so the structure of the energy bands is highly sensitive to whether the number of flux quanta per unit cell is rational or irrational. This can be seen most clearly in the energy level diagrams calculated for  $p$  up to about 50 by Hofstadter [15] for a modulation with square symmetry, and by Claro and Wannier [16] for a modulation with hexagonal symmetry. The quantum number associated with the Hall current gives a useful way of classifying the energy gaps in this sort of diagram, and the study of periodic modulations sheds some light on the problem of a random substrate. There are not yet any experiments to which this theory is applicable, but it is likely that some experiments on two-dimensionally modulated layers will be done soon.

Studies of this problem have been made by various authors [17-19]. We found that from the Bloch wave function  $\psi_{k,h}$  the Hall

conductance of a sub-band is given by the integral over the Brillouin zone

$$t = \frac{1}{2\pi} \int d\mathbf{k} \left\{ \left\langle \frac{\partial \psi}{\partial k_1} \right| \frac{\partial \psi}{\partial k_1} \right\rangle - \left\langle \frac{\partial \psi}{\partial k_2} \right| \frac{\partial \psi}{\partial k_2} \right\} \quad (2.1)$$

This is a topological invariant which can be shown to be an integer by using Stokes' theorem to reduce it to an integral round the perimeter of the Brillouin zone, and then the periodicity of the Hamiltonian in the Brillouin zone can then be used to show that the integrand is just the derivative of a phase round the perimeter. A nonzero value of the Hall current implies that the wave function cannot be written as a continuous single valued function satisfying periodic boundary conditions in the unit cell, and therefore well-behaved Wannier functions do not exist for a sub-band with nonzero Hall current. We derived, with some difficulty, the general relation

$$pt + qs = r \quad (2.2)$$

for the Hall current  $t$  in the  $(r-1)$ th gap; all these quantities are integers. This is equivalent to Streda's [18] expression

$$te/h = \rho n / dB, \quad (2.3)$$

where  $n$  is the electron density. For an incommensurate flux density, for which  $p/q$  would have to be replaced by an irrational number, the equation equivalent to 2.2 has a unique solution, but for a rational flux density this equation obviously gives a value of  $t$  which is only determined modulo  $q$ . For the modulation with simple rectangular symmetry we argued that  $s$  should be as small as possible, and this determines the solution uniquely, and apparently correctly. In the case of a modulation with hexagonal symmetry, with its minima at points of sixfold symmetry, there is an additional restriction that  $s$  and  $t$  cannot both be odd. It turns out, however, that  $s$  does not always have the lowest possible magnitude, as can be seen from an inspection of the energy level diagram in Claro and Wannier [16]. The gap for  $p=5, q=1, r=4$  clearly corresponds to  $t=0, s=4$ , not to  $t=1, s=-1$ , for example.

In an indirect fashion this model can shed some light on the idea that in a random potential the Hall current is all carried at one singular energy. A slowly varying potential is one in which  $p$  is much larger than  $q$ . For  $q=1$  it is certainly true that  $t$  is zero below the center of the Landau level and unity above the center, for the square lattice, so that all the Hall current is carried by the central sub-band or pair of sub-bands. If  $q$  is larger than unity each of the sub-bands carries a nonzero current, but it is still true that the sub-bands fall into approximately  $p/q$  groups, with each group other than the central group carrying no total Hall current. The energy gaps within groups are very small compared with the energy gaps between groups. For more rapid modulations, so that  $p$  and  $q$  are of comparable magnitude, the Hall current varies in a rather exotic manner from gap to gap. It is generally true that the larger gaps correspond to smaller Hall currents, but there is no obvious sign that the current is carried in one particular part of the spectrum.

### 3. Fractional Quantization

The discovery of fractional quantization[20] served to undermine the complacency of theorists even further. Recent work seems to show clearly that the Hall conductance of high mobility inversion layers at very low temperatures is precisely  $1/3$ [21], and can probably be other exact fractions, of  $e^2/h$ [22]. So clean an experimental result demands a clear theoretical explanation, and promises to lead to a lot of new and unexpected physics, but, in my opinion, there is so far no theory which matches the elegance of the experimental results.

There are a few things that are generally agreed. In the first place, since the integer Hall quantization is observed in lower mobility devices and the fractional effect is observed in very high mobility devices, and since integer quantization appears to be an almost inevitable consequence of a theory of noninteracting electrons in a weak substrate potential, it seems reasonable to suppose that fractional quantization is a result of the dominance of electron-electron interactions over the effects due to disorder. It is a natural extension of this observation that a model in which the degeneracy of the Landau levels is broken by the Coulomb interaction between electrons, but the substrate potential and transitions to other Landau levels are ignored, should be sufficient to show fractional quantization. It is also clear that any mechanism which makes rational fraction occupation of the Landau level energetically favorable will go a long way towards explaining fractional quantization. The argument from the Lorentz transformation shows that, provided the electrons are not locked to the substrate, a one third full Landau level will carry one third of a quantum of Hall current. Equation 2.3 also shows that if the occupancy of the Landau level is what determines the energy, then it will also give an appropriate fractional Hall current.

Two types of theories which are in accord with the principles outlined in the previous paragraph have been studied. There are models in which there is some sort of charge density wave, and those in which there is no charge density wave. It is natural to expect a charge density wave in such a system, since at very high magnetic fields or very low electron densities the system behaves classically and forms a hexagonal lattice. Yoshioka and Fukuyama[23] and Yoshioka and Lee[24] are among the many authors who have studied this problem recently. There are two major difficulties with this approach, however. The first is that a charge density wave is likely to be pinned by substrate inhomogeneities, as it is in other systems, and should require some minimum electric field to free it from the substrate[25]. The second is that there does not seem to be any particular stability associated with simple fractional occupation of the Landau level, or, equivalently, with the commensurability of the electron lattice and the flux quantum. It can be seen why this is from the type of energy band diagram shown in Claro and Wannier[16]. If there is one electron per unit cell the Fermi energy lies in a gap that extends from the bottom left to the top right of the diagram, and it is easy to show that if the Fermi energy is in a gap the energy is an analytic function of the magnetic field, and so there can be no commensuration energy in a mean field theory. There are gaps that close at simple rational values of the flux density, but it is hard to see how these could lead to enough stable fractional occupations to explain the observed results, or how pinning could be avoided with such a mechanism.

A rather different version of the charge density wave mechanism has been proposed by Haldane[26]. In this model the lattice is locked to commensurate values by the reduced energy of defects such as vacancies and interstitials which occurs when the lattice spacing is commensurate with the flux. The lattice is rigid, and free to carry the Hall current by sliding over the substrate, and it is only the defects that get pinned to the substrate.

Yoshioka, Halperin and Lee[27] have carried out a calculation for up to six electrons in a single Landau level whose degeneracy is broken by the Coulomb interaction. They found some signs of the  $1/3$  quantization even in such a small system, but no charge density wave.

The theory of Laughlin[28] does not involve a charge density wave. In this theory the wave function for the lowest Landau level is written in the form

$$\prod_{i < j} (z_i - z_j)^p \exp(-\sum_i |z_i|^2 / 4 \ell^2), \quad (3.1)$$

where  $z = x - iy$  and  $p$  is odd, so that the level has a  $1/p$  occupation. This gives a specially low energy for commensurate occupation, but has no variations in charge density to provide a pinning mechanism, so it should give a  $1/p$  Hall quantization. It is not immediately obvious how this can be generalized to give fractional occupation with denominator greater than unity, but Anderson[29] has shown how this can be done. The state described by eq. 3.1 has a broken symmetry, and there are  $p-1$  equivalent states that can be generated

from this state by gauge transformations. States with fractional occupation  $q/p$  can be produced by taking the product of  $q$  of these equivalent states.

Our own approach to this problem [30,31] has some features in common with the work of Laughlin [28], although our approach is quite different. We have tried to use conventional many-body techniques to deal with this problem in which the complete degeneracy of the partially occupied Landau level is broken by the Coulomb interaction. The difficulty in comparison with the more usual sort of theory is that the splitting between the energy levels is itself produced by the perturbation, so there is no variable parameter that gives the ratio of the perturbation to the unperturbed energy denominators. On the other hand there is a high degree of symmetry that can be exploited to simplify calculations. In our work so far we have used the Landau gauge, but the symmetric gauge could be used without it making any essential difference, and in that gauge it is easier to compare our results with Laughlin's. We assume that there is some suitable unperturbed ground state in which some fraction of the one-particle states in the Landau level are occupied and the rest are unoccupied. We then use many-body techniques to calculate the self-energies of the various one-particle states. If the occupied states are chosen in a regular manner, so that, for example, one state is occupied and the next  $p-1$  states are unoccupied through the whole array of one-particle states allowed by the boundary conditions, we find an energy gap between the hole and the particle states which stabilizes the  $1/p$  occupation and an enhanced correlation energy. This, like Laughlin's state, has a broken symmetry with  $p$  equivalent ground states. Unfortunately in the present state of the theory we find even denominators as well as the odd denominators found both by the experimentalists and by Laughlin. Tao [31] has generalized the work to cases in which the denominator is greater than unity. If the techniques of many-body theory can be adapted successfully to deal with this problem it will be much easier to calculate the effects of disorder and nonzero temperature.

#### Acknowledgements

I am grateful to Dr. R. Tao for many useful discussions. I am also grateful to the many people who have sent me preprints of their work. This work was supported in part by the National Science Foundation under grant number DMR79-20795.

#### References

- [1] K. von Klitzing, G. Dorda and M. Pepper, *Phys. Rev. Lett.* 45(1980)498
- [2] T. Ando, Y. Matsumoto and Y. Umura, *J. Phys. Soc. Japan* 39(1973)279
- [3] H. Aoki and T. Ando, *Solid State Commun.* 38(1981)1079
- [4] R. E. Prange, *Phys. Rev. B* 23(1981)4802
- [5] D. J. Thouless, *J. Phys. C* 14(1981)3475
- [6] R. E. Prange and R. Joynt, *Phys. Rev. B* 25(1982)2943
- [7] R. B. Laughlin, *Phys. Rev. B* 23(1981)5632
- [8] E. Abrahams, P. W. Anderson, D. C. Licciardello and T. V. Ramakrishnan, *Phys. Rev. Lett.* 42(1979)673
- [9] F. Wegner, *Zeits. f. Phys.* B36(1980)209
- [10] S. Hikami, *Phys. Rev. B* 24(1981)2671
- [11] T. Ando, *Surface Sci.* 113(1982)182
- [12] S. Luryi and R. F. Kazarinov, *Phys. Rev. B* 27(1983)1386
- [13] S. A. Trugman, preprint
- [14] H. Levine, S. B. Libby and A. M. M. Pruisken, preprint
- [15] D. R. Hofstadter, *Phys. Rev. B* 14(1976)2239
- [16] F. H. Claro and G. H. Wannier, *Phys. Rev. B* 19(1979)6068
- [17] D. J. Thouless, M. Kohmoto, M. P. Nightingale and M. den Nijs, *Phys. Rev. Lett.* 49(1982)405
- [18] P. Streda, *J. Phys. C* 15(1982)L717
- [19] D. Yoshioka, *Phys. Rev. B* 27(1983)3637
- [20] D. C. Tsui, H. L. Stormer and A. C. Gossard, *Phys. Rev. Lett.* 48(1982)1559
- [21] D. C. Tsui, H. L. Stormer, J. C. M. Hwang, J. S. Brooks and M. J. Moughton, preprint
- [22] H. L. Stormer, A. Chang, D. C. Tsui, J. C. M. Hwang, A. C. Gossard and W. Wiegmann, preprint
- [23] D. Yoshioka and H. Fukuyama, *J. Phys. Soc. Japan* 47(1979)394
- [24] D. Yoshioka and P. A. Lee, *Phys. Rev. B* 27(1983)4986
- [25] H. Fukuyama and P. M. Platzman, *Phys. Rev. B* 25(1982)2934
- [26] F. D. M. Haldane, preprint
- [27] D. Yoshioka, B. I. Halperin and P. A. Lee, *Phys. Rev. Lett.* 50(1983)1219
- [28] R. B. Laughlin, *Phys. Rev. Lett.* 50(1983)1395
- [29] P. W. Anderson, *Phys. Rev. B* to be published
- [30] R. Tao and D. J. Thouless, *Phys. Rev. B* to be published
- [31] R. Tao, preprint

The Ground State of the 2d Electrons in a Strong Magnetic Field  
and the Anomalous Quantized Hall Effect

D. Yoshioka<sup>(a)</sup>, B. I. Halperin<sup>(b)</sup>, and P. A. Lee<sup>(c)</sup>

<sup>(a)</sup> Institute for Solid State Physics, The University of Tokyo  
Roppongi, Minato ku, Tokyo 106, Japan

<sup>(b)</sup> Department of Physics, Harvard University  
Cambridge, Massachusetts 02138, U.S.A.

<sup>(c)</sup> Department of Physics, Massachusetts Institute of Technology  
Cambridge, Massachusetts 02139, U.S.A.

Abstract

Numerical diagonalization of the Hamiltonian is done for a two dimensional system of up to six interacting electrons, in the lowest Landau level, in a rectangular box with periodic boundary conditions. It is found that the ground state is not a Wigner crystal but a liquid-like state. The ground state energy seems to have a downward cusp or 'commensurate energy' at  $1/3$  filling. Although the nature of the ground state is still not clear, the magnitude of the cusp is consistent with the experimentally observed anomaly in  $\sigma_{xx}$  and  $\sigma_{xy}$  at  $1/3$  filling by Tsui, Stormer and Gossard (Phys. Rev. Lett. 48 (1982)1559). Several properties of the ground state are also investigated.

1. Introduction

Two dimensional electron system in a strong magnetic field without the Coulomb interaction has highly degenerate energy spectrum due to the Landau quantization. The mutual Coulomb interaction should have a large effect on such a system, and it was believed before the discovery of the anomalous quantized Hall effect(1-3) that when the Landau level is partially filled, a charge density wave (CDW) state, which is essentially a Wigner crystal, is formed at zero temperature(4,5). Since the anomalous quantized Hall effect is observed only in samples with high mobility, and since the behavior of  $\sigma_{xx}$  and  $\sigma_{xy}$  indicates impurity effects are not important, it is clear that the Coulomb interaction is essential to this phenomenon and that the anomalous quantized Hall effect is caused by the property of the ground state of two dimensional electrons with Coulomb interaction. However we cannot explain the phenomenon by the formation of the CDW state. Because firstly the total energy of the CDW state is a smooth continuous function of the filling factor of the Landau level  $\nu$ (6), while we need some kind of anomaly at  $\nu=1/3$  to have finite width for the plateau in Hall conductivity  $\sigma_{xy}$  at  $1/3e^2/h$ . Secondly the CDW state is expected to be pinned easily by the impurities, and the pinning makes  $\sigma_{xx}$  quantized not into fractional of  $e^2/h$  but into integer times  $e^2/h$ (7,8). Thus the observation of the anomalous quantized Hall effect requires the discovery of the true ground state for interacting two dimensional electrons in a strong magnetic field. What we must do is to show the existence of the true ground state that is not the CDW state, to clarify the nature of the ground state (which will be a new kind of an ordered state), and to explain the anomalous quantized Hall effect.



We have investigated finite systems to find the ground state. We consider a few electrons in a rectangular cell with periodic boundary conditions. When the size of the cell and number of electrons are small, we can numerically diagonalize the Hamiltonian, and we can obtain the energy and wave function of every eigenstate. In this way we have found that the ground state is not a CDW state but a liquid-like state and that the ground state energy as a function of  $\nu$  deviates downward at simple rational values of  $\nu$  from a smooth interpolation. This investigation does not tell us what is essential for the ground state, so we cannot tell with confidence the behavior of the ground state energy for an infinite system. However if this downward deviations of the ground state energy at simple rational values of  $\nu$  remain for the infinite system as dips in the ground state energy, the anomalous quantized Hall effect can be explained.

Recently Laughlin proposed a trial wave function for  $\nu=1/p$ , where  $p$  is an odd integer (10). Unless  $\nu$  is too small, his wave function also represents a liquid-like state. We investigate the relationship between his wave function and our ground state wave function.

## 2 The ground state for finite systems

We consider a rectangular cell with periodic boundary conditions in the  $x$ - $y$  plane, the boundary of which is given by  $x=0$ ,  $x=a$ ,  $y=0$  and  $y=b$ . A magnetic field  $B$  is applied parallel to the  $z$ -axis. We assume that the magnetic field is so strong that the cyclotron energy  $\hbar\omega_c$  is much larger than typical energy for the Coulomb interaction  $e^2/\epsilon l$ ,  $\epsilon$  the dielectric constant and  $l=(\hbar c/eB)^{1/2}$  the Larmor radius. Then it is a good approximation

to consider only the lowest Landau level. The boundary condition requires that the area of the cell  $ab$  should be  $2\pi l^2 m$ , where  $m$  is an integer. Then the single electron wave function in the Landau gauge,  $A=(0, Bx)$  is given by

$$\phi_j(r) = \left(\frac{1}{b\sqrt{\pi}l}\right)^{1/2} \sum_{k=-\infty}^{\infty} \exp\left\{i\frac{(X_j + ka)y}{l^2} - \frac{(X_j + ka - x)^2}{2l^2}\right\}. \quad (1)$$

Here integer  $j$ ,  $(1 \leq j \leq m)$ , specifies the state, and  $X_j = 2\pi l^2 j/b$  is the  $x$ -coordinate of the center of the cyclotron motion.

When there are  $n$  electrons in this cell, the filling factor  $\nu$  is  $n/m$ . The basis  $n$ -electron wave function is specified by the occupation of the single-electron state:  $(j_1, j_2, \dots, j_n)$ . The total number of the bases is  $\binom{m}{n}$ , and all these bases are degenerate without the Coulomb interaction. The Coulomb interaction mixes these bases, and lifts the degeneracy. Hence we need to diagonalize large Hamiltonian matrices.

The symmetry of the system makes the calculation easier. The total momentum in the  $y$ -direction,  $J = j_1 + j_2 + \dots + j_n \pmod{m}$  is conserved due to the translational symmetry along the  $y$ -axis. Hence the dimension of the Hamiltonian for each  $J$  is approximately  $m^{-1} \binom{m}{n}$ . Two values of  $J$  which differ by a multiple of  $n$  are equivalent due to the translational symmetry along the  $x$ -axis. Hence when  $m$  and  $n$  have no common factor, the energy spectrum of the Hamiltonian is independent of  $J$  and every eigenenergy is at least  $m$ -fold degenerate. On the other hand when  $m$  and  $n$  have a common factor, the states are less degenerate and the ground state is realized only at certain choices of  $J$ . For example at  $m=12$  and  $n=4$ , the three-fold degenerate ground state is found at  $J=2, 6$  and  $10$ . Due to the electron-hole symmetry the system with  $\nu=n/m$  is equivalent to that with  $\nu=(m-n)/m$ . Our

calculations are done for  $\nu \leq 0.5$  and extended to  $\nu > 0.5$  using this symmetry. Finally due to the rotational symmetry the cell with aspect ratio  $a/b$  is equivalent to that  $b/a$ . Hence the calculations are done only for aspect ratio  $a/b \geq 1$ .

Since we are interested in the ground states near  $\nu=1/3$ , the actual diagonalization is done mainly for  $n=4, 5$  and  $6$  and  $0.25 \leq m, m=\nu n \leq 0.5$ , except for  $n=6$  where we calculate only up to  $m=20$ . The ground state energy per electron for the choice of aspect ratio  $a/b=n/4$  is shown in fig.1. (This choice of  $a/b$  seems to give approximate local minimum in the energy). The energy is not a smooth function of  $\nu$  for each  $n$ . When  $m$  and  $n$  have a common factor, the energy becomes lower than a smooth interpolation through every point for each  $n$ . The lowering of the energy is most noticeable at  $\nu=1/3$  and  $\nu=1/2$ . At  $\nu=1/3$  the lowering of the energy or the magnitude of the 'commensurate energy' is almost independent of  $n$ . On the other hand at  $\nu=1/2$  the commensurate energy seems to exist only for  $n=4$  and  $6$  and not for  $n=5$ . This difference may indicate that for the infinite system the commensurate energy or a dip in energy remains at  $\nu=1/3$ , where the anomalous quantized Hall effect is observed, and does not remain at  $\nu=1/2$ , where the effect is not observed, although our system is too small to draw such a conclusion.

To investigate the nature of the ground state, we calculate the pair correlation function  $g(\underline{r})$ .

$$g(\underline{r}) = \int d^2 \underline{r}_1 \langle \rho(\underline{r} + \underline{r}_1) \rho(\underline{r}_1) \rangle_N, \quad (2)$$

where  $\rho(\underline{r})$  is the density operator and  $\langle \rangle_N$  means the normal product. A graph of  $g(\underline{r})$  of the ground state for  $n=4$  and  $m=12$  is shown in fig.2 together with that for one of the excited states.

The  $g(\underline{r})$  for the excited state is almost identical to that of the triangular CDW state obtained by the Hartree-Fock approximation for the infinite system. Hence we identify this state to be the CDW state. On the other hand that of the ground state is quite different from that of the CDW state. The  $g(\underline{r})$  has peaks at  $\underline{r}=(\pm a/2, 0)$  and  $(0, \pm b/2)$ , but not at  $\underline{r}=(\pm a/2, \pm b/2)$  where we would expect to have peaks if the state were a square CDW state. Moreover the shape of the peaks is different from the gaussian peak of the CDW state. This behavior of the  $g(\underline{r})$  suggests that the ground state is a liquid-like state. Overall behavior of  $g(\underline{r})$  of the ground state for other value of  $m$  for  $n=4$  is qualitatively the same. The  $g(\underline{r})$ 's of the ground states for  $n=5$  and  $n=6$  also show liquid-like structure.

For  $n=4$  we find the CDW states at even  $m$ . The energy of the CDW states become minimum at  $a/b=2/\sqrt{3}$  as expected, since at this aspect ratio the CDW state has the hexagonal symmetry. These energies are also shown in fig.1. They seem to lie on a smooth curve, which is consistent with the result of the Hartree-Fock calculation for the infinite system(6). This fact indicates that the dips in the ground state energy are not due to the boundary effect, but come from the intrinsic nature of the ground state.

### 3. Discussion

In the previous section we found that for a finite system the ground state is not the CDW state but a liquid-like state and the ground state energy is especially low at  $\nu=1/3$ . If we extrapolate the present result and speculate that even for an infinite system the ground state is a liquid-like state and has a dip at  $\nu=1/3$  (and possibly at other simple rational values), we can explain the anomalous quantized Hall effect. The dip in the

ground state energy means the existence of an energy gap in the quasi-particle excitation spectrum at  $\nu=1/3$ . That the ground state at  $\nu=1/3$  is only threefold degenerate, in contrast to the highly degenerate ground state for other value of  $\nu$  in the vicinity of  $1/3$ , suggests collective modes also have a gap at  $\nu=1/3$ . Then it will be possible that the liquid-like ground state flows without dissipation, and  $\sigma_{xx}$  is given by the same value as that of free electrons, i.e.  $(1/3)e^2/h$ .

As for the origin of the finite width of the plateau, namely that the quantized value is realized in a finite width of the magnetic field, we can give two explanations. The first explanation is the following. When the filling factor is near  $1/3$ , the ground state is composed of the  $\nu=1/3$  state plus quasi-particle or quasi-hole excitations. If these excitations are localized by impurities, they do not contribute to  $\sigma_{xx}$ , and  $\sigma_{xx}$  is given by  $(1/3)e^2/h$ . If this explanation is correct the width of the plateau should become narrower for a sample with better mobility.

The other explanation is the following. As pointed out by Baraff and Tsunetsugu, the density of the two-dimensional electrons in GaAs-GaAlAs heterojunction is not fixed, but should be determined so as to minimize the total energy of the two dimensional electrons and electrons at the donor levels in the GaAlAs. When the ground state energy is a smooth function of  $\nu$ , the density of the two-dimensional electrons is a smooth, slowly varying function of  $B$ . However at  $\nu=1/3$  the ground state energy per particle has a dip, and when  $\nu$  approaches  $1/3$ , rapid change of the density resulting into pinning of  $\nu$  at  $1/3$  for a finite width of the magnetic field is expected. To estimate the width let us replace the dip in the ground state energy per particle by a  $\delta$ -function singularity,  $-\delta E \delta(\nu - 1/3)$  (12). Then the width of the plateau is

determined by the competition between the energy gain  $n_0 \delta E$ , where  $n_0$  is the electron density at  $\nu=1/3$ ,  $n_0 = (1/3)(2\pi l^2)^{-1}$ , and the charging energy  $2\pi L_d(e\delta n)^2/\epsilon$  to transfer  $\delta n = (\nu - 1/3)/2\pi l^2$  electrons across a depletion layer of thickness  $L_d$ . If we extract a rough estimate of  $\delta E = 0.008(e^2/\epsilon l)$  from fig.1, and we use  $L_d = 240\text{\AA}$  and  $\epsilon = 68\text{\AA}$  ( $B = 15\text{T}$ ), this would lead to a full width of the Hall plateau at  $\nu=1/3$  of  $\Delta\nu/\nu \approx 0.15(L/L_d)^{1/2} \approx 0.16$ , which is consistent with current experiments. In this case the width depends on the thickness of the depletion layer  $L_d$  and independent of the mobility of the sample as long as the ground state is not destroyed. It should also be noticed that if the plateau comes solely from this mechanism, we will never observe the anomalous quantized Hall effect in Si-MOS, where the electron density is fixed externally. Returning to the experiment on GaAs-GaAlAs heterojunction, we notice the magnitude of  $\delta E$  is also consistent with the observed temperature dependence of  $\sigma_{xx}$  and  $\sigma_{xy}$ . The plateau in  $\sigma_{xy}$  and the dip in  $\sigma_{xx}$  begin to appear around  $T = 5\text{K}(2)$ , which is of the same order as  $\delta E/k_B = 1.5\text{K}$ .

Now let us compare our ground state with the trial wave function by Laughlin (10). Since the gauge and the boundary condition are different, we cannot compare the wave functions directly. However there are some evidences which suggest the agreement of the wave functions. Firstly there is a good agreement of the ground state energy. The difference between Laughlin's estimate and the present result for  $n=4$  system is about 0.1% at  $\nu=1/3$  and 0.5% at  $\nu=1/5$ . Secondly the short range behaviors of the wave functions show qualitative agreement. The  $g(\underline{r})$  of the ground state at  $\nu=1/3$  (fig.2(a)) shows a strong depression near origin in contrast to the parabolic  $r$ -dependence for the  $g(\underline{r})$  of the CDW state (fig.2(b)). This is in qualitative

accordance with Laughlin's wave function, which vanishes as  $z, z_i \rightarrow 0$  when  $|z, z_i|$  tends to zero. The same strong depression is seen for  $q(\underline{r})$  of the ground state for  $\nu \leq 1/3$  for each  $n$ . On the other hand for  $\nu > 1/3$ , the  $r$ -dependence of  $q(\underline{r})$  near origin is always parabolic. This behavior suggests that for  $\nu \leq 1/3$  the ground state is made up of Laughlin's  $1/3$  state plus excitations.

However there is a slight disagreement between Laughlin's wave function and our wave function. As a function of one of the electrons, the zeros of Laughlin's wave function coincide with the positions of the other electrons, and around each of these zeros the phase of the wave function changes by  $2\pi/\nu(13)$ . In other words there is a  $2\pi/\nu$  vortices at each position of other electrons. There is no other vortex in the system. On the other hand usually there are  $n$  zeros in our system, each zero being a  $2\pi$  vortex. For  $\nu \leq 1/3$  three  $2\pi$ -vortices, one of which is bound to an electron, gather and form a triplet of  $2\pi$ -vortices. If this triplet merged into a single  $6\pi$ -vortex, our state would be identical to that of Laughlin's. However except for special configurations of electrons there are finite separations of vortices in a triplet of the order of 0.1a or 0.1b, even in the configuration in which the maximum of the wave function is realized. This finite size of the triplet is in disagreement with Laughlin's wave function. However the appearance of the triplet always and only for  $\nu \leq 1/3$  is in qualitative agreement. Hence we think Laughlin's wave function is essentially the same as our ground state wave function at  $\nu = 1/3$ , the slight discrepancy, the finite size of the triplet, being either due to the boundary condition of our system or due to the fact that Laughlin's wave function is a good approximation to the ground state but not the exact ground state.

It is expected that as  $\nu \rightarrow 0$  the CDW state or the crystalline state becomes the ground state. We performed the numerical diagonalization of the Hamiltonian for  $n=4$  down to  $\nu=0.1$  to investigate the cross over of the ground state. We find that the liquid-like state remains the ground state in the whole range of  $\nu$  we have investigated. However the difference between the two states becomes smaller for smaller  $\nu$ , and an extrapolation of the data suggests a cross over near  $\nu=0.075$  in accordance with the expectation, although the numerical value of the cross over point should not be taken literally.

In conclusion we have found that the new liquid-like state is the ground state of the two-dimensional electrons in a strong magnetic field in a wide range of the filling factor  $\nu$  ( $0.1 \leq \nu \leq 0.9$ ); that the properties of this new ground state are consistent with the observed anomalous quantized Hall effect. We investigated the relationship between the present ground state and Laughlin's wave function, and found a qualitative agreement. However we need further investigation to clarify what is essential for the new liquid-like ground state, and what type of order is realized in the ground state, if it is an ordered state.

#### Acknowledgement

The authors thank M.A. Paalanen, H.L. Stormer, and D.C. Tsui for discussion of the experimental data. This work was supported in part by National Science Foundation Grant No. DMR 82-07431, and by U.S. Joint Services Electronics Program Grant No. DAAG 29 83-K-0003.

# References

- (1) D.C. Tsui, H.L. Stormer, and A.C. Gossard, Phys. Rev. Lett. **48** (1982) 1559.
- (2) H.L. Stormer, D.C. Tsui, A.C. Gossard, and J.C.M. Hwang, proceedings of the 18th International Conference on Physics of Semiconductor (to be published)
- (3) H.L. Stormer, A. Chang, D.C. Tsui, J.C.M. Hwang, A.C. Gossard, and W. Wiegmann, Phys. Rev. Lett. **50** (1983) 1953.
- (4) H. Fukuyama, P.M. Platzman, and P.W. Anderson, Phys. Rev. **B19** (1979) 5211.
- (5) D. Yoshioka and H. Fukuyama, J. Phys. Soc. Jpn. **47** (1979) 394.
- (6) D. Yoshioka and P.A. Lee, Phys. Rev. **B27** (1983) 4986.
- (7) H. Fukuyama and P.M. Platzman, Phys. Rev. **B25** (1982) 2934.
- (8) D. Yoshioka, Phys. Rev. **B27** (1983) 3837.
- (9) D. Yoshioka, B.I. Halperin, and P.A. Lee, Phys. Rev. Lett. **50** (1983) 1219.
- (10) R.B. Laughlin, Phys. Rev. Lett. **50** (1983) 1395.
- (11) G.A. Baraff and D.C. Tsui, Phys. Rev. **B24** (1981) 2274.
- (12) This replacement of the dip by a  $\delta$ -function is justified if the width of the dip is narrower than the width of the plateau.
- (13) B.I. Halperin, Helvetica Physica Acta (to be published) (Proceedings of the Conference of the Condensed matter Division of the European Physical Society, Lausanne, March 1983).

# Figure Captions

Fig.1 The energies per particle vs the fractional filling of the first Landau level. The dashed and dotted lines respectively show energy of the electron and hole crystals (the CDW state) resulting from the Hartree-Fock approximation for the infinite system. Open squares, closed circles, and open circles show the ground state energies for  $n=4, 5$ , and 6 electrons for  $\nu \leq 1/2$  and  $n=4, 5$ , and 6 holes for  $\nu > 1/2$ . Closed squares show the CDW state for the  $n=4$  system. The solid line drawn through the  $n=5$  ground state is a guide to the eye only.

Fig.2 Perspective view of the pair correlation function  $g(r)$  for  $n=4$  and  $m=12$  system: (a): that of the ground state and (b): that of an excited state identified as the CDW state. The axes are normalized by the dimension of the cell:  $X=x/a$  and  $Y=y/b$ .

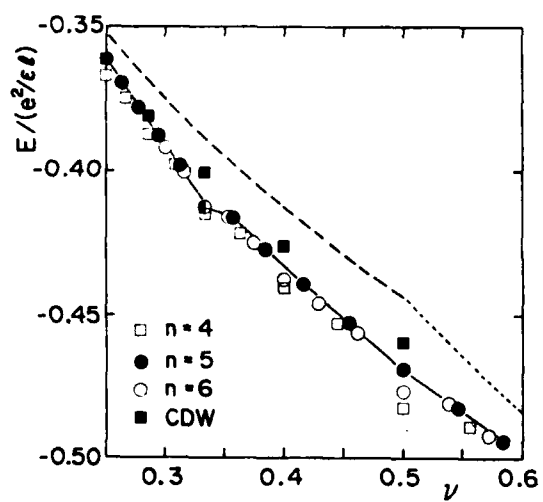


Fig. 1

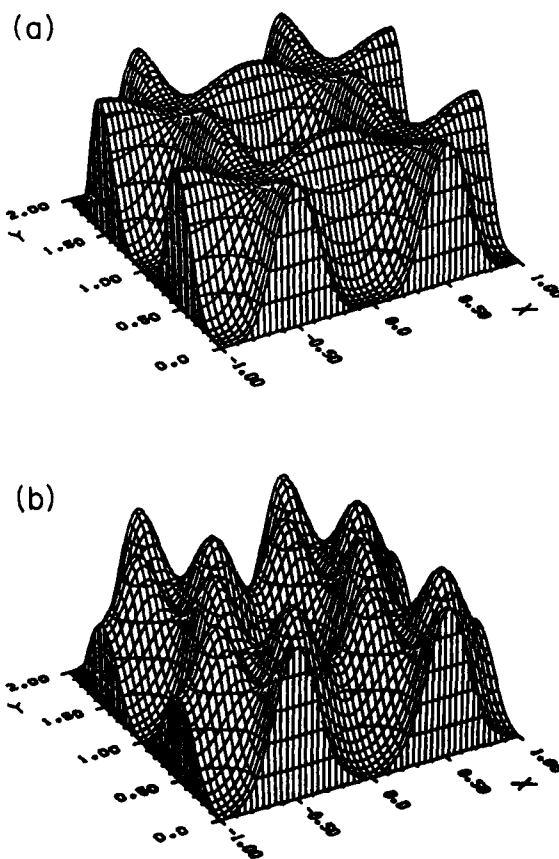


Fig. 2

Anomalous Quantum Hall Effect

R.B. Laughlin

Lawrence Livermore National Laboratory,  
Livermore, CA 94550

- An Invited Paper -

246

Two-Dimensional Magnetism

M. Pomerantz

IBM Thomas J. Watson Research Center,  
Yorktown Heights, NY 10598

- An Invited Review -

247

# THERMOELECTRIC POWER OF SUPERLATTICES

By

Lionel Friedman  
GTE Laboratories, Inc.  
40 Sylvan Road  
Waltham, MA 02254

## Abstract

The low temperature thermoelectric power of a doped superlattice as a function of the Fermi energy (band filling) locates the positions of the edges of the minibands. The thermoelectric power is anisotropic according to whether the temperature gradient is along or perpendicular to the superlattice axis: for momentum relaxation rates proportional to the density of final states and for the Fermi energy in the gap between minibands, it vanishes in the former case, but not in the latter. For the Fermi level near the tops of the minibands, a sign reversal is predicted indicative of hole-like behaviour.

## Introduction

Layered structures with precise interfacial and dimensional control made possible by molecular beam epitaxy (MBE) are the subject of much current interests. The spatial quantization of the electronic energy levels in such single or multiple quantum well structures has been observed in optical absorption (1). When the quantum wells are sufficiently close that there is a spatially periodic, finite overlap of the electronic wave functions of adjacent wells, one has a bona-fide superlattice. The resulting zone folding and broadening of the discrete electronic levels into narrow minibands was the basis for the early predictions of negative differential resistance and Bloch oscillations by Esaki and Tsu (2), and later predictions of nonlinear optical properties of superlattices (3). While analogous phenomena have been observed for the phonon spectra (4), it has not yet been seen for electrons (or holes). However, with continued improvement in growth and interfacial quality made possible by MBE, the electronic miniband

structure will likely be realized (5). For this case, it is shown in the present paper that the low temperature thermoelectric power as a function of the Fermi level (band filling) maps out the location in energy and widths of the minibands, thereby providing basic information about the band structure and density of states distribution of a superlattice. Additionally, information is provided about the scattering mechanisms operative.

The standard form of the electron's dispersion in a superlattice is free-electron-like parallel to the layers, and tight-binding-like perpendicular to the layers, viz:

$$E(k_{||}, k_{\perp}) = \frac{\hbar^2 k_{||}^2}{2m^*} + t(1 - \cos k_{\perp} d), \quad (1)$$

where  $m^*$  is the conduction band effective mass,  $t$  is the transfer integral (half the bandwidth) in the perpendicular direction, and  $d$  is the superlattice period.

The density of states corresponding to eqn. (1) is (6)

$$n_{SL}(e) = \frac{m^*}{\sqrt{2} \hbar^2 d} \times \begin{cases} \cos^{-1} \left( 1 - \frac{e}{t} \right) & 0 < e < 2t \\ \frac{e}{2t} & e > 2t \end{cases} \quad (2)$$

At  $T=0$ , impurities introduced by uniform or modulation doping yield carriers which fill the density of available states. For partial filling of the lowest miniband, the carrier density  $N$  corresponding to a Fermi energy  $\zeta$  is given by

$$N = \frac{m^* t}{\sqrt{2} \hbar^2 d} \left\{ - \left( 1 - \frac{\zeta}{t} \right) \cos^{-1} \left( 1 - \frac{\zeta}{t} \right) + \left[ 2 \left( \frac{\zeta}{t} \right) - \left( \frac{\zeta}{t} \right)^2 \right]^{1/2} \right\} \quad (3)$$

The thermoelectric power  $S$  of a degenerate electron gas may be written (7)

$$S = \frac{e^2}{3} k_B^2 T \left\{ \frac{1}{n(e)} \frac{\partial n(e)}{\partial e} + \frac{1}{v_1^2} \frac{\partial \sqrt{v_1^2}}{\partial e} + \frac{1}{\tau(e)} \frac{\partial \tau(e)}{\partial e} \right\} \quad (4)$$

where  $n(e)$  is the density of states,  $\sqrt{v_1^2}$  is the square of the electron's velocity in the direction of the external temperature gradient averaged over the Fermi surface  $e = \zeta$ , and  $\tau(e)$  is the energy-dependent momentum relaxation time.



Eqn. (4) requires that (1)  $k_B T \ll \epsilon$ , and (2) that the energy dependent quantities be slowly varying on the scale of  $k_B T$ . These conditions will be investigated immediately below.

The logarithmic derivative of  $n_{SL}(\epsilon)$  is found to vary smoothly with  $\epsilon$  through the miniband, but to diverge at the band extrema as

$$\frac{1}{n_{SL}} \frac{\partial n_{SL}}{\partial \epsilon} = \begin{cases} (\tau/2\delta)^{-1} & , \delta \ll 1 \\ (\tau\pi)^{-1} (2\delta')^{-1/2} & , \delta' \ll 1, \\ 0, & \delta > 2 \end{cases} \quad (5)$$

where  $\delta = \tau/\tau$ ,  $\delta' = (2-\delta)$ . The behaviour through the miniband is shown in Fig. 1. However, when the energy variation is sufficient that condition (2) above is violated, the quantity is averaged over an energy interval  $\sim k_B T$  and does not diverge. But for layers sufficiently thin to show superlattice banding, e.g. a typical GaAs-GaAl<sub>x</sub>As<sub>1-x</sub> superlattices ( $d \sim 50\text{\AA}$ - $70\text{\AA}$ ), Kronig-Penney calculations yield bandwidths  $2t \sim 60$ - $120$  meV (3). Since  $k_B T$  in low temperature thermoelectric power measurements can be made significantly smaller than this, most of the variation through the band will be discernable, except very close to the miniband edges. Of course for  $\delta > 2$  in the "gap",  $\partial n_{SL}/\partial \epsilon = 0$ . Thus the positions of the miniband edges are indicated. We also find that for carrier densities  $10^{16}$ - $5 \times 10^{17} \text{ cm}^{-3}$ , condition (1) is also satisfied for typical superlattice configurations.

Turning next to the second term in the brackets of eqn. (4), there are two cases according to whether the temperature gradient is parallel or perpendicular to the layers. For the first case,  $v_1 = \hbar k_x/m^*$ , it is found that

$$\frac{1}{v_1^2} \frac{\partial v_1^2}{\partial \epsilon} = \frac{1}{t} \frac{1}{(\delta-1)\cos^{-1}(1-\delta) + (2\delta-2)^{1/2}} \left[ \cos^{-1}(1-\delta) + \frac{(1-\delta)}{(2\delta-2)^{1/2}} \frac{1}{\cos^{-1}(1-\delta)} \right], \delta < 2$$

$$= t^{-1}(\delta-1), \delta > 2$$

(6)

250

while in the second case,  $v_1 = (\tau d/\hbar) \sin k_x d$ ,

$$\frac{1}{v_1^2} \frac{\partial v_1^2}{\partial \epsilon} = \frac{1}{2t} \frac{1}{(2\delta-2)^{1/2} (1-\delta) - \cos^{-1}(1-\delta)} \left[ \frac{(2\delta-2)^{1/2} (1-\delta)^2 - (2\delta-2)^{1/2}}{\cos^{-1}(1-\delta)} \right], \delta < 2$$

$$= 0, \delta > 2$$

(7)

Both eqn. (6) and (7) tend to diverge as  $\delta^{-1}$  at the bottom of the band, and as  $-(\delta')^{1/2}$  at the top of the band, i.e. a sign reversal indicative of hole-like behaviour is found here. Their behaviour are very similar and is shown in Fig. 1.

The removal of the divergences just at the band edges occurs for the same reasons as for the density of states.

Finally, we consider the third term in the brackets of eqn. (4). In contrast to the bulk or an isolated quantum well, the momentum relaxation rates are not known for all the scattering mechanisms of interest in the case of a true superlattice. Unlike the quantum well case, there is a density of final states with momenta along the superlattice axis into which the carrier can scatter. One result derived for a superlattice is that of deformation potential scattering under the usual assumptions of elastic scattering and phonon equipartition (6). For this case  $\tau_{DP}^{-1}(\epsilon) \sim n_{SL}(\epsilon)$ , the logarithmic derivative of  $\tau_{DP}^{-1}$  exactly cancels the first term of eqn. (4), and the entire contribution to  $S$  comes from eqns. (6) and (7), exhibiting the sign reversals at the tops of the minibands. On the other hand, if energy independent rates characteristic of a quantum well (infinite potential barriers) are assumed (8), the logarithmic derivative of  $\tau^{-1}$  vanishes, and the contributions to  $S$  are the sums of eqns. (5), (6), and (7). In this case, the sign reversals at the tops of the minibands do not occur. Also, as shown by eqns. (5), (6), and (7) for the case  $\delta > 2$  (Fermi energy above the top of the lowest miniband), these contributions to  $S$  vanish when the temperature gradient is along the superlattice axis, but not when it is parallel to the layers. The reason is that there is no coherent transport of carrier kinetic energy perpendicular to the

251

layers when the Fermi level is in the gap between minibands. If rates proportional to the density of final states multiplied by the carrier energy to some power  $\epsilon^p$  are assumed (the latter characterizing the energy dependence of the matrix element), then an additional slowly varying term  $\sim p/\epsilon$  contributes for both orientations of the thermal gradient, and  $S$  never vanishes for the Fermi level in the "gap". However, the tendency of  $S$  to "diverge" at the miniband extrema occurs in all cases, indicating the location in energy of the miniband edges.

#### References

1. R. Dingle, in *Festkörperprobleme (Advances in Solid State Physics)*, edited by H. J. Queisser (Pergamon/Vieweg, Braunschweig, 1975) vol. 15, p. 21
2. L. Esaki and R. Tao, *IBM J. Research and Development*, 14 (1970) 61
3. W. L. Bloss and L. Friedman, *Appl. Phys. Lett.* 41 (1982), 1023
4. C. Colvard, R. Merlin, M. V. Klein, and A. C. Gossard, *Phys. Rev. Letters* 45 (1980) 298.
5. L. L. Chang and L. Esaki, *Proc. Third International Conf. on Electronic Properties of Two-Dimensional Systems*, Surface Science (1980).
6. J. P. Palmier and Y. Ballini, *J. Physique* 41 (1980) L539
7. D. K. C. MacDonald, *Thermoelectricity: An Introduction to the Principles* (John Wiley and Sons, 1962).
8. B. K. Ridley, *J. Phys. C* 15 (1982) 5899

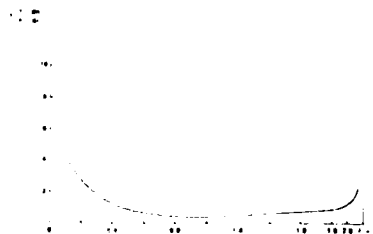


Figure 1: Logarithmic Derivative of Superlattice Density of States vs. Energy.

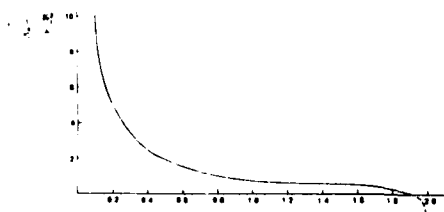


Figure 2: Logarithmic Derivative of Energy of Transport vs. Energy.

Thermoelectric Effects in Silicon MOSFETs  
in High Magnetic Fields

R.P. Smith, H. Closs\*, and P.J. Stiles  
Brown University, Providence, Rhode Island 02912, USA  
\*present address: INPE, 12200 S.J. dos Campos, Sao Paulo, Brazil

**ABSTRACT:** The thermopower in quantized Hall systems has been suggested to be a sensitive probe of electron transport. We performed experiments on [100] silicon MOSFETs at temperatures of 1.8 K to 4.25 K, temperature differences of 0.01 K to 0.5 K, and magnetic inductions of 8 tesla. Results are presented which clearly show mobility edges within Landau levels and also a signal which is apparently due to the temperature dependence of the edge states.

Introduction:

The thermoelectric effect is often used to examine the nature of electronic states in conducting systems, yet to date it has not been used in studying quantized Hall systems. It is of particular interest in these systems for a number of reasons. First, the thermopower is very sensitive to the presence of mobility edges [1], and it has been suggested that large numbers of localized states are the cause of the width of Hall steps. Also, it has been suggested that there is a thermopower which is due to the temperature dependence of the conducting edge states [2], so measurements should be a good test of that theory of quantized Hall conduction. Finally, if an appreciable thermoelectric effect does exist it may affect the very high accuracy quantum Hall studies now being done in several laboratories.

Results are presented of studies of thermoelectric voltages in [100] silicon inversion layers. The temperatures of the sample range from 1.8 K to 4.25 K while the temperature gradients for the reported results range from 0.01 K to 0.1 K. The data clearly show mobility edges within Landau levels and also appear to show a signal corresponding to the edge states' temperature dependence. Transverse data is presented as well. All of

these results are preliminary in nature; more complete data will be presented soon.

Theory:

As was mentioned above, Girvin and Jonson proposed the existence of a new type of thermopower based on the temperature dependence of the states edges of the inversion layer. They predict that the thermopower should reach maxima when the chemical potential is at mid-level and that these maxima should equal  $-\ln 2 (k_B T) / (1 + 1/2)$  where  $l$  is the Landau level index. They also predict that in the absence of impurity scattering the transverse component of the thermopower should equal zero.

A thermopower can also result from the presence of a mobility edge [1,3]. This type of thermopower occurs when the Fermi level is near the mobility edge and the temperature gradient causes an inhomogeneous distribution of carriers in the extended states.

Large numbers of localized states have been suggested to be the reason for the widths of Hall steps in two dimensional systems. The thermopower should be a good probe of the location of the transitions from localized to extended states and may well give information on the numbers of extended states in mostly localized regions and vice-versa. According to Fritzsche's results [3] and assuming a reasonably high number of localized states a thermopower of the order of  $100 \mu V/K$  can be expected.

Experiment:

The metalization mask for the sample is shown in fig. 1. The thermoelectric voltage was measured on the long Hall bar. The temperature gradients were determined by combining data from the small

Corbino geometry devices with the known  $a/l^3$  dependence of the thermal conductivity at low temperatures. The constant  $a$  is a function of the material, the sample's geometry, and its surfaces. It was determined empirically and may be a large source of error in the experiments. All of the MCFETs are on (100) silicon and have mobilities of about 4500 cm<sup>2</sup>/V-sec at 4.2 K. There are no diffused regions at the ends of the Hall bar that serve as heaters. Temperature gradients are created by clamping the sample at one end and passing an electrical current through the heater at the opposite end. The entire apparatus is then heated and pumped down to about  $10^{-5}$  torr to reduce any extraneous thermal losses.

Heat was applied with an AC voltage at 7 Hz. The temperatures at the clamp range from 1.6°K to 4.2°K, and the applied heat raises the sample temperature from 0.15°K for the 4.2°K data to 0.35°K for the 1.6°K data at the peaks of the heater signal.

#### Results:

The longitudinal component of the thermopower is shown in fig. 2. The locations of the mobility edges are clearly shown by the peaks and dips in the thermopower. There are large numbers of localized states below  $\epsilon = 4 \pm 0.8$  and above  $\epsilon = 4 \pm 1.5$  where  $l$  is an integer. The indexing counts each spin and valley split level individually, but conductance data (not shown) shows only weak spin splitting. The structure in the centers of the levels indicates that there are large numbers of localized states at the edges of spin split levels. The relative weakness of this structure is probably due to some overlap of levels along with the coexistence of extended and localized states in these regions.

The transverse component of the thermal voltage is also shown in

fig. 2. It is not known why the signal is so large for the low indices. It seems reasonable that the reduction in signal in the longitudinal case for small indices and the corresponding rise in the magnitude of the transverse case may be due to the larger influence of impurity scattering for the lower indices.

The temperature dependence of the thermopower as measured from the source to the drain is shown by the two curves in fig. 3. The broad features in the 4.2°K data are thought to be due to, in addition to the mobility edge signal, the thermopower proposed by Girvin and Jonson [1]. Measuring the thermal voltage from the source to the drain is expected to give some combination of the longitudinal and transverse components of the thermopower because of the fact that the diffused regions will tend to change the apparent conductivity between the two sides near the ends of the sample. This is reflected in the 1.8 K data.

The method for measuring temperature gradients has not yet been perfected, so there is an uncertainty of 25 to 50% in the absolute values of the stated temperature gradients and thermopowers. This uncertainty does not carry over to relative comparisons.

#### Conclusions:

The thermopower has been shown to be a sensitive probe of the nature of electronic conduction in a quantized two-dimensional electron gas. At low temperatures, the longitudinal component of the thermopower clearly marks the locations of mobility edges, and it may be possible to obtain better information on the relative numbers of localized and extended states in the future. At around 4.2°K the signal predicted by Girvin and Jonson becomes dominant.

Future plans include using higher mobility samples, which may yield more information in the first few levels, especially for the transverse data. Lower temperatures and higher fields can also be used. A direct comparison between the number of localized states derived from the thermopower and from  $\rho_{xx}$  and  $\rho_{xy}$  in the same sample will also be made.

#### Acknowledgements:

The authors wish to thank R.G. Wheeler and his coworkers for help and advice in preparing samples along with Keith Warner, William Patterson, Dale Syphers, and Ray Zeller of Brown University.

This work was supported by the NSF under contract DMR-8211238.

#### References:

- [1] M. Cutler and N.F. Mott, Phys. Rev. 181 (1969)pp. 1336-1340.
- [2] S.M. Girvin and M. Jonson, J. Phys. C:Solid State Phys., 15 (1982) pp. 1147-1151.
- [3] H. Fritzche, Sol. State Comm. 9 (1971) pp. 1813-1815.
- [4] W.S. Hurst and D.R. Frankl, Phys. Rev. 186 (1969)pp. 801-810.
- [5] A.K. McCurdy, H.J. Meris, and C. Elbaum, Phys. Rev. B2 (1970)pp.4077-4083.

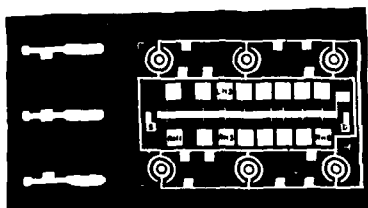


Fig 1. Metalization mask for sample. Longitudinal data was taken between RH1 and RH8; transverse data between RH3 and LH3. The probes contact the inversion layer at the small bumps on the Hall bar alongside the marked contacts. S and D denote the source and drain.

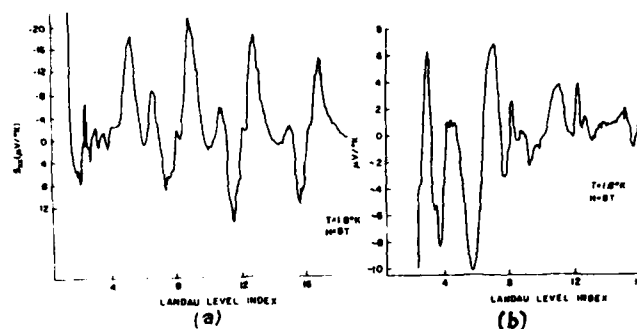


Fig. 2. (a) Longitudinal (RH1-RH8) thermopower. The sample was modulated at 7 Hz, with a temperature gradient of about  $0.1^{\circ}\text{K}$ . (b) Transverse (RH3-LH3), taken under the same conditions as (a).

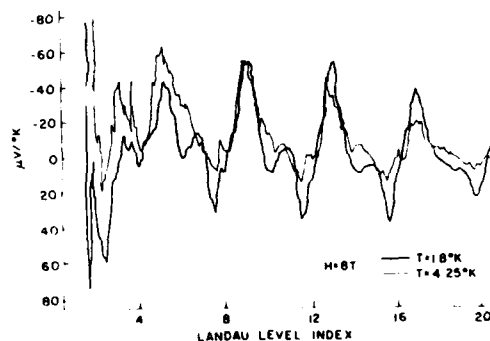


Fig. 3. Source-Drain thermopower. The  $1.8^{\circ}\text{K}$  data was taken under the same conditions as above; the  $4.25^{\circ}\text{K}$  data was taken with a temperature difference of  $0.01^{\circ}\text{K}$ .

# ANALYSIS OF QUANTIZED HALL RESISTANCE AT FINITE TEMPERATURES

B. Tausendfreund and K. v. Klitzing  
Physik-Department, Technische Universität München  
D-8046 Garching, Fed. Rep. of Germany

## Abstract

High resolution measurements of the Hall resistivity  $\rho_{xy}$  within the Hall plateaus show that the slope is finite at finite temperatures but decreases exponentially with inverse temperature. This behavior is observed even in a temperature range where the resistivity  $\rho_{xx}^{\min}$  is only weakly temperature dependent due to scattering processes interpreted as variable range hopping.

A characteristic feature of the quantized Hall resistance is the appearance of plateaus in the Hall resistance as a function of the magnetic field or the gate voltage<sup>/1/</sup>. These plateaus are explained by a pinning of the Fermi level in the gap (mobility gap) between two Landau levels by a reservoir of localized electrons. A large number of calculations indicate that localized states in the tails of the Landau levels are responsible for the observations<sup>/2-6/</sup>, but also trap states outside the channel of the 2DEG or edge states may contribute to the development of plateaus<sup>/7,8/</sup>. Information about the density of states in the plateau region and their contribution to the Hall effect at finite temperature is not available. In this paper we present measurements of the resistivity components  $\rho_{xx}$  and  $\rho_{xy}$  on silicon MOSFETs and GaAs-Al<sub>x</sub>Ga<sub>1-x</sub>As heterostructures in the temperature range

1.5 K < T < 10 K at filling factors  $\nu = N_s h/eB$  close to an integer  $i$  ( $N_s$  = surface carrier density).

High resolution data for  $\rho_{xy}$  in the plateau region are obtained using an a.c. bridge<sup>/9/</sup>. Fig. 1 shows experimental results for a silicon MOSFET. The resistivity  $\rho_{xx}$  close to the filling factor  $i = 8$  is plotted in the upper part of this figure for different substrate bias voltages or after illumination with an infrared LED. The variation of  $\rho_{xy}$  as a function of the gate voltage is shown in the lower part of Fig. 1. These data demonstrate that a quantitative analysis of the shape of Hall plateaus is difficult because an anomalous minimum in  $\rho_{xy}$  (which disappears at higher temperatures) is visible at a filling factor slightly smaller than a completely filled Landau level. The depth of this minimum increases drastically, if the threshold voltage is changed by infrared illumination or substrate bias voltage. Calculations show that the corrections due to the finite aspect ratio of the devices<sup>/10/</sup>, which reduce  $\rho_{xy}$  if the Hall angle deviates from 90°, are not responsible for the minima. We believe that inhomogeneities lead to the observed structures.

For a quantitative analysis of the experimental curves we used only measurements where the Hall resistivity  $\rho_{xy}$  shows no anomalous structures. This means that  $\rho_{xy}$  varies approximately antisymmetrically relative to the gate voltage of a fully occupied Landau level (this condition is always obtained at not too low temperatures because the minimum shown in Fig. 1 disappears rapidly with increasing temperature). Under this condition, the minimal slope  $d\rho_{xy}/dN_s$  seems to be the adequate quantity for the characterization of the so-called Hall plateaus. In the temperature range where  $\rho_{xx}^{\min}$  is thermally activated<sup>/11,12/</sup>,  $d\rho_{xy}/dN_s$  is directly proportional to  $\rho_{xx}^{\min}$ . This is shown in Fig. 2 where  $\rho_{xx}^{\min}$  has been changed by a factor of  $10^3$  by varying the temperature of the magnetic field. The one-to-one relation between  $\rho_{xx}^{\min}$  and  $d\rho_{xy}/dN_s$  can be explained within the model that only the

extended states close to the center of the Landau levels contribute to  $\rho_{xx}$  and  $\rho_{xy}$  and that a variation  $dN_s$  in the carrier density corresponds to a temperature and magnetic field independent variation of the Fermi energy  $dE_F$ . Calculations show that both  $\rho_{xx}$  and  $d\rho_{xy}/dN_s$  are determined by the same exponential factor  $\exp(-\Delta E/2kT)$  where  $\Delta E$  is equal to the cyclotron energy for an idealized system, but is usually smaller due to the spin-splitting and a finite linewidth of the extended states.

Theoretically, the ratio  $(d\rho_{xy}/dN_s) : \rho_{xx}^{\min}$  depends on the density of states  $D_1$  in the mobility gap. Preliminary calculations on the basis of an elliptic form for the density of extended states and an energy independent contribution  $D_1$  of localized states yield a relatively large value of  $D_1 > 0.1 D_0$  ( $D_0$  = density of states without magnetic field). However, this result depends on the model used for the calculation and may be unrealistic.

It is known that at low temperatures  $\rho_{xx}^{\min}(T)$  deviates from a thermally activated behavior<sup>13/</sup>. This can be interpreted as an additional contribution to the scattering rate by variable range hopping. Such a contribution is not visible in Hall effect measurements as shown in Fig. 3. The slope  $d\rho_{xy}/dN_s$  decreases exponentially with decreasing temperature even in the temperature range where  $\rho_{xx}^{\min}$  is only weakly temperature dependent. The activation energy deduced from  $d\rho_{xy}/dN_s(T)$ -data (Fig. 3) at high magnetic fields ( $B > 10$  T) agree within  $\pm 3\%$  with the cyclotron energy  $\hbar\omega_c$  minus spin-splitting  $\Delta s$ . Measurements at lower magnetic field values ( $B = 8.1$  T for silicon MOSFET and  $B = 4.1$  T for GaAs-Al<sub>x</sub>Ga<sub>1-x</sub>As heterostructure) yield  $\Delta E$ -values which are up to 20% smaller than calculated from  $\hbar\omega_c - \Delta s$ . Such a reduction in the activation energy has been obtained from an analysis of the exponential part in the  $\rho_{xx}(T)$  curves, too, and may originate from the broadening of the Landau levels.

In conclusion, the analysis of the slope  $d\rho_{xy}/dN_s$  or  $d\rho_{xy}/dB$  of the

Hall plateaus at helium temperature demonstrates that this slope shows an activated behavior corresponding to  $d\rho_{xy}/dN_s \sim \exp(-\Delta E/2kT)$ . At high magnetic fields ( $B > 10$  T for high-mobility silicon MOSFETs)  $\Delta E$  agrees with the energy gap between discrete Landau levels. This activated behavior is visible even in the temperature range where the resistivity  $\rho_{xx}^{\min}$  is dominated by a scattering process interpreted as variable range hopping. This result supports the conception that hopping contributes less to Hall effect than one would expect from normal conductivity.

The work has been supported by the Stiftung Volkswagenwerk.

#### References

- 1) K. v. Klitzing and G. Ebert in: Proc. of the 16th Int. Conf. on Physics of Semicond., Montpellier 1982, Ed. M. Averons (North-Holland Publ. Comp., Physica 117B + 118B (1983), p. 682)
- 2) R.E. Prange, Phys. Rev. B 23, 4802 (1981)
- 3) H. Aoki and T. Ando, Solid State Commun. 38, 1079 (1981)
- 4) T. Ando, Surf. Science 113, 182 (1982)
- 5) J.T. Chalker, this conference
- 6) W. Brenig, to be published
- 7) G.A. Baraff and D.C. Tsui, Phys. Rev. B 24, 2274 (1981)
- 8) H. Bando, Solid State Commun. 1983 (to be published)
- 9) K. v. Klitzing, B. Tausendfreund, H. Obloh, and T. Herzog, Lecture Notes in Physics 177, 1 (1983)
- 10) K. v. Klitzing, Advances in Solid State Physics XXI, 1 (1981)
- 11) Th. Englert and K. v. Klitzing, Surface Science 73, 70 (1978)
- 12) R.J. Nicholas, R.A. Stradling, S. Askenazy, P. Perrier, and J.C. Portal, Surface Science 73, 106 (1978)
- 13) G. Ebert, K. v. Klitzing, C. Probst, E. Schuberth, K. Ploog, and G. Weimann, Solid State Commun. 45, 625 (1983)

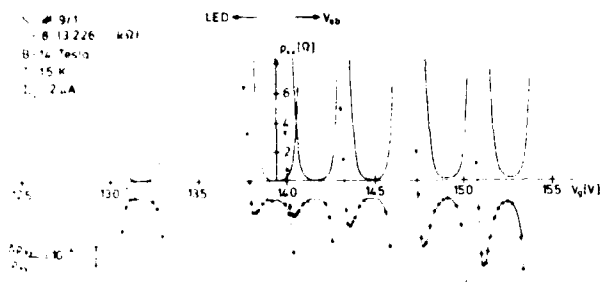


Fig. 1: Resistivities  $\rho_{xx}$  and  $\rho_{xy}$  close to the filling factor  $i = 8$  for different substrate bias voltages ( $V_{sb}$ ) or after illumination with an infrared LED.

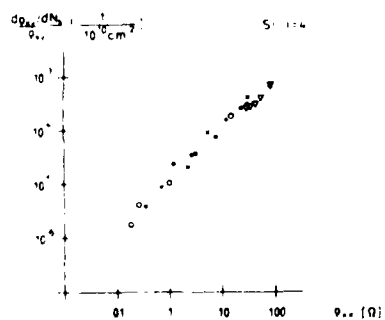


Fig. 2:  
Minimal slope of the Hall resistance  $d\rho_{xy}/dV_g \sim d\rho_{xy}/dN_s$  as a function of the minimal resistivity  $\rho_{xx}$ . The magnetic field is varied between 8.4 T < B < 13 T, the temperature between 1.5 K < T < 4.2 K, and the substrate bias voltage between -9 V <  $V_{sb}$  < 0 V.

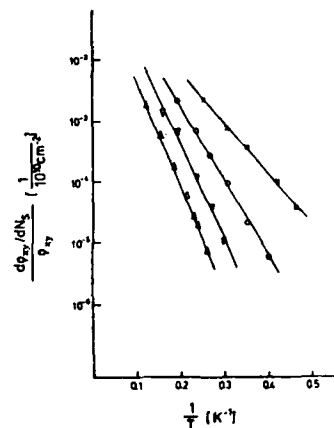
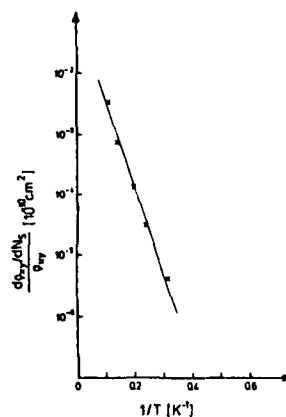
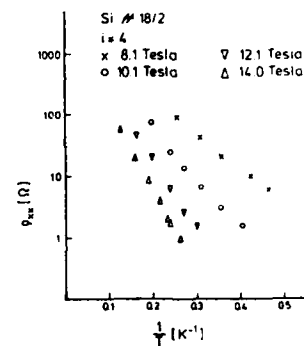
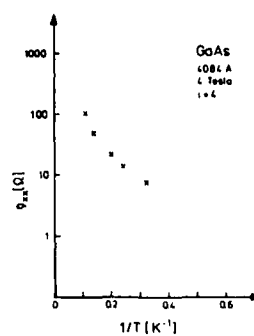


Fig. 3:  $\rho_{xx}^{\min}$  and minimal slope  $d\rho_{xy}/dN_s$  (or  $d\rho_{xy}/dB \sim -d\rho_{xy}/dN_s$ ) as a function of inverse temperature ( $1/T$ ) for a GaAs-Al<sub>x</sub>Ga<sub>1-x</sub>As heterostructure and a silicon MOSFET.  $d\rho_{xy}/dN_s$  remains activated even if  $\rho_{xx}^{\min}$  is saturated due to variable range hopping.



QUANTUM HALL EFFECT AND HOPPING CONDUCTION  
IN  $\text{In}_{1-x}\text{Ga}_x\text{As-InP}$  HETEROJUNCTIONS AT LOW TEMPERATURE

Y. Guldner<sup>x</sup>, J.P. Hirtz<sup>\*\*\*</sup>, A. Briggs<sup>\*\*\*\*</sup>, J.P. Vieren<sup>\*\*</sup>, M. Voos<sup>\*\*</sup>,  
and M. Razeghi<sup>\*\*\*\*</sup>

<sup>\*\*</sup> Groupe de Physique des Solides de l'E.N.S., 24 rue Lhomond, 75005 Paris, France.

<sup>\*\*\*\*</sup> L.C.R., Thomson-C.S.F., 91401 Orsay, France.

<sup>\*\*\*</sup> C.R.T.B.T. and S.N.C.I., C.N.R.S., 38042 Grenoble, France.

ABSTRACT

We report investigations of the temperature dependence of the quantum Hall effect in modulation doped  $\text{In}_{1-x}\text{Ga}_x\text{As-InP}$  heterojunctions. The diagonal conductivity  $\sigma_{xx}$  is studied at several minima of the magneto-resistance  $\rho_{xx}$  between 50 mK and 2 K. A hopping conduction mechanism is observed when the Fermi level is in the tail of the Landau levels.

Hall effect measurements on a two-dimensional electron gas (TDEG) show that the Hall resistivity at low temperature and high magnetic field presents plateaus which are equal to the quantized values  $\rho_{xy} = h/ie^2$ , where  $i = 1, 2, \dots$  is the number of filled Landau levels. Simultaneously, the magneto-resistance  $\rho_{xx}$  vanishes. The Quantum Hall Effect (QHE) was first observed in Si MOSFET's<sup>1</sup> and, then, in modulation doped GaAs-Al<sub>x</sub>Ga<sub>1-x</sub>As<sup>2</sup> and  $\text{In}_{1-x}\text{Ga}_x\text{As-InP}$ <sup>3</sup> heterojunctions. This effect implies that the Fermi level is pinned between Landau levels over finite ranges of magnetic field B. In strong magnetic fields the TDEG Landau level energy separation becomes large compared to the Landau level linewidth, and only the tails of adjacent levels overlap. The electrons whose energies fall in these tails are localized due to disorder<sup>4</sup>, and the localized states are separated from the extended states in the center of each Landau level by a mobility edge. The pinning of the Fermi level  $E_F$  is due to the existence of such localized states and, when  $E_F$  is in a mobility gap between two Landau levels, the conductivity  $\sigma_{xx}$  drops to zero as the temperature is decreased, the conduction occurring by variable range hopping

at very low temperature. Quite recently, interesting low temperature magneto-transport studies below 1 K have been reported in GaAs-Al<sub>x</sub>Ga<sub>1-x</sub>As<sup>5-8</sup> and  $\text{In}_{1-x}\text{Ga}_x\text{As-InP}$ <sup>9</sup> heterojunctions. We want to report here recent investigations of the temperature dependence of the QHE and  $\sigma_{xx}$  performed down to 50 mK in modulation-doped  $\text{In}_{1-x}\text{Ga}_x\text{As-InP}$  heterojunctions and the observation of a variable range hopping conduction  $\sigma_{xx}$  in the vicinity of the magneto-resistance minima.

The  $\text{In}_{1-x}\text{Ga}_x\text{As-InP}$  heterojunctions, which correspond to  $x = 0.53$ , were grown by low-pressure metalorganic chemical vapor deposition<sup>10</sup> on (100) semi-insulating Fe-doped substrates. The InP layer (2000 Å thick) was n-type with  $N_D - N_A \sim 3 \times 10^{16} \text{ cm}^{-3}$ . The  $\text{In}_{1-x}\text{Ga}_x\text{As}$  layer was also n-type with  $N_D - N_A \sim 1.5 \times 10^{15} \text{ cm}^{-3}$  and its thickness was equal to 1 μm. The electron densities and the mobilities at 4.2 K were  $4.5 \times 10^{11} \text{ cm}^{-2}$  and  $33,000 \text{ cm}^2 \text{ V}^{-1} \text{ sec}^{-1}$  (sample 1), and  $3 \times 10^{11} \text{ cm}^{-2}$  and  $80,000 \text{ cm}^2 \text{ V}^{-1} \text{ sec}^{-1}$  (sample 2). Usual Hall bridges were used to measure  $\rho_{xx}$  and  $\rho_{xy}$ . The sample was cooled in a dilution refrigerator, and the magnetic field B, perpendicular to the interface, was provided by a superconducting coil and could be swept continuously from 0 to 9 T.

Figure 1 shows data obtained at 1.85 K and 55 mK for  $\rho_{xy}$  and  $\rho_{xx}$  as a function of B for a current equal to  $10^{-8} \text{ A}$  in sample 1. The temperature dependence of the QHE is essentially characterized by an increased width of the  $\rho_{xy}$  plateaus and by a narrowing of the associated  $\rho_{xx}$  peaks when T is decreased. We have investigated particularly the width of the  $\rho_{xy} = h/4e^2$  plateau between 4.2 K and 50 mK. As shown in the inset of Figure 1 (a), this width ranges with an accuracy of the order of 0.5 %, from 30 % to 80 % of its largest possible value obtained from the midpoints of the adjacent steps. A similar variation is obtained in sample 2 for the  $\rho_{xy} = h/2e^2$  plateau which occurs in the same magnetic field region (Fig. 2). At low temperature  $\rho_{xx}$  decreases with decreasing temperature even at the Shubnikov-de Haas peaks, where, for quantum numbers  $n > 2$ , the logarithmic dependence  $\delta\sigma_{xx} = 0.8 \times 10^{-5} \ln T$  (who) is observed between 0.2 and 2 K. This dependence, previously observed in GaAs-Al<sub>x</sub>Ga<sub>1-x</sub>As heterojunctions<sup>5</sup>, may be due to Coulomb interactions in the TDEG under high magnetic field as pointed out by Girvin et al.<sup>11</sup>.

Completely different results are observed for the  $\sigma_{xx}$  minima as presented in Fig. 3 (a) which shows, in sample 1, the temperature dependence of  $\sigma_{xx}$  at three  $\rho_{xx}$  minima, namely between the  $n = 2$  and  $n = 3$  (curve A), the  $n = 1$  and  $n = 2$  (curve B), and the  $n = 1$  spin-split (curve C) Landau levels (see Fig. 1). Curves A, B and C correspond to  $B = 3.3, 4.95$  and  $6.3 \text{ T}$ , respectively. It can be seen that the data can be fitted to the following expression over a wide range of  $\sigma_{xx}$  between 50 mK and 1 K:

$$\rho_{xx} = \frac{1}{\sigma} \exp \left( -\frac{T_0}{T} \right)^{1/2} \quad (1)$$

This behaviour, recently reported in GaAs-Al<sub>x</sub>Ga<sub>1-x</sub>As heterojunctions<sup>7,8</sup>, was derived by Ono<sup>12</sup> for a hopping conduction in a two-dimensional electron gas under high magnetic field, using gaussian localization for states close to the edge of the broadened Landau levels. Such a good agreement would not be obtained over this range of temperature for  $\rho_{xx} = \exp(-T_0/T)^{1/3}$  which corresponds to the Mott's law for a TDEG at zero magnetic field and was reported by Stormer et al.<sup>13</sup> in GaAs-Al<sub>x</sub>Ga<sub>1-x</sub>As heterojunctions in a narrower temperature range.  $T_0$  in Eq. 1 is given by<sup>12</sup>:

$$k T_0 = \frac{V_c + B}{D(E_F)g} \quad (2)$$

where  $D(E_F)$  is the density of states at the Fermi energy and  $V_c$  is a constant of the order of unity which is related to the critical concentration of the percolation problem<sup>12</sup>. From our results, we obtain  $T_0 = 11.70$  and  $7.8$  K for curves A, B and C respectively. This difference is not explained by the magnetic field dependence of  $T_0$ , but by the variation of the density of states  $D(E_F)$  at the  $\rho_{xx}$  minima A, B and C. Fig. 3(b) shows the resistivity  $\rho_{xx}$  in the vicinity of the three minima at 0.2 K. For the A and C minima,  $\rho_{xx}$  does not drop to zero because the overlap between the tails of the adjacent Landau levels is important and, as a consequence, the corresponding values for  $T_0$  are small. For the minimum B, the resistivity drops to zero, the overlap between the Landau level  $n=2$  and 1 being very small, and  $T_0$  is larger. If the percolation constant is assumed to be  $V_c = 1$ , the density of states  $D(E_F)$  can be deduced from  $T_0$ . At the minimum B, Eq. (2) leads to a value  $D(E_F) = 1.3 \times 10^{11} \text{ meV}^{-1} \text{ cm}^{-2}$  which is an unrealistic value, much higher than the density of states without magnetic field which is  $2.1 \times 10^{10} \text{ meV}^{-1} \text{ cm}^{-2}$  in the case of In<sub>0.53</sub>Ga<sub>0.47</sub>As and which represents, in any case, an upper limit for the density of states at the  $\rho_{xx}$  minima. This discrepancy which has been first pointed out by Ebert et al. in GaAs-Al<sub>x</sub>Ga<sub>1-x</sub>As heterojunctions<sup>8</sup>, shows that Eq. (2) is probably not correct.

Finally, it is noteworthy that the hopping conductivity is not only observed at the  $\rho_{xx}$  minima but over the entire Hall plateau region. For instance, curve D in Fig. 3(a) shows the conductivity  $\sigma_{xx}$  at  $B = 4.6$  T which corresponds to the onset of the  $\rho_{xy} = h/4e^2$  plateau at 1.85 K (Fig. 1(a)). It is clear that the data are well fitted to Eq. (1) with a value  $T_0 \sim 23$  K which is three times smaller than  $T_0$  at the B point. Nevertheless, it is

important to point out that the results at the D point could also be interpreted with the  $\exp(-T_0/T)^{1/3}$  Mott's law corresponding to an exponential localization. These observations confirm that the Hall plateaus occur when the Fermi level  $E_F$  lies in the localized states in the tails of the Landau levels while the Hall steps appear when  $E_F$  is in the extended states in the center of each Landau level<sup>14</sup>. The observation of a plateau width reaching about 80 % of its largest possible value at low temperature shows that most of the electron states are localized for the lowest indices Landau levels as already observed in GaAs-Al<sub>x</sub>Ga<sub>1-x</sub>As heterojunctions<sup>5,8</sup>.

#### REFERENCES

- (1) K. von Klitzing, G. Dorda and M. Pepper, Phys. Rev. Lett. 45 (1980) 494.
- (2) D.C. Tsui and A.C. Gossard, Appl. Phys. Lett. 38 (1981) 550; D.C. Tsui, H.L. Störmer and A.C. Gossard, Phys. Rev. Lett. 48 (1982) 1559.
- (3) Y. Guldner, J.P. Hirtz, J.P. Vieren, P. Voisin, M. Voos and M. Razeghi, J. Phys. Lett. (Paris) 43 (1982) L613.
- (4) T. Ando, Surface Sci. 113 (1982) 182.
- (5) M.A. Paalanen, D.C. Tsui and A.C. Gossard, Phys. Rev. B25 (1982) 5566.
- (6) G. Ebert, K. von Klitzing, C. Probst and K. Ploog, Solid State Commun. 44 (1982) 95.
- (7) K. von Klitzing and G. Ebert in Proceedings of the 16th International Conference on the Physics of Semiconductors, Montpellier (1982), Physica 117B and 118B (1983) 682.
- (8) G. Ebert, K. von Klitzing, C. Probst, E. Schuberth, K. Ploog and G. Weimann, Solid State Commun. 45 (1983) 625.
- (9) A. Briggs, Y. Guldner, J.P. Vieren, M. Voos, J.P. Hirtz and M. Razeghi, Phys. Rev. B 27 (1983) 6549.
- (10) M. Razeghi, P. Hirtz, J.P. Larivain, R. Blondeau, B. de Cremoux and J.P. Duchemin, Electron. Lett. 17 (1981) 643.
- (11) S.M. Girvin, M. Jonson and P.A. Lee, Phys. Rev. B 26 (1982) 1651.
- (12) Y. Ono, J. Phys. Soc. Japan 51 (1982) 237.
- (13) H.L. Störmer, D.C. Tsui and A.C. Gossard, Phys. Rev. B 25 (1982) 1405.
- (14) R.E. Prange, Phys. Rev. B 23 (1981) 4802; H. Aoki and T. Ando, Solid State Commun. 38 (1981) 1079.

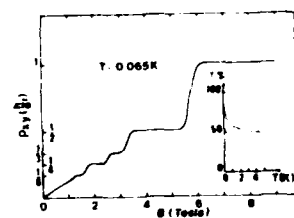
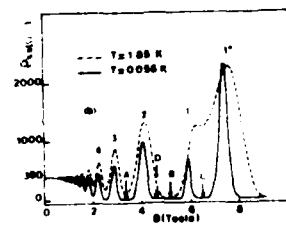
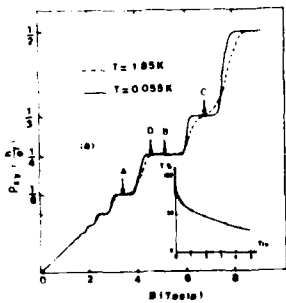


Figure 1

(a) Hall resistance  $\rho_{xy}$  as a function of  $B$  at different temperatures in sample 1. The inset gives as a function of temperature the ratio of the width of the  $\rho_{xy} = h/4e^2$  plateau to its maximum possible width, as defined in the text.

(b) Magneto-resistance  $\rho_{xx}$  as a function of  $B$  at different temperatures. The corresponding Landau levels are noted  $l^+$ ,  $l^-$ ,  $2$ ,...

Figure 2

Hall resistance as a function of  $B$  in sample 2. The inset shows, as a function of  $T$ , the ratio of the width of the  $\rho_{xy} = h/2e^2$  plateau to its maximum possible width.

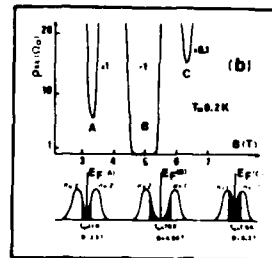
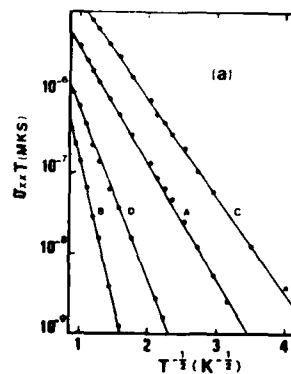


Figure 3

(a) Temperature dependence in sample 1 of  $\sigma_{xx}$  at  $\rho_{xx}$  minima A, B, C and at the point D, as defined in the text.

(b)  $\rho_{xx}$  in the vicinity of the minima A, B, C at 0.2 K. Schematic diagram of the density of states at the magnetic field at which these minima occur. The hatched areas represent the localized states.

# THE QUANTUM HALL EFFECT: A SUM RULE

J. T. Chalker

Institut für Theoretische Physik, Universität Heidelberg,  
Philosophenweg 19, D-6900 Heidelberg, FRG

## Abstract

The influence of disorder on the Hall conductivity of a two-dimensional electron gas in a strong magnetic field is examined by studying the scattering of a single particle from an arbitrary potential in crossed electric and magnetic fields. The Hall current in a large system is shown to be unaffected by 'islands' of disorder.

## Introduction

The measurements by von Klitzing, Dorda and Pepper (1) of the low temperature Hall conductivity of silicon inversion layers in intense magnetic fields demand a simple theoretical interpretation. Attempts in this direction proceeded in two stages. Firstly, the system is modeled by a two-dimensional electron gas and it is argued that the density of states in energy consists of a series of Landau levels, broadened by substrate disorder. If the electron states in the tails of the levels are localised and those near the centre are extended, at least on the scale of the sample size, then the Hall conductivity as a function of electron density will rise whilst extended states are filled and show a plateau when the Fermi energy is varied within a region of localised states. Secondly, the observed plateau values of the Hall conductivity, integer multiples of  $-e^2/h$ , are simply those of an idealised system, without scattering, in which the Fermi energy lies between Landau levels. The

problem is now to understand why this result is unaffected by the scattering processes active in a real material. Approaches taken have been of three types: Linear response theory has been used to discuss the influence of disorder on the Hall conductivity (2,3,4); the gauge symmetry of the problem has been examined (5,6,7); and it has been shown by explicit solution that the presence of a single delta-function scattering centre does not change the Hall current (8).

In the present paper a sum-rule is derived for scattering from an arbitrary static potential which leads to the conclusion that a disordered background potential does not alter the Hall current in a non-interacting, two-dimensional electron gas. If some electron states are localised by the potential, the remaining, extended states carry an extra current which exactly compensates (9).

## The scattering problem

Consider the scattering of electrons moving in two dimensions under the influence of a uniform, perpendicular magnetic field and an in-plane electric field. The appropriate Hamiltonian is

$$H = -\frac{1}{2} \frac{\partial^2}{\partial x^2} + \frac{1}{2} \left( i \frac{\partial}{\partial y} - x \right)^2 - V(x) + V(x, y) \quad (1)$$

where units have been chosen so that the cyclotron length, cyclotron energy and magnitude of the electric charge are all unity, and the Landau gauge has been selected. The external electric potential,  $V(x)$ , is translationally invariant in the direction of the Hall current (the  $y$  direction) and monotonic in the direction of the field. The Hall potential is chosen to be less than the cyclotron energy:  $V(\infty) - V(-\infty) < 1$ . A scattering region, which is of finite extent but otherwise arbitrary, is represented by the potential  $V(x, y)$ .

The spectrum of the pure system ( $V(x,y) = 0$ ) consists of a series of Landau levels broadened by the electric field. Each eigenstate is extended and carries a current parallel to the  $y$  axis. A very unusual property is that no two states are degenerate in energy: the electric field lifts degeneracies associated with symmetry under spatial rotations, and the magnetic field breaks time-reversal invariance (10). The eigenstates in the absence of scattering,  $\psi^0(x,y)$ , can be labeled by their energy,  $E$ , or by their  $y$ -momentum and Landau level,  $k$  and  $n$ . Their functional form is

$$\psi_{kn}^0(x,y) = e^{iky} \phi_{kn}(x) \quad (2)$$

The presence of a scattering potential may give rise to bound states and will also modify the extended states. Suppose that a particle prepared in the state  $\psi^0$  is incident on the scattering centre from  $y = -\infty$ . The absence of degeneracies severely restricts the type of scattering possible and, far beyond the centre, the wavefunction,  $\psi$ , differs from that in the absence of scattering by, at most, a phase factor.

$$\psi(x,y) \sim \begin{cases} \psi^0(x,y) & y \rightarrow -\infty \\ e^{i\phi} \psi^0(x,y) & y \rightarrow +\infty \end{cases} \quad (3)$$

A second quantity which is relevant in characterising the scattering process is the time delay (or advance) an electron experiences in passing the scattering centre. Our central result is that the phase change and time delay induced by scattering are not independent quantities. Let  $\psi_E^0$  and  $\psi_E$  be eigenstates at the energy  $E$ , as introduced above, normalised to carry unit current. The time delay is

$$t = \iint_{-\infty}^{\infty} dx dy \{ |\psi_E|^2 - |\psi_E^0|^2 \} \quad (4)$$

274

The right-hand side can be written, by using  $1 = \frac{d}{dE} (E' - E) \Big|_E$ , replacing  $E\psi_E$  with  $\mathcal{H}\psi_E$  and integrating by parts to obtain

$$t = \frac{d\phi}{dE} \quad (5)$$

It is clear that the time delay is related to effect of disorder on the Hall current carried by an eigenstate at the energy,  $E$ , whilst the derivative of the phase shift,  $d\phi/dE$ , reflects the influence of disorder on the density of states. In the final section this connection is formulated more precisely.

#### The Hall conductivity

A single scattering centre in an infinite system has an infinitesimal effect on the density of states. We therefore treat a system similar to that discussed above, but with periodic boundary conditions applied in the  $y$  direction between  $y = -M/2$  and  $y = M/2$ . The length  $M$  is chosen sufficiently large for a given  $V(x,y)$  that the wavefunctions of the infinite system are close to their asymptotic behaviour at  $y = \pm M/2$ . This should not be a serious restriction since corrections decay as (polynomial)  $\times e^{-y^2/4}$  in the region  $V(x,y) = 0$ .

The eigenstates of the finite system consist of the bound states of the infinite system together with extended states at those energies for which

$$Mk + \phi_n(k) = 2\pi \times \text{integer} \quad (6)$$

The number of states in the  $n^{\text{th}}$  Landau level with momenta in the range  $(k, k + \Delta k)$  is therefore

$$N(k) \Delta k = \frac{M}{2\pi} \left\{ 1 + M^{-1} \frac{d\phi}{dk} \right\} \Delta k \quad (7)$$

275

The current carried by each eigenstate is, on normalising the wavefunctions within the finite system,

$$j(k) = M^{-1} j^0(k) \left\{ 1 + M^{-1} \frac{dE}{dk} t \right\}^{-1} \quad (8)$$

where  $M^{-1} j^0(k)$  is the current in the absence of a scattering centre. The relation between the time delay and the phase shift allows the current to be expressed as

$$j(k) = M^{-1} j^0(k) \left\{ 1 + M^{-1} \frac{d\phi}{dk} \right\}^{-1} \quad (9)$$

so that the total current carried by states within a small energy range is

$$J(k) \Delta k = \frac{i}{2\pi} j^0(k) \Delta k \quad (10)$$

which is independent of  $V(x,y)$ .

The presence of disorder may thus influence both the density of extended states and the current carried by each state, but these effects cancel when the contribution to the Hall current from a range of energies is considered. Equation (10) may be integrated and conventional units restored to show that, when the extended states of  $n$  Landau levels are occupied, the Hall conductivity is  $-ne^2/h$ .

#### References

- (1) K. von Klitzing, G. Dorda and M. Pepper, Phys. Rev. Lett. **45** (1980) 494
- (2) M. Aoki and T. Ando, Solid State Comm. **38** (1981) 1079
- (3) D. J. Thouless, J. Phys. C **14** (1981) 3475
- (4) P. Streda, J. Phys. C **15** (1982) L 717
- (5) R. B. Laughlin, Phys. Rev. B **23** (1981) 5632

- (6) B. I. Halperin, Phys. Rev. B **25** (1982) 2185
- (7) Y. Imry, J. Phys. C **15** (1982) L 271
- (8) R. E. Prange, Phys. Rev. B **23** (1981) 4802
- (9) J. T. Chalker, J. Phys. C, to appear
- (10) R. E. Prange and R. Joynt, Phys. Rev. B **25** (1982) 2943

#### Acknowledgements

I am indebted to Professor F. Wegner for stimulating discussions. The financial support of the Science and Engineering Research Council is gratefully acknowledged.

# The Effect of Interface Charge on the Quantum Hall Effect\*

J. E. Furneaux and T. L. Reinecke  
Naval Research Laboratory, Washington, D.C. 20375 USA

## Abstract

The effects of variable oxide charge on quantum Hall plateaus have been studied using Si MOSFETs which have driftable Na ions in the oxide. Interesting and unusual behaviors have been observed for both the widths and positions of the various plateaus in the Hall resistivity as functions of increasing interface charge. The origin of these effects is discussed in terms of a picture based on localized electron states in the inversion layer.

The quantum Hall effect (QHE) in the two-dimensional electron gas (1) confined at the Si-SiO<sub>2</sub> interface in metal-oxide-semiconductor field-effect transistors (MOSFETs) has been of considerable experimental and theoretical interest recently (2)(3). It is observed that the Hall resistivity has flat steps with values  $\rho_{xy} = h/ie^2$ ,  $i=1,2, \dots$  corresponding to filled Landau, spin and valley levels as a function of increasing gate voltage. The magnetoresistivity  $\rho_{xx}$  vanishes for gate voltages in the steps. It is generally thought that these plateaus are associated with localized electron states in the band tails of the Landau and spin levels. These states pin the Fermi level for increasing gate voltage. The microscopic nature of the localized states and their effects on the QHE however are not yet well understood (2).

The purpose of the present work is to investigate the effects of well characterized changes in interface charge and the associated localized electron states on the QHE. MOSFET samples with mobile positive charge in the gate oxide are very attractive candidates for these studies. Hartstein and

Fowler (4) have found that for each positive charge drifted to the interface, a bound impurity state is created at the Si-SiO<sub>2</sub> interface. By drifting the mobile positive charges to the interface it is possible to vary the number of interface charges  $N_{ox}$  in a given sample. Experimentally, the width in gate voltage of the flat Hall plateau is generally determined from the region for which  $\rho_{xy} = h/ie^2 \pm \Delta$  where  $\Delta$  is a small quantity associated with the experimental resolution. A similar criterion is used here in an AC technique which allows us to use very low excitation current (100 nA). At a constant field of 13T and at T=1.35K we have measured  $\rho_{xx}$ ,  $\rho_{xy}$ ,  $d\rho_{xx}/dn$  and  $d\rho_{xy}/dn$  as a function of  $V_G$  using an experimental configuration similar to that of Fang and Fowler (5). The width of the Hall step was taken to be the width of the region in inversion layer density  $n$  for which  $d\rho_{xy}/dn < 3.5 \times 10^5 \Omega \text{cm}^{-2}$ . The  $\Delta$  corresponding to this criterion is  $\sim 10$ .

The results of these studies are shown in Figs. 1-3. In Fig. 1 the widths of the Hall steps are seen to be approximately proportional to the number of oxide charges drifted to the Si-SiO<sub>2</sub> interface for small drifts in high mobility samples. The Hall plateau widths fall on universal curves linear in  $1/\mu$  at high mobilities as seen in Fig. 2 where the mobilities  $\mu$  are measured at 4.2K and  $H=0$ . The parameter  $1/\mu$  provides a measure of scattering in the inversion layer (6). A notable feature of these data is the difference in behavior between the plateaus associated with the full Landau levels and the plateaus associated with the full spin levels. The spin plateaus grow in width more slowly than the Landau level plateaus. A similar behavior is observed (Fig. 2) as a function of  $1/\mu$  for high mobility samples ( $\mu B^2 > 12$ ).

A remarkable feature of these data is shown in Fig. 3. The positions in gate voltage of the spin plateaus are found to move with respect to the positions of the full Landau plateaus for increased oxide charge at the interface. In order to determine precisely the position of a given plateau, the temperature was chosen such that  $\rho_{xx}$  shows well defined minima rather than flat regions. Measurements of  $\rho_{xx}$  versus  $V_G$  were made at a number of magnetic

fields between 8T and 13T and apparent thresholds for the full spin and full Landau levels were obtained from the usual fan diagrams (3). The positions of these thresholds were then compared to the conductivity threshold,  $V_{TC}$ , at 77K and are shown in Fig. 1. The amount of drifted interface charge was determined by  $\Delta N_{OX} = eC\Delta V_{TC}$  where  $C$  is the capacitance per unit area of the MOSFET. It can be seen that for  $\Delta N_{OX} = 4 \times 10^{11} \text{ cm}^{-2}$  the full Landau level positions do not move with respect to the conductivity threshold within experimental error. The minima associated with filled spin levels however move closer to minima for the next full Landau levels. The positions of the  $\rho_{xx}$  minima associated with the filled valley levels behave like those for the filled spin levels and will be discussed separately (7).

The effects of varying oxide charge on the quantum Hall plateaus are now discussed in terms of a picture of localized states in the inversion layer (2). Increased interface oxide charge leads to greater potential fluctuations there and hence to greater localization. Thus the increased widths with increasing oxide charge in Figs. 1 and 2 are consistent with a picture of Hall plateaus arising from localized inversion layer states. More specifically at  $N_{OX} = 5.5 \times 10^{11} \text{ cm}^{-2}$  the  $\text{Na}^+$  forms a localized hydrogenic state in the inversion layer (4). The combined  $\text{Na}^+$  and localized electron then give rise to the interface potential fluctuation.

The different shifts of plateaus for full spin and Landau levels (Fig. 3) and the differences in their widths as functions of oxide charge (Figs. 1,2) is especially remarkable. In order for there to be an apparent shift in a  $\rho_{xx}$  minimum it is necessary not only that the adjacent band tails overlap but also that they shift with respect to one another in such a way that the increased overlap is asymmetrical. The data for the filled Landau level in Fig. 3 therefore suggests that the band tails do not overlap significantly with the previous spin level. The upward shift of the filled spin plateau is consistent with a picture (7) in which the interaction of the band electrons with the electrons localized at the  $\text{Na}^+$  depends on spin. The interaction between the

electrons in the lower spin state of a Landau level with the localized electron state is stronger because of their orthogonality, and the resulting shift is asymmetrical because screening decreases this interaction as the band fills. The interaction with these localized electrons causes the mobility edges of the lower spin bands to move more with interface charge, and increased screening causes the upper mobility edge in each band to be affected less. These effects give the different increases of the spin and Landau Hall plateaus seen in Figs. 1 and 2.

#### References

- \*Partially supported by an Office of Naval Research contract
- (1) K. Von Klitzing, G. Dorda, and M. Pepper, Phys. Rev. Lett. 45 (1980) 494.
- (2) Proceedings of the 4th International Conference on Electronic Properties of Two-Dimensional Systems, ed. Frank Stern (North-Holland, Amsterdam, 1982) and references therein.
- (3) Tsuneya Ando, Alan B. Fowler and Frank Stern, Rev. Mod. Phys. 54 (1982) 437 and references therein.
- (4) A. Hartstein and A. B. Fowler, Phys. Rev. Lett. 34 (1975) 1435.
- (5) F. F. Fang and A. B. Fowler, Phys. Rev. 169 (1968) 619.
- (6) H. L. Störmer, D. C. Tsui, A. C. Gossard, in Electronic Properties of Two-Dimensional Systems, ed. Frank Stern (North-Holland, Amsterdam, 1982), p. 32.
- (7) J. E. Furneaux and T. L. Reinecke, to be published.

Fig. 1. The width of the Hall plateaus plotted versus drifted interface charge. The open symbols are the Landau level widths and the filled-in symbols are the spin level widths. Each point is a composite of data at six different substrate biases giving the plotted error bars.

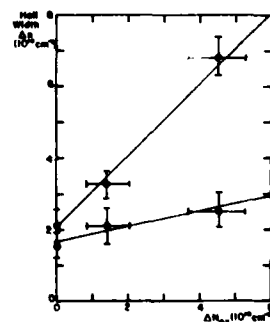




Fig. 2 The normalized width of the Hall plateaus plotted versus normalized inverse mobility. A) The widths of the spin plateaus; B) The widths of the Landau plateaus. The density associated with a nondegenerate Landau level is  $n = 3.166 \times 10^{11} \text{ cm}^{-2}$ . The straight lines are approximate fits to the high mobility data which go through the origin as expected from localization due to potential fluctuations. The different symbols indicate different substrate biases:  $\circ = +1 \text{ V}$ ,  $\square = 0 \text{ V}$ ,  $\Delta = -1 \text{ V}$ ,  $\bullet = -2 \text{ V}$ ,  $\blacksquare = -4 \text{ V}$ ,  $\blacktriangle = -8 \text{ V}$ .

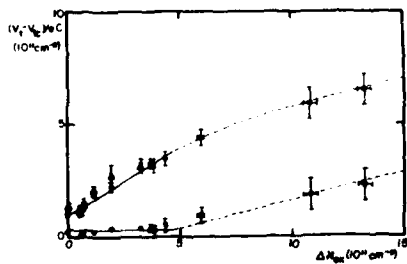
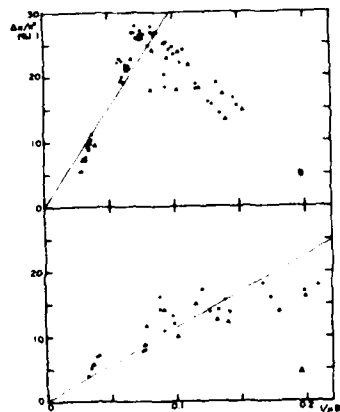


Fig. 3 The normalized positions of the  $p_{xx}$  minima relative to the conductivity thresholds  $V_{xx}^{LC}$  plotted versus added interface charge  $\Delta N_{ox}$ . The upper curve is the spin and valley level positions and the lower curve is the Landau level positions. The dashed curve indicates the region for which the electrons associated with the impurities are banded and thus where the measurement of  $\Delta N_{ox}$  is less reliable.

# Plateaus in the Quantized Hall Resistance Without Localized States\*

T. L. Reinecke  
Naval Research Laboratory  
Washington, D.C. 20375

and

B. D. McCombe  
Department of Physics, State University of New York at Buffalo  
Buffalo, New York 14260

The role of the channel contacts in giving rise to plateaus in the quantized Hall resistivity of the inversion layer electron system in  $\text{Ga}_{1-x}\text{Al}_x\text{As}/\text{GaAs}$  heterostructures and in Si MOSFETs is discussed. It is shown that under certain circumstances this effect can make a significant contribution to the plateau widths particularly in the case of the heterostructures.

The quantized plateaus in the Hall resistivity of the two-dimensional inversion layer electron systems as a function of magnetic field  $B$  in  $\text{Ga}_{1-x}\text{Al}_x\text{As}/\text{GaAs}$  heterostructures and as a function of gate voltage  $V_G$  in Si MOSFETs have attracted much interest recently. The so-called "integer" plateaus correspond to the filling of Landau levels, and the "subinteger" plateaus to the opening of a gap in the electronic spectrum due to many-body effects. The widths of these plateaus are generally thought to be caused by localized states which pin the Fermi energy  $\epsilon_F$  in the band tails of the Landau levels or at the edges of the many-body gap (1). The microscopic origin of the plateau widths, however, is not yet well understood.

Several considerations suggest that another mechanism in addition to that from localized states may contribute to the plateau widths. The low temperature widths of plateaus in high mobility  $\text{Ga}_{1-x}\text{Al}_x\text{As}/\text{GaAs}$  heterojunctions (2) are generally found to be considerably greater than those in lower mobility Si

MOSFETs (3). On the other hand, the interface disorder and thus the localization should be less for the heterojunction than for the Si-SiO<sub>2</sub> interface. Secondly, both subinteger plateaus corresponding to small gaps in the energy spectrum and also substantial widths for the integer plateaus are observed in the same high mobility heterostructure devices (4).

The channels of the devices in which these resistivities are measured have heavily doped, degenerate n-type contacts diffused into the semiconductor material. The number of electrons in them and in the associated metallizations is sufficiently large to provide effectively infinite reservoirs for the channel electrons. The experiments are done under so-called "cold, dark" conditions in which the thermal equilibrium of the inversion layer with the depletion layer and with the bulk semiconductor, which is established at higher temperatures, is no longer maintained at the low temperatures.

Consider first the Hall conductivity of a  $\text{Ga}_{1-x}\text{Al}_x\text{As}/\text{GaAs}$  heterostructure for increasing magnetic field. Charge which moves from the inversion layer into the contacts is expected to remain near the inversion layer in order to reduce its electrostatic field energy, and it should affect the potential energy of the inversion layer electrons in only a small region corresponding to a "fringing field" near the contacts. Thus in the region away from the contacts the band bottom for the inversion layer system and  $\epsilon_F$  remain fixed as functions of density, the latter being specified by the value of the chemical potential in the contact.

The Hall conductivity in the relaxation time approximation is  $\sigma_{xy} = ne/B$  where  $n$  is the inversion layer density per unit area. In high mobility heterojunction devices the Landau levels should be narrow. At  $T=0$  if  $\epsilon_F$  lies between Landau levels, then for increasing  $B$  charge flows from the contacts into the inversion layer, and  $\sigma_{xy}$  remains constant with a value  $\sigma_{xy} = Le^2/h$  where  $L$  is the number of filled levels. When a Landau level passes through  $\epsilon_F$  its charge is transferred abruptly into the contact. At arbitrary temperatures the chemical potential of the inversion layer system measured from the band

bottom remains constant and is given to good approximation by that for an ideal two-dimensional electron gas (5). The resulting  $\sigma_{xy}$  is shown in Fig. 1 for zero Landau level width and no localization. The broad plateaus are seen at low temperature, and as  $T$  increases to  $k_B T/\hbar\omega_c \sim 0.2$  they disappear. This temperature dependence is similar to that seen in experiment (6). The effects of finite band width and of localized states are such as to improve this agreement.

In the case of Si MOSFETs charge will flow between the contacts and the inversion layer as a function of  $V_G$ . In many, but not all, of these devices there is an additional contact at the back of the semiconductor which is kept at constant electrostatic potential and chemical potential with respect to the channel contacts. As a result when  $\epsilon_F$  lies between Landau levels a small change in  $V_G$  ( $\sim 0.05$  volts for a typical device) moves the next Landau level to  $\epsilon_F$ , and the resulting contribution to the plateau width is small (of the order of 5% of the ideal zero temperature width). On the other hand, for MOSFETs which effectively lack such a contact to the back of the semiconductor, the contribution of the present mechanism to the plateau width will be similar to that for the case of the heterojunction.

The present analysis suggests experiments to distinguish the present mechanism from that arising from localized states as the origin of plateaus in the quantized Hall resistivity. These include contactless conductivity studies and experiments using high mobility MOSFETs which do not have back contacts.

#### References

\* Supported in part by ONR Contract Number N0001481MR10136 (T.L.R.) and ONR Contract Number N0001481K0219 (R.D.M.)

- (1) see e.g. Proceedings of the 4th International Conference on Electronic Properties of Two-Dimensional Systems, ed. Frank Stern (North Holland, Amsterdam, 1982) and references therein.

- (2) M. A. Paalanen, D. C. Tsui, and A. C. Gossard, Phys. Rev. B **25**, 5566 (1982).
- (3) K. von Klitzing, G. Dorda, and M. Pepper, Phys. Rev. Lett. **45**, 454 (1980).
- (4) H. L. Störmer, A. Chang, D. C. Tsui, J. C. M. Huang, A. C. Gossard, and W. Wiegman, Phys. Rev. Lett. **50**, 1953 (1983) and references therein.
- (5) A. Isihara and D. Y. Kojima, Phys. Rev. B **19**, 846 (1979); A. Isihara, Solid State Commun. **46**, 265 (1983).
- (6) H. L. Störmer, D. C. Tsui, A. C. Gossard, and J. C. Huang, Physica **117B/118B**, 688 (1983).

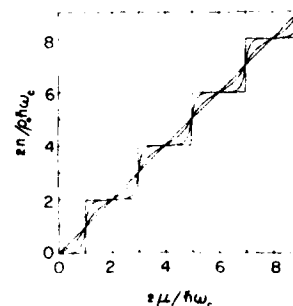


Fig. 1. The Hall conductivity  $\sigma_{xy}$  versus  $1/B$  for an ideal  $\text{Ga}_{1-x}\text{Al}_x\text{As}/\text{GaAs}$  heterojunction.  $\sigma_{xy} = en/B$  is shown on the vertical axis where  $p_0 = m/\hbar^2$  is the uniform density of states of the inversion layer electrons of effective mass  $m$ , and  $\omega_c = eB/m$ , the cyclotron frequency. The temperatures are given by  $k_B T/\hbar\omega_c = 0.01$  (broad plateaus), 0.05, 0.2, 10 (no plateaus). The chemical potential  $\mu$  is effectively constant. Spin splitting of the Landau levels has been neglected.

On the Theory Quantum Hall Effect in 2-D

Ote Gummich and J. Hajdu  
Institut für Theoretische Physik,  
Universität zu Köln, D-5000 Köln 41,  
W. Germany

The influence of a point impurity on the Hall conductivity of a finite system is investigated. It is shown that the bound state contribution vanishes exponentially in the thermodynamic limit for a completely filled Landau band.

We show that for an infinite system containing noninteracting electrons and uncorrelated statistically distributed impurities the isothermal Hall conductivity exactly coincides with the classical free electron result. This result is in agreement with Streda's analysis, which indicates that the linear response Hall conductivity reduces to the isothermal one as long as the Fermi energy lies in an energy-gap.

Some aspects of non-ergodicity which are presumably significant for the quantum Hall effect are discussed.

# NON-EQUILIBRIUM BEHAVIOUR OF THE TWO-DIMENSIONAL ELECTRON GAS IN THE QUANTIZED HALL RESISTANCE REGIME OF $\text{GaAs}/\text{Al}_{0.3}\text{Ga}_{0.7}\text{As}$

F. KUCHAR  
Institute für Festkörperphysik der Universität Wien, and Ludwig Boltzmann  
Institute, Vienna Austria.

G. BAUER  
Institute für Physik, Montanuniversität, Leoben, Austria.

G. WEIMANN, H. BURKHARD  
Forschungsinstitut der Deutschen Bundespost, Darmstadt, FRG.

Experiments concerning geometrical effects and the non-equilibrium behaviour of  $\rho_{xx}$  and  $\rho_{xy}$  under pulsed current conditions were performed in  $\text{GaAs}/\text{Al}_{0.3}\text{Ga}_{0.7}\text{As}$ . A sharp transition from the quantized Hall resistance state to the classical state in a very narrow critical current range is observed in  $\rho_{xx}$  when the Fermi level is midway between two Landau levels. Under this condition  $\rho_{xy}$  is independent of the current intensity. Spike-shaped voltage ( $\rho_{xx}$ ) instabilities are observed just below and at the critical current.

## 1. INTRODUCTION

The quantized Hall resistance (1) can be observed in two-dimensional electron systems (2DES) when the Fermi level lies between two adjacent Landau levels. The value of the conductivity component  $\sigma_{xy}$  which is observed to be  $-ie^2/h$  (....filling factor) coincides with the value according to the classical formula  $\sigma_{xy} = -ne/B$  when the lower one of the two Landau levels is fully occupied. In actual samples the situation becomes complicated due to facts like the presence of impurities, the finite extension of the 2DES and the electrical contacts. Attempts to include these facts into a theoretical treatment (reviewed in Refs. 2 and 3) are criticized by Hajdu (3) as giving no conclusive arguments for the importance of the finite dimensions of the 2DES (4) or for the precision of the quantized Hall resistance when the Fermi level is not in an energy gap but in the range of localized states (5, 6, 7).

The experimental results on  $\text{GaAs}/\text{Al}_{0.3}\text{Ga}_{0.7}\text{As}$  as reported in this paper do demonstrate the effect of the finite dimensions and of the current contacts. In the non-equilibrium experiments with current

pulses up to 1 mA the change from the quantized Hall resistance state to the classical state is observed. It also allows to locate very exactly the magnetic field strength where the Fermi level is midway between two adjacent Landau levels.

## 2. EXPERIMENTAL

The epitaxial  $\text{GaAs}$  and  $\text{Al}_{0.3}\text{Ga}_{0.7}\text{As}$  layers of standard layer thicknesses (8) were grown on Cr doped substrates in a commercial VARIAN Gen II MBE system. Concentration and mobility of the 2D electrons were  $2 \times 10^{11} \text{ cm}^{-2}$  and  $1.1 \times 10^5 \text{ cm}^2/\text{Vs}$ , respectively, at 2.1 K. A Mesa structure with side arms was produced photolithographically (dimensions see Fig. 1). In the non-equilibrium experiment current pulses of length between 250 ns and 5 ns were applied to the sample. Current-voltage characteristics with a 100 kohm resistor in series with the sample were recorded using sampling techniques. D.C. measurements concerning the potential and current distribution were performed under constant current conditions with drastically different length/width ratios  $L/W$  of 4.3 and 0.23 on the same sample.  $L/W=0.23$  was verified by using the central side arms of the  $L/W=4.3$  geometry as current contacts.

## 3. EXPERIMENTAL RESULTS

### 3.1 D.C. Measurements

Recordings of the Hall voltage  $V_H$  and of the voltage drop  $V_x$  in the longitudinal direction versus magnetic field are shown in Fig. 1 ( $L/W=4.3$ ). The insert shows the numbering of the contacts. In the case  $L/W=0.23$  the following voltage drops are measured in the magnetic field range of the  $i=2$  plateau:

$$V_{13} = V_{27} = V_{34} = 0 \text{ and } V_{12} = V_{37} = V_{47} = V_H (\text{polarity } B^+)$$

$$V_{13} = V_{27} = V_{47} = 0 \text{ and } V_{12} = V_{37} = V_{34} = V_H (\text{polarity } B^-)$$

Reversing the polarity of the current changes  $V$  to  $-V$  but leaves the potential distribution unchanged. These results mean that the Hall voltage appears in one corner at each current contact. With reversed polarity of the magnetic field it appears in the opposite corners. With negligible contact resistance the Hall voltage is also observed between the current contacts. An analogous potential distribution is observed with  $L/W = 4.3$ .

These observations can be understood on the basis of considerations of the potential and current distribution in rectangular samples (9, 10). For a Hall angle  $\theta = 90^\circ$  the potential and current distributions are sketched in Fig. 2. The contacts are equipotential

lines and the current direction has to be perpendicular to the electric field direction. As a consequence, close to a contact the current lines are parallel to it and turn by  $90^\circ$  in the corner opposite to the one where the electric field is highest. This field corresponds to the Hall voltage. The current would only flow through the centre part of the layer if most of the equipotential lines did end in the contacts. A consequence would be that the voltage between the current contacts would be much smaller than the Hall voltage ( $V_{12} \approx 0$  in the case  $L/W=4.3$ ). This is in contradiction to the experimental observations.

### 3.2 Non-equilibrium Experiments

Figure 3 shows the dependence of the Hall voltage  $V_{45}$  and of the longitudinal voltage drop  $V_{56}$  on the current intensity at  $B=4.4$  T and  $T=2$  K, measured 250  $\mu$ s after application of the current pulse ( $L/W=4.3$ ). At a critical current,  $I_{cr}$ ,  $V_{56}$  (proportional to  $\rho_{xx}$ ) jumps by about 1 kOhm within a few percent of increase of the current. At  $T=4.2$  K  $I_{cr}$  is by 10% lower. The value of  $I_{cr}$  is of the same order of magnitude as measured by Ebert and v.Klitzing (11) in a d.c. experiment on a comparable sample.

Spike-shaped instabilities of the voltage  $V_{56}$  appear at certain current intensities just below  $I_{cr}$  and are particularly strong within the steep increase at  $I_{cr}$ . Their temporal spacing is about 50-200  $\mu$ s below  $I_{cr}$  and narrower at  $I_{cr}$ . Their amplitude is up to about 20% of the height of the voltage pulse just above  $I_{cr}$ .

The  $\rho_{xx}$  jump is steepest at 4.4 T which corresponds to the Fermi level  $E_F$  being midway between the  $N=0$  and the  $N=1$  Landau level. The Hall voltage is proportional to the current (constant  $\rho_{xy}$ ) particularly also in the range where the  $\rho_{xx}$  jump occurs. The behaviour of  $V_{45}$  below  $I_{cr}$  depends on the quality of the contacts as also reported in Ref. (11). It does not affect the qualitative appearance of the  $\rho_{xx}$  jump. However, it has a weak influence on the time dependence of it. The strongest time dependence observed was a decrease of  $I_{cr}$  by 3% when sampling the current pulse at 5 ns instead at 250  $\mu$ s; the d.c. value of  $I_{cr}$  was another 3% lower. Increasing values of  $\rho_{xx}$  below the  $\rho_{xx}$  jump tend to weaken the time dependence.

The spatial distribution of the  $\rho_{xx}$  jump is demonstrated in Fig. 4. The voltage drops  $V_{51}$  and  $V_{61}$  are measured between potential probes and current contact. At low current intensities these observations reflect the situation of Fig. 2. With the polarity  $B^-$  the Hall

voltage appears between contact 6 and 1. The behaviour of  $V_{41}$  and  $V_{31}$  is analogous for opposite magnetic field polarities. The  $\rho_{xx}$  jump is not observable close to the current contacts.

The effect of changing the magnetic field from the  $E_F$ -midway situation ( $B_{1/2}$ ) is shown in Fig. 5. The steepness of the increase of  $V_{56}$  is weakened and  $I_{cr}$  is reduced;  $\rho_{xy}$  is no longer independent of the current intensity. Above  $I_{cr}$ ,  $\rho_{xy}$  decreases when  $B < B_{1/2}$  and increases when  $B > B_{1/2}$  approaching values according to the classical formula  $\rho_{xy} = B/ne$ .

### 4. DISCUSSION

The transition from the quantized Hall resistance state to the classical state visible in  $V_{45}$  is steepest when the Fermi level is midway between two Landau levels ( $B_{1/2}$ ). Under this condition  $\rho_{xy}$  cannot change with current since  $\rho_{xy}(\text{quant.}) = \rho_{xy}(\text{classical})$ . In the geometrical picture of Fig. 2, this means that the Hall angle  $\theta$  changes to a value significantly smaller than  $90^\circ$  but still close to  $90^\circ$ . Consequently the potential distribution changes and locks to one according to the classical  $\rho_{xy}$  value. In the middle of the sample  $V_{45}$  has to be finite in this case (equipotential lines cross the lateral boundaries of the sample outside the region close to the end contacts in Fig. 2). In the corners the situation is different due to the bending of the equipotential lines. Consider Fig. 4, polarity  $B^-$ : At  $I > I_{cr}(V_{51})$  no additional equipotential lines related to the jump of  $V_{51}$  cross the boundary between contacts 6 and 1. For the polarity  $B^-$  the  $\rho_{xx}$  jump is superimposed on the Hall voltage ( $V_{61} = V_H$ ).

The following two facts have to be considered for the interpretation of the spatial origin of the  $\rho_{xx}$  jump:

(a) Since the electron current flows very close to the edge of the layer the current density is very high.

(b) In the corners the electric field is very high (A singularity (10) should not occur due to the non-zero value of  $\rho_{xx}$ ).

A scaling of  $I_{cr}$  with the width of the layer, as approximately observed by Ebert and v.Klitzing (11), not necessarily proves the  $\rho_{xx}$  jump to be a bulk effect. It could also be caused by a dependence of the current density (a) or the field (b) on the width of the layer.

Possible mechanisms for the transition of the 2D electrons from predominantly localized states (Hall plateaus) to delocalized states (classical behaviour) are impact ionization by a small number of delocalized electrons or tunnelling between two adjacent Landau levels. The time constants involved are apparently smaller than 100  $\mu$ s. The weak time de-

pendence observed in our experiments cannot be excluded to be a thermal effect (increasing the lattice temperature decreases  $I_{cr}$ ).

An understanding of the non-equilibrium behaviour, particularly of the sharp transition at  $B_{1/2}$ , primarily needs the development of a detailed theory of the equilibrium Hall effect. Since the current flows close to one edge of the layer the inclusion of edge states (7) in the theoretical treatment is definitely necessary. For a further investigation of the temporal development of the transition pulsed current experiments on a shorter time scale are in preparation.

#### REFERENCES

- (1) K.v.Klitzing, G.Dorda and M.Pepper, Phys.Rev.Letters **45**,494(1980).
- (2) B.I. Halperin, Helvetia Physica Acta (to be published).
- (3) J.Hajdu, in: Lecture Notes in Physics, Vol.177,Ed.G.Landwehr (Springer,1983) p.23.
- (4) B.I.Halperin, Phys.Rev.B25,2185(1982).
- (5) R.B.Laughlin, Phys.Rev.B23,5622 (1981).
- (6) H.Aoki and T.Ando, Solid State Commun.38,1079 (1981).
- (7) D.J.Thouless, J.Phys.C14,3475 (1981).
- (8) K.v.Klitzing and G.Ebert,Physica 117B/118B,682 (1983).
- (9) H.Weiss in: Semiconductors and Semimetals, Vol.1,Ed. R.K.Willardson and A.C.Beer (Academic Press,1966) p315.
- (10) R.W.Rendell and S.M.Girvin, Surface Sci.113 (1982).
- (11) G.Ebert, K.v.Klitzing, K.Ploog, and G.Weimann (to be published).

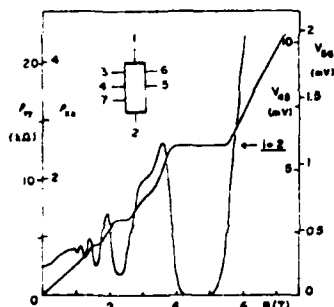


Fig.1 Hall voltage  $V_{45}$  and  $\rho_{xy}$  as well as voltage drop  $V_{56}$  and  $\rho_{xx}$  vs magnetic field. Side arms (width 0.32 mm, spacing 2.7 mm) not shown on inset. Sample area  $8.7 \times 2 \text{ mm}^2$ .  $T = 2.1 \text{ K}$ .

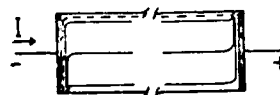


Fig.2 Qualitative picture of the electron current (broken line) and potential distribution (full lines) in a rectangular sample for a Hall angle of  $90^\circ$ . The current contacts (black areas) cover the whole width.

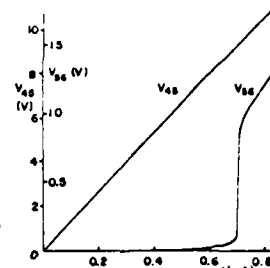


Fig.3 Hall voltage  $V_{45}$  and voltage drop  $V_{56}$  vs current sampled at  $t = 250 \text{ } \mu\text{s}$ .  $B = 4.4 \text{ T}$ ,  $T = 2.1 \text{ K}$ .

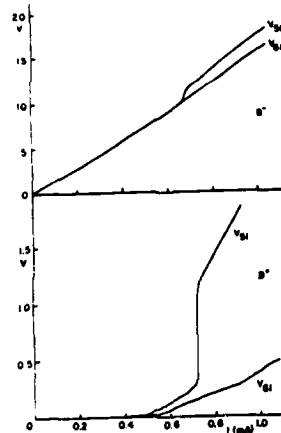


Fig.4 Longitudinal voltage drops  $V_{51}$  and  $V_{61}$  vs current for both field polarities  $B^+$  and  $B^-$ .  $B = 4.4 \text{ T}$ ,  $T = 2.1 \text{ K}$ ,  $t = 250 \text{ } \mu\text{s}$ .

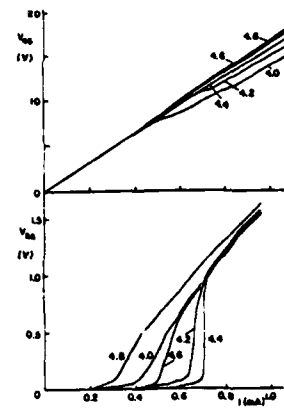


Fig.5  $V_{45}$  and  $V_{56}$  vs current for different values of the magnetic field (T) in the plateau region  $i = 2$ .  $T = 2.1 \text{ K}$ ,  $t = 250 \text{ } \mu\text{s}$ .

# QUANTUM OSCILLATIONS IN SMALL RINGS AT LOW TEMPERATURES

Yuval Gefen and Joseph Imry

Department of Physics and Astronomy, Tel Aviv University, Tel Aviv 69978,

Israel

and

M. Ya. Azbel

I. B. M. Research Center, Yorktown Heights, N.Y., 10598, U.S.A.

## Abstract

The transmission coefficient of two terminals of an effectively one-dimensional (1D) ring with arbitrary scatterers is calculated exactly as a function of enclosed magnetic flux,  $\phi$ . At low temperatures, where the inelastic diffusion length is larger than the size of the ring, its conductance follows from the Landauer formula. Oscillations of the conductance as a function of the characteristics of the scatterers and of  $\phi$  are found. The period of the oscillations in the magnetoresistance is  $\phi_0 = hc/e$ , though for weak scattering higher harmonics may develop. The oscillations persist even when the elastic scattering is strong. A consequence of this calculation is the inapplicability of the classical addition of resistances in the quantum case. Conditions for the observability of these effects are discussed.

We consider the quantum conductance of two effectively one-dimensional (1D) parallel resistors, which is equivalent to two-terminal ring geometry (see Fig. 1). The complex transmission amplitude of this device was recently calculated in Ref. 1 and is given by

$$P = \frac{t_1 t_2 (t_1' + t_2') + t_1 (r_2 - 1)(1 - r_1') + t_2 (r_1 - 1)(1 - r_2')}{(t_1 + t_2)(t_1' + t_2') - (2 - r_1 - r_2)(2 - r_1' - r_2')} \quad (1)$$

where  $r_i, r_i', t_i$  ( $i=1, 2$ ) are the reflection amplitudes for right going and left going waves and the transition amplitudes through the  $i^{\text{th}}$  barrier, which represents the  $i^{\text{th}}$  resistor in a similar manner to previous works on the 1D localization problem (2,3). A simple model for the two splitters was used following Shapiro (4). The transmission coefficient  $\tilde{T}$  is given by  $|\tilde{T}|^2$ . In the case where the diameter of the ring is smaller than the appropriate inelastic diffusion length,  $L_T$ , its conductance is given by the Landauer formulae

$$G = (e^2/h) \frac{\tilde{T}}{1 - \tilde{T}} \quad (2)$$

Let us first consider the case with no magnetic flux ( $\phi=0$ ). Even in this case  $\tilde{T}$  may exhibit oscillations as a function of the phases of the  $t$ 's and  $r$ 's. In Figs. (2) we show some representative results of the dependence of  $\tilde{T}$  on the relative phase,  $\alpha$ , between  $t_1$  and  $t_2$ , for various magnitudes of  $t_1$  and  $t_2$  (note that  $r_i, r_i'$  are determined up to a phase by  $|r_i|^2 + |t_i|^2 = 1$  and by  $-t_i/t_i' = r_i/r_i'$ ). In these figures we chose  $t_1, r_1$  and  $ir_1'$  to be real, and  $t_2 = |t_2| \exp(i\alpha)$ . We note the substantial oscillations as a function of  $\alpha$ . For a given value of the larger  $|t|$  these oscillations are in general largest when  $|t_1| = |t_2|$ . Even when, say,  $|t_2| \ll |t_1|$ , the oscillations persist and may be quite large. It turns out that for these quantum systems the combined resistance of two parallel resistors is in many cases smaller than expected from Ohm's law. In fact, the addition of a parallel larger resistor with the same phase,  $\alpha$ , makes the combined resistance larger than that of the original (smaller) resistor. For the case of equal resistors,  $R$ , when  $\alpha=0$  the combined parallel resistance is  $R$ . Likewise we have found that the smallest resistance of  $n$  parallel resistors each having a resistance  $R$ , with a similar symmetry splitter, is also equal to  $R$ .



These observations suggest interesting effects of the temperature (or other phase breaking mechanisms) dependence of the combined resistance. Once  $t_T$  becomes much smaller than the size of the ring, the common parallel Ohm's law should, of course, apply. Thus, a decrease of the resistance with increasing temperature is expected in many cases. This may offer a partial explanation for the "negative TCR" obtained in the localization theory.

We now turn on a magnetic flux,  $\phi$ . In general  $\tilde{R}$  is periodic with a period  $\phi_0$ , although one can find specific conditions to enhance the effect of the higher harmonics and turn the effective periodicity into  $\phi_0/2$ . Our effect is thus different from the one reported in Refs. (5) and (6). In Fig. (3) we show the dependences of  $\tilde{R}$  on  $\phi = \phi_0 \alpha$  for various values of the  $t$ 's. The combined resistance of two equal parallel resistors,  $R$ , with equal phases at a zero magnetic flux ( $\alpha=0$ ), oscillates as a function of  $\phi$  between  $R$  and  $\infty$ . Again for a given value of the larger  $|t|$  these oscillations are in general largest when  $|t_1| = |t_2|$  (Figs. 3a, 3c). When  $|t_2| \ll |t_1|$ , the oscillations in  $\tilde{R}$  still persist, but they are of the order of  $|t_2|^2 / |t_1|^2$  (Fig. 3b). In all these cases the combined resistance is larger than the value expected from Ohm's law. The sensitivity of the oscillations to  $\alpha$  is exemplified in Figs. (3d-g). The shallow minimum in  $\tilde{R}$  (Fig. 3a) means that higher harmonics have developed. For very large  $|t_1|$ , varying  $\alpha$  introduces a clear second harmonic (periodicity of  $\phi_0/2$ ). We don't know whether this build-up of the second harmonic ( $\log t_1 \approx 1$  is related to the weak scattering limit (5) in which the periodicity is  $\phi_0/2$ ). Clearly, higher harmonics are also possible. A full understanding of the dependence of the oscillations on the parameters must await further study.

The experimental realizability of the above effects is discussed in Ref. (1). It was argued that with the present available technology it

should be possible to detect the oscillations studied here. We emphasize that a 2D semiconducting ring, such as a MOSFET ring with a width of a few hundred Å, might be suitable for the observation of these effects. Small measuring currents are needed due to the necessity not to heat the electrons and the requirement that the generated field  $E$  will be such that the length  $(7) \tau_E = (\hbar D / e E)^{1/3}$  be larger than the ring diameter. Small currents will also reduce the number of electrons participating in the process. To avoid electron-hole interference effects one may use systems where one type of carriers is localized or is less mobile. This happens e.g. for donor levels, and may also be achieved by appropriate band structure effects.

This work was partially supported by the National Council for Research and Development, Israel and the K.F.A. Jülich, Germany, and by the U.S.-Israel Binational Science Foundation (BSF), Jerusalem, Israel.

#### References.

- (1) Y. Gefen, Y. Iary and M. Ya. Azbel, to be published.
- (2) R. Landauer, I.B.M. J. Res. Div. 1 (1959) 223; Phil Mag. 21 (1970) 863.
- (3) P. W. Anderson, D. J. Thouless, E. Abrahams and D. S. Fisher, Phys. Rev. B22 (1980) 3519.
- (4) B. Shapiro, Phys. Rev. Lett. 50 (1983) 747.
- (5) B. L. Altshuler, A. G. Aronov and B. Z. Spivak, Pis'ma Zh. Eksp. Teor. Fiz. 33 (1981) 101 [Sov. Phys. JETP Lett. 33 (1981) 94].
- (6) D. V. Sharvin and Yu. V. Sharvin, Pis'ma Zh. Eksp. Teor. Fiz. 34 (1981) 295 [Sov. Phys. JETP Lett. 34 (1981) 273]; B. L. Altshuler, A. G. Aronov, B. Z. Spivak, D. Yu. Sharvin and Yu. V. Sharvin, Pis'ma Zh. Eksp. Teor. Fiz. 35 (1982) 476 [JETP Lett. 35 (1982) 588].
- (7) M. Kaveh, M.J. Uren, R.A. Davies and M. Pepper, J. Phys. C 14 (1981) L413.

# Figure Captions.

**Fig. 1.** Schematic picture of the system  $\Phi$  is the magnetic flux through the system.

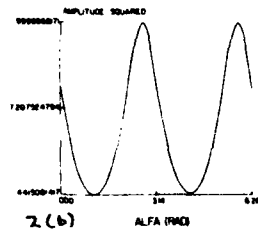
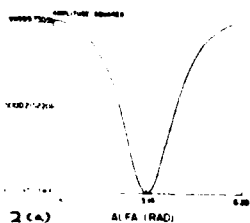
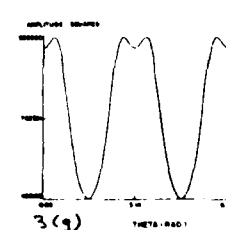
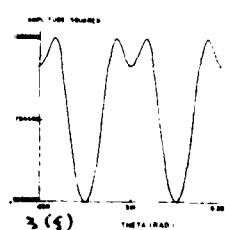
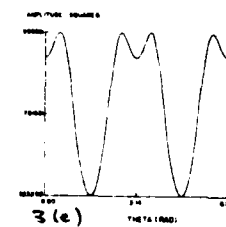
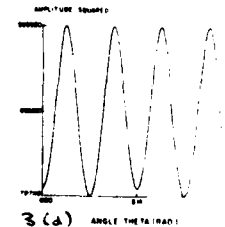
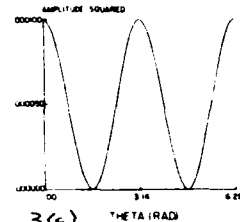
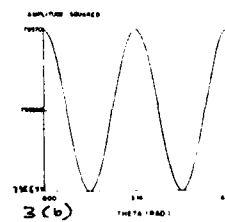
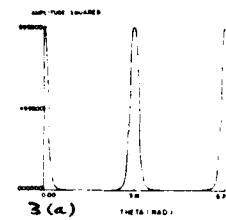
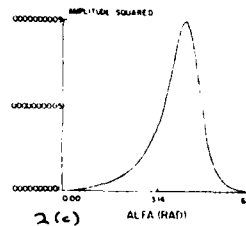
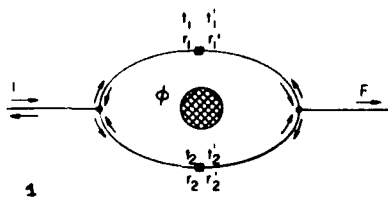
**Fig. 2.** The transmission coefficient versus  $\alpha$ , for

- (a)  $|t_1| = |t_2| = 0.99999$ ;
- (b)  $|t_1| = 0.99999$ ,  $|t_2| = 0.00001$ ;
- (c)  $|t_1| = |t_2| = 0.00001$ ;

These amplitudes and their phase are discussed in the text.

**Fig. 3.** The transmission coefficient as a function of the magnetic flux, represented by  $\theta$ .

- (a)  $|t_1| = |t_2| = 0.9999$ ,  $\alpha = 0$ ; (b)  $|t_1| = 0.99999$ ,  $|t_2| = 0.00001$ ,  $\alpha = 0$ ; (c)  $|t_1| = |t_2| = 0.01$ ,  $\alpha = 0$ ;
- (d)  $|t_1| = |t_2| = 0.99999$ ,  $\alpha = \pi/2$ ;
- (e)  $|t_1| = |t_2| = 0.99999$ ,  $\alpha = \pi/3$ ;
- (f)  $|t_1| = |t_2| = 0.99999$ ,  $\alpha = \pi/3$ ;
- (g)  $|t_1| = |t_2| = 0.99999$ ,  $\alpha = \pi/4$ .



# THE COMPLEX CAPACITANCE OF SI INVERSION LAYERS IN THE QUANTIZED RESISTANCE REGIME

L. C. Zhao\*, B. B. Goldberg, D. A. Syphers and P. J. Stiles  
Brown University, Providence, Rhode Island 02912, USA

## ABSTRACT:

We report the results of an examination of the complex capacitance of SI inversion layers at low temperatures and kHz frequencies in the quantized resistance regime. We also discuss the results for the capacitance without a magnetic field and in a non-quantizing magnetic field. We find that the one dimensional diffusion model as discussed by Stern is adequate for the discussion of the latter cases, but does not describe the quantizing case. A description is given which may be a basis for deriving the density of states and the contribution of both the localized and extended states.

The study of the quasi-two dimensional electron gas in inversion layers has a long history [1], [2]. The earliest studies were of the Shubnikov-de Haas effect (SdH). Later, results from magneto-capacitance experiments were reported [3], [4]. The recent observation of the quantized Hall effect [5] has brought additional focus on the properties of such systems. Most information on the density of states has been determined from the SdH effect, a non-equilibrium property of the electron gas. The recent observations of the de Haas-Van Alphen effect [6] in a SI inversion layer and in a (Ga,Al)As/GaAs multilayer structure [7] are expected to give information on the density of states via the study of the magnetization, an equilibrium effect.

The capacitance and interface conductance of MOS structures have been widely studied [8] under the usual conditions of no magnetic field at room temperature. The technique has been very useful in determining the density of states. However, until recently little work has been done under the conditions of our experiments [9].

Voschenkov and Zemel [4] (VZ) examined the magneto-capacitance of inversion layers in SI at low temperatures. They studied the complex admittance of circular SI MOSFETs at kHz frequencies. The admittance exhibited structure due to the quantization of the two dimensional electron gas into highly degenerate Landau levels. The low density of states at the Fermi level in between Landau levels results in a large reduction in the inversion layer capacitance (really the differential capacitance) and hence in the total capacitance.

303

While exploring both the real and imaginary part of the magneto-capacitance, VZ did not analyze in detail the results due to the Landau levels per se. They illustrated that this complex capacitance is a strong function of frequency.

We have shown previously that the picture of the charging and discharging of the inversion layer-gate capacitor is of a one dimensional diffusive nature when  $\mu H$  is less than one. These results are illustrated in fig. 1. The behavior of the real and the imaginary parts of the capacitance as a function of the parameter  $fRC$  is within a few percent of that predicted by Stern in his treatment [10]. He uses what is essentially a one dimensional diffusion (1DD) model. It is important to note that in this treatment the ratio of the real part to the imaginary part at the peak is about 1.4, and is about one for all greater values of  $fRC$ . Our results for both linear and circular samples indicate that the ratios in the above regions may be as large as 100x that expected from the Stern model.

The samples that we used had oxide thicknesses between 500 and 2000 Å and dimensions ranging from  $600 \times 200 \mu m^2$  to  $500 \times 3750 \mu m^2$ . Peak mobilities ranged from 3000 to 12000  $cm^2/V\cdot s$ . The capacitance was measured from 10 Hz to 1 MHz although we focus on the results between 1.5 kHz to 65 kHz in this report. Data was taken with magnetic fields as high as 8 T and at temperatures as low as 1.2 K.

The source and substrate are connected and the drain is connected to the source via a small resistor to measure the conductance of the sample. The capacitance is measured between the common connection and the gate under computer control. The computer records the gate voltage, real and imaginary components of the capacitance signal and the conductance in real time.

The results in the quantized resistance region are distinctly different than those in other regions. For the long samples we plot the real and imaginary parts of the capacitance,  $C_{re}$  and  $C_{im}$ , and the admittance versus magnetic field for three densities in fig. 2. The resistances in all three cases are low enough that we are in the low  $fRC$  region of fig. 1. Negative

304

magnetoresistance is seen in the admittance curve at low fields and is appropriately reflected in the capacitance. This relative behavior between  $Q_{RE}$ ,  $C_{JM}$  and admittance which is designated as normal behavior, holds for magnetic fields less than about 6T ( $\mu H < 1.5$ ). However, above that field the results are strikingly different. Notice the opposite behavior of  $Q_{RE}$  and  $C_{JM}$  for  $l=2$  with the peak in admittance for  $n=7.2 \times 10^{11} \text{ cm}^{-2}/\text{V-s}$ . This is the anomalous behavior observed in the quantized resistance (QR) region.

In fig. 3 we plot the same parameters at fixed magnetic field versus filling factor  $\nu$ . Notice that temperature smears the behavior of all three. Although we are on the low fRC side of the  $C_{JM}$  peak, there is a peak in  $C_{JM}$  at  $l=2,4$ . For  $l=3$ , there is a weaker peak in admittance and one observes a peak in  $Q_{RE}$  and a minimum in  $C_{JM}$ , the normal behavior. Such has not been seen previously. Note the characteristic peak in  $C_{JM}$  at  $l=0.5$ . There is no characteristic structure at  $l=1$  at this field and temperature.

The results for the short samples show that the imaginary part of the capacitance increases in the QR region as expected, and often exhibits the double hump structure shown in fig. 4. Most samples exhibit more symmetric structure than the one chosen for this figure. We assert that the resistance is symmetric about the minimum in  $Q_{RE}$ , and therefore the maximum in  $C_{JM}$  on either side of the minimum in  $Q_{RE}$  (double hump structure) implies we are near the maximum in  $C_{JM}$  versus fRC. Yet, the measured dc resistance is low, much lower than any resistance calculated with the application of the 1DD model.

In the regime where  $\mu H < 1$ , it appears that the only deviations from the 1DD model are caused by localized states. For the QR regime the behavior is much different. We show  $Q_{RE}$ , fRC and R as a function of  $f$  in a log log plot in fig. 5. First notice that the values of fRC and  $Q_{RE}$  are only weakly dependent on  $f$ . We arrived at this value of fRC by inverting the ratio of  $Q_{RE}$  to  $C_{JM}$  via the Stern model. We obtained R from the values of  $Q_{RE}$  and fRC. However, the measured value of  $R_{SD}$  is 12 k $\Omega$ . The R derived above varies about as  $f^{-1}$ , not unusual for conduction via localized states. In comparing

Stern's value of R from fRC at the peak in  $C_{JM}$  to the value calculated from our data at 60 kHz, we see that the former is about 10x larger.

At 10T, the extended states are apt to be a few meV below the Fermi energy. Thus the empty states at the Fermi energy require tens of kT activation energy, and hence the inversion layer cannot be charged rapidly via the extended states. We conclude that in the QR:

1. The only charging of the inversion layer is via the dissipative localized to localized state conduction process;
2. The similar results for long and circular samples further confirms that  $R_{SD}$  plays little if any role at low temperatures and at moderate to high frequencies;
3. There is a critical value of  $\mu H$  or  $\omega \tau$  which is necessary for the QR regime. It appears to be about 1.5. Below this value the capacitance behaves normally;
4. Real structure exists at the  $l=3$  valley splitting and the observed normal behavior indicates that under the present conditions, extended states are at least within a few kT if not at the Fermi energy;
5. To explain our results we probably need:
  - a. To treat the system as involving a two dimensional diffusion flow;
  - b. A proper treatment of the capacitance of localized states;
  - c. A resistance for charging of the localized states that has  $R \sim \tau^{-1}$  for an open structure.

We would like to thank R. Zeller for his help and the National Science Foundation for partial support of this work. We would also like to thank R. Wagner, Y. Takeishi, and A. B. Fowler for samples.

\* Permanent address: Shanghai Univ. of Science and Technology, Shanghai, PRC

#### REFERENCES:

- [1] A. B. Fowler, F. F. Fang, W. E. Howard and P. J. Stiles, Phys. Rev. Lett. 16, 901 (1966)
- [2] For a general review see T. Ando, A. B. Fowler and F. Stern, Rev. of Mod. Phys. 54, 437 (1982)
- [3] M. Kaplitt and J. N. Zemel, 306 Rev. Lett. 21, 212 (1968)

- [4] A. M. Voschenkov and J. N. Zemei, Phys. Rev. B9, 4410 (1974)
- [5] K. von Klitzing, G. Dorda and M. Pepper, Phys. Rev. Lett. 45, 494 (1980)
- [6] F. F. Fang and P. J. Stiles, submitted to the Phys. Rev.
- [7] H. L. Stormer, T. Haavasoja, V. Narayanasurti, A. C. Gossard and W. Wiegmann, to be published
- [8] For a review see MOS Physics and Technology edited by E. H. Nicollian and J. R. Brews, 1982 (John Wiley and Sons, Inc., New York)
- [9] L. C. Zhao, D. A. Syphers, B. R. Goldberg and P. J. Stiles, submitted to SSC
- [10] F. Stern, unpublished IBM Internal report, 1972

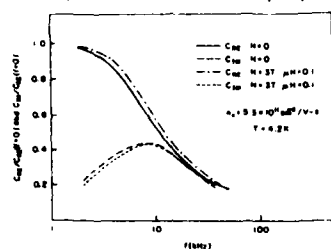


Fig. 1. Measured  $C_N$  and  $G_N$  as a function of frequency for (IRC).

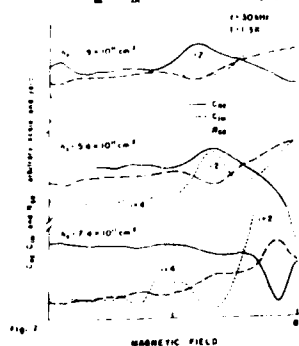


Fig. 2.  $C_N$ ,  $G_N$  and  $R_N$  versus magnetic field for three different carrier densities. The oscillatory behavior is due to the Landau level filling factor.

307

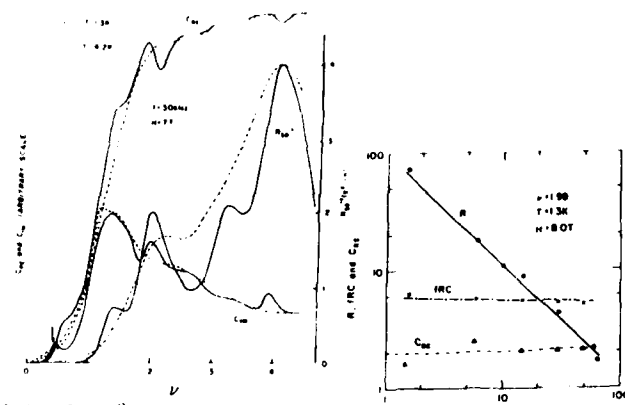


Fig. 3.  $C_N$ ,  $G_N$  and  $R_N$  versus filling factor for the long sample. Notice the normal behavior for  $\nu=1$  and the anomalous behavior for  $\nu=2, 3$ .

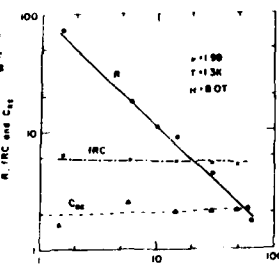


Fig. 4.  $C_N$ ,  $G_N$  and  $R_N$  versus frequency for the short sample. This double loop structure is thought to be due to the  $C_N$  peak at the 100 MHz.

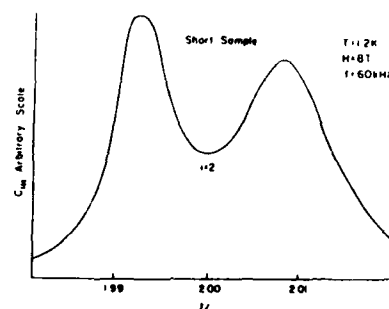


Fig. 5.  $C_N$  versus filling factor and temperature for the short sample. This double loop structure is thought to be due to the  $C_N$  peak at the 100 MHz.

308

Use of Capacitance Techniques in the study of Two-Dimensional  
Layers in Silicon MOSFETs

R. E. Goodall, R. J. Higgins, J. P. Harrang,  
University of Oregon\*

Capacitance techniques have been developed to study the density of states and conductivity tensor components in the n-type inversion layer of Si MOSFETs at T=1.4K and 8-9T using both Corbino and bar geometries. As first demonstrated by Kaplit and Zemel<sup>1</sup>, the capacitance signal shows radical fluctuations when the Fermi level is between Landau levels, even where the conductivity vanishes. In order to extend the technique to study the Quantum Hall Effect a model for the device which relates the real and imaginary parts of the capacitance signal to the density of states is used to test various forms for  $D(E)$  as well as fit the level broadening. The analysis is also applied to apparent changes in the localized state density that are observed when a substrate bias is applied.

\*Work supported by NSF Grant S0WR 81-19550 and the  
Tektronix Foundation

<sup>1</sup>M. Kaplit and J. M. Zemel, Phys. Rev. Lett. 21, p212.

# ALLOY SCATTERING LIMITED MOBILITY OF TWO DIMENSIONAL ELECTRON GAS FORMED IN $\text{In}_{0.53}\text{Ga}_{0.47}\text{As}$

P.K. Basu and B.R. Nag  
 CAS in Radio Physics and Electronics, University of Calcutta  
 92 Acharya Prafulla Chandra Road, Calcutta 700 009 INDIA

A theory of alloy scattering of 2DEG is developed. Calculations for  $\text{In}_{0.53}\text{Ga}_{0.47}\text{As}$  indicate that alloy scattering is more dominant than impurity and surface roughness scattering and the calculated mobility at 4.2 K comes close to the experimental value.

## 1. Introduction

$\text{In}_{0.53}\text{Ga}_{0.47}\text{As}$  is considered to be a prospective material for extending the frequency range of operation of Two-dimensional Electron Gas FETs (TSGFETs) (1) as the bulk saturation velocity is the highest (2) in this material. electron transport in 2DEG in  $\text{InGaAs}$  is therefore receiving extensive attention and recently Bastalezy et al (3) have presented the mobility values. The 2DEG in the  $\text{InGaAs}$  is separated from impurities in a doped  $\text{InAlAs}$  layer by an undoped spacer. The 2D concentration and mobility are found to be independent of temperature from 2 to 77 K and the mobility at 4.2 K is about  $9.5 \times 10^4 \text{ cm}^2 \text{V}^{-1} \text{S}^{-1}$ . Since at low temperatures phonon scattering is insignificant and the role of impurity scattering is reduced by the spacer, the mobility is expected to be limited by alloy and surface roughness scattering. The theory of alloy scattering of 2DEG is not, however, available in the literature. In this paper, we have worked out a theory of alloy scattering of 2DEG and applied the theory to estimate the role of alloy scattering in comparison to impurity and surface roughness scattering

in limiting the mobility. The theory and the results are presented below.

## 2. Theory

We assume that the 2DEG occupy the lowest subband and the wave function of the electrons is

$$\psi = S^{-1/2} (\frac{1}{2} b^3)^{1/2} z \exp(-bz/2) \exp(i\vec{k} \cdot \vec{r}) \quad (1)$$

S is the surface area and b is the variational parameter (4). The scattering potential, which is the difference of the actual potential at site A or B and the perfectly periodic virtual potential, is assumed to be a spherically symmetric square well with height  $\Delta E$  and radius  $r_0$  (5,6). The potential at  $(\vec{r}, z)$  due to a well at  $(\vec{r}_i, z_i)$  may be expressed as

$$V(\vec{r}, z) = \sum_i 2\pi \Delta E \frac{r_0 J_1(qr_0)}{q} [1 - H(z_i \pm r_0)] \exp[i\vec{q} \cdot (\vec{r} - \vec{r}_i)] \quad (2)$$

where  $J_1$  is the Bessel function of first order (7) and H is a step function ( $H(x) = 0$  ( $>$ ) 0)

The total transition probability from a state  $\vec{k}$  to another state  $\vec{k}'$  may be written by using Eqs.(1) and (2) as

$$P(\vec{k}, \vec{k}') = \frac{(2\pi)^3}{S^2 k} (\Delta E r_0)^2 \left| \frac{J_1(qr_0)}{q} \right|^2 \frac{N}{b} F(z_i) x(1-x) \delta(\epsilon_{\vec{k}'} - \epsilon_{\vec{k}}) \quad (3)$$

where N is the number of sites per unit volume and the A and B sites in the crystal  $A_x B_{1-x}$  are assumed to be randomly distributed in the ratio  $x:1-x$ . Also

$$F(z_i) = \frac{1}{4} \int_{br_0}^{\infty} \{ (y_1^2 + 2y_2 + 2) e^{-y_1} - (y_1^2 + 2y_2 + 2) e^{-y_2} \}^2 dy \quad (4)$$

$$y_1 = y + br_0 ; y_2 = y - br_0$$

When the radius  $r_0$  is small,  $qr_0 \ll 1$ , and  $J_1(x) \approx x/2$  (7).

One then obtains for the relaxation time

$$\frac{1}{\tau(k)} = \frac{m^* (\pi \Delta E r_s^2)^2}{k^3} \frac{N_D}{b} F(x_i) x(1-x) \quad (1)$$

Calculation of mobility using  $\tau(k)$  is standard (8) and the mobility is independent of temperature.

### 3. Results and Discussions

We have made an estimate of the mobilities limited by alloy, impurity and surface roughness scattering by using Eq.(5) and the expressions given by Takeda et al (9) and by Ando (10). The following values of parameters are used :-

$$\begin{aligned} m^* &= 0.042 m_0; \quad \epsilon(\text{InGaAs}) = 13.78 \epsilon_0; \quad \epsilon(\text{InAlAs}) = 12.65 \epsilon_0; \\ N_D &= 10^{18} \text{ cm}^{-3}; \quad x_1 = 80 \text{ \AA}; \quad d = 15 \text{ \AA}; \quad \Delta = 4.3 \text{ \AA}; \\ \Delta E &= 0.42 \text{ eV}; \quad r_0 = (\sqrt{3}/4) a_0; \quad a_0 = 5.868 \text{ \AA} \end{aligned}$$

In the above,  $N_D$  is the donor concentration in InAlAs,  $x_1$  is the thickness of the spacer,  $d$  and  $\Delta$  are, respectively, the mean square height and lateral spatial decay length connected with surface roughness (10) and  $a_0$  is the lattice constant. The values of  $d$  and  $\Delta$  correspond to Si-SiO<sub>2</sub> interface and we have taken these values in the present case, in the absence of any other reported values.

The calculated values of mobility as a function of 2D concentration, presented in Fig.1, indicate that impurity scattering limited mobility is about 10 times and the surface roughness scattering limited mobility is about 25 times higher than the alloy scattering limited mobility in the experimental condition ( $n_{2D} \approx 7 \times 10^{11} \text{ cm}^{-2}$ ). This observation and the fact that the experimental mobility is independent of temperature, indicate that alloy scattering is the most dominant process in the experimental situation.

There exists in the literature a good deal of controversy (2,4) about the choice of the potential  $\Delta E$ . In the bulk, its value is determined from the best fit to either the low temperature ohmic mobility or the high field mobility data. The low-temperature ohmic mobility is influenced also by impurity scattering, the strength of which cannot be ascertained correctly due to uncertainty in the value of compensation ratio. This, in turn, makes the estimate of  $\Delta E$  quite uncertain. The above results for 2D systems, however, indicate that a proper analysis of 2D mobility may lead to a better estimate of  $\Delta E$ , or at least of the product ( $\Delta E r_0$ ). A correct estimate of this product by using the present analysis is not possible, since in the experiment, two subbands are populated. If we assume, however, that intersubband scattering is absent and the mobilities in two subbands are equal, the above values of  $\Delta E$  and  $r_0$  give a close agreement between calculation and the experimental value at 4.2 K. (indicated by a dot in Fig.1).



# References

- (1) D. Delagebeaudeuf and N.T. Linh, *IEEE Trans. Electron Dev.* **29** (1982) 955, and references therein.
- (2) M.A. Littlejohn, J.R. Hauser, T.H. Glisson, D.K. Ferry, and J.W. Harrison, *Solid State Electron.* **21** (1978) 107.
- (3) A. Kastalsky, R. Dingle, K.Y. Chang and A.Y. Cho, *Appl. Phys. Lett.* **41** (1982) 274.
- (4) F. Stern and W.E. Howard, *Phys. Rev.* **163** (1967) 816.
- (5) L. Nordheim, *Ann. Phys. (Leips)*. **2** (1931) 607.
- (6) J.W. Harrison and J.R. Hauser, *Phys. Rev. B* **13** (1976) 5351.
- (7) H. Abramowitz and I.A. Stegun (Eds.), *Handbook of Mathematical Functions*, Dover Publ. Inc., N.Y. 1970.
- (8) P.K. Basu and B.R. Nag, *Phys. Rev. B* **22** (1980) 4849.
- (9) Y. Takeda, H. Kamei and A. Sasaki, *Electron Lett.* **18** (1982) 309.
- (10) T. Ando, *J. Phys. Soc. Japan*, **43** (1977) 1616.
- (11) D. Chattopadhyay, S.K. Sutradhar and B.R. Nag, *J. Phys. C* **14** (1981) 891.

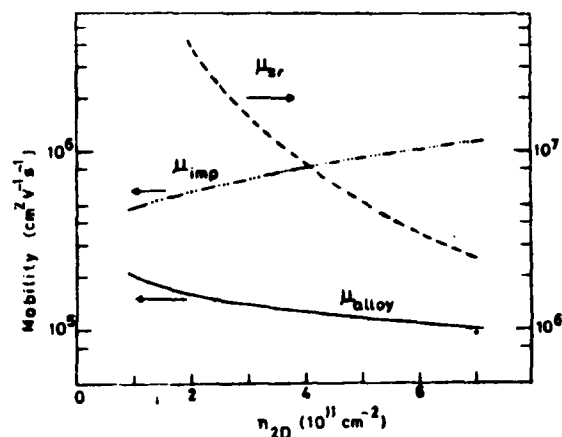


Fig.1 Mobilities limited by alloy ( $\mu_{\text{alloy}}$ ), impurity ( $\mu_{\text{imp}}$ ) and surface roughness ( $\mu_{\text{sr}}$ ) scattering in 2DEG formed in  $\text{In}_{0.53}\text{Ga}_{0.47}\text{As}$  at 4.2 K as a function of 2D concentration ( $n_{2D}$ ). The experimental value is indicated by a dot.

PHONON SCATTERING OF ELECTRONS IN QUASI-ONE-DIMENSIONAL  
AND QUASI-TWO-DIMENSIONAL QUANTUM WELLS

F.A. Riddoch and B.K. Ridley,  
Department of Physics,  
University of Essex,  
Wivenhoe Park, Colchester,  
Essex, U.K.

ABSTRACT

The present work is an extension of previous analysis for quasi-2-D wells to quasi-1-D wells. Analytic expressions are determined for the scattering rate due to the deformation potential interaction, and numerical results (scattering and momentum-relaxation rates) are presented for polar optical mode scattering. We calculate the rates as a function of energy, and compare our results with the bulk solutions and with those for 2-D wells.

The scattering and momentum-relaxation rates for polar optical mode scattering are shown to be considerably enhanced over the bulk result, the threshold of emission being very abrupt. The latter suggests the existence of an intrinsic n.d.r. The possibility of a negative momentum-relaxation rate is shown to exist for low energy associated with motion parallel to the barriers.

We describe an electron confined between potential interfaces (quasi-1-D well) at  $x=0$ ,  $x=L_x$  and  $y=0$ ,  $y=L_y$  by the wave function

$$\psi = \frac{2}{V} U_{k_x}(x) U_{k_y}(y) U_{k_z}(z) e^{ik_x x} \sin(k_y y) \sin(k_z z) \quad (1)$$

where  $k_y = n_y \pi / L_y$ , and  $k_z = n_z \pi / L_z$ . Here  $V$  is the electron-cavity volume, and  $k_x$  is the  $x$ -component of the total electron wave vector  $k$ . (For the 2-D case the  $x, y$  component of  $k$  is expressed as  $k$ ).

The energy associated with the state  $\psi$  is

$$E_x = \frac{\hbar^2 k_x^2}{2m^*} + n_y^2 \frac{\hbar^2}{2m^* L_y^2} + n_z^2 \frac{\hbar^2}{2m^* L_z^2} \quad (2)$$

The density of states, for given spin associated with a particular

$n_y, n_z$  is

$$N(E_x) = \frac{m^* \hbar^2}{2^{3/2} \hbar^2 k_x L_y L_z} \quad (3)$$

The total scattering-rate is computed from

$$W(k_x) = \sum_{n_y, n_z} W(k_x, n_y, n_z, m_y, m_z) \quad (4)$$

where the sum is over all final sub-band numbers  $m_y, m_z$ , subject to energy conservation.

In the case of deformation-potential scattering the evaluation of  $W(k_x)$  is straightforward. For scattering by acoustic phonons

$$W(k_x) = \sum_{n_y, n_z} \frac{(2+\delta_{n_y, n_z})(2+\delta_{n_z, n_z}) \hbar^2 k_x^2 N(E_x)}{2\hbar C_L} \quad (5)$$

(absorption plus emission)

and for optical mode scattering

$$W(k_x) = \sum_{n_y, n_z} \frac{(2+\delta_{n_y, n_z})(2+\delta_{n_z, n_z}) \hbar^2 D_o^2 [n(\omega_o) N(E_x + \hbar\omega_{eff}) + (n(\omega_o)+1) N(E_x - \hbar\omega_{eff})]}{4\omega_o} \quad (6)$$

where  $\mathcal{E}$  = deformation potential,  $C_L$  = elastic constant,  $D_o$  = optical deformation constant,  $\rho$  = mass density and

$$\hbar\omega_{eff} = \hbar\omega_o \left[ (n_y^2 - m_y^2) \frac{L_y^2}{L_x^2} + (n_z^2 - m_z^2) \frac{L_z^2}{L_x^2} \right] \quad (7)$$

Here, the upper sign denotes absorption and the lower denotes emission.

Upon comparing eqns. (5) and (6) with the results for 2-D wells (1)

and the bulk (3) we see that  $W(k)$  is directly dependent upon the form of the density of states.

The polar mode scattering and momentum relaxation rates (neglecting screening) for a 2-D and a 1-D well for which  $L_y = L_z$  are shown in Figs. 1 and 2. To allow convenient comparison with the quasi-2-D results and the bulk result we consider absorption and emission separately and express  $W(k)$  as normalized rates

$$W^*(k) = \frac{4\pi e^2 \hbar}{\epsilon^2 D_o} \left( \frac{\hbar}{2m^* \omega_o} \right)^2 \frac{W(k)}{n(\omega_o) + 1/2} \quad (8)$$

Here,  $\epsilon_p^{-1} = \epsilon^{-1} - \epsilon_s^{-1}$  and  $\epsilon_s, \epsilon_p$  are the high-frequency and static permittivities. The momentum-relaxation rate,  $\tau$ , is normalized in the same manner. As in the 2-D case, the 1-D results are clearly dominated by the form of the density of states, the onset of emission being very abrupt. At the onset of emission there is an equal amount of forward and backward scatter; indeed,  $W_r$  (emission) is unity at this point. This means that for quantum-wells there will be more equal forward and backward scatter at the onset of emission than in the bulk. As in the 2-D case, the disparity of scattering rates above and below the threshold for emission supports the possibility of an intrinsic negative differential resistance (4).

For larger well widths inter-sub-band scattering will occur at lower kinetic energy. Figs. 3 and 4 (2-D and 1-D respectively) show the intra-sub-band contribution to the polar mode total rate for an electron in the lowest but one sub-band for a wider well. It is clear that intra-sub-band scattering is dominant. However, due to the form of the density of states associated with transitions in the 1-D well, inter-sub-band scattering, unlike the situation in 2D, actually becomes dominant for the threshold energies for scattering to higher sub-bands.

A calculation of the intra-sub-band polar mode momentum relaxation rate associated with absorption for 1-D wells utilizing the momentum conservation approximation of (1) had previously indicated that this may be negative, and this curious result is investigated in more detail. Fig. 5 shows the variation of intra-sub-band scattering and momentum relaxation rates (absorption) with  $E_{O2}/\hbar\omega_0$ , appropriate for an electron with thermal energy at 130°K in GaAs. For well-widths such that  $E_{O2}/\hbar\omega_0 < 0.433$  inter-sub-band scattering is permitted, so this section of the graph is not indicative of the total scattering-rate.

However for  $E_{O2}/\hbar\omega_0$  in the range 0.433 to 1.32 the model predicts that the momentum relaxation rate is indeed negative. This implies that for energies below the emission threshold, for a range of well-widths, the electrons may gain momentum on average from the lattice before rapidly losing their momentum upon reaching the emission threshold. This suggests a relationship with 1-D charge density waves (5) in the non-degenerate limit. The effect appears simply to arise out of the bias in favour of forward scattering which is characteristic of polar scattering.

#### REFERENCES

- (1) B.K. Ridley, J. Phys. C: Solid St. Phys. **15** (1982) 5899.
- (2) F.A. Riddoch and B.K. Ridley, J. Phys. C: Solid St. Phys.
- (3) B.K. Ridley, Quantum Processes in Semiconductors (O.U.P., Oxford, 1982) p.99 and p.109.
- (4) B.K. Ridley, J. Phys. C: Solid St. Phys. **16** (1983).
- (5) H. Fröhlich, Proc. Roy. Soc. **A223** (1954) 296.

#### Acknowledgement

This work was funded by the U.S. Office of Naval Research.

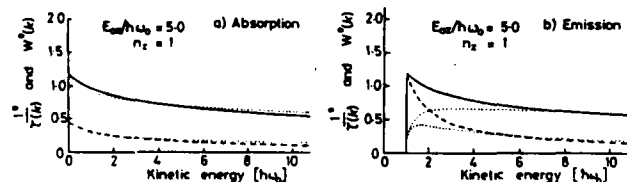


Fig. 1: Polar optical mode scattering rates (solid lines) and momentum-relaxation rates (broken lines) as a function of kinetic energy relative to the lowest sub-band minimum for an electron in the lowest sub-band of a quasi-2-D well. The bulk curves for scattering rate and momentum relaxation rate are indicated by the upper and lower dotted lines, respectively.

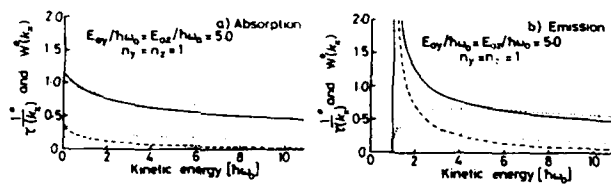


Fig. 2: Polar optical mode scattering rates (solid lines) and momentum-relaxation rates (broken lines) as a function of kinetic energy relative to the lowest sub-band minimum for an electron in the lowest sub-band of a quasi-1-D well. The bulk curves are indicated as in Fig. 1.

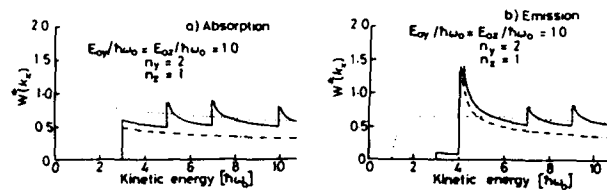


Fig. 4: Polar optical mode scattering rates (solid lines) as a function of kinetic energy relative to the lowest sub-band minimum for an electron in the lowest but one sub-band of a quasi-1-D well. The intra-sub-band contribution to the total is given by the dash-dotted line. The dotted line depicts the bulk rate.

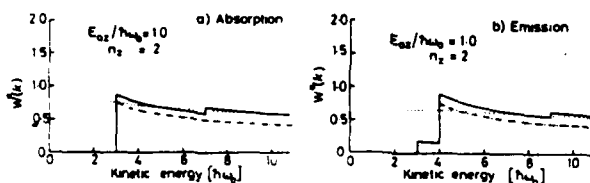


Fig. 3: Polar optical mode scattering rates (solid lines) as a function of kinetic energy relative to the lowest sub-band minimum for an electron in the lowest but one sub-band of a quasi-2-D well. The intra-sub-band contribution to the total is given by the dash-dotted line. The dotted line depicts the bulk rate.

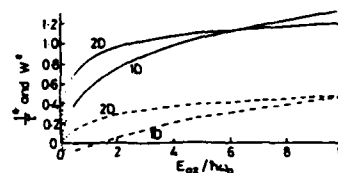


Fig. 5: Intra-sub-band scattering rates (solid lines) and intra-sub-band momentum-relaxation rates (broken lines) as a function of  $E_{0z}/\hbar\omega_0$  for an electron in the lowest sub-band of quasi-2-D and quasi-1-D ( $L_y = L_z$ ) wells. For the 2-D well  $E_x/\hbar\omega_0 = 0.3$ , and for the 1-D well  $E_x/\hbar\omega_0 = 0.3$ . The dotted portion of the curves indicate the range where inter-sub-band scattering is also permitted.

# INTERBAND SCATTERING IN MOBILITY IN GaAs-GaAlAs HETEROSTRUCTURES

Nguyen Toan Thang(a), G. Fishman  
Groupe de Physique des Solides de l'E.N.S., Université Paris VII,  
2 place Jussieu  
F-75251 Paris Cedex 05, France

The energy levels and the wave-functions of GaAs-Ga<sub>1-x</sub>Al<sub>x</sub>As heterostructures are quite different from those of multiple quantum wells: for an Al concentration below about 0.25 and for standard densities, many subbands are below the Fermi level, some of them are mainly in GaAlAs and the others mainly in GaAs. We present realistic calculations of the mobility in this case as a function of donor concentration and buffer width. The interband scattering lowers the mobility by a factor of three when the spacer thickness is zero but only some tens of percent when the spacer thickness is 100 Å.

## 1. Introduction

The influence of spacer width on mobility is now well understood in multiple quantum wells (1-3). In that case the calculation is made easy because the wave functions which correspond to bound energy levels of a quantum well have a similar shape: the electrons are mainly inside the quantum well, and in fact the calculation is very much simplified if the probability of finding an electron outside the well is assumed negligible, which is

322

reasonable in a quantum well. Because of this shape the mobility calculation taking into account the intersubband scattering is tedious but not difficult. It is worth noting that for usual electronic densities at most the two lowest subbands (so-called "0" and "1") can be populated.

The situation can be quite different in a simple heterostructure if the Al concentration  $x$  is below about 0.25, so that freeze-out should not be expected in the GaAlAs. Let us recall briefly the geometry of the samples of interest. The donors are located between  $z = 0$  and  $z = d_2$  (we keep the usual notation of quantum wells) in GaAlAs. Between  $z = d_2$  and  $z = d_2 + d_3$  there is the undoped spacer layer (always in GaAlAs). Beyond  $z = d_2 + d_3$  the GaAs layer begins up to the total sample thickness  $d_2 + d_3 + d_4$ . Contrary to the quantum well case, the electrons are only in a narrow channel of the GaAs near the interface between GaAs and GaAlAs. We have taken the conduction band discontinuity  $\Delta E_c = 0.22$  eV,  $d_2 = 600$  Å and  $d_3 = 0, 50$ , and  $100$  Å, and for the potential we have taken the boundary conditions that  $V = 0.33$  eV for  $z = 0$ , and  $V = V_0 = 0.2$  eV at  $z = d_2 + d_3 + 2200$  Å. As shown in Ref. 4, there can be a lot of energy levels below the Fermi level. The aim of this contribution is to show how a mobility calculation can be made in practice in such a case and to point out the main differences from a quantum well.

## 2. Method and results

In principle we should take into account all the levels. However, on the one hand only two of them correspond to wave functions mainly centered in GaAs and on the other hand the mobility in GaAlAs is known (5) to be weak in comparison with that of GaAs. Then a calculation without any adjustable parameter treating the two kinds of electrons (in GaAs and in GaAlAs) on the same footing would have no meaning. These reasons lead us to take into account only the electrons for which the wave function is mainly in GaAs assuming that the electrons in GaAlAs give a negligible contribution to the mobility. Furthermore we cannot assume that all donors are active (no ionization scattering).

323

nor that the number of donors is equal to the number of free electrons in GaAs. This is depicted in Fig. 1 and indicates one of the main differences from the quantum well case. In order to calculate the number and distribution of active donors in the GaAlAs we use a classical model in which the calculated values of the potential at the surface of GaAlAs and at the GaAlAs-GaAs interface and the calculated number of electrons in the GaAlAs layer are combined with a Schottky approximation for the charge distribution to give the thicknesses of the two depletion layers at the surface and at the doped GaAlAs/undoped spacer layer interface. On the other hand the full quantum mechanical calculation gives the Fermi wave-vector needed to calculate the mobility.

For quantum wells simple approximations of wave functions lead to a calculation of the scattering times  $\tau_s$  and  $\tau_y$  of subbands 0 and 1 by a simple integral. Unfortunately such simplifications do not seem possible here especially for the first excited subband. In fact we find that when only one subband is populated, even very simple approximations (such as  $\delta$ -functions) give almost correct results, whereas when two subbands are occupied, simple approximations lead to erroneous results.

Our results are shown in Fig. 2 which exhibits the mobility as a function of total donor density (not as a function of electron density) with spacer width  $d_s$  as a parameter. Comparing with similar results in quantum wells we note that (i) these results have the same qualitative features, especially the relative jumps of the mobility at the onset of population of the first excited subband are decreasing when the spacer thickness is increasing; (ii) these jumps do not occur for the same value of doping. If we compare our results with the experimental data of Ref. 4, we do not find the same electron transfer (Ref. 4); this weakens the relevance of a direct comparison between the measured and calculated mobility.

In conclusion, we have pointed out the conceptual differences between a mobility calculation in a multiple quantum well system and a simple

heterojunction structure of finite size when more than one subband is taken into account. We have shown how reasonable approximations can simplify the problem and have presented results of such a calculation.

#### References

- (\*) On leave of absence from Center for Theoretical Physics, Nghia Do Tu Lien, Hanoi, Vietnam
- (1) S. Mori and T. Ando, J. Phys. Soc. Japan 48 (1980) 265
- (2) H.L. Stormer, A. Pinsuk, A.C. Gossard, and M. Wiegmann, Appl. Phys. Lett. 38 (1981) 691
- (3) G. Fishman and D. Calecki, Physica 117B and 118B (1983) 744, and to be published
- (4) B. Vinter, this conference
- (5) e.g. T. Ishikawa, J. Saito, S. Sasa, and S. Miyamizu, Jap. J. Appl. Phys. 21 (1982) L675
- (6) H.L. Stormer, A.C. Gossard, and M. Wiegmann, Solid State Commun. 41 (1982) 707

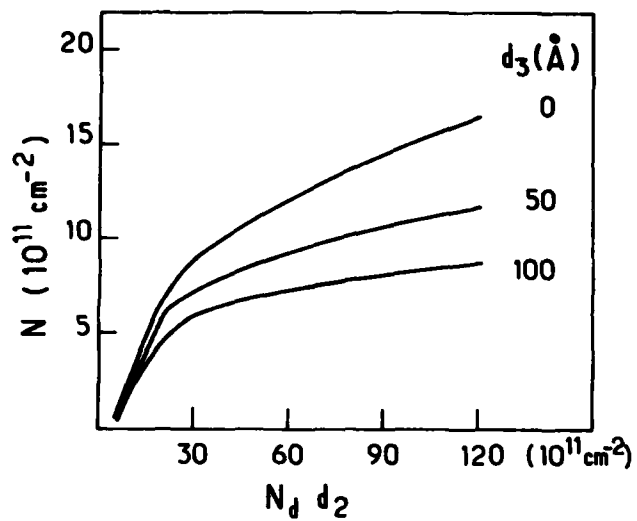


Fig. 1: Density  $N$  of the GaAs part of electrons belonging to the channel as a function of total number  $N_d d_2$  of donors in GaAlAs, with undoped spacer layer thickness  $d_3$  as parameter.  $d_2 = 400 \text{ \AA}$ .

326

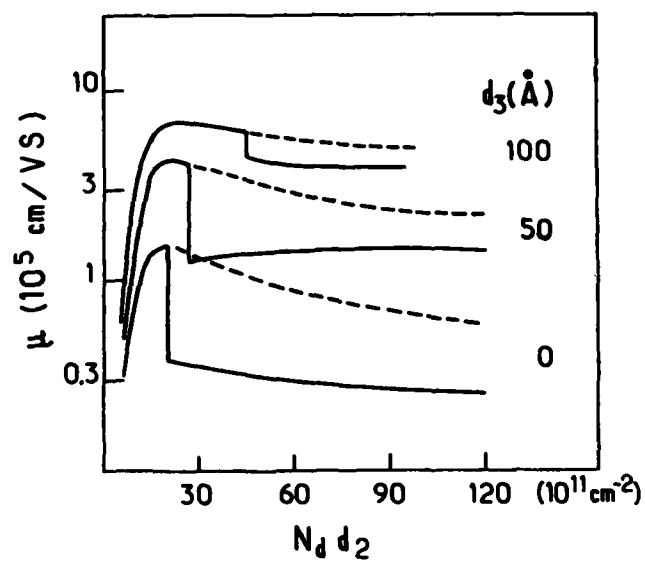


Fig. 2: Calculated mobility of electrons belonging to the channel as a function of total number of donors in GaAlAs. Full curves: intersubband scattering included; dashed curves: mobility of lowest subband only. For  $d_3 = 100 \text{ \AA}$  at the highest doping three channel subbands are correlated.

327

the plasmon wavevector or integer multiples  $n$  of it. The DC properties of the gate are unaltered by leaving a high resistivity metal gate electrode, which is transparent for FIR radiation ( $\sim 50\text{Å}$  Ti or NiCr). This method allowed the verification of the plasmon dispersion relation up to wave vectors of  $0.1 k_F$  /8/ by coupling plasmons with  $n=4$  to gratings of  $a = 1\mu\text{m}$ . Deviations from the classical dispersion relation due to finite interelectron spacing, due to correlation effects or due to finite inversion layer thickness have been studied theoretically /1,9-11/. First evidence of a wave-vector dependent "plasmon-mass" was reported by Heitmann et al. /12/ at high wave vectors (up to  $0.1 k_F$ ).

The method of coupling photon and plasmon via a metallic grating allowed furthermore the observation of magneto-plasmons /7/, of plasmons in hole space charge layers on silicon /13/ and, recently, of interactions of 2D-plasmons with intersubband resonances /14/.

In multilayered structures, in addition to the wave vector parallel to the 2D system, also a component perpendicular to the interfaces exists. These plasmon modes were observed for the first time by means of light-scattering in GaAs-AlGaAs-multilayers by Olego et al. /15/. A different experimental approach to 2D plasmons was initiated by Tsui et al. /16/, who excited plasmons by passing a current through the 2D system and observed narrow-band FIR emission due to radiative decay of 2D plasmons via the metallic grating. This excitation was recently shown to be a thermal effect resulting from the heating of the 2D electron gas in the electric field /17/. The thermodynamic equilibrium of electrons and plasmons by microscopic excitation was qualitatively shown to be due to Coulomb scattering in the system /18/. In this paper we will review the recent work on FIR emission from thermally excited plasmons. In addition the plasmon contribution to the specific heat of a 2D system is discussed; the thermal background radiation will be used for determining electron temperatures.

## II. FIR-EMISSION FROM THE "FREE" 2D-ELECTRON SYSTEM

### Theory

In the following we discuss the optical properties of a free 2D electron system, in the absence of a magnetic field, regarding only the lowest parabolic subband filled with  $n_s$  electrons of effective mass<sup>\*</sup>. Their optical properties can be described by a complex dynamical conductivity  $\sigma(\omega)$ , where the specific form of  $\sigma(\omega)$  depends on the approximation made. For Si-MOSFET's in the metallic density regime ( $n_s > 1.10^{12}\text{cm}^{-2}$ ) it has been shown experimentally by Allen et al. /19/ that  $\sigma(\omega)$  in the frequency range of 0 to  $40\text{cm}^{-1}$  can be well approximated by the Drude expression

$$\sigma(\omega) = \frac{\sigma_0}{1 - i\omega\tau} \quad (3)$$

with  $\sigma_0$  taken from DC-measurements as  $\sigma_0 = n_s e^2 \tau / m^*$ . The absorptivity of a 2D electron system is calculated using the boundary conditions for the electric and magnetic field, giving

$$A(\omega) = \frac{4F}{(2 + F)^2} \quad (4)$$

where  $F = \text{Re}\sigma(\omega)/c_0 c$ . In the presence of a dielectric medium on one side of the 2D carrier system, the absorptivity is changed according to

$$A(\omega) = \frac{4F}{(\sqrt{\epsilon} + 1 + F)^2} \quad (5)$$

where  $\epsilon$  is the lattice dielectric constant of the substrate. For the classical electrodynamical calculation of the coupling photon - plasmon via a periodic grating structure, one has to calculate the response of a 2D car-



## TWO-DIMENSIONAL PLASMONS AND FAR INFRARED EMISSION

Ralph A. Höpfel, Erich Gornik  
Institut für Experimentalphysik  
Universität Innsbruck  
AUSTRIA

### Abstract

The experimental work on plasmons in two-dimensional (2D) carrier systems is briefly reviewed. Thermal excitation of the collective modes in a 2D electron system by applying a voltage along the system is described quantitatively. We present results of far infrared emission experiments from n-Si-inversion layers, using a grating coupler for the radiative decay of the 2D plasmons. The contribution of two-dimensional plasmons to the specific heat of a 2D carrier system is discussed. From the thermal background far infrared emission electron temperatures in Si-MOSFET's can be determined. Results in the range  $2K < T < 30K$  are compared with other methods of electron temperature measurements.

### 1. INTRODUCTION:

The dispersion relation of two-dimensional plasmons was first calculated by F. Stern /1/ who found a dependence of the plasma-frequency on the wave-vector  $k$ , written in first order ( $k \ll k_p$ ) as

$$\omega_p^2 = \frac{n_s e^2 k}{2m^* \epsilon_0 \epsilon} \quad (1)$$

( $n_s$ ... 2D electron concentration,  $\epsilon$ ... dielectric constant of the surrounding medium). This relation was later modified for a real MOS-structure taking into account screening by a metallic gate in the distance  $d$  of the 2D electron system /2-4/ resulting in

$$\omega_p^2 = \frac{n_s e^2 k}{m^* \epsilon_0 (\epsilon_{Si} + \epsilon_{ox} \cdot \coth(k \cdot d))} \quad (2)$$

Two-dimensional plasmons were observed for the first time by Grimes and Adams /5/ in the 2D plasma formed by electrons in image-potential-induced surface states on liquid helium. The authors produced standing waves in the rf-range (50 - 200 MHz) and measured the absorption of the 2D electron system. By relating the resonant frequencies to the integer numbers of knots in the cell, the dispersion relation (1) could be verified.

Plasmons in n-inversion layers of Si-MOS-structures were observed in far-infrared (FIR) transmission experiments /6,7/. Since the phase-velocity of the plasmons is always smaller than the velocity of light, the momenta of photon and plasmon have to be matched in a proper way. For this purpose the gate of the MOS-device is altered to a metallic grating of periodicity  $a$  which allows an exchange of momenta  $n \cdot 2\pi/a$ . Since the photon momentum is much smaller than that of the 2D plasmon of same frequency, coupling is achieved when the grating wave vector  $k = 2\pi/a$  is equal to

rier system to a periodic electric field  $\vec{E} = \vec{E}_0 e^{i(kx - \omega t)}$ . In the electrostatic limit, Poisson's equation in conjunction with the equation of continuity leads to a dynamical conductivity  $\sigma(\omega, k)$ , which is now a function of frequency and wave vector [20].

$$\sigma(\omega, k) = \frac{\sigma(\omega)}{1 - \frac{\sigma(\omega)}{\epsilon_0} \frac{k}{\epsilon_0 \omega} \coth(kd)} \quad (6)$$

Poles of  $\text{Re}(\sigma(\omega, k))$  for  $\omega = 0$  give an implicit dispersion relation for the 2D-plasmon, which is identical with eq. (2). For the absorption of FIR radiation polarized parallel to the grating wave-vector the strength of the spatially modulated field components acting at the 2D system have to be calculated; this leads to a factor  $\alpha < 1$ , which depends on the geometrical design and the distance of the coupling grating to the inversion layer as discussed extensively in ref. [20]. The absorptivity due to plasmon excitation is thus given by

$$A(\omega) = \frac{4\pi}{(\epsilon_0^2 + 1 + F)^2} \quad \text{with } F = \alpha \cdot \text{Re}(\sigma(\omega, k)) / \epsilon_0 c \quad (7)$$

The FIR-emission from the 2D system can be calculated if thermodynamic equilibrium is assumed: If electrons and plasmons are excited to a temperature  $T$  according to their quantum statistics, the emission from the system is given by

$$I(T, \omega) = I_{\text{BB}}(T, \omega) + A(\omega), \quad (8)$$

where  $I_{\text{BB}}(\omega)$  is the emission of a blackbody of temperature  $T$ . The real amount of thermal plasmon excitation and the problems arising especially at higher temperatures will be discussed in section III.

#### Experiment

The FIR-emission set-up is schematically shown in figure 1: The emitting sample (MOSFET) and the detector (high purity n-GaAs:  $N_D - N_A = 1.3 \times 10^{14} \text{ cm}^{-3}$ ,  $N_D + N_A = 2.5 \times 10^{14} \text{ cm}^{-3}$ ) are mounted in a brass waveguide immersed in liquid Helium. A schematic cross-section of the MOSFET is shown in the insert: Upon the semitransparent Ti-Gate ( $\sim 50 \text{ \AA}$ , area  $2.5 \times 2.5 \text{ mm}^2$ ) Al-gratings (thickness 1000 Å) of periods 3  $\mu\text{m}$ , 2  $\mu\text{m}$  and 1.5  $\mu\text{m}$  are evaporated using optical contact lithography and lift-off-technique. The grating wave-vector defines the momentum of the plasmon which can be coupled out. The gate voltage  $V_G$  and thus the electron concentration  $n_s$  is swept so that the plasma frequency according to eq. (2) is tunable. The 2D electron system is heated by applying electric source-drain-pulses of 0.5 V to 10 V to the MOSFET's which have mobilities around  $10,000 \text{ cm}^2/\text{Vs}$ . The detector signal is correlated with the pulse frequency using a Lock-In-amplifier. The spectral detector response is shown in figure 3a: The photoconductivity peak at 4.4 meV ( $\sim 35.5 \text{ cm}^{-1}$ ) splits up into three lines in the magnetic field. At  $B_0 = 0$  the detectors' responsivity is in the order of  $10^6 \text{ V/W}$ .

Figure 2 shows the main results of the emission experiments: The detector signal is plotted as a function of the electron concentration for two values of grating wave-vector. The heating pulses are 12 V/cm in both cases. Upon a background of broadband FIR emission from hot electrons - discussed in section IV - a peak from the 2D plasmon can be seen, that changes its position, linewidth and amplitude for different grating periods. From the  $\omega(k)$ -relation (eq.(2)) it can be identified as the plasmon peak, which is described by eq. (7) both in amplitude and in linewidth: The smaller plasmon signal at  $a = 1.5 \mu\text{m}$  (lower curve) is due to a lower coupling efficiency  $\alpha$  and a lower electron concentration  $n_s$  giving a smaller value of the resonance in  $\text{Re}(\sigma(\omega, k))$ .

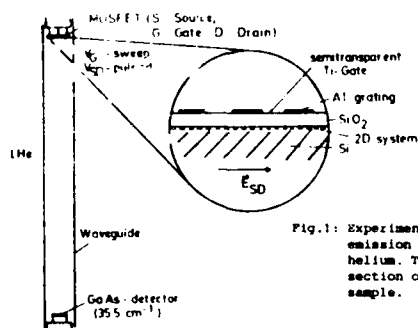


Fig.1: Experimental setup for the FIR-emission experiments in liquid helium. The insert shows a cross-section of the FIR emitting MOS-sample.

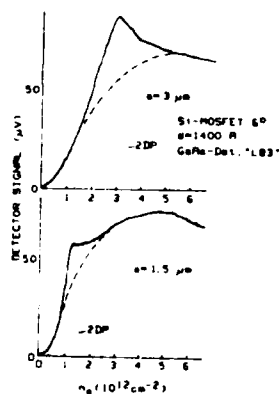


Fig.2: Signal of the GaAs-detector ( $35.5\text{ cm}^{-1}$ ) as a function of  $n_s$  for two different grating periods. Dashed line: background emission from experiments without gratings, dotted lines: 2D plasmon

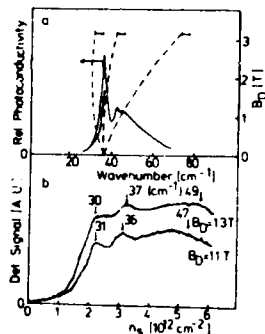


Fig.3: Photoconductivity spectrum of the n-GaAs-detector and its magnetic field dependence (a). Detector signal as a function of electron concentration for two values of detector magnetic field (b).

We performed experiments in the electron concentration range of  $1$  to  $4 \times 10^{12}\text{ cm}^{-2}$  and in the electric field range of  $2$  to  $4\text{ V/cm}$ . This corresponds to electron temperatures of  $2$  up to  $30\text{ K}$  above Helium bath temperature. In this whole range the model of thermal excitation showed up to describe well the experiment. In order to prove the model also at frequencies above  $35.5\text{ cm}^{-1}$ , we used the GaAs-detector in the magnetic field, where the photoconductivity peak splits up into 3 lines, as shown in fig. 3a. In fig. 3b the spectra at  $B_D = 1.1$  and  $1.3\text{ T}$  are shown, the frequencies detected by this method are indicated by arrows; they exactly prove the dispersion relation (2).

#### Magnetoplasmons

In a magnetic field the dispersion of a two-dimensional plasma wave is modified according to [2,21/

$$\omega_{mp}(k) = [\omega_p^2(k) + \omega_c^2]^{1/2} \quad (9)$$

This leads for a given detector frequency to a shift of the resonant photoconductivity peak to lower  $n_s$ , as it is shown in the spectra of fig. 4: The inverted triangles give the  $n_s$ -position of the  $4.4\text{ meV}$ -magnetoplasmon according to eq. (9). The position of the magnetoplasmon resonance follows the theoretical calculation. The intensity of the signal, however, decreases strongly with increasing magnetic field. This effect can be explained by the classical theory based on  $\sigma(\omega, k, B)$  [7/]. The carrier mobility is decreased due to Landau quantisation, leading to a strongly decreased dynamical conductivity as well as carrier heating. The oscillatory FIR emission at  $7.5\text{ T}$  is due to probably four oscillatory effects in the magnetic field, which cannot be quantitatively separated, since they are not all yet experimentally observed separately: The input

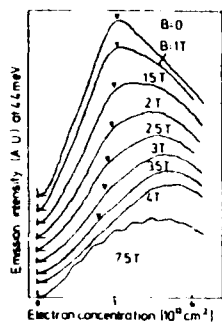


Fig.4: Spectra of the plasmon emission at different magnetic fields taken with the GaAs-detector ( $35.5 \text{ cm}^2$ ). The inverted triangles give the  $n$ -positions of the magneto plasmon according to eq.(9).

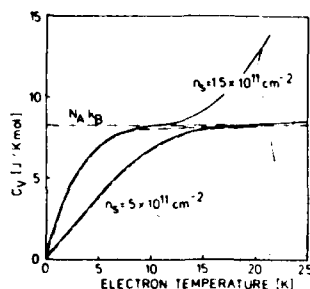


Fig.5: Molar specific heat of a 2D carrier system: Free carrier value ( $C_{v,el}$ , dashed lines) and plasmon contribution ( $C_{v,pl}$ , dotted lines) to the total specific heat ( $C_{v,tot}$ ).

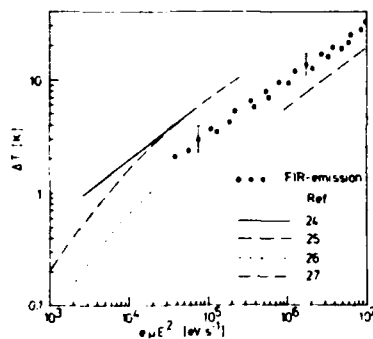


Fig.6: Experimentally obtained electron temperature behaviour from FIR-broadband emission in comparison to previous  $T_t$ -measurements.

power as well as  $n(\omega)$  oscillate due to oscillations of the conductivity, oscillations of acoustic phonon scattering and the specific heat [22], which both cause an oscillatory carrier temperature, are predicted.

### III. THE SPECIFIC HEAT OF THE FREE 2D ELECTRON SYSTEM

The spectral energy density of the longitudinal 2D plasmons can be calculated with Bose-Einstein statistics. For an arbitrary plasmon dispersion relation  $\omega(k)$ , the plasmon energy density is given by

$$U(\omega(k), T) = \int u(\omega(k), T) d\omega,$$

where the spectral energy density  $u(\omega(k), T)$  is

$$u(\omega(k), T) = \frac{1}{(2\pi)^2} \int \frac{\hbar \omega(k) k (\delta k / \delta \omega) dy}{\exp[\hbar \omega(k) / k_B T] - 1} \quad (10)$$

$y$  is the polar angle in the two-dimensional  $k$  space and  $(\delta k / \delta \omega)$  is the inverse of the group velocity of the plasmon  $\omega(k)$ .  $T$  denotes the electron temperature.

With the known energy density (eq.(10)) one can calculate the specific heat of the 2D plasmons: For a pure 2D plasma dispersion -  $\omega^2$  proportional to  $k$  - we obtain for the molar plasmon specific heat

$$C_{v,pl} = - \frac{dU}{dT} \frac{N_A}{n_B} = N_A k_B \left( \frac{T}{T_0} \right)^2 \int_0^{n_{crit}} \frac{x^2 e^x dx}{(e^x - 1)^2}, \quad (11)$$

where

$$T_0 = \frac{\hbar \omega}{k_B} = \left( \frac{n_B^2 \pi}{m^2 \epsilon_0^2 (\epsilon_{st} + \epsilon_{ox})^2} \right)^{1/4}$$

and  $\omega_{crit} = \hbar \omega_{crit} / k_B T$ .  $N_A$  denotes the Avogadro number and  $\omega_{crit}$  the critical frequency (cutoff frequency), where the dispersion relation of the plasmon crosses the single-particle excitation regime. There the plasmon does not exist any more as a well-defined mode. The temperature  $T_0$  is characteristic for the low-temperature plasmon specific heat. Typical values of  $T_0$  for Si are, e.g., 328 K for  $n_s = 1 \times 10^{12} \text{ cm}^{-2}$  and 35 K for  $n_s = 1.5 \times 10^{11} \text{ cm}^{-2}$ . At low temperatures and high densities  $\omega_{crit}$  can be replaced by  $\omega$ . In this regime the plasmon specific heat increases with  $T^4$  and decreasing  $n_s$ . At high temperatures and low densities the plasmon specific heat would be of the order of the free-electron specific heat, which is limited by  $N_A k_B$ . However, the plasmon and single-particle contributions to the total specific heat cannot be simply added, since the kinetic energy of electrons as single particles and their collective motion cannot be considered completely independent. In addition the upper limit  $\omega_{crit}$  becomes finite and limits the value of  $C_{v,pl}$ . Therefore eq. (11) describes the plasmon contribution to the total specific heat of the system only at low temperatures and high densities. We expect, however, the total specific heat of the electron system to exceed the free-electron-gas value as a result of plasmon generation at low densities and high temperatures, since the restoring forces in the plasma oscillations increase the time-averaged energy of the system.

In fig. 5 the calculated  $T$ -dependences of the free carrier specific heat  $C_{v,el}$  in comparison to the plasmon contribution  $C_{v,pl}$  are plotted for two values of  $n_s$ . At  $n_s = 5 \times 10^{11} \text{ cm}^{-2}$  the plasmon contribution is negligible, at  $n_s = 1.5 \times 10^{11} \text{ cm}^{-2}$ , however, the plasmon specific heat should give a significant contribution to the total specific heat of the electron system, which exceeds the Dulong-Petit limit already at temperatures of about 10 K.

#### IV. ELECTRON TEMPERATURES IN SI-MOSFET's

FIR emission from the inversion layer of the Si-MOSFET's brings a new method of determining electron temperatures. Since the broadband FIR absorption by the 2D electron system is known experimentally [19] and theoretically (eq. (4)), the absolute emission intensity of FIR-radiation from the 2D electron system according to eq. (8) represents a direct measure for the electron temperature  $T$ .

In these experiments we used MOSFET's with transparent gate electrodes and a GaAs-detector, whose responsivity at  $35.5 \text{ cm}^{-1}$  has been determined accurately by using a Carbone-glass-bolometer as a reference source [23]. The 2D electron system is heated by applying electric source-drain pulses of 0.5 V up to 10 V to the MOSFET's. Simultaneously the current-voltage characteristics of the MOSFET's is measured to determine the  $n_s$ - and field dependent mobilities of the samples for the calculation of the input power  $e\mu E^2$  and the dynamical conductivity  $\text{Re}\sigma(\omega)$ .

We investigated MOS-samples with different mobilities from 2,000 up to 10,000  $\text{cm}^2/\text{Vs}$ . In fig. 6 the electron temperatures evaluated according to eq. (8) are plotted versus the input power  $e\mu E_{SD}^2$  which, in equilibrium situation, is equal to the power loss of the hot electron gas. In the figure also the slope for  $\Delta T \propto (e\mu E^2)^{1/2}$  is indicated. As a result the electric heating  $\Delta T$  is in the whole range of temperature exactly proportional to the square root of the input power respectively the power loss  $e\mu E^2$ . We can therefore express the electron heating as a function of the input power  $e\mu E^2$  quantitatively as

$$\frac{\Delta T}{(e\mu E^2)^{1/2}} = (1.2 \pm 0.3) \cdot 10^{-2} \text{ K } \mu^{1/2} (\text{eV})^{-1/2} \quad (12)$$

This result is close to the electron temperature measurements made at low electron temperatures by Fany and Fowler /24/, Kawaji and Kawaguchi /25/ and Hönlein and Landwehr /26/, as indicated in fig. 6, and somewhat higher than those obtained from subband emission /27/. FIR-emission is the first method that can give results in the whole temperature range of 2 K up to more than 30 K. The linear dependence of  $\Delta T$  on  $(\mu E^2)^{1/2}$  is predicted by recent theories of acoustic phonon scattering in 2D systems /28,29/ up to electron temperatures of at least 50 K.

With the method of FIR-broadband-emission we were furthermore able to measure the effect of increased carrier heating /26,30/, when a negative substrate bias is applied. The effect is due to a decreased channel width /29/ and an influence of  $\text{SiO}_2$  phonon modes /26/.

In conclusion, we emphasize that FIR emission from heated carriers in 2D systems is a powerful tool to study electronic excitations in two dimensions, such as plasmons, subband excitations etc., since only the electron system is heated, and other excitations of the device are not disturbing in the experiments. Up to now only spontaneous emission from thermally excited plasmons could be experimentally achieved. This means that in all experiments thermodynamic equilibrium of plasmons and electrons was given. A non-equilibrium specific excitation of plasmons would be of interest since the radiative decay efficiency is quite high. There are theoretical calculations of amplification of plasmons in 2D systems, e.g. /31/. Promising possibilities of non-equilibrium excitation would be drifting carriers - exceeding the phase velocity of the plasma wave or interacting strongly with the grating, in analogy to travelling wave tubes. High drift velocities in GaAs/AlGaAs-heterostructures up to  $3 \times 10^7$  cm/s have been reported /32/, which are already equal to the phase velocities of 2D plas-

mons at low electron concentrations. Striking experiments on plasmon-generation by drifting carriers can therefore be expected in the near future.

#### Acknowledgements

The MOS-samples were made at Bell-Laboratories, Murray Hill, USA, and kindly provided by Prof. D.C. Tsui, Princeton University. This work was supported by the Fonds zur Förderung der wissenschaftlichen Forschung, Wien, Austria (Projekt S 22/05) and by the European Research Office, London.

# REFERENCES

- 1 F. Stern, Phys.Rev.Lett. 18 (1967) 546.
- 2 A.V. Chaplik, Zh. Eksperim.Teor.Fiz. 62 (1972) 746, Soviet Phys.-JETP 35 (1972) 395.
- 3 M.Nakayama, J.Phys.Soc.Japan 36 (1974) 393.
- 4 A. Equiluz, T.K. Lee, J.J. Quinn, K.W. Chiu, Phys.Rev.B 11 (1975) 4989.
- 5 C.C. Grimes, G. Adams, Phys.Rev.Lett. 36 (1976) 145.
- 6 S.J. Allen, D.C. Tsui, R.A. Logan, Phys.Rev.Lett. 38 (1977) 980.
- 7 T.N. Theis, J.P. Kotthaus, P.J. Stiles, Solid State Commun. 24 (1977) 273.
- 8 T.N. Theis, J.P. Kotthaus, P.J. Stiles, Solid State Commun. 26 (1978) 603.
- 9 D.E. Beck, P. Kumar, Phys.Rev.B 13 (1976) 2859.
- 10 M. Jonson, J.Phys.C 9 (1976) 3055.
- 11 A.K. Rajagopal, Phys.Rev.B 15 (1977) 4264.
- 12 D. Heitmann, J.P. Kotthaus, E.G. Mohr, Solid State Commun. 44 (1982) 715.
- 13 E. Batke, D. Heitmann, A.D. Wieck, J.P. Kotthaus, Solid State Commun. 46 (1983) 269.
- 14 A.D. Wieck, E. Batke, D. Heitmann, J.P. Kotthaus, this conference.
- 15 D.J. Olego, A. Pinczuk, A.C. Gossard, W. Wiegmann, Phys.Rev.B 25 (1982) 7867.
- 16 D.C. Tsui, E. Gornik, R.A. Logan, Solid State Commun. 35 (1980) 875.
- 17 R.A. Höpfel, E. Vasa, E. Gornik, Phys.Rev.Lett. 49 (1982) 1667.
- 18 R.A. Höpfel, E. Gornik, A.C. Gossard, W. Wiegmann, Proc. 16th Int. Conf. on "The Physics of Semiconductors", Montpellier, France, 1982, edited by M. Averous (North Holland Amsterdam, 1983) p. 646.
- 19 S.J. Allen, D.C. Tsui, F. De Rosa, Phys.Rev.Lett 35 (1975) 1359.
- 20 T.N. Theis, Surface Sci. 98 (1980) 515.
- 21 N.J. Hornig, M.M. Yildiz, Ann.Phys. 97 (1976) 216.
- 22 M. Zawadzki, this conference.
- 23 R.A. Höpfel, E. Vasa, E. Gornik, to be published.
- 24 F.F. Fang, A.B. Fowler, J.Appl.Phys. 41 (1970) 1825.
- 25 S. Kawaji, Y. Kawaguchi, Proc.Int.Conf.on "The Application of High Magnetic Fields in Semiconductor Physics", Grenoble 1982, p. 53, Lecture Notes in Physics Vol. 177 (ed. G. Landwehr), Springer 1983.
- 26 M. Hönlein, G. Landwehr, Surface Sci. 113 (1982) 260 and priv. commun.
- 27 E. Gornik, D.C. Tsui, Solid State Electronics 21 (1978) 139.
- 28 Y. Shiiba, J. Nakamura, J.Phys.Soc. Japan 50 (1981) 114.
- 29 E. Vasa, R.A. Höpfel, E. Gornik, to be published.
- 30 K.M. Chao, R.G. Wheeler, Surface Sci. 98 (1980) 210.
- 31 A.V. Chaplik, Surface Sci. 113 (1982) 353, and this conference.
- 32 Y. Inuishi, Int.Conf.on Solid State Devices, Tokyo 1982.

INTERACTION BETWEEN ELECTRONIC AND PHONON RAMAN  
SCATTERING IN HOLE SPACE CHARGE LAYERS ON SILICON

M. Baumgartner and G. Abstreiter

Physik-Department, Technische Universität München  
8046 Garching, Fed. Rep. of Germany

Abstract

The interaction of quasi-continuous electronic excitations in hole space charge layers of Si with the optical phonons is investigated. The induced asymmetric broadening of the one-phonon line can be understood as a quantum mechanical interference of the continuum excitations with the discrete energy state. The lineshape is directly related to electron-phonon interaction matrix elements.

Resonant inelastic light scattering has been used recently to investigate the subband structure of hole accumulation layers in Si-MOS-structures<sup>1,2/</sup>. The measured subband splittings are found to be in surprisingly good agreement with self-consistent Hartree calculations of Bangert<sup>3/</sup>. With increasing surface hole concentrations the experimental lines broaden considerably. For  $N_s \approx 5 \times 10^{12} \text{ cm}^{-2}$  a more or less structureless continuum is observed which extends to energies as high as 100 meV. The extreme broadening of the hole subband excitation lines is mainly caused by strongly different  $k_{\parallel}$ -dispersion of the individual subbands and also by the contribution of various subbands. The transitions involved are shown schematically in Fig. 1. In the present communication we want to report on the interaction of these quasi-continuous electronic excitations with the optical phonons at  $\approx 65 \text{ meV}$ .

343

It is well known that when a discrete energy state is superimposed on a broad continuum the phenomenon of resonant interference may occur. This effect has been studied extensively in bulk-Si with heavy acceptor doping<sup>4/</sup>. In the nonpolar material Si plasmon-phonon coupling is negligible because the optical phonons at  $k \approx 0$  do not split into LO and TO components. The phonons, however, couple with the electronic excitations via the deformation potential mechanism. These effects are usually small but have been observed directly in Raman scattering. They appear as a shift and broadening of the phonon lines, which is caused by the formation of a quasi-particle consisting of a phonon dressed with single-particle electronic excitations. The quasi-particle has a self-energy. Its real part is the energy shift, its imaginary part the additional broadening introduced by the carriers. The lineshape is described by the Fano-Breit-Wigner formula where the intensity is given by<sup>5/</sup>

$$I \sim \frac{(Q + \epsilon)^2}{1 + \epsilon^2} \quad (1)$$

with  $\epsilon = (\omega - \omega_0 - \Delta\omega_0)/\Gamma$  and  $Q = (V T_p/T_e + \Delta\omega_0)/\Gamma$ .  $Q$  is the asymmetry parameter,  $\Gamma$  the broadening,  $\omega_0$  the phonon frequency without carriers, and  $\Delta\omega_0$  the frequency shift.  $Q$  depends on  $\Gamma$  and  $\Delta\omega_0$  and on the electron phonon matrix element  $V$ , as well as on the ratio of the Raman matrix elements of pure phonon and pure electronic scattering  $T_p/T_e$ .  $Q$ ,  $\Gamma$  and  $\Delta\omega_0$ , which can be determined experimentally, are directly related to the microscopic properties of the system.

These types of interactions have now been studied in connection with the hole subband structure at Si-surfaces. The experiments have been performed in back-scattering geometry, using the 3.48 eV emission line of a  $\text{Kr}^{+}$ -ion laser. This energy is close enough to the  $E_0^v$  gap of Si in order to fulfill the resonance condition for electronic light scattering. The laser penetration depth is of the order of 100 Å, and thus comparable to the width of the surface space charge layer. The effect of a hole accumulation layer on the

344



optical phonons in Si is shown in Fig. 2. The dashed line represents a Raman spectrum of pure Si under flatband conditions. The solid line is observed when a gate voltage  $V_g = -50$  V ( $N_s \approx 1 \times 10^{13} \text{ cm}^{-2}$ ) is applied to the MOS-capacitor sample. The interaction between the electronic continuum excitations and the one-phonon line manifests itself in a decrease of the phonon intensity, which is concomitant with a slightly asymmetric broadening of the phonon line.

The dependence of the phonon peak height on the gate voltage is shown more explicitly in the insert of Fig. 2. While no change is found when a positive gate voltage is applied, the phonon intensity decreases by as much as 15% when a hole space charge layer is formed (negative gate voltage). Both the decreasing intensity and the asymmetric broadening are seen more clearly in Fig. 3 where we plot the difference of the Raman spectra as obtained with a phase sensitive technique. The gate voltage is switched periodically between the desired values. The differential spectrum shows a strong negative signal at the energy of the optical phonons ( $\approx 65$  meV) which gives directly the decrease of the phonon intensity. Both on the low and high energy side the positive signals reflect the increased scattering intensity in the wings of the phonon line. The different amplitudes are caused by the asymmetric broadening.

In order to obtain the parameters  $Q$ ,  $\Delta\omega_0$ , and  $\Gamma$  quantitatively the spectra have been fitted to equation (1). Without carriers good agreement is obtained for  $Q \approx 400$  and  $\Gamma = 0.13$  meV,  $\Gamma$  being the halfwidth of the phonon line at half maximum. At  $V_g = -50$  V we find  $Q = 60_{-20}^{+10}$  and  $\Gamma = (0.17 \pm 0.01)$  meV for the scattering configuration used. The points in Fig. 2 represent the calculated lineshape. The frequency shift  $\Delta\omega_0$  is found to be smaller than 0.01 meV. The carrier-induced broadening is directly proportional to the electron-phonon interaction matrix element  $V$ . The interference parameters can be varied by changing the carrier concentration. In order to calculate  $Q$ ,  $\Gamma$ , and  $\Delta\omega_0$  explicitly, the combined density of states for the electronic transitions and

their contribution to the broadening has to be known. This requires extensive subband calculations including the dispersion in the whole two-dimensional  $k_{\parallel}$ -space. Such calculations are not yet available. The asymmetry parameter  $Q$  is also related to the ratio  $T_p/T_e$ . This can be determined independently from the measured scattering intensities. It, however, depends on the surface orientation and on the scattering configuration.

In conclusion, we have demonstrated that the effect of free carrier excitations in hole space charge layers on the optical phonons of the nonpolar semiconductor Si can be measured with Raman spectroscopy. The analysis of the induced changes of the one-phonon lineshape yields microscopic information on electron-phonon interactions in surface space charge layers.

#### Acknowledgments

This work has been supported by the Deutsche Forschungsgemeinschaft via Sonderforschungsbereich 128.

#### References:

- 1) G. Abstreiter, U. Claessen, and G. Tränkle, Solid State Comm. **44**, 673 (1982)
- 2) M. Baumgartner and G. Abstreiter (to be published)
- 3) E. Bangert (unpublished) (1975);  
E. Bangert, K. v. Klitzing, and G. Landwehr, Proc. 12<sup>th</sup> Int. Conf. Phys. Semicond. (ed. by M.H. Pilkuhn), p. 714, Stuttgart (1974)
- 4) See for example:  
F. Cerdeira, T.A. Fjeldly, and M. Cardona, Phys. Rev. **B 8**, 4734 (1973)
- 5) U. Fano, Phys. Rev. **124**, 1866 (1961)

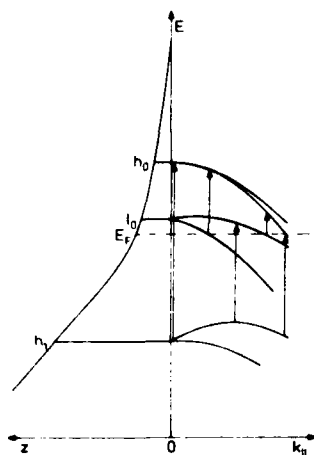


Fig. 1: Valence band diagram for a hole space charge layer in Si.  $h_0$ ,  $l_0$ , and  $h_1$  denote the heavy-hole and light-hole-like subbands. The arrows indicate various possible subband transitions yielding a quasi-continuous background over a wide energy region.

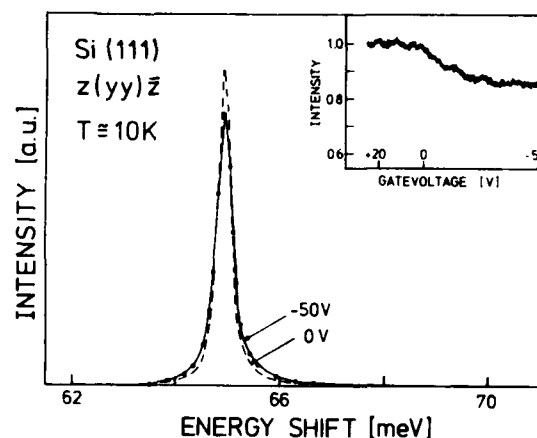


Fig. 2: Comparison of the one-phonon Raman line of Si with and without a hole space charge layer at the surface. The points represent a calculated lineshape. The insert shows the decrease of the phonon intensity with applied gate voltage.

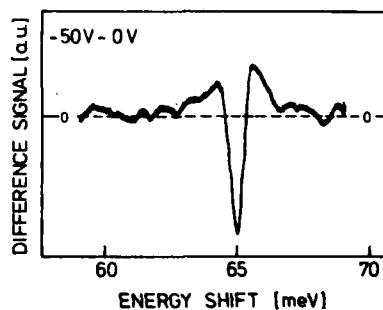


Fig. 3: Differential Raman spectrum which shows directly the space charge layer induced changes of the optical phonon line in Si.

# INTERFACE OPTIC PHONONS AND MAGNETO-PHONON EFFECT IN POLARizable DOUBLE-HETEROSTRUCTURES

R. Lassnig and W. Zawadzki\*  
Institut für Experimentalphysik  
Universität Innsbruck, AUSTRIA

\*Institute of Physics  
Polish Academy of Sciences, 02668 Warsaw, POLAND

The properties of interface longitudinal optical phonons and their interaction with electrons confined in double-heterostructures are derived, the latter representing an intermediate step between single heterostructures and superlattices. We discover a continuous transition from two- to three-dimensional interaction. The results are discussed in relation with experimental observations of the magnetophonon effect.

## INTRODUCTION

In recent years there has been an increasing interest in the interaction between low energy electrons and the elementary excitations of solids in the presence of interfaces. In the case of polar crystals the electrons couple to bulk as well as interface optic phonon modes. Semiconductor heterostructures and superlattices therefore represent an ideal tool for the investigation of interface phonon properties.

Shortly after the first observation of resonant magneto-phonon effects in GaAs-AlGaAs heterostructures (1) Nicholas et al. (2) performed similar experiments on GaInAs-InP superlattices, this material being a good candidate for the detection of interface optic phonons.

The interaction Hamiltonian for a completely two-dimensional electron gas with interface optic phonons for a semiconductor-insulator structure has been derived by Tzoar (3). In the present paper we generalize his approach to double-heterostructures (DHS) between arbitrary polar semiconductors, for realistic wave functions spread out in z-direction. The DHS has been chosen, since on the one hand the single heterostructure represents only a limiting case of the former. On the other hand, the difference to a superlattice is not very great, especially if the insulating layer of the superlattice is not too thin. The results are compared with new experiments of Portal et al. (4).

## PHONON STRUCTURE

In order to determine the phonon structure in a DHS we make use of the energy loss method, comparing the classical and the quantum mechanical rate of energy loss of a test charge. The interfaces are taken parallel to the (x,y) plane at  $z = \pm d/2$  and the bulk dielectric functions of the layer and the surrounding material are denoted by  $\epsilon_m$  and  $\epsilon_s$ , respectively. The symmetry of the problem allows working in the  $(q_x, z)$ -space, which makes the calculations simple.

At first the potential induced by a test point charge moving in the  $z=0$  plane with velocity  $v_x$  is derived. In order to account for the dielectric discontinuities at  $z = \pm d/2$  image charges  $q_m$  and  $q_s$  are introduced. Since they are no real charges, their value and position depends on the position  $z$  of the observer. The potential ansatz is

$$\phi(q_x, z) = \frac{e\delta(\omega - q_x v_x)}{8\pi^2 q_x} \begin{cases} [e^{-q_x z} + \alpha_m (e^{-q_x(d-z)} + e^{-q_x(d+z)})]/\epsilon_m & \dots |z| < d/2 \\ [e^{-q_x z} (1 + \alpha_s) + \alpha_m e^{-q_x(z-d)}]/\epsilon_s & \dots z > d/2 \end{cases} \quad (1)$$

From the Maxwell conditions, requiring that both the potential and the dielectric displacement are continuous across the interface, one obtains

$$\alpha_m = -\alpha_s = \frac{(\epsilon_m - \epsilon_s)}{\epsilon_s(1+\gamma) + \epsilon_m(1-\gamma)} \quad , \quad \gamma = e^{-q_x d} \quad (2)$$

Setting  $z=0$ , the classical energy loss of the test charge is (3)

$$\frac{dW}{dt} = \lim_{v \rightarrow 0} \text{ev} \phi(x, z, t) = 2e \int d^2 q_x \int_0^\infty d\omega \text{Im} \phi(q_x, \omega) \quad (3)$$

$$\text{Im} \phi(q_x, \omega) = \frac{e\delta(\omega - q_x v_x)}{8\pi q_x} \left[ \frac{(1-\gamma)\epsilon(\epsilon_m)}{(1+\gamma)} - \frac{4\gamma}{(1+\gamma)} \delta(\epsilon_s(1+\gamma) + \epsilon_m(1-\gamma)) \right] \quad (4)$$

Eqs. (3,4) are now compared with the quantum mechanical rate of energy loss. In terms of the destruction operators  $b_2$  and  $b_3$  the electron-phonon interaction is specified in the following form:

$$V_{ph}^{(2)} = \sum_{q_x} i q_x x (e^{-q_x(d/2-z)} + e^{-q_x(d/2+z)}) v_2 b_2 + \text{h.c.} \quad \dots |z| < d/2 \quad (5)$$

$$V_{ph}^{(3)} = \sum_{q_x} i q_x x \sum_{n=1}^\infty \sin((z/d - 1/2)n\pi) v_3 b_3 + \text{h.c.} \quad \dots z > d/2 \quad (6)$$

$V_{ph}^{(3)}$  is the bulk potential characterized by a restricted number of phonon modes in z-direction.  $V_{ph}^{(2)}$  describes the pair of two-dimensional phonons from the two interfaces. Writing the matrix element for one-phonon emission as  $\langle H_{int} \rangle$ , the quantum mechanical expression for the rate of energy loss is

$$\frac{dN}{dt} = \frac{2\pi}{h} \sum_q |\langle H_{int} \rangle|^2 \delta(\omega - q_z v_z) \quad (7)$$

In the following we restrict ourselves to the situation where the layer and the surrounding material are of single-mode type:

$$\epsilon_{m,s}(\omega) = \epsilon_{m,s} (\hbar^2 \omega^2 - L_{m,s}^2) / (\hbar^2 \omega^2 - T_{m,s}^2) \quad (8)$$

where  $\epsilon_m$ ,  $L$  and  $T$  denote the high frequency dielectric constant, the longitudinal and the transverse optic phonon energy, respectively. In this case one obtains two interface phonon modes, characterized by the frequencies  $\omega_s$  and the interaction strengths  $V^2$ :

$$\omega_s^2 = (p \pm \sqrt{p^2 - (\epsilon_m^{-1} + \epsilon_s^{-1}) (\epsilon_m^{-1} T_m^2 + \epsilon_s^{-1} T_s^2)}) / (\epsilon_m^{-1} + \epsilon_s^{-1}) \quad (9)$$

$$p = [\epsilon_m^{-1} (T_m^2 + L_m^2) + \epsilon_s^{-1} (T_s^2 + L_s^2)] / 2, \quad \epsilon_m^{-1} = \epsilon_m^{-1} (1 - \gamma), \quad \epsilon_s^{-1} = \epsilon_s^{-1} (1 + \gamma) \quad (10)$$

$$(V_s^2)^2 = e^2 \hbar \omega_s f_s / A q_z \quad (11)$$

$$f_s = \pm (\hbar^2 \omega_s^2 - T_m^2) (\hbar^2 \omega_s^2 - T_s^2) / 4 \hbar^2 \omega_s^2 (\omega_s^2 - \omega_m^2) (\epsilon_m^{-1} + \epsilon_s^{-1}) \quad (12)$$

where  $A$  denotes the normalization area. The bulk interaction is given by

$$(V_s)^2 = \frac{e^2}{A} \frac{\hbar L_m}{d \epsilon_m} \left(1 - \frac{T_m^2}{L_m^2}\right) \frac{1}{q_z^2 + (n\pi/d)^2} \quad (13)$$

#### MAGNETOPHONON EFFECT AND EFFECTIVE POTENTIALS

In a previous paper (5) we have derived the following expression for the magneto-phonon contribution to the conductivity  $\sigma_{xx}$  for a quasi two-dimensional electron gas:

$$\sigma_{xx} = \frac{e^2}{\hbar k_B T} n_s (n_s + 1) \frac{1}{2} \sum_{n,m} \sum_q q^2 V_{eff} |J_{nm}(q_z^2/2)|^2 \cdot I_{nm} \quad (14)$$

$$V_{eff} = \frac{e^2 \hbar \omega}{4 A q_z} \left( \frac{1}{\epsilon_m} - \frac{1}{\epsilon_0} \right) F(q_z) \quad (15)$$

$$F(q_z) = \frac{q_z}{\pi} \int dq_z |\rho(q_z)|^2 / (q_z^2 + q_z^2) \quad (16)$$

$$|J_{nm}(a)|^2 = \frac{n!}{m!} a^{m-n} e^{-a} |L_{m-n}^{m-n}(a)|^2 \quad m > n \quad (17)$$

$$I_{nm} = [f(E_n - \hbar \omega) - f(E_n)] / (1 + \frac{E_n - E_n - \hbar \omega}{2T}) \quad (18)$$

where  $n_s$  and  $f(E)$  denote the Bose and Fermi distribution functions for optic

phonons and electrons.  $E_n$  stands for the energy of an electron in Landau level  $n$ ,  $r$  is the level width,  $l^2 = \hbar c / e H$ ,  $\rho(q_z)$  is the Fourier transform of the electronic charge density  $\rho(z)$  and the functions  $L_n^{m-n}$  are associated Laguerre polynomials, which are equal to 1 for  $n=0$ . In the above expression the Fröhlich interaction has been treated as three-dimensional, and  $k_B T \gg \Gamma$  has been assumed. The form factor  $F$  depends on the spreading of the electron wave function in  $z$ -direction and is equal to one for a completely two-dimensional electron gas. The factor  $I_{nm}$  becomes large if the Landau levels  $n$  and  $m$  are separated by the phonon energy  $\hbar \omega$ , which is the usual magneto-phonon resonance condition.

Interface phonon effects show up in a different effective interaction and smaller phonon energies than in the bulk case. If the distance between the DHS interfaces is not too large, the lowest electric subband can be described by the following wave function:

$$\psi(z) = \sqrt{2/d} \sin((z/d - 1/2)n\pi) \quad (19)$$

The corresponding interface and bulk effective potentials are

$$V_{eff}^{(2)} = \frac{e^2 \hbar \omega_s f_s}{A q_z} \pm \frac{4(1 - e^{-\alpha})}{(1 + \alpha^2/4\pi^2)}, \quad \alpha = q_z d \quad (20)$$

$$V_{eff}^{(b)} = \frac{e^2 \hbar L_m}{A q_z \epsilon_m} \left(1 - \frac{T_m^2}{L_m^2}\right) \frac{64}{9\pi^2} \frac{\alpha}{(1 + \alpha^2/\pi^2)} \quad (21)$$

where the bulk effective potential  $V_{eff}^{(b)}$  has been approximated (within one percent) by the interaction with the longest wavevector phonon with  $q_z = n\pi/d$ .

#### RESULTS AND DISCUSSION

By a comparison of the classical and the quantum mechanical energy loss of a test charge the energy spectrum and the interaction strength of LO phonons in polar double-heterostructures has been determined. The numerical calculations are performed for a  $\text{Ga}_{0.5}\text{In}_{0.5}\text{As}$  layer embedded in  $\text{InP}$ . Although it is well known (6) that  $\text{GaInAs}$  is a two-mode material, the lower mode is neglected for simplicity, since for the given composition it couples much weaker to the electrons than the upper mode. The material constants are taken to be  $L_m = 34$ ,  $T_m = 31.7$ ,  $L_s = 43$ ,  $T_s = 37.6$  (all in meV),  $\epsilon_m = 11.35$  and  $\epsilon_s = 9.56$ .

Generally it can be said the properties of the DHS phonons depend essentially on the dimensionless parameter  $\alpha = q_z d$  describing the relation of the layer thickness  $d$  to the phonon wavelength  $\sim 1/q_z$  parallel to the interface.

Fig. 1a shows the phonon energy spectrum as a function of  $q$ , revealing the characteristic features of DHS phonons. The full line corresponds to the bulk phonon energy, the dashed and the dotted lines to the higher (InP) and lower two-dimensional phonons. Whereas in the case of a single interface the interface phonon energies are independent of the momentum  $q$ , the DHS phonon energies vary with the momentum and the layer thickness. For  $qd \ll 1$ , i.e. for relatively long phonon wavelengths, the DHS phonon corresponding to the layer material (GaInAs) is damped down to the TO phonon energy  $\hbar\omega_{TO}$ . At the same time the InP-like mode approaches the bulk energy value. On the other hand, for relatively small wavelengths ( $qd \gg 1$ ), the DHS phonon energies converge to the single interface phonon energies, which is the single heterostructure limit.

Fig. 1b shows the two-dimensional form factors  $F_z$  and  $F_d$ , defined as  $V_{eff}^{(2+)}(b)$  and  $V_{eff}^{(b)}$  (Eq. 15, with  $F=1$ ). They are compared with the three-dimensional form factor  $F$  (circles) and represent a reasonable measure for the effective coupling. Just as for the energies, the interaction of the InP-like phonon approaches the three-dimensional value for  $qd \rightarrow 0$ , describing the transition from two- to three-dimensional electron-phonon interaction.

For the GaInAs modes it can be seen that over the whole regime the bulk interaction is considerably stronger than the interface interaction. This is due to the fact that the DHS phonon energy is closer to the TO phonon energy, which corresponds to weak polarity.

To interpret magneto-phonon effects, the integration Eq. (14) has to be performed numerically. In the present work, however, a more qualitative comparison is given preference: Consider a  $0 \rightarrow m$  magnetophonon resonant situation, where the phonon energy is a multiple of the cyclotron resonance energy ( $\hbar\omega_c = m\hbar\omega_{ph}$ ). If the two-dimensional form factors  $F$  are slowly varying, as indicated in Fig. 1b, the expression under the integral Eq. (14) has a relatively pronounced maximum at  $q_z^2 = 2m+1$ . Determining  $q_z^2$  from the resonance condition, this corresponds to  $q_z^2 = 2m^2 \omega_c / \hbar(1+1/2m)$ , which is magnetic field independent and for  $\text{Ga}_{0.5}\text{In}_{0.5}\text{As}$ , where the effective mass  $m^*$  is 0.04 to 0.05, is of the order of  $q_z^2 = 1/50 \text{ \AA}^{-2}$ . Since  $q_z^2$  denotes the momentum value, for which the resonant interaction is strongest,  $\omega_c(q_z^2 d)$  can be interpreted as the typical DHS phonon frequencies involved.

Studying magnetophonon effects in  $\text{Ga}_{0.47}\text{In}_{0.53}\text{As}$ -InP superlattices (for  $d=80$ , 100 and 150 Å and InP-layers of 400 Å) Portal et al. (4) detected two series of

oscillations. For the lower GaInAs series they found  $\hbar\omega_c = 33.6$  (32.9) meV for a 150 (80) Å sample. The decrease towards lower  $d$ -values can be well explained by the increasing influence of interface phonons for  $d \rightarrow 0$ . Weighing the phonon energies (Fig. 1a) with the interaction strengths (Fig. 1b) for  $q^2 = q_z^2 d$  one obtains  $\hbar\omega_c = 33.7$  (33.2) for the 150 (80) Å sample. In addition interface grading should further reduce the phonon energies.

For the higher InP-like mode the energy was found around the bulk value. Theoretically, one expects a lower energy. However, the phonon energy varies with the momentum and, as can be seen in Fig. 1b, the form factor is considerably larger for low momenta. Therefore the range of effective phonon energies is quite large, between 40.5 and 43 meV, so that the resonance is expected to be broadened, but around 41 to 41.5 meV. The remaining discrepancy to the experiment is possibly due to shortcomings in the description of nonparabolicity.

#### ACKNOWLEDGEMENTS

This work was partially sponsored by the Fonds zur Förderung der wissenschaftlichen Forschung, Proj. Nr. S22/05. The authors wish to thank Prof. Erich Gornik for his interest in this work and Prof. Jean-Claude Portal for informative discussions and for making his work available to us prior to publication.

#### REFERENCES

- (1) D.C. Tsui, Th. Englert, A.Y. Cho and A.C. Gossard; Phys. Rev. Lett. 44, 1980 (1980)
- (2) R.J. Nicholas, M.A. Brummel, J.C. Portal, M. Razeghi, M.A. Poisson; Int. Conf. on the Appl. of High Magn. Fields in Semic., Grenoble 1982 (Springer 1983)
- (3) N. Tzoar; Surf. Science 84, 440 (1979)
- (4) J.C. Portal, J. Cisowski, R.J. Nicholas, M.A. Brummel, M. Razeghi, M.A. Poisson; J. Phys. C, July 1983
- (5) R. Lassnig and W. Zawadzki; to be published in J. Phys. C
- (6) M.H. Brodsky and G. Lucovsky; Phys. Rev. Lett. 21, 990 (1968)

Fig. 1: Phonon energies (a) and form factors (b) for a  $\text{Ga}_{0.5}\text{In}_{0.5}\text{As}$ -InP double-heterostructure as a function of  $aq_z d$ .

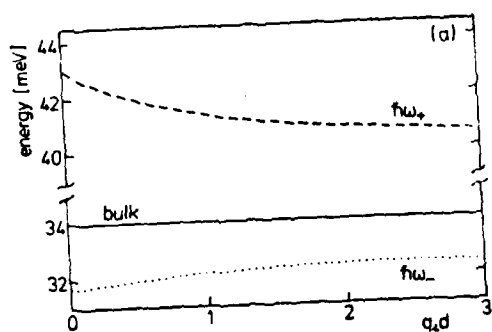


FIGURE 24

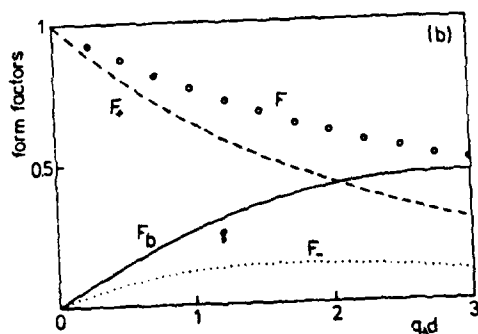


FIGURE 24

CYCLOTRON RESONANCE STUDIES OF SCREENING AND POLARON EFFECTS  
IN GaAs-AlGaAs HETEROSTRUCTURES

M.Seidenbusch, G.Lindemann, R.Lassnig, J.Edlinger and E.Gornik  
Institut für Experimentalphysik  
Universität Innsbruck  
AUSTRIA

**Abstract**

Polaron and screening effects in a two-dimensional electron gas (2DEG) as present in GaAs-AlGaAs heterostructures are determined by cyclotron transmission measurements. The experimental data for the cyclotron mass are well described by a nonparabolicity model. A strong reduction of polaron effects as compared to the bulk GaAs case is demonstrated. An influence of screening effects on the cyclotron resonance linewidth is observed.

**INTRODUCTION**

Recently Das Sarma (1) has predicted that polaron effects are enhanced for a 2DEG as compared to the three dimensional (3D) case.

Horst et al. (2) have performed Cyclotron Resonance (CR) studies in InSb inversion layers for the 0-1 Landau transition through the reststrahlen region and confirmed the predicted increased polaron interaction. However this is in contrast to subband resonance studies performed by Scholz et al. (3) in CdHgTe-accumulation layers, who found reduced polaron effects as compared to bulk CdHgTe. This controversy remains unexplained until yet.

We have investigated the influence of polaron effects on the effective mass of electrons in high mobility GaAs inversion layers as present in GaAs-AlGaAs heterostructures. By using CR transitions with energies well below the optical phonon energy we use a three level method which has been successfully applied at investigations in bulk GaAs (4). In high purity bulk GaAs electrons were heated up by electric fields to occupy higher Landau levels (LL) and several transitions were observed simultaneously. From the analysis of the different LL transitions polaron effects and contributions from nonparabolicity were separated. Both effects were found to be approximately of the same size in good agreement with theoretical calculations (4,5).

In the 2D system different transitions are induced by varying the filling factor. In addition we have studied the influence of screening effects on the CR linewidth.

**RESULTS**

CR absorption measurements were performed using a FIR lasersystem with wavelengths between 200 and 96  $\mu\text{m}$ . Samples with a concentration of  $n_1 = 2.5 \times 10^{11} \text{ cm}^{-2}$  and  $n_2 = 4.1 \times 10^{11} \text{ cm}^{-2}$  and mobilities of  $\mu_1 = 220,000 \text{ cm}^2/\text{Vs}$  and  $\mu_2 = 320,000 \text{ cm}^2/\text{Vs}$  were used.

The electron concentration ( $n_s$ ) was varied by illumination with a LED (6) and monitored by SDH-measurements.

In a 2DEG the number of states per LL is given by the magnetic field. The Fermi level shows an oscillatory behaviour for a given concentration with varying field. The position of the Fermi level is characterized by the filling factor  $\nu$ , defined as the number of electrons divided by the number of states within one Landau level. For  $\nu$  smaller than 1, the Fermi level is within the lowest LL ( $0^{\text{th}}$ ) and only CR transitions 0-1, for  $\nu$  closed to 2 only transitions 1-2 are possible. The observable transitions are therefore unambiguously determined by  $\nu$ . By illumination of the heterostructure with a GaAsP-LED the 2D electron concentration as well as  $\nu$  is increased and different Landau transitions are induced. CR transmission experiments were performed at several laser wavelengths with  $\nu$  as an experimental parameter. Fig.1 shows typical transmission spectra as a function of the magnetic field for the wavelength of 96  $\mu\text{m}$ . Before the illumination the electron concentration is  $2.8 \times 10^{11} \text{ cm}^{-2}$  ( $\nu=0.66$ ). With increasing filling factor ( $>1$ ) a shift of the resonance position to a higher magnetic field is observed. This shift can be explained due to a superposition of different CR transitions. Since we change the carrier concentration by LED illumination we have to investigate first the light effect on the band structure. We assume that the increase of the 2D carrier concentration results from two processes. First from an excitation of electrons from deep impurities in the AlGaAs (6,7) causing a deepening of the interface potential and second from the generation of electron-hole pairs in the depleted p-GaAs region, which are separated in the depletion field; the holes compensate the ionized acceptors, the electrons increase the 2D concentration. The compensation of the depletion charge results in a decrease of the interface potential. The change in the potential well influences the subband energy which can be monitored via a change in the

effective mass. Since the energy gap  $\epsilon_g$  in GaAs is large, nonparabolicity effects are small and the electric and magnetic contributions can be easily estimated.

We solve Zawadzki's nonparabolicity equation for the 2D electron system (8). The electric potential  $V$  in the inversion is calculated in Hartree-approximation by a variational ansatz using the well-known Stern-Howard trial functions. We find that the relevant terms describing the total energy  $\epsilon$  and the nonparabolicity can be expressed in the following way (9):

$$\epsilon = \langle T \rangle + \langle V \rangle + \epsilon_n \left( 1 - \frac{2\langle T \rangle}{\epsilon_g} \right) \text{ with } \epsilon_n = \frac{\hbar^2 q^2}{2} + \sqrt{\frac{\hbar^2 q^2}{4} + \epsilon_g \hbar \omega_c \left( n + \frac{1}{2} \right)}. \quad (1)$$

The brackets  $\langle T \rangle$  and  $\langle V \rangle$  denote the expectation values (10) of the kinetic and potential energy in  $z$ -direction respectively. The electric contribution to nonparabolicity enters by changes into the form of the potential  $\langle V \rangle$ . The third term represents the magnetic field contribution to nonparabolicity.

We have calculated the influence of the illumination on the cyclotron effective masses  $m_c(0-1)$ ,  $m_c(1-2)$  with this model. Fig. 2 shows the calculated influence of the increase of the electron concentration by light illumination on the effective cyclotron mass.

We start with an electron concentration ( $n_s$ ) of  $2.8 \times 10^{11} \text{ cm}^{-2}$  and a depletion charge ( $N_D$ ) of  $0.5 \times 10^{11} \text{ cm}^{-2}$ . First  $N_D$  is diminished by illumination leaving  $m_{CR}(0-1)$  really constant. A further increase in  $n_s$  leads to a continuous increase of  $m_{CR}(0-1)$ . The total mass increase due to nonparabolicity is about 20% when changing  $n_s$  from  $2.8 \times 10^{11}$  to  $5.9 \times 10^{11} \text{ cm}^{-2}$  indicated by the arrow in Fig. 2. In analogy to the 3D case polaron effects and nonparabolicity are determined from the magnetic field shift of the (1-2) transition in respect to the transition (0-1). This shift is derived from a comparison of the magnetic field positions at a filling factor  $\nu < 1$  and  $\nu > 2$  where the different transitions are observed individually.

In Fig. 3 we have plotted the experimentally (from the transmission minima) derived cyclotron mass  $m_{exp}^*$  as a function of  $\nu$ . The mass remains constant from  $\nu = 0.6$  to 1 and from 1.6 to 2. From  $\nu = 1$  to 1.6 a continuous increase due to the superposition of the transitions 0-1 and 1-2 is observed.

The dashed theoretical curve is calculated using the nonparabolicity model of Eq. 1 and taking into account the superposition of the individual transitions. In the full theoretical curve in addition the effect of the changed band structure, caused by the increased electron concentration is in-

cluded. A good agreement between the experimental data and the theory is found. The 2D experimental results can thus be well described by a nonparabolic bandstructure model taking into account the selfconsistent electric potential in the inversion layer varying with the electron concentration. The inclusion of the compensation of the depletion charge due to LED illumination improves the agreement, but does not substantially change the result. We cannot identify any significant polaron contribution to the observed experimental spectra. The strong reduction of polaron effects is clearly demonstrated by comparison with the 3D results, where the equivalent LL splittings are about a factor of 2 larger.

In addition we have investigated the CR linewidth as a function of  $\nu$ . A variation of the linewidth with  $\nu$  was first observed by Englert et al. (11). Our results confirm this observation. We have found a linewidth of  $1.9 \text{ cm}^{-1}$  at  $\nu = 0.66$  and  $2.5 \text{ cm}^{-1}$  at  $\nu = 1$ . This increase is due to a reduction of the screening of the ionized impurity scattering. The experimental result can be well fitted by theoretical calculations using the same impurity concentration derived from the effective mass analysis (12).

We conclude that the polaron interaction is significantly reduced in the 2D case by occupation and screening effects for energies below the optical phonon energy. The variation of screening effects with the filling factor is proven by a CR linewidth analysis and well described by theoretical calculations.

#### ACKNOWLEDGEMENTS

This work was partially sponsored by the Fonds zur Förderung der Wissenschaftlichen Forschung, Austria, Projekt Nr. S 22/05.

#### REFERENCES

- (1) S. Das Sarma, Solid State Commun., to be published.
- (2) M. Horst, U. Merkt and J.P. Kotthaus, Phys. Rev. Lett. 50 (1983) 754.
- (3) J. Scholz, F. Koch, Z. Ziegler, H. Maier, Solid State Commun. 46 (1983) 665.
- (4) G. Lindemann, R. Lassnig, W. Seidenbusch, E. Gornik, Phys. Rev. B, to be published.
- (5) G. Lindemann, W. Seidenbusch, R. Lassnig, J. Edlinger, E. Gornik, 16th Conference on Phys. Semicond., Montpellier (1982).
- (6) H.L. Störmer, R. Dingle, A.C. Gossard, W. Wiegmann and M.D. Sturge, Solid State Commun. 29 (1979) 705.
- (7) A.K. Saxena, Solid State Electronics 25 (1982) 127.
- (8) W. Zawadzki, J. Phys. C: Solid State Phys. 16 (1983) 229.
- (9) R. Lassnig, W. Zawadzki, reported in the same conference.
- (10) T. Ando, A.B. Fowler and F. Stern, Rev. of Modern Physics 54 (1982) 466.
- (11) Th. Englert, I.C. Maan, Ch. Uihlein, D.C. Tsui, A.C. Gossard, 16th Int. Conf. on Phys. Semicond., Montpellier (1982).
- (12) R. Lassnig, E. Gornik, Solid State Commun., in press.



AD A147 163

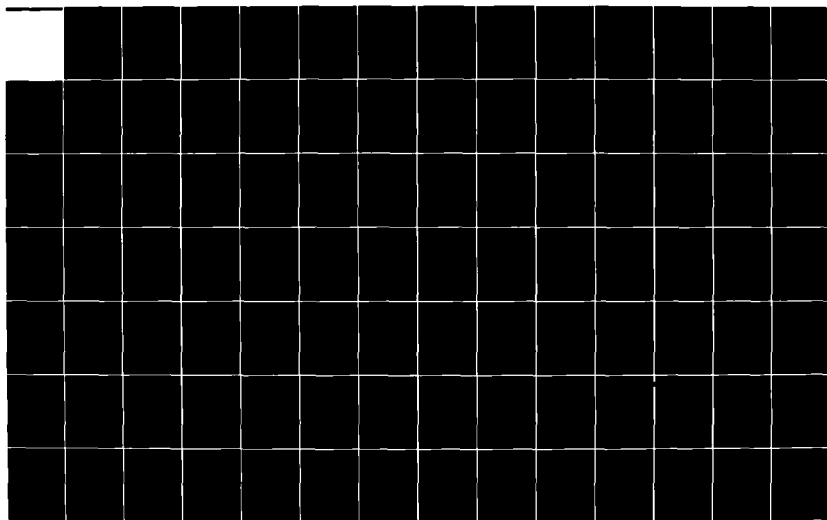
INTERNATIONAL CONFERENCE ON ELECTRONIC PROPERTIES OF  
TWO DIMENSIONAL SYSTEMS (5TH) HELD AT OXFORD ENGLAND ON  
5-9 SEPTEMBER 1983(11) OXFORD UNIV (ENGLAND) 1983

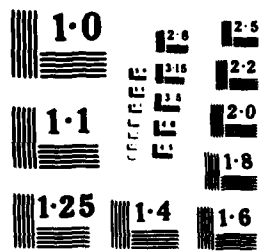
3/4

UNCLASSIFIED

F/G 9/3

NL





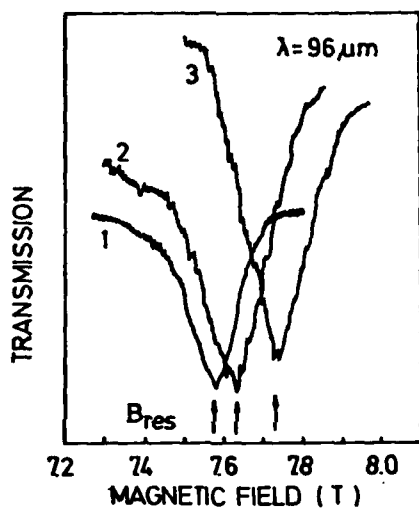


Fig.1:  
CR-Transmission spectra  
at a wavelength of  $96 \mu\text{m}$   
for different values of  
the filling factor.  
1)  $\nu = 0.66$   $B_{\text{res}} = 7.57 \text{ T}$   
linewidth =  $1.9 \text{ cm}^{-1}$   
Transition 0-1  
2)  $\nu = 1.3$   $B_{\text{res}} = 7.63 \text{ T}$   
linewidth =  $2.49 \text{ cm}^{-1}$   
Transition 0-1 and 1-2  
3)  $\nu = 1.62$   $B_{\text{res}} = 7.73 \text{ T}$   
linewidth =  $2.77 \text{ cm}^{-1}$   
Transition 1-2

Fig.3:  
Dependence of the cyclotron mass on the filling factor.  
The continuous increase between 1 and 1.6 is due to the superposition of the  
transitions 0-1 and 1-2.  
dashed curve: theoretical curve using the nonparabolicity model  
full curve: in addition the changed band structure is included

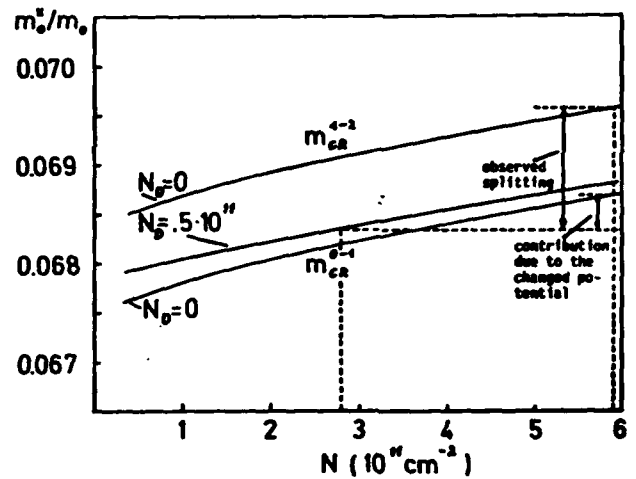
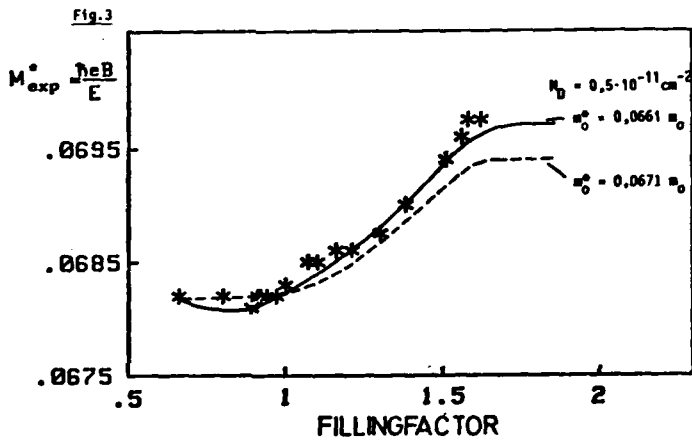


Fig.2:  
Calculated dependence of the effective cyclotron mass on the electron con-  
centration. A detailed explanation is given in the text.



# CYCLOTRON RESONANCE AND POLARON EFFECTS IN A 2DEG IN GaInAs

M.A. Brummell<sup>\*</sup>, R.J. Nicholas<sup>\*</sup>, L.C. Brunel<sup>†</sup>, S. Huan<sup>‡</sup>, M. Baj<sup>‡</sup>,

J.C. Portal<sup>§</sup>, M. Raseghi<sup>¶</sup>, M.A. di Forte-Poisson<sup>¶</sup>, K.Y. Cheng<sup>¶</sup> and A.Y. Cho<sup>¶</sup>

<sup>\*</sup>Clarendon Laboratory, Parks Road, Oxford OX1 3PU, U.K.

<sup>†</sup>S.N.C.I.-C.N.R.S., 166X, 38042 Grenoble, France

<sup>‡</sup>Laboratoire de Physique des Solides, I.N.S.A., 31077 Toulouse, France

<sup>§</sup>Laboratoire Central de Recherche, Thomson-C.S.F., 91401 Orsay, France

<sup>¶</sup>Bell Laboratories, Murray Hill, New Jersey 07974, U.S.A.

Cyclotron resonance results from GaInAs-InP heterojunctions and superlattices and GaInAs-AlInAs heterojunctions in fields up to 18T are reported. For low frequencies, the effective mass is compared with the predictions of  $k \cdot p$  theory, and the resonance linewidth is fitted to finite range scattering theories. At higher frequencies, the linewidth increases dramatically, while the effective mass deviates from its low-frequency value. These effects are attributed to resonant polaron coupling.

The subject of polaron coupling in two dimensional systems has caused considerable theoretical<sup>(1,2)</sup> and experimental interest<sup>(3-5)</sup> recently. In this paper we report cyclotron resonance studies of the 2DEG in GaInAs at frequencies up to and above the optic phonon values. We have studied both superlattices and heterojunctions of GaInAs-InP, grown by LP-MOCVD at the Thomson-C.S.F. Laboratories<sup>(6)</sup>, and heterojunctions of GaInAs-AlInAs, grown at Bell Laboratories by M.B.E.<sup>(7)</sup>. Firstly we shall consider the linewidths and effective masses in the relatively low frequency regime where polaron coupling is not significant, and then we shall go on to examine the polaron effects at higher frequencies.

Fig. 1 shows typical experimental recordings of transmission for a GaInAs-AlInAs heterojunction, with  $n = 8 \times 10^{11} \text{ cm}^{-2}$  and  $\mu = 90,000 \text{ cm}^2 \text{ V}^{-1} \text{ s}^{-1}$  at 4.2K. A plot of the resonance positions as a function of magnetic field (Fig. 2) is accurately linear, with a constant effective mass of  $0.049 m_0$ , as predicted by three band  $k \cdot p$  theory<sup>(8)</sup> in the expression

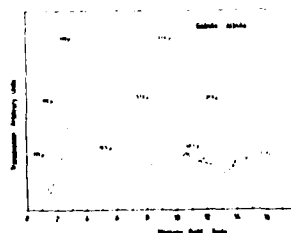


Fig. 1 shows typical experimental recordings of the transmission of a GaInAs-AlInAs heterojunction at frequencies up to  $265 \text{ cm}^{-1}$  and a temperature of 4.2 K. The transmission scales are not the same for the different wavelengths.

$$\frac{1}{m^*} = \frac{1}{m_0} \left( 1 + \frac{K_2}{E_g} [(2L+2)\hbar\omega_c + 2E_{11}] \right) \quad (1)$$

where  $m_0$  is the band edge mass,  $E_g$  is the band gap,  $L$  is the quantum number of the initial Landau level,  $E_{11}$  is the energy due to motion parallel to the field, and  $K_2$  is a factor,  $-0.85$  for GaInAs, which is determined by the band gap and spin orbit splitting. For Fermi energies  $E_F > \hbar\omega_c$ , the factor  $(2L+2)\hbar\omega_c$  is almost constant, and hence the constant effective mass. Similar measurements on a GaInAs-InP heterojunction with  $n = 3 \times 10^{11} \text{ cm}^{-2}$  and  $\mu \sim 90,000 \text{ cm}^2 \text{ VS}^{-1}$  at 4.2 K give a constant effective mass of  $0.047 m_0$  up to 6T, above which there is a small increase in mass consistent with Eq.(1). A more pronounced example of this is seen in Fig. 3, in which results are shown for a  $150 \text{ \AA}$  GaInAs-InP quantum well with  $n = 1.2 \times 10^{11} \text{ cm}^{-2}$ . The first few low field results give a mass of  $0.040 m_0$ , after which the deviation from the pure linear dependence is quite obvious. This value is somewhat low compared with the generally accepted bulk band edge mass of  $0.041 m_0$ <sup>(9)</sup> but is probably due to an excess of In in such thin layers.

Ando<sup>(10)</sup> has calculated that the value of  $E_{11}$  to be used in Eq.(1) for the lowest subband in heterojunctions is approximately  $E_0/3$ , where  $E_0$  is the energy of the lowest subband, which may be calculated from the simple Hartree expression<sup>(11)</sup>. This leads to the prediction of low field cyclotron masses of  $0.0465 m_0$  and  $0.0435 m_0$  for the two heterojunctions respectively, in significant disagreement with the experimental values. This is

not altogether surprising in view of some recent measurements on bulk GaInAs<sup>(12)</sup>, which suggest that Eq. (1) underestimates the non-parabolic corrections to the mass by a factor of approximately two.

The magnetic field dependence of the cyclotron resonance linewidth ( $\Gamma$ ) is shown in Fig. 4a,b,c for the same three samples. This is plotted as a function of  $B^{1/2}$ , to facilitate comparison with linewidth theories which predict a value of  $\Gamma_0 = 0.65(B/\mu)^{1/2}$  (in T) for short range scatterers<sup>(11,13)</sup>. At higher fields the linewidths fall well below these values, as observed recently in GaAs-GaAlAs systems<sup>(14,15)</sup>, however no oscillatory behaviour<sup>(15)</sup> was seen. For all three cases it was found that the field dependence could be very well described in terms of finite range Gaussian scattering centres, with a value of  $\Gamma$  given by<sup>(16,17)</sup>

$$\Gamma = \frac{\Gamma_0}{(1+r^2)^{3/2}}, \quad \beta^2 = \frac{2a^2}{L^2} = \frac{2a^2 eB}{\hbar} \quad (2)$$

where  $L$  is the radius of a cyclotron orbit and the range,  $a$ , was found to be 35 Å and 40 Å for the AlInAs- and InP- heterojunctions respectively, and 55 Å for the GaInAs-InP superlattice. These values are rather smaller than the screening length in GaInAs (75 Å)<sup>(11)</sup> but are comparable to the width of the graded interface in the MOCVD layers<sup>(18)</sup>. At still higher fields the cyclotron frequency approaches the optic phonon frequencies, with the result that the linewidth shows a very pronounced resonant increase, which may be seen to fall again for the highest frequency used with the AlInAs-heterojunction.

Our recent magnetophonon measurements<sup>(19-21)</sup> have shown that the electron-phonon interaction in GaInAs is strongly dependent upon the particular structure being studied. AlInAs-GaInAs structures are dominated by 'InAs' like L.O. phonons at 235 cm<sup>-1</sup><sup>(20)</sup>, in agreement with the results presented here, where the resonance linewidth has a sharp peak at around 240 cm<sup>-1</sup>, and has decreased again to almost its impurity limited value by

265 cm<sup>-1</sup>. Both of the InP-GaInAs structures show a similar resonant increase in linewidth, but there is no decrease at 265 cm<sup>-1</sup>, since the 'GaAs' L.O. phonon at 271 cm<sup>-1</sup> is dominant for these structures<sup>(21)</sup>. The picture is much less clear for the resonance positions, and hence effective masses. For the AlInAs-GaInAs heterojunction there is a discontinuity at 240 cm<sup>-1</sup>, with the higher frequency peaks occurring at a lower field, and hence giving a lower mass than the extrapolation of the low field results (Fig. 2). This is consistent with the expected behaviour, seen in bulk materials<sup>(22)</sup>, of a shift occurring above the optic phonon frequency. There is however no displacement of the resonance to higher fields at frequencies below the optic phonon. For the GaInAs-InP superlattice there is a similar discontinuity at around 240 cm<sup>-1</sup>, however in this case the resonances are strongly shifted to higher fields at frequencies just below the 'GaAs' L.O. phonon (Fig. 3) at 271 cm<sup>-1</sup>. There are several possible causes for this difference in behaviour. The very different electron-optic phonon coupling strengths in the two structures must play a role, but it should also be noted that the electron concentration in the AlInAs-heterojunction is much higher, leading to the occupation of the next highest electric sub-band, and possibly very different magneto-plasma effects. Das Sarma<sup>(2)</sup> has also shown recently that the polaron coupling is decreased by screening. Another point is that the superlattice is very close to a fractional occupancy of  $\nu = 1/3$  by 13 T. This rather confusing picture mirrors the results on other systems; in InSb, increases in linewidth on going above the optic phonon frequency have been observed, together with a decrease in mass<sup>(3)</sup>, but for HgCdTe<sup>(4)</sup>, no evidence of an effective mass discontinuity was found, and for GaAs heterojunctions it has been claimed that polaron contributions to the mass, at frequencies well below the L.O. phonon, are significantly less than for the bulk.<sup>(5)</sup>

**Acknowledgement:** M.A. Brummell was supported by an S.F.R.C. CASE scholarship in collaboration with the C.E.C. Risc Research Centre. We would like to thank Dr. J.P. Duchemin and Dr. T.P. Pearsall for useful discussion.

#### References

1. S. Das Sarma and A. Madhukar, *Phys. Rev.* **B22** (1980) 2823
2. S. Das Sarma, *Phys. Rev.* **B27** (1983) 2590
3. M. Horst, U. Merkt and J.P. Kotthaus, *Phys. Rev. Lett.* **50** (1983) 754
4. J. Scholz, F. Koch, J. Ziegler and H. Maier, *Solid State Commun.* **46** (1983) 665
5. G. Lindemann, W. Seidenhuach, R. Lasenig, J. Edlinger and E. Gornik, *Physica* **117B & 118B** (1983) 649
6. M. Razeghi, J.P. Hirtz, J.P. Lariivain, R. Blondeau, B. de Cremoux and J.P. Duchemin, *Electron Lett.* **17** (1981) 641
7. K.Y. Cheng, A.Y. Cho, T.J. Drummond and H. Morok, *Appl. Phys. Lett.* **40** (1982) 147
8. F.D. Palik, G.S. Picus, S. Teitler and R.P. Wallis, *Phys. Rev.* **122** (1961) 475
9. R.J. Nicholas, S.J. Sessions and J.C. Portal, *Appl. Phys. Lett.* **37** (1980) 178
10. T. Ando, *J. Phys. Soc. Japan* **51** (1982) 3893
11. T. Ando, A.B. Fowler and F. Stern, *Rev. Mod. Phys.* **54** (1982) 437
12. C.K. Sarkar, D.Phil Thesis (University of Oxford, 1983) and to be published.
13. G. Abstreiter, J.P. Kotthaus, J.F. Koch and G. Dorda, *Phys. Rev.* **B14** (1976) 2480
14. P. Voisin, Y. Guldner, J.P. Vieren, M. Voos, J.C. Maan, P. Delescluse and N.T. Linh, *Physica* **117B & 118B** (1983) 634
15. Th. Englert, J.C. Maan, Ch. Uehlein, D.C. Tsui and A.C. Gossard, *Solid State Commun.* **46** (1983) 545
16. M. Prasad and S. Fujita, *Physica* **91A** (1978) 1
17. C.K. Sarkar and R.J. Nicholas, *Surf. Sci.* **113** 326 (1982)
18. R. Bisaro, G. Laurencin, A. Friederich and M. Razeghi, *Appl. Phys. Lett.* **50** (1982) 978
19. J.C. Portal, J. Cisowski, R.J. Nicholas, M.A. Brummell, M. Razeghi and M.A. Poisson, *J. Phys. C: Solid State* **16** L573
20. M.A. Brummell, R.J. Nicholas, J.C. Portal, K.Y. Cheng and A.Y. Cho, *J. Phys. C: Solid State Phys.* **16** (1983) L579
21. J.C. Portal, G. Gregoris, M.A. Brummell, R.J. Nicholas, M. Razeghi, M.A. di Forte-Poisson, K.Y. Cheng and A.Y. Cho. This conference. (*Surf. Sci.*)
22. C.W. Litton, R.B. Dennis and S.D. Smith, *J. Phys. C: Solid State Phys.* **2** (1969) 2146

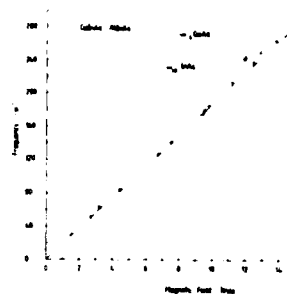


Fig. 2 shows the resonance field for the different laser frequencies in a GaInAs-AlInAs heterojunction. The straight line represents the low-frequency effective mass of 0.049  $m_0$ , and it can be seen that considerable deviation from this occurs near the LO phonon frequencies.

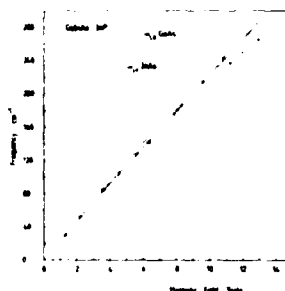


Fig. 3 shows the resonance field as a function of frequency for a 150 Å GaInAs-InP superlattice. The broken line represents the low-frequency mass of 0.040  $m_0$  and non-parabolicity can be seen above 3T because of the low electron concentration, as predicted by k.p. theory. Again, there is deviation from the expected mass values near the LO phonon frequencies.

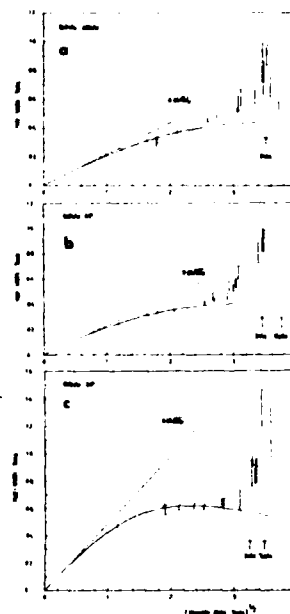


Fig. 4 shows the resonance linewidths plotted against  $\omega$ . Broken lines show the short range scattering limit and solid lines are calculated from finite range scattering theory. The plots are: (a) a GaInAs-AlInAs heterojunction, fitted to a scattering range of 35 Å; (b) a GaInAs-InP heterojunction with a range of 40 Å; (c) a 150 Å GaInAs-InP superlattice with a range of 55 Å. In all cases the linewidth increases dramatically at frequencies near the LO phonons and in (a) there is a definite maximum at the 'InAs' frequency. This is consistent with magnetophonon results: the dominant interaction is with 'InAs' modes in GaInAs-AlInAs and 'GaAs' modes in GaInAs-InP.

# STRUCTURAL AND ELECTRONIC PROPERTIES OF $\text{PbTe}/\text{Pb}_{1-x}\text{Sn}_x\text{Te}$ SUPERLATTICES

K.E. Ambrosch, H. Clemens, E.J. Fantner, G. Bauer  
 Institut für Physik, Montanuniversität Leoben, A-8700 Leoben,  
 M. Kriechbaum, P. Aepfer  
 Institut für Theoretische Physik, Universität Graz, A-8010 Graz,  
 Austria  
 R.J. Nicholas  
 Clarendon Laboratory, University of Oxford, Oxford OX1 3PU, England

## Abstract

$\text{PbTe}/\text{Pb}_{1-x}\text{Sn}_x\text{Te}$  ( $x = 0.12$ ) superlattices (d: 300–2000 Å, up to 40 layers) were produced by modified hot wall technique. The films were analysed by X-ray diffractometry and it turns out that the p-PbSnTe layers are under tensile strain. Shubnikov-de Haas and cyclotron resonance measurements were performed. An analysis within the framework of the envelope function approach yields information on the electronic subbands and their anisotropy.

## 1. Introduction

Semiconductor heterostructures and superlattices have been prepared by molecular beam epitaxy (MBE) for a variety of III-V/III-V and also for IV/III-V systems (1). Recently, Kinoshita et al. (2) and Clemens et al. (3) succeeded in preparing superlattices of a IV-VI/IV-VI system, namely  $\text{PbTe}/\text{PbSnTe}$  by using a rather simple type of vapor phase epitaxy, the hot wall epitaxy (HWE). In this paper, quantum transport and cyclotron resonance experiments on  $\text{PbTe}/\text{Pb}_{1-x}\text{Sn}_x\text{Te}$  ( $x = 0.12$ , up to 40 layers) are described. An empirical tight binding calculation shows, that these structures do not form type II superlattices. Using this information an analysis was performed within the framework of the envelope-function approach (4) taking into account the detailed band structure of the L-point of the Brillouin zone.

## 2. Experimental and Results

$\text{PbTe}$  and  $\text{Pb}_{1-x}\text{Sn}_x\text{Te}$  layers were grown alternatively by a modified hot wall technique on cleaved  $\text{BaF}_2(111)$  substrates (3). The layer thicknesses range from 300...2000 Å, with up to 40 layers deposited on a 1000 Å  $\text{PbTe}$  layer with a thickness of about 4000...5000 Å on the  $\text{BaF}_2$ -substrate. The growth conditions were chosen to yield  $\text{PbTe}$  layers with electron concentrations of  $n = 0.5...3 \times 10^{17} \text{ cm}^{-3}$  and  $\text{Pb}_{1-x}\text{Sn}_x\text{Te}$  layers with hole concentrations of  $p = 2...10 \times 10^{17} \text{ cm}^{-3}$ . For large differences of the electron and hole concentration, either mobile holes in the  $\text{PbSnTe}$  layers or electrons in both the  $\text{PbTe}$  and

$\text{PbSnTe}$  layers are present depending on the relative position of the band edges. Layer thicknesses were selected by two limitations: (i) the lower boundary was limited by the gradients due to diffusion of the constituents, (ii) the upper was determined by the mean free path of the free carriers to achieve a transition from superlattice to bulk behavior. The layers were analysed by X-ray diffractometry to check the layer composition and also by probing the Sn-profile using Auger spectroscopy and SIMS techniques (5). Due to the fact that the difference in lattice constants of  $\text{PbTe}/\text{Pb}_{0.88}\text{Sn}_{0.12}\text{Te}$  is  $1.62 \cdot 10^{-2} \text{ Å}$ , ( $T = 300 \text{ K}$ ,  $(a_1 - a_2)/a_1 = 2.5 \cdot 10^{-3}$ ) this system forms a strained superlattice. In order to investigate these strains in the temperature range 20–300 K, the lattice constants of different crystallographic lattice planes inclined under various angles with respect to the  $[111]$  growth direction were measured (6). The difference in lattice constants is completely accommodated by misfit strain. At  $T = 300 \text{ K}$ ,  $\text{PbTe}$  exhibits a compressive,  $\text{PbSnTe}$  a tensile strain of  $1.75 \cdot 10^{-3}$  in the  $(111)$  film plane. At 20 K, the substrate induced strain causes an additional tensile distortion of the  $\text{PbSnTe}$  layers ( $\epsilon = 2.25 \cdot 10^{-3}$ ), whereas the strain in the  $\text{PbTe}$  layers is reduced to  $0.25 \cdot 10^{-3}$ . Shubnikov-de Haas experiments were performed at  $T = 2 \text{ K}$  and  $4.2 \text{ K}$  and as an example Fig. 1 shows results for samples CIE1 ( $40 \times 500 \text{ Å}$ ) and D2C ( $10 \times 2000 \text{ Å}$ ). The periods of the SH oscillations of the  $d = 500 \text{ Å}$  sample and their dependence on the tilt angle  $\theta(\mathbf{k}, [111])$  turn out to be different from the bulk behavior which is already found for the  $d \approx 700 \text{ Å}$  sample.

Fig. 2 shows results of far infrared transmission as a function of magnetic field in  $\mathbf{B} \parallel \mathbf{E} \parallel [111]$  geometry ( $B_{\parallel}$ ). Two cyclotron resonances are observable, the light mass resonance being rather weak. In this sample ( $d = 500 \text{ Å}$ ) the carriers are situated in the p-PbSnTe layers, where due to the tensile strain a redistribution within the 4 L-valleys occurs. For  $B$  in the plane of the layers ( $B_{\perp}$ ), the  $d = 500 \text{ Å}$  samples do not exhibit cyclotron resonances. For  $d \geq 700 \text{ Å}$  tilted orbit resonances and hybrid resonances appear, according to the usual bulk behavior.

## 3. Theory

The type of superlattice to be expected for these structures is determined by the relative positions of the gaps of the two constituent materials. First an empirical LCAO calculation (7) was performed for bulk  $\text{PbTe}$  and  $\text{SnTe}$  by setting up a tight binding

Hamiltonian for the outermost valence s and p states, including first- and second nearest neighbor interactions. A linear interpolation in the spirit of the virtual crystal approximation yielded the band edges of  $\text{Pb}_{1-x}\text{Sn}_x\text{Te}$  mixed crystals with a zero gap at  $x=0.16$ . The relevant parameters of the two constituents of the present superlattices are shown in Table 1. Investigating the charge transfer in the  $\text{PbTe}/\text{p-PbSnTe}$  heterojunction gives a depletion length of roughly 3000 Å which is larger than the width of each layer in all samples. Therefore all electrons will combine with the holes leaving a positively charged PbTe layer and a net hole concentration of  $2 \cdot 10^{17} \text{ cm}^{-3}$  in the PbSnTe layer. The resulting superlattice band structure is shown in Fig. 3. The electrostatic potential is given by

$$V_{\text{PbTe}} = N_A (d/2)^2 / 2\epsilon_{\text{PbTe}} \quad (1)$$

which for a layer width  $d = 500$  Å yields  $V_{\text{PbTe}} = 0.87$  and  $V_{\text{PbSnTe}} = 0.45$  meV. The energy dispersion relation for the superlattice was calculated in the framework of the envelope function approach (4). The Hamiltonian appropriate for a narrow gap at the L point neglecting the far bands is (6)

$$\begin{bmatrix} E_c - E & h_{cv} \\ h_{cv}^* & E_v - E \end{bmatrix} f = 0 \quad (2)$$

with  $E_c, E_v$  the band edge energies appropriate for each constituent, with

$$h_{cv} = P_1 \sigma_1 k_1 + P_2 (\sigma_1 k_1 + \sigma_2 k_2), \quad f = (f_1 \dots f_4) \quad (3)$$

$\sigma_1$  denote the Pauli matrices, and  $\hat{1}_1, \hat{1}_2$  refer to the main valley axis and two perpendicular directions. The continuity of the Schrödinger function requires all  $f_i$  to be continuous across the boundaries and the superlattice periodicity  $D = d_A + d_B$  imposes the Bloch condition

$$f_i(x + D) = e^{iKD} f_i(x) \quad (4)$$

whence the energy dispersion  $E(K, K_y, K_z)$  is determined as given in (4) for the [111] valley and the valleys oblique to [111].

A noteworthy feature is the infinite mass in [111] direction, a consequence of the fact that the energy lies within the gap of one constituent and of the high thickness of the layer. The surface of constant energy is a circular cylinder for the [111] valley and an elliptical one for the oblique valleys. Its per-

pendicular masses depend weakly on layer thickness with the small mass decreasing with increasing layer thickness and the large mass being roughly constant for energies in the gap of one layer. The density of states is similar to a two-dimensional electron gas

$$\rho(E) = \frac{1}{2\pi} \frac{2\pi}{D} q_v \frac{m^*}{\hbar^2} \quad (5)$$

The magnetic field is introduced via the commutator relation

$$\hat{r} \times \hat{k} = -i\ell^2 \quad (6)$$

( $\ell$  cyclotron length,  $\ell^2 = \hbar/eB$ ). It turns out that for energies close to the band edge of layer A and within the gap of sufficiently thick layer B (2100 Å) the superlattice Landé factor is equal to the bulk Landé factor of layer A.

The calculation of the dispersion relation for quantizing magnetic fields in arbitrary direction is a difficult numerical task. We therefore restricted ourselves to  $B_{\perp}$ . Again, for the oblique valleys the continuity condition across the boundary cannot be treated in a simple way. As an approximation the oblique valleys were therefore treated as being perpendicular to [111]. In a strict two band model of the IV-VI materials the Landé splitting is exactly equal to the Landau splitting. In the fan charts Fig. 5 the horizontal lines represent the single degenerate 0<sup>+</sup> level pertaining to each subband, whereas the next curves are doubly degenerate.

#### 4. Discussion

The dependence of the SdH amplitudes on  $\theta$  is explained by the cylinders of constant energy as predicted by the model. Also the cyclotron resonance data in Faraday and Voigt geometry are in qualitative agreement, especially also for magnetic field parallel to the layers. Based on an analysis appropriate to a two dimensional electron gas (8) the minima of the SdH oscillations were plotted into the fan chart (Fig. 5). The density of states for  $B_{\perp}$  consists as in the two dimensional case of a series of  $\delta$ -spikes with the maximum number of carriers in each spike proportional to the magnetic field:  $1/(D2\pi\ell^2)$ . The total number of carriers calculated from the Fermi level in Fig. 5 is  $p \approx 4 \cdot 10^{17} \text{ cm}^{-3}$  in agreement with design parameters. The superlattice subband system for the [111] valley is shifted by about 10 meV with respect to the subband system of the oblique valleys in agree-



ment with the measured strain data. We are aware of the fact that with decreasing magnetic field the Fermi level position is influenced by the [111] valley. However, the size of this effect is comparable to the error introduced by the idealized fan chart. We consider the fact that the magnetoresistance and magnetocapacitance data show weak structure for the  $\mu_0$  case in samples with periods more than  $\lambda \approx 700 \text{ \AA}$  as a transition from superlattice to bulk effects, which is reasonable by considering the size of the cyclotron radius. The disappearance of superlattice effects for the  $2000 \text{ \AA}$  sample for all orientations of  $\mu_0$  is attributed to the mean free path being about  $1000 \text{ \AA}$  for the experimental conditions. This model is also in agreement with the measured cyclotron masses. For the oblique valleys allowance has to be made for the simplified geometry in the present calculations for the magnetic field case.

#### Acknowledgement

We thank Prof. G. Föhler for stimulating discussions. High field CR data were obtained in collaboration with M. von Ortenberg, Grenoble. Work supported by Fonds zur Förderung der wissenschaftlichen Forschung, Österreich.

#### References

1. e.g. H. Störmer, J. Phys. Soc. Jap. **49** Suppl. A, 1013 (1980) and references cited therein; J. C. Maan, Lecture Notes in Physics **177**, 163 (1983).
2. M. Kinoshita et al., J. Appl. Phys. **51**, 5845 (1980); M. Kinoshita, S. Takaoka, K. Murase and H. Fujiyasu, Proc. 2<sup>nd</sup> Symp. MBE, Tokyo: MBE-CST-2 (1987) p. 61.
3. H. Clemens, E. J. Fantner, G. Bauer, Rev. Sci. Instr., in print.
4. G. Bastard, Phys. Rev. B **25**, 7594 (1982).
5. We thank R. Maier, RWTH Aachen for performing the AES and SIMS-analysis of our specimens.
6. E. J. Fantner, H. Clemens, G. Bauer, Advances in X-Ray Analysis, **27** in print.
7. P. Kocavar, to be published.
8. G. Bauer, Lecture Notes in Physics **133**, 427 (1980).
9. T. Ando, A. Fowler, F. Stern, Rev. Mod. Phys. **54**, 437 (1982).

Table 1. Relevant material parameters

	$E_c$	$E_v$ (eV)	$n$ (cm <sup>-3</sup> )	$E_F - E_v$ (meV)	$E_F - E_c$	$E$
$\text{Pb}_{0.99}\text{Sn}_{0.12}\text{Te}$	-1.40	-4.50	$n = 1.10^{17}$	10		1300
$\text{SnTe}$	-4.42	-4.54	$p = 4.10^{17}$		19	2500
	-4.20	-4.51				

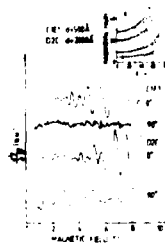


Fig. 1

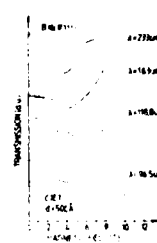


Fig. 2



Fig. 3

Fig. 1: Shubnikov-de Haas oscillations vs magnetic field for sample C1E1 and D2C;  $\theta = 0^\circ$  and  $90^\circ$  respectively. Insert: dependence of fundamental magnetic fields on  $\theta$ ;  $\circ$  experimental data, full lines: according to  $B_F \cos \theta$ .

Fig. 2: Cyclotron resonances of sample C1E1 for various far infrared laser wavelengths.

Fig. 3: Superlattice bandstructure: a) bulk properties, b) solid line: complete charge transfer, dotted line: electrostatic potential of homogeneously distributed positive and negative charges of density  $2.10^{17} \text{ cm}^{-3}$  included (not drawn to scale).

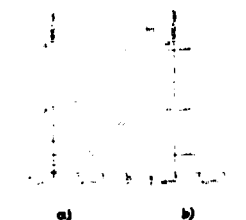


Fig. 4

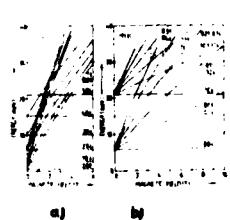


Fig. 5

Fig. 4: Energy vs  $k$  for  $K[111]$  and  $K[211]$  (solid line),  $K[011]$  (broad dashed) and  $K[011]/\sqrt{2} + [211]/\sqrt{6}$  (narrow dashed).  $d_A = d_B = 500 \text{ \AA}$ ,  $d = d_A + d_B$ ,  $E_A^0 = 0$ ,  $E_B^0 = -110$ ,  $E_C^0 = 30$ ,  $E_V^0 = -160 \text{ meV}$ ; a) [111] valley, b) oblique valleys.

Fig. 5: Fan charts of subbands and Landau states: a) [111] valley and b) oblique valleys. Notation: e.g. 00+ indicates lowest subband, lowest Landau state, spin down. Dash dotted lines: Fermi level as a function of field. Plot a has to be shifted upwards with respect to b by 10 meV in energy because of effects due to strain.

role played by the electron-acoustic phonon interaction in silicon inversion layer is provided by a series of beautiful experiments<sup>17</sup> on the ballistic phonon absorption by Hensel et al. Bergmann has recently argued<sup>18</sup> convincingly that electron-acoustic phonon interaction is possibly the dominant low temperature inelastic scattering mechanism for conduction electrons in thin metallic films. This is important in interpreting experimental data<sup>19</sup> on weak localization. Electron-LO phonon interaction plays<sup>20</sup> a significant role in the inelastic light scattering experiments on the GaAs-AlGaAs superlattice system because of the coupling<sup>9,10</sup> between the LO-phonons and the intersubband plasmons. Other III-V space charge layer systems are expected to behave the same way. Magneto-phonon anomalies in the magnetoresistance have been observed<sup>21</sup> by a number of groups in GaAs systems. A magneto-optical anomaly has recently been observed<sup>22</sup> in the cyclotron resonance experiment on InSb inversion layer by Horst et al. They attribute this effect to LO-phonon-Landau level coupling based on an earlier theoretical prediction<sup>6</sup> of Das Sarma and Madhukar. Nicholas et al. observed<sup>23</sup> an interesting variation in the cyclotron mass with the cyclotron frequency in InSe accumulation layers. Even though a quantitative theory for this observation does not exist, a possible candidate for the phenomenon is the electron-LO phonon interaction effects in the presence of free carriers.

Screening effects continue to play an important role in the understanding of various physical phenomena of these systems. This is expected since these systems are metallic in the sense of having well defined Fermi surfaces (actually Fermi circles in two dimensions). Also for the accessible carrier density range ( $10^{11} \text{ cm}^{-2} < n_0 < 10^{13} \text{ cm}^{-2}$ ) in these systems Thomas-Fermi wavenumber ( $q_{TF}$ ) is usually larger than the Fermi wavenumber ( $k_F$ ) producing strong screening. This last statement is actually more applicable to silicon space charge layers rather than to the III-V systems where lighter carrier mass makes  $k_F$  larger. Screening is an important factor in determining the

relative importance between the electron-electron interaction and the weak localization contributions to the recently discovered 'logarithmic' conductivity in the two dimensional electron systems.<sup>19</sup> Very recent developments in the theory of screening in two dimensional electronic systems include a self-consistent local density functional calculation<sup>24</sup> of impurity screening in silicon inversion layer, calculation<sup>25,26</sup> of two dimensional screening including impurity scattering effects and a theory<sup>27</sup> of screening near the mobility edge.

In many physical situations screening by free carriers affects electron-phonon interaction effects in an important way. A recent example is provided by the calculated<sup>7</sup> reduction in the polaronic effects in GaAs heterostructure due to screening by the free carriers. This is in agreement with a number of recent experimental findings.<sup>28-30</sup> In principle electron-phonon interaction effects in two dimensional electron systems are always coupled with screening effects and theoretical calculation should include the two effects on equal footing.

The rest of this paper is organized as follows: Section II will cover aspects of electron-acoustic phonon interaction, electron-LO phonon interaction is taken up in Section III, screening effects are covered in Section IV, future theoretical prospects are briefly discussed in Section V with a conclusion in VI.

## II. Electron-Acoustic Phonon Interaction

The most spectacular effect of the electron-acoustic phonon interaction on bulk electronic systems (metals) is perhaps the phenomena of superconductivity. A surface analog of the superconductivity in quasi-two dimensional electron system has been investigated<sup>5,31</sup> and detailed calculation including realistic electron-acoustic phonon interaction parameters predicts<sup>32</sup> a transition temperature of around 10 mK in silicon electron inversion layers. Since electron-acoustic phonon interaction in silicon is rather weak (particularly in the presence of free carrier screening) earlier investigations<sup>31</sup>

ELECTRON-PHONON INTERACTION AND SCREENING EFFECTS IN  
QUASI-TWO DIMENSIONAL ELECTRON SYSTEMS

S. Das Sarma  
Center for Theoretical Physics  
University of Maryland  
College Park, Maryland 20742

Abstract

Aspects of electron-phonon interaction and screening effects in quasi-two dimensional electron systems (e.g. inversion and accumulation layers; semiconductor heterostructures and superlattices) are reviewed with particular emphasis on recent developments. Theoretical and experimental results are compared where ever possible. Differences with the bulk three dimensional systems are pointed out and prospects for future theoretical efforts are outlined.

374

Introduction

In this paper some of the recent developments in the effects of the electron-phonon interaction and screening on quasi-two dimensional electron systems will be reviewed. The article will concentrate mostly on developments that took place after the Fourth International Conference on the Electronic Properties of Two Dimensional Systems held in New London, New Hampshire (August 1981). For references to earlier work (not covered by this article) the reader should consult the proceedings<sup>1</sup> of the New London Conference and the excellent review article<sup>2</sup> by Ando, Fowler and Stern.

Early interest<sup>2,3</sup> in the electron-phonon interaction in quasi-two dimensional electronic systems arose in the context of the transport behavior of silicon electron inversion layers which at room temperatures is limited basically by the electron-acoustic phonon interaction. Screening effects were also among the important early considerations<sup>2,4</sup> in understanding the transport in inversion layers at low temperatures since scattering of the carriers by the charged impurity centers at the interface contribute significantly to the resistivity of these systems. Transport study in these systems is still an active area of research where both electron-phonon interaction and screening effects play important and essential roles. However, the introduction of heterostructures and superlattices made mostly from the weakly polar compound semiconductor materials of the III-V series has made the electron-LO phonon interaction an essential ingredient in our understanding of the physical properties of the quasi-two dimensional electron systems. Also the focus of the current activities is not just the transport properties of these systems. Theoretically electron-phonon interaction has been invoked in the discussion of a number of phenomena including superconductivity,<sup>5</sup> magneto-phonon anomalies,<sup>6</sup> polaronic effects,<sup>7</sup> subband structure,<sup>8</sup> light scattering spectroscopy,<sup>9,10</sup> cyclotron resonance,<sup>11</sup> specific heat anomaly,<sup>12</sup> inelastic life-time effects,<sup>13</sup> phonon absorption,<sup>14</sup> interface traps<sup>15</sup> and charge density waves.<sup>16</sup> Clear experimental evidence for the

375

concentrated on a novel mechanism of superconductivity based on electron-acoustic plasmon interaction. However detailed analysis<sup>32</sup> eventually showed that in the region of parameter values (electron density etc.) where the superconducting transition temperature is the highest, electron-acoustic phonon interaction is the dominant mechanism driving the superconductivity. So far experimental efforts to observe superconductivity in quasi-two dimensional electronic systems occurring near semiconductor surfaces and interfaces have failed.

One of the interesting recent developments in the electron-acoustic phonon interaction effects in two dimensional electron systems has been the observation<sup>17,33</sup> of ballistic phonon absorption by the two dimensional degenerate electron gas in the (100) Si inversion layer system. In these experiments one measures the absorption of ballistic phonons passing through the two dimensional electron gas in the inversion layer. The measured absorption gives a direct estimate of the electron-acoustic phonon interaction matrix elements and is a potential powerful tool for probing the Fermi surface in these systems. Recent theoretical calculation by Hensel et al.<sup>14,33</sup> shows that inclusion of the interference effects (in solving the Fresnel problem for elastic waves obliquely incident on the multi-element planar system) in the inversion layer geometry is crucial in a quantitative explanation for the measured phonon absorption which were originally<sup>17</sup> thought to be too large. However the improved theory<sup>14</sup> using the known bulk deformation potential for silicon is in reasonable agreement with the experimental results. Kelly has recently considered<sup>34</sup> the effect of finite temperature on the phonon absorption. One of the interesting prospects is to use the ballistic phonon absorption as a probe to study Fermi surface instability in the two dimensional electron gas. There are predictions<sup>35</sup> for exchange-correlation driven valley-occupancy phase transitions in silicon inversion layers with critical temperature<sup>36</sup> in the 1-10 K range. These transitions should manifest themselves in a variable temperature ballistic phonon

absorption experiment. Experiment has so far been performed at a fixed temperature of 2 K.

In bulk metals electron-acoustic phonon interaction manifests itself in the renormalization of a number of electronic properties (e.g. specific heat, cyclotron resonance etc.). In an important paper<sup>37</sup> Prange and Kadanoff analysed which electronic properties are affected by the electron-acoustic phonon interaction and which are not. Basically a density of state mass is renormalized by the electron-acoustic phonon interaction but a conductivity mass is not.<sup>37</sup> The basis of the Prange-Kadanoff analysis is Migdal's theorem<sup>38</sup> asserting the smallness of the electron-acoustic phonon vertex correction in three dimensional metals. Even though the analysis of Prange and Kadanoff was restricted to three dimensional systems, it is easy to show that their conclusions are equally valid in two dimensional systems provided Migdal's theorem holds. There is a problem<sup>39</sup> about the applicability of Migdal's theorem in silicon inversion layers due to the smallness of the Fermi energy in these systems ( $E_F$  is typically comparable with the Debye energy). These questions have not been investigated in any kind of details. However the practicality and the relevance of these fundamental issues to actual experimental situation may be limited since the electron-acoustic phonon renormalization is found<sup>40</sup> to be very small in leading order calculation of the effective mass in silicon inversion layers. Smallness of the electron-phonon coupling in silicon and strong screening by the inversion layer electrons make such renormalization effects much less important quantitatively than the corresponding electron-electron interaction effects.<sup>2</sup>

One recent theoretical calculation<sup>12</sup> suggests that the temperature dependence of the electronic specific heat in a two dimensional electronic system could be quite different from the corresponding three dimensional case due to electron-acoustic phonon interaction effects. In particular a many-body calculation<sup>12</sup> including the electron-phonon self energy effect gives the following electronic specific heat,

$$C_v(T) = \gamma T^{1/2} [1 + b(T/T_F)^2 \ln(T/T_D)], \quad (1)$$

where  $\gamma = \gamma_0 (1+\lambda) = \frac{1}{3} \pi^2 k_B^2 m^*$  is the renormalized electronic specific heat constant ( $m^*$  is the renormalized electron effective mass),  $T_F$  and  $T_D$  are respectively the Fermi and the Debye temperatures and the positive constant  $b$  is given by

$$b = (3\pi/40) (1/1-2\lambda) (v_F/S)^2 (v_F/v_{TF})^2. \quad (2)$$

In Eq. (2)  $\lambda$  is the effective dimensionless electron-acoustic phonon interaction strength ( $0 < \lambda < 0.5$ ) and  $v_F$ ,  $v_{TF}$ ,  $S$  are the Fermi, Thomas-Fermi and the renormalized sound velocities of the two dimensional system. It must be emphasized that the second term in Eq. (1) comes with an opposite sign to the corresponding term in the three dimensional system.<sup>41</sup> Thus  $C_v(T)$  in two dimensional will have a weak local minimum at low temperatures due to the logarithmic term rather than a weak maximum as in the three dimensional system. This interesting many-body effect is perhaps difficult to observe because of the smallness of the electronic specific heat in most of the two dimensional electron systems.

Finally, electron-acoustic phonon interaction is claimed<sup>42</sup> to play a significant role in the nonohmic carrier transport in silicon inversion layers. The energy loss of the hot carriers can be used<sup>42</sup> to obtain information about the electron-acoustic phonon interaction in these two dimensional electron systems.

### III. Electron-LO Phonon Interaction

Most of the discussions in the last section on the electron-acoustic phonon interaction in quasi-two dimensional electron system is based on silicon inversion layer system. Electron-optical phonon interaction is, however, not of much significance in silicon. Most of the work involving electron-LO phonon interaction in quasi-two dimensional electron system is on the III-V semiconductor systems like GaAs heterostructure, GaAs-Al<sub>x</sub>Ga<sub>1-x</sub>As

superlattice, InSb space charge layer etc. All these materials are weakly polar (Frohlich coupling constant is around 0.1 for these materials) in nature. However this weak coupling may very well give rise to some interesting observable effects particularly because interaction effects are usually enhanced in systems of lower dimensionality.

Electron-LO phonon interaction is usually discussed within the context of a Frohlich model which employs a continuum approximation. It has recently been shown<sup>7</sup> that electron-LO phonon interaction modifies the energy  $E(k)$  of a

two dimensional electron from the simple parabolic relation  $E(k) = \hbar^2 k^2 / 2m$  to,

$$E^*(k) = E(k) - \alpha \hbar \omega_{LO} K' - O(\alpha^2) \quad (3)$$

where  $K$  is the complete elliptic integral of the first kind and  $q = (2m\omega_{LO}/\hbar)^{1/2}$  with  $\omega_{LO}$  as the LO-phonon frequency. Eq. (3) signifies a polaronic mass enhancement in two dimension from  $m$  to,

$$m^*(k) = m \left( 1 + \frac{\pi\alpha}{8} + \frac{9\pi\alpha}{128\omega_{LO}} \cdot \frac{\hbar^2 k^2}{2m} \right). \quad (4)$$

The polaronic binding energy in two dimension is given by,<sup>7,43</sup>

$$E_0 = -\alpha \hbar \omega_{LO} / 2. \quad (5)$$

These results (Eqs. 3-5) are obtained on the basis of leading order Rayleigh-Schrodinger perturbation theory for a single parabolic electron (no screening) interacting with the polar lattice. Very recently these calculations have been extended<sup>44</sup> to include the second order term in the coupling constant  $\alpha$  and the non-parabolicity of the bare electron. These effects turn out to be small for GaAs heterostructure systems.

Comparing the polaronic effective mass correction (Eq. 4) and the binding energy (Eq. 5) with the corresponding three dimensional results (in three

dimensions:  $m^*(k) = m \left( 1 + \frac{\alpha}{6} + \frac{3\alpha}{40\hbar\omega_{LO}} \frac{\hbar^2 k^2}{2m} \right)$  and  $E_0 = \alpha\hbar\omega_{LO}$ , one concludes that polaronic effects are appreciably enhanced in two dimensional systems. For example the effective mass is enhanced by a factor of  $\frac{3\pi}{4} = 2.4$  and the binding energy is enhanced by a factor of  $\frac{\pi}{2} = 1.6$ . Also the polaron-induced non-parabolicity correction in the effective mass (i.e. the  $k^2$  term in Eq. 4) is enhanced by a factor of 2.95. These results are quite consistent with our intuitive expectations that interaction effects are more important in systems of lower dimensionality. However, careful experimental search (using cyclotron resonance) for the polaron mass correction in GaAs heterostructure<sup>28</sup> and also in HgCdTe space charge layer<sup>30</sup> have failed to observe any appreciable mass renormalization. In fact Lindemann et al.<sup>28</sup> in their work on GaAs heterostructure concluded that the polaron mass correction in two dimensional system is at least a factor of three smaller than the corresponding result in bulk GaAs. This is an order of magnitude smaller correction than what Eq. 4 would suggest. Also, HgCdTe has a reasonably high polar coupling ( $\alpha = 0.3$  for HgCdTe as against 0.07 for GaAs) and so one would have expected appreciable polaron correction in the two dimensionally confined carriers in HgCdTe space charge layer.

These negative experimental results have recently been explained<sup>7</sup> theoretically on the basis of a simple model that includes screening of the electron-LO phonon interaction by the two dimensionally confined carriers. It has been shown that strong screening by the electrons in the heterostructure reduces the polaron mass correction from that given by Eq. 4. In addition the fact that the carriers in these systems are quasi-two dimensional in their character (i.e. they are confined in a region of finite width) further

reduces the polaronic effects. These results are shown in Figs. 1 and 2. In Fig. 1, the mass correction (at  $k = 0$ )  $\Delta M_{2D} = (m^* - m)$  is shown as  $\Delta M_{2D}' = \Delta M_{2D}/\Delta M_{3D}$ , scaled with respect to the corresponding three dimensional Frohlich result without any screening. The parameter  $\beta (= b/q_0)$  gives the effective width of the two dimensional carriers with  $1/b$  as the average width of the confined electrons and the parameter  $\gamma (= q_{TF}/q_0)$  gives the effective screening in the system with  $q_{TF} (= 2\pi e^2/\hbar k^2)$  as the Thomas-Fermi screening wavenumber in two dimensions. The solid curves are the results for the quasi-two dimensional system whereas the dashed curves ( $\beta = \infty$ ) give the purely two dimensional limits. Results as a function of  $\beta$  for various values of the screening strength ( $\gamma = 0, 1, 2, 3$  etc.) including the unscreened  $\gamma = 0$  situation are shown. It is clear from this figure that the polaronic mass correction may be reduced appreciably from that given by Eq. 4. In particular the experimental situation<sup>28</sup> for the GaAs heterostructure corresponds to  $\beta = 1.0$  and  $\gamma = 0.85$  giving  $\Delta M_{2D}' = 0.4$  which is in agreement with the experimental results. In Fig. 2 the corresponding quasi-two dimensional polaronic binding energy,  $c_r (= E_0^{2D}/E_0^{3D})$  is shown as a function of  $\beta$  and  $\gamma$ . Again screening and finite width effects appreciably reduce polaronic corrections.

In contrast to the above experiments<sup>28-30</sup> reporting negligible polaronic effects in two dimensional electronic systems, one recent paper<sup>22</sup> reports the observation of a marked discontinuity in the cyclotron resonance energies and linewidths in InSb electron inversion layer in the vicinity of the LO-phonon energy. These features have been attributed to resonant electron-LO phonon interaction effects in the two dimensional electron system. A detailed theory for the resonant electron-LO phonon interaction effect in two dimensional electronic systems has been worked out<sup>6,45</sup> a few years ago. The recent experiment observations<sup>22</sup> are qualitatively quite consistent with the theoretical predictions<sup>6</sup> about the magneto-optical anomalies in two

dimensionally confined carriers around  $\omega_c = \omega_{LO}$ . A fully quantitative theory for the magneto-optical anomalies including the finite width of the carrier wave-function and the screening effects does not exist at the present time.

The basic idea of the resonant electron-phonon coupling is rather simple.<sup>6</sup> Around  $\omega_c = \omega_{LO}$ , two states of the system given by an electron in the  $(N-1)$ th Landau level plus one LO-phonon and only an electron in the  $N$ th Landau level are degenerate and hence even a weak electron-LO phonon coupling will become important at this resonance lifting the degeneracy and thus splitting the  $N$ th level into two levels  $N_+$  and  $N_-$  which will have an energy difference proportional to the effective electron-LO phonon coupling in the system. Cyclotron resonance above and below the LO-phonon frequency will thus be different. In principle one should be able to observe both the split levels in an experiment, however one of the levels may be pushed into the reststrahlen band around  $\omega_{LO}$  and hence may become unobservable. Clearly in an experiment where the cyclotron frequency,  $\omega_c$  is varied through the LO-phonon frequency  $\omega_{LO}$ , one would see a transition to the  $N_-$  level for  $\omega_c < \omega_{LO}$  and a transition to the  $N_+$  level for  $\omega_c > \omega_{LO}$  (the other levels will be in the reststrahlen band). Thus cyclotron effective mass will be higher than the usual cyclotron mass for frequency below the LO-phonon frequency and will be lower above  $\omega_{LO}$ . This discontinuity is exactly what is being observed experimentally.<sup>22</sup> Linewidth should also be higher for  $\omega_c > \omega_{LO}$  because real emission of LO-phonons becomes allowed increasing the decay channel of the excited electron. It has been shown theoretically<sup>6</sup> that such resonant electron-LO phonon interaction induced anomalies should be much stronger in two dimensionally confined carriers compared with the three dimensional systems due to the lack of a wave-vector in the  $z$ -direction and the concomitant sharpness of the Landau levels. Magneto-phonon anomalies<sup>21</sup> in the magnetoresistance which have been observed in GaAs heterostructure is another example of such resonant electron-LO phonon coupling in two dimensional electronic systems.

A different aspect of the electron-LO phonon coupling in these systems is the dielectric coupling<sup>10</sup> of macroscopic electric fields due to the LO-phonons and the plasmons associated with the intersubband transitions between different quantum levels in the space charge layer. This is very similar to the well-studied<sup>46</sup> plasmon-LO phonon coupling in the doped bulk compound semiconductor systems. In principle LO-phonons can couple to both the intrasubband plasmons involving two dimensional oscillations within a quantum level and the intersubband plasmons which involve motion of electrons perpendicular to the plane of two dimensional confinement. However the coupling of LO-phonons to the intrasubband plasmons has not been observed because the plasmon energy (usually below 10 meV) is way below the LO-phonon energy (about 35 meV in GaAs). On the other hand coupling of LO-phonons to intersubband plasmons has very important effects on the inelastic light scattering spectrum by these systems. This subject has recently been reviewed<sup>47</sup> by Pinczuk and Worlock.

One important point regarding the electron-phonon coupling in these quasi-two dimensional systems is that the electrons seem always to couple to the bulk phonons of the relevant material. This is clearly true for the electron-LO phonon coupling where experiments like resonant magneto-phonon anomalies<sup>21,22</sup> and inelastic light scattering spectroscopy<sup>20</sup> unambiguously identify the energies of the relevant LO-phonon modes which always turn out to be the bulk three dimensional (rather than the interface two dimensional) phonon modes. This is presumably because the interface phonons decay within a small distance of the interface whereas the electronic wave-function in these systems is usually peaked at a distance larger than the typical decay length of the interface phonons.

#### IV. Screening Effects

A number of situations where inclusion of the screening effects in the theory is crucial to the understanding of the experimental results have already been mentioned in connection with the electron-phonon interaction phenomena. Examples are electron effective mass renormalization due to

electron-phonon interaction effects both for the acoustic<sup>40</sup> and for the optical<sup>7</sup> phonons. This section will concern itself with aspects of screening effects in quasi-two dimensional electron systems are not related to electron-phonon interaction phenomena.

One of the important recent developments in the understanding of screening effects in quasi-two dimensional electron systems is the recent work<sup>24</sup> of Vinter on the non-linear screening around a static impurity charge center in the (100) silicon inversion layer. Within a local density functional formalism Vinter calculates the self-consistent potential around the charged impurity and gets very good agreement with the experimentally<sup>48</sup> determined scattering rates in the dilute impurity concentration limit. He also shows that there is only one four-fold occupied bound state associated with the impurity charge center. This is a reflection of the strong screening in the system. In fact, Vinter finds that this four-fold-degeneracy is not lifted even if spin- or valley-density functional methods are used. Vinter's work clearly shows the importance of keeping screening effects in calculating the bound states associated with the charged impurity center, particularly in the high carrier density limit. Similar self-consistent density-functional calculations have not been performed in any other quasi-two dimensional electronic system.

While Vinter's self-consistent-local-density-functional calculation gives a good picture for the screening effects in the limit of high carrier density ( $N_5$ ), it clearly becomes inadequate when the charged impurity density ( $N_1$ ) is large. In particular Vinter's calculation is strictly valid for the single impurity problem (the "dilute" limit) and the calculated mobility ( $\mu$ ) at zero temperature has the form,

$$\mu^{-1} = a N_1, \quad (6)$$

where the coefficient  $a \equiv a(N_5)$  is independent of the impurity density  $N_1$ . This is true in the Born approximation or single-site-scattering type theories where scattering by individual impurity centers is treated independently.

These approximations are valid only in the limit of  $N_1 \ll N_5$ . On the other hand experiment<sup>48</sup> clearly shows that the mobility in (100) silicon electron inversion layer due to charged impurity scattering at low temperatures has the following form,

$$\mu^{-1} = a N_1 + b N_1^2, \quad (7)$$

where the coefficient  $b \equiv b(N_5)$  is very small when  $N_1 \ll N_5$ . Vinter's results are valid in that limit.

Recently a self-consistent screening theory<sup>25</sup> has been developed which explains the experimental<sup>48</sup> results very well over a wide range of  $N_5$  and  $N_1$ . The theory includes the effects of impurity scattering on the screening function. In particular scattering effects reduce<sup>25,26</sup> screening in a way rather similar to the reduction of screening at finite temperatures.<sup>49</sup> This is only understandable since both scattering (even at  $T = 0$  K) and finite temperature effects smear<sup>50</sup> the electronic Fermi distribution function around  $k = k_F$ . This is directly reflected in the rounding of the sharp corner in the two dimensional screening function around  $k = 2 k_F$ . Since  $2k_F$  - scattering is the dominant scattering mechanism limiting mobility, such scattering effects on screening can significantly reduce mobility particularly for higher values of  $N_1$ . In Fig. 3 the effect of impurity scattering (finite mean free path) on the screening is shown by depicting the static polarizability function  $\Pi(k)$  as a function of the wavenumber  $k$  for three different values of the mean free path  $l k_F = \infty, 10$  and  $2$  including the non-interacting ( $l = \infty$ ) situation first calculated by Stern.<sup>51</sup> The scattering has been treated in Born approximation in this calculation. The long wavelength value  $\Pi(k = 0)$  gives the density of states of the electrons in the presence of impurity scattering.

The self-consistency aspect in the screening function arises from the fact that while scattering determines screening through the polarizability function, scattering strength itself is determined by the screened Coulomb



interaction. Thus screening and scattering should be obtained together self-consistently. The self-energy correction due to electron-impurity interaction in the Born approximation is given by,

$$\begin{aligned} M(k, \omega + i\epsilon) &= N_i \frac{d^2 p}{(2\pi)^2} \left| U(k - p) \right|^2 G(p, \omega + i\epsilon) \\ &= \Delta(k, \omega) - i \Gamma(k, \omega), \end{aligned} \quad (8)$$

where  $U(k)$  is the screened electron-impurity interaction and  $G$  is the electronic Green's function. The screening is usually treated in the random phase approximation. The broadening  $\Gamma(k, \omega)$  turns out<sup>50</sup> to be not a very strong function of  $k$  and  $\omega$ . The theory<sup>25</sup> calculates the self-energy and the screened interaction self-consistently and then uses the self-consistently screened interaction  $U(k)$  to obtain the mobility.

In Fig. 4 the electronic level broadening is shown as a function of impurity density  $N_i$  both for the simple Thomas-Fermi screened interaction (dashed line) and for the self-consistently screened interaction (solid line). Obviously the Thomas-Fermi result is linear in  $N_i$  whereas the self-consistent result has higher order  $N_i$  corrections. In Fig. 5 the inverse of the mobility is shown as a function of  $N_i$  for the simple Born approximation theory (dashed line) that is linear in  $N_i$  and for the self-consistent result (solid line) that is in excellent agreement with the experimental results and with Eq. (7). The calculated<sup>25</sup>  $N_i$ -dependence of the coefficients  $a$  and  $b$  is also in good agreement with the experimental results. The specific theoretical results are for the silicon (100) electron inversion layer system so that a comparison with the experimental<sup>48</sup> results can be made.

For  $N_i \ll N_g$ , the self-consistent theory and the simple theory give basically the same results whereas for  $N_i \sim N_g$  the self-consistency in screening is important. A real desirable theoretical improvement will be the

inclusion of exchange-correlation effects<sup>40</sup> into the self-consistent scattering-screening formalism.<sup>25</sup> This however involves incorporating level broadening effects into a local-density-functional screening formalism. This is a difficult theoretical problem.

Screening in the two dimensional electronic system in the presence of a strong perpendicular magnetic field must include scattering effects self-consistently<sup>52,53</sup> since the electronic density of states is singular in the absence of level broadening. Such calculations suggest<sup>52</sup> that screening is a function of the filling factor and in particular screening is a maximum when the Landau level is half-filled and is a minimum when the level is full. These theoretical predictions have recently been confirmed experimentally<sup>54</sup> in GaAs heterostructure system.

There have been a number of efforts<sup>55-57</sup> in going beyond the random phase approximation in calculating the screening in two dimensional electronic systems. However the experimental consequences of such many-body corrections on the dielectric function are difficult to assess.

#### V. Future Prospects

A number of challenging theoretical questions remain open as has been indicated in the earlier sections of this paper. An important problem is to consider the electron-phonon interaction effects in the presence of full dynamical screening by the two dimensional carriers. The situation in the presence of a strong magnetic field also needs to be investigated in more quantitative details. Inelastic life time of the two dimensional electrons due to electron-phonon interaction effects is another unsolved theoretical problem. Possible importance of the electron-phonon vertex correction in these systems is another difficult and unsolved theoretical problem.

In screening, the important issue is to develop a theory that incorporates both Vinter's self-consistent-local-density-functional calculation<sup>40</sup> and the recently developed<sup>25</sup> scattering-screening self-consistent formalism. Such a theory will be able to describe the charged-impurity-

scattering-limited mobility in these systems for a wide range of values of  $N_1$  and  $N_2$ . Another unsolved theoretical problem is the screening by bound or localized electrons in quasi-two dimensional electronic systems. A lot of experimental data<sup>58</sup> on impurity binding in silicon inversion layer exists and can be used as a guide to estimate the screening by bound electrons in these systems.

#### VI. Conclusion

Aspects of electron-phonon interaction and screening effects in quasi-two dimensional electron systems have been reviewed in this paper with the emphasis on current developments in semiconductor systems. Among the topics that have been left out almost completely from this paper are electron-phonon interaction effects on transport properties of the two dimensional systems. This paper concentrates mostly on low temperature properties where real phonons are absent and the electron-phonon interaction effect on transport is rather small. However, in modulation doped GaAs-Al<sub>x</sub>Ga<sub>1-x</sub>As heterostructures, electron-phonon interaction is virtually the only scattering mechanism limiting mobility.<sup>59</sup> Charge (or, spin) density wave transition and possible phonon softening is an important ingredient<sup>60</sup> in the physics of layered compounds (e.g. TaSe<sub>2</sub>). These systems have not been considered in this review at all. Electrons on liquid-helium surface have also been left out of this article.

#### Acknowledgements

The author gratefully acknowledges the hospitality of the Semiconductor Physics Group at the IBM Thomas J. Watson Research Center where part of this review has been written. He also wishes to thank A. B. Fowler, E. Gornik, D. R. Grempel, J. C. Hensel, J. F. Koch, V. Korenman, J. P. Kotthaus, R. E. Prange, P. Stern and B. Vinter for helpful discussions. The work is supported in part by National Science Foundation through Grant No. NSF-DMR 8208819.

#### References

1. Surf. Sci. **113** (1982).
2. T. Ando, A. B. Fowler and P. Stern, Rev. Mod. Phys. **54** (1982) 437.

3. H. Ezawa, S. Kawaji and K. Nakamura, Japan J. Appl. Phys. **13** (1974) 126.
4. F. Stern and W. E. Howard, Phys. Rev. **163** (1967) 816.
5. W. Hanke and M. J. Kelly, Phys. Rev. Lett. **45** (1980) 1203.
6. S. Das Sarma and A. Madhukar, Phys. Rev. B **22** (1980) 2823.
7. S. Das Sarma, Phys. Rev. B **27** (1983) 2590.
8. G. Kawamoto, R. K. Kalis and J. J. Quinn, Surf. Sci. **98** (1980) 589;  
T. S. Rahman, D. L. Mills and P. S. Riseborough, Phys. Rev. B **23** (1981) 4081.
9. E. Burstein, A. Pinczuk and D. L. Mills, Surf. Sci. **98** (1980) 451.
10. S. Das Sarma, App. Surf. Sci. **11/12** (1982) 535.
11. B. Horowitz and A. Madhukar, Solid State Commun. **32** (1979) 695;  
M. Prasad, T. K. Srinivas and S. Prjita, Surf. Sci. **73** (1978) 505.
12. D. R. Grempel and S. Das Sarma, Phys. Rev. B **25** (1982) 7826.
13. S. Das Sarma, unpublished.
14. J. C. Hensel, B. I. Halperin and R. C. Dynes, Bul. Am. Phys. Soc. **28** (1983) 324.
15. C. T. White and K. L. Ngai, Surf. Sci. **98** (1980) 227.
16. M. J. Kelly, Solid State Commun. **27** (1978) 717.
17. J. C. Hensel, R. C. Dynes and D. C. Tsui, Surf. Sci. **113** (1982) 249 and Phys. Rev. B (in press).
18. G. Bergmann, Solid State Commun. **46** (1983) 347.
19. M. Pepper (this conference); R. C. Dynes, Surf. Sci. **113** (1982) 510.
20. A. Pinczuk, J. M. Worlock, H. L. Stormer, R. Dingle, W. Wiegmann and A. C. Gossard, Solid State Commun. **36** (1980) 43; G. Abstreiter, Ch. Zeller and K. Ploog in *Gallium Arsenide and Related Compounds*, 1980, edited by H. W. Thim (Institute of Physics, Bristol) pp. 741.
21. D. C. Tsui, Th. Englert, A. Y. Cho and A. C. Gossard, Phys. Rev. Lett. **44** (1980) 341; M. A. Brummel, R. J. Nicholas, J. C. Portal, M. Raseghi and M. A. Poisson, Physica **118 B** (1983) 753.

22. M. Horst, U. Merkt and J. P. Kotthaus, Phys. Rev. Lett. 50 (1983) 754.
23. R. J. Nicholas, E. Kress-Rogers, J. C. Portal, J. Galibert and A. Chevy, Surf. Sci. 113 (1983) 339.
24. B. Vinter, Phys. Rev. B 26, (1983) 6808 and references therein.
25. S. Das Sarma, Phys. Rev. Lett. 50 (1983) 211.
26. T. Ando, J. Phys. Soc. Japan 51 (1982) 3215.
27. P. A. Lee, Phys. Rev. B 26 (1982) 5882.
28. G. Lindemann, W. Seidenbush, R. Lassing, J. Edlinger and E. Gornik, Physica 118 B & C (1983) 649.
29. G. Kido, N. Miura, H. Ohno and H. Sakaki, J. Phys. Soc. Japan 51 (1982) 2168.
30. J. Scholz, F. Koch, J. Ziegler and H. Maier, Solid State Commun. 46 (1983) 665.
31. Y. Takada, J. Phys. Soc. Japan 45 (1978) 786.
32. M. J. Kelly and W. Hanke, Phys. Rev. B 23 (1981) 112 and 924.
33. J. C. Hensel, this conference.
34. M. J. Kelly, J. Phys. C 16 (1983) L 517.
35. W. L. Bloss, L. J. Sham and B. Vinter, Phys. Rev. Lett. 43 (1979) 1529.
36. S. Das Sarma and B. Vinter, Phys. Rev. B 26 (1982) 960.
37. R. E. Prange and L. P. Kadanoff, Phys. Rev. 134 A (1964) 566.
38. A. B. Migdal, Sov. Phys.-JETP 7 (1958) 996.
39. A. Madhukar, Solid State Commun. 24 (1977) 11.
40. B. Vinter, Phys. Rev. B 13 (1976) 4447.
41. G. M. Eliashberg, Sov. Phys.-JETP 16 (1963) 780.
42. T. Henggebauer and G. Lendwehr, Phys. Rev. B 21 (1980) 702.
43. J. Sak, Phys. Rev. B 6 (1972) 3981.
44. S. Das Sarma and B. A. Mason, to be published.
45. A. Madhukar and S. Das Sarma, Surf. Sci. 98 (1980) 135.
46. B. B. Varga, Phys. Rev. A 137 (1965) 1986.
47. A. Pinczuk and J. M. Worlock, Surf. Sci. 113 (1982) 691 and Physica 118 B & C (1983) 637.
48. A. Hartstein, A. B. Fowler and M. Albert, Surf. Sci. 98 (1980) 181.
49. P. Madaque, Surf. Sci. 73 (1978) 296.
50. S. Das Sarma and B. Vinter, Phys. Rev. B 24 (1981) 549 and Surf. Sci. 113 (1982) 176.
51. F. Stern, Phys. Rev. Lett. 18 (1967) 546.
52. S. Das Sarma, Solid State Commun. 36 (1980) 357 and Phys. Rev. B 23 (1981) 4592.
53. T. Ando, J. Phys. Soc. Japan 43 (1977) 1616.
54. Th. Englert, J. C. Maon, Ch. Vihlein, D. C. Tsui and A. C. Gossard, Solid State Commun. 46 (1983) 545 and J. Vac. Sci. Technol. B 1 (1983) 427.
55. M. Jonson, J. Phys. C 9 (1976) 3055.
56. P. Madaque, Sol. State Commun. 26 (1978) 133.
57. A. Czachor, A. Holas, S. R. Sharma and K. S. Singwi, Phys. Rev. B 25 (1982) 2144.
58. A. B. Fowler and A. Hartstein, Philos. Mag. B 42 (1980) 949.
59. P. J. Price, Ann. Phys. 133 (1981) 217.
60. F. J. DiSalvo, Surf. Sci. 58 (1976) 297.

# Figure Captions

Fig. 1: Shows the polaronic mass correction in quasi-two dimensional systems as a function of the width parameter  $\beta$  ( $= b/q_0$ ) for different values of the screening parameter  $\gamma$  ( $= v/q_0$ ).

Fig. 2: Shows the polaronic binding energy in quasi-two dimensional system as a function of parameter  $\beta$  for different values of  $\gamma$ .

Fig. 3: Shows the polarizability  $\pi(k)$  expressed in the units of the long wavelength ion interacting polarizability function. Results for three different values of the parameter  $k_p$  ( $= \pi, 10, 2$ ) are shown.

Fig. 4: Shows the level broadening  $\Gamma$  in Si(100) electron inversion layer as a function of impurity density ( $N_i$ ) for a fixed value of carrier density ( $N_0$ ).

Fig. 5: Inverse mobility  $\mu^{-1}$ , is shown as a function of  $N_i$  for a fixed value of  $N_0$ . The full curve is the result of the self-consistent screening theory whereas the dashed curve is the simple Born approximation result that is linear in  $N_i$ . The experimental points from Ref. 48 are also shown.

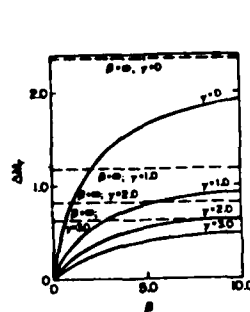


Fig. 1

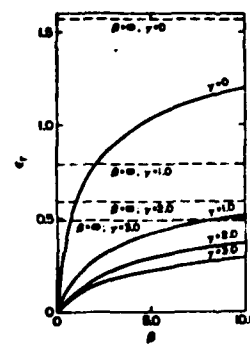


Fig. 2

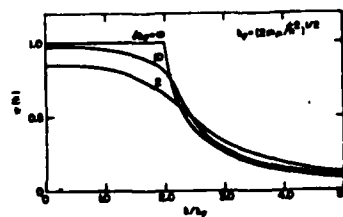


Fig. 3

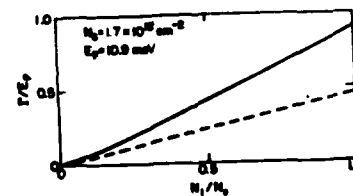


Fig. 4

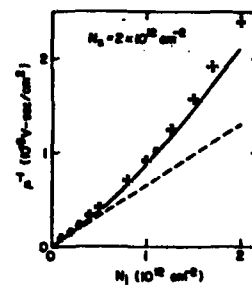


Fig. 5

# INFRARED STUDIES OF THE GaAs/(GaAl)As 2DFG

Z. Schlesinger, J. C. M. Hwang, S. J. Allen, Jr. and H. L. Stormer

Bell Laboratories  
Murray Hill, New Jersey 07974

H. Le

Francis Bitter National Magnet Lab  
Cambridge, Mass 02139

## ABSTRACT

Cyclotron resonance, (CR), of electron space charge layers produced in GaAs/(GaAl)As heterostructures has been studied with magnetic fields up to 20T and frequencies from d.c. to the TO optic phonon frequency. Anti level crossing of Landau levels and electric subband transitions, cyclotron line splitting at a magnetic field determined by the 2D electron density, and pinning of the cyclotron resonance and localization in a low mobility, low density samples have been investigated.

\* \* \* \* \*

The electron space charge layer formed in a selectively doped GaAs/(GaAl)As heterostructure<sup>1,2</sup> (Fig. 1) has emerged as an interesting model system in which to study magneto transport in two dimensions. The observations of plateaus in the quantized Hall resistance at fractional occupation of Landau levels was totally unexpected<sup>3</sup> and conditional on the high mobilities<sup>4</sup> that can be achieved in this system. To learn more about these high mobility 2D systems we have studied cyclotron resonance, (CR), in a variety of samples. Although the original goal of this research was to examine the behavior of CR at fractional occupation of the lowest Landau level, a number of remarkable observations have been made at more modest magnetic fields and densities and we explore them here.

### A. Subband - Landau level Coupling

If the magnetic field is tipped slightly with respect to the sample normal, it is possible to induce a coupling between the motion parallel to the surface, Landau levels, and the perpendicular subband levels.<sup>5,6</sup> Figure 2 shows a classic anti level crossing between the CR and electron subband transition. The splitting is proportional to the tip angle  $\theta$  as shown in Fig. 3.

396

By applying a voltage to a gate electrode on the back of a thinned sample, the electric subband transition energy can be Stark tuned. Fig. 4 shows the experimental variation of the electric subband transition energy and electron density with gate voltage. The solid line is an estimate of the theoretical tuning rate assuming a triangular potential well<sup>7,8</sup> model of the interface fixed only by depletion layer charges. Inclusion of the Hartree term will decrease the slope of the theory line improving the agreement with experiment.

Although the spectra are probed with the electric field in the plane of interface, the anti level crossing occurs at the frequency of the depolarization shifted electric subband transition. (Any uniform, ( $q=0$ ), infrared excitation can only sense this depolarization shifted energy.) A precise measure of the angle dependence of the splitting should give the electric dipole matrix element between these two states and provide a critical test of models of electric subband states in this system.

### B. CR Line Splitting

At lower magnetic fields samples such as the aforementioned reveal another unrelated and totally unexpected CR line splitting or broadening, which does not depend on small tip angles of the magnetic field with respect to the sample normal. Fig. 5 shows the evolution of the spectra for a sample with electron density  $n_s = 3.9 \times 10^{11}/\text{cm}^2$ . CR peak frequencies and the conductivity as a function of magnetic field are shown in Figure 6. The 2D electron density is obtained from the Shubnikov-de Haas oscillations in  $\sigma_{xx}$ .

Although previous studies in this range of magnetic field and density report a line broadening when the Landau levels are just filled,<sup>9</sup> we find that this broadening/splitting depends sub-linearly on the 2D electron density (Figure 7). The solid line in Figure 7 is proportional to  $n_s^{1/4}$ . This rules out filling factor as a critical parameter and suggests that electron-electron interactions play a critical role.

At elevated temperatures  $\geq 20^\circ\text{K}$  the doublet shown in Fig. 5 collapses to a single line narrower than the combined width seen at 1.3K.

397

The ability of electron-electron interactions to effect CR once translational symmetry has been broken by impurity scattering has been discussed by Fukuyama et al.<sup>10</sup> Platzman et al.<sup>11</sup> have shown that dynamic screening can lead to varied line shapes, but it is not clear that the systematics revealed here will emerge from these theories in a convincing way.

### C. Pinning of CR in Low Mobility Samples

Although the position of the line broadening/splitting does not depend on mobility the character of the splitting discussed in the last section does depend on this parameter. If we examine a sample with low density and mobility, which shows strong negative magneto-resistance, we find that the CR exhibits a pinned behavior<sup>12</sup> over a wide field range. However, at sufficiently low magnetic fields the resonance does not hang up at the pinning frequency, as would be expected if the electron gas were in fact trapped or exponentially localized. Rather, it drops below the expected CR line position and gives rise to a broad resonance with heavy mass. This behavior may be related to that described in the previous section.

At elevated temperatures,  $\approx 30^\circ\text{K}$ , the "pinned" behavior disappears giving a broad resonance that follows the expected linear CR frequency versus magnetic field behavior.

### Summary

We have tried to indicate the wealth of phenomena that has been revealed in the high frequency magneto transport (CR) of this system. Despite the high mobility and apparent model nature of the 2DEG in GaAs a number of features have emerged that are not easily understood. The coupling of the CR and subband transitions is the notable exception. However, the line splitting at a critical field and the pinning in low density/mobility samples require some detailed theoretical modeling before we can lay claim to properly understanding magneto transport in two dimensions.

### Acknowledgment

We would like to acknowledge the assistance of K. Baldwin and A. Savage in sample preparation and F. DeRose for taking some of the spectra. All work above 8T was performed at the Francis Bitter National Magnet Lab at M.I.T. where B. L. Brandt, L. O. Rubin, P. A. Wolff, and B. Lax lent considerable support and aid.

### REFERENCES

1. A. R. Cho, *J. Vac. Sci. Technology* **16**, 275 (1979).
2. R. Dingle, H. L. Sluiter, A. C. Gossard and W. Wiegmann, *Appl. Phys. Letters* **33** 665 (1978); H. Sluiter, R. Dingle, A. C. Gossard, W. Wiegmann and M. D. Sturge, *Solid State Commun.* **29**, 705 (1979); R. Dingle, H. L. Sluiter, A. C. Gossard and W. Wiegmann, *Surface Sci.* **90**, 90 (1980).
3. D. C. Tsui, H. L. Sluiter and A. C. Gossard, *Phys. Rev. Lett.* **48**, 1599 (1982).
4. H. L. Sluiter, A. Chang, D. C. Tsui, J. C. M. Hwang, A. C. Gossard and W. Wiegmann, *Phys. Rev. Letters* **50**, 1953 (1983).
5. W. Benngel and J. F. Koch, *Phys. Rev. Lett.* **40**, 1736 (1978).
6. T. Ando, *Phys. Rev. B* **20**, 2106 (1979).
7. F. Stern, *Phys. Rev.* **85**, 489 (1972).
8. T. Ando, A. B. Fowler and F. Stern, *Rev. Mod. Phys.* **54**, 437 (1982).
9. Th. Englert, J. C. Moon, Ch. Urbain, D. C. Tsui and A. C. Gossard, *Int'l Conf. on the Physics of Semiconductors*, Montpellier, France (1982).
10. H. Fukuyama, Y. Kusunoto and P. M. Platzman, *Phys. Rev. B* **24**, 4980 (1979).
11. P. M. Platzman, M. J. Hoon and T. Toner, *Int'l Conf. on Electronic Properties of 2D Systems*, Birmingham (1977).
12. B. A. Wilson, S. J. Allen, Jr., and D. C. Tsui, *Phys. Rev. B* **24**, 3887 (1981).

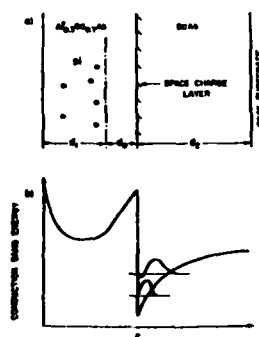


Fig. 1. Relatively doped GaAs/AlGaAs interface.  
(a) Geometry of interface including subband distances,  $d_0$ , to donor impurities. For the sample discussed in the text  $d_0 \approx 320 \text{ \AA}$ ,  $d_1 \approx 700 \text{ \AA}$  and  $d_2 \approx 1 \text{ \mu}$ .  
(b) Conductance band edges and lowest subband levels.

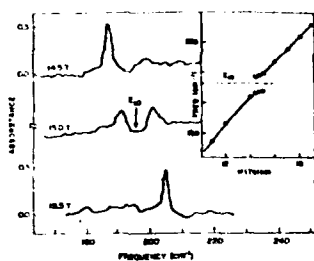


Fig. 2. Cyclotron resonance at level crossing. Three cyclotron resonance spectra taken at the indicated fixed fields and a gate voltage  $V_g = -15$  Volts are shown. At 15 V two absorption peaks of comparable magnitude are present. The insert shows the frequency of the observed absorption peaks (at  $V_g = 0$  Volts) as a function of magnetic field.

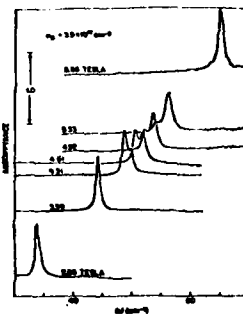


Fig. 5. Anomalous Cyclotron Linesplitting. Cyclotron absorbance spectra for  $V = 1.2$  V and 2D electron density  $1.9 \times 10^{11} \text{ cm}^{-2}$  are shown for several values of the magnetic field, B. An unsplitting of the cyclotron resonance absorption line is observed at  $B = 45$  G.

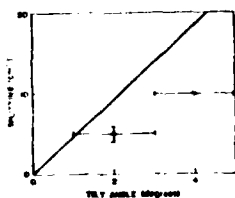


Fig. 3. Splitting vs Tilt Angle. The splitting of the two peaks observed in the cyclotron resonance spectrum at the level crossing is shown for two angles. The straight line is an estimated theoretical splitting (Eq. 7) due to the tilting of the magnetic field away from the surface normal.

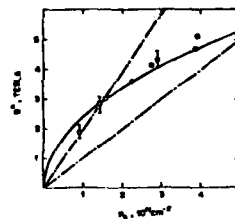


Fig. 6. Splitting Field vs 2D Density. The magnetic field at which the cyclotron linesplitting or linewidth maximum occurs is plotted as a function of 2D electron density. The points roughly follow a  $B_c \propto n_s^{1/2}$  dependence (solid line). Lines of constant Landau level filling factor for  $n = 1$  and 2 are shown for reference (dashed lines).

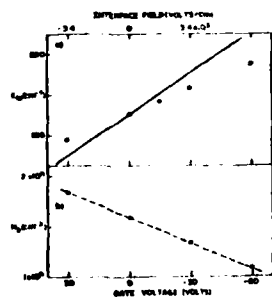


Fig. 4. Stark shift of the  $n = 1$  subband transition. (a) The effect of a dc gate voltage on the  $n = 1$  subband transition energy,  $E_{10}$ , is shown. The straight line is the calculated shift for a triangular potential. (b) Area density of the 2DES as a function of gate voltage is shown.

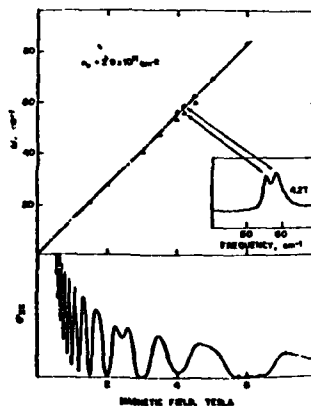


Fig. 7. Cyclotron Resonance and Magnetotransport. (a) The frequencies at which absorption peaks occur for each magnetic field value are plotted for  $V = 1.2$  V. The straight dot-dashed line gives the frequency of the single CH peak seen at 30 K. The insert shows a sample CH spectrum at 1.2 K from the field at which roughly equal peak height occurs. The 2D electron density is  $1.9 \times 10^{11} \text{ cm}^{-2}$ . (b) Probable-Adams oscillations measured with a two contact fixed voltage technique are shown. The 2D electron density is obtained to within a few percent from the periodicity in  $B^{-1}$ .

# ELECTRIC SUBBANDS IN THE LIMIT $E_G \rightarrow 0$

J. Scholz and F. Koch

Physik-Department, Technische Universität München

8046 Garching, Fed. Rep. of Germany

and

J. Ziegler and H. Maier

Telefunken Electronic, 7100 Heilbronn, Fed. Rep. of Germany

## Abstract

The subband energy separations  $E_{01}$  and  $E_{12}$  are shown to depend sensitively on the energy gap  $E_G$  when tunneling overlap of the surface-bound electron with a filled valence-band state becomes possible.

## Introduction

In a number of recent publications electronic subbands in an accumulation layer on  $\text{Hg}_{1-x}\text{Cd}_x\text{Te}$  with  $x \sim 0.2$  have been studied. In particular, subband energy separations have been determined in far-infrared resonance experiments<sup>1/</sup>.

It has been speculated for some time that for  $\text{Hg}_{1-x}\text{Cd}_x\text{Te}$  with its small and  $x$ -dependent  $E_G$  one should be able to observe the effects of a surface-potential-induced coupling of the conduction and valence band states. The point has most recently been made by Takada et al. in ref. /2/. From a realistic, self-consistent potential calculation for the subbands the authors have estimated that tunneling overlap of the surface electrons with the valence band states becomes significant when  $x \lesssim 0.2$ . The electric-field-induced tunneling is responsible for band-mixing. Such band-band interaction is included in principle also in the very lucid formulation by Zawadzki<sup>3/</sup> of the subbands and resonant excitation for narrow-gap semiconductors.

To date there exists no satisfactory numerical evaluation of subband energies in the band-mixing situation. The Takada et al. calculation<sup>2/</sup>, which explicitly ignores this effect, gives a subband separation for  $\text{Hg}_{1-x}\text{Cd}_x\text{Te}$  which is only weakly dependent on  $x$  when the latter varies between 0.17 and 0.32. The energy  $E_1 - E_0 \approx E_{01}$  is calculated as  $\sim 35$  meV for surface density  $N_s = 1 \times 10^{12} \text{ cm}^{-2}$ . It decreases as  $E_G$  increases with  $x$ , an effect that one may link with the increasing  $m^*$ . In the triangular potential-well description,  $E_{01}$  is proportional to  $(m^*)^{-1/3}$ . For comparison with this  $E_{01}$  of 35 meV we note that the gap energy at 4.2 K varies approximately linearly from  $\sim 10$  meV at  $x = 0.17$  to  $\sim 60$  meV for  $x = 0.20$ .

## The Experiments

We became aware of a very significant  $N_s$ -dependence of a given resonance transition such as  $E_{01}$  or  $E_{12}$  by comparing the subband excitation on different samples. Thus the detector-type samples with anodically oxidized surface layers (as in ref. /1/) gave  $N_s$ -values which were typically a factor of 2 - 3 less than comparable lacquer-type samples with different  $x$ -values in the surface region. The fact that the stoichiometric composition  $x_s$  of the surface layer for anodically-oxidized  $\text{Hg}_{1-x}\text{Cd}_x\text{Te}$  differs significantly from the bulk-value  $x_b$  has now been established from surface cyclotron resonance and subband spectroscopy<sup>4/</sup>. The present work is not concerned with such differences but seeks to establish the experimental facts as to how the subband energies depend on  $E_G$ .

For this purpose we work with a series of "lacquer-type" samples prepared from material with  $x$ -values 0.171, 0.181, and  $x = 0.200$ , as determined from density analysis. The sample surface is polished in a bromine-methanol solution and coated with an insulating lacquer immediately afterwards. A thin gate electrode ( $\sim 100 \text{ \AA}$  nichrome) is evaporated onto the lacquer. Because there is no significant difference of surface CR (in the limit  $N_s \rightarrow 0$ ) and the corresponding volume CR on such samples we conclude that for such samples  $x_s \approx x_b$ .



A check of the volume CR serves to confirm the above  $x$ -values to an accuracy of the order of  $\pm 0.02$ .

The subband resonance on the various samples is observed in a  $45^\circ$  reflection (R) geometry and recorded as a derivative  $dR/dV_G$  for  $\hbar\omega = 10.5, 12.9, 17.6$ , and  $30.2$  meV. Fig. 1 shows such resonance data for  $17.6$  meV. The resonance structures on the Drude-type background are not as sharp and well-resolved in Fig. 1 as for the case of the previously published detector-sample data<sup>(1)</sup>. Nevertheless by carefully observing the evolution of the signals with  $\hbar\omega$  and  $N_s$  we arrive at the assignment of the peaks as in the figure. Transitions marked  $\sim$  are the depolarization-shifted, perpendicularly-excited modes. The unmarked transitions represent true subband energy splittings. In Fig. 2 we have collected the resonance data obtained for the four values of  $\hbar\omega$  in order to construct curves of subband energy vs.  $N_s$  for each of the different materials.

To illustrate how sensitively the separations  $E_{01}$  and  $E_{12}$  depend on  $x$  at a fixed density  $N_s = 1 \times 10^{12} \text{ cm}^{-2}$  we have constructed the following table using the data from Fig. 2.

$x$	$E_G(\text{meV})$	$E_{01}(\text{meV})$	$E_{12}(\text{meV})$
0.200	60	46	16
0.181	28	30	14
0.171	10	16	$\sim 9.5$

Table 1: Subband energies for surface density  $N_s = 1 \times 10^{12} \text{ cm}^{-2}$

The data in the table must be contrasted with the calculation in ref. /2/, which gives  $E_{01}$  and  $E_{12}$  nearly independent of  $x$  in the range  $0.17 \leq x \leq 0.20$ . For p-type material with  $N_A - N_D = 10^{15} \text{ cm}^{-3}$ , Takada et al.<sup>/2/</sup> give  $E_{01}$  35 meV and  $E_{12} \sim 18$  meV. The discrepancy of theoretical and experimental values is unusually large. Moreover the theory does not properly describe the sensitive dependence of the subband energies on  $E_G$ . We note that the

level separation  $E_{01}$  in the table decreases by a factor 3, while energy  $E_{12}$  changes by only  $\sim 40\%$ .

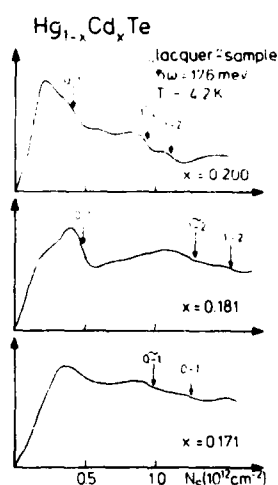


Fig. 1: Subband resonances observed as a reflection-derivative ( $dR/dV_G$ ) signal at  $\hbar\omega = 17.6$  meV

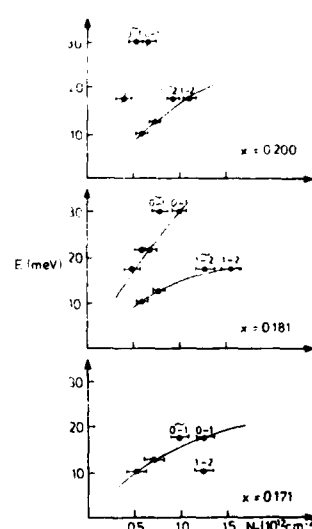


Fig. 2: Subband energies  $E_{01}(0-1)$  and  $E_{12}(1-2)$  vs.  $N_s$  for different  $x$ .

For the case of several occupied subbands it must be kept in mind that the resonances are not strictly energies between the bottoms of a pair of levels. Because the  $k_y = 0$  transitions are blocked by occupancy effects, the resonance is a weighted contribution for finite  $k_y$ . The energy difference, however, in comparing with the  $k_y = 0$  result from ref. /2/ is not nearly as large as the discrepancy. The "finite  $k_y$ "-shift for InSb and InAs has turned out to be only a few percent.

### Discussion and Conclusions

The experimental evidence in Table I for an influence of  $E_G$  on the subband energies is clear-cut. The effect is much stronger than the theory in ref. /2/ allows. Moreover, it has a different sign than one may expect from the dependence of  $m^*$  on  $E_G$ . The subband separations decrease with narrowing of the band-gap. We suggest that this is *prima facie* evidence of band-mixing via the tunneling interaction.

In the absence of subband calculations which treat band-mixing we are free to speculate about the consequences of having a significant overlap of the electron subband wave-function with the filled state in the valence band. The overlap is most important for the  $n = 0$  groundstate as sketched in Fig. 3. The higher lying,  $n = 1$  or  $2$  levels need not even coincide with a filled state of the valence band. Since both the conduction and valence band states, whose wavefunctions overlap in the figure, have the Bloch function  $|s\rangle$  and  $|p\rangle$  admixture of a typical narrow-gap semiconductor, we have a situation in which electrons with the same "quantum numbers" are in the same region of space. Pauli exclusion must be operative in this situation. The effect could be to reduce the  $|s\rangle$  and  $|p\rangle$  admixture that comes from the  $\vec{k} \cdot \vec{p}$ -perturbation, with the subband state becoming more  $s$ -like and the valence electron more  $p$ -like. The net effect, as suggested by the observations, is that there is a level repulsion in which the  $n = 0$  state in Fig. 3 is pushed up.  $E_{01}$  is decreased as a result. Moreover, it is decreased more than the corresponding separation  $E_{12}$  as Table I shows.

It is interesting to note that the tunneling effect, which in principle allows the electron to leak out of the surface potential well, results in raising the  $n = 0$ , groundstate energy. Tunneling into an empty valence band state should lower and broaden the surface subband energy. Level repulsion thus applies only to the case of a filled valence band.

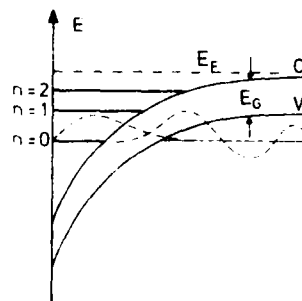


Fig. 3: Sketch of the surface potential well with  $n = 0, 1, 2$  subbands. The tunneling overlap of valence and conduction band wave-functions is largest for  $n = 0$ .

Enough for the speculations! The subband spectroscopy evidence for a band-mixing effect is clear-cut. It is time for a quantitative theory, perhaps along the line of the theory in ref. /3/.

### References:

- 1) J. Scholz, F. Koch, H. Maier, and J. Ziegler, *Solid State Commun.* **45**, 39 (1983)
- 2) Y. Takada, K. Arai, and Y. Uemura, in "Physics of Narrow-Gap Semiconductors" (Lecture Notes in Physics, Vol. **152**, Springer, 1982)
- 3) W. Zawadzki, *J. Phys. C* **16**, 229 (1983)
- 4) J. Scholz, *Doctoral Dissertation*, TU München (1983);  
E. Schindlbeck, *Diplom Thesis*, TU München (1983).

# Intersubband Resonance of Holes and Interaction with 2D-Plasmons on Si

A. D. Wieck, E. Batke, D. Heitmann, and J. P. Kotthaus  
Institut für Angewandte Physik, Universität Hamburg  
Juniusstraße 11, 2000 Hamburg 36, F. R. Germany

## Abstract

Intersubband resonances of holes have been investigated on the high symmetry surfaces of silicon for a wide range of frequencies (30-400  $\text{cm}^{-1}$ ) and charge densities ( $1-8 \times 10^{12} \text{cm}^{-2}$ ) with Fourier transform spectroscopy. Spectra are measured in transmission with the far infrared radiation polarized parallel to the Si-SiO<sub>2</sub> interface and allow a detailed analysis of excitation strength and resonance lineshape. Also possible interactions of energetically low lying subband resonances and 2D-plasmons have been studied.

Intersubband resonances in electron space charge layers on Si have been studied in great detail experimentally and theoretically [1]. In contrast there exist only little information on the more complex surface bandstructure of holes [2-7]. Using Fourier transform spectroscopy we have studied hole intersubband resonances on the three principal surfaces of Si(100), (110) and (111) for a wide range of frequencies (30-400  $\text{cm}^{-1}$ ) and charge densities ( $1-8 \times 10^{12} \text{cm}^{-2}$ ). Here we restrict ourselves to the discussion of the results on the (110)-surface, which is especially interesting because of its anisotropy.

Because of the warped energy contours of the valence bands and the nonparabolic subbandstructure intersubband resonances can be excited with electric field components parallel to the surface and thus can be observed in normally transmitted radiation. Experiments are performed on MOS-capacitors at 4 to 15 K. Typical sample parameters are: gate diameter 4-5 mm, gate resistance 500  $\Omega/\square$ , substrate resistivity 20  $\Omega\text{cm}$ , oxide thickness 45 nm. Both, accumulation layers in p-type substrates and quasi accumulation layers in band gap illuminated n-type samples are investigated and yield essentially the same results.

Typical experimental spectra of the relative change in transmission  $-\Delta T/T = -[T(V_G) - T(V_T)]/T(V_T)$  with  $V_G$ =gate voltage and  $V_T$ =threshold voltage are shown in Fig. 1. The intersubband resonance is superimposed on the 2D-Drude absorption and shifts with increasing charge density  $N_s$  to higher wavenumbers. The different strength of the Drude absorption in Fig. 1 for the different polarization is caused by the anisotropic mass of the (110) surface [8]. Our data also show that the excitation strength of the intersubband resonance is significantly different for both directions of polarization. However, within the experimental accuracy the peak position is not affected by the polarization. We like to note, that our transmission measurements are calibrated and thus make possible direct comparison with theoretical excitation strengths. Our frequency domain study allow also direct analysis of the resonance lineshape. Subtracting the Drude background, the intersubband resonance is found to be strongly asymmetric. This reflects the fact, that for holes the energies  $E_i(\vec{k}, \sigma)$  of different subbands  $i$  show different depen-

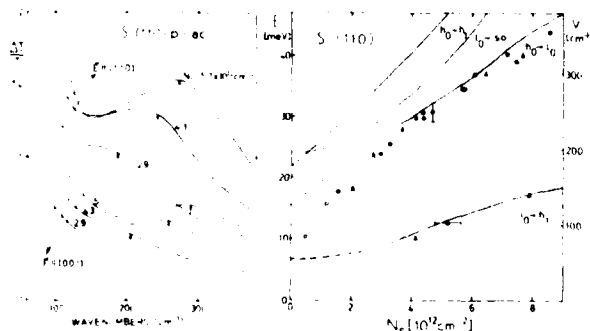


Fig. 1

Fig. 1: Frequency dependent intersubband resonance excitation on p-accumulation layers of Si (110) for different charge densities  $N_s$  and polarization of the infrared electric field parallel to [001] and [110].

Fig. 2: Hole intersubband resonance positions for Si (110). Full symbols (•, Δ) show data for two typical samples. Positions (Δ) have been extracted from laser spectroscopy. (□) are experimental results from /3/. Lines indicate theoretical resonance energies at  $\vec{k}=0$  according to /5/. (e.g.  $l_0 \rightarrow h_1$ , means a transition from the lowest light hole subband  $l_0$  to the first excited heavy hole subband  $h_1$ , s. o. means spin orbit split off subbands.) Dashed lines indicate the density regime where  $l_0$  is not occupied.

dence on the wavevector  $\vec{k}$  and also split for different spin orientations  $\sigma$  for  $\vec{k} \neq 0$  /5/. Experimentally we find that the linewidth increases with increasing charge density  $N_s$ , which is consistent with increasing dispersion effects for higher  $N_s$ .

Experimental resonance positions are plotted in Fig. 2. For different samples data coincide within  $\pm 1.5$  meV. They compare well with calculations of Bangert et al. /5/ and correspond to a transition from the lowest heavy hole subband  $h_0$  to the lowest light hole subband  $l_0$ . Deviations of experimental and theoretical resonance energies at low charge densities  $N_s$  can be explained by two effects, first that many body correction are not included in the theory /5/ and second that the calculations are carried out for inversion conditions whereas our experiments are performed on accumulation layers. Both effects become important at low densities. For low densities, extrapolation of our data also agrees with experimental results of /3/. In laser transmission experiments we also detect a second transition at low energies, which compares with a  $l_0 \rightarrow h_1$ -transition of /5/. The excitation strengths of this transition is comparatively weak. Possible reasons are a low occupation of the  $l_0$ -subband, matrix element effects and perhaps also the fact, that the light hole energy contours are rather isotropic and little nonparabolic. For comparison we wish to note briefly that on Si (100) we observe a transition which compares well to a  $l_0 \rightarrow h_1$  transition in /5/. On Si (111) we see a weak structure that agrees with a  $l_0 \rightarrow h_1$  transition of /5/ but the main observed resonance cannot be easily identified. The good agreement of theoretical resonance energies with the experimental data for many transitions remains

surprising, since all theoretical data are evaluated for  $k=0$ , thus  $k$ -dispersion effects are not included in the comparison of experiment and theory.

On samples with periodically structured gates 2D-plasmons can be excited with FIR-radiation. Recently, 2D-plasmons have been observed in hole space charge layers /8/. With presently available grating fabrication techniques plasmon wavevectors  $q$  about  $2 \times 10^5 \text{ cm}^{-1}$  can be achieved, which corresponds to plasmon frequencies of about  $150 \text{ cm}^{-1}$  at charge densities  $N_s \sim 5 \times 10^{12} \text{ cm}^{-2}$ . Since in hole space charge layers energetically relatively low lying intersubband resonances exist, it is possible to obtain coincidence of the plasmon energy and an intersubband spacing at the same density. At the (110) surface the  $1_0-h_1$  transition coincides with the plasmon dispersion for plasmon wavevectors  $q \approx 1.2 \times 10^5 \text{ cm}^{-1}$  at densities about  $5 \times 10^{12} \text{ cm}^{-2}$ . For this transition we find on many samples with periodically structured gates a more pronounced excitation strength in comparison with samples without grating if the intersubband resonance occurs within the linewidth of the plasmon excitation. Also deviations of the measured plasmon dispersion from the  $\sqrt{N_s}$ -dependence in the crossing regime give evidence for an interaction of plasmon and intersubband resonances. However, more experiments are necessary to achieve a quantitative understanding. Also, if gratings with smaller periodicities and corresponding higher plasmon wavevectors and energies become available, it is interesting to study these interactions in electron space charge layers with much sharper resonances.

We like to thank E. Bangert for access to unpublished calculations, W. Beinvoigt of Siemens, Munich for supplying oxidized wafers and the Deutsche Forschungsgemeinschaft for financial support.

#### References

- /1/ For a recent review see for example:  
T. Ando, A. B. Fowler, and F. Stern, Rev. Mod. Phys., 54, 437 (1982).
- /2/ P. Kneschaurek, A. Kamgar, and J. F. Koch, Phys. Rev. B 14, 1610 (1976).
- /3/ A. Kamgar, Solid State Commun. 21, 823 (1977)
- /4/ G. Abstreiter, U. Claessen and G. Tränkle, Solid State Commun. 44, 673 (1982).
- /5/ E. Bangert, K. v. Klitzing, and G. Landwehr, Proc. 12th Int. Conf. Phys. Semiconductors, p. 714 Stuttgart (1974) and E. Bangert, unpublished preprint.
- /6/ F. J. Ohkawa and Y. Uemura, Prog. Theor. Phys. Suppl. 57, 164 (1975).
- /7/ F. J. Ohkawa, J. Phys. Soc. Japan 41, 122 (1976)
- /8/ E. Batke, D. Heitmann, A. D. Wieck and J. P. Kotthaus, Solid State Commun. 46, 269 (1983).

# PHOTOCONDUCTIVITY ON GaAs-Al<sub>x</sub>Ga<sub>1-x</sub>As HETEROSTRUCTURES

D. Stein, G. Ebert, and K. v. Klitzing  
Physik-Department, Technische Universität München  
8046 Garching, Fed. Rep. of Germany  
and  
G. Weimann

Forschungsinstitut der Deutschen Bundespost beim FTZ  
6100 Darmstadt, Fed. Rep. of Germany

## Abstract

The variation of the resistivity  $\rho_{xx}$  of GaAs-Al<sub>x</sub>Ga<sub>1-x</sub>As heterostructures at  $T = 1.5$  K under far-infrared or microwave irradiation is analyzed as a function of the magnetic field. The observed resonances are attributed to cyclotron resonance and electric-dipole induced electron spin resonance.

Photoconductivity measurements on semiconductors, which are often more sensitive than absorption measurements, are mainly used for the detection of optical transitions between sharp energy levels. In this paper we present photoconductivity measurements on GaAs-Al<sub>x</sub>Ga<sub>1-x</sub>As heterostructures as a function of the magnetic field under microwave or far-infrared illumination.

The samples have standard Hall geometry and consist of  $1.5 \mu\text{m}$  undoped GaAs on insulating GaAs, a spacer of undoped Al<sub>0.3</sub>Ga<sub>0.7</sub>As, 60 nm Si-doped Al<sub>0.3</sub>Ga<sub>0.7</sub>As, and 20 nm undoped GaAs. The two-dimensional carrier densities are about  $2.3 \times 10^{11} \text{ cm}^{-2}$  and  $4.6 \times 10^{11} \text{ cm}^{-2}$  for a spacer of 14 nm and 5 nm, respectively. The variation of the resistivity  $\rho_{xx}$  due to infrared radiation ( $\lambda = 118 \mu\text{m}$  and  $\lambda = 337 \mu\text{m}$ ) or microwaves in the frequency range 12 GHz - 35 GHz is measured as a function of the magnetic field. Photovoltaic signals

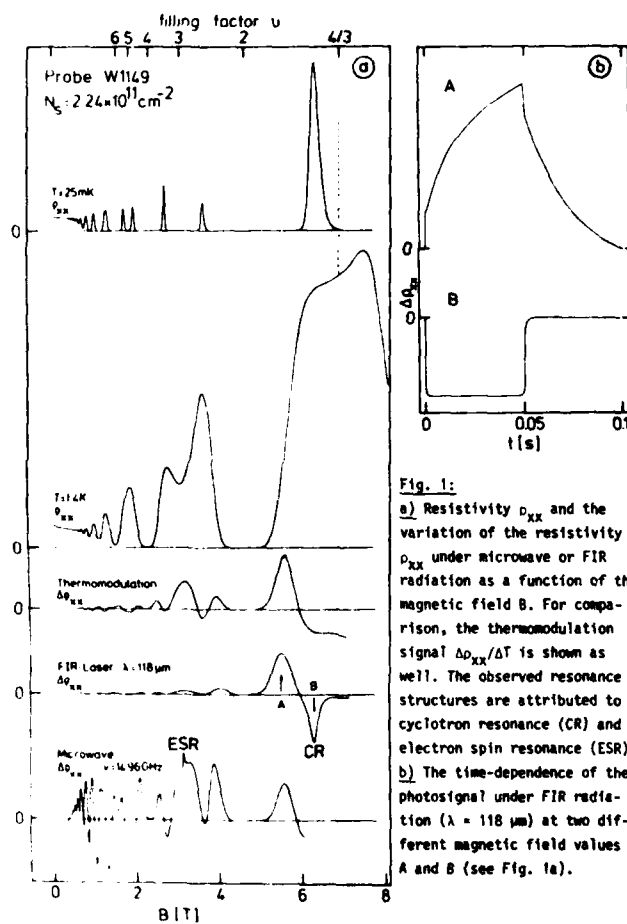


Fig. 1:  
a) Resistivity  $\rho_{xx}$  and the variation of the resistivity  $\rho_{xx}$  under microwave or FIR radiation as a function of the magnetic field  $B$ . For comparison, the thermomodulation signal  $\Delta\rho_{xx}/\Delta T$  is shown as well. The observed resonance structures are attributed to cyclotron resonance (CR) and electron spin resonance (ESR).  
b) The time-dependence of the photosignal under FIR radiation ( $\lambda = 118 \mu\text{m}$ ) at two different magnetic field values A and B (see Fig. 1a).

are eliminated by analyzing the variation of the photosignal under a.c. conditions with an additional lock-in amplifier. The temperature in all photoconductivity experiments was typically 1.5 K.

A survey of experimental data is shown in Fig. 1a. The upper two curves are Shubnikov-de Haas measurements for different temperatures. At  $T = 25$  mK the spin splitting of the Landau levels  $n = 1$  and  $n = 2$  are clearly resolved, whereas the structure visible at a filling factor  $\nu = 4/3$  at  $T = 1.4$  K disappears below 300 mK. Since photoconductivity data are usually influenced by a bolometric signal, the thermomodulation signal  $d\rho_{xx}/dT$  is shown in Fig. 1a, too.

The measurements under FIR radiation show usually a strong enhancement of the photosignal at the magnetic field of cyclotron resonance<sup>1,2</sup>. However, if the resonance lies in the plateau region ( $\rho_{xx} = 0$ ), the absorption process is not visible in photoconductivity. This means that the lifetime of photoexcited carriers is extremely small. The time-dependence of the photosignal (Fig. 1b) demonstrates that at least two different processes with different time constants contribute to  $\Delta\rho_{xx}$ . The amplitude and the sign of the contributions vary independently with magnetic field. The signal with a time constant of more than 10 ms is attributed to a modulation of the lattice temperature, whereas the fast response originated from an electronic process which leads to a change in the electron distribution function and in the simplest case to a variation in the electron temperature. We have no explanation for the fact that at the magnetic field position B (cyclotron resonance field) only the fast photosignal is visible. This result may indicate that radiative recombination is very effective under this condition. The photosignals plotted in Fig. 1a are obtained at a chopper frequency of  $f = 900$  Hz and correspond to the fast photosignal.

With microwave radiation, a new sharp resonance appears around  $B = 3$  T at  $\nu = 14$  GHz, as shown in the lowest curve of Fig. 1a. This signal is

416

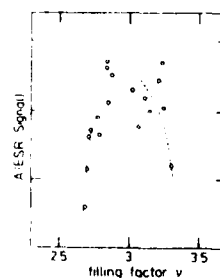


Fig. 2: Amplitude of the ESR signal (normalized relative to the background signal) as a function of the filling factor  $\nu$ .

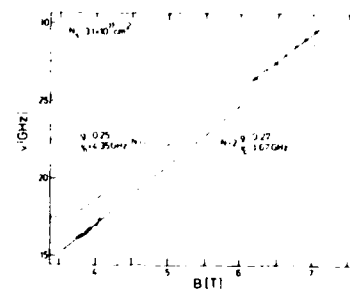


Fig. 3: Magnetic field positions of the ESR signal at different microwave frequencies  $\nu$  for filling factors close to 3 ( $N = 1$ ) and 5 ( $N = 2$ ). The tilt angle of the magnetic field is  $\phi \approx 50^\circ$ . The straight lines are characterized by the offset  $\nu_0$  and the slope  $g\mu_B/h$ .

attributed to spin resonance of free electrons (ESR) in the two-dimensional system. In principle any absorption process within the device may influence the resistivity of the two-dimensional electron gas (2DEG), but the following results indicate that the observed resonances are really connected with electronic states of the 2DEG:

- a) The resonance can only be observed, if the Fermi energy is located between spin-split levels. The amplitude of the signal has a maximum at filling factors close to  $\nu = 3$  and  $\nu = 5$ . (The magnetic field for  $\nu = 1$  is outside the experimental range and at  $\nu = 7, 9, 11$ , etc. the spin-splitting is not resolved.) A typical result is shown in Fig. 2 where the normalized amplitude of the ESR signal is plotted as a function of the filling factor. The amplitude relative to  $\nu = 3$  is reduced by more than one order of magnitude at  $\nu < 2.5$  and  $\nu > 3.5$ .

417

b) The resonance condition is a function of the Landau quantum-number  $N$ , as shown in Fig. 3. For  $N = 1$  (filling factor close to  $\nu = 3$ ) the observed resonance obeys the law  $\nu = 4.35 \text{ GHz} + 0.25 \mu_B/\hbar$ , whereas for  $N = 2$  the relation  $\nu = 1.67 \text{ GHz} + 0.27 \mu_B/\hbar$  is obtained.

These experimental data demonstrate that the observed resonance under microwave radiation is connected with the electronic properties of the 2DEG and can be explained as electric-dipole induced electron spin resonance<sup>/3/</sup>.

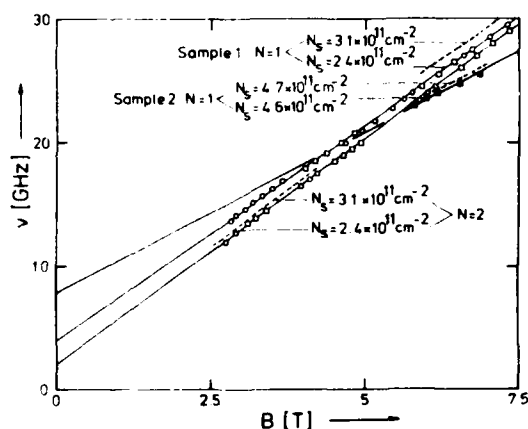


Fig. 4: Summary of the ESR fields  $B$  at different frequencies  $\nu$  for two samples, Landau quantum numbers  $N = 1$  and  $N = 2$ , and different surface carrier densities due to different cooling processes.

A summary of all experimental data related to the ESR signal is shown in Fig. 4. The magnetic field positions of the resonance are plotted as a function of the microwave frequency. In order to follow the resonance structure over a wide range of magnetic field, different tilt angles  $\phi$  between the magnetic field direction and the surface normal have been used for the

measurements on sample 1, whereas the data for sample 2 are obtained at  $\phi = 0^\circ$ . The dotted lines correspond to measurements on the same device but higher surface carrier density  $N_s$  obtained after another cooling process from room temperature to helium temperature. A shift of the resonance energy to higher frequencies is also observed, if the carrier density of the 2DEG is increased by infrared radiation<sup>/4/</sup>. The extrapolation to zero magnetic field gives always a finite excitation energy.

All these experimental data are compatible with spin resonance of free electrons in the two-dimensional system. Especially the lifting of the spin-degeneracy at  $B = 0 \text{ T}$  for a two-dimensional system without inversion symmetry has been predicted theoretically<sup>/5,6/</sup>, but a quantitative theory is not available. A discussion of the experimental data on the basis of electron spin resonance will be published separately<sup>/4/</sup>.

This work has been supported by the Deutsche Forschungsgemeinschaft (SFB 128).

#### References:

- 1) C.F. Lavine, R.J. Wagner, and D.C. Tsui, *Surf. Science* **113**, 112 (1982)
- 2) J.C. Maan, Th. Englert, D.C. Tsui, and A.C. Gossard, *Appl. Phys. Letters* **40**, 609 (1982)
- 3) F. Kuchar and M. Kriechbaum, *Proc. Int. Conf. "Application of High Magnetic Fields in Semiconductor Physics"*, *Lecture Notes in Physics* **177**, 309 (1983)
- 4) D. Stein, K. v. Klitzing, and G. Weimann, to be published
- 5) Y. Uemura, *Japan J. Appl. Phys. Suppl.* **2**, Pt 2, 17 (1974)
- 6) G.E. Margues and L.J. Sham, *Surf. Science* **113**, 131 (1982)



Properties of n-i-p-i Doping Superlattices in III-V and IV-VI Semiconductors

G.H. Döhler and P. Ruden

Max-Planck-Institut für Festkörperforschung,  
Heisenbergstrasse 1, 7000 Stuttgart 80

We discuss the unusual electronic properties of n-i-p-i doping superlattices, i.e. semiconductors modulated by periodically alternating n- and p- doping. The work on these systems involving GaAs as a host material is briefly reviewed. New features which are to be expected from doping superlattices using IV-VI semiconductors as host materials are then presented. It is shown that the different electronic structure of these materials leads to doping superlattice properties which are qualitatively different from those observed in III-V materials. The effect of a magnetic field on the electronic states is also discussed. Finally we propose a new hetero- n-i-p-i superlattice which combines the tunability of doping superlattices with the absence of impurity scattering of modulation doped hetero superlattices and allows for the observation of the subband structure in luminescence experiments.

1. Introduction

The first successful experiments on n-i-p-i doping superlattices have initiated a steadily growing interest in this new type of semiconductor superlattices. Those experiments of a few years ago were able to confirm the theoretical predictions of very unusual electronic properties characteristic of n-i-p-i superlattices. Then, and also in most of the work done subsequently, GaAs was used as a host material.

The term "n-i-p-i superlattice" was introduced by one of us (G.H.D.) in his first theoretical investigation of the electronic properties of semiconductors with doping superlattices (1,2). It originally signified a periodic sequence of n- and p-doped layers,

separated by intrinsic (i-) layers. The term is now used for the whole class of doping superlattices, even if no intrinsic layers are incorporated. The major results of the original study (1,2) and of a few subsequent papers (3-5) can be summarized as follows:

- 1) The superposition of the periodic space charge potential of the impurities to the crystal potential of the host material reduces the effective band gap  $E_g^{eff}$  by an amount which depends on the design parameters of the superstructure (period length and doping profiles).
- 2) This effective band gap is an "indirect gap in real space" since electronic states near the bottom of the conduction band are shifted by half a superlattice period with respect to hole states near the top of the valence band.
- 3) The spatial separation between electrons and holes causes a large increase in the recombination lifetimes. The lifetimes depend on the design parameters on an exponential scale. Large deviations of the two-dimensional electron concentration  $n^{(2)}$  in the n-layers and of the hole concentration  $p^{(2)}$  in the p-layers from the thermal equilibrium values are metastable. The non-equilibrium charge carrier distributions can be characterized by different quasi-Fermi levels  $\phi_n$  and  $\phi_p$ , respectively. In other terms, the carrier concentration in a given n-i-p-i crystal is tunable.
- 4) The free carriers in the n- and p-layers partially compensate the fixed impurity space charge. In this way they reduce the amplitude of the periodic space charge potential increase the effective band gap. Thus,  $E_g^{eff}$  is also a tunable quantity which can be varied by changing the non-equilibrium carrier concentrations  $n^{(2)}$  and  $p^{(2)}$ .
- 5) Electrons and holes in the respective layers form a dynamical-

ly two-dimensional many-body quantum system. The subband structure is also tunable by variation of the carrier concentration.

- e) The tunability of carrier concentration and electronic structure, which is a unique feature of this class of semiconductors, results in exotic properties such as tunable bipolar conductivity, tunable luminescence and absorption coefficient, and tunable elementary excitations.

Although these properties seem quite appealing from the point of view of basic physics as well as for exciting device applications, their experimental investigation became possible only many years later, when GaAs n-i-p-i crystals were grown by molecular beam epitaxy (MBE) by Ploog and coworkers (6). This was particularly surprising because the n-i-p-i system does not contain any interfaces and, therefore, represents a simpler structure than the compositional superlattices (7) which had already been studied extensively at that time.

Within a rather short period the experimental studies on n-i-p-i crystals have confirmed most of the theoretical predictions. The investigations include the electrical and/or optical tuning of two-dimensional conductivity (8,9), luminescence (10,12), optical gain (13), absorption coefficient (14), 2-D subband structure and charge and spin-density excitations (10,15,16). In all cases tunability over a wide range was possible and was found to be in quantitative agreement with the theory, which was simultaneously extended (17-19). The theoretical and experimental work on GaAs n-i-p-i structure has been reviewed several times during the last year (20-24). In Ref. 24 and Ref. 25, also the various device aspects which derive from the tunability of the optical and electrical properties have been discussed. Therefore, we refer to one of those reviews for details of the state of the art in this field.

The objective of the present paper is a preview on our future theoretical studies which, we hope, will soon be followed (or even accompanied) by further experiments. So far most experiments on n-i-p-i crystals and, implicitly, most of the theoretical studies, have been restricted to GaAs as the host material. A particularly appealing property of n-i-p-i structures, however, is just the fact, that there is almost no restriction with respect to the choice of the host material. The only condition is that a preparation technique is available which allows for sufficiently well controlled periodic n- and p-doping during the growth process.

Although, there is an enormous flexibility for designing n-i-p-i structures with very different properties made from the same host material but with different superlattice period and doping profiles, the choice of different host materials provides a new dimension of flexibility. In the first part of this paper we will show how strongly the features of new n-i-p-i systems may differ from their GaAs counterparts. In a discussion of the electronic structure and of some of the resulting properties of n-i-p-i superlattices in IV-VI compound crystals, it will become obvious that such systems can be much more suitable for the observation of phenomena which involve both, electron and hole subbands. In addition we will see that many new n-i-p-i phenomena originate from the many-valley band structure of this host material. In the second part we will discuss a few examples of extensions of the original n-i-p-i concept. There we will combine alternating n- and p-doping with a periodic modulation of composition. With respect to their electronic properties such systems feature both the unique tunability of the electronic structure of n-i-p-i crystals and the high mobility of modulation-doped compositional superlattices (26).

## 2. IV-VI compound n-i-p-i crystals

The electronic properties of the binary and ternary IV-VI compounds of the elements Sn and Pb, and S, Se and Te are characterized by a narrow, direct band gap  $E_g^0$  at the L-point, with nearly equal and small transverse conduction and valence band masses  $m_{c,t}$  and  $m_{v,t}$ . The anisotropy ratio  $K$  between longitudinal and transverse masses is rather large in most cases and it may differ considerably between conduction and valence band valleys. The values of the static dielectric constant are extremely high. Finally, impurities don't form bound states in these materials (27,26). In the following we will restrict ourselves to PbTe as a typical member of this family. PbTe can be grown with well controlled deposition rate in the (111) direction by hot-wall-epitaxy on BaF<sub>2</sub> substrates (29,30). Doping concentrations of n- and p-type of  $10^{18} \text{ cm}^{-3}$  can be achieved by intentional non-stoichiometry. Each Pb vacancy forms a double negatively charged defect whose charge is neutralized by two holes in the valence band. The Te vacancies behave correspondingly, generating a double positively charged defect and two free electrons in the conduction band. A PbTe n-i-p-i crystal can then be grown by periodic n- and p-doping just as in the case of GaAs.

The electronic structure, however, becomes quite different due to the different material parameters of the host crystal. We consider, for the sake of simplicity, a n-i-p-i structure with constant and equal (net) n- and p-doping  $n_D$  and  $n_A$  in the respective layers. The layers are assumed to be of equal thickness  $d_n = d_p = d/2$  with no intrinsic layers between them. The fixed charge density  $2|e|n_D$  and  $-2|e|n_A$  in the doping layers causes a periodic parabolic space charge potential of amplitude

$$V_0 = (4\pi e^2 n_D / \epsilon_0) (d/4)^2 \quad (1)$$

which modulates the conduction and valence band edges in real space

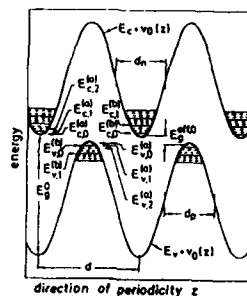


Fig. 1 Schematic real-space energy diagram of a IV-VI compound n-i-p-i crystal with doping superstructure along one of the (111)-directions. A symmetric configuration with  $n_D = n_A$  and  $d_n = d_p = d/2$  (i.e. zero thickness of the intrinsic layers) is assumed. The electronic subband energies are nearly symmetric for corresponding conduction and valence band valleys. The band edges are indicated by full lines for the b- and by dashed lines for the a-valleys. The value of the effective band gap  $E_g^{\text{eff}}$  is tunable within wide limits by carrier injection or photoexcitation, as in GaAs n-i-p-i crystals.

as indicated in Fig. 1. From Eq. (1) it follows that the superlattice period and/or the doping concentration in PbTe n-i-p-i's have to be considerably larger than in their III-V counterparts in order to obtain values of  $V_0$  which are comparable with the band gap  $E_g^0$  of the host material. The reason for that is the static dielectric constant  $\epsilon_0 = 1500$  (at  $T = 0 \text{ K}$ ), which is by more than two orders of magnitude larger than that of GaAs. Thus, the situation shown in Fig. 1 with a modulation of the band edges such that the effective band gap in the ground state

$$E_g^{\text{eff},0} = E_g^0 - 2V_0 \quad (2)$$

nearly vanishes can be realized with  $d_n = d_p = 200 \text{ nm}$  if  $2n_D = 2n_A = 10^{18} \text{ cm}^{-3}$ . We have used  $E_g^0 = 190 \text{ meV}$  for the PbTe band gap at  $T = 0 \text{ K}$ . For the lowest electron and hole subbands whose wave functions are confined to a single parabola and whose energies are small enough for the non-parabolicity of  $\epsilon(k)$  in momentum space to be negligible, we obtain the harmonic oscillator energies as subband edges (20-24)

$$E_{c,v}^{(i)} = E_g^0 - 2V_0 + \hbar \omega_c^{(i)} (u+1/2); u = 0, 1, 2, \dots; i = a \text{ or } b$$

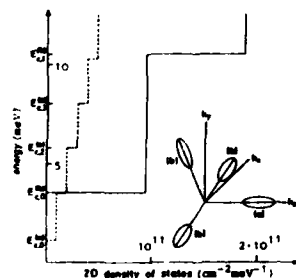
$$E_{v,v}^{(j)} = -\hbar \omega_v^{(j)} (v+1/2); v = 0, 1, 2, \dots; j = a \text{ or } b \quad (3)$$

where

$$\omega_c^{(i)} = (4\pi e^2 n_D / \kappa_0 m_{c,z}^{(i)})^{1/2} \quad (4)$$

$$\omega_v^{(j)} = (4\pi e^2 n_A / \kappa_0 m_{v,z}^{(j)})^{1/2}$$

We see, that the subband spacings are less affected than the space charge potential by the huge dielectric constant, since  $\kappa_0$  enters with 1/2-power in Eqs. (4). Eqs. (3) and (4) reflect the multivalley bandstructure of the host material and the anisotropy of the valleys. By convention the a-valleys are those, whose energy ellipsoids are oriented along the direction which coincides with the z-direction (valley degeneracy factor  $g_v^{(a)} = 1$ ) whereas the b-valleys correspond to the band extrema at the three other L-points (degeneracy factor  $g_v^{(b)} = 3$ ; see inset in Fig. 2). The values for the relevant effective masses  $m_{c,z}^{(i)}$  and  $m_{v,z}^{(j)}$  can be derived from the corresponding transverse and longitudinal masses by the expressions given by Stern and Howard (31) for conduction subbands in Ge space-charge layers with (111) surface orientation. The same applies to the masses  $m_{c,x}^{(i)}$ ,  $m_{c,y}^{(i)}$ ,  $m_{v,x}^{(j)}$  and  $m_{v,y}^{(j)}$  for motion in the x-y plane (i.e. parallel to the layers) and the resulting two-dimensional densities of states per



subband  
 $N_c^{(i)} = g_v^{(i)} (m_{c,x}^{(i)} m_{c,y}^{(i)})^{1/2} / (\pi \hbar^2)$   
 $N_v^{(j)} = g_v^{(j)} (m_{v,x}^{(j)} m_{v,y}^{(j)})^{1/2} / (\pi \hbar^2) \quad (5)$   
 Fig. 2 Density of states diagram for the conduction subbands in a PnTe n-i-p-i crystal grown in (111)-direction with donor concentration  $n_D = 5 \times 10^{11} \text{ cm}^{-3}$ . Dashed line: (a)-valley subbands. Full line: (b)-valleys. The inset shows the orientation of the L-point valleys in momentum space.

In Fig. 2 the density of states diagram for the conduction subbands is shown for  $2n_D = 10^{18} \text{ cm}^{-3}$ .

We note that the calculated electronic structure in the present system represents much less an idealization than in the case of a typical III-V compound n-i-p-i structure. Due to the absence of bound impurity states and due to the very efficient screening of the impurity potentials which results from the high value of the static dielectric constant, impurity bands, subband broadening effects and random potential fluctuations will be extremely small in comparison to the subband spacings. Therefore, the presence of impurities does not significantly restrict the observation of effects related to two-dimensional subbands, in contrast to the case of the hole subbands in GaAs n-i-p-i crystals.

Another remarkable consequence of the huge static dielectric constant is the weak interaction between the carriers at energies sufficiently below the optical phonon energies. Hartree, exchange, and correlation contributions to the subband energies are negligible in many cases where they are of crucial importance in III-V n-i-p-i superlattices.

In order to illustrate this observation we compare the ratios of the compensating space charge density -  $|e|n(z)$  at the center of an n-type layer to the fixed impurity space charge density. For the two systems we assume a two-dimensional carrier concentration such that the first excited subband just begins to be populated and we neglect all self-consistent corrections to the space charge potential due to the mobile carriers. A simple calculation yields the result

$$n(z=0)/n_D = 8\pi (m_c/m_i) (a_{\text{Bohr}}^{\text{eff}}/a) (E_D/\hbar\omega_c) \quad (6)$$

where  $a$  is the decay length of the harmonic oscillator wave function and  $E_D$  the binding energy of the hydrogen like effective

mass donor. The numerical values at  $n_D = 10^{18} \text{ cm}^{-3}$  are

$$n(z=0) / n_D = \begin{cases} 1^7 & \text{for GaAs} \\ 0.02 & \text{for PbTe} \end{cases} \quad (7)$$

These results demonstrate that a non-self-consistent calculation (without the Hartree corrections) will provide a completely incorrect result for the case of GaAs, whereas the selfconsistency corrections are negligibly small in PbTe for the present example. From the density of states diagram in Fig. 2 we see, that  $n(z=0) / n_D$  is still significantly  $< 1$  at the carrier concentration where the population of the first excited subband of the b-valleys starts and where the two-dimensional carrier concentration is already  $\approx 10^{12} \text{ cm}^{-2}$ .

From the latter result we deduce that many properties of PbTe n-i-p-i crystals can be calculated analytically by using the harmonic oscillator wave functions as the solutions of the z-dependent part of the Schrödinger equation. In the following we will discuss the transitions between conduction and valence subbands and the magnetic field effects as two instructive examples. These two examples may also serve as a demonstration of the qualitatively new properties of this group of n-i-p-i crystals.

### 2.1. Conduction to valence band transitions

Electron-hole recombination lifetimes are generally very large in PbTe n-i-p-i crystals, just as in GaAs doping superlattices. Their actual values depend on the design parameters of the structure and on the degree of excitation.

Recently, we have derived an approximate, analytical expression for the life-time enhancement resulting from the spatial separation of electrons and holes (22). This expression has been applied successfully to GaAs n-i-p-i's (20). It is,

however, interesting to note, that this expression represents a better theoretical description of the situation in PbTe n-i-p-i's and that it implies interesting consequences:

The transition probability for interband recombination between carriers in the lowest subbands, as obtained from a calculation of the overlap between the spatially shifted harmonic oscillator envelope wave functions, reads (22)

$$\tau_{nipi} / \tau_{bulk} \approx [(\omega_c^{(i)} + \omega_v^{(j)}) / (\omega_c^{(i)} \omega_v^{(j)})^{1/2}] \exp(8V_0 / (\hbar\omega_c^{(i)} + \hbar\omega_v^{(j)})) \quad (8)$$

where  $\omega_c^{(i)}$  and  $\omega_v^{(j)}$  are the harmonic oscillator frequencies, of the i-th and j-th conduction and valence band valleys obtained from eqs. 4. The numerical values obtained from eqs. 8 are very different for transitions between (a) or (b) valleys. (Note, that optical (a)-to-(b)-transitions are forbidden by the k-selection rule). For  $n_D = n_A = 10^{18} \text{ cm}^{-3}$ , and  $2V_0 = 40 \text{ meV}$  (corresponding to  $d_n = d_p = 90 \text{ nm}$  we obtain

$$(\tau_{nipi} / \tau_{bulk})_a \approx e^{35} \approx 10^{15} \quad (9)$$

$$\text{and} \quad (\tau_{nipi} / \tau_{bulk})_b \approx 10^5 \quad (10)$$

This means that the luminescence intensity increases by about 10 orders of magnitude when the population of the (b) valleys begins upon increase of the total carrier concentrations  $n^{(2)}$  and  $p^{(2)}$  in the conduction and hole subbands.

This is true, if all the electrons and all the holes are in their respective thermal equilibrium described by the quasi

level levels  $\epsilon_n$  and  $\epsilon_p$ , respectively. This situation can be realized, for instance, in the case of electroluminescence with electron and holes injected via selective electrodes (11).

If the crystal is excited by absorption of light the distribution of carriers in the (a) and (b) valleys depends on the polarization of the absorbed light, on the relaxation processes, and on the lifetimes for (a)-(b) intervalley scattering. Moreover, a frequency variation of the exciting light provides an interesting tool for influencing the distribution of photoexcited carriers within the (a) and (b) valleys.

For photon energies  $\hbar\omega < E_g^0$  the absorption coefficient due to interband transitions between (b) valleys is much larger than between (a) valleys, again, because of the much larger overlap between the relevant subband wave functions.

If, finally, we consider that the position of the luminescence spectra provides information about the effective energy gap, and therefore about the carrier concentrations  $n^{(2)}$  and  $p^{(2)}$ , we realize, that interesting new phenomena can be studied by absorption, photoconductivity, and photo- or electroluminescence experiments. We are not aware of any other systems where reduction of symmetry yields such dramatic differences in behavior between (a) and (b) valley carriers.

## 2.2. Magnetic field induced peculiarities

The effects of magnetic fields, both, normal and perpendicular to the layers, turn out to be quite unique in PbTe n-i-p-i crystals.

A magnetic field normal to the layers will shift the charge carriers from the (a) valleys to the (b) valleys, since the Landau level splitting

$$\Delta \hbar \omega_{n,(H_z)}^{(i)} = \hbar e H_z / (\omega_{n,x}^{(i)} m_{n,y}^{(i)} c^2)^{1/2}, \quad i=a,b; \quad n=v,c \quad (11)$$

and the spin splitting

$$\Delta \epsilon_{sp,n}^{(i)} = g_{n,z}^{(i)} \mu_B H_z \quad (12)$$

increase faster for the (a) than for the (b) valleys. Because of the small electric subband spacing the first quantum limit reached with increasing  $H_z$ -field will correspond to a population of the lowest Landau level in several (electric) subbands, if  $n^{(2)}$  is of the order of  $10^{12} \text{ cm}^{-2}$ . Only at considerably higher magnetic fields the final quantum limit (all carriers populating the lowest Landau level within the lowest subband with spin down orientation) will be reached. This situation implies interesting consequences for the magnetoabsorption in the PbTe n-i-p-i's.

A magnetic field parallel to the layers has two important consequences. At relatively moderate magnetic fields  $H_y$  the curvature of the magnetic potential

$$v_{H_y}^{(i)}(z) = (e H_y / c)^2 m_{n,z}^{(i)-1} z^2 / 2, \quad n=c,v; \quad i=a,b \quad (13)$$

exceeds the curvature of the space charge potential. The value of the subband spacing, given by

$$\Delta \hbar \omega_{(z)}^{(i)} = \hbar \{ [8 \pi e^2 n_i / \kappa_0 \cdot (e H_y / c)^2] / m_{n,z}^{(i)} \}^{1/2}, \quad (i) = (c), (v), (a) \quad (14)$$

increases strongly and becomes dominated by the magnetic field. The subband wave functions, however, are essentially pinned at the center of the doping layers, due to the large amplitude

of the space charge potential. Their position shifts only slightly in  $z$ -direction with increasing momentum of the free motion perpendicular to the  $H_H$ -field. The overlap between electrons and holes in adjacent  $n$ - and  $p$ - layers, however, decreases dramatically due to decreasing localization length of the harmonic oscillator wave functions. Therefore a strong tunability of the recombination lifetimes by the  $H_H$  field parallel to the layers results.

We have discussed only a few remarkable properties which we predict for this new kind of doping superlattices. We hope, however, that we have been able to demonstrate that choosing a new host material does not merely imply the application of the established concept to a different system. We have tried to show that interesting new physics results from the investigations of those structures.

### 3. Hetero- $n-i-p-i$ - superlattices

The observation of two-dimensional effects other than those related to disorder and localization is generally influenced in an unfavorable manner by the indispensable presence of impurities in doping superlattices. Therefore, we have proposed a few years ago a modified version of the original concept, the "hetero  $n-i-p-i$  structure" which combines the high mobility of modulation doped compositional superlattices with the unique tunability of modulation of band gap and carrier concentration in the  $n-i-p-i$  superlattices (32). Recently this system has been realized and the expected behavior, was observed (33).

The version of a hetero-  $n-i-p-i$  structure just mentioned consists essentially of a normal doping superlattice with thin intrinsic layers of a smaller bandgap material interspersed

in the middle of the doped layers. This particular structure is probably the most suitable one for electrical experiments where large lifetimes are required or for studies of the luminescence or absorption by vertical optical transitions within the layers of the smaller band gap material. The point of particular interest in the latter case concerns the time dependence of the carrier concentration in the layers. Depending on the design of the structure, on the excitation energy and intensity an increasing net electron and hole concentration will pile up fast or slowly in the low band gap layers due to various kinds of transitions between adjacent layers.

A different version of a hetero  $n-i-p-i$ , is shown in Fig. 3. Electrons and holes are spatially separated from both types of impurities, just as in the former structures. Therefore we expect again only small impurity induced subband broadening effects for the electron and hole subbands. The modulation of the band edges in the present version, however, differs strongly from the former one. Electrons and holes are closer

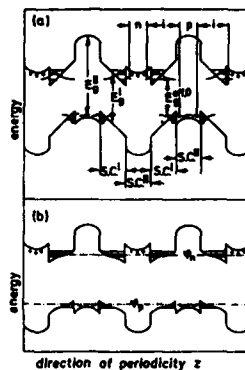


Fig.3 Example of real space energy diagram of a "hetero  $n-i-p-i$  crystal" consisting of semiconductors  $s.c.I$  and  $s.c.II$  with superposition of a  $n-i-p-i$  doping structure. (a): Ground state. The zeroth electron and heavy-hole subband envelope wave functions are indicated schematically. (b): Excited state with increased effective band gap and different quasi-Fermi levels  $\epsilon_n$  and  $\epsilon_p$  for electrons and holes, respectively.

together in real space and energetically they are no longer separated by potential barriers involving the larger band-gap material. Thus, the present structure behaves much more like a conventional n-i-p-i crystal with respect to its tunable absorption and luminescence. The luminescence spectrum, however, should be much narrower as the subbands are no longer broadened due to random fluctuation of the impurity distribution. Moreover, we will observe transitions into hole subbands, in contrast to the conventional III-V compound n-i-p-i crystal, where the holes are in the acceptor impurity band. Note also, that the vertical recombination processes, which are the dominant ones at excitation energies in the range  $E_g^I < \hbar\omega < E_g^{II}$  in the previously discussed hetero n-i-p-i, are completely suppressed in the present one.

#### Acknowledgment

We would like to thank G. Bauer, H. Fujijasu, and P. Vogl for stimulating discussions.

#### References

- (1) G.H. Döhler, *phys. stat. sol. (b)* **52** (1972) 79
- (2) G.H. Döhler, *phys. stat. sol. (b)* **52** (1972) 533
- (3) G.H. Döhler, *Surface Science* **73** (1978) 97
- (4) G.H. Döhler, *J. Vac. Sci. Technol.* **16** (1979) 851
- (5) G.H. Döhler and K. Ploog, *Prog. Crystal Growth Charact.* **2** (1979) 145
- (6) K. Ploog, A. Fischer and H. Künzel, *J. Electrochem. Soc.* **128** (1981) 400
- (7) R. Dingle, in *Festkörperprobleme: Advances in Solid State Physics*, Ed. H.J. Queisser (Vieweg, Braunschweig, 1975), Vol. **XV**, p. 21, L. Esaki and L.L. Chang, *Thin Solid Films* **36** (1976) 285; M. Voos and L. Esaki, Springer Ser. Solid State Sci. **24** (1981) 292
- (8) K. Ploog, H. Künzel, J. Knecht, A. Fischer, and G.H. Döhler, *Appl. Phys. Lett.* **38** (1981)
- (9) H. Künzel, G.H. Döhler and K. Ploog, *Appl. Phys. A* **27** (1982) 1

- (10) G.H. Döhler, H. Künzel, U. Olego, K. Ploog, P. Ruden, and H.J. Stolz, *Phys. Rev. Lett.* **47** (1981) 864
- (11) H. Künzel, G.H. Döhler, P. Ruden and K. Ploog, *Appl. Phys. Lett.* **41** (1982) 852
- (12) H. Jung, G.H. Döhler, H. Künzel, K. Ploog, P. Ruden and H.J. Stolz, *Sol. Stat. Commun.* **43** (1982) 291
- (13) H. Jung, G.H. Döhler, E. Göbel and K. Ploog, *Appl. Phys. Lett.*, in press
- (14) G.H. Döhler, H. Künzel, and K. Ploog, *Phys. Rev. B* **25** (1982) 2616
- (15) Ch. Zeller, B. Vinter, G. Abstreiter and K. Ploog, *Phys. Rev. B* **26** (1982) 2124
- (16) G. Fasol, P. Ruden, K. Ploog, submitted for publication
- (17) P. Ruden and G.H. Döhler, *Phys. Rev. B* **27** (1983) 3538
- (18) P. Ruden and G.H. Döhler, *Phys. Rev. B* **27** (1983) 3547
- (19) G.H. Döhler and P. Ruden, to be published
- (20) G.H. Döhler, in *Festkörperprobleme: Advances in Sol. Stat. Phys.*, Ed. P. Grosse (Vieweg, Braunschweig, 1983), Vol. **XXIII**, p. ....
- (21) G.H. Döhler, *Jap. J. of Appl. Phys.* **22**, Suppl. **22-1** (1983) 29
- (22) G.H. Döhler, *J. Vac. Sci. Technol.*, in press
- (23) G.H. Döhler and K. Ploog, in *Synthetic Modulated Structure Materials*, L.L. Chang and B.C. Giessen, (Academic Press, N.Y.) to be published.
- (24) G.H. Döhler, in: *The Technology and Physics of Molecular Beam Epitaxy*, Eds. E.H.C. Parker and M.G. Dowsett (Plenum, New York, 1984)
- (25) G.H. Döhler, in *Collected Papers of MBE-CST-2*, R. Ueda, Ed, Tokyo, (1982) p. 20
- (26) H.L. Störmer, R. Dingle, A.C. Gossard, W. Wiedmann and R.A. Logan, *Institute of Physics Conference Series* **43**, (1978) 557; S. Niyamizu and T. Kimura, *J. Vac. Sci. Technol.*, in press
- (27) D.L. Mitchell and R.F. Wallis, *Phys. Rev.* **151** (1966) 581
- (28) G. Martinez, M. Schlüter, and M.L. Cohen, *Phys. Rev. B* **11** (1975) 651
- (29) H. Kinoshita, T. Sakashita, and H. Fujijasu, *J. Appl. Phys.* **52** (1981) 2869
- (30) H. Liemans, E.J. Fantner, and G. Bauer, *Rev. of Sci. Instr.*, June 1983
- (31) F. Stern and W.E. Howard, *Phys. Rev.* **163** (1967) 816
- (32) G.H. Döhler, *Physica Scripta* **24** (1981) 430
- (33) H. Künzel, A. Fischer, J. Knecht, and K. Ploog, *Appl. Phys. A* **30** (1983) 73



MAGNETO-OPTICAL STUDIES OF TWO-DIMENSIONAL  
ELECTRONS IN MQW HETEROSTRUCTURES

J. M. Worlock, <sup>(a)</sup> A. C. Maciel, <sup>(b,c,d)</sup> A. Petrou, <sup>(b,c)</sup> J. H. Perry, <sup>(b,c)</sup>  
R. I. Aggarwal, <sup>(c,e)</sup> M. Smith, <sup>(b,c)</sup> A. C. Gossard, <sup>(f)</sup> and W. Wiegmann, <sup>(f)</sup>

The two topics covered in this report are 1) determination of the cross section for Landau level Raman scattering and a new explanation for this "forbidden" scattering; and 2) new spectra of photoluminescence by MQW electrons in magnetic fields, showing behavior related to electron exchange energy, and competition for dominance in the valence band between confinement and magnetic field effects.

In this report, we discuss two aspects of our studies of two-dimensional (2D) electrons in multi-quantum well (MQW) heterostructures. We have performed magneto-Raman and photoluminescence experiments on MQW samples of GaAs-AlGaAs grown by molecular beam epitaxy using the technique of modulation doping to produce clean, well defined 2D electron layers.<sup>1</sup>

In the first part, we present the results of measurements of absolute cross sections for Raman scattering by both intersubband (IS) and cyclotron resonance (CR) modes, and compare these with a new theory for interband magneto-optical transitions which we believe explains the forbidden CR scattering.

In the second part, we show spectra of photoluminescence and their variation with magnetic field, and discuss these qualitatively in terms of many body effects in the electron system, and competition between quantum-well

confinement and the magnetic field in determining the valence band states.

Since our first observation of Landau level (or CR) Raman scattering,<sup>2</sup> we have searched for an explanation for this forbidden scattering, while continuing to make experiments designed to limit the theoretical search. In this quest, we have measured the absolute cross sections, at resonance, for both IS and CR modes.<sup>3,4</sup> These were obtained by comparison with the known cross section for optical phonons in silicon.<sup>5</sup> We concentrated on a high mobility sample,  $\mu = 90,000 \text{ cm}^2/\text{voltsec.}$ , with  $n_s = 5 \times 10^{11} \text{ electrons/cm}^2$ . Working at 2K and 8 Tesla, we determined the following cross sections ( $\text{cm}^2$  per electron): IS ( $F_{01}$  transition),  $\sim 1.5 \times 10^{-21}$ ; and CR,  $\sim 1.0 \times 10^{-21}$ . We have shown<sup>4</sup> that the maximum theoretical cross section  $(d\sigma/d\Omega)_{\text{max}}$  for an electron in GaAs, assuming all envelope function overlap matrix elements are unity, is  $1.0 \times 10^{-19} \text{ cm}^2$ , using a resonant energy denominator of 10 meV, which is consistent with our resonance measurements. The cross section for CR scattering is thus about one percent of this theoretical maximum, so we cannot tolerate any really small overlap matrix elements. The crucial factor<sup>6</sup> in the matrix element is

$$I_{n,m} = \langle f_n(x) | f_m(x + \ell^2 q) \rangle,$$

where  $f_n$  and  $f_m$  are the Landau oscillator wave functions in conduction and valence band;  $\ell^2$  is the square of the magnetic length,  $\ell^2 = \hbar c / eH$ ; and  $q$  is the component of optical wave vector perpendicular to  $H$ . The "forbiddenness" of first order CR scattering comes from the fact that  $\lim_{q \rightarrow 0} I_{n,m} = \delta_{n,m}$ , i.e., interband optical transitions preserve Landau level index, in the limit of small  $q$ . In our experiments, for the scattered beam,  $q^2$  is very small, but for the incident laser beam, at 8T,  $q \ell \approx 0.091$ , which gives  $|I_{0,1}|^2 \approx 0.004$  and  $|I_{1,2}|^2 \approx 0.008$ , when the overlap integral  $I_{n,m}$  is evaluated<sup>6</sup> for finite  $q$ . These are a bit small, but the right order of magnitude to explain our measured cross sections. We note that  $\ell$  becomes larger at lower fields, which helps to explain why our cross sections are larger at small fields, in spite of the fact that many electrons hide in the lower Landau levels, unavailable

<sup>(a)</sup> Bell Laboratories, Holmdel, NJ  
<sup>(b)</sup> Physics Department, Northeastern Univ., Boston, MA  
<sup>(c)</sup> National Magnet Laboratory, MIT, Cambridge, MA  
<sup>(d)</sup> Present Address: Clarendon Laboratory, Oxford Univ., Oxford, England  
<sup>(e)</sup> Physics Department, MIT, Cambridge, MA  
<sup>(f)</sup> Bell Laboratories, Murray Hill, NJ

for promotion, and hence do not participate in CR scattering.

Now we turn our attention to the second half of our paper. MWM samples have long been studied by luminescence, and the literature is far too vast to be reviewed here. Our contribution is to subject these samples to sizable magnetic fields. Our motivation was to study electron structure at extremely high fields and low temperatures in the hope of contributing to the understanding of the quantum Hall effect. As we shall see, we are still some distance from this goal, but we believe we can show already some interesting phenomena.

Figure 1a shows spectra of one MWM sample, with a rather high electron concentration  $n_e = 6 \cdot 10^{11}$  electrons/cm<sup>2</sup> in each quantum well of thickness 20 Å. The incident illumination is 30 milliwatts of 5145 Å laser light (0.15 watts/cm<sup>2</sup>), linearly polarized, and the crystal is held at 2K. This is the same MWM sample analyzed by Pinczuk, et al., at this conference.<sup>7</sup>

The zero field spectrum displays roughly the shape we would expect from the built-in electrons recombining with photo-excited holes: a low energy onset somewhere near the bandgap  $E_g$  and an exponential thermal tail beyond the energy  $E_g + E_F$ . Analysis of the high energy tail gives us an electron temperature of  $\sim 35K$ .

In the presence of a magnetic field, the electron continuum breaks into Landau levels, and we see peaks in our recombination spectrum (a textbook example) corresponding to transitions from electron Landau levels  $n = 0, 1, 2, \dots$  to some valence band states, occupied according to Boltzmann statistics, by the photo-injected holes. We note also that the luminescent efficiency increases, and that the broadening is reduced as field is increased. The zero field MWM value of 3 meV reduces to 0.7 meV - 0.8 meV at the extreme field of 15T shown in Figure 1b. At 15T, for this sample only one Landau level is occupied, though both spin components are present. The spectra are now circularly polarized and the single (0-0) transition has split into two components.

Figure 2 shows how the first few spectral peaks develop with H. Roughly, but very roughly, they increase in energy as  $(n + \frac{1}{2})\hbar\omega_c$  where  $(\omega_c/H \approx 1.7\text{meV/Tesla})$  is the cyclotron frequency for an electron in GaAs, and  $n$  is the Landau level index. If the valence band were uncomplicated, and if the electrons' energies were not affected by exchange, we would expect the recombination peaks to have a common zero field origin at  $E_g + E_{\text{confinement}}$  and then to increase as  $(n + \frac{1}{2})(\hbar\omega_c + \hbar\omega_v)$  with  $\omega_v$  the hole cyclotron frequency. The only measurement of cyclotron resonance in two-dimensionally confined holes<sup>8</sup> gives a hole mass on the order of  $0.4 m_e$ , implying  $\omega_v \approx 1/6 \omega_c$ . The expected slopes of the transitions shown would be, in units of  $\hbar\omega_c$ : 0.58, 1.74, 2.90, and 4.06. In contrast, the measured slopes are 1.07, 2.10, 3.27, and 4.20. Beyond a few Tesla the slopes do decrease to more respectable values, and eventually the single lines split into two polarized components.

The following factors will be important in analyzing our spectra.

1) Electron exchange energy must change with field. Indeed oscillations in exchange energy on the order of several meV are expected as the Fermi level passes through Landau levels.<sup>9</sup> 2) The valence band is, in fact, four-fold degenerate, and two effects are fighting for dominance in breaking this degeneracy: a) confinement in the quantum wells, which gives hole level spacings on the order of a few meV; and b) the magnetic field, which alone gives the complicated but well honored energies derived by Luttinger.<sup>10</sup> We believe that at high magnetic fields, the holes will finally simplify and follow Luttinger. An indication that this happens is that the luminescence becomes split and circularly polarized. When the hole states are finally understood, it will be possible to use the recombination energy to study simply the electronic behavior in high magnetic fields.

Acknowledgments: We thank P. A. Wolff, A. Pinczuk, and J. Shah for helpful discussions; and L. Rubin and the staff of the National Magnet Laboratory for cooperation and hospitality. The National Magnet Laboratory is supported by the National Science Foundation. This work was also supported in part by the Office of Naval Research, under contract N-00014-81-K-651, and the National Science Foundation, under grant.

# References

- (1) A. C. Gossard, in: Thin Films: Preparation and Properties, K. N. Tu and R. Rosenberg, eds. Academic Press (1981).
- (2) J. M. Worlock, A. Pinczuk, Z. J. Tien, C. H. Perry, H. L. Störmer, R. Dingle, A. C. Gossard, W. Wiegmann, and R. L. Aggarwal, *Solid State Commun.* **40**, (1981) 867, and Z. J. Tien, Ph.D. Thesis, Northeastern Univ. (1981).
- (3) J. M. Worlock, A. C. Maciel, C. H. Perry, Z. J. Tien, R. L. Aggarwal, A. C. Gossard and W. Wiegmann, in: Application of High Magnetic Fields in Semiconductor Physics, C. Landwehr, editor, Springer-Verlag (1983) p. 186.
- (4) A. C. Maciel, J. M. Worlock, C. H. Perry, R. L. Aggarwal, A. C. Gossard, and W. Wiegmann, *Bull. A.P.S.* **28**, (1983) 448, and to be published.
- (5) M. Cardona, M. H. Grimsditch, and D. Olego, in: Light Scattering in Solids, J. L. Birman, H. Z. Cumming and K. K. Rebane, editors, Plenum Press (1979) p. 249.
- (6) J. M. Worlock, *Solid State Commun.* to be published.
- (7) A. Pinczuk, J. Shah, H. L. Störmer, R. C. Miller, A. C. Gossard, and W. Wiegmann, this conference.
- (8) H. L. Störmer, A. Chang, Z. Schlesinger, D. C. Tsui, A. C. Gossard, and W. Wiegmann, *Phys. Rev. Letters* **51**, (1983) 000.
- (9) Th. Englert, D. C. Tsui, A. C. Gossard, and Ch. Uthlein, *Surface Science* **113**, (1983) 295.
- (10) J. M. Luttinger, *Phys. Rev.* **102**, (1956) 1030.

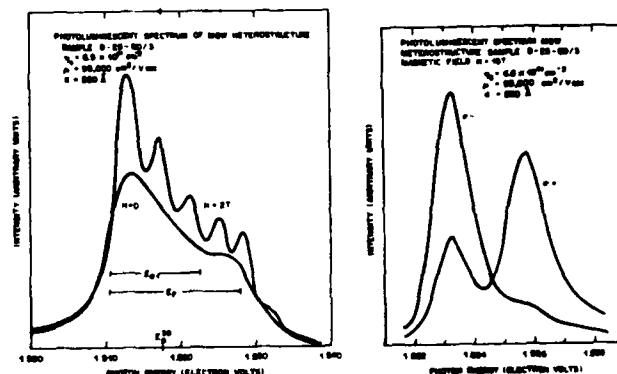
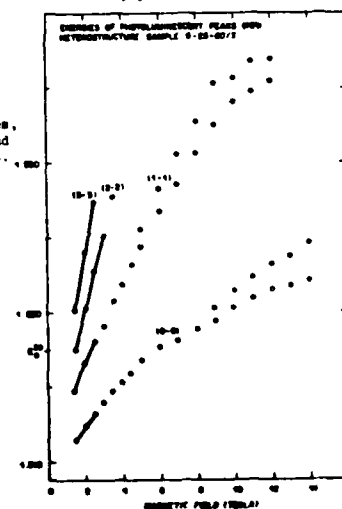


Figure 1: Photoluminescent spectra of 2D electrons in MQW heterostructure. a) The electron continuum (H=0) breaks into Landau levels (H=2T) with increase in luminescent efficiency. b) At the highest fields (15T) luminescence has two narrow circularly polarized components.

Figure 2: Energies of photoluminescent peaks versus magnetic field showing large initial slopes, curvature toward lower slopes, and splitting into polarized doublets.



# INVESTIGATION OF OPTICAL PROCESSES IN A SEMICONDUCTOR 2D ELECTRON PLASMA

A. Pinezuk and Jasdeep Shah  
Bell Laboratories, Holmdel, NJ 07733  
R. L. Stenger, E. C. Miller, A. C. Gossard and W. Wegmann  
Bell Laboratories, Murray Hill, NJ 07974

We have studied intrinsic optical emission and excitation processes associated with 2D plasmas in modulation-doped GaAs - (AlGa)As quantum-well heterostructures. The emission spectra indicate considerable energy gap renormalizations, assigned to many-body interactions, and large breakdown of the parity selection rule for the optical matrix element in quantum-wells. In spite of the high electron density, in excitation spectra we find evidence of final-state electron-hole interactions.

In this communication we report an investigation of optical processes across the energy gaps of modulation-doped (1), GaAs - (AlGa)As quantum-well heterostructures. In emission and in luminescence excitation spectra we have identified the intrinsic recombination and absorption processes associated with electrons confined in the GaAs quantum wells. Our research reveals remarkable behavior of 2D plasmas in semiconductors that has not been reported in previous studies of free electrons in semiconductor heterostructures (2,3) and doping superlattices (4).

We find that emission spectra are dominated by intrinsic recombination processes involving vertical transitions between electrons in the conduction band and photoexcited holes in the valence band states. The spectral shapes can be fitted in terms of 2D densities of states and the equilibrium occupation factors for electrons and holes. The energy gaps determined by this analysis show relatively large renormalizations, comparable to the Hartree energies. These findings indicate that many-body phenomena in these 2D electron systems may be more important than those calculated at higher densities (5).

Unexpected behavior is observed in emission and excitation spectra. In the luminescence excitation spectra we observe structure that suggest final-state electron-hole interactions in the optical absorption processes. This occurs in spite of the fact that the screening lengths of plasmas in our samples are

only  $\sim 50\text{\AA}$ . In emission spectra we find evidence of a large breakdown of the parity selection rule for the optical matrix element.

The measurements were carried out in three GaAs - (Al<sub>x</sub>Ga<sub>1-x</sub>)As multiple quantum-well heterostructures, grown by molecular beam epitaxy and modulation doped with Si donors (1). The sample parameters are given in Fig. 1.  $d_1$  is the thickness of the GaAs wells,  $d_2$  that of the doped (Al<sub>x</sub>Ga<sub>1-x</sub>)As larger and  $d_3$  that of the undoped (Al<sub>x</sub>Ga<sub>1-x</sub>)As spacer introduced to enhance the electron mobility (6). Characterization of the 2D plasmas in these samples was carried out by Hall effect, Shubnikov-de Haas oscillations (1) and inelastic light scattering (7) measurements. Substantial occupation of the two lowest conduction subbands is observed in samples 9-25-80(2) and 9-25-80(3). In sample 8-4-81(3) light scattering spectra indicate that occupation of a second subband is much smaller (below  $0.3 \times 10^{11} \text{cm}^{-2}$ ). Luminescence was excited by means of an LD-700 dye laser, continuously tunable between 6850Å and 8250Å. Incident power densities were about  $5 \times 10^{-3} \text{W/cm}^2$ . All measurements were carried out with the samples immersed in superfluid He. Figure 1 shows luminescence spectra from the three samples. The major structures occur between 8100Å and 8250Å. The weaker emission observed at longer wavelengths is associated with impurities and will not be considered here. In the assignment of the emission between 8100Å and 8250Å we focus on the fact that spectra from samples 9-25-80(2) and 9-25-80(3) show well defined doublet structures. These are the samples in which there is substantial occupation of two conduction subbands. This characteristic behavior indicates that emission originates in recombination processes that are associated with the electron plasmas confined in the GaAs quantum-wells. This assignment also explains the separations between the two components of the doublets. They are  $\sim 13 \text{ meV}$  apart, an energy that is close to the spacing between the lowest subbands determined from Shubnikov-de Haas and light scattering measurements.

Optical absorption processes were studied by means of luminescence excitation spectra. In addition to a step-like onset of absorption, these spectra show structure in the form of maxima and minima with a relative amplitude that can be as large as  $\sim 15\%$ . These observations point to final-state interactions in the absorption processes. However, the effects are here much smaller than the excitons observed in undoped quantum-wells (3,8). They are also found to broaden with increasing temperature, and are not observable for temperatures above  $\sim 50^\circ \text{K}$ .

we observe characteristic separations between emission and excitation spectra. Figure 2 compares the spectra measured in sample 9-25-80(3). The energy difference between the maximum in the emission spectrum and the onset of absorption, indicated as  $E_{\text{ABS}}$  in the excitation spectrum, has been represented as

$$E_F(1+m_e/m_h) \quad (1)$$

where  $E_F$  is the Fermi energy of the 2D plasma. For the conduction band effective mass we have used  $m_e = 0.068 m_0$  (9). Quantitative agreement with the separation shown in Fig. 2 is obtained with  $m_h = 0.42 m_0$ . This value is close to the hole mass determined in p-type, modulation-doped, GaAs - (AlGa)As heterostructures (10).

All these behaviors are characteristic of absorption and emission processes across the forbidden energy gap. Thus, we have fitted the emission spectra with the lineshape function

$$I(\hbar\omega) = A \int_0^\infty p(E) g_e(E) g_h(E) \delta(E - \hbar\omega) dE \quad (2)$$

where  $\omega$  is the emitted photon energy and  $E$  represents the transition energies.  $g_e$ ,  $g_h$  is the Fermi function for the electrons.  $F_h(E)$  is the Boltzman factor for the photoexcited holes. Electrons and holes are assumed to be at the same temperature  $T$ .  $p(E)$  is the 2D density of states. We have assumed parabolic bands and taken  $p(E)$  as a step function at the energy gap  $E_G$ . This is a good approximation since the valence bands are known to be highly non-parabolic. Homogeneous broadening is considered in  $\delta(E - \hbar\omega)$  by means of a damping parameter  $\Gamma_h$  (in higher mobility samples  $\Gamma_h \leq 1$  meV). Inhomogeneous broadening is included in  $p(E)$ .  $A$  is a constant factor, adjustable in the numerical analysis.

We find that Eq. (2) gives excellent fits to the measured emission spectra. Figure 2 shows the results obtained in sample 9-25-80(3). Two terms are required, one for each of the occupied conduction subbands. They are the dashed curves in Figure 2. The full line is the total fit. The adjusted value of the energy gap and the separation between the two terms are indicated in the figure. An inhomogeneous broadening of  $\Gamma_h = 1.5$  meV is used in order to fit the low energy tail of the spectra. We find that the carrier temperature also needs to be considered as an adjustable parameter. This is

not surprising, since illumination at very low power levels can induce significant heating of carriers in semiconductors (11). The adjusted value of  $T$  depends on  $m_e$  and  $m_h$ . For  $m_e = 0.068 m_0$  and  $m_h = 0.42 m_0$  we obtain  $T = 6^\circ\text{K}$ . It is remarkable that the adjusted value of  $E_G = 1.5095$  eV is lower than the energy gap of intrinsic bulk GaAs ( $E_G = 1.518$  eV) (12). We have estimated  $E_G$  within the Hartree approximation using the conduction energy levels calculated by Fishman (13) and valence band energy levels obtained in a parabolic-well approximation. We found  $E_G = 1.528$  eV, a value that indicates a renormalization of the energy gap, assigned to many-body interactions, of  $\sim 25$  meV. This renormalization is comparable to the Hartree energy ( $\sim 30$  meV). It indicates that in our density range ( $n \sim 5 \times 10^{11} \text{ cm}^{-2}$ ) many-body effects are significant for the 2D plasmas confined in GaAs quantum wells. At higher densities the Hartree energies are expected to become more important (5).

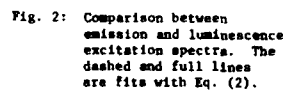
The emission band shown in Fig. 2 at an energy  $E_{01} = 13$  meV above the major band is assigned to recombination transitions from first excited conduction subband to ground valence subband states. The assignment is based on the fact that  $E_{01}$  is very close to the conduction subband spacings determined by light scattering and Shubnikov-de Haas oscillations ( $E_{01} \sim 11.5$ –13 meV). This emission violates the parity selection rule for the optical matrix element in quantum-wells (14). Breakdown of the parity selection rule has been previously observed in luminescence from photoexcited plasmas (3) and in light scattering spectra (7). Our results show that the effect is unexpectedly large. The ratio between parity forbidden and parity allowed matrix elements determined from the data in Fig. 2 is 0.5.

In summary, the investigation of optical processes reveals fundamental behavior of 2D plasmas confined in GaAs quantum-wells. We have observed phenomena like energy gap renormalization, final state interactions and large breakdown in the parity selection rule for the optical matrix in quantum-wells. We anticipate that these results will stimulate interest in optical studies of 2D plasma behavior in semiconductor heterostructures.

**Acknowledgements:** We thank P. A. Wolff for numerous discussions. G. D. Amiller and K. Baldwin provided technical assistance.

## 446

- 447



# CYCLOTRON RESONANCE OF TWO-DIMENSIONAL ELECTRONS

## IN $\text{Al}_{1-x}\text{Ga}_x\text{As}/\text{GaAs}$ HETEROJUNCTION

K. Muro, S. Mori and S. Marita

Department of Material Physics, Faculty of Engineering Science  
Osaka University, Toyonaka, Osaka 560, Japan

S. Miyamizu and K. Nanbu

Fujitsu Laboratories Ltd., Ono, Atsugi, Kanagawa 243-01, Japan

Peculiar behaviours of two-dimensional electron gas in the cyclotron resonance have been studied using a high mobility FET of  $\text{Al}_{1-x}\text{Ga}_x\text{As}/\text{GaAs}$  heterojunction. The results are fairly well explained by the calculated results based on the theoretical model assuming the long-range scatterers scheme by Ando. However, we find remaining discrepancies between the experimental and the calculated results which have possibility to be ascribed to some electron-electron correlation effects in the system.

## 1. Introduction

Cyclotron resonance (CR) experiments [1] so far performed on Si-MOS inversion layer have revealed some specific properties of two-dimensional (2D) electron system, especially in the quantum limit. These results have been discussed in a variety of theoretical models: trapped electron model, pinned charge density wave model and so on. However, the correspondence between the experimental results and the theoretical ones have been not necessarily made clear. On the other hand, we have extended the CR study to a new 2D system,  $\text{Al}_{1-x}\text{Ga}_x\text{As}/\text{GaAs}$  heterojunction FET [2,3]. Though the characteristics of CR in the quantum limit resemble those in Si-MOS inversion layer in such aspects as the high energy shift of resonance peaks, and their temperature-dependence [3], there are some differences between the two systems.

In the present work, detailed CR spectra of the 2D heterojunction electrons are measured over wide ranges of electron density, magnetic field and temperature, and the results are discussed in comparison with the calculation, according to the model presented by Ando [4].

The samples and the experimental setup used were almost the same as those described in previous reports [2,3]. However, in the first study [2] the too high-frequency gate voltage modulation ( $\sim 1\text{kHz}$ ) brought some erroneous results, and in the second study [3] under static gate voltages, unfavourable baseline shift and additional structure appeared in the spectra. Therefore, in the present experiment, the gate voltage modulation technique with slow repetition rate ( $\sim 130\text{Hz}$ ) was adopted and the transmission signals after a sufficient delay time ( $3\sim 4\text{ msec.}$ ) were picked up, in order to obtain good fidelity and improved S/N ratio.

## 2. Results and Discussion

Typical CR spectra for 118.8 and 170.6  $\mu\text{m}$  laser lines observed at 4.2K are shown in Fig.1 for various electron densities,  $n_s$ , or filling factors,  $\nu = (n_s/2 \times 10^{12})$ , where  $\ell = (r\hbar/eH)^{1/2}$ , (the cyclotron radius). The peak frequency shifts,  $\omega_c - \omega_b$ , from the bulk CR frequency,  $\omega_b$ , (which corresponds to the bulk mass;  $m_b = 0.0675m_0$ ), and the linewidths are shown against the filling factor,  $\nu$ , in Fig.2.

On the other hand, Landau level width,  $\Gamma_n$ , and CR width,  $\Gamma_n^*$ , calculated theoretically by Ando and Uemura [5], and Prasad and Fujita [6], assuming a scattering potential with a gaussian form;  $V(r) = V_0 \exp(-r^2/d^2)$ , are shown in Fig.3 as a function of parameter  $\alpha$ . Here,  $\alpha = (d/\ell)$  is the normalized range of scattering potential by the cyclotron radius  $\ell$ . The theory about the CR lineshape presented by Ando [4] shows that CR under the long-ranged scattering potential ( $\alpha \geq 1$ ) can be described as an inhomogeneously broadened system, and gives the CR linewidths with a similar  $\alpha$ -dependence to those by Prasad and Fujita, though the former does not show the explicit form. In a long-ranged scatterer schemes ( $\alpha \geq 1$ ), the CR linewidth  $\Gamma_n^*$  depends on the Landau quantum number,  $n$ , that is; on the filling factor  $\nu$ , and decreases with increasing magnetic field.

By comparing the resonance field- and filling factor- dependences of the

CR linewidth (shown in Fig.2) with the theoretical ones, we derived the range of scattering potential to be  $150 \sim 200 \text{ \AA}$ . These long-ranged scattering potential can be reasonably ascribed to the ionized donors in Si-doped AlGaAs layer beyond the undoped AlGaAs interlayer with a thickness of  $60 \text{ \AA}$ , if we take into account the wavefunction thickness of the 2D electron,  $\sim 100 \text{ \AA}$ , and the average distance of donors in the doped AlGaAs layer,  $\sim 100 \text{ \AA}$ .

The CR lineshape is numerically calculated according to the equation (1,12) in ref.[4] for the dynamical conductivity  $\sigma_{xx}(\omega)$ . The lineshapes of partially occupied lowest Landau level for  $\nu=2$  calculated are shown in Fig.4(a), assuming that  $d \sim 200 \text{ \AA}$  and  $l \sim 100 \text{ \AA}$  which corresponds to the spectra at  $118.8 \text{ \mu m}$  in Fig.1. Although observed spectra are obtained against magnetic field, we can interpret the magnetic field axis as a frequency axis, but reversing the direction, because the CR linewidth is sufficiently narrow in the present experiments.

The calculated spectra have a bell-shape due to the elliptic density of states in self-consistent Born approximation [5], which is in contrast with the nearly Lorentzian lineshape of the observed spectra. However, the vaning of the spectra from high field (low frequency) side and the subsequent peak shift with decreasing filling factor in the experiment are deduced in the theoretical frame work by Ando [4].

As seen in Fig.1 and Fig.2, the vaning of the CR spectra (peak shift to higher frequency) occurs even in the region  $\nu > 1$ , and this tendency becomes prominent with decreasing magnetic field. This effect is qualitatively understood by taking into account the incomplete spin splitting of the broadened Landau levels. Figure 4(b) shows the calculated spectra for  $\nu < 2$ , where the spin splitting,  $\Delta$  is equal to one half of the ground Landau level width,  $\Gamma_0$ . In the present experimental condition ( $\alpha \sim 1.5 \sim 2$ ), the ground Landau level width  $\Gamma_0$  is estimated to be  $7 \sim 9 \text{ cm}^{-1}$  and scarcely depends on the magnetic field, and therefore the present CR lineshape profiles with changing the

filling factor is consistent with the enhanced effective g-value;  $\sim 5$  (e.g.  $g \sim 14$  at  $6 \text{ Tesla}$ ) reported as an experimental result [7].

Figures 5(a) and (b) show the observed temperature dependence of the CR spectra for  $118.8 \text{ \mu m}$  laser-incidence at  $\nu \sim 0.64$  and the corresponding theoretical lineshape calculated assuming  $\alpha=2$ , respectively. The spreading out of the CR spectra to higher field from the spectra at  $4.2 \text{ K}$  with increasing temperature is considered to be caused by the thermal distribution within the inhomogeneous broadened Landau level in the above theoretical model. However, the experimental peak shift seems to be much larger than the theoretically expectation.

In the above descriptions, we have examined the characteristics of the observed CR spectra, in the light of the theoretical model by Ando [4] under the long ranged scatterers scheme, and known that some aspects can be understood successfully.

However, we find following remaining discrepancies between the experimental and theoretical results; 1) observed CR lineshapes are rather Lorentzian in contrast with the bell-shape in the theory, 2) a part of the spectra at  $\nu < 1$  protrudes out to lower field from the full spectra at  $\nu=1$ , being inconsistent with the theory [4] and this tendency becomes prominent in high magnetic fields and at lower temperatures, 3) the temperature shift of the CR spectral peak at  $\nu < 1$  is much larger than that expected from the thermal distribution in the lowest Landau level.

The problem 1) may be improved to employ a more realistic density of states than the elliptic one in the theory. While, 2) and 3) seem to be difficult to be understood in the framework of one electron theory, and are possibly ascribed to some many body effects (the screening [8] or the correlation effects [9,10] in the 2D-electron system) or other origins.

Englert et al. [11] have observed the oscillation of CR linewidth as a function of filling factor  $\nu$  and ascribed it to the screening effects [8].



In the present experiment, we have not observed such an oscillation, as seen in Fig.2, and the discrepancies (2), and (3) cannot be explained by introducing the screening effects as described by Das Sarma [8].

Though the observed discrepancies (2) and (3) seem to have the character associated with the pinned charge density wave model [10], the whole feature of the present results cannot be, as described previously [3], explained by the model. In order to solve the above mentioned problems of 2D electron system, further detailed CR experiments with high mobility samples in high magnetic fields are strongly requested.

#### References

- [1] B.A. Wilson, S.J. Allen, Jr. and D.C. Tsui, Phys. Rev. B24 (1981) 5987.
- [2] K. Muro, S. Narita, S. Hiyaizumi, K. Nanbu and H. Hashimoto, Surface Sci. 113 (1982) 321.
- [3] S. Narita, K. Muro, S. Mori, S. Hiyaizumi and K. Nanbu, Proc. Intern. Conf. Appl. High Magnetic Field to Semicond. Phys. (Grenoble, 1982) p.194.
- [4] T. Ando, J. Phys. Soc. Japan 38 (1975) 989.
- [5] T. Ando, Y. Temura, J. Phys. Soc. Japan 36 (1974) 959.
- [6] M. Prasad and S. Fujita, Physica 91A (1978) 1.
- [7] Th. Englert, D.C. Tsui, A. Gossard and Ch. Uihlein, Surface Sci. 113 (1982) 295.
- [8] S. Das Sarma, Solid State Commun. 36 (1980) 357.
- [9] H. Fukuyama, P.M. Platzman and P.W. Anderson, Phys. Rev. B19 (1979) 5211.
- [10] H. Fukuyama, and P.A. Lee, Phys. Rev. B18 (1978) 6245.
- [11] Th. Englert, J.C. Maan, Ch. Uihlein, D.C. Tsui and A.C. Gossard, Proc. Intern. Conf. Phys. Semicond. (Montpellier, 1982) p.631.

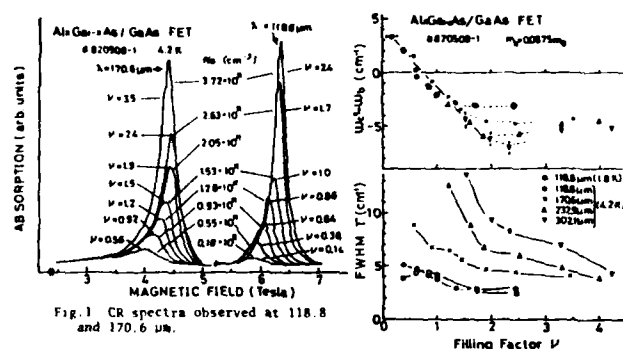


Fig.1 CR spectra observed at 118.8 and 170.6 μm.

Fig.2 CR frequency shift and linewidth versus  $\nu$ .

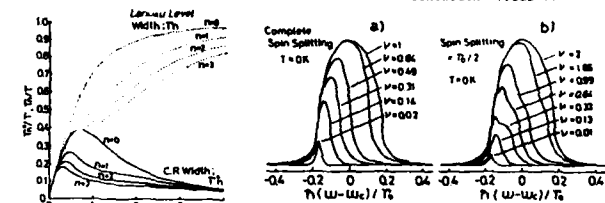


Fig.3 Theoretical Landau level width  $\Gamma_n$  and CR linewidth  $\Gamma$  as a function of  $\alpha$ .

Fig.4 CR lineshapes for different  $\nu$ , calculated with the theory by Ando [4] assuming  $\alpha=2$  and  $T=0K$ . a)  $\Delta \geq 2\Gamma_0$  b)  $\Delta = \Gamma_0/2$ .

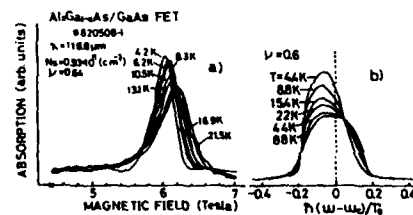


Fig.5 Temperature dependence of (a) CR lineshapes for  $\nu=0.64$  observed at 118.8 μm and (b) theoretical ones calculated for  $\alpha=2$ ,  $\Delta \geq 2\Gamma_0$ .

# SURFACE CYCLOTRON RESONANCE IN A STRONG $B_{||}$

Wen-qin Zhao, C. Mazurek, and F. Koch  
Physik-Department, Technische Universität München  
D-85346 Garching, Fed. Rep. of Germany

and

J. Ziegler and H. Maier  
Telefunken Electronic, 7100 Heilbronn, Fed. Rep. of Germany

## Abstract

We discuss the cyclotron resonance of carriers in a surface accumulation layer on  $Hg_{1-x}Cd_xTe$  for a magnetic field in the sample plane.

## Introduction

Cyclotron resonance (CR) of volume carriers in a semiconductor can be observed in either a  $B_{\perp}$  (Faraday)- or  $B_{||}$  (Voigt)-configuration, the latter in the extraordinary mode with current  $j \perp$  to  $B_{||}$ . If the experimental energy  $\hbar\omega$  is much greater than the plasma energy  $\hbar\omega_p$ , the two resonances are quite similar. For finite  $\omega_p/\omega$  there is expected a plasma-shift in the Voigt configuration according to the relation  $\omega = \sqrt{\omega_c^2 + \omega_p^2}$ .

Electrons in a 2-dimensional surface layer are usually studied with  $B_{\perp}$ . For the case of a strong  $B_{||}$  and a finite width of the surface charge layer, however, there is also possible a CR-like excitation of the surface layer in an extraordinary-mode Voigt-geometry. The criterion for the existence of this mode is roughly that the cyclotron radius is smaller than the charge-layer width. Next to volume carrier CR and  $B_{\perp}$ -surface CR, the  $B_{||}$ -mode in a surface layer is a "CR-experience of the third kind". In the work of surface layers on  $PbTe$ <sup>[1]</sup> such  $B_{||}$ -surface CR was first observed. More recently it has been studied for  $InSb$  surface layers<sup>[2]</sup> and for  $InAs$ <sup>[3]</sup>.

## Basic Ideas

It suffices to give a qualitative description of the subband levels in a strong  $B_{||}$ , and to contrast the  $B_{||}$ -surface CR from what has in earlier work been described as subband-resonance shifted by a  $B_{||}^{3/4}$ .

In the absence of  $B_{||}$  the surface layer electrons occupy a system of subband levels in an approximately triangular potential-well as in Fig. 1a. Most carriers occupy the  $n = 0$  groundstate with the minimal binding length  $z_0$ . For a  $B_{||}$  without a surface electric field  $E_{\perp}$  the situation is shown in part b. Except for electron orbits whose center coordinate is less than the cyclotron radius away from the surface the energy is independent of this coordinate. For Fig. 1a the 2 degrees of freedom of motion parallel to the surface give a constant density of states for each electric subband, which is filled to some appropriate  $E_F$  in the surface layer. In the case of 1b there is the one-dimensional density of states associated with the parallel momentum  $k_{||}$ . Fig. 1c is an approximate description of the spectrum of states in the crossed  $E_{\perp}$  and  $B_{||}$ -fields, assuming a relatively weak  $E_{\perp}$  and neglecting screening in the surface layer. The  $n = 0$  groundstate electrons are spread most deeply into the semiconductor. The density of these states is one-dimensional.

The physical picture that we suggest for the experimental observations of the  $B_{||}$  surface-CR on  $Hg_{1-x}Cd_xTe$  is one, where for typical fields  $B_{||}$  most surface electrons occupy magnetic-like states on the  $z = 0, 1, \dots$  etc. straight lines. Such carriers move on spiral paths within the width of the surface charge layer. The latter must be several times greater than the quantum limit orbit diameter (256 Å in 1 T). The density of electrons in the layer is graded, decreasing with the number of states available with increasing depth  $z$ . To the extent that electronic states are predominantly determined by the  $B_{||}$ -field, the selection rule for their excitation is expected to be cyclotron-resonance-like. Resonance should be observable in a surface rf field perpendicular to  $B_{||}$ . By contrast, the  $B_{||}$ -shifted subband resonance in ref. [3] was observed in an

rf electric field polarized perpendicular to the surface. For the strongly non-parabolic conduction band states of  $\text{Hg}_{1-x}\text{Cd}_x\text{Te}$ , we expect that the effective mass of the  $B_y$ -resonance is an indicator of the energy of the electronic state in the band.

#### Experimental Results and Discussion

To illustrate the  $B_y$ -surface CR we give here a number of results obtained with n-type  $\text{Hg}_{1-x}\text{Cd}_x\text{Te}$  ( $n \sim 1.5 \times 10^{15} \text{ cm}^{-3}$ ,  $x \sim 0.2$ ) that are intended to show the characteristics of the effect. A more detailed description will follow.

##### a) Three Cyclotron Resonances

Fig. 2 shows the conventional volume CR in the uppermost curve. It is observed in the extraordinary Voigt geometry under conditions for which  $\omega_p \ll \omega$ . The evaluation of the line width gives an  $\omega\tau \sim 24$ . The line position is that of the quantum limit  $0^+ \rightarrow 1^+$  transition for an  $x \sim 0.206$ . The volume resonance is followed by the  $B_y$ -surface resonance for  $N_s = 7 \times 10^{11} \text{ cm}^{-2}$ , recorded as a change in transmission with on-off modulation of the surface layer. The resonance is observed for a plane-parallel slab ( $d \sim 10 \mu\text{m}$ ) and the lineshape is certainly affected by standing-wave interference. It is a relatively sharp line dominated by resonance contributions at the position of the volume resonance. It is evident that these can only be transitions of the  $0 \rightarrow 1$  type in Fig. 1c. The dominant part must come from the  $k_y = 0$  states. Transitions at finite  $k_y$  and between the other levels are expected to contribute to the absorption on the high field side. A complete lineshape interpretation requires knowledge of the exact spectrum of the states in Fig. 1c including spin-orbit splitting, nonparabolicity, etc. The  $B_y$ -resonance originates from a layer in which the 3-d density is of order  $10^{17} \text{ cm}^{-3}$  and  $\hbar\omega_p \approx 10 \text{ meV}$ . From the subband resonance with perpendicular excitation we know to expect a sizeable plasma-shift. There is no comparable effect on the  $B_y$ -surface CR. The very last trace in Fig. 2 is the previously reported  $B_z$ -surface CR<sup>1/5/</sup>. In addition to a contribution from volume carriers near 2.4 T, this resonance is dominated by the two cyclotron transitions from the surface subbands  $n = 0$  and 1 as labelled. Their mass

values are strongly  $N_s$ -dependent and they reflect the subband binding energy and occupancy.

##### b) $N_s$ -Dependence of $B_y$ -Surface CR

The  $B_y$ -resonance amplitude and lineshape depend on the  $N_s$  of the surface layer. The peak position is largely independent of  $N_s$ . Particularly for low excitation energy  $\hbar\omega$  (and consequently low  $B_y$ ) there are structures on the resonance that change with  $N_s$ . Fig. 3 is an example of such curves for  $\hbar\omega = 10.5 \text{ meV}$ . The linewidth tends to increase with rising  $N_s$ . The linewidth and lineshape changes indicate varying contributions from states other than  $z = 0$  and  $k_y = 0$  in Fig. 1c. Because the  $B_y$ -field is quite small for 10.5 meV, the states are expected to be more subband-like. The limit  $B_y \rightarrow 0$  is, of course, the normal  $N_s$ -dependent subband resonance. With  $B_y$  small, the resonance is expected to shift with  $N_s$  according to the perturbation-theory ideas discussed in ref. /3/.

##### c) Amplitudes of the $B_y$ -Resonance

There is an unusual and marked dependence of the resonance amplitude on  $N_s$ , different for each of the frequencies  $\hbar\omega$ . Typical signal strengths are a few percent of the transmitted intensity. Fig. 4 shows that the signal grows linearly with  $N_s$  only at the lowest  $\hbar\omega$ . At the highest  $\hbar\omega$  the resonance signal is much smaller and nearly constant in amplitude. Because of the plane-parallel slab geometry, standing-wave effects make difficult a comparison between the frequencies, but the  $N_s$ -dependences for given  $\hbar\omega$  are quite distinct. In constructing Fig. 4 the maximum height of the resonance has been plotted. With the lineshape changes as in previous Fig. 3, this procedure is not necessarily an appropriate description of signal strength.

##### d) Frequency Dependence: Polaron Effects?

In studying the  $B_y$ -CR at different  $\hbar\omega$ , we have searched for evidence of resonant polaron effects. The VCR signal in Fig. 2 shows the distinct lowering of  $m_c^*$  at 17.6 meV by  $\sim 8\%$  as reported in ref. /5/. The SCR in  $B_z$  fails to show a comparable effect. The  $B_y$ -resonance shifts by a small amount, if judged

solely by peak position. It remains to give a proper description of the line-shape in order to identify uniquely a resonant polaron effect in  $B_{||}$ -surface CR.

#### Conclusions

The  $B_{||}$ -surface CR is yet another and distinctly different resonance mode of the surface layer. It may roughly be treated as free carrier resonance in a slab with density of order  $10^{17} \text{ e/cm}^3$ . Nevertheless, the unusual lineshape and amplitude effects will require a more detailed analysis for a proper description. An outstanding question that needs to be addressed is why there is apparently no plasma-shift of the resonance in the high-density surface layer. We recall that the subband excitation in perpendicular excitation is considerably shifted by such plasma effects<sup>16</sup>.

#### References

- 1) H. Schaber and R.E. Doezema, Phys. Rev. B 20, 5257 (1979)
- 2) J.H. Crasemann, U. Merkt, and J.P. Kotthaus, Phys. Rev. submitted for publication
- 3) J.C. Mean, Application of High Magnetic Fields in Semiconductor Physics, Proceedings, Lecture Notes in Physics, Vol. 177, p. 163 (Springer, 1983)
- 4) W. Beinvogl, A. Kamgar, and F. Koch, Phys. Rev. B 14, 4274 (1976)
- 5) J. Scholz, F. Koch, J. Ziegler, and H. Maier, Sol. State Commun. 45, 665 (1983)
- 6) J. Scholz, F. Koch, J. Ziegler, and H. Maier, Sol. State Commun. 45, 39 (1983)

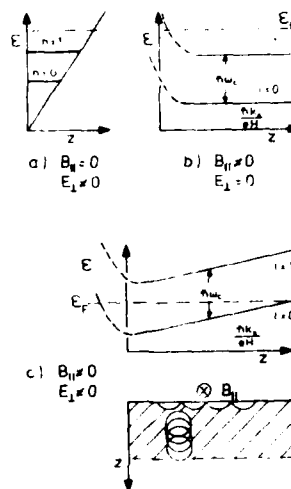
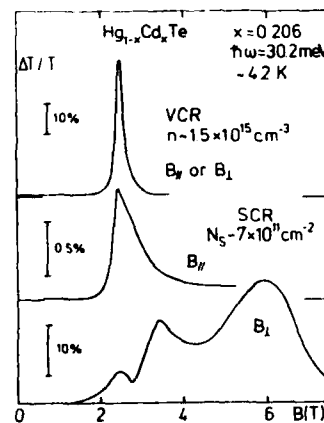


Fig. 1:

Quantized electronic states in various configurations of the surface electric field  $E_L$  and the magnetic field  $B_{||}$ . In 1c are drawn the cyclotron-like orbits in the surface charge layer that correspond to transitions  $z = 0$  to  $z = 1$ .

Fig. 2:

Cyclotron resonances from bulk carriers (VCR) and surface carriers (SCR) in  $\text{Hg}_{1-x}\text{Cd}_x\text{Te}$ . The sample thickness is  $\sim 10 \mu\text{m}$ , so that the number of volume carriers is twice  $N_s$ .



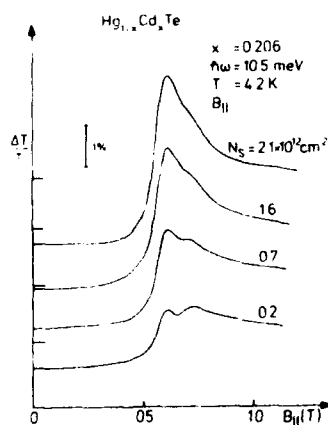


Fig. 3: The B -surface CR at various densities  $N_s$ .

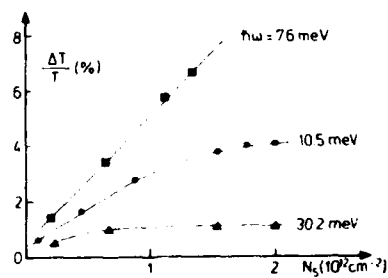


Fig. 4: Resonance amplitude vs.  $N_s$  for different frequencies.

# SUBBANDS IN BACK-GATED HETEROJUNCTIONS

B. Vinter

Division Composants Microonde,

THOMSON-CSF, Domaine de Corbeville,

R.P. 10, F-91401 Orsay, France

The subband structure at low temperature of an  $\text{Al}_x\text{Ga}_{1-x}\text{As}/\text{GaAs}$  heterojunction in which the density is modulated by a gate on the GaAs substrate has been calculated with full account of tunnelling between the two sides of the junction. The results show that when the first excited subband is occupied, the number of electrons in the lowest subband remains essentially constant independent of back-gate voltage, in agreement with a recent experiment. Comparison of the calculated density at which the first excited subband starts being occupied with the experiment indicates that the doping impurities behave quite differently in AlGaAs than in GaAs, even for an Al concentration of 0.22.

## 1. Introduction

Impurities like Si which produce shallow donor levels in GaAs are known to behave differently in  $\text{Al}_x\text{Ga}_{1-x}\text{As}$ . Thus, at an Al concentration  $x$  of 0.2, Hall effect measurements (1-4) show a binding energy of more than 50 meV. In accordance with this finding, calculations on electronic properties of AlGaAs/GaAs heterojunctions have assumed that electrons in the AlGaAs are frozen out (5,6), so that the Fermi level (7) and the two-dimensional subbands on the GaAs side lie well below the bottom of the conduction band in the GaAs.

However, for Al mole fractions below about 0.25, the binding energy is

found (1-3) to be just as small as in GaAs, and one would not expect such difference from the hydrogenic-like behaviour of shallow donors. In this case freeze-out should not occur in doped samples and the electrons in the AlGaAs should be free. In accordance with these considerations we have performed calculations on heterojunctions in which all donors are taken to be ionized and all conduction electrons free, also on the AlGaAs side of the junction. Furthermore we have taken into account the (usually very small) thickness of the AlGaAs layer which quantizes the motion of the electrons in the AlGaAs perpendicular to the heterojunction interface. Consequently the potential for the electrons in the junction forms the familiar case of a double well with the conduction band discontinuity giving rise to the barrier between the two wells.

For the actual calculations we have employed a fairly standard Hartree approximation in which we neglect the differences in permittivity and in effective mass of electrons in AlGaAs and GaAs. The effective mass Schrödinger equation and Poisson's equation are solved self-consistently to calculate the subband energies, wave-functions, the total electronic charge and its distribution in the heterojunction. Compared with other similar Hartree calculations the main difference is that we do not fix the electronic charge in the channel from the start but calculate it as a function of the conduction band energies on the boundaries. At the surface of AlGaAs there is a barrier of approximately 0.33 eV (7) and in the GaAs substrate away from the channel the potential is determined by the back-gate potential and/or the doping of the substrate. Rather than trying to model this potential in the substrate, we have assumed a certain boundary value of the conduction band energy at a point far away from the junction but close enough that effects of non-intentional doping of the substrate can be neglected. The effect of a change in back-gate voltage is then to alter the boundary value. Details of the calculation can be found in (8).

## 2. Results and discussion

In Fig. 1 we show some characteristic results. The  $\text{Al}_{0.6}\text{Ga}_{0.4}\text{As}$  layer is 60 nm thick and highly doped,  $N_D = 2 \times 10^{18} \text{ cm}^{-3}$ , so that one would expect strong degeneracy in the bulk. The conduction band discontinuity is taken to be  $\Delta E_c = 0.22 \text{ eV}$  and the boundary condition in the substrate is taken to be  $V = V_0 = 0.4 \text{ eV}$  in the plane 180 nm from the  $\text{AlGaAs/GaAs}$  interface. The Fermi level  $E_F = 0$ . The total number of electrons in the system is found to be  $N = 9.45 \times 10^{12} \text{ cm}^{-2}$  but most are in the  $\text{AlGaAs}$  layer:  $N_{\text{AlGaAs}} = 6.90 \times 10^{12} \text{ cm}^{-2}$ . Many subbands are occupied but inspection of the subband wavefunctions shows that in most cases a subband can be considered belonging to either the  $\text{AlGaAs}$  potential well or the  $\text{GaAs}$  well, since the wave-function has its probability almost exclusively in one well. Thus, two occupied subbands  $E_0$  and  $E_1$  can be identified as subbands in the  $\text{GaAs}$  channel with electrons of high mobility, whereas the others are in the  $\text{AlGaAs}$  with low mobility. We have calculated the wave-functions and charge distributions for several doping levels and several thicknesses of undoped  $\text{AlGaAs}$  spacer layers, and these results serve as input for the calculation of mobilities presented in another paper at this conference (9).

If we now change the back-gate voltage, i.e. we alter the energy of the conduction band in the substrate, the subband energies change as shown in Fig. 2. We find the expected double-well behaviour: the subbands belonging to the  $\text{AlGaAs}$  stay almost constant, whereas the  $\text{GaAs}$  levels increase with increasing back-gate potential, and because the barrier is very narrow in this high-doping case, the subbands repel each other where they would otherwise have crossed. Most interesting, however, is the observation that as long as the first excited subband  $E_1$  belonging to  $\text{GaAs}$  is occupied, the ground subband energy  $E_0$  and occupation remain almost constant. This agrees with the experiment of Störmer et al. (10) and shows that even though the number of electrons in the channel increases, i.e. for decreasing  $V_0$ , the separation  $E_1 - E_0$  decreases, when the electrons are induced by the back-gate.

The density for onset of occupation of the first excited subband is found to be  $N_{\text{th}} = 1.5 \times 10^{12} \text{ cm}^{-2}$ , which is considerably higher than the  $8.7 \times 10^{11} \text{ cm}^{-2}$  observed experimentally. As argued in (8) it is difficult to account for this discrepancy simply by allowing for fairly large inaccuracies of the sample parameters, so based on comparison with this single experiment one would have to conclude that the donors are not simply shallow when the doping is high, even for a low Al mole fraction for which other experiments give no indication of unusual behaviour (1-3). A more systematic study is called for, but certainly the double-well behaviour described here should be realizable by a suitable choice of sample parameters.

## References

- (1) T. Ishikawa, J. Saito, S. Sasa, and S. Miyazawa, *Jap. J. Appl. Phys.* 21 (1982) 1675.
- (2) D. H. Collins, D. F. Mars, R. Fischer, and C. Kocot, *J. Appl. Phys.* 54 (1983) 857.
- (3) J. J. Yang, L. A. Moudy, and M. I. Simpson, *Appl. Phys. Lett.* 40 (1982) 244.
- (4) K. Hess, M. Morkoc, M. Shichijo, and B. G. Streetman, *Appl. Phys. Lett.* 35 (1979) 469.
- (5) T. Ando, *J. Phys. Soc. Japan* 51 (1982) 3893, *ibid.* 51 (1982) 3900.
- (6) P. J. Price and F. Stern (to be published in *Surf. Sci.*)
- (7) D. Delagebeaudeuf, M. Lavirotte, P. Delescluse, Pham N. Tung, J. Chaplart, and Nguyen T. Linh, *Electron. Lett.* 18 (1982) 103.
- (8) B. Vinter, *Solid State Commun.* (to be published).
- (9) Nguyen T. Thang, R. Fishman, and B. Vinter (this conference).
- (10) H. L. Störmer, A. F. Gossett, and M. Wiegmann, *Solid State Commun.* 41 (1982) 707.

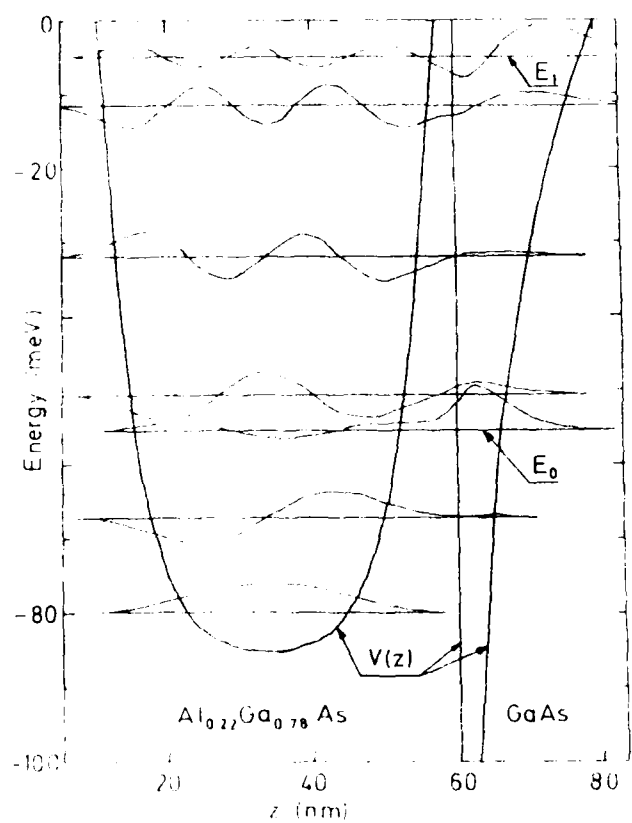


Fig. 1: Self-consistent potential  $V(z)$ , energy levels, and wave-functions for a potential of  $V_0 = 1.4$  eV at  $z_0 = 240$  nm. The Fermi level is at 0, and two subbands belonging to the channel  $E_0$  and  $E_1$  are occupied.

465

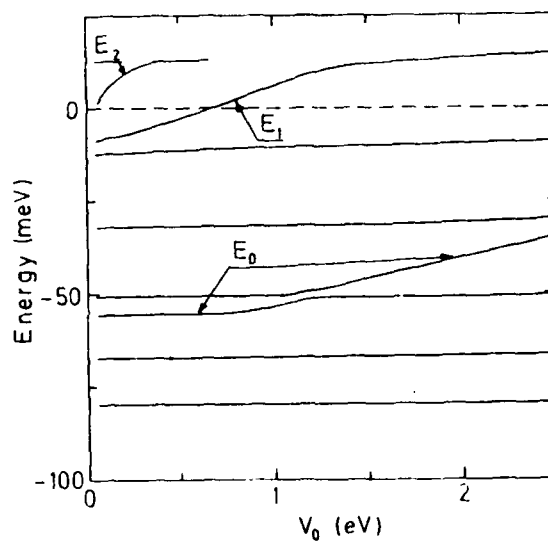


Fig. 2: Subband energy levels as a function of potential energy  $V_0$  at  $z_0 = 240$  nm. Three subbands belonging to the channel  $E_0$ ,  $E_1$ ,  $E_2$  are indicated.

466



# PLASMON AND INTERSUBBAND MODES OF A SUPERLATTICE - CLASSICAL VERSUS QUANTUM LIMITS

By

W. L. Bloss  
GTE Laboratories  
Waltham, MA 02254

The collective plasmon oscillations of a semiconductor superlattice in the quantum limit are calculated including subband structure. For finite well dimensions, superlattice plasmons with dispersion relation similar to the results of previous theories are found. We also predict the existence of a new collective mode involving charge depolarization associated with intersubband transitions that can propagate along the superlattice axis. These collective plasmon oscillations are also investigated in the classical limit where the electron de Broglie wavelength is smaller than the well dimension. Here the symmetric and antisymmetric slab modes associated with a metallic layer are shown to couple into bands when arranged in a superlattice. The bands along the superlattice axis formed from these slab modes in the classical limit are shown to correspond to the superlattice plasmon and intersubband superlattice plasmon modes in the quantum limit. Results for the interaction of light with the superlattice plasmons will also be presented.

## I. Introduction and Results

Recent advancements in the field of molecular beam epitaxy (MBE) have made it possible to grow semiconductor superlattices with extremely sharp, high quality interfaces with dimensions ranging from tens to hundreds of Angstroms (1). Doped or modulated doped GaAs-GaAlAs structures form a superlattice of electron (or hole) layers because of the band gap discontinuities between the conduction and valence bands. In recent publications, ourselves (2) and others (3) have investigated the collective plasmon modes of such a superlattice complex in the limit that the confining well width is less than the electron de Broglie wavelength so that quantization effects are important and barrier widths large enough so that electron wave function overlap is negligible. In this limit, the electron gas in the layers is confined in the subband levels in the direction along the superlattice axis, but is free electron like in the x, y directions.

Each layer independently behaves as a 2-D electron gas. P. Stern (4) has shown that such a 2-D electron gas is capable of supporting plasmon oscillations with dispersion quite different from the bulk,  $\omega_p^{2D} = \left( \frac{2\pi n e^2}{m} \right)^{1/2}$ . It has been shown that the 2-D plasmons of each layer when arranged in a superlattice can couple via the long-range Coulomb force to give rise to a band of Bloch-like plasmon oscillations along the superlattice axis (the so-called superlattice plasmons). (5)

Our approach consists of diagonalizing the dielectric matrix for a system consisting of a periodic array of electron (or hole) layers interacting Coulombically. In the limit, that the well width of the electron gas layers approaches zero, we obtain the dispersion relation (5) for the superlattice plasmon modes

$$\omega = \omega_p^{2D} \left[ \frac{1 - e^{-2qd}}{1 - 2e^{-qd} \cos kd + e^{-2qd}} \right]^{1/2} \quad (1)$$

where  $\omega_p^{2D}$  is the 2-D plasmon, d is the superlattice periodicity, k is the wavevector component along the superlattice axis and q is the perpendicular component (parallel to the layers). We note that for qd and kd  $\rightarrow 0$ , this reduces to the usual plasmon dispersion for an anisotropic system,  $\omega = \omega_p \cos \theta$ , where  $\theta$  is the angle the wavevector makes with the layer and  $\omega_p$  is an effective 3-D plasmon,  $\omega_p^2 = \frac{4\pi n e^2}{m d}$ ; n being a 2-D density. Recent experimental verification of the acoustic behaviour ( $\omega \sim q$ , for kd fixed and qd  $\rightarrow 0$ ) of these plasmon modes has been obtained by Olego, et. al. (6) via light scattering. In fact, in their experiment the well separation was about 1000Å, indicating that the long range Coulomb interaction is still extremely important even at very large distances.

Our formalism, via the dielectric matrix defined on site and subband indices, allows for the inclusion of subband effects. In particular, we have shown that the well-known charge depolarization shift of an intersubband excitation (in a single 2-D layer system) will also couple Coulombically when arranged in a superlattice. We state here our result for the dispersion of these intersubband modes since it

will be needed later.

$$\omega^2 = \epsilon_{10}^2 + \frac{4\pi e^2 \epsilon_{10} k_{10}}{c} \left[ 1 - \frac{q^2 \epsilon_{10}^2}{k_{10}^2} \left( \frac{1 - e^{-2qd}}{1 - 2e^{-qd} \cosh kd + e^{-2qd}} \right) \right] \quad (2)$$

where  $\epsilon_{10} = \epsilon_1 - \epsilon_0$ ,  $\epsilon_{10}$  is a dipole matrix element, and  $k_{10}$  is a Coulomb matrix element (7). Other effects such as coupling to LO-phonons (2), magnetic field (2), and diatomic-like superlattices (8) (electron-hole or dual density superlattices) giving rise to optic and acoustic-like modes have also been considered. Here, we extend our calculations to the classical limit where layer widths are large compared to the de Broglie wavelength and can be treated as metallic-like slabs.

A metal-semiconductor interface is capable of supporting surface plasmon modes if one medium has a positive dielectric constant and the other a negative dielectric constant. These surface modes are propagating along the interface but decay exponentially away from the interface. A metal slab supports surface plasmons at each interface and these surface plasmons interact to produce symmetric and antisymmetric surface plasmon modes. Our model consists of a superlattice of such slabs with a periodicity  $l$ , layer widths  $a$  and  $b$ , and dielectric constants  $\epsilon_a(\omega)$  and  $\epsilon_b(\omega)$ , respectively, which are taken to be the 3-D dielectric constants of the isotropic, homogeneous medium with no spatial dispersion (see Fig. 1). We show that the symmetric and antisymmetric surface plasmon modes of a single layer (slab) couple into corresponding symmetric and antisymmetric plasmon bands when arranged in a superlattice.

Our theory proceeds parallel to previous theories for the collective oscillations of the coupled surface plasmon modes of a finite layer media except here we extend the calculation to a periodic array of metallic-like layers. In what follows, the dielectric constants for the two media are specialized to be  $\epsilon_a(\omega) = \epsilon_a$  and  $\epsilon_b(\omega) = \epsilon_b \left( 1 - \frac{\omega_p^2}{\omega^2} \right)$ ; that is, alternating semiconductor and metallic-like layers. After applying the boundary conditions, continuity of  $E_x$  and  $D_x$  and periodicity, we find the following equation describing the coupled surface plasmon bands.

$$\cos kl = \alpha^+ \beta^+ \cosh [(K_a - K_b)a + K_b l] + \alpha^- \beta^- \cosh [(K_a + K_b)a - K_b l] \quad (3)$$

where  $\alpha^{\pm}$  and  $\beta^{\pm}$  are defined as

$$\alpha^{\pm} = 1/2 \left( 1 \pm \frac{\epsilon_b(\omega) K_a}{\epsilon_a(\omega) K_b} \right) \quad \beta^{\pm} = 1/2 \left( 1 \pm \frac{\epsilon_a(\omega) K_b}{\epsilon_b(\omega) K_a} \right) \quad (4)$$

and  $K_{a,b}^2 = q^2 - \frac{\omega^2}{c^2} \epsilon_{a,b}(\omega)$ , appropriate for interface modes. We consider now the non-retarded limit ( $qc \gg \omega$ ) and from eqn. (3) find for the dispersion relation for the coupled surface plasmon modes

$$\omega_{\pm}^2 = \frac{\omega_p^2}{2} \left\{ \frac{(\epsilon_a - \epsilon_b) \pm \epsilon_a \sqrt{n^2 - n^2}}{2\epsilon_a \epsilon_b - (\epsilon_a^2 + \epsilon_b^2)n} \right\} \quad (5)$$

where  $n = \sinh qa \sinh qb$  and  $n = \cosh k - \cosh qa \cosh qb$ . Here, the  $+$ ( $-$ ) branch corresponds to the coupling of the symmetric (antisymmetric) surface plasmon modes of a single slab into a band along the superlattice axis. In Fig. (2), we plot eqn. (5) along the superlattice axis for  $qa = 0.5$  and  $qb = 0.5$ . We note that for  $qa \rightarrow \infty$  (slabs widely separated), eqn. (5) reduces to

$$\omega_{\pm}^2 = \frac{\omega_p^2}{2} (1 \pm a^{-qb}) \quad (6)$$

the symmetric and antisymmetric modes of a single slab. We now consider the plasmon dispersion as the metallic slab layer width goes to zero ( $qb \rightarrow 0$ ). In this limit, one finds for the collective plasmon modes,

$$\omega_{\pm}^2 = \frac{\omega_p^2}{2} \left\{ 1 \pm \left( 1 + \frac{qb \sinh qa}{\cosh k - \cosh qa} \right) \right\} \quad (7)$$

The symmetric (+) branch is identical to the previous result for the superlattice plasmon eqn. (1). If one defines an effective plasmon frequency  $\omega_{p,eff}^2 = \frac{4\pi e^2 N_{10}^2}{\epsilon}$  and an effective length as  $b_{eff} = \frac{2\epsilon_{10}^2}{k_{10}}$ , it follows that the antisymmetric (-) branch of eqn. (7) is identical to the intersubband plasmon mode of eqn. (2) to within a factor that is a quantization energy. This is physically correct since the superlattice plasmon mode sets up a charge distribution along the layer and maps onto the charge density of the symmetric mode in the  $b \rightarrow 0$  limit, whereas the intersubband excitation has an induced charge density normal to the plane of the layer and maps onto the antisymmetric mode.

We have also investigated the interaction of the superlattice plasmon eqn. (1) with light (the retarded limit). One solves Maxwell's equations including the

response of the 2-D layered superlattice. Alternatively, the result can also be derived from the  $b \rightarrow 0$  limit of the classical result eqn. (3). Details will be presented elsewhere. The dispersion relation for the coupled superlattice plasmon polarization mode for  $|\vec{k}| \rightarrow 0$  and  $K^2 = q^2 + k^2$  is found to be

$$\omega^2 = \frac{1}{2} \left[ \frac{c^2 k^2}{\epsilon} + \omega_p^2 \pm \sqrt{\left[ \frac{c^2 k^2}{\epsilon} + \omega_p^2 \right]^2 - \frac{4c^2 \omega_p^2 k^2 \cos^2 \theta}{\epsilon}} \right] \quad (8)$$

where  $\theta$  is the angle  $\vec{k}$  makes with the electron layers. For  $\theta = 90^\circ$ , that is wavevector along the superlattice, we find  $\omega^2 = \frac{c^2 k^2}{\epsilon} + \omega_p^2$ . For  $\theta = 0^\circ$ , the modes are uncoupled.

#### References

1. A. Y. Cho and J. R. Arthur, *Prog. Solid State Chem.* **10**, 157 (1975).
2. L. L. Chang and L. Esaki, *Prog. Cryst. Growth Char.* **2**, 3 (1979).
3. W. L. Bloss and E. M. Brody, *Solid St. Comm.* **43**, 523 (1982).
4. S. Das Sarma and I. J. Quinn, *Phys. Rev.* **B25**, 7603 (1982).
5. F. Stern, *Phys. Rev. Lett.* **18**, 546 (1967).
6. A. L. Fetter, *Ann. Phys.* **88**, 1 (1974).
7. D. Olego, A. Pinzuk, A. C. Gossard, and W. Wiegman, *Phys. Rev.* **B25**, 7867 (1982).
8. W. L. Bloss, *Solid St. Comm.* **46**, 143 (1983).
9. W. L. Bloss, *Solid St. Comm.* **44**, 363 (1983).

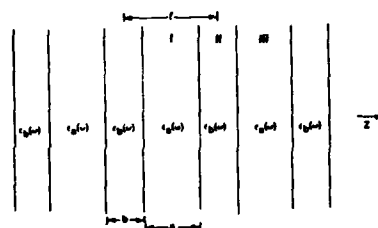
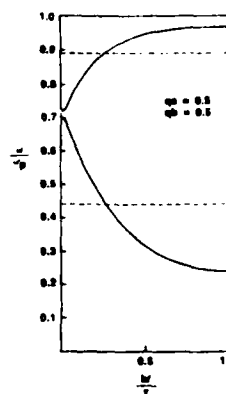


Figure 1: A superlattice composed of layers arranged periodically with dielectric constants  $\epsilon_a(\omega)$  and  $\epsilon_b(\omega)$ , widths  $a$  and  $b$ , and periodicity  $t$ .

Figure 2: Plot of the plasmon dispersion relation along the superlattice axis eqn. (5) for the coupled surface plasmon modes for  $qa=0.5$  and  $qb=0.5$ . The top (bottom) band corresponds to the antisymmetric (symmetric) modes of oscillation. The dotted lines are the single slab symmetric and antisymmetric modes. The formation into bands is evident.



# THEORY OF RESONANT POLARONS IN NARROW GAP SEMICONDUCTORS

R. Lassnig and W. Zawadzki  
Institut für Experimentalphysik  
Universität Innsbruck  
AUSTRIA

Resonant magneto-polarons are calculated for two-dimensional electron systems in narrow gap semiconductors, using a variational model for the electronic band structure. The results are compared with recent experimental findings, indicating that the resonant polaron interaction between adjacent Landau levels is not reduced by many-body effects.

## INTRODUCTION

Since the discovery of resonant polarons in the magneto-absorption of InSb (1) the electron-optic phonon interaction in polar semiconductors has become subject of extensive studies. In strong magnetic fields the peak structure of the electronic density of states leads to pronounced resonance phenomena. Recently Horst et al. (2) reported the first observation of resonant polaron pinning in two-dimensional (2D) systems, performing two-level cyclotron resonance (CR) experiments on InSb inversion layers.

The aim of the present paper is to describe theoretically resonant magneto-polarons in 2D electron systems including nonparabolicity effects. At first we develop a variational model for the 2D energy levels in narrow gap semiconductors. Assuming discrete Landau levels, the polaron interaction is then included applying Wigner-Brillouin perturbation theory. This approach is adequate, if one is mainly interested in the position of the polaron energy levels, and if the width of the involved Landau levels is not too large. The inclusion of finite level widths in the calculation of the magnetoabsorption, which has been carried out by Das Sarma and Madhukar (3) for parabolic bands, is straightforward.

The calculations are performed for InSb inversion layers and discussed in relation with the experimental data of ref. (2).

## THEORY

We use a two-level k-p band model for a narrow gap semiconductor in which the s-like  $\Gamma_6$  conduction level is separated by the energy gap  $E_g$  from the p-like  $\Gamma_8$  level. The slowly varying potential within the inversion layer

$U(z)$  is taken in the Hartree approximation. We fix the magnetic field  $H$  in the  $z$ -direction. The resulting 4x4 matrix equation is solved by substitution (4). Describing the motion parallel to the interface by harmonic oscillator wave functions the resulting equation for the first component of the  $z$ -dependent envelope function becomes

$$\left\{ c_n - \frac{\hbar^2}{2m_0} \frac{d^2}{dz^2} - \frac{1}{c_g + c - U} \frac{\hbar^2}{2m_0} \frac{dU}{dz} \frac{d}{dz} + \frac{1}{c_g} (c - U)(c_g + c - U) \right\} |\varphi_r\rangle = 0 \quad (1)$$

$$c_n = \hbar\omega_c(n + \frac{1}{2}) + \frac{1}{2} |g_0^s| \mu_B H, \quad r, n = 0, 1, 2, \dots \quad (2)$$

$$U(z) = \frac{e}{\kappa_0} (N_d z + \sum_r N_r (z - z_r^0) \rho_r(z^0) dz^0) \quad (3)$$

$m_0^s$  and  $g_0^s$  denote the effective mass and spin splitting factor at the band edge and  $\omega_c = eH/m_0^s c$ .  $\kappa_0$  is the static dielectric constant of the semiconductor and  $N_d$  is the depletion charge. The indices  $r$  and  $n$  characterize electric and magnetic subbands, respectively, and  $N_r$  and  $\rho_r(z)$  stand for the absolute population and the normalized charge density in the electric subband  $r$  (we set  $N_{inv} = \sum N_r$ ). Multiplying Eq. (1) from the left side with  $\langle \varphi_r |$  and integrating one obtains easily a quadratic equation for the energies:

$$c = -c_g/2 + \langle U \rangle_r + \frac{c_g}{2} \sqrt{1 + 4(\langle T \rangle_r + c_n)/c_g - 4\delta^2/c_g^2} \quad (4)$$

$$\delta^2 = \langle (U - \langle U \rangle_r)^2 \rangle_r + \frac{\hbar^2}{2m_0^s} \langle \frac{c_g}{c_g + c - U} \cdot \frac{dU}{dz} \frac{d}{dz} \rangle \quad (5)$$

The factor  $\delta^2/c_g^2$  is very small and therefore neglected in the following. The brackets  $\langle T \rangle_r$  and  $\langle U \rangle_r$  signify the expectation values of the kinetic and potential energy in  $z$ -direction, respectively. For brevity only expressions for the zeroth electric subband are given, using the well-known Stern-Howard variational wave functions:

$$\varphi_0 = \sqrt{b^3/2} z e^{-bz/2} \quad (6)$$

If only the lowest electric subband is occupied, the calculation is particularly simple, leading to (5)

$$\langle T \rangle = \frac{\hbar^2 b^2}{8m_0^s}, \quad \langle U \rangle = \frac{3e^2}{\kappa_0 b} (N_d + \frac{11}{32} N_{inv}) \quad (7)$$

Inserting  $\langle T \rangle$  and  $\langle U \rangle$  in Eq. (4) and minimizing the energy  $c(b)$  with respect to  $b$  gives a third order equation for  $b^2$ , which can be solved analytically:

$$b^* = (\sqrt{q^2 + p^2} + \sqrt{q^2 - p^2}) \cdot b_0^* \quad (8a)$$

$$b_0^* = 12m_0^* e' (N_d + \frac{11}{32} n_{inv}) / \kappa_0 \hbar^2 \quad (8b)$$

$$p = \frac{\hbar^2 b_0^*}{6m_0^* \epsilon_g}, \quad q = (1 + \frac{4\epsilon_n}{\epsilon_g})/2 \quad (8c)$$

In the case of weak nonparabolicity, such as in GaAs-AlGaAs heterostructures, the factor  $b$  can be well approximated by the parabolic value  $b_0$ .

If higher electric subbands are occupied, the calculation becomes somewhat more tedious, especially since the populations  $N_p$  are not fixed. Comparing our model with calculations of Takada et al. (6) using the same material parameters we have found that the results are very close for the zeroth and the first electric subband.

As has been demonstrated by Lax (7) for the three-dimensional case, the phonon interaction  $V_{ph}$  is included in the nonparabolicity equations in the following way:

$$\epsilon = -\frac{\epsilon_g}{2} + \langle U \rangle + \frac{\epsilon_g}{2} \sqrt{1 + 4(\langle T \rangle + \epsilon_u + V_{ph})/\epsilon_g} \quad (9)$$

Since the Fröhlich interaction is small relative to the subband energies, Eq.(9) can be expanded to:

$$\epsilon = -\frac{\epsilon_g}{2} + \langle V \rangle + \frac{\epsilon_g}{2} \sqrt{1 + \frac{4}{\epsilon_g} (\langle T \rangle + \epsilon_u)} + \frac{V_{ph}}{\sqrt{1 + 4(\langle T \rangle + \epsilon_u)/\epsilon_g}} \quad (10)$$

We consider only the interaction between a level characterized by  $n$  with his adjacent level  $(n-1)$  and neglect interface phonon effects. Starting from the unperturbed energies  $\epsilon_n$  and  $\epsilon_{n-1}$ , Wigner-Brillouin perturbation theory gives for the energy shift  $\Delta\epsilon_n$  of the level  $n$ :

$$\Delta\epsilon_n = \sum_q \frac{|M_{fi}(q)|^2}{\Delta\epsilon_n + \epsilon_n - \epsilon_{n-1} - \hbar\omega_L} \cdot \frac{1}{\sqrt{1 + 4(\langle T \rangle + \epsilon_u)/\epsilon_g}} \quad (11)$$

$$|M_{fi}|^2 = \frac{1}{q^2} |\rho_r(q_z)|^2 \cdot \frac{\hbar}{n} e^{-a} \left[ \frac{dL_n(a)}{da} \right]^2 \quad (12)$$

$$V_q^* = \frac{1}{2q^2} \cdot \left( \frac{1}{\kappa_u} - \frac{1}{\kappa_0} \right) \frac{e^2 \hbar \omega_L}{V} \quad (13)$$

where  $a = q_1^2 l^2 / 2$ ,  $l = (\hbar c / eH)$  and the functions  $L_n(a)$  are Laguerre polynomials.  $\rho_r(q_z)$  denotes the Fourier transform of the charge density  $\rho_r(z)$ .

As usual, the denominator in Eq.(11) becomes resonant for  $\epsilon_n = \epsilon_{n-1} + \hbar\omega_L$ , when the energy separation of the two levels is equal to the LO phonon energy  $\hbar\omega_L$ . The energy denominator is momentum independent, and the

$q_z$ -summation can be performed analytically:

$$\Delta\epsilon_n = \frac{C_0 I_n(\sqrt{2}/1b)}{\Delta\epsilon_n + \epsilon_n - \epsilon_{n-1} - \hbar\omega_L} \quad (14)$$

$$I_n(x) = \frac{2}{\sqrt{\pi n}} \int_0^\infty d\alpha \sqrt{\alpha} e^{-\alpha} \left[ \frac{dL_n(\alpha)}{d\alpha} \right]^2 \frac{(1 + \frac{9}{8} \sqrt{\alpha} x + \frac{3}{8} \alpha x^2)}{(1 + \sqrt{\alpha} x)^2} \quad (15)$$

$$C_0 = \frac{e^2 \hbar \omega_L}{8\sqrt{2\pi}} \left( \frac{1}{\kappa_u} - \frac{1}{\kappa_0} \right) \frac{1}{\sqrt{1 + 4(\langle T \rangle + \epsilon_u)/\epsilon_g}} \quad (16)$$

Evaluating the last integral Eq.(15) numerically, a simple quadratic equation for  $\Delta\epsilon_n$  is obtained, the two solutions representing the upper and lower polaron branch. The result is expressed in terms of the energy separation  $\hbar\omega_L$  of the splitted level  $n$  from the unperturbed level  $(n-1)$ , which corresponds to the measurable CR energy:

$$\hbar\omega_L = \frac{1}{2} [(\epsilon_n - \epsilon_{n-1} + \hbar\omega_L \pm \sqrt{(\epsilon_n - \epsilon_{n-1} - \hbar\omega_L)^2 + 4C_0^2 I_n(\sqrt{2}/1b)})] \quad (17)$$

The effective mass  $m^*$  is as usual defined as  $m^* = m_0^* \omega_c / \omega_L$ .

## RESULTS AND DISCUSSION

In the theoretical part we have demonstrated that a simplification of the nonparabolicity and polaron model is possible without loosing much accuracy. The kinetic terms  $\langle T \rangle$ ,  $\epsilon_u$  and  $V_{ph}$  appear together under the square root in Eq.(9). The expansion Eq.(10) shows that the polaron interaction is decreased relative to the parabolic case.

The calculations have been performed assuming that the electric subband occupation numbers are not altered at high magnetic fields. Although this assumption appears unrealistic, the description of the detailed Landau level filling at high densities is too complex and does not give much more information. The material parameters are taken to  $\kappa_0 = 17.9$ ,  $\kappa_u = 15.7$ ,  $m_0^* = 0.0135$  and  $|g_0^*| = 51$ .

Fig.1 shows the experimental data (2) for the zeroth subband compared with two versions of the theory. The dashed lines indicate the calculation corresponding to the measured density of  $N_{inv} = 2 \cdot 10^{11} / \text{cm}^2$ . In this case more than one Landau level is filled at lower magnetic fields and the theoretical mass does not increase apart from the polaron resonance, as it is the energy-dependent mass at the Fermi energy. It can be seen, however, that

the observed mass does increase with the magnetic field. Therefore the solid lines show a calculation using a lower density,  $N_{inv}=10^{11}/cm^2$ , for which practically over the whole considered regime only the lowest Landau level is occupied. The agreement with the experiment is much better and the resonant polaron anomaly is described excellently.

Fig.2 shows the comparison between the experiment (2) and the theory for a higher charge density, at which two electric subbands are occupied. The calculation is performed for  $N_{inv}=6 \cdot 10^{11}/cm^2$ , which is again lower than the experimentally determined density ( $N_{inv}=1.1 \cdot 10^{12}/cm^2$ ). Also at this density several Landau levels are occupied and the resulting effective masses are almost independent of the magnetic field, apart from the resonant anomaly. It can be seen that for the first electric subband the agreement between the theory and the experiment is quite convincing. For the zeroth electric subband the agreement is somewhat worse and it is not quite clear, why the experimentally measured mass value increases so strongly with the magnetic field below the resonance. Concerning the polaron effect, a good agreement is obtained if the theoretical curve is somewhat shifted down.

In the present work we have not included the influence of occupation number and screening effects on the polaron interaction. However the experimental data are quantitatively well described, indicating that many-body effects do not reduce the resonant polaron interaction between adjacent Landau levels at the Fermi energy.

#### ACKNOWLEDGEMENTS

This work was partially sponsored by the Fonds zur Förderung der Wissenschaftlichen Forschung, Austria, Projekt Nr. S 22/05. The authors wish to thank Prof. Gornik for stimulating discussions.

#### REFERENCES

- (1) D.H.Dickey, E.J.Johnson, D.M.Larsen; Phys.Rev.Lett.18 (1967) 599.
- (2) M.Horst, U.Merkt, J.P.Kotthaus; Phys.Rev.Lett.50 (1983) 754.
- (3) S.Das Sarma, A.Madhukar; Phys.Rev.B 22, 6 (1980) 2823.
- (4) M.Zawadzki; J.Phys.C: Solid State Physics 16 (1983) 229.
- (5) T.Ando, A.B.Fowler, F.Stern; Rev.Mod.Phys.54, 2 (1982) 466.
- (6) Y.Takada, K.Arai, Y.Uemura; Physics of Narrow Gap Semicond., Linz, Austria 1981, p.101; edited by E.Gornik, H.Heinrich, L.Palmethofer.
- (7) B.Lax; in "Polarons in Ionic Crystals and Polar Semicond.", edited by J.T.Devreese, p.756, Antwerpen 1972.

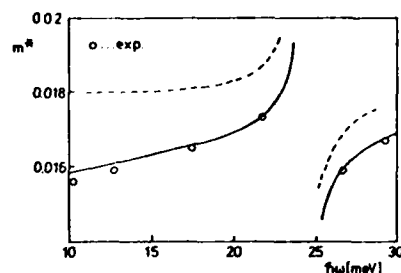


Fig.1: Cyclotron resonance effective mass as a function of the transition energy  $h\nu$ , calculated for  $N_{inv}=2 \cdot 10^{11}/cm^2$  (dashed lines) and  $N_{inv}=10^{11}/cm^2$  (full lines) and compared with the experimental data of ref.(2).

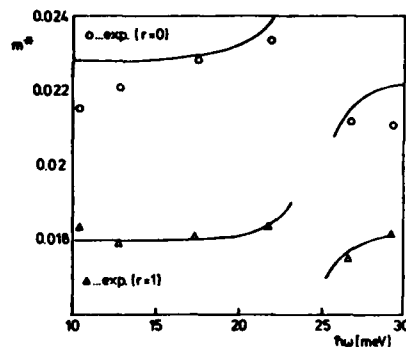


Fig.2: Cyclotron resonance effective mass for two electric subbands as a function of the transition energy  $h\nu$ , for  $N_{inv}=6 \cdot 10^{11}/cm^2$  and compared with the experimental data of ref.(2). The upper curves correspond to the zeroth electric subband and the lower to transitions in the first electric subband.

# Intrasubband Plasma Modes of a Semi-Infinite Superlattice:

## A New Type of Surface Wave.\*

Gabriele F. Giuliani,<sup>†</sup> Guoqi Qin,<sup>‡</sup> and J. J. Quinn

Brown University, Providence, Rhode Island 02912, USA

Dispersion relations are derived for the bulk and surface plasma modes of a model semi-infinite superlattice. The model consists of a periodic array of two-dimensional electron layers embedded in a material of dielectric constant  $\epsilon_0$ , terminating at the interface with a homogeneous medium of dielectric constant  $\epsilon_1$ . The bulk modes form a continuum, and the surface mode, which exists only for wavelengths shorter than a critical value, can occur either above or below the bulk continuum depending on the ratio of  $\epsilon_1$  to  $\epsilon_0$ .

The simplest model<sup>1</sup> of a superlattice which can correctly describe the bulk and surface intrasubband plasma modes consists of a semi-infinite array of two-dimensional electron gas layers located at  $z = la$ , where  $l = 0, 1, 2, \dots$ . These layers are embedded in a medium of background dielectric constant  $\epsilon_0$ , and the space  $z < 0$  is occupied by an insulator of dielectric constant  $\epsilon_1$ . In this model the miniband structure of the superlattice is ignored; only the ground subband and the intrasubband collective modes are considered.

The most straightforward way<sup>2</sup> to obtain the electromagnetic modes of the system is to write down the general solution of the wave equation in each region and to impose standard boundary conditions. For a p-polarized wave the solution in the  $l$ th layer can be written

$$E(y, z+la, t) = e^{iqy - i\omega t} \left[ 0, E_l^+ e^{i\beta z} + E_l^- e^{-i\beta z}, -q\beta^{-1}(E_l^+ e^{i\beta z} - E_l^- e^{-i\beta z}) \right] \quad (1)$$

Here  $0 < z < a$ ,  $q$  is wavevector along the layers,  $\beta = (c^{-2}\epsilon_0\omega^2 - q^2)^{1/2}$ , and  $E_l^\pm$  are the amplitudes of the forward and backward going waves (or growing and decaying waves if  $\beta$  is imaginary). To describe the bulk modes of an infinite

superlattice we need only assume that

$$E_l^+ = \exp(ikla) E_0^+ \quad (2)$$

where  $|k| \leq \pi/a$ . This is simply a statement that the field associated with the mode satisfies Bloch's theorem since it is a solution of a wave equation in a periodic structure. Using Eqs. (1) and (2), and imposing the standard boundary conditions that  $E_y$  be continuous at  $z = la$ , and that the discontinuity in  $D_z = \epsilon E_z$  at  $z = la$  be equal to  $4\pi\rho$ , where  $\rho$  is the induced charge density on the plane  $z = la$ , gives

$$\left[ iEv_q \chi(q, \omega) / qc \right] \frac{\sinh i\beta a}{\cosh i\beta a - \cos ka} = 1 \quad (3)$$

Here  $v_q = 2\pi e^2/q$  and  $\chi(q, \omega)$  is the polarizability of the two-dimensional electron gas. In the non-retarded, or electrostatic limit ( $cq \gg \omega$ ),  $\beta \rightarrow iq$ , and Eq. (3) is identical to the dispersion relation  $\omega = \omega(q, k)$  obtained by Das Sarma and Quinn<sup>1</sup> by a somewhat more complicated method.

The intrasubband plasma modes described by Eq. (3) form a band whose maximum (for a given value of  $q$ ) occurs at  $\omega_+(q) = \omega(q, k=0)$  and whose minimum occurs at  $\omega_-(q) = \omega(q, k=\pi/a)$ . For all values of  $k$  other than  $k = 0$ , the modes start out for very small values of  $q$  with linear dispersion. The continuum of bulk modes is shown as the upper shaded region in Fig. 1, a plot of frequency vs  $qa$ .

To describe surface modes<sup>3</sup> we make the assumption that

$$E_l^+ = \exp(-\alpha la) E_0^+ \quad (4)$$

for  $l > 0$ , where  $\alpha$  has a positive real part. This corresponds to an excitation which decays exponentially with distance from the surface  $z=0$ . Eq. (1) still holds for  $z > 0$ , but for  $z < 0$  the solution of the wave equation must be of the form

$$E(y, z, t) = e^{iqy - i\omega t} (0, 1, -iq\delta_0^{-1}) E_0 e^{\delta_0 z} \quad (5)$$

Here  $p_0 = (q^2 + \omega_p^2/c^2)^{1/2}$  reduces to the value  $q$  in the electrostatic limit, and only the decaying wave solution has non-vanishing amplitude. The boundary conditions are once again that  $E_y$  must be continuous, and that the discontinuity in  $D_z = E_z$  must be equal to  $4\pi p$  at  $z=ka$  for  $k=0,1,2,\dots$ . The dispersion relation can be written

$$\left[ \frac{1}{\epsilon_s} + \frac{1}{\epsilon_0} \right] \left[ \frac{1}{\epsilon_s} + \frac{1}{\epsilon_0} \right] + \left[ \frac{1}{\epsilon_s} + \frac{1}{\epsilon_0} \right] \left[ \frac{1}{\epsilon_s} + \frac{1}{\epsilon_0} \right] = 0. \quad (6)$$

Here  $k$  is simply the complex value of  $k$  which is the solution of Eq. (3) for the particular values of  $q$  and  $\omega$ , and  $\epsilon_s = \frac{1}{2}(\epsilon_s + \epsilon_0)$ . The solution of Eq. (6), which must be obtained numerically, depends quite critically on the ratio of  $\epsilon_s$  to  $\epsilon_0$ . For  $\epsilon_s > \epsilon_0$  a surface wave solution exists above the continuum of bulk modes for  $q$  larger than a critical value  $q^*$ . For  $\epsilon_s < \epsilon_0$  a surface wave solution exists below the bulk continuum for  $q > q^*$ . The solid curve in Fig. 1 shows the surface wave dispersion for the case in which  $\epsilon_s = 5$  and  $\epsilon_0 = 20$ . The values of  $q^*$  can be obtained analytically by requiring that Eqs. (5) and (3) (with  $k=0$  or  $k=\pi/a$ ) be satisfied simultaneously. This leads to the result

$$q^* = a^{-1} \ln \left[ \frac{\epsilon_s + \epsilon_0}{\epsilon_s - \epsilon_0} \right]. \quad (7)$$

The insert in Fig. 1 shows an enlargement of the region in which the surface mode intersects the continuum at  $q^*$ . The value of the decay parameter  $\alpha$  is given by

$$\alpha = a^{-1} \ln \left[ \frac{1 + \sinh(\gamma) \sqrt{\epsilon_s - 1}}{1 - \sinh(\gamma) \sqrt{\epsilon_s - 1}} \right], \quad (8)$$

where  $\gamma = \cosh qa - \omega^2(\omega_p^2/2\epsilon_0) qa \sinh qa$ . For  $\epsilon_s > \epsilon_0$   $\alpha$  is real and approaches zero as  $q \rightarrow q^*$  from above. For  $\epsilon_s < \epsilon_0$   $\alpha$  has an imaginary part equal to  $i\pi/a$ .

Again the real part of  $\alpha$  approaches zero as  $q \rightarrow q^*$  from above. This behavior is shown in Fig. 2, a plot of the real part of  $\alpha a$  vs  $qa$  for the same  $\epsilon_0, \epsilon_s$  as in Fig. 1.

It is interesting to note that these surface plasma modes, in contrast to

those of a three-dimensional material<sup>4,5</sup>, do not suffer Landau damping. In a three-dimensional jellium-like metal the single particle energy is a continuous function of wavevector. Because the presence of the surface relaxes the condition of conservation of the normal component of wavevector, a surface plasmon can always decay into a single electron-hole pair. This is not true in the superlattice because the energies associated with motion normal to the layers are quantized. It is impossible to conserve energy and parallel component of wavevector in the creation of an electron-hole pair by an elementary excitation lying outside the single particle continuum. For the simple model used in this note, the single particle continuum consists of that portion of the  $\omega$ - $q$  plane in which  $\omega < \hbar q(k_F + q/2)/2m$ . The single particle continuum appears as the lower shaded region in Fig. 1. For the model considered in reference 6, there are a number of "two-dimensional" electronic subbands separated by energy  $\hbar\omega_{no}$  from the ground subband, and there can exist a set of intersubband collective modes. In that case, there are additional regions of the single particle continuum defined by  $\hbar q(k_F + q/2)/2m + \omega_{no} < \omega < \hbar q(k_F + q/2)/2m + \omega_{no}$  for each subband separation  $\omega_{no}$ . Collective surface excitations lying outside the single particle continuum are unable to decay into a single electron-hole pair and are thus not subject to Landau damping. Therefore, in high mobility semiconducting superlattices, these surface modes should have a very long lifetime.

A good candidate for possible observation of the surface polariton modes discussed here is the GaAs/Al<sub>x</sub>Ga<sub>1-x</sub>As superlattice system. In this system the background dielectric function  $\epsilon_s$  is not a constant, but it is a function of frequency:  $\epsilon_s(\omega) = \epsilon_s(\omega) (\omega^2 - \omega_L^2) (\omega^2 - \omega_T^2)^{-1}$ , where  $\epsilon_s(\omega)$  is the high frequency dielectric constant, and  $\omega_L$  and  $\omega_T$  are the longitudinal and transverse optical phonon frequencies respectively. By taking account of the frequency dependence of  $\epsilon_s(\omega)$ , one finds a system of coupled intersubband plasmon-optical phonon modes. Both bulk bands and surface excitations exist.<sup>7</sup>



Because the surface polaritons are non-radiative, they do not couple directly to light. In order to observe the modes in optical absorption or reflectance it will be necessary to destroy the translation invariance along the surface by, for example, producing a grating on the surface. The grating spacing  $\ell$  should satisfy the inequality  $\ell < 2\pi q^{-1}$ ; this is in the range of thousands of  $\text{\AA}$  and should not be difficult to achieve. Resonant Raman scattering and electron energy loss spectroscopy appear to be possible techniques for observing these surface polariton. In these experiments large momentum transfer along the surface is possible, so that values of  $q$  greater than  $q^*$  can be attained.

The authors would like to thank Dr. G. Gonzalez de la Cruz and Dr. A. C. Teolis for stimulating discussions.

#### REFERENCES

- Supported in part by National Science Foundation Grant DMR 812069.
- On leave from the Scuola Normale Superiore, Pisa, Italy.
- † Visiting scholar from Nanking University, China
- 1. A. L. Fetter, *Ann. Phys.* **81**, 367 (1973); S. Das Sarma and J. J. Quinn, *Phys. Rev.* **B25**, 7603 (1982).
- 2. K. W. Uhle and J. J. Quinn, *Phys. Rev.* **B9**, 4727 (1974).
- 3. E. Burstein, "Polaritons", edited by E. Burstein and F. DeMartini, (Pergamon Press Inc., N.Y. 1974) pg. 1.
- 4. H. Ritchie, *Phys. Rev.* **106**, 874 (1957); R. A. Stern and R. A. Farrell, *Phys. Rev.* **120**, 130 (1960).
- 5. R. Fuchs and K. L. Kliewer, *Phys. Rev.* **B2**, 2270 (1971); D. E. Beck, *Phys. Rev.* **B4**, 1555 (1971).
- 6. A. Teolis, G. Gonzalez de la Cruz, and J. J. Quinn, *Solid State Comm.*, **66**, 779, (1983); G. Gonzalez de la Cruz, A. Teolis, and J. J. Quinn, *J. Chem. Phys. Solids*, to appear.
- 7. G. Giuliani and J. J. Quinn, to be published.

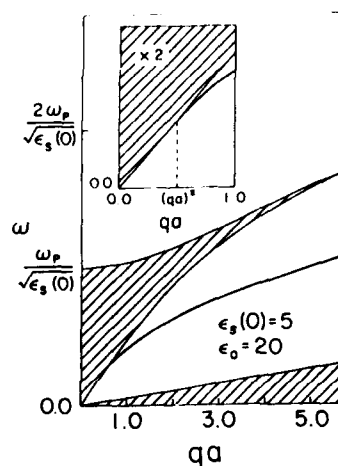


FIGURE 1.

A plot of frequency vs.  $qa$ , the product of wavenumber parallel to the layers and superlattice spacing. The upper shaded region is the band of bulk intrasubband plasmons. The lower shaded region is the single particle continuum. The surface polariton mode is the solid line which intersects bulk plasmon continuum at  $(qa)^*$  as shown in the inset. Here  $\epsilon_s$  is taken to have a value of 5 and  $\epsilon_0$  a value of 20.

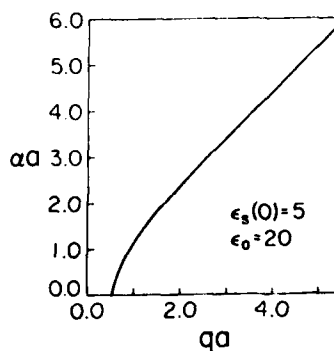


FIGURE 2.

A plot of the real part of  $qa$  vs.  $qa$  for the case in which  $\epsilon_s=5$  and  $\epsilon_0=20$ . For large values of  $q$ ,  $a$  is proportional to  $q$ , but  $a$  vanishes at  $q=q^*$ .

TWO DIMENSIONAL MAGNETOPHONON RESONANCE IN GaInAs-InP and GaInAs-AlInAs  
HETEROJUNCTIONS AND SUPERLATTICES

J.C. Portal\*, G. Gregoris\*, M.A. Brummell\*, R.J. Nicholas\*, M. Razeghi<sup>†</sup>,  
M.A. di Forre-Poisson<sup>‡</sup>, K.Y. Cheng<sup>§</sup> and A.Y. Cho<sup>§</sup>

\*Laboratoire de Physique des Solides, I.N.S.A., 31077 Toulouse, France,  
and S.N.C.I.-C.N.R.S., 166X, 38042 Grenoble, France.

†Clarendon Laboratory, Parks Road, Oxford, OX1 3PU, England.

‡E.C.R., Thomson-C.S.F., 91401 Orsay, France.

§Bell Laboratories, Murray Hill, New Jersey 07974, U.S.A.

Abstract

We report the observation of magnetophonon resonance in GaInAs-InP heterojunctions and measurements of the temperature dependence of the oscillations. A single series of oscillations due to scattering by the 'GaAs-like' mode of GaInAs is seen, in contrast to GaInAs-InP superlattices, where scattering from InP phonons is also observed, and GaInAs-AlInAs heterojunctions, where coupling to 'InAs-like' modes only is seen. This behaviour is discussed in terms of long-range phonon interactions and interface phonons.

Magnetophonon resonance is an extremely powerful tool in the study of electron-phonon interactions in semiconductors. In two recent letters, we have shown how the dominant electron-LO phonon scattering processes are quite different in the two-dimensional gases formed in GaInAs-InP superlattices and in GaInAs-AlInAs heterojunctions<sup>(1,2)</sup>. In this paper we report the observation of magnetophonon resonances in GaInAs-InP heterojunctions, where the scattering observed is different again, but quite consistent with the changes observed with increasing quantum well thickness in the superlattices.

The optic phonon modes of Ga<sub>0.47</sub>In<sub>0.53</sub>As have been studied by a number of workers<sup>(3-6)</sup>, who have found two L.O. phonons at 233 cm<sup>-1</sup> and 271 cm<sup>-1</sup>.

The dielectric constant for a material with two sets of optic phonon modes is

$$\epsilon = \epsilon_{\infty} + (\epsilon' - \epsilon_{\infty}) \frac{\omega_{TO}^2 (\omega_{TO}^2 - \omega^2)}{(\omega_{TO}^2 - \omega^2)^2 + \gamma^2 \omega^2} + (\epsilon_0 - \epsilon') \frac{\omega_{LO}^2 (\omega_{LO}^2 - \omega^2)}{(\omega_{LO}^2 - \omega^2)^2 + \gamma^2 \omega^2} \quad (1)$$

485

where  $\omega_{TO}$  and  $\omega_{LO}$  are the two TO phonon frequencies,  $\epsilon_0$  and  $\epsilon_{\infty}$  are the low and high frequency dielectric constants,  $\gamma$  and  $\gamma'$  are damping parameters, and  $\epsilon'$  is defined by the generalised Lyddane-Sachs-Teller relations

$$\frac{\epsilon'}{\epsilon_{\infty}} = \frac{\omega_{LO}^2}{\omega_{TO}^2}, \quad \frac{\epsilon_0}{\epsilon'} = \frac{\omega_{LO}^2}{\omega_{TO}^2} \quad (2)$$

The oscillator strengths associated with each mode are  $(\epsilon_0 - \epsilon')$  and  $(\epsilon' - \epsilon_{\infty})$ . For Ga<sub>0.47</sub>In<sub>0.53</sub>As this gives 0.82 for the 'InAs-like' mode at 233 cm<sup>-1</sup> and 1.58 for the 'GaAs-like' mode at 271 cm<sup>-1</sup>. It is thus not surprising that magnetophonon measurements on bulk GaInAs have shown that the dominant scattering is by 'GaAs-like' phonons<sup>(7)</sup>, although recent measurements have detected some trace of oscillations due to 'InAs-like' modes<sup>(8)</sup>.

Magnetophonon measurements were made on several GaInAs-InP heterojunctions grown at the Thomson-C.S.F. Laboratories by the LP-MOCVD technique<sup>(9)</sup>, with electron concentrations of  $3.5 \times 10^{11}$  cm<sup>-2</sup> and typical mobilities of 8000 cm<sup>2</sup> V<sup>-1</sup> s<sup>-1</sup> at 300 K and 30 000 cm<sup>2</sup> V<sup>-1</sup> s<sup>-1</sup> at 77 K. The oscillations were detected by standard second-derivative techniques and a typical series of curves, taken at lattice temperatures between 80 K and 300 K, is shown in Fig. 1. Rotation of the sample relative to the field at several temperatures showed that the resonances were two-dimensional up to 300 K.

The oscillations observed form a single series with a fundamental field,  $hB_N$ , of 14.4 T. Using the measured cyclotron mass of  $m^* = 0.048 m_0$ <sup>(10)</sup> with a small correction for non-parabolicity<sup>(11)</sup>, the phonon energy can be deduced from

$$\hbar\omega_{LO} = \hbar\omega_c = \frac{\hbar e H_N}{m^*} \quad (3)$$

where  $\omega_c$  is the cyclotron frequency. This gives a phonon energy of 278 cm<sup>-1</sup>, which may be reduced slightly by a resonant polaron contribution to the effective mass; this has been ignored as there is some uncertainty over its magnitude in two dimensional systems, but it is thought to be small, of order 1%<sup>(1,2,11,12)</sup>. The dominant scattering would thus appear to be by

486

'GaAs-like' phonons in bulk GaInAs. It can be seen from Fig. 1 that an additional peak at 10.2  $\mu$  appears at lower temperatures. The amplitudes of this peak and the  $N = 2$  magnetophonon oscillation are plotted in Fig. 2. The magnetophonon peak is visible over the whole temperature range studied, and has a maximum at 150 K, while the extra peak only appears below 220 K and increases monotonically with decreasing temperature. Magnetophonon amplitudes fall at low temperatures due to the decreasing LO phonon population, and at high temperatures the oscillations become increasingly damped due to additional broadening of the Landau levels. The extra peak is thought to be the remains of the  $N = 1$  Shubnikov-de Haas oscillation; at such high temperatures the Shubnikov-de Haas amplitude falls off less quickly than expected from classic  $X/\sinh X$  relation ( $X = 2\pi^2 kT/\hbar\omega_c$ ) since  $\hbar\omega_c$  is no longer much less than  $\hbar\omega_c$ .

Fig. 3 shows magnetophonon oscillations in all three GaInAs two-dimensional systems studied to date: heterojunctions and superlattices of GaInAs-InP and heterojunctions of GaInAs-AlInAs. The significant feature of the superlattice results is the appearance of a second series of oscillations which increases in amplitude as the quantum well thickness is reduced, becoming comparable in amplitude with the main series at a well thickness of 80 Å. This series cannot be the remains of the Shubnikov-de Haas oscillations, as the amplitude increases with temperature in the range 100-160 K, and the fundamental field is much too high. The main series gives a phonon energy at 268  $\text{cm}^{-1}$ , and is due to scattering by the 'GaAs-like' mode at GaInAs, while the second series gives a phonon energy of 350  $\text{cm}^{-1}$ , corresponding to the LO phonon of InP<sup>(4,13)</sup>. As the well thickness is reduced, electrons are confined closer to the GaInAs-InP interface, and scattering by InP phonons becomes more significant. The heterojunctions represent the limit of infinite quantum well thickness, when the InP phonon scattering has become too weak to detect. The details of the InP phonon - GaInAs electron interaction are not clear. Both the finite

screening of the InP phonon field in the GaInAs<sup>(14,15)</sup> and the penetration of the electron wavefunction into the InP could lead to scattering. Grading of the interface region or interface phonons may also play a role.

Results from the GaInAs-AlInAs heterojunctions are very different; only one series of oscillations is observed (Fig. 3), corresponding to a phonon energy of 235  $\text{cm}^{-1}$ . This is thought to be due to the existence of degenerate 'InAs-like' modes on both sides of the interface, causing stronger coupling to the electron gas. The oscillator strength ( $e_0 - e'$ ) of the 'InAs' mode in AlInAs is 1.27, greater than the value of 0.82 in GaInAs.

The results show that the electron-phonon interactions in the three systems studied are strongly dependent upon the interface, but do not provide any evidence for interface phonons as such. The interface phonon energies may be deduced by equating the dielectric constant at the interface,  $(\epsilon_1 + \epsilon_2)/2$ , to zero, where  $\epsilon_1$  and  $\epsilon_2$  are the dielectric constants of the two materials calculated from Eq.(1). The frequencies and oscillator strengths deduced are shown in Table 1. For the GaInAs-InP system the interface phonon energies seem significantly too low to account for the series observed, while for the GaInAs-AlInAs heterojunctions the bulk and interface 'InAs' modes are degenerate. This would seem to explain the dominance of 'InAs' phonon scattering in this system, since the interface phonon oscillator strength is not obviously dominant for the 'InAs' mode.

In conclusion we may say that the scattering of a 2DEG in GaInAs by LO phonons may be controlled so that the dominant interaction is with one of the three phonon modes 'InAs', 'GaAs' or 'InP'. The three cases correspond to:

- (i) 'InAs' dominance in GaInAs-AlInAs heterojunctions and probably superlattices.
- (ii) 'GaAs' dominance in GaInAs-InP heterojunctions or quantum wells of thickness greater than  $\sim 100\text{\AA}$ .
- (iii) 'InP' dominance in GaInAs-InP quantum wells of thickness less than  $\sim 100\text{\AA}$ .

Table 1 shows the frequency in  $\text{cm}^{-1}$  followed by the oscillator strength for all bulk and interface LO phonons in the two systems.

mode	'InAs'	'GaAs'	'InP'	'AlAs'
<b>Bulk Phonons</b>				
GaInAs	233/0.8	271/1.6		
InP			349/3.0	
AlInAs	286/1.2			369/1.4
<b>Interface Phonons</b>				
GaInAs-InP	228/0.4	261/0.8	328/1.5	
GaInAs-AlInAs	234/1.0	265/0.8		359/0.7

#### References

1. J.C. Portal, J. Giszewski, R.J. Nicholas, M.A. Brummell, M. Razezghi and M.A. Poisson, *J. Phys. C: Solid State Phys.* **16** (1983) L573
2. M.A. Brummell, R.J. Nicholas, J.C. Portal, K.Y. Cheng and A.Y. Cho, *J. Phys. C: Solid State Phys.* **16** (1983) L579
3. M. Brodsky and G. Lucovsky, *Phys. Rev. Lett.* **21** (1968) 990
4. C. Pickering, *J. Electron. Mater.* **10** (1981) 901
5. A. Pinczuk, J.M. Worlock, R.E. Nahory and M.A. Pollack, *Appl. Phys. Lett.* **31** (1978) 461
6. K. Kuwamoto and K. Katoda, *Appl. Phys. Lett.* **40** (1982) 826
7. R.J. Nicholas, S.J. Sessions and J.C. Portal, *Appl. Phys. Lett.* **37** (1980) 128
8. C.K. Sarkar, D.Phil. thesis, Oxford University (1983)
9. M. Razezghi, J.P. Hirtz, J.P. Larivain, R. Blondeau, B. deCremoux and J.P. Duchemin, *Electron. Lett.* **17** (1981) 641
10. M.A. Brummell, R.J. Nicholas, J.C. Portal, S. Huan, J.C. Portal, M. Razezghi, M.A. diPorte-Poisson, K.Y. Cheng and A.Y. Cho, this conference.
11. D. Englert, D.C. Tsui, J.C. Portal, J. Beerens and A.C. Gossard, *Solid State Commun.* **44** (1982) 1301
12. S. das Sarma, *Phys. Rev. B* **27** (1983) 2590
13. A. Mooradian and G.B. Wright, *Solid State Commun.* **4** (1966) 431
14. K. Hess and P. Vogl, *Solid State Commun.* **30** (1979) 807
15. M.A. Brummell, R.J. Nicholas, J.C. Portal, M. Razezghi and M.A. Poisson, *Proc. 16th Int. Conf. on the Physics of Semiconductors 1982, Physica B* **118** (1983) 753

**Acknowledgement:** M.A. Brummell was supported by an S.E.R.C. CASE Studentship in collaboration with the G.E.C. Rivet Research Centre. We would like to thank Dr. J.P. Duchemin and Dr. T.P. Pearsall for useful discussions.

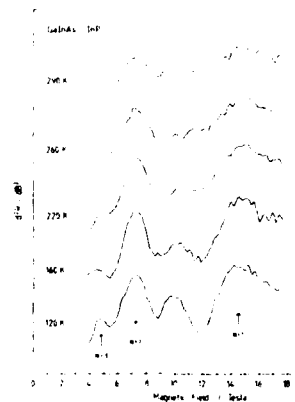


Fig. 1 shows magnetophonon oscillations in a GaInAs-InP heterojunction as a function of temperature. The extra peak at lower temperatures is thought to be the  $N = 1$  Shubnikov-de Haas peak.

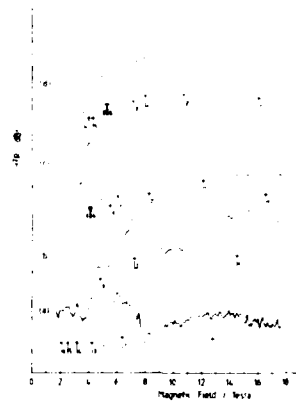


Fig. 3 shows magnetophonon oscillations in the three systems studied. (a) shows a single series due to 'InAs' phonons in a GaInAs-AlInAs heterojunction; (b) shows a single series in a GaInAs-InP heterojunction due to 'GaAs' phonons; (c) shows results for a 150Å GaInAs-InP superlattice where, in addition to the main series due to scattering by 'GaAs' phonons, there is a weaker second series due to scattering by 'InP' phonons (resonance indices shown primed); (d) shows results for an 80Å GaInAs-InP superlattice, where the two series due to 'GaAs' and 'InP' phonons are approximately equal in intensity. The masses in the two superlattices differ from each other, and from the heterojunctions due to non-parabolicity.

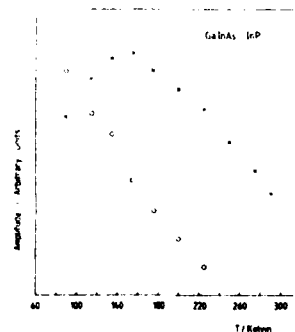


Fig. 2 shows the amplitudes of the  $N = 2$  magnetophonon resonance (crosses) and the extra peak (circles) as a function of temperature.

# RESONANT TUNNELING IN DOPING QUANTUM WELL STRUCTURES

Ch. Zeller and G. Abstreiter

Physik-Department, Technische Universität München

8046 Garching, Fed. Rep. of Germany

and

K. Ploog

Max-Planck-Institut für Festkörperforschung

7000 Stuttgart, Fed. Rep. of Germany

## Abstract

The resonant tunneling of electrons through the forbidden gap into discrete subband states is studied in pnp-GaAs quantum well structures. Transitions into different electric subbands in the conduction band are observed in the derivative curves of the I-V characteristics. The concept of a tunnel triode structure is proposed which is based on resonant tunneling via electronic states of a two-dimensional system.

Tunneling experiments for the investigation of subband energies have been performed so far only for accumulation layers on degenerate semiconductors<sup>1/</sup> and in Si-MOS structures<sup>2/</sup>. In those experiments the region through which the carriers tunnel consisted of a very thin insulating layer. Quantum mechanical tunneling processes have also been observed in double barrier structures formed by thin layers of semiconductors with different band gaps (e.g. GaAs and  $\text{Al}_x\text{Ga}_{1-x}\text{As}$ )<sup>3/</sup>. It is well known, however, that tunneling of carriers can also occur through the forbidden energy gap of a homogeneous semiconductor from conduction to valence band states and vice versa, using heavily doped np-junctions<sup>4/</sup>. Also the possibility of bipolar transport

between n- and p-layers of doping superlattices has been discussed briefly more than ten years ago<sup>5/</sup>. In the present work we report on the observation of resonant tunneling through the forbidden gap into subband states of a two-dimensional system in the conduction band using ultrathin pnp-GaAs triode structures.

The samples grown by molecular beam epitaxy consist of an ultrathin (40 nm to 70 nm) n-GaAs layer imbedded in two thick ( $\sim 500$  nm) p-GaAs layers. Si and Be are used as n- and p-type dopants, respectively. The doping concentration  $N_D = N_A \geq 1 \times 10^{18} \text{ cm}^{-3}$  leads to a nearly parabolic one-dimensional space-charge potential well with approximately equidistant subbands in the conduction band of the n-type layer. In the ground-state of the systems the Fermi energy in the conduction band is finite, i.e. a few subbands are occupied (see Fig. 1b). Selective ohmic contacts to the different layers are formed by alloying small Sn and Sn/Zn balls as  $n^+$ - and  $p^+$ -electrodes, respectively.

The carrier density in the potential well can be varied by applying a voltage  $U_{np}$  between the selective electrodes. The potential well is then shifted with respect to the Fermi level  $\phi_p$  in the p-type layers. In Fig. 1 the situation is shown schematically for different values of  $U_{np}$ . For  $U_{np} = 0$  the Fermi levels in the p- and n-type layers are equal, and the occupation of electric subbands depends on the design parameters. With reverse bias ( $U_{np} < 0$ ) the carrier concentration gets depleted, the depth of the potential well, however, is increased (Fig. 1a). The tunnel probability for electrons from valence band states to the empty subbands depends on the density of states. Consequently, this reflects the step-like behavior of the two-dimensional system in the n-type layer. A forward bias ( $U_{np} > 0$ ), on the other hand, decreases the depth of the potential well, and the quasi-Fermi level for electrons  $\phi_n$  is increased. Electrons can now tunnel from the occupied subbands into the hole states above  $\phi_p$  (Fig. 1c). If the applied potential

$e(\phi_n - \phi_p)$  exceeds  $\epsilon_n$ , direct tunneling processes are no longer possible (Fig. 1d).

In order to observe directly the tunnel current we have carefully studied the I-V characteristics of several pnp-GaAs structures. In Fig. 2 results are shown as obtained for a sample with  $N_D = N_A = 2 \times 10^{18} \text{ cm}^{-3}$  and the thickness of the n-type layer of  $d_n = 70 \text{ nm}$ . The top curve is the direct I-V trace measured for a large voltage range to show the overall behavior of the np-characteristics. The two lower curves are the first and second derivative observed in the region  $-200 \text{ mV} \leq U_{np} \leq 100 \text{ mV}$ . The more sensitive derivative spectra exhibit a sequence of peaks, with a separation of approximately  $31 \text{ meV}$ . At  $0 \text{ V}$  an additional dip is observed which is related to a weak zero bias anomaly whose strength varies from sample to sample. This effect causes some distortions of the subband tunnel structure around  $0 \text{ V}$ . The spacing of the peaks in the derivative curves is explained by changes of the tunnel current which occur whenever a subband is shifted through the Fermi level  $\phi_p$  in the valence band.

The observed structures can be compared with self-consistent calculations of the potential well and the subband energies. Using the given design parameters of the sample we obtain a Fermi energy for the unexcited state  $\epsilon_n = 73 \text{ meV}$ . Consequently one should reach the condition that the lowest subband moves through the Fermi level in the valence band at  $U_{np} = 73 \text{ mV}$ . This is marked in Fig. 2 by the large arrow. It coincides extremely well with the strongest peak observed in the derivative curves. The small arrows mark the calculated subband separations as obtained for those subbands which are closest to  $\phi_p$  and are therefore responsible for the structures in the tunnel current. The energy difference is increasing with applied negative bias voltage. For  $U_{np} > 0$  only the lowest subbands are involved in the tunneling processes. Their energy separation is of the order of  $20 \text{ meV}$ . At  $U_{np} = -180 \text{ mV}$

we find a separation between subbands five and six of about  $35 \text{ meV}$ . Except for the dip at  $0 \text{ V}$  there is good agreement between theory and the measured peak structures.

We have also observed some structures for applied voltages where direct tunneling between valence band- and subband states is no more possible. They are probably caused by deep impurity levels both above the valence band and below the conduction band edge. Some of these levels are also seen in photoluminescence spectra of the same samples<sup>/6/</sup>.

The present experiments have been performed on samples with relatively low doping concentrations ( $N_D = N_A \leq 4 \times 10^{18} \text{ cm}^{-3}$ ). For these values the direct tunneling probability through the band gap is weak. Consequently, the structures were observed only in the derivative curves but not in the direct I-V characteristic. A strong increase of the tunnel current is expected for higher doping concentrations, which, however, requires an improved contact technology. With the presently diffused contacts the leakage current becomes too high. One solution is the incorporation of masking techniques into the molecular beam epitaxy system. Another possibility is the application of well-defined ion implantation for highly resistive areas around the contact regions. The fabrication of such devices opens a wide field for applications which, for example, make use of resonant tunneling from one p- to the other p-region via real electronic states of a two-dimensional system in the n-type layer.

#### Acknowledgements:

We wish to thank A. Fischer for the expert help in sample preparation. The work has been supported by the Deutsche Forschungsgemeinschaft via SFB 128 and by the Bundesministerium für Forschung und Technologie of the Federal Republic of Germany.

# References:

- 1) D.C. Tsui, Phys. Rev. B 4, 4438 (1971); D.C. Tsui, G. Kaminsky, and P.H. Schmidt, Phys. Rev. B 9, 3524 (1974)
- 2) U. Kunze and G. Lautz, Surface Science 113, 55 (1982)
- 3) L.L. Chang and L. Esaki, Appl. Phys. Lett. 24, 593 (1975)
- 4) L. Esaki, Phys. Rev. 109, 603 (1958)
- 5) G.H. Döhler, Phys. Status Solidi B 52, 533 (1972)
- 6) H. Jung (unpublished)

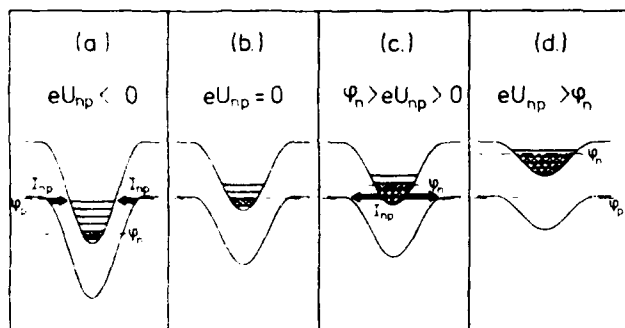


Fig. 1: Variation of the band edges in a pnp-GaAs structure.  $\epsilon_p$  and  $\epsilon_n$  are the quasi-Fermi energies in the valence and in the conduction band, respectively. The arrows indicate possible tunneling processes which involve electric subbands in the conduction band.

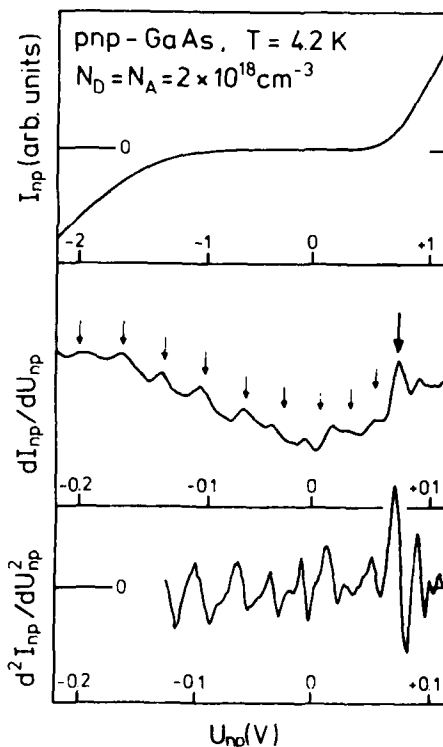


Fig. 2: Direct I-V characteristic and its first and second derivative of a pnp-GaAs sample. Note the different scales of the  $U_{np}$ -axis. For discussion see text.

# COLLECTIVE MODES OF TYPE II SEMICONDUCTOR SUPERLATTICES\*

A. Tselis<sup>†</sup>, G. Gonzalez de la Cruz<sup>††</sup> and J. J. Quinn  
Department of Physics, Brown University, Providence, RI 02912 USA

## ABSTRACT

A general formulation is developed to describe the electronic collective modes of a type II superlattice as exemplified by the InAs/GaSb system. Dispersion relations are evaluated in the limit of weak coupling between different intersubband excitations and the intrasubband modes.

In this paper, we investigate the electronic collective excitations of type II semiconductor superlattices. For many purposes, type I superlattices can be thought to consist of a periodic array of quasi-two-dimensional electron layers, while type II superlattices can be thought of as a periodic array of alternating quasi-two-dimensional electron and hole layers. A typical example of the latter is the InAs/GaSb system, in which the conduction band edge of InAs is below the valence band edge of GaSb. This results in the transfer of electrons from the GaSb layers to the InAs layers, leaving holes behind in the GaSb.

The model used to describe the electronic structure of the type II superlattice is the following. Each quasi-two-dimensional layer is labelled by an integer (the layer index,  $l$ ). This index is even for electron layers (which contain  $n_e$  electrons per unit area, of effective mass  $m_e$  and charge  $-e$ ) and odd for hole layers (which contain  $n_h$  holes per unit area, of effective mass  $m_h$  and charge  $+e$ ).

The eigenvalues and eigenfunctions of the unperturbed system are taken to be

$$\epsilon_{nl}(k) = \epsilon_{nl} + \frac{\hbar^2 k^2}{2m_l} \quad (1)$$

$$\phi_{nl}(\vec{r}) = e^{i\vec{k} \cdot \vec{\rho}} \phi_{nl}(z - la)$$

Here,  $n$  is a subband index,  $l$  the layer index, " $a$ " the layer separation, and  $\vec{k}$  and  $\vec{\rho}$  are two-dimensional wavevector and position vectors within a layer, respectively. The envelope functions  $\phi_{nl}(z)$  are considered to be known functions,  $\phi_n(z)$  for all electron layers and  $\eta_n(z)$  for hole layers. In this model, electrons (or holes) are free to move along their layer, but their motion normal to the layer is quantized by the superlattice potential. No transfer of carriers from layer to layer is allowed, so the minibands of the periodic superlattice potential are flat.

To obtain the electronic collective modes of the system, we introduce an external perturbing potential of the form

$$v_{\text{ext}}(\vec{r}, t) = v_{\text{ext}}(\vec{q}, \omega, z) e^{i\omega t - i\vec{q} \cdot \vec{\rho}} \quad (2)$$

This external disturbance gives rise to a total, self-consistent potential  $v$  which is the sum of the external potential, a Hartree potential  $v^H$ , and an exchange-correlation potential  $v^{\text{xc}}$ . The change in density  $\delta n$  caused by the self-consistent potential is calculated by linear response theory; it is given by

$$\delta n(\vec{q}, \omega, z) = \sum_{n'l'} \Pi_{nn'}^{(l)} \langle n | v_l(q\omega) | n' \rangle \phi_{n'l}(z-la) \phi_{n'l}(z-la) \quad (3)$$



Here, we have assumed that there is no overlap of the wavefunctions in adjacent layers, and introduced the symbol

$$\epsilon_{mm'}^{(l)} = \frac{1}{k} \int d\mathbf{r} \frac{f[\epsilon_{ml}(\mathbf{k}+\mathbf{q})] - f[\epsilon_{m'l}(\mathbf{k})]}{\epsilon_{ml}(\mathbf{k}+\mathbf{q}) - \epsilon_{m'l}(\mathbf{k}) - \hbar\omega} \quad (4)$$

the irreducible polarizability of the  $l$ -th layer. The symbol  $\langle m|v_l|m' \rangle$  stands for the matrix element of  $v(q, \omega, z)$  between the  $m$  and  $m'$  subbands on the  $l$ -th layer. The Hartree and exchange-correlation potentials are given by

$$v^H(q, \omega, z) = \frac{2\pi e^2}{q} \int dz' e^{-q|z-z'|} n(q, \omega, z') \quad (5)$$

$$v^{xc}(q, \omega, z) = \frac{v_{xc}^{(n)}}{\Delta n} \Delta n(q, \omega, z) \quad (6)$$

where  $v_{xc}^{(n)}$  is the exchange-correlation functional.

By combining these equations, we can obtain a relation between matrix elements of the external potential  $v^{ext}$  and matrix elements of the self-consistent potential  $v$ . This relation can be thought of as a matrix equation in which subband indices label the matrix elements. It contains the same information as the non-local dielectric function  $\epsilon(z, z'; q, \omega)$ , which provides an integral relation between the external potential at position  $z$  and the self-consistent potential at position  $z'$ .

The condition for self-sustaining collective modes is obtained by requiring that the self-consistent  $v$  remain finite when  $v^{ext}$  is set equal to zero. This condition, together with the ansatz that

$$\begin{aligned} \langle n|v_l(q, \omega)|0 \rangle &= e^{ik_z z_l} \langle n|v_0(q, \omega)|0 \rangle \quad \text{for } l \text{ even} \\ \langle n|v_l(q, \omega)|0 \rangle &= e^{ik_z (l-1)a} \langle n|v_1(q, \omega)|0 \rangle \quad \text{for } l \text{ odd} \end{aligned} \quad (7)$$

leads to an infinite determinantal equation whose roots give the collective mode frequencies as a function of  $q$  and  $k$ . Limitations of space permit us to display only some simple special cases. It is convenient to label the electron subbands  $n=0, 1, 2, \dots$  and the hole subbands  $n'=0', 1', 2', \dots$ . The rows and columns of the determinant will then be labelled  $0, 0', 1, 1', 2, 2', \dots$ . In the remainder of this note, we will neglect the coupling between intra- and intersubband modes, and between different intersubband pairs. In that case the determinant is diagonal in  $2 \times 2$  blocks.

In the limit of weak-coupling between the layers, where the layers are far apart in the sense that  $qa \gg 1$ , the modes consist of purely two-dimensional plasmons and collective intersubband excitations occurring independently on each layer.<sup>4</sup>

In the strong-coupling limit, where the layers are close together ( $qa \ll 1$ ), we obtain coupled 2D electron-hole plasmons, and coupled intersubband electron-hole modes. The former have been discussed elsewhere,<sup>2</sup> but we display the two bands of intrasubband plasmons in Fig. 1 for the sake of completeness. The coupled intersubband electron-hole modes have frequencies to  $O(q^2)$  given by

$$\omega_{\pm}^2 = \frac{1}{2} [\omega_{no}^2 + \omega_{n'o'}^2] \pm \frac{1}{2} \sqrt{[\omega_{no}^2 - \omega_{n'o'}^2]^2 + 4v_n^2 \left( \frac{e}{\epsilon_0} \frac{\Delta n}{\Delta n_0} S(q) \right)^2} \quad (8)$$

where  $\Delta n_0$  is the separation between the  $n$ -th and ground electron subbands, and

$$\omega_{no}^2 = \omega_{no}^2 (1 + \alpha_n - \beta_n - v_n S(q))^2 \quad (9)$$

Here,  $\alpha_n, \beta_n$  give the depolarization and excitation shifts respectively, and  $v_n = (4\pi e^2 / \epsilon_0 \Delta n_0) |z_{no}|^2$ .  $S = \sinh(2qa) \cosh 2qa - \cosh 2ka$  and  $S' = S \coth ka / \cosh(qa)$  are structure factors describing the coupling be-

tween adjacent layers. The barred quantities are defined in the same way as the unbarred ones, except that they refer to the hole layers. The two frequencies in (8) corresponds to the in-phase and out-of-phase motion of the electrons and holes within a supercell (note the analogy with the phonon modes of a linear diatomic chain). In the weak-coupling limit ( $qa \gg 1$ ),  $S=1$ ,  $S'=0$  and we obtain separate electron or hole intersubband modes. In the strong-coupling limit with  $k=0$ , so that the motions in all the supercells are in phase,  $Sq=S'q=1/a$ , and eq. (8) yields coupled softened electron-hole intersubband modes. For  $k \neq 0$ , on the other hand, we find the interesting result that

$$\begin{aligned} \omega_+^2 &= \omega_{no}^2 (1 + \bar{\alpha}_n - \bar{\beta}_n) + O(q^2), \\ \omega_-^2 &= \omega_{no}^2 (1 + \bar{\alpha}_n - \bar{\beta}_n) + O(q^2), \end{aligned}$$

where the coupling occurs only in the coefficients of  $q^2$ .

In Fig. (1) a qualitative sketch showing both the intra- and intersubband excitation bands is presented. These collective modes can be detected by light-scattering and infrared absorption measurements on type II systems such as InAs/GaSb. Light-scattering techniques are more suitable for an unambiguous identification of the modes, since these methods allow measurement of the dispersion of the modes by appropriate changes in the angle of incidence.

Calculations on the effects of magnetic fields and the electron-phonon interaction, as well as the transverse modes, have been done and will be presented elsewhere.

#### REFERENCES

\* Supported in part by National Science Foundation Grant DMR 81 21062.

† Present Address: Physics Department, Purdue University, West Lafayette, Indiana 47907 U.S.A.

†† Present Address: Departamento de Física, CINVESTAV-IPN, APTDO POSTAL 14-740, 07000 MEXICO

1. A. Tselis and J. J. Quinn, Surf. Sci. **113**:362(1982).
2. S. Das Sarma and J. J. Quinn, Phys. Rev. **225**:7603(1982); W. Bloss, Solid State Comm. **44**:363(1982).

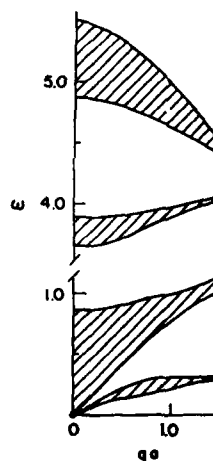


Figure 1. A qualitative sketch of the frequency of the intra- and intersubband collective modes as a function of  $qa$ . The ordinate is in units of  $10^{13} \text{ sec}^{-1}$ . Both intra- and intersubband modes form a pair of bands whose boundaries are at  $k=0$  or  $k=\pi/2a$ . The four bands are shown as the cross-hatched regions.

Optical and Electrical Properties of  $\text{PbTe-Pb}_{1-x}\text{Sn}_x\text{Te}$   
 Superlattices Prepared on KCl by a HWE

H. Fujiyasu and A. Ishida  
 Graduate School of Electronic Science and Technology,  
 Shizuoka University, Hamamatsu, 432, Japan

H. Kuvabara  
 College of Engineering, Shizuoka University,  
 Hamamatsu, 432, Japan

S. Shimomura, S. Takaoka and K. Murase  
 Department of Physics, Faculty of Science, Osaka University,  
 Toyonaka, Osaka, 560, Japan

The infrared transmittances of  $\text{PbTe-Pb}_{0.8}\text{Sn}_{0.2}\text{Te}$  superlattices prepared on KCl substrates by a hot wall epitaxy were measured at 200 K and their absorption edges are compared with the theoretical calculations. In addition results of transverse magnetoresistances and cyclotron resonance are given.

#### 1. Introduction

Since the first proposition of the one-dimensional superlattice by Esaki and Tsu (1), many works involving various kinds of superlattices (SLs) (2~4) have been reported.  $\text{PbSnTe}$  is a narrow gap semiconductor with electrons or holes, both of which have very light effective masses and large changes of the energy gap should be expected by making SLs using this semiconductor.

Recently  $\text{PbTe-Pb}_{0.8}\text{Sn}_{0.2}\text{Te}$  SLs have been prepared on the  $\text{BaF}_2$  (111) cleaved surfaces by the hot wall epitaxy (HWE) and their quantum size effects were investigated by our group (5~7).  $\text{PbSnTe}$  has many valley band structures and the features of the electronic states of the SLs are somewhat complicated, because in the growth condition mentioned above the axis of SL is along [111] and two kinds of subband with light and heavy effective masses occur. For the reduction of this complication or an application of the SL to  $\text{PbSnTe}$  laser (8), preparations of the SLs on such a substrate as a KCl (100) surface are desired. We succeeded in making the SLs ( $n$  or  $p = 10^{17} \sim 10^{18} \text{ cm}^{-3}$  and 45~270 layers) and will report experimental results of their optical and electrical properties with theoretical analysis.

#### 2. Sample preparation

In the early stage of our experiments on making  $\text{PbSnTe}$  SLs, it seemed that the  $\text{PbSnTe}$  thin film growth on the KCl substrate was not easy compared with that on the  $\text{BaF}_2$  substrate. The thermal expansion coefficient of KCl is much greater than that of  $\text{BaF}_2$  and it was difficult to make flat thin film of it on the KCl substrate heated at rather low temperature (250°C). But in the

progress of our works it was found that the surface of the grown film even on the KCl substrate was much improved by using a flip-flop growth method (discretely growing). In our method of making  $\text{PbTe-PbSnTe}$  SLs using HWE one must stop growing of film in a interval between  $\text{PbTe}$  and  $\text{PbSnTe}$  layer growths, where two hot wall systems for  $\text{PbTe}$  and  $\text{PbSnTe}$  are used, i.e. this is one kind of the flip-flop growth method.

The first buffer  $\text{PbTe}$  layer with a thickness of about 500 Å was grown on the KCl substrate cleaved along the (100) plane. The thickness is much thinner compared with that in the early stage because of the reason mentioned above. Periodic layers of the  $\text{PbTe-Pb}_{0.8}\text{Sn}_{0.2}\text{Te}$  SLs were successively grown on the buffer layers. SLs prepared are classified into two groups; i.e. one group (A); the thickness of a  $\text{PbSnTe}$  layer (width of potential well) is 40~400 Å, while that of the  $\text{PbTe}$  layer (barrier width) is constant (200 Å) and the other group (B): the former is constant (60 Å), while the latter is 40~300 Å. The surfaces of the SLs obtained in this way were almost specular in appearance. The substrate temperature during growth was 260°C and  $\text{Te}$  reservoir temperatures were adjusted to be 300 and 310 °C to obtain  $n$  and  $p$ -type samples, respectively.

#### 3. Experimental results and discussions

[Optical properties] The infrared transmittances of the SLs of group (A) were measured at 200 K and their results are shown in Fig. 1-a. For the materials used both masses of electrons and holes are very light and the Burstein-Moss effect obscures the fundamental absorption edges. To avoid this effect, all the measurements were carried out at the rather high temperature. Curves 2~6 show the transmittances of SLs, while 1 and 7 show those of a  $\text{PbTe}$  and a  $\text{Pb}_{0.8}\text{Sn}_{0.2}\text{Te}$  layers, respectively. Total thickness of the SL was fixed to be 2.8  $\mu\text{m}$ . It is apparently seen that absorption edges are shifted towards high energy with decrease in the thickness of the  $\text{PbSnTe}$  layer in the SL. The energy level or wavenumber of the quantum state in the potential well of the conduction band increases with this change. Similar variation should occur in the valence band and the energy separation between ground states in the conduction and valence bands increase with this change, assuming that the barrier height of the valence band ( $\Delta E_v$ ) is nearly equal to that of the conduction band ( $\Delta E_c$ ).

To analyze the transmittances the absorption coefficients were calculated from the curves in the Fig. 1-a. Absorption edge energies  $E_g$  were obtained and are shown in Figs. 1-b and 1-c for the groups (A) and (B), respectively. The materials used are narrow gap semiconductors and the potential well depth (barrier height) should be small. So tunneling effect with changing the

thickness of the PbTe layer (barrier width) were examined and their results are shown in the Fig. 1-c for the group (B). In these analyses the Kronig-Penney and the Kane's models were used. Absorption coefficients  $\alpha$ s depend usually on the density of empty states of the two-dimensional systems. Temperature dependences of the transmittances were measured and some humps were appeared in the  $\alpha$  curves obtained from the transmittance curves as shown in Fig. 2. The humps become to be seen sharp at high temperature due to increase in the density of empty states. Thus one can estimate positions of the energy of the optical transition between excited subbands ( $N=2$ ).

[Magnetoresistance] To ascertain two-dimensional conduction of carriers confined in the quantum well transverse magnetoresistance of p-type ( $p=2 \times 10^{18} \text{ cm}^{-3}$ ) PbTe (200 Å)-Pb<sub>0.8</sub>Sn<sub>0.2</sub>Te (200 Å) SL was measured at 77 K and  $B=12 \text{ kG}$  and are shown in Fig. 3. The magnetoresistance varies as  $\Delta\rho/\rho_0 \propto \cos\theta$ , here  $\theta$  is angle between the magnetic field  $B$  and the direction of SL ( $\{100\}$ ). It decreases almost to zero at  $\theta=90^\circ$ . Longitudinal magnetoresistance was also measured and was found to be very small. These resistances should become some magnitudes for such a single crystal as a n-type Ge due to many valley band structures with ellipsoidal constant energy surfaces at L points. From the above discussions holes are found to be confined in the quantum well of the SL.

[Cyclotron resonance] To investigate electronic motion of the SLs the cyclotron resonance (CR) was measured at 4.2 K using a 337  $\mu\text{m}$  HCN laser. Angular dependences of CR absorption spectra and of CR mass  $M_c$  for the n-type PbSnTe (40 Å)-PbTe (200 Å) SL are shown in Figs. 4-a and 4-b, respectively. In the Fig. 4-b broken lines were obtained theoretically assuming  $E_c/\Delta E_v=1$ . If one assume it  $\sim 1/4$ , their coincidence becomes good with each other. But its validity of the latter assumption is not now clear, even though there should be some strains in the interfaces of the SLs. In any way, CR radius becomes 500 Å with Fermi energy  $E_F=10 \text{ meV}$ ,  $m^* \approx 0.017 m_0$  and  $B_0=10 \text{ kG}$ , and it is much larger than the length of one period of the SL (240 Å). It is noticed that CR was observed even in the condition and observed masses are lighter than the conduction band edge mass of PbTe. In addition, transverse ( $\theta=90^\circ$ ) and longitudinal magnetoresistance were observed to some extent. These facts show that some quantum subbands appear between the top of the barrier (bottom of the conduction band of PbTe) and the bottom of the quantum well (bottom of the conduction band of Pb<sub>0.8</sub>Sn<sub>0.2</sub>Te).

#### 4. Summary

The infrared transmittances of PbTe-Pb<sub>0.8</sub>Sn<sub>0.2</sub>Te superlattices prepared on the KCl substrate by a hot wall epitaxy were measured at 200 K and the fundamental absorption edges can be explained by the theoretical calculations

using the Kronig-Penney model, taking into account the many valley band structures with ellipsoidal constant energy surfaces and the non-parabolicity of the electronic state. For a p-type sample transversal magnetoresistance was measured and two-dimensional motion of holes confined in the quantum well was ascertained. For a n-type sample cyclotron resonance was measured at 4.2 K and observed cyclotron masses are compared with the theoretical values. To clarify natures of the PbTe-PbSnTe superlattices in more detail more experimental studies as cyclotron resonance are required.

#### References

- (1) L. Esaki and R. Tsu, IBM J. Res. Dev. 14 (1970) 61.
- (2) A.Y. Cho, Appl. Phys. Lett. 19 (1971) 467.
- (3) L. Esaki, L.L. Chang, W.E. Howard and V.L. Rideout, Proc. 11th Int. Conf. on the physics of Semiconductors, Warsaw, Poland, 1972, PWN-Polish Scientific Publishers, Warsaw, Poland, 1972, p.431.
- (4) G.H. Döhler, Phys. Status Solidi, B52 (1972) 533.
- (5) H. Kinoshita and H. Fujiyasu, J. Appl. Phys. 51 (1980) 5845.
- (6) H. Kinoshita, H. Fujiyasu, A. Ishida and H. Kuwabara, Proc. 4th Int. Conf. on the Physics of Narrow Gap Semiconductors, Springer Verlag, Berlin, Heidelberg 1982 p.368.
- (7) H. Kinoshita, S. Takaoka, K. Murase and H. Fujiyasu, Proc. 2nd. Int. Symp. on MBE and Clean Surface Techniques, Japan Society of Appl. Phys. 1982 p. 61.
- (8) F.J. Bryant, M. Ekin-Uddin, J. Reed and E.L. Thomas, Infr. Phys. 22 (1982) 97.

Fig. 1 The infrared transmittances of various kinds of PbTe-Pb<sub>0.8</sub>Sn<sub>0.2</sub>Te SLs at 200 K (1-a). Variations of the optical absorption edge energy as a function of Pb<sub>0.8</sub>Sn<sub>0.2</sub>Te (1-b) and PbTe layer thicknesses (1-c) compared with the theoretical values using the Kronig-Penney model. For the samples 3, 5 and 6 in the Fig. 1-a, PbTe ununiform films ( $\sim 8 \mu\text{m}$ ) were deposited onto the tops of the SLs in order to diminish interference fringes near the absorption edges.

Fig. 2 Energy dependences of  $\alpha(\hbar\omega)$  for the PbTe (200 Å)-Pb<sub>0.8</sub>Sn<sub>0.2</sub>Te (400 Å) SL at the temperatures 77 (A), 200 (B) and 280 (C) K. Broken lines (a), (b) and (c) show the theoretical density of empty states corresponding to (A), (B) and (C).

Fig. 3 Results of the transversal magnetoresistance of the p-type ( $p=2 \times 10^{18} \text{ cm}^{-3}$ ) PbTe (200 Å)-Pb<sub>0.8</sub>Sn<sub>0.2</sub>Te (200 Å) SL at 77 K.

Fig. 4 Angular dependences of CR spectra (4-a) and of CR mass (4-b) at 4.2 K for the n-type ( $n=9 \times 10^{16} \text{ cm}^{-3}$ ) PbTe (200 Å)-Pb<sub>0.8</sub>Sn<sub>0.2</sub>Te (40 Å) SL.

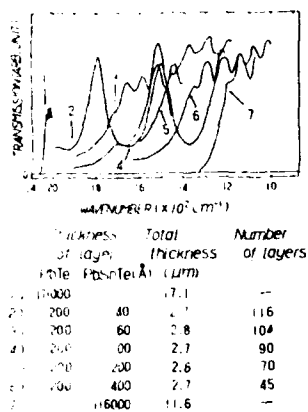


FIGURE 1a (ABOVE)  
FIGURE 1b (ABOVE RIGHT)  
FIGURE 1c (RIGHT)  
FIGURE 2 (BELOW)

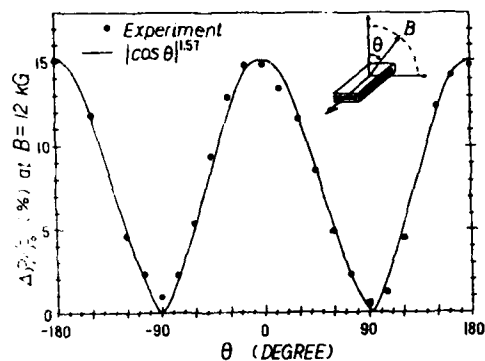
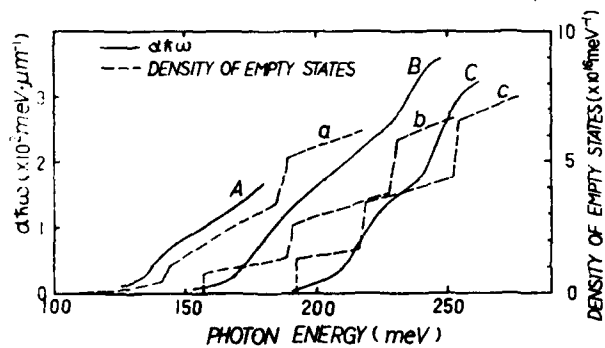
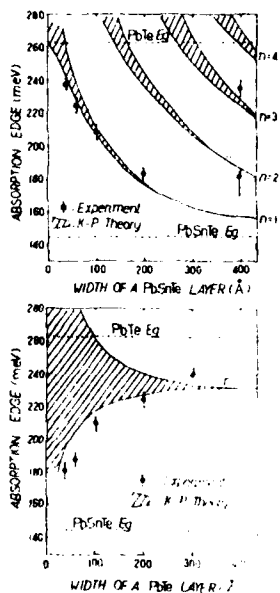


FIGURE 3

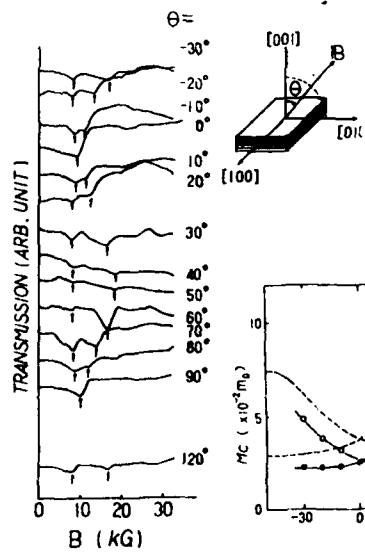


FIGURE 4a

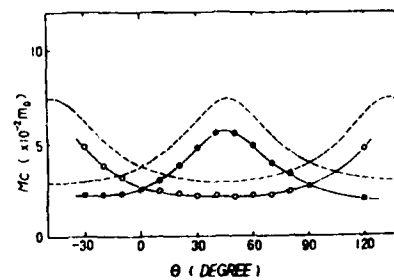


FIGURE 4b

PHOTOLUMINESCENCE AND EXCITATION SPECTROSCOPY IN  
COUPLED GaAs-Ga(Al)As QUANTUM WELLS

C. Delalande, U.O. Ziemelis, G. Bastard, M. Voos  
Groupe de Physique\* des Solides de l'Ecole Normale Supérieure  
24 rue Lhomond, 75231 Paris Cedex 05, France

A.C. Gossard and W. Wiegmann  
Bell Laboratories, Murray Hill, New Jersey 07974 USA

Abstract

We address the subject of virtual bound states (resonances) in a coupled quantum well, GaAs-Ga(Al)As structure grown by molecular beam epitaxy. The behaviour of bound hole states and hole resonances is calculated in the envelope function approach for a double well system with well (GaAs) widths ranging from 0 to 200 Å and a fixed barrier (Ga<sub>0.84</sub>Al<sub>0.16</sub>As) width of 12 Å, taking into account band non-parabolicity and the spin-orbit energies of the host materials. Experimental results based on excitation spectroscopy measurements and pertaining to the existence of a transition involving a virtual bound hole state are presented for a system consisting of 40 periods of two 45 Å GaAs wells separated by 12 Å Ga<sub>0.84</sub>Al<sub>0.16</sub>As barriers. We also discuss briefly the evolution of the photoluminescence and excitation spectra in the 2 to 40 K temperature range.

The development of techniques such as molecular beam epitaxy has made it possible to grow single crystal structures approaching atomic dimensions and numerous studies of quantum effects in these systems have been carried out [1]. In particular, Dingle et al. [2] have conducted optical absorption measurements in coupled multi-well GaAs-Ga(Al)As structures, which indicate splitting of single well bound states due to inter-well coupling. We report the first observation of this phenomenon based on excitation spectroscopy measurements in a GaAs-Ga(Al)As double well sample (see Fig. 1a). We also present the first

\* Laboratoire associé au CNRS.

calculations of the level structure associated with a coupled well system based on the envelope function approach, which include in a natural way band non-parabolicity and various boundary condition intricacies at the interface. Our calculations indicate that one of the four peaks observed in the excitation spectrum is due to an optical transition between a bound electron state and a light hole virtual bound state.

In the envelope function approach [3,4], for zero wavevector in the layer plane, the envelope function  $f_S$  associated with the  $S$  periodic part of the Bloch function is the solution of a non-parabolic hamiltonian of the Kane type, in which the  $\Gamma_4$ ,  $\Gamma_5$  and  $\Gamma_6$  edges shift at the GaAs-Ga<sub>1-x</sub>Al<sub>x</sub>As interfaces by the amounts  $V_S$ ,  $V_P$  and  $V_G$  respectively. Following Dingle [1], we have used  $V_S = 1060$  x and  $V_P = V_G = -197$  x. Bound electron (e) and hole (h) states occur for energies  $\epsilon_e < V_S$  and  $\epsilon_h < V_P$  respectively. Since we are dealing with identical wells (of width  $L$ ), the bound states are odd or even with respect to the midpoint of the centrally located barrier (of width  $h$ ). For energies corresponding to the continuum spectra ( $\epsilon_e > V_S$  or  $\epsilon_h > V_P$ ) one searches for transmission resonances. The transmission coefficient of a double well structure is given by :

$$T(\epsilon) = \left\{ 1 + \frac{1}{4} \left( \xi - \frac{1}{\xi} \right)^2 \sin^2 k_w L \left[ 2 \cos k_w L \cos k_b h - \left( \xi + \frac{1}{\xi} \right) \sin k_w L \sin k_b h \right]^2 \right\}^{-1} \quad (1)$$

where  $k_w$  and  $k_b$  are the wavevectors and  $\xi$  is the ratio of the probability currents in the well and the barrier.  $\xi$ ,  $k_w$  and  $k_b$  are easily deduced from the dispersion relations of the host materials. Resonances (twice degenerate) occur for :

$$k_w L = p\pi, \quad p \text{ integer} \quad (2)$$

$$\cos k_w L \cos k_b h - \frac{1}{2} \left( \xi + \frac{1}{\xi} \right) \sin k_w L \sin k_b h = 0 \quad (3)$$

As  $k_b \rightarrow 0$  resonances of the first kind converge towards the even bound states at the same energy ( $\epsilon_e = V_S$ ,  $\epsilon_h = V_P$ ), whereas resonances of the second kind converge in the same limit towards the odd bound states. Note that resonances

(3) would correspond to a superlattice state with wavevector  $\pi/2(L, h)$  if the  $(L, h)$  basis was infinitely repeated. On the other hand, the condition  $k_{\parallel}L = \pi$  is that obtained for a single well structure. Each resonance can be described as a virtual bound state corresponding to an accumulation of density probability in the double well structure. The present analysis shows that the double well structure exhibits virtual bound states either clamped on a single well or delocalized over the whole double well.

The calculations predict, for the structure under investigation ( $L_1 = 45 \text{ \AA}$ ,  $h = 12 \text{ \AA}$ ,  $x = 0.16$ ), that two electronic levels and two heavy hole levels are bound, however only a single light hole level (the symmetric one) is predicted to occur within the valence band barrier ( $V_p = 29.9 \text{ meV}$ ). The light hole resonance, which occurs in the continuum at  $4 \text{ meV}$  from  $V_p$  is calculated to be relatively narrow ( $5 \text{ meV}$ ). This resonant level is the continuation of the antisymmetric ( $AS_1$ ) light hole bound level after it has merged with the valence continuum. As the well width is increased ( $x$  and  $h$  being fixed),  $AS_1$  becomes bound for  $L_1 > 50 \text{ \AA}$ . Figure 2 shows the predicted behaviour of the bound and virtual hole states as a function of  $L_1$  for the system of interest ( $h = 12 \text{ \AA}$ ,  $x = 0.16$ ). The calculated level structure and the allowed transitions for ground state ( $n = 1$ ) electrons and holes are shown in Fig. 1b. Since the conduction and valence band edges have opposite parities, electric dipole optical transitions are allowed only between states with envelope functions having the same symmetries with respect to the midpoint of the central barrier.

Figure 3 shows the observed excitation and photoluminescence spectra at 2 and 40 K. A dye (LD 700) laser, pumped by the all-lines (red) output of a cw  $\text{Kr}^+$  laser, was used as a tunable excitation source. The photoluminescence was analysed with a  $1/4 \text{ m}$  monochromator and detected by a cooled photomultiplier (S1 photocathode) using conventional lock-in techniques. The calculated transition energies agree well with the energies of the excitation spectrum peaks and allow the immediate assignment of a specific transition to each peak (see Figs. 1b and 3). Peaks A, B and C correspond to transitions between bound elec-

tron and bound hole states. Peak D is assigned to an optical transition between a light hole virtual bound state (resonance) and the asymmetric electron state. We have varied the  $L_1$  and  $x$  parameters in the theoretical calculations over ranges greater than the growth error ranges of  $L_1$  ( $45 \pm 2.5 \text{ \AA}$ ) and  $x$  ( $0.16 \pm 0.02$ ) and we find that the light hole level of interest remains unbound. The peak assignments for the excitation spectrum were verified by circular polarization measurements of the photoluminescence signal (fixed energy) generated by circularly polarized excitation (scanned in energy) /6,7/.

At 2 K, the photoluminescence associated with the coupled wells consists of a single peak ( $\alpha$  - full width at half maximum :  $16 \text{ meV}$ ) shifted by  $13 \text{ meV}$  from the lowest energy peak (A) of the excitation spectrum. As the sample temperature is increased from 2 to 40 K, a second line ( $\beta$ ) appears in the photoluminescence spectrum on the high energy side of  $\alpha$ , separated from the latter by approximately  $10 \text{ meV}$ .  $\beta$  dominates  $\alpha$  in intensity for temperatures greater than about 30 K. Over the range of temperatures studied, the excitation spectra associated with peaks  $\alpha$  and  $\beta$  are identical, confirming that both peaks are associated with the double well structure. Circular polarization measurements of the photoluminescence indicate that both  $\alpha$  and  $\beta$  arise from the recombination of electrons with heavy holes.

The behaviour of the photoluminescence with increasing sample temperature suggests that one or both of the recombining states responsible for  $\alpha$  can be associated with a shallow trap ; the  $\beta$  luminescence is then interpreted as due to the recombination of free excitons. Under this hypothesis, the appearance of  $\beta$  is due to the thermal de-trapping of the trapped species. Work is continuing to test this hypothesis and identify the trap or binding centre associated with the  $\alpha$  luminescence.

#### References

- // R. Dingle, *Festschriftprobleme XV, Advances in Solid State Physics*, edited by H.J. Queisser (Pergamon/Vieweg, Braunschweig, 1975) p.21.

- /2/ R. Dingle, A.C. Gossard and W. Wiegmann, Phys. Rev. Lett. 34 (1975) 1327.  
 /3/ S. White and L. Sham, Phys. Rev. Lett. 47 (1981) 879.  
 /4/ G. Bastard, Phys. Rev. B 24 (1981) 5693.  
 /5/ R. Dingle, W. Wiegmann and C.H. Henry, Phys. Rev. Lett. 33 (1974) 827.  
 /6/ R.C. Miller, D.A. Kleinman, W.A. Norland, Jr. and A.C. Gossard, Phys. Rev. B 22 (1980) 863.  
 /7/ C. Weisbuch, R.C. Miller, R. Dingle, A.C. Gossard and W. Wiegmann, Solid State Commun. 37 (1981) 219.

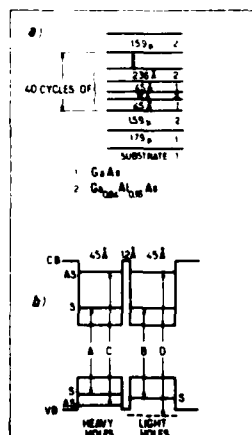


Figure 1 : (a) Schematic illustration of the sample structure. The 236 Å thick barriers which separate individual double well periods are sufficiently thick to prohibit inter-period tunneling. Details of sample growth are presented in Ref./5/.

(b) Schematic representation of calculated level structure and allowed transitions for ground state ( $n=1$ ) electrons and holes. The transition labels A, B, C and D refer to the excitation spectrum peak assignments (see Fig. 3). Symmetric and antisymmetric levels are labelled S and AS respectively. All hole levels continue across both wells - they are separated here simply for the sake of clarity. The hole resonance is indicated by a dashed line.

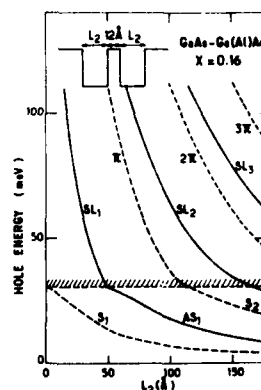


Figure 2 : Calculated energies for light hole bound and resonance states as a function of well thickness in the double well  $\text{GaAs-Ga}_{0.84}\text{Al}_{0.16}\text{As}$  system with  $h = 12 \text{ Å}$ . The hatched horizontal line indicates the valence continuum edge. Bound states are labelled according to symmetry, S : symmetric, AS : antisymmetric; subscripts indicate  $n$  values. Resonance states are labelled according to type, SL : superlattice (Eq.3) or pr : "single well" (Eq.2).

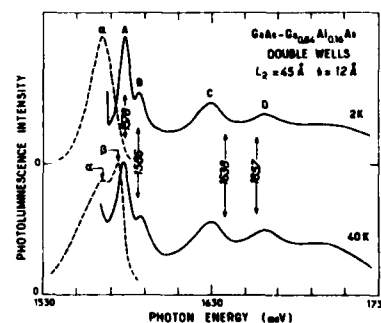


Figure 3 : Excitation (full line) and photoluminescence (broken line) spectra of the two-coupled-well sample at 2 and 40 K. The monochromator set energies were 1565 meV and 1555 meV for the 2 and 40 K excitation spectra respectively. The sharp rise in intensity below peak A is due to the coincidence of the dye laser and monochromator set energies. Theoretically predicted peak positions are indicated by arrows; calculated peak energies are given in meV. Both photoluminescence spectra were excited with 1630 meV light.



# Effects of Electron Heating on the Two-Dimensional Magnetotransport in GaAlAs/GaAs Heterostructures

H. Sakaki, K. Hirakawa, J. Yoshino, S.P. Svensson,<sup>44</sup>  
Y. Sekiguchi, T. Hotta, S. Nishi and N. Miura<sup>45</sup>

Institute of Industrial Science, University of Tokyo  
Institute for Solid State Physics, University of Tokyo<sup>4</sup>  
7-22-1 Roppongi, Minato-ku, Tokyo 106, Japan

Modulation doped AlGaAs/GaAs heterostructures are known to exhibit very high electron mobility at low temperatures. Hence, this system plays an important role in high-speed-device applications as well as in such fundamental studies as quantized Hall effect (QHE); this high mobility feature is effective in minimizing the Landau level broadening and provides an idealized condition for QHE. However, high-mobility electrons are easily accelerated by electric field and therefore one needs to clarify the effects of electron heating on various transport phenomena. In this work, we study at 4.2K both the Shubnikov-de Haas (SdH) effect and QHE at different current levels and show that

1. even a weak electric field ( $E_0 \sim 0.1 \text{ V/cm}$ ) heats up the electrons to a level where the resonant emission of optical phonons gets important, and also that
2. such a heating affects also the QHE and the appropriate choice of current level is important in maximizing the Hall voltage plateau width.

AlGaAs/GaAs heterojunctions studied here were grown by MBE and their mobilities are typically  $70,000 \text{ cm}^2/\text{Vs}$  at 10K. Figure 1 shows one example of SdH oscillations (solid lines) for two different electric fields  $E_0$ . If we assume that electron temperature  $T_e$  is determined by analyzing the damping of SdH oscillations,  $T_e$  is found to rise from 4.2K to 15K when the field  $E_0$  is raised only up to 1V/cm. One notices also in Fig.1 the appearance of an extra peak structure at  $B=12\text{T}$  when  $E_0$  is raised to 1.5V/cm. This extra peak can be ascribed to the resonant emission process of optical phonons  $\hbar\omega_{LO}$  between the two Landau levels, since such a peak appears always at  $12\text{T}$ , irrespective of samples with different electron concentrations. Moreover, its position ( $12\text{T}$ ) coincides with the position of the second harmonic peak ( $\hbar\omega_{LO} = 2\hbar\omega_{ac}$ ) of the magnetophonon resonance, which was observed at higher temperature, 173K (the broken curve in Fig.1). It is noteworthy that such a resonant phonon emission occurs even in the range of very low electron temperature ( $T_e \sim 15\text{K}$ ), where the electron mobility deviates only a very little from its low-field value.

Similarly, the electron heating was found to affect dramatically the QHE as shown in Fig.2. Note that the plateau width decreases when the current level exceeds  $2\mu\text{A/cm}$ . This results from the rise of electron temperature. When the current level is set too low ( $< 30\mu\text{A/cm}$ ), however, there appears on the edge of each plateau a peak-and-valley structure, suggesting the need of choosing the optimum current level for QHE measurement. Although the origin of this side structures is not clear at present, this suggests the complex nature of localization in this system.

<sup>44</sup> On leave from Dept. of Physics, Chalmers Univ. of Tech., Göteborg, Sweden

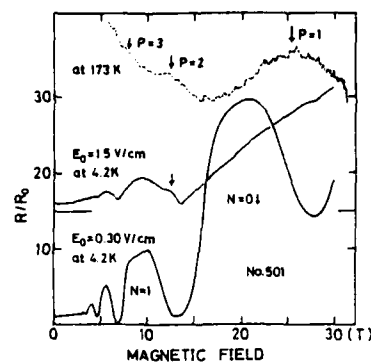


Fig.1 Electric field dependence of magnetoresistance at 4.2K (solid curves) and 173K (broken curve).

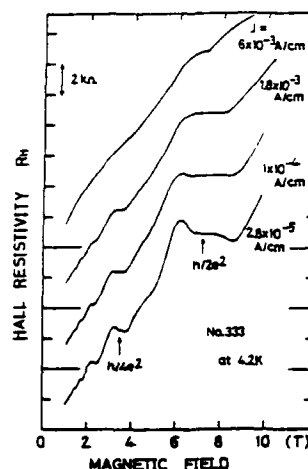


Fig.2 Electric field dependence of Quantized Hall Effect at 4.2K.

# NEGATIVE MAGNETORESISTANCE OF (100) n-Si-MOSFETS UNDER SUBSTRATE BIAS

W. Monlein and G. Landwehr

Max-Planck-Institut für Festkörperforschung, Hochfeld-Magnetlabor Grenoble, F-38042 Grenoble, and Physikalisches Institut der Universität Würzburg, D-8700 Würzburg.

**Abstract:** We have determined the inelastic scattering time  $\tau_c$  from magnetoconductance experiments as a function of substrate bias at a constant Fermi energy.  $\tau_c$  increases with small substrate biases but decreases at higher  $V_{sb}$ . The results are compared with the energy relaxation time  $\tau_r$  as a function of substrate bias.

It has been shown that the negative magnetoresistance in a two dimensional electron system can well be explained by a delocalization of weakly localized electrons as described by a theory developed by Altshuler et al. (1) and Hikami et al. (2) on the basis of Anderson localization and electron-electron interaction. Kawaguchi et al. (3) extracted the inelastic scattering time  $\tau_c$  by fitting the theory to the experimentally observed magnetoconductance in (100)-Si-MOSFETs. In this paper we describe the results of an investigation of the influence of a negative substrate bias on the magnetoconductance of a (100)-Si-MOSFET at a constant Fermi energy.

The application of a negative substrate bias enhances the depletion layer charge and squeezes the z-dependent part of the electron wave function. In addition the average distance  $\langle z \rangle$  of the electrons from the interface is decreased resulting in a reduced mobility  $\mu$ . It should be noted, that for substrate biases  $V_{sb}$  up to -14 V used in the present experiment  $\langle z \rangle$  was not larger than 0.1  $\mu m$  or 5 % of the average extension of the wave function. The sample under investigation had a length to width ratio of 8 with potential probes 100  $\mu m$  apart. Changes of the substrate bias were made at elevated

temperatures and were checked by monitoring the threshold voltage  $V_{th}$  as deduced from the Shubnikov-deHaas effect. The carrier density was held constant at  $N_s = 4.2 \cdot 10^{12} cm^{-2}$  by adjusting the gate voltage. The source drain field was kept well below 0.1 V/cm in order to avoid carrier heating.

Fig. 1 shows the magnetoconductance at two different temperatures. The lines represent the closest fit to the formula:

$$\Delta\sigma = \sigma(B) - \sigma(0) = -\frac{n_v a e^2}{2\pi\hbar} \left[ \psi\left(\frac{1}{2} + \frac{1}{8\tau}\right) - \psi\left(\frac{1}{2} + \frac{1}{8\tau_c}\right) - \ln \frac{\tau}{\tau_c} \right] \quad (1)$$

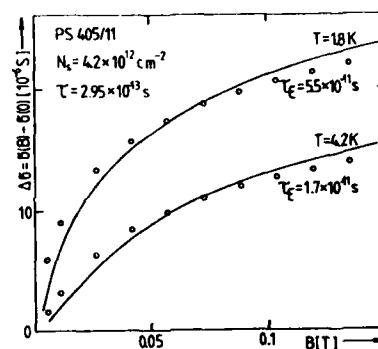


Fig. 1

as proposed by Hikami et al. (2). Here  $a = 4DeB/\hbar = \frac{4\mu_F B}{\hbar}$  with  $\mu$  = mobility,  $\epsilon_F$  = Fermi energy,  $B$  = magnetic field,  $\tau_c$  and  $\tau$  are the inelastic and elastic scattering times, respectively,  $\psi$  is the digamma function,  $n_v = 2$  = valley degeneracy, and  $\alpha$  is an empirical parameter depending on the spin orbit interaction, magnetic scattering, intervalley scattering and Coulomb interaction. Here we have chosen  $\alpha = 0.3$ . Although no perfect agreement between experiment and theory could be achieved, we extracted the inelastic scattering time  $\tau_c$ . This seems to be justified because the deviations were the same for all substrate biases. Thus the fitting procedure should at least yield reliable results for the relative change of  $\tau_c$  with substrate bias as shown in Fig. 2. At small values of the substrate bias  $\tau_c$  increases slightly for both  $T = 1.8$  K and 4.2 K. This result is in agreement with that obtained by Wheeler et al. (4) for higher mobility samples. At higher substrate biases  $\tau_c$  decreases for  $T = 1.8$  K and increases for  $T = 4.2$  K.

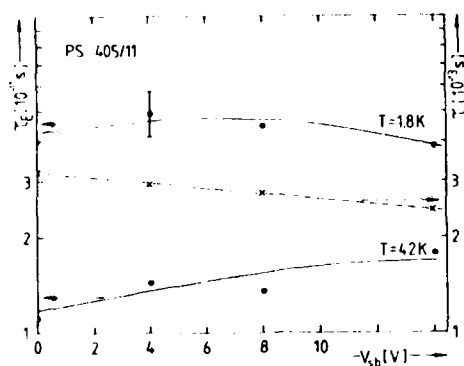


Fig. 2

nature of  $\tau_e$  we determined the energy relaxation time  $\tau_r$  from energy loss experiments under substrate bias at the same sample. If the electron temperature concept is valid,  $\tau_r$  is defined by

$$\frac{d\epsilon}{dt} = -\frac{1}{\tau_r} (\epsilon(T_C) - \epsilon(T)) = P \quad (2)$$

where  $d\epsilon/dt$  is the average energy loss of an electron per unit time,  $\epsilon(T)$  is the average electron energy and for  $k_B T \ll \epsilon_F$  we have

$$\epsilon(T) = \frac{\pi^2}{6} \frac{(k_B T)^2}{\epsilon_F} \quad (3)$$

We then can determine  $\tau_r$  to be

$$\tau_r = \frac{\pi^2 k_B^2}{6 \epsilon_F} (T_C + T) \frac{(T_C - T)}{P}$$

The determination of  $P$  is described elsewhere in detail (5). It should be noted that the  $T_C$  determination from the Shubnikov-deHaas effect yields consistent results with the  $T_C$  determination from the negative magnetoresistance effect under substrate bias.

In Fig. 3 we plotted  $\tau_r$  as a function of the substrate bias for two different

The broken line indicates the influence of an increased surface roughness scattering on the elastic scattering time  $\tau$  as deduced from the mobility. In order to get insight in the microscopic

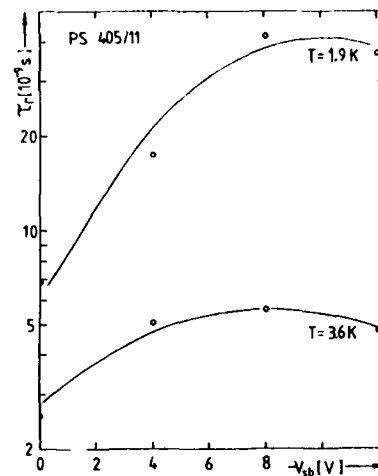


Fig. 3

lattice temperatures  $T$ . At low substrate biases  $\tau_r$  shows a considerable increase of nearly one decade for  $T=1.9$  K, reaching a maximum at approx.  $-8$  V and decreasing slightly for higher substrate biases. Fig. 4 shows the slopes of  $\tau_r - T^{-2}$ , indicating an increase of  $r$  from  $-1.5$  to  $-3$  at  $V_{sb} \approx -9$  V. For the substrate biases at the maximum both  $\tau_r$  and  $r$  are in good agreement with the surfon theory of electron-phonon scattering by Shinba et al. (6). However, at zero substrate bias both  $\tau_r$  and  $r$  are reduced. A detailed discussion of these results will be published elsewhere. In addition Fig. 4 shows the  $V_{sb}$  dependence of the slopes of  $\tau_e - T^{-2}$ . At  $V_{sb} = -14$  V  $p$  drops to  $-1$ , whereas at  $V_{sb} = 0$  V  $p = 1.5$  in agreement with results of Kawaguchi et al. (3). This completely different behaviour of the temperature dependence of  $\tau_r$  and  $\tau$  under substrate bias indicates, that the electron-phonon interaction is not the dominating inelastic scattering mechanism in the theory of weak localization in the temperature range of the present experiments. The reduction of  $p$  with increasing negative bias is, however, in agreement with the concept of e-e-scattering in a dirty 2D-system.

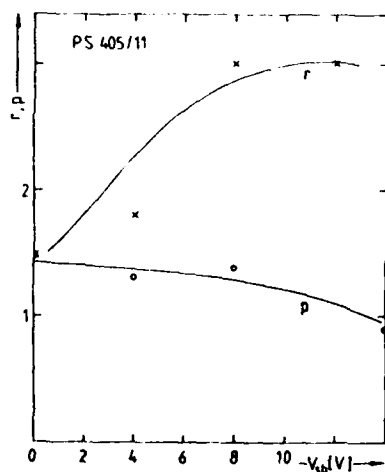


Fig. 4

#### References

- (1) B. L. Altshuler, D. Khmel'nitskii, A. I. Larkin and P. A. Lee, Phys. Rev. B 22 (1980) 5142.
- (2) S. Hikami, A. I. Larkin and Y. Nagaoka, Progr. Theoret. Phys. 63 (1980) 707.
- (3) Y. Kawaguchi and S. Kawaji, J. Phys. Soc. Japan 48 (1980) 699.
- (4) R. G. Wheeler, K. K. Choi, A. Goel, Surf. Sci. 113 (1982) 523.
- (5) W. Hönlein and G. Landwehr, Surf. Sci. 113 (1982) 260.
- (6) Y. Shinba, K. Nakamura, M. Fukuchi and M. Sakata, J. Phys. Soc. Japan 51 (1982) 157.

#### Figure Captions

Fig. 1: Magnetoconductance of a (100)-Si-MOSFET for two lattice temperatures  $T$ . The solid lines represent the closest fit of expression (1) with  $\alpha = 0.3$ .

Fig. 2: Substrate bias dependence of the inelastic scattering time  $\tau_e$  for two lattice temperatures  $T$  at a constant Fermi energy. The broken line indicates the substrate bias dependence of the elastic scattering time  $\tau$ .

Fig. 3: Substrate bias dependence of the energy relaxation time  $\tau_p$  for two lattice temperatures.

Fig. 4: Substrate bias dependence of the exponents  $p$  in  $\tau_e \sim T^{-p}$  and  $r$  in  $\tau_p \sim T^{-r}$ .

EFFECT OF MAGNETIC FIELD ON THE BINDING ENERGY OF A HYDROGENIC  
IMPURITY CENTER IN QUANTUM WELL STRUCTURES

Ronald L. Greene

Department of Physics, University of New Orleans, New Orleans, LA 70148, USA

and

K. K. Bajaj

Air Force Wright-Aeronautical Laboratories  
AFWAL/AADR, Wright-Patterson Air Force Base, Ohio 45433, USA

ABSTRACT

We report a first calculation of the binding energy ( $E_B$ ) of the ground state of a hydrogenic donor associated with the first subband in GaAs quantum well sandwiched between two semi-infinite layers of  $\text{Ga}_{1-x}\text{Al}_x\text{As}$  as a function of the potential barrier height (or equivalently of Al concentration  $x$ ) and the size of the quantum well in the presence of an arbitrary magnetic field. We assume, for the sake of illustration, that the positively charged impurity ion is located at the center of the well. Furthermore, the applied magnetic field is assumed to be parallel to the axis of growth. We follow a variational approach in which the trial wave function used is expanded in terms of an appropriate gaussian basis set. For a given value of  $x$  and a magnetic field we calculate the value of  $E_B$  as a function of the GaAs quantum well size ( $L$ ). As expected, we find that for a given value of the magnetic field,  $E_B$  is larger than its value in zero field. It is known<sup>(1)</sup> that for a given value of  $x$ , in a zero magnetic field,  $E_B$  increases as  $L$  is reduced till it reaches a maximum value and then drops to bulk  $\text{Ga}_{1-x}\text{Al}_x\text{As}$  value as  $L$  goes to zero. In the presence of a magnetic field we find essentially similar behavior except that the maximum value of  $E_B$  is larger and it takes place at a smaller value of  $L$ . The variation of  $E_B$  as a function of  $L$  for different values of  $x$  and of the magnetic field will be discussed. The relevance of our results to magneto-optical and magneto-transport phenomena in quantum well structures will be pointed out. The dependence of  $E_B$  on the location of the donor ion along the axis of growth will be mentioned.

1. Ronald L. Greene and K. K. Bajaj, Solid State Commun. 45, 825(1983)

# OPTICAL STUDIES OF SEMICONDUCTOR SUPERLATTICES

Paul Voisin

Groupe de Physique des Solides de l'Ecole Normale Supérieure  
24 rue Lhomond, 75231 Paris Cedex 05, France

## Abstract

We review here some of the most striking optical properties (basically absorption and luminescence) of both Type I and Type II superlattices built up from III-V semiconductor compounds.

## 1 - INTRODUCTION

Though superlattices (SL) were at first conceived (1) from the point of view of their transport properties along the growth axis, most of the interest has up to now been focused on their optical properties and on the quasi-two dimensional transport in the layers plane. In this paper, we shall review some of the most striking results obtained in studying the fundamental optical properties exhibited by undoped binary superlattices built up from III-V compounds. These structures consist in a periodic stacking of very thin alternate layers of two different - but closely lattice-matched - semiconductors A, B. The realization of such modulated structures with extremely sharp interfaces (having, ideally, a compositional discontinuity over one monolayer), has at first been allowed by the development of Molecular Beam Epitaxy (MBE) (2), but it is now established that near-atmospheric pressure epitaxy by Metal Organic Chemical Vapor Deposition (MOCVD) can also be used (3). In the x, y directions of the layers plane, the periodicity is a, the lattice parameter of A and B, while along the growth (z) axis, the period is the sum  $d = L_A + L_B$  of the A and B layers thicknesses. Thus the SL Brillouin zone has a "normal" extension  $2\pi/a$

in the x, y directions and a much smaller extension  $2\pi/d$  in the z direction. The potential in the superlattice is the sum of the potentials in the A and B materials and of a square wave shaped superpotential which arises from the electron affinity and bandgap difference between A and B. For the conduction band for example, the layers of one material - say A - form a series of square shape potential wells which confine the conduction states. The quantized confinement energies are of the order of :

$$E_n = n^2 \hbar^2 \pi^2 / 2m_A^* L_A^2 \quad (1)$$

To each of these quantized levels corresponds a two dimensional density of states  $m^*/\hbar^2$ . The associated wave functions are mainly localized in the A layers, with evanescent wings in the adjacent B layers. These potential wells are separated by the potential barriers formed by the layers of the B material. Tunneling of electrons through these potential barriers leads to the formation of subbands having small but finite widths, which are the SL conduction bands. Thus, superlattices present a duality of aspects, the quantum well aspect with its associated notions of quantized confinement energies, two dimensional densities of states and wave functions localization, and the superlattice aspect, with the strong anisotropy of the Brillouin zone and the resulting smallness of the bandwidths in the z direction. As for the superpotential associated with the valence band, the effective mass dependence in Eq.(1) shows that the degeneracy of the host  $\Gamma_6$  valence band is lifted in the SL, the heavy hole states having smaller confinement energies than the light hole states. Indeed, a more careful analysis (4) shows that the  $|3/2, \pm 3/2\rangle$  (heavy holes) and  $|3/2, \pm 1/2\rangle$  (light holes) states are strictly uncoupled at  $k_z = (k_x, k_y) = 0$ . This is no longer true for finite  $k_z$ . To our knowledge, the problem of the adequate hole masses with respect to the in-layer motion is actually not fully resolved, at least from the experimental point of view. Also, it is clear that two SL configurations may occur, as illustrated in Fig.1 :

- (i) Either the successive layers of the same material (say A) are

quantum wells for both conduction and valence states. This situation (Type I SL's) is met in the  $\text{Al}_{1-x}\text{Ga}_x\text{As}/\text{GaAs}$  system, by far the most studied. In a type II SL, both the electron and hole wave functions are localized in the A layers.

(ii) Or the layers of the A material confine the conduction band states while those of the B material confine the valence band states. InAs/GaSb SL's belong to this second category (Type II SL's). In such a structure, the electron and hole wave functions are spatially separated.

Up to now, most of the optical studies in type I systems have been performed on "multi-quantum well" (MQW) structures for which the superlattice aspect is of secondary importance. On the other hand, InAs/GaSb superlattices generally display conduction subband widths of a few tens of meV, and they present some three dimensional character.

In the next section, we compare the selection rules or interband transitions in Type I and Type II SL's, as obtained (5) in the envelope function description of these structures. Then we examine the informations obtained from optical absorption and excitation spectroscopy (section III) and the results of luminescence studies (section IV) in both types. Some other experiments are reviewed in section V.

## II - OPTICAL SELECTION RULES IN THE ENVELOPE FUNCTION APPROXIMATION

Consider two consecutive A, B layers, and let  $P_A$ ,  $P_B$  be the planes bisecting the A, B layers. The product  $R_B R_A$  of two reflections  $R_A$  and  $R_B$  with respect to  $P_A$  and  $P_B$  respectively is equal to a translation  $\tau_d$  of the SL period  $d = L_A + L_B$ . We are dealing with direct band gap III-V compounds and we assume that only the usual  $\Gamma_A$ ,  $\Gamma_B$  and  $\Gamma_d$  host band edges contribute significantly to the SL wave functions. In the envelope function scheme, the SL wavefunctions associated with the conduction (e) or valence (h) subbands of index n are written as :

$$\psi_{n,q,k_z}^{e,h}(\vec{r},t) = \frac{1}{\sqrt{S}} \sum_{\vec{r}} e^{i\vec{k}_\perp \cdot \vec{r}} U_{\vec{r}}(\vec{r}_\perp, z) f_{n,\nu,q,k_z}^{e,h}(z) \quad (2)$$

$\vec{r}_\perp$  and  $k_z$  are two-dimensional vectors in the layer planes of area S, and q is the SL wave vector in the z direction.  $U_{\vec{r}}$  is the periodic part of the  $\nu^{\text{th}}$  host Bloch function and  $f_{\vec{r}}$  is the associated envelope function, which is slowly varying at the scale of a.  $f_{\vec{r}}$  is solution of a 1d effective hamiltonian  $H_{\vec{r}}$ .

$R_A$ ,  $R_B$  and  $\tau_d$  commute with  $H_{\vec{r}}$  but not with each other. We have  $[R_B, R_A] = (\tau_d^2 - 1)\tau_d^{-1}$ ,  $[R_A, \tau_d] = R_B(\tau_d^2 - 1)$ , and  $[R_B, \tau_d] = (1 - \tau_d^2)R_A$ . In the Bloch representation, the  $f_{\vec{r}}$ 's are eigenfunctions of  $H_{\vec{r}}$  and  $\tau_d$ , with eigenvalues  $e_{n,q}^{e,h}$  and  $e^{iqd}$ , respectively. At  $q = 0$  and  $q = \pi/d$ , all these commutators vanish, and we can choose the Bloch envelope functions  $f_{\vec{r}}$  as eigenfunctions of  $R_A$  and  $R_B$ . The eigenvalues are  $\pm 1$ , corresponding to wave functions which are even or odd with respect to  $P_A$ ,  $P_B$ . Now, the relation  $R_B R_A f_{\nu,q} = e^{iqd} f_{\nu,q}$  shows that the parity with respect to the centers of one type of layers must be the same at  $q = 0$  and  $q = \pi/d$ , while the parity with respect to the centers of the other type of layers must be opposite at  $q = 0$  and  $q = \pi/d$ . This is easily seen in Table I. For an electromagnetic wave propagating parallel to the SL axis, the interband matrix element  $M_{nm}$  becomes, in this effective mass treatment, proportional to a sum of  $\rho_{\nu\nu'}$  optical matrix elements between the quickly varying functions  $U_{\vec{r}}$  multiplied by the overlap integrals between the slowly varying envelope functions :

$$M_{nm}(q, k_z) = \sum_{\nu, \nu'} \rho_{\nu\nu'} \int_{-d/2}^{+d/2} f_{\nu n q k_z}^{e,h} f_{\nu' m q k_z}^{e,h} dz \quad (3)$$

where we have made use of the wave vector conservation for interband transitions in any perfect solid. For transitions between the few low-lying subbands, and as long as non-parabolicity effects are not dramatic, only  $\nu \equiv$  conduction (S-like) and  $\nu' \equiv$  valence (P-like) come into play. For a heavy hole to conduction subband transition,  $\rho_{\nu\nu'}$  is then proportional to  $\frac{1}{\sqrt{2}} \langle S | p_x | X \rangle$ , while for transitions from a light hole subband,  $\rho_{\nu\nu'}$  will be  $\sqrt{3}$  smaller.

For type I systems, we assume that  $f_{n,q}^e$  and  $f_{m,q}^h$  retain the same sym-

symmetry with respect to  $P_A$  at both  $q = 0$  and  $q = \pi/d$ . Then, if the transition is parity-allowed at  $q = 0$  ( $n-m$  even), it will remain parity allowed at  $q = \pi/d$ , as illustrated in Fig. 1(a) for the ground wave function case  $n = m = 1$ . On the other hand, in a type II SL,  $f_{n,q}^e$  (resp.  $f_{m,q}^h$ ) is expected to retain the same parity with respect to  $P_A$  (resp.  $P_B$ ) at both  $q = 0$  and  $q = \pi/d$ . If the transition is parity allowed at  $q = 0$  (say that  $f_{n,q}^e$  and  $f_{m,q}^h$  are even with respect to  $P_A$ , like in Fig. 1(b)), then this transition becomes parity forbidden at  $q = \pi/d$  because in the integral in Eq. (3),  $f_{n,q}^e$  remains even with respect to  $P_A$  whereas  $f_{m,q}^h$  becomes odd with respect to the same plane. More generally, we find that in type I SL's,  $M_{nm}(q,k)$  almost does not depend on  $(k,q)$ , is parity-forbidden if  $n-m$  is odd, and parity-allowed if  $n-m$  is even, the  $n = m$  transitions being by far the most intense. In type II SL's, the interband matrix element depends strongly on  $q$ . The transitions which are parity-allowed at  $q = 0$  ( $n-m$  even) become parity-forbidden at  $q = \pi/d$ , and vice-versa. In a wide range of practical situations, we find :

$$M(q,k_x) = \frac{1}{2} [M(0,k_x) + (-1)^{n-m} \cos qd] \quad (4)$$

Note that transitions with  $n-m = 0$  or  $n-m \neq 0$  will a priori have comparable strengths, always small compared to that of a  $n = m$  transition in a type I SL. Finally, in the case of type II SL's, the selection rule relies basically on the phase coherence of at least one the Bloch envelope functions  $f_e$ ,  $f_h$ , and thus could be relaxed if both the conduction and valence subband widths become smaller than their scattering induced broadening. On the opposite, the selection rules for type I systems are essentially those of the isolated quantum well.

### III - OPTICAL ABSORPTION AND EXCITATION SPECTROSCOPY

One of the most striking evidence of the quantization of the energy levels in  $Al_{1-x}Ga_xAs/GaAs$  MQW's was obtained from optical absorption measurements (6,7). The transmission spectra exhibit a series of sharp exciton peaks

separated by absorption plateaus characteristic of the constant two-dimensional density of states (see Fig. 2). For very thin ( $< 200 \text{ \AA}$ ) layers, the first exciton peak is clearly splitted, which results from the difference between the heavy and light hole confinement energies. From fits of such data, the offsets of the hosts bands  $\Delta E_c$  and  $\Delta E_v$  were determined as  $\Delta E_c = 0.85 \Delta E_g$  and  $\Delta E_v = 0.15 \Delta E_g$ , where  $\Delta E_g$  is the difference between the band gaps of  $Al_xGa_{1-x}As$  and  $GaAs$  ( $\Delta E_g = 374 \text{ meV}$  for  $x = 0.3$ ). The small value of  $\Delta E_v$  is consistent with the prediction from the common anion argument (8). However, in the absence of a careful treatment of the heavy and light hole exciton, the accuracy of this determination is perhaps questionable. In particular, from the assignment of 2S excitons absorption, Miller et al (9) have recently concluded that the "light" hole exciton should have a slightly larger binding energy than the "heavy" hole exciton. Finally, the reported figures for the absorption coefficients (6) are in qualitative agreement with the calculated values (see below). Moreover, the parity selection rule (section II) seems fully obeyed since weak  $\Delta n = 2$  and no symmetry forbidden transitions are observed. Similar informations on the shape of the absorption coefficient are obtained from excitation spectroscopy. This technique was used (10) to determine the origin of the excitonic absorption linewidth. From their data, Weisbuch et al (10) concluded that this linewidth is governed by intralayer thickness fluctuations which appear to be essentially one monolayer in height and a few hundreds of  $\text{\AA}$  in lateral size.

Optical absorption measurements were also performed in  $InAs/GaSb$  superlattices grown by MBE (11,12). The very small absorption coefficients and the spectral position of the absorption edges clearly revealed the type II nature of these SL's and also the very original relative position of the hosts band edges. Indeed, the interpretation of the data shown in Fig. 3 implies that the  $InAs$  conduction band lies about 150 meV below the top of the  $GaSb$  valence band, as predicted from the comparison of the electron affinities. Two major consequences result from this situation : (i) the  $InAs$   $\Gamma_6$  conduction band always strongly interact with the  $GaSb$   $\Gamma_6$  light hole band, which is the very



reason for the "large" bandwidths in these SL's. (ii) The SL band gap (defined as the energy difference between the first conduction ( $E_1$ ) and heavy hole ( $HH_1$ ) subbands), which decreases with increasing layers thicknesses, reaches actually negative values when the sum of the electron and heavy hole confinement energies become smaller than 150 meV, which is the case for periodicities larger than 180 Å and equal layer thicknesses. The extrapolation of interband magnetooptical transitions towards negative energies (13-15) gave direct evidence of this configuration (Fig.4). The absorption spectra of semiconducting InAs/GaSb SL's shown (12) in Fig.3 exhibit step-like structures which are attributed to transitions between the various valence and conduction subbands. In agreement with the selection rules of section II, transitions with  $\Delta n = 0$  or  $\Delta n \neq 0$ , and  $\Delta n$  even or odd present equivalent strengths. Note also that the reported absorption coefficients are in good agreement with detailed calculations (15). The absence of exciton peaks in these spectra should not be regarded as an indication of poor sample quality. In fact, no excitonic effect should be expected in these structures, as the spatial separation of the carriers in a type II SL results in a drastic reduction of the binding energy of an electron-hole pair (16).

More recently, it was found that SL's with good crystalline quality can be grown from host materials with a rather important lattice mismatch (4a/a of a few percents) (17-19). Photocurrent spectroscopy was used to determine the energy gap of various strained layers SL's (18,19), but the reported data can hardly establish the two-dimensional character of these structures. We have investigated the optical absorption at low temperature in MBE grown GaSb/AlSb MQW's (20) where  $a/a_s = 0.65\%$ . These structures (21) consist of thin (50 to 200 Å) GaSb layers separated by thick (500 to 1000 Å) AlSb barriers. The transmission spectra shown in Fig.5 exhibit the step like behaviour characteristic of a two dimensional density of states, and from the series of absorption steps, it is clear that the involved conduction band states are those associated with quantized electron states in the GaSb layers. The intriguing

feature is that the absorption edges are observed at energies significantly smaller than those expected for simple GaSb quantum wells. However, the type I nature of this system is definitely established by the consideration of the order of magnitude of the absorption coefficients. For transitions between a heavy hole ( $HH_1$ ) and a conduction ( $E_j$ ) states, the band to band absorption coefficient on the two-dimensional plateau reads (5) :

$$K_{ij}(h\nu) = \frac{e^2}{4\pi\epsilon_0\epsilon_r^{1/2}m_0\hbar^2cv} \mu P^2 \frac{l_{ij}^2}{d} Y(h\nu - E_j - HH_1 - E_g) \quad (5)$$

where  $h\nu$  is the photon energy, and  $\mu$  the electron-hole reduced mass with respect to the in-layer motion.  $P$  is the Kane matrix element, whose value is  $2P^2/m_0 = 23$  eV.  $l_{ij}$  is the electron-hole wave functions overlap which, to a good approximation, is simply  $\delta_{ij}$  in the type I case, and has much smaller values in the type II case.  $E_g$  is the energy difference between the relevant band edges, from which the confinement energies  $E_j$  and  $HH_1$  are measured. The numerical estimates of Eq.(5) in the type I scheme together with the computation of the energy levels of the system (4) leads to an acceptable fit to our data, provided an effective bandgap  $E_g^{eff}$  about 50 meV smaller than that of bulk GaSb is introduced. This effect is interpreted by considering that the 0.65 % lattice mismatch is mostly accommodated by straining the thin GaSb layers, which stretch in the layer plane directions to conform with the thick AlSb layer lattice. Estimate of the bandgap shrinkage due to this biaxial tensile stress gives 50 meV, which compares favorably with the observed  $E_g^{GaSb} - E_g^{eff}$ .

#### IV - LUMINESCENCE

The luminescence of bulk GaAs is dominated by impurity effects, even for impurity concentrations below  $10^{15} \text{cm}^{-3}$ . In sharp contrast, the luminescence from GaAs/Al<sub>x</sub>Ga<sub>1-x</sub> MQW's usually present only one dominating line, eventually accompanied by a low energy tail and various small structures (7) (Fig.2). The line widths are often rather large ( $\geq 10$  meV) and essentially sample dependent. This description rules for the luminescence emitted along  $x$ . To our knowledge,

no systematic comparison of the luminescences emitted along  $z$  and perpendicular to  $z$  has been carried out though they should - and indeed seem to be (22,23) - different. Strong arguments have been presented (7), which support the interpretation of this main luminescence line in terms of intrinsic free excitons recombination inhomogeneously broadened by intralayer thickness fluctuations. Recent picosecond spectroscopy measurements (24) have brought further confirmation of this interpretation. The shoulder on the high energy side of the main peak (Fig.2) is attributed (7) to the recombination of light hole excitons. Recently, the low energy part of equivalent spectra was interpreted by Miller et al (25) in terms of conduction band-acceptor recombination. The problem of a coulombic center in a quantum well was studied theoretically by Bastard (26) for infinite depth wells. The effect of finite depth, which was included in recent studies (27,28), does not alter significantly the practical conclusions of Ref.26 for acceptors. A systematic search for impurity effects has been reported by Miller et al (25), who concluded to a good agreement with Bastard's calculations. Somewhat different spectra reported by Lambert et al (29) also show a close agreement with this theory.

The temperature dependence of the luminescence spectrum of a  $27 \text{ \AA} / 44 \text{ \AA}$  semiconductor InAs/GaSb SL is shown in Fig.6. The luminescence consists of a main line accompanied by a low energy tail which tends to saturate with increasing excitation level (15,30). The high energy side of this line reflects the increasing carrier temperature as the lattice temperature is increased. The position of the line at low temperature is in close agreement with the calculated band gap. All these observations support the interpretation in terms of band to band recombination. Further confirmation is obtained from the analysis of the lineshapes (15). The fit of the  $T = 300 \text{ K}$  data is shown in Fig.7(a). The theoretical lineshape is rather sensitive to the conduction band width  $\Delta E_c$ , as well as to the influence of the interband optical matrix element, as shown in Fig.7(b). From the fit we deduce  $\Delta E_c = 60 \pm 15 \text{ meV}$ , in close agreement with the calculated value. The effective carrier temperature of  $370 \text{ K}$

should be regarded as indicative only, since non-parabolicity was not included in the lineshape calculations. At low temperatures, the fits (15) clearly exhibit a hot electron effect, as often observed in small gap materials, especially when the excitation energy is far above the band gap, which was actually the case. In our experiments, the effective carrier temperature is found to be in the range of  $50 \text{ K}$  and to increase slightly with the excitation level. At low excitation, a low energy tail develops and at intermediate temperatures forms sometimes a distinct shoulder at  $\sim 35 \text{ meV}$  below the band gap. In our system, the acceptors in the  $p$ -type GaSb layers ( $N_A - N_D \sim 10^{14} \text{ cm}^{-3}$ ) are expected to give an energy band extending from  $16$  to  $32 \text{ meV}$  above  $HH_1$  (26,30) while two monolayers fluctuations of the InAs layers thickness should give rise to a continuum of states extending up to  $40 \text{ meV}$  below  $E_1$  (4). Donors in the InAs layers (which are  $n$ -type) and GaSb layers fluctuations would give bound levels with binding energies of  $\sim 4 \text{ meV}$  and  $\sim 6 \text{ meV}$ , respectively. No attempt was made to fit the low energy part of the spectra since such a work requires extensive information on the densities of states, optical matrix elements, etc..., which are not experimentally available.

Various data on the luminescence of GaSb/AlSb superlattices have been reported (31,32). In recent investigations of high quality samples, we observed at low temperature a luminescence line centered  $30$  to  $40 \text{ meV}$  below the exciton peak seen in absorption. Its width ( $20$  to  $40 \text{ meV}$ ) increases with decreasing GaSb layer thicknesses. Luminescence is likely to arise from conduction band to acceptor recombination, this interpretation being consistent with the  $p$ -type ( $N_A - N_D \sim \text{a few } 10^{14} \text{ cm}^{-3}$ ) nature of the layers.

#### V - OTHER STUDIES

Numerous studies of other optical properties of SL's or MQW's have been reported, which cannot be extensively discussed here. The early study of the wavelength dependence of the intensity of resonant Raman scattering by LO phonons in GaAs MQW's (33) have provided information on the two-dimensional

density of states and level quantization. Resonant inelastic light scattering techniques have been extensively used to determine both single particle and collective excitations in modulation doped GaSb/Al<sub>x</sub>Ga<sub>1-x</sub>As MQW's (34). Various effects of an external electric field on the optical properties of GaAs/Al<sub>x</sub>Ga<sub>1-x</sub>As MQW's have been reported. Mendez et al (35) have observed a red shift and a strong quenching of the luminescence when an electric field of a few  $10^5$  V cm<sup>-1</sup> is applied parallel to z. The first effect is qualitatively understood while the other does not seem to be explained. Recently, Chenla et al (36) have reported a ~ 10 meV red shift of the 300 K excitonic absorption when an electric field ( $\sim 1.6 \cdot 10^5$  V cm<sup>-1</sup>) is applied in the layer plane, which is attributed to a Stark excitonic effect.

#### Conclusion

The study of the optical properties (basically absorption and luminescence) of various SL systems have certainly brought the most precise information on their electronic properties, which present indeed a variety of original phenomena. However, despite the considerable number of works devoted to optical studies of superlattices, some fundamental questions are still unresolved. Among them, we will quote the considerable enhancement of intrinsic recombination in GaAs/Al<sub>x</sub>Ga<sub>1-x</sub>As MQW's with respect to bulk materials and the problem of the valence band dispersion relations in the layer plane. It is therefore clear that additional optical investigations would certainly be helpful.

#### Acknowledgements

L.L. Chang, L. Esaki, C. Weisbuch and their respective co-workers are thanked for the kind authorization of reproducing some figures from their original publications, and for helpful conversations. I am also indebted to M. Voos and C. Bastard for a number of valuable discussions.

#### References

\* Laboratoire associé au CNRS.

- (1) L. Esaki and R. Tsu, IBM J. Res. Dev. **14**, 61 (1970).
- (2) See for example A. Cho, NATO School on MBE and Heterostructures, Erice (Italy), March 1983, to be published (Martinus Nijhoff Publishers, The Netherlands).
- (3) R.D. Dupuis, P.D. Daphus, M. Holonyak and R.M. Kolbas, Appl. Phys. Lett. **35**, 487 (1979); P.M. Frijlink and J. Maluenda, Japan. J. Appl. Phys. L **21**, 574 (1982); Y. Guldner, J.P. Vieren, P. Voisin, M. Voos, M. Razeghi and H.A. Poisson, Appl. Phys. Lett. **40**, 877 (1982).
- (4) G. Bastard, Phys. Rev. B **24**, 5693 (1981), B **25**, 7584 (1982); see also G. Bastard, in Ref.2.
- (5) P. Voisin, G. Bastard and M. Voos, to be published in Phys. Rev. B (1983).
- (6) R. Dingle, W. Wiegmann and C.H. Henry, Phys. Rev. Lett. **33**, 827 (1974); R. Dingle in Festkörperprobleme XV - Advances in Solid State Phys., Ed. H.J. Queisser (Pergamon Vieweg 1975), p.21.
- (7) C. Weisbuch, R.C. Miller, R. Dingle, A.C. Gossard and W. Wiegmann, Solid State Comm. **37**, 219 (1981).
- (8) W.A. Harrison, J. Vac. Sci. Technol. **14**, 1016 (1977).
- (9) R.C. Miller, D.A. Kleinman, W.T. Tsang and A.C. Gossard, Phys. Rev. B **24**, 1134 (1981); see also R.L. Greene and K.K. Bajaj, Solid State Comm. **45**, 831 (1983).
- (10) C. Weisbuch, R. Dingle, A.C. Gossard and W. Wiegmann, Solid State Comm. **38**, 709 (1981).
- (11) G.A. Sai-Maleas, L.L. Chang, J.M. Welter, C.A. Chang and L. Esaki, Solid State Comm. **27**, 935 (1978).
- (12) L.L. Chang, G.A. Sai-Maleas, L. Esaki and R.L. Aggarwal, J. Vac. Sci. Technol. **19**, 389 (1981).
- (13) Y. Guldner, J.P. Vieren, P. Voisin, M. Voos, L.L. Chang and L. Esaki, Phys. Rev. Lett. **45**, 1719 (1980).

- (14) J.C. Maan, Y. Guldner, J.P. Vieren, P. Voisin, M. Voos, L.L. Chang and L. Esaki, Solid State Comm. 39, 683 (1981).
- (15) P. Voisin, Thèse de Doctorat d'Etat, Orsay, May 1983.
- (16) G. Bastard, Phys. Rev. B 26, 1974 (1982).
- (17) J.W. Matthews and A.E. Blakeslee, J. Cryst. Growth 29, 73 (1975) and 32, 265 (1976).
- (18) I.J. Fritz, R.M. Biefeld and G.C. Osbourn, Solid State Comm. 45, 323 (1983).
- (19) I.J. Fritz, L.R. Dawson and T.E. Zipperian, J. Vac. Sci. Technol. B1(2), 387 (1983).
- (20) C.A. Chang, H. Takaoka, L.L. Chang and L. Esaki, Appl. Phys. Lett. 40, 983 (1982).
- (21) P. Voisin, G. Bastard, M. Voos, F.E. Mendez, C-A Chang, L.L. Chang and L. Esaki, J. Vac. Sci. Technol. B1(2), 409 (1983).
- (22) N. Holonyak, W.D. Laidig, B.A. Vojak, H. Hesse, J.J. Coleman, P.D. Dapkus and J. Bardeen, Phys. Rev. Lett. 45, 1703 (1980).
- (23) R.C. Miller, C. Weisbuch and A.C. Gossard, Phys. Rev. Lett. 46, 1042 (1981).
- (24) J. Hegarty, M.D. Sturge, C. Weisbuch, A.C. Gossard and W. Wiegmann, Phys. Rev. Lett. 49, 930 (1982).
- (25) R.C. Miller, A.C. Gossard, W.T. Tsang and O. Munteanu, Phys. Rev. B 25, 3871 (1982).
- (26) G. Bastard, Phys. Rev. B 24, 4714 (1981).
- (27) R.L. Greene and K.K. Bajaj, Solid State Comm. 45, 825 (1983).
- (28) C. Mailhot, Y.C. Chang and T.C. McGill, Phys. Rev. B 26, 4449 (1982).
- (29) B. Lambert, B. Deveaud, A. Regreny and G. Talalaeff, Solid State Comm. 43, 443 (1982).
- (30) P. Voisin, G. Bastard, C.E.T. Gonçalves da Silva, M. Voos, L.L. Chang and L. Esaki, Solid State Comm. 39, 79 (1981).

- (31) N. Naganuma, Y. Suzuki and N. Okamoto, Int. Symp. GaAs Related Compounds, Oiso (1981); Inst. Phys. Conf. Series 63, 125 (1981).
- (32) E.E. Mendez, C-A. Chang, H. Takaoka, L.L. Chang and L. Esaki, J. Vac. Sci. B1(2), 152 (1983).
- (33) P. Manuel, C.A. Sai-Halasz, L.L. Chang, C-A. Chang and L. Esaki, Phys. Rev. Lett. 37, 1701 (1976).
- (34) A. Pinczuk and J.M. Worlock, Proc. 16<sup>th</sup> Int. Conf. Phys. Semicond., (Ed. by M. Averous, North Holland, 1983), p.637.
- (35) E.E. Mendez, G. Bastard, L.L. Chang and L. Esaki, Phys. Rev. B 26, 7101 (1982).
- (36) D.S. Chemla, T.C. Damen, D.A.B. Miller, A.C. Gossard and W. Wiegman, Appl. Phys. Lett. 42, 864 (1983).

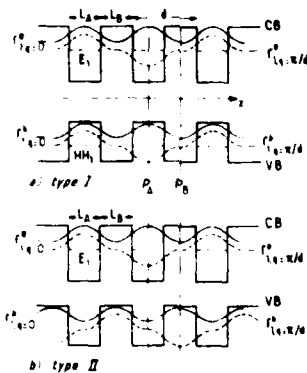


Fig. 1 : Schematic band diagram and envelope functions of the ground states at  $q = 0$  and  $q = \pi/d$  for (a) type I and (b) type II SL's.

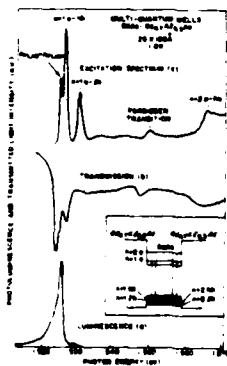


Fig. 2 : Photoluminescence (a) absorption (b) and excitation spectra (c) in 188 Å thick GaAs quantum wells (from Ref. 7).

	$R_A$	$R_B$
$q=0$ ( $R_B R_A = 1$ )	$+1$	$+1$
$q=\pi/d$ ( $R_B R_A = -1$ )	$-1$	$-1$

Table I : truth table of the parity statement

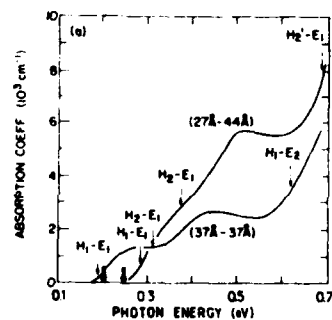


Fig. 3 : Absorption spectra of two InAs/GaSb semiconductor superlattices (from Ref. 12).

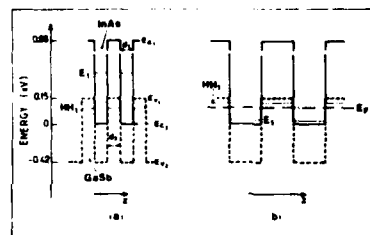


Fig. 4 : Schematic band diagram and semiconductor (a) to semimetal (b) transition in InAs/GaSb superlattices

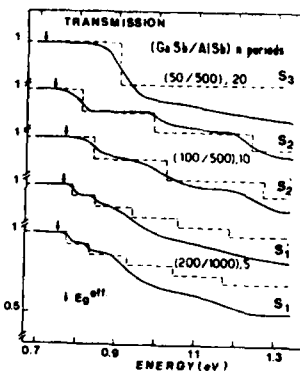


Fig. 5 : Transmission spectra of GaSb/AlSb MQW's. The sample  $S_1$  and  $S_2$  belong to a different series of growths (from Ref. 21).

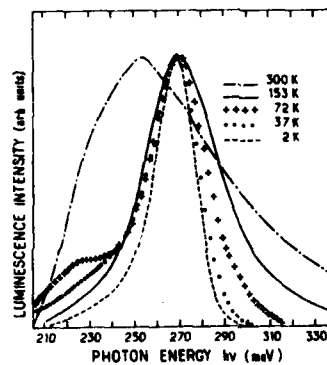


Fig. 6 : Temperature dependence of the luminescence spectrum of a 27 Å/44 Å InAs/GaSb SL, in the "high" excitation level regime (from Ref. 30).

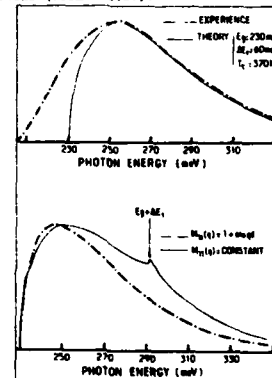


Fig. 7 : (a) Fit of the room temperature spectra of Fig. 6. (b) Influence of the optical matrix element  $M(q)$  on the theoretical lineshape.

Landau levels and Magneto-optics of  
Semiconductor Superlattices

A. Fasolino and M. Altarelli

Max-Planck-Institut für Festkörperforschung,  
D-7000 Stuttgart 80,  
Federal Republic of Germany

and

Max-Planck-Institut für Festkörperforschung,  
Hochfeld-Magnetlabor, B.P. 166X  
F-38042 Grenoble Cedex, France

Abstract

The many-band envelope-function approximation to the band structure of semiconductor superlattices is extended to include an external magnetic field perpendicular to the layers. The Landau level structure for InAs-GaSb superlattices is computed, with emphasis on the "semimetallic" range of layer thicknesses etc. The Landau levels display striking deviations from linear behavior as function of the field. The theoretical results compare favourably with magneto-optical experiments in the far infrared.

There has been much interest on the electronic properties of type-II semiconductor superlattices, like InAs-GaSb. Experiments [1-2] indicate a semimetallic state for periods  $d \approx 180 \text{ \AA}$ , when the lowest conduction-like subband sinks through the highest heavy-hole-like subband. However, calculations in the many-band envelope-function approximation predict small hybridization gaps (1-10 meV) throughout the Brillouin zone, therefore ascribing the observed semimetallic behavior to extrinsic effects [3].

Most information about these systems comes from magneto-optical experiments [2,4]. In order to compare these experi-

ments with theory, however, it is necessary to calculate the Landau levels in detail. In fact, it becomes clear by considering a simple model of two coupled bands with opposite curvature, that the hybridized bands are strongly non-parabolic, and therefore that a free-electron-like linear behavior of the Landau levels in the magnetic field cannot be expected. Consider indeed the band structure given for  $k$  in the  $(x,y)$  plane by the following matrix

$$H(k) = \begin{bmatrix} \Delta/2 - \alpha k^2 & P(k_x + ik_y) \\ P(k_x - ik_y) & -\Delta/2 + \beta k^2 \end{bmatrix} \quad (1)$$

in which a hole-like band is an energy  $\Delta$  above a conduction-like one, the two being coupled by a  $k \cdot p$  term with matrix element  $P$ . Adding a field  $B$  in the  $z$  direction, one obtains solutions in terms of harmonic oscillator eigenfunctions of the form  $(c_1 \psi_n, c_2 \psi_{n-1})$  where  $c_2 = 0$  for  $n = 0$  and  $c_1, c_2 \neq 0$  for  $n = 1, 2, \dots$ . The eigenvalues as function of the field are sketched in fig. 1. The band coupling introduces strong deviations from linearity for all Landau levels except the  $n = 0$ , which is purely hole-like. This simple model provides good qualitative insight for the realistic calculations described in the following.

We represent each constituent with a six-band model, i.e. the spin-up and spin-down s-like conduction-band, and the fourfold  $j = 3/2$  valence-band set split into heavy-hole and light-hole bands at  $k \neq 0$ . The split-off  $j=1/2$  bands are not explicitly included, but their contribution to conduction band mass and g-factor is introduced, following Roth et al. [5]. We modify the method of Ref. [3], to include an external magnetic field along  $z$ , the growth

axis of the superlattice. This is achieved by (a) replacing  $\vec{k}$  by  $\vec{k} - (e/c) \vec{A}$  in the Hamiltonian of each constituent; (b) adding a spin-dependent term to the conducting band diagonal elements, which become:

$$H_{cc} = \epsilon_c + \frac{1}{2m^*} (\vec{k} - (e/c) \vec{A})^2 + \frac{g^*}{2mc} \vec{\sigma} \cdot \vec{B} \quad (2)$$

where

$$1/m^* = (1/m) (1 + \frac{2P^2}{3m(E_c - E_v + \Delta)}), \quad g^* = 2 - \frac{m}{m^*} \quad (3)$$

and  $\Delta$  is the spin-orbit splitting; (c) introducing the additional valence-band terms proportional to the parameter  $x$ , as shown by Luttinger [6] (the other parameter  $q$  is very small and is neglected). It is then no longer possible to decouple the  $6 \times 6$  system into "spin-up" and "spin-down" levels. Furthermore, the new  $\vec{k}$ -dependent terms (step (a) modify the current operator and therefore the boundary conditions at the interfaces [3]). The motion parallel to the layers is described by a six-component eigenvector:

$$\vec{\psi}_n = (c_1 \psi_n, c_2 \psi_{n-1}, c_3 \psi_{n+1}, c_4 \psi_n, c_5 \psi_n, c_6 \psi_{n+2}) \quad (4)$$

with  $n = -2, -1, 0, 1, \dots$  and vanishing coefficients for  $n < -1$  for components with negative oscillator index.

Numerical calculations for InAs-GaSb were performed using the band parameters obtained in Ref. [7-8] by bulk experiments, and an energy step of 0.150 eV between the bottom of the InAs conduction band and the top of the GaSb valence band [1]. The results presented here are obtained in the flat-band approximation. In Fig. 2, we compare the computed cyclotron resonance transition energy of an n-type semiconducting superlattice with  $d_{\text{InAs}} = 65 \text{ \AA}$ ,

$d_{\text{GaSb}} = 80 \text{ \AA}$  with experiment [2]. The good agreement could not be obtained without the split-off band correction to the electron mass, Eq. (3).

Turning to  $d > 180 \text{ \AA}$  superlattices, we show in Fig. 3 the Landau levels of a  $d_{\text{InAs}} = 120 \text{ \AA}$ ,  $d_{\text{GaSb}} = 80 \text{ \AA}$  superlattice at the zone center ( $k_z = 0$ ) and at the zone boundary ( $k_z = \pi/d$ ). Notice the qualitative similarity to the simple model of Fig. 1 for  $k_z = 0$ , and the prominent deviations from the linear behavior of the Landau levels previously assumed to interpret the magneto-optical spectrum of this system [4].

In Fig. 4 we compare the computed transition energies, compatible with the selection rule  $\Delta n = \pm 1$ ,  $\Delta k_z = 0$ , and with a Fermi-level position corresponding to a slight n-type doping, with experiments [4] for the same superlattice. The agreement is quite good, in view of the absence of adjustable parameters and of the flat-band approximation. Notice that the theory accounts for the deviation from linearity of the transition beginning just above 6T, and that transitions between high  $n$  Landau levels tend to fall on top of one another in the low  $B$  region, to form the strong transition indicated as electron cyclotron resonance in Ref. [4]. The experimental points in the low  $B$ , high  $E$  region correspond in our picture to transitions across the gap visible in Fig. 3 (a), which is particularly sensitive to the flat-band approximation.

In conclusion, the agreement is encouraging and provides support to the results of the calculations at zero field and to the conclusions drawn from them.

Further comparison of theory and magneto-optical experiments for other samples is in progress.

# References

- [1] See e.g. L.L.Chang, J.Phys.Soc.Japan 49, Suppl.A,997(1980)
- [2] J.C. Maan, in: Infrared and millimeter Waves, (Ed.K.J. Button (Academic, New York, 1983) vol.8 p.387 and references therein
- [3] M. Altarelli, Phys. Rev. B 28, in press (1983)
- [4] J.C. Maan, Y. Guldner, J.P. Vieren, P. Voisin, M. Voos, L.L.Chang and L. Esaki, Solid State Commun. 39, 683 (1981)
- [5] L.M. Roth, B. Lax and S. Zwerdling, Phys. Rev. 114, 90 (1959)
- [6] J.M. Luttinger, Phys. Rev. 102, 1030 (1956)
- [7] C.R. Pidgeon, D.L. Mitchell and R.N. Brown, Phys. Rev. 154, 737 (1967)
- [8] K. Suzuki and N. Miura, J.Phys.Soc.Japan 39, 148 (1975)

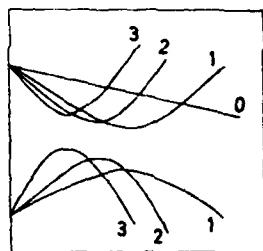


Fig. 1  
Energy level vs magnetic field for a two-band model with k.p interaction. The quantum number  $n$  (see text) are indicated

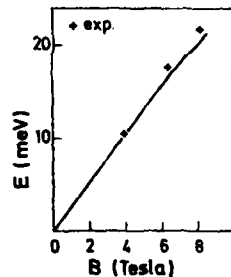


Fig. 2  
Computed transition energy for a  $d = 65 + 80 \text{ Å}$  InAs-GaSb superlattice (solid line). Experimental points are shown by crosses.

Fig. 3  
Landau levels of an InAs-GaSb superlattice for  $d = 120 + 80 \text{ Å}$ . (a)  $k_z = 0$ , (b)  $k_z = \pi/d$ . The quantum number  $n$  is indicated (see text).

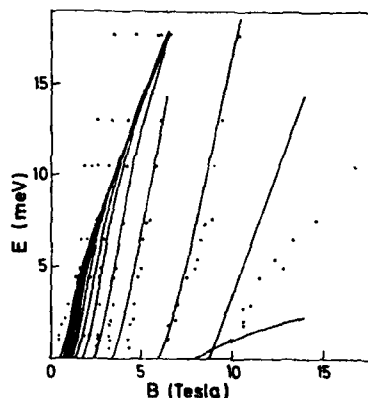
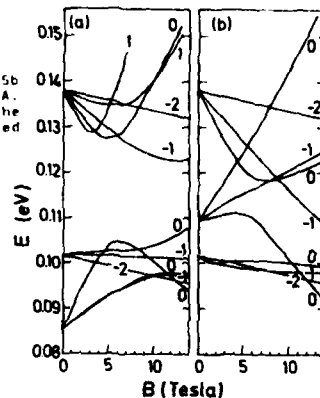


Fig. 4  
Solid lines: predicted optical transition energies for an n-type InAs-GaSb superlattice with  $d = 120 + 80 \text{ Å}$  as a function of magnetic field. Dots: experimental transition energies (from Ref. [4]).



SELF CONSISTENT VARIATIONAL CALCULATIONS AND ALLOY SCATTERING  
IN SEMICONDUCTOR HETEROJUNCTIONS

G. Bastard

Groupe de Physique des Solides de l'Ecole Normale Supérieure\*  
24 rue Lhomond, 75231 Paris Cedex 05, France

Abstract

We report the results of self consistent variational calculations for the ground and first excited states of semiconductor heterojunctions. The calculations have been performed for the electric quantum limit in the Hartree approximation and applied to the Ga(Al)As-GaAs and InP-In(Ga)As modulation doped heterostructures. Charge transfers from the doped barrier to the conducting channel are discussed. The alloy scattering for InP-In(Ga)As heterojunctions is calculated to limit the channel mobility to  $3 \times 10^5 \text{ cm}^2/\text{Vs}$  if the bulk value ( $0.6 \text{ eV}$ ) for the strength of the alloy potential is retained.

There exist two kinds of lattice-matched modulation doped heterojunctions (M.D.H.J.): the conducting channel can be primarily located within a binary semiconductor (e.g. the Ga(Al)As-GaAs M.D.H.J.'s) or within a ternary random alloy (e.g. InP-In(Ga)As M.D.H.J.'s). The low temperature mobility of Ga(Al)As-GaAs M.D.H.J. can be very high (in excess of  $10^6 \text{ cm}^2/\text{Vs}$ ) whereas up to now InP-In(Ga)As M.D.H.J.'s have shown mobility lower than  $10^5 \text{ cm}^2/\text{Vs}$ . It may be of interest to scrutinize whether alloy disorder, the basic difference between InP-In(Ga)As and Ga(Al)As-GaAs M.D.H.J.'s, can be an efficient scattering mechanism.

We need first to calculate the wavefunctions  $\chi_1, \chi_2$ , bound states energies  $E_1, E_2$  of the ground and first excited two-dimensional subbands which are formed between the interface and the self consistent electrostatic potential. Recently, Stern /1/ and Ando /2/ have solved this problem numerically within the Hartree and density functional approximations respectively. Here we present the results of a variational self consistent treatment performed for the Electric Quantum Limit in the Hartree approximation. We have generalized Fang and Howard wavefunctions /3/ to allow the penetration of the  $\chi$ 's in the barrier of finite height  $V_b$ .

\* Laboratoire associé au Centre National de la Recherche Scientifique

$$\chi_1(x) = \begin{cases} M_1 \exp(\kappa_1 x/2) & ; x < 0 \\ N_1 (x+a_0) \exp(-bx/2) & ; x > 0 \end{cases} \quad \chi_2(x) = \begin{cases} M_2 \exp(\kappa_2 x/2) & ; x < 0 \\ N_2 (x+a_0) \exp(-cx/2) & ; x > 0 \end{cases} \quad (1)$$

In addition to (1) and Poisson equation, the electrostatic potential is prescribed:

$$(N_d - N_A) \epsilon_d = N_A \omega + n_s + N_{dep} \quad (2)$$

where  $N_{dep} = n_s \epsilon_d$  is the depletion charge in the channel,  $\epsilon_d$  the acceptor depletion length,  $n_s$  the 2D sheet carrier concentration,  $N_d$  the volume concentrations of donors (Si in Ga(Al)As) and  $N_A(n_s)$  residual acceptor concentrations in the barrier (channel).  $\omega$  is the width of the spacer layer (non-intentionally doped) which is inserted between the doped part of the barrier and the 2D gas to enhance mobility. At thermal equilibrium, the chemical potential  $\mu$  is constant throughout the whole structure. At  $T = 0$ , in the EQL, we have therefore:

$$E_1 + \frac{\pi^2 n_s^2}{6} = V_b - \epsilon_b - \frac{2\pi e^2}{\kappa} (n_s + N_A \omega + N_{dep}) \left[ 2\omega + \frac{(n_s + N_A \omega + N_{dep})}{N_d - N_A} \right] + \frac{2\pi e^2}{\kappa} N_A \omega^2 + \frac{4\pi e^2}{\kappa} n_s \frac{M_1^2}{K_1^2} = \mu \quad (3)$$

In (3),  $\epsilon_b$  is the donor binding energy in the barrier and  $\kappa$  the relative dielectric constant assumed to be the same in both semiconductors. Since the wavefunction marginally leaks into the barrier, we can decouple the Poisson + Schrödinger equations from the electrical neutrality + thermal equilibrium conditions (2,3): the penetration of the  $\chi_1$  wavefunction is so small that no overlap practically exists between the 2D gas electron states and the bound donor states, substantiating the concept of donor depletion length. For the same reason, the exact shape of the electrostatic potential within the barrier will not influence the  $E_1$  binding energy. Therefore, we can first solve the Schrödinger and Poisson equations for a given  $n_s$  neglecting (2-3). In a second step, knowing the functional dependence  $E_1(n_s)$  we will determine the equilibrium  $n_s$  satisfying (2,3) for a specified heterostructure geometry ( $N_d, N_A, \omega$ ). The acceptor depletion length  $\epsilon_d$  has been approximated by  $(\kappa E_g / 2\pi e^2 n_s)^{1/2}$  where  $E_g$  is the bandgap of the well-acting material.

Despite the small wavefunction penetration in the barrier, the finiteness of  $V_b$  considerably lowers  $E_1$  with respect to the value  $E_1^\infty$  obtained for the same  $n_s$  but infinite  $V_b$ . For instance, consider a Ga(Al)As-GaAs H.J. with

$V_b = 0.3$  eV,  $m_{GaAs} = 0.07 m_0$ ,  $m_{Ga(Al)As} = 0.088 m_0$ ,  $\bar{x} = 13$ . Let  $P_b = \int_0^d \chi_1^2(x) dx$  be the integrated probability density for the electron to be in the barrier. We have found  $P_b = 1.15\%$ ;  $E_1 = 51.8$  meV;  $E_2 = 64.9$  meV for  $n_e = 5 \times 10^{11} \text{ cm}^{-2}$  and  $N_{dep} = 0.46 \times 10^{11} \text{ cm}^{-2}$ . These values are in good agreement with Stern's results [1] who found  $P_b = 1.11\%$ ;  $E_1 = 51.9$  meV and  $E_2 = 63.63$  meV for the same material parameters.  $E_1$  is affected by  $N_{dep}$ . For the H.J. under consideration and  $n_e = 4 \times 10^{11} \text{ cm}^{-2}$ ,  $E_1$  increases from 43 meV to 50.5 meV when  $N_{dep}$  increases from  $0.46 \times 10^{11} \text{ cm}^{-2}$  ( $n_a = 10^{18} \text{ cm}^{-3}$ ) to  $1.38 \times 10^{11} \text{ cm}^{-2}$  ( $n_a = 9 \times 10^{18} \text{ cm}^{-3}$ ). The residual acceptor concentration in the channel more severely affects the energy position of the first excited subband  $E_2$ , assumed to be empty in the E.Q.L. This is expected since  $\chi_2$  is orthogonal to  $\chi_1$  and therefore is very small in the region where the  $E_1$  electrons contribute to the electrostatic potential is important. For a given  $N_{dep}$ , the difference  $\mu - E_1$  increases more rapidly with  $n_e$  than  $E_2 - E_1$  does; and for some critical  $n_e^c$ ,  $E_2$  becomes populated. We show on Fig. 1 the  $N_{dep}$  dependence of  $n_e^c$  in Ga(Al)As-GaAs H.J.'s with  $V_b = 0.3$  eV. The two empty circles are Ando's results [2] obtained within the density functional approximation. For residual p type GaAs channels ( $N_{dep} \sim 5 \times 10^{10} \text{ cm}^{-2}$ ) we see that there exists a good agreement between our simplified model and Ando's refined treatment. Differences are larger at very low  $n_e$  indicative of the weaknesses of variational procedure for excited states (especially when they are weakly bound). Notice in Fig. 2 the steep increase of  $n_e^c$  with  $N_{dep} \geq 10^{10} \text{ cm}^{-2}$ .

Once  $E_1(n_e)$  is determined, we can solve the equilibrium conditions (2,3) for specified  $N_A$ ,  $N_D$ ,  $w$ ,  $\epsilon_b$ . We show on Fig. 2 the  $w$  dependence of the transferred 2d charge  $n_e$  in Ga(Al)As-GaAs M.D.H.J.'s for  $N_D = 7 \times 10^{17} \text{ cm}^{-3}$ ,  $V_b = 0.3$  eV and three compensating acceptor concentrations  $N_A$ . We have taken  $\epsilon_b = 0$  based on the assumption of hydrogenic Si donors. There is however a recent report [4] showing a very strong increase of  $\epsilon_b$  above 25% Al concentration in Ga(Al)As alloys. Also shown on Fig. 2 are Drummond et al results [5]. We see that there is a tendency towards the presence of residual acceptors in Ga(Al)As. More recently, Störmer et al [6] have used wider Ga(Al)As spacers and higher Si

doping level ( $N_D = 2 \times 10^{18} \text{ cm}^{-3}$ ) resulting in remarkably low  $n_e$  (black circles on Fig. 3). It is not impossible to find a suitable  $N_A$  which would fit these  $n_e$ 's. However, with  $N_D = 2 \times 10^{18} \text{ cm}^{-3}$ , the  $N_A$ 's would be in excess of  $10^{18} \text{ cm}^{-3}$  and it would be impossible to account for the very high mobilities found by Störmer et al in their low  $n_e$  samples. At the moment, we do not see how to positively correlate the measured  $n_e$  with the charge transfer effects as described by Eqs. (1-4).

In InP-In(Ga)As M.D.H.J.'s, the band discontinuity is not very well known ( $V_b = 0.53$  eV [7] or  $V_b = 0.3$  eV [8]). In any event, these heterostructures are quite similar to the Ga(Al)As-GaAs ones except that the conducting channel is located in the ternary random alloy  $\text{In}_{0.53}\text{Ga}_{0.47}\text{As}$ . The 2D electrons will be scattered by the short range alloy fluctuation. Assuming the alloy is perfectly random, we obtain in the E.Q.L. at  $T = 0$  K

$$\frac{1}{\tau} = \frac{\pi}{\hbar} x(1-x) \Omega_0 \langle \delta V \rangle^2 \int_0^d \chi_1^2(x) dx \quad (4)$$

where  $\pi = 0.047 m_0$ ,  $x = 0.47$ ,  $\Omega_0 = (5.87 \text{ \AA})^3$  and  $\langle \delta V \rangle$  is the strength of the scattering potential. Retaining the bulk value  $\langle \delta V \rangle = 0.6$  eV [9], we have calculated the mobility limited by alloy scattering versus the 2D concentrations  $n_e$ . The results are shown on Fig. 3 together with the calculated  $E_1$  energies for  $V_b = 0.53$  eV (solid curves) and  $V_b = 0.3$  eV (dashed curves). To calculate  $E_1$ , quasi-accumulation condition has been retained ( $N_{dep} = 10^7 \text{ cm}^{-2}$ ). The mobility curves are independent of the precise value of  $V_b$  whereas, as expected, larger  $V_b$  leads to larger  $E_1$ . The calculated mobility decreases from  $3.5 \times 10^4 \text{ cm}^2/\text{V.s.}$  to  $\sim 1.5 \times 10^4 \text{ cm}^2/\text{V.s.}$  when  $n_e$  increases from  $10^{11}$  to  $10^{12} \text{ cm}^{-2}$ . The alloy scattering is therefore very efficient when the conducting channel is located in the ternary alloy. In the reverse situation (e.g. alloy scattering occurring in the Ga(Al)As barrier for Ga(Al)As-GaAs M.D.H.J.) this scattering mechanism is rather ineffective [2] due to the small penetration of the wavefunction in the barrier. Although the assumption of total randomness is an upper bound for scattering efficiency and despite the possible deviation of  $\langle \delta V \rangle$  from its measured bulk

AD-A147 163

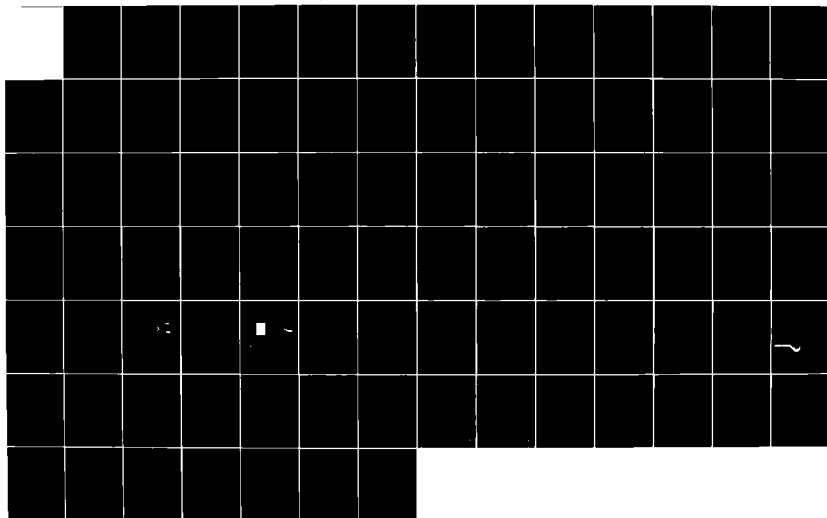
INTERNATIONAL CONFERENCE ON ELECTRONIC PROPERTIES OF  
TWO DIMENSIONAL SYSTEMS (5TH) HELD AT OXFORD ENGLAND ON  
5-9 SEPTEMBER 1983(1) OXFORD UNIV (ENGLAND) 1983

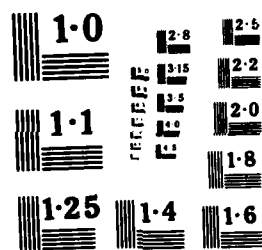
4/4

UNCLASSIFIED

F/G 9/3

NL





value, it seems hard to imagine that low temperature mobility of InP-In(Ga)As M.D.H.J. may exceed those found in the Ga(Al)As-GaAs system.

#### References

- /1/ F. Stern, Bull. American Phys. Soc. **28**, 447 (1983) and private communication.
- /2/ T. Ando, J. Phys. Soc. Japan **51**, 3893 (1983) and **51**, 3900 (1982).
- /3/ F.F. Fang and W.E. Howard, Phys. Rev. Lett. **16**, 797 (1966).
- /4/ T. Ishikawa, J. Saito, S. Sasa, S. Hiyamizu, Japanese Journ. Appl. Phys. **21**, L.675 (1982).
- /5/ T.J. Drummond, W. Kopp, M. Keever, B. Morkoç, A.Y. Cho, J. Appl. Phys. **53**, 1023 (1982).
- /6/ H.L. Störmer, A. Chang, D.C. Tsui, J.C.M. Hwang, A.C. Gossard, W. Wiegmann preprint (1983).
- /7/ Y. Guldner, J.P. Vieren, P. Voisin, M. Vooß, M. Razeghi, M.A. Poisson, Appl. Phys. Lett. **40**, 877 (1982).
- /8/ R.J. Nicholas, M.A. Brummell, J.C. Portal, M. Razeghi, M.A. Poisson in "Application of High Magnetic Fields in Semiconductor Physics" edited by G. Landwehr, Springer Verlag, Lecture Notes in Physics, Berlin Heidelberg (1983).
- /9/ J.R. Hayes, A.R. Adams, P.D. Greene in "GaInAsP Alloy Semiconductors" edited by T.P. Pearsall, John Wiley and Sons, New York (1982).
- /10/ J. Saito, K. Nanbu, T. Ishikawa, S. Hiyamizu, Japanese Journ. Appl. Phys. **22**, L.79 (1983).

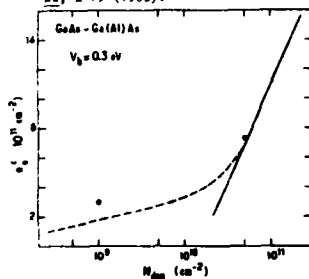


Fig. 1 : Critical concentration  $n_c^c$  versus 2d concentration of fixed space charges in GaAs  $N_{dep}$ . Open circles are Ando's results /2/. For  $n > n_c^c$ ,  $E_z$  becomes populated.

550

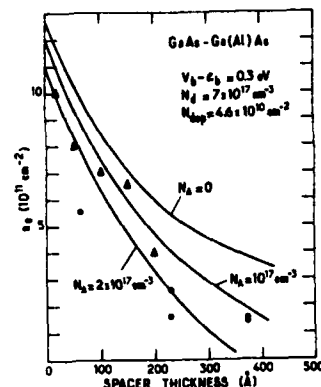


Fig. 2 : Calculated 2d. concentration  $n_s$  versus spacer thickness in GaAs-Ga(Al)As M.D.H.J.'s for three compensating acceptor concentrations  $N_A$  (solid lines) in Ga(Al)As. Symbols correspond to experiments : triangles /5/ ; black circles /6/ ; open circle /10/.

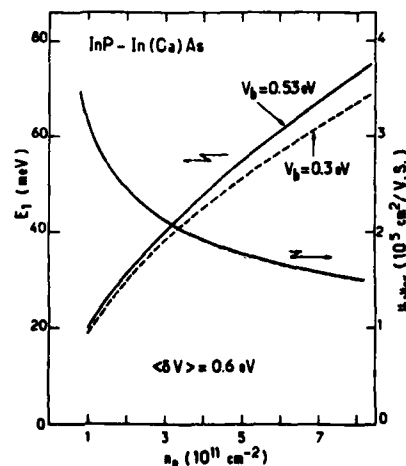


Fig. 3 :  $n_s$  dependence of the mobility limited by alloy scattering (right scale) and binding energy of the ground subband (left scale) in InP-In(Ga)As M.D.H.J. Solid lines :  $V_b = 0.53$  eV. Dashed lines :  $V_b = 0.3$  eV.

551

Photoluminescence from "Spike Doped" Hydrogenic Donors  
in  $\text{Al}_{0.3}\text{Ga}_{0.7}\text{As-GaAs}$  Quantum Wells\*

B. V. Shanabrook and J. Comas  
Naval Research Laboratory  
Washington, D.C. 20375 USA

Abstract

We have performed photoluminescence (PL) measurements on  $\text{GaAs-Al}_{0.3}\text{Ga}_{0.7}\text{As}$  superlattices where Si donors have been selectively doped at the center of the non-interacting quantum wells. A PL feature is shown to be donor related and is attributed to the radiative recombination of an electron of a neutral donor at the center of a quantum well with a heavy hole. Furthermore, our measurements indicate that the binding energy of the electron bound at a neutral donor is slightly larger than that of a coupled electron heavy hole exciton and, in addition, is significantly larger than that observed for donors in bulk GaAs. These observations are in substantial agreement with recent theoretical calculations.

Introduction

Recently, the nature of the wavefunctions and binding energies of hydrogenic impurities confined in quantum wells has been theoretically explored [1-3]. Two of the main conclusions of these investigations are (a) the predicted sensitivity of the impurity binding energy to the location of the impurity in the quantum well and secondly, (b) that impurities placed at the center of the well exhibit significantly larger binding energies than those of impurities in bulk material. Of course, one physically expects that the magnitude of these effects will be the largest and therefore the easiest to observe experimentally when the Bohr orbit of the hydrogenic impurity is comparable to the quantum well width ( $L_z$ ). Since donors in GaAs are well

described by the hydrogenic approximation (i.e., very small central cell corrections) and, in addition, exhibit rather large Bohr orbits (100 Å), it appears that  $\text{GaAs-Al}_{0.3}\text{Ga}_{0.7}\text{As}$  quantum wells could serve as a model system to test the concepts mentioned above in (a) and (b). Previous studies [4] have investigated the properties of shallow acceptors in GaAs quantum wells. However, in this case, a quantitative comparison between experimental results and existing theories is hampered by the inadequate description of acceptors in GaAs by the hydrogenic model.

Sample	No.	Table I			
		$L_z(\text{\AA})$	$x$	$n(\text{cm}^{-3})$	$E(\text{eV})$
MBE	187	$150 \pm 10$	$.28 \pm .02$	undoped	1.534
MBE	160	$150 \pm 10$	$.28 \pm .02$	$1 \times 10^{16}$	1.533
MBE	159	$150 \pm 10$	$.28 \pm .02$	$1 \times 10^{16}$	1.536

Results and Discussion

We have prepared a variety of  $\text{GaAs-Al}_{0.3}\text{Ga}_{0.7}\text{As}$  superlattices by the MBE technique. In all cases, the width of the  $\text{Al}_{0.3}\text{Ga}_{0.7}\text{As}$  layers were greater than 150 Å and, therefore, the assumption of isolated quantum wells is justified. Furthermore, to be able to investigate experimentally the peculiar properties of impurities confined in quantum wells and mentioned above in (a) and (b), we have tried to incorporate donor atoms at particular locations in the quantum wells. The width of the doping spike ( $L_d$ ) was estimated by the product of the time that the shutter of the MBE Si effusion cell was open and the growth rate of the epitaxial layer. The possibility of donor segregation during growth or diffusion indicates that  $L_d$  is only a lower limit for the actual width of the doping spike. Shown in Fig. 1 is the photoluminescent response obtained from three  $\text{GaAs-Al}_{0.3}\text{Ga}_{0.7}\text{As}$  superlattices. The major difference between these samples is the doping concentration of a 50 Å wide Si donor doping spike incorporated at the center of the quantum well. The doping concentrations and other relevant material properties of these samples are summarized in Table I. Small changes in either the Al concentration of the ternary semiconductor or

the width of the GaAs quantum wells result in small differences between the PL energies obtained from different samples. Therefore, the energy scales of the PL spectra displayed in Fig. 1 have been shifted relative to one another (by less than 3 meV) to bring the peak positions of PL which arise from similar radiative recombination processes into correspondence. The actual energy position of the PL may be determined by summing the quantity  $E$  (given in Table 1) and the  $X$  value given by energy scale of Fig. 1. Previous measurements [4] have indicated that radiative recombination of intrinsic excitons composed of electrons coupled to either heavy (e-hh) or light (e-lh) holes are the dominant photoluminescent processes which occur in undoped quantum wells. A comparison between the spectral position, shape and width of the PL spectrum obtained from the undoped superlattice (MBE 187) with what has been reported in the literature [4] indicates that the PL peaks occurring at  $X = 0$  meV and  $X = 7$  meV arise from radiative recombination of e-hh and e-lh, respectively. When a 50 Å doping spike of Si donors is incorporated into the center of the multi-quantum well, a PL feature shown in Fig. 1 at  $X = -1.5$  meV becomes more intense relative to the e-hh emission. This observation is in agreement with the PL spectra obtained from seven different samples grown with similar  $L_z$  values but with differing Si doping concentrations and strongly suggests that donors are involved in the recombination process responsible for the PL at  $X = -1.5$  meV. In analogy with the donor-related PL features that are known to occur in bulk GaAs [5], we suggest that this PL peak arises from either the recombination of a heavy hole with an electron of a neutral donor (D-hh) or a donor bound electron-heavy hole exciton (D(e-hh)).

Shown in Fig. 2 are the changes observed in the PL spectra obtained from sample MBE 160 with variations of excitation laser power. The maximum intensity of the donor-related PL feature at 1.531 eV of Fig. 2 ( $X = -1.5$  meV in Fig. 1) exhibits an approximately linear variation with changes in laser power while a slightly faster variation is observed for e-hh emission at 1.533 eV. If the PL at 1.531 eV was created by a recombination process whose initial

state involved the capture of a coupled electron-heavy hole exciton, as one might expect for D(e-hh) [5], and if the intensity of the e-hh PL was a measure of the steady state concentration of the coupled electron heavy hole excitons (as is true to first order with changes of laser power), then the PL occurring at 1.531 eV and 1.533 eV would be expected to exhibit similar changes in PL intensity with changes in laser power. Since we do not observe this behavior, we suggest that the PL feature at 1.531 eV arises from the D-hh recombination mechanism. Time-resolved or temperature dependent PL measurements will provide additional tests of the above-proposed emission process. The D-hh recombination mechanism had been suggested previously by other workers [6]. However, for reasons not understood, the band edge PL features they report exhibit significantly wider energy distributions and larger shifts in PL peak positions with changes in laser power than those observed in our samples.

We have prepared seven spike doped superlattices with various quantum well widths ( $L_z$ ) between 80-540 Å. In all cases, a donor related peak occurs 1-2 meV below the e-hh PL and this feature is interpreted as arising from radiative recombination of a heavy hole and an electron trapped at a neutral donor. A theoretical calculation of the PL response resulting from a D-hh recombination mechanism in a uniformly donor doped GaAs quantum well has indicated that two peaks should occur in the PL spectrum [3]. The lower (higher) energy peak which involves donors at the center (edge) of the well would occur just below (above) the e-hh emission [1,2,7]. Since this emission we observe always occurs slightly below the e-hh PL peak (1-2 meV), we conclude that we are observing D-hh recombination from donors at the center of the quantum well. This conclusion is also consistent with the location of the doping spike that one would surmise from the growth procedure. The rather constant energy separation between the D-hh and e-hh PL indicates that the exciton and the donor are affected in a similar fashion by the confinement imposed by the quantum wells. Because the Bohr orbits of neutral donors and

free excitons in bulk GaAs are rather similar (100 Å versus 120 Å, respectively), this behavior is not unexpected. The combination of our PL emission energies with the width of the quantum wells and a theoretical calculation [7] leads us to conclude that the binding energy of electrons bound to donors at the center of the quantum well varies from 6 meV to 10 meV for  $L_z$  widths between 540 Å and 60 Å. These values are somewhat lower but in substantial agreement with recent theoretical calculations [1,2].

We have also selectively doped three multi-quantum wells ( $L_z = 150$  Å) with Si donor doping spikes at the edges of the quantum wells. From two of these samples, a PL peak appears 2 meV above the e-hh transition. A similar feature is also observed in the PL spectrum shown in Fig. 1 for the undoped sample. The simplest interpretation for the origin of this peak which is consistent with the doping profile and theoretical calculations would suggest that this emission is probably associated with a D-hh transition involving donors at the edge of the quantum well. However, these samples also yield a systematic growth in the intensity of the PL feature we have associated with donors located at the center of the quantum well and therefore it appears that the donors are either diffusing or segregating over a distance of at least 50 Å during crystal growth. This observation is rather interesting in that it suggests that measurements of extrinsic PL in multiquantum wells may provide useful information about the diffusion and (or) segregation of impurity atoms over distances which cannot be measured by other experimental probes.

#### References

\* Partially supported by the Office of Naval Research.

1. R. L. Greene and K. K. Bajaj, *Solid State Commun.* **45** (1983) 825.
2. C. Mailhot, Y. Chang and T. C. McGill, *Phys. Rev. B* **26** (1982) 4449.
3. G. Bastard, *Phys. Rev. B* **24** (1981) 4714.
4. R. C. Miller, A. C. Gossard, W. T. Tsang and O. Munteanu, *Phys. Rev. B* **25** (1982) 3871 and references therein.
5. R. Ulbrich and B. Moreth, *Solid State Commun.* **14** (1974) 331.
6. B. Lambert, B. Deveaud, A. Regreny and G. Talalaeff, *Solid State Commun.* **63** (1982) 443.
7. R. L. Greene and K. K. Bajaj, *Solid State Commun.* **45** (1983) 831.

Fig. 1. The PL spectra obtained from 3 different multi-quantum well samples where MBE 187 is undoped and MBE 159 and 160 have been selectively donor doped at concentrations of  $1 \times 10^{16} \text{ cm}^{-3}$  and  $1 \times 10^{15} \text{ cm}^{-3}$ , respectively. The actual energy scale of the spectra are determined by the sum of E, a quantity defined in Table I, and X.

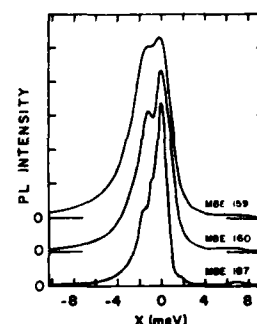
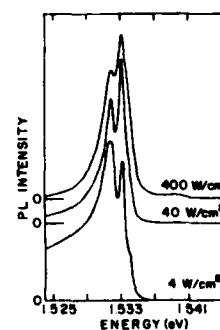


Fig. 2. A comparison of the PL spectra obtained from MBE 160 with the indicated excitation power of 6471 Å radiation.





# Magnetic Breakdown in GaAlAs/GaAs Quantum Well Structures

J. Yoshino, H. Sakaki and T. Hotta

Institute of Industrial Science, University of Tokyo  
7-22-1 Roppongi, Minato-ku, Tokyo 106, Japan

**Abstract:** The Shubnikov-de Haas oscillations of various GaAs/GaAlAs quantum well structures are studied at 4.2K by applying the strong magnetic field parallel to the layers. A series of oscillations are found to appear, when the diameter of cyclotron orbits becomes comparable to or smaller than the well width. A simple theory of such magnetic breakdown phenomena is presented and is shown to explain the observed oscillations quite satisfactorily.

## §1 Introduction

It is well known that electrons confined in ultra thin semiconductor layers such as Si-MOS inversion layers and GaAlAs/GaAs quantum well structures have characteristic of quasi-two dimensional electron gas (2DEG) systems. In such 2D system Shubnikov-de Haas (SdH) effect is known to be anisotropic in the sense that the oscillatory magnetoresistance is dominated by the normal component  $B_z$  of the magnetic field, and is scarcely affected by the tangential component  $B_y$ . It is because the quantum wells in which electrons are confined are very thin usually and interrupt the cyclotron motion. One should consider, however, that the widths of actual quantum wells are finite. Hence, if an extremely strong magnetic field is applied in parallel to the layer plane and if the diameter of the cyclotron motion becomes comparable to the layer thickness, we expected the electrons to complete the cyclotron motion. Although these magnetic breakdown phenomena are of fundamental importance, practically no work has been done so far except one preliminary experiment (1) and a few theoretical (2, 3) studies. In this paper we present the first systematic study of the magnetic breakdown phenomena. In particular, we demonstrated experimentally the presence of such breakdown phenomena in various GaAs/AlGaAs quantum-wells. In addition we show that the observed oscillations can be well explained by the theory, in which both the quantum well potential and the harmonic potential of magnetic fields are taken into account.

## §2 Description of Our Experimental Methods and Results

Since the radius  $r$  of cyclotron motion for the  $l$ th Landau level is given by  $r = (h/eB)^{1/2} (2l+1)^{1/2}$  the cyclotron radius for  $l=0$  gets as small as 65Å at  $B=15$  Tesla. Hence, the magnetic breakdown is expected in relatively low magnetic field range ( $B < 15$  Tesla), if the quantum wells widths  $L_z$  are chosen far greater than 130Å. For this reason, we prepared various  $\text{Ga}_{1-x}\text{Al}_x\text{As/GaAs}$  quantum wells (QW) with the well widths ranging from 250Å to 500Å. A care was taken to dope only the GaAs well layers with Si donors. This doping profile creates nearly-ideal square potential wells. All the samples were grown by molecular beam epitaxy on Cr doped semi-insulating GaAs substrates. Two kinds of samples were measured. One had 35 periods of 500Å GaAs well and 500Å GaAlAs barrier layers (No.393), while the other had 40 periods of 250Å GaAs and 250Å GaAlAs layers (No.404). Each sample was shaped into standard Hall bar geometry, 50 $\mu\text{m}$  wide and 600 $\mu\text{m}$  long, by mesa etching technique. Potential probes on this Hall bar were placed at two positions which were 200 $\mu\text{m}$  away from the end electrodes. From Hall measurement at 77K, electron mobilities were found to be 1600 $\text{cm}^2/\text{V s}$  and 2000 $\text{cm}^2/\text{V s}$  respectively. These relatively low values are due to the heavy doping in GaAs well layers. The Fermi energy of electrons in the ground level  $E_F - E_0$  are determined from the measured period of SdH oscillations at 4.2K, and found to be 56 meV in 500Å-well sample and 72 meV 250Å-well sample. The SdH oscillations were measured at 4.2K by passing the constant current along the x-axis. The direction  $\theta$  of magnetic fields with respect to the layer (x-y) plane was varied between the normal direction ( $B_z, \theta=0^\circ$ ) and the parallel direction ( $B_y, \theta=90^\circ$ ). The results of such angular dependence measurement are shown in Fig.1. The SdH oscillation of 500Å-well sample is found to be essentially isotropic. However in the low field region the peaks shifted slightly toward the lower magnetic field as  $\theta$  is increased. This suggests the diameter of cyclotron motion is smaller than 500Å in most of

the field. On the other hand, the SdH oscillation of 250Å-well sample clearly exhibited anisotropic nature (Fig.1(b)). The general tendency of this anisotropy is in accordance with the simple 2D picture. But the simple theory cannot explain the presence of an extra oscillation when  $B \geq 12$  Tesla and the magnetic field is parallel to the layer.

### 3. Theoretical Formulation and Discussion

For simplicity, we consider the case, in which the magnetic field applied is parallel to the layer ( $y$ ). We put the quantum well potential  $V(z)$  along  $z$ -coordinate and choose the vector potential as  $A = (Bz, 0, 0)$ ; then the Hamiltonian  $H$  can be described as

$$H = \frac{1}{2m^*} (P_x + eA)^2 + V(z) \quad (1)$$

where  $m^*$  is the effective mass. As is well known, Hamiltonian  $H$  and momentum operator  $P_x$  and  $P_y$  can be commuted. Hence if we indicate each quantum number as  $n_k x$  and  $n_k y$ , Schrödinger equation is reduced to the following one dimensional form.

$$\left\{ -\frac{\hbar^2}{2m^*} \frac{d^2}{dz^2} + V(z) + \frac{1}{2} m^* \omega_c^2 (z - Z_0)^2 \right\} \psi = \epsilon \psi \quad (2)$$

$$Z_0 = -\frac{\hbar k_y}{eB}, \quad \epsilon = E - \frac{\hbar^2 k_y^2}{2m^*}, \quad \omega_c = \frac{eB}{m^*}$$

where  $E$  is the total energy of electrons and  $Z_0$  is the coordinate of the center of cyclotron motion. When the barrier width is wide enough to ignore the interaction of adjoining wells, we can treat each of quantum wells separately and the potential is given as follows.

$$V(z) = \begin{cases} 0 & |z| > a/2 \\ -V_0 & |z| \leq a/2 \end{cases} \quad (3)$$

in which  $a$  means the well width. As is well known, the energy levels in the absence of quantum well potential  $V(z)$  are those of harmonic oscillators,

which are degenerate for different quantum number  $Z_0$ . In the quantum well, however, such degeneracy is resolved because of the presence of the  $z$  dependent potential  $V(z)$ . Figure 2 shows the energy eigenvalues  $\epsilon$  of 500Å quantum well structures calculated numerically as function of  $Z_0$  at  $B=6$  Tesla and 10 Tesla. Since the oscillatory behaviour of resistivity  $\Delta\rho(B)$  results from the oscillatory change of state density  $D(E,B)$  at Fermi energy  $E_F$  it is possible to predict at which magnetic fields  $B$  the resistivity peaks appear, as long as we calculate the position of the peaks in the state density  $D(E,B)$ . Although the exact form of the state density function  $D(E,B)$  can be obtained only by counting all the states  $\epsilon(Z_0, k_y)$  having different values of  $Z_0$  and  $k_y$ , one can readily see in Fig.2 that the peak positions of the state density are given simply by the eigenvalues  $\epsilon$  at  $Z_0=0$  and  $k_y=0$ . Hence, we calculate the energy levels  $\epsilon(Z_0=0, k_y=0)$  as functions of magnetic field  $B$ . The result for 500Å-well structure is shown in Fig.3. At low magnetic field limit, the calculated energy levels are found to approach asymptotically to those levels which are determined by the quantum well potential. In contrast, the energy levels at high magnetic field approach to those of harmonic oscillator,  $E = \hbar\omega_c(n+1/2)$ , which would be expected from the shape of Hamiltonian. Since the Fermi energy  $E_F$  does not depend on magnetic field so strongly we assume here that  $E_F - E_0$  of 500Å-well sample is constant ( $\approx 52$ meV). Then the position of resistivity peaks can be easily predicted from Fig.3, because  $\Delta\rho(B)$  should show peaks whenever one of the calculated energy levels in Fig.3 crosses  $E_F$ . The triangles in Fig.4 are the peak positions calculated for 500Å-well sample by this method. For comparison, Landau plot of measured peaks and dips at  $\theta=0^\circ$  and  $\theta=90^\circ$  are shown by solid and blank circles, and found to be explained by the present model. Note especially that the peaks for high Landau-indices ( $n=4$  and 3) shift considerably toward the lower magnetic field direction, in accordance with the theory. A similar calculation has been extended to the

250A-well structure. Figure 5 shows the calculated energy levels as function of magnetic field  $B$  for  $\theta=90^\circ$ . In the case of 250A-well, the bounding of well potential is so strong that the energy level is not changed by magnetic field drastically. If one assumed here that the Fermi energy is constant, then the first resistivity peak is predicted appear at about 16 Tesla. The experimental results shown in Fig.1(b) exhibit no peaks for  $\theta=90^\circ$  up to 14 Tesla, in accordance with this simple theory.

In summary, we have shown by the systematic experiment that oscillatory changes of resistivity appear in GaAs/GaAlAs quantum well structures under the parallel magnetic field when the diameter of cyclotron motion becomes comparable to or less than the well width. The observed oscillations are shown to be well explained by the theory and can be viewed as clear evidence of magnetic breakdown phenomena in quantum wells.

The authors are very grateful for the comments of and discussions with Professor T. Ando and Professor S. Kawaji and the valuable co-operation of Y. Sekiguchi and K. Hirakawa. The work is partly supported by the Grant-in-Aid for the Special Promotion Research from the Ministry of Education, Science and Culture.

#### References

- (1) L.L. Chang, H. Sakaki, C.A. Chang and L. Esaki, Phys. Rev. Lett. 38 (1977)1489.
- (2) K. Nakao, J. Phys. Soc. Japan 46(1979)1669.
- (3) T. Ando, J. Phys. Soc. Japan 50(1981)2978.

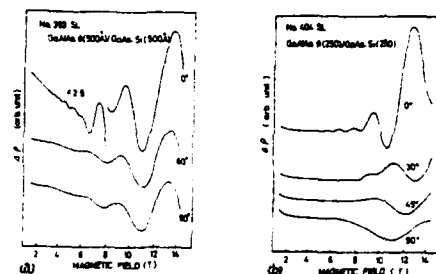


Figure 1. Angular dependence of SDH oscillation on a 500A-well sample (a) and a 250A-well sample (b). The angle is measured from the normal to the quantum well plane.

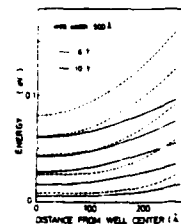


Figure 2. The dependence of energy levels in 500A-well structure vs quantum number  $Z_0$  (see text).

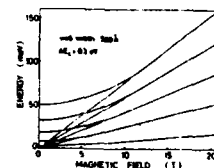


Figure 3. Energy levels in 500A-well structure. The thin lines show the Landau levels in free space.

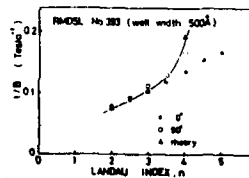


Figure 4. The inverse of magnetic field ( $1/B$ ) at which  $\Delta P(B)$  shows maxima is plotted as a function of Landau index  $n$ . In experimental results (circles) dip positions are also indicated.

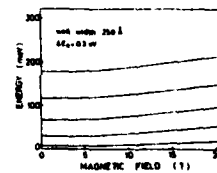


Figure 5. Energy levels in 250A well structure are shown as function of magnetic field.

# deHaas-van Alphen Effect in Silicon Inversion Layers

F.F. Fang

IBM Thomas J. Watson Research Center  
Yorktown Heights, New York 10598

and

P. J. Stiles

Brown University  
Providence, R.I. 02912

## ABSTRACT

The magnetic susceptibility of the Si inversion layer electrons was measured for the field up to 15T. Ideally, the system is expected to become totally quantized with discontinuous magnetization between discrete magnetic levels. In order to detect the small oscillatory magnetic signals (deHaas-van Alphen effect), we have devised a geometry of the MOS field effect sample structure whose magnetic pick-up is directly above the periphery of the gate electrode. The change of magnetization is provided by the modulation of the gate voltage.  $(dM/dn_g)$  for (100) Si inversion layer was measured at 1.5 K and frequency up to 100 KHz. The detected signals were found to have the expected frequency dependence and the expected spikes between magnetic levels. We also expect quantized steps characterized by integer unit of double effective Bohr magneton  $(e\hbar/m^*c)$  in each magnetic level which has not been discerned so far with the present sensitivity of the measurements.

The two dimensional electron gas (2DEG) systems as typified by the inversion layers in Si MOSFETs have been studied extensively<sup>(1)</sup>. Magnetic quantum oscillations have been studied primarily in the Shubnikov-de Haas effect (SdH) and in oscillations in the capacitance. The recent observation and identification of the quantized Hall effect in these systems<sup>(2)</sup> has led to much renewed theoretical and experimental interest in this area. The SdH effect is a measure of a non-equilibrium property of the 2DEG. The system is probed under electric field perturbation and understood in terms of current transport. In this paper, we report some preliminary results in the oscillatory magnetization experiments in Si inversion layers.

The oscillatory magnetization in three dimensions is known as the deHaas-van Alphen (dHvA) effect. It is a measure of *one* of the thermodynamic properties of the electronic system in a quantizing magnetic field. The dynamic scattering process enters only in the effect through the modification of the self energy.

Consider a 2DEG with an electron concentration  $n_e(\text{cm}^{-2})$ , the free energy  $F$  in a quantizing magnetic field  $H$  is given by

$$F = E_0 n_e + \sum_{l=1}^n (n - \frac{1}{2}) \hbar \omega_c N_l + (n + \frac{1}{2}) \hbar \omega_c (n_e - n N_l) \quad (1)$$

where  $n$  is the Landau level quantum index,  $E_0$  is the ground state energy of the two dimensional subband,  $\omega_c = (e\hbar/m^*c)$  is the cyclotron frequency for electrons with mass  $m^*$  parallel to the surface and

$$N_l = (\xi_{v,s} c \hbar) / (\hbar c) \quad (2)$$

is the density of states of a single Landau level with  $\xi_{v,s}$  being the valley and spin degeneracy. For simplicity and without loss of generality, we have ignored spin and valley splitting, temperature and collision broadenings. The magnetization  $M$  is then given by

$$M = \frac{\partial F}{\partial H} = \sum_{l=1}^n (n - \frac{1}{2}) 4\beta^* N_l - n(n + \frac{1}{2}) 4\beta^* N_l + (n + \frac{1}{2}) 2\beta^* n_e \quad (3)$$

where  $\beta^* = e\hbar/2m^*c$  is the effective Bohr magneton. Fig. 1 shows the normalized free energy and magnetization as a function of the normalized electron density  $n_e/N_l$  where integers,  $n$ , designate the filling of the particular Landau levels. The kinks in the free energy and the discontinuities in the magnetization at integer values of  $n_e/N_l$ , respectively are the result the delta function density of states of the Landau levels in an ideal 2D system.

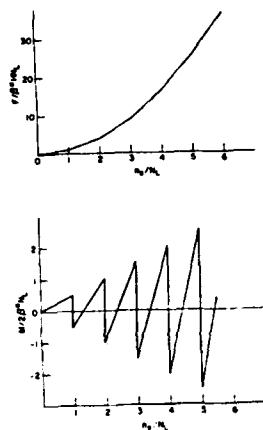


Fig. 1 Normalized electron free energy and magnetization as a function of the normalized electron density  $n_0/n_0^*$  in a constant quantizing magnetic field where the integer  $n$  designates the number of filled Landau levels.

Since the spin and valley equally divide the Landau level density, these figures represent approximately the well resolved spin and valley splitting spectra of  $M$  if one replaces  $N_L$  by  $eH/hc$ , and  $\omega_c = eH/\zeta_{v,s} m^*c$ . An analytical account for the spin splitting in a size-quantized 2D system using odd and even integer representations was given by Gurevich and Shik<sup>1</sup> and by Kao et al.<sup>2</sup>

Since  $N_L$  is about  $2.4 \times 10^{11} \text{ cm}^{-2}$  for  $H=10\text{T}$ , for a spin and valley resolved level, the total magnetization for a typical sample of  $10^{-2} \text{ cm}^2$  is of the order of  $10^{-9} \text{ erg/gauss}$  which is difficult to detect. We chose to measure the change of  $M$  with respect to the carrier concentration  $n_0$ . The method is to modulate the gate voltage and measure the magnetically induced signal in a pick-up coil which is placed on the periphery of the gate electrode. Phase detection techniques were employed for the induced signal at modulation frequencies up to 100 KHz.

566

Fig. 2 shows schematically the sample and measurement configurations. The active gate and pick-up coil geometry are shown in Fig. 3. The Si substrate is  $100 \Omega \cdot \text{cm}$  p-type (100). The inversion layer has the shape of twenty  $25 \mu\text{m} \times 500 \mu\text{m}$  fingers. The gate is N doped polycrystalline Si. The gate oxide thickness  $\delta_{ox}$  is 437 Å. Around the inversion layer, the Si wafer is N-type doped degenerate to provide the access for the inversion layer electrons. On top of the gate electrode, there is a 520 Å CVD oxide layer. The pick-up coil surrounds the gate electrode and is  $5 \mu\text{m}$  wide Al on top of the CVD oxide. On the same wafer, there is a monitoring FET with  $W$  and  $L$  dimensions equal to 250 and  $25 \mu\text{m}$  respectively with the same gate and oxide structure as the dHVA samples.

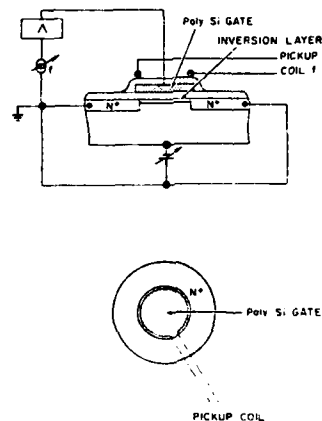


Fig. 2 Schematic diagrams of the sample and measuring configurations.

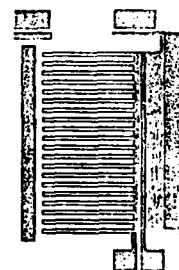


Fig. 3 The gate and pick-up coil geometry of the actual sample. Heavily doped N-type region surrounding the inversion layer under the gate.

The dHVA effect is observed as a voltage induced in the pick-up coil due to the time rate of change of the flux induced by the time dependent magnetization of the inversion layer electrons. We modulate the electron density sinusoidally such that

567

$$V(t) = \frac{d\phi}{dt} = -\frac{A}{c} C_{ox} \frac{dM}{dn_s} \frac{dV}{dt} \quad (4)$$

where  $A$  is the total area under the gate,  $C_{ox} = \kappa/4\pi d_{ox}$  is the specific gate capacitance and  $V$  is the time varying part of the gate voltage with  $\kappa$  being the dielectric constant of the gate oxide. The primary contribution to the induced voltage is derived from the magnetization of the electrons near the pick-up coil, and the area under the gate. Also it can be shown that for a rectangular shaped field effect inversion layer structure with the long and narrow dimensions  $W$  and  $L$  respectively, the characteristic charging time is proportional to  $L^2$ . These are the reasons for the shape of the sample shown in Fig. 3 used for the high frequency modulation experiment.

We note from Eq. 3 that

$$\frac{dM}{dn_s} = (n + \frac{1}{2})\hbar e/m^*c \quad (5)$$

and the pick-up signal is given by

$$|V(t)| = A(n + \frac{1}{2})\hbar C_{ox} \omega V_{g0}/m^*c \quad (6)$$

where  $\omega$  and  $V_{g0}$  are the gate modulating frequency and amplitude respectively.

A schematic of the behavior of  $dM/dn_s$  as a function of  $n_s/N_L$  is shown in Fig. 4. We thus expect quantized plateaus in steps of the double effective Bohr magneton,  $\hbar e/m^*c$ , for each quantum number  $n$ .

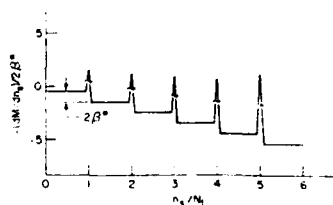


Fig. 4. Schematic of the expected behavior of  $dM/dn_s$  as a function of the normalized electron density  $n_s/N_L$  in a constant magnetic field.

Typical results for the induced pick-up coil as a function of gate voltage are shown in Fig. 5. The conductance of the monitoring FET is shown also. It can be seen that the spike structure observed in the induced voltage occurs at positions where Landau levels are filled, as expected. The results of a crude check for the amplitude dependence on frequency and modulation amplitude are as expected. For fixed frequency, the relative size of the different spikes depends on two competing conditions. The first is: the increasing size at higher densities as illustrated in Fig. 5, whereas the increasing scattering rate with respect to increasing density is expected to decrease the size at higher densities. As can be seen, the latter dominates the spike structure which disappears completely at the highest densities studied. It can also be seen from Fig. 4 that the plateau structure predicted for the low scattering regime is not observed. Clearly, our present signal to noise ratio is not adequate to resolve the quantum step of double effective Bohr Magnetron.

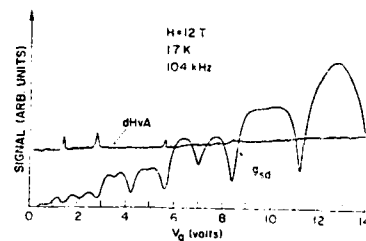


Fig. 5. The dHvA signal detected from the pick-up coil as a function of the gate voltage at  $H=12$  T,  $T=17$  K and modulation frequency at 104 kHz. Also shown is the 50% modulation in channel conductance  $G_{ch}$  of a companion FET. The expected dHvA spikes between magnetic levels are clearly seen.

One concern in such a quasi-DC experiment is that in fact there are frequency effects present. After all, we are charging and discharging a capacitor structure. We are in an open structure geometry and expect that the appropriate resistance for charging the capacitor between Landau layers is the quantized resistance<sup>5</sup>. From the results of the monitoring structure we can see that the quantized admittance is a linear function of the Landau levels filled. Any charging effect should have a similar dependence. However, it can be seen that the experimental results do not behave in that fashion. We note that the size of the  $n=2$  structure is about the same size as that for  $n=4$ . Further the  $n=6$  is missing while the  $n=8$  and  $n=12$  are visible. We conclude that although there may be some vestigial effects due to the frequency, such effects can not be a major cause of the observed structure.

#### REFERENCES

- (1) For a review of 2D electron system see, for example, T. Ando, A.B. Fowler and F. Stern, *Rev. Mod. Phys.* 54, 437 (1982).
- (2) K. v. Klitzing, G. Dorda and M. Pepper, *Phys. Rev. Lett.* 45, 494 (1980).
- (3) L.E. Gurevich and A. Ya. Shuk, *Sov. Phys. JETP* 27, 1006 (1968).
- (4) Y.H. Kao, Y.S. Wav and S.Y. Wang, *Phys. Rev. Lett.* 26, 390 (1971).
- (5) F.F. Fang and P.J. Stiles, *Phys. Rev. B* (to appear).

Magnetization Measurements on  
a Two Dimensional Electron System

T. Haavasoja, H. L. Störmer, D. J. Bishop,  
V. Narayanamurti, A. C. Gossard and W. Wiegmann

Bell Laboratories  
Murray Hill, New Jersey 07974 U.S.A.

We have measured the deHaas-van Alphen oscillations in a 2D electron system of GaAs-(AlGa)As superlattices from 0 to 5T at 1.5K. The amplitude of the oscillations together with known density distribution implies for the Landau levels a half-width of  $\sim 2$  meV, which roughly agrees with the width calculated from the zero field mobility of  $19000 \text{ cm}^2/\text{Vs}$ . We have observed eddy current relaxation times up to 300s at  $T \sim 0.4\text{K}$  suggesting the resistivity of the material to be as low as  $\rho_{xx} \approx 10^{-10} \Omega/\square$  corresponding to a 3D resistivity of  $\rho \approx 10^{-16} \Omega \text{ cm}$ .

There is considerable interest in determining the density of states (DOS) of two-dimensional electron systems (2DES) in order to comprehend in more detail the Quantized Hall Effect (QHE) (1,2) and the Zero Resistance State (ZRS) (3). So far experimental techniques have been limited to magneto-transport, magneto-capacitance and cyclotron resonance, all of which reveal aspects of the DOS only in an indirect way. However, the DOS can be determined directly from a measurement of the field dependent magnetic moment of a 2DES (4).

We have measured for the first time the oscillating magnetic moment, i.e. deHaas-van Alphen effect, of a 2DES from 0 to 5T at  $T \sim 1.5\text{K}$ . From the amplitude of the oscillations we can estimate the halfwidth of the Landau levels to be  $\sim 2$  meV, which is comparable to their spacing  $\hbar\omega_c$  ( $\sim 5$  meV at 3T). The

samples consist of modulation-doped GaAs-(AlGa)As superlattices of 172 GaAs 2D layers of thickness  $143 \text{ \AA}$  and average carrier concentration  $n = 8.2 \times 10^{11} \text{ cm}^{-2}$  with total area of  $\sim 33.2 \text{ cm}^2$ .

The magnetic moment  $\mu$  was measured with a commercial SQUID magnetometer up to 5T at 1.5K. The experimental data of  $\mu$  are shown in Fig. 1 together with the Shubnikov-deHaas  $\rho_{xx}$  and Hall Resistance  $\rho_{xy}$  data from a portion of the same sample. If the electron density  $n$  is constant and the DOS consists of a set of  $\delta$ -functions at Landau levels, we expect the magnetic moment to exhibit sawtooth-type oscillations periodic in inverse magnetic field  $1/B$ . Whenever a Landau level becomes completely filled, the Fermi energy jumps abruptly to the next level resulting in a discontinuity in the magnetic moment of magnitude  $\Delta\mu = \hbar en/m^*$  (4). The amplitude of  $\Delta\mu$  becomes highly damped at low fields mainly due to local inhomogeneities in  $n$  and due to a finite width of Landau levels. Under these conditions only the fundamental frequency of the sawtooth shape remains. Since  $\rho_{xx}$  is in the ZRS when the Fermi energy is between two Landau levels, oscillations of  $\mu$  and  $\rho_{xx}$  should be  $90^\circ$  out of phase as can be verified from Fig. 1.

We have determined the density distribution  $P(n)$  of our  $\mu$  sample by measuring the density gradients of several specimens at the periphery of our sample. The approximate full width at half maximum of  $P(n)$  is  $1.1 \times 10^{11} \text{ cm}^{-2}$  or 13% of the average  $n$  value. The average magnetic moment of the whole sample is

$$\langle \mu \rangle = \int_0^\infty \mu(n) P(n) dn \quad (1)$$



with

$$\nu(n) = -\frac{2}{\partial B} \int_0^\infty \frac{E D(E, B)}{1 + e^{(E-E_F)/kT}} dE, \quad (2)$$

where the DOS is  $D(E, B) = (2eB/h) \sum_{i=0}^\infty f(E - \hbar\omega_c(i+1/2)) / f(E) dE = 1$ . If we approximate the shape function  $f(E)$  by a Gaussian  $f(E) = \exp(-E^2/2\Gamma^2)$ , and use the observed  $P(n)$  it turns out that  $\Gamma$  must be chosen  $\sim 2$  meV in order to be able to approximate the data using Eq. 1.

The value of the fitted  $\Gamma \sim 2$  meV may be compared to the cyclotron frequency  $\hbar\omega_c = \hbar eB/m^* = 1.65 \times B$  (meV/T). The width estimated from the zero field mobility of 19000 cm<sup>2</sup>/Vs roughly agrees with our  $\Gamma$ . However, cyclotron resonance measurements on similar kinds of samples indicate a halfwidth of  $\Gamma \sim 1$  meV (5). This apparent disagreement may arise from the fact that our measurement of  $\nu$  is a true DC measurement. Whence we might expect to couple also to the localized electron states, which are expected to amount to a considerable fraction of the total number of electronic states. From the plateau widths at the  $\rho_{xy}$  data of Fig. 1 we can deduce that for  $B > 4$  T the ratio of localized to delocalized states is  $\gg 1$  for  $T \ll 1$  K.

We have extended the measurements of  $\nu$  up to 11 T with a modified Faraday balance technique (6). It turned out that the measurement of  $\nu$  must be performed under true DC conditions in order to avoid contributions to the magnetic moment due to eddy currents in field regions when the 2DES is in the ZRS. The sensitivity of this technique in DC mode is not yet sufficient to detect the small oscillations of  $\nu$ . Nevertheless, we were able to observe decay times of eddy currents as long as 300 ns at

$\sim 0.4$  K. Time constant of this length suggests that the resistivity of the material is as low as  $10^{-10}$   $\Omega/\square$  corresponding to a 3D resistivity of  $\rho \approx 10^{-16}$   $\Omega$  cm. The above value of  $\rho_{xx}$  is more than three orders of magnitude lower than the value reported earlier by Tsui et al. (7).

The magneto-transport of the superlattice was measured with an ordinary Hall rig. Contacts to all layers were provided by diffusing In into the sample at the position of the current and voltage probes. Assuming equal distribution of the total current over all the 172 layers the Hall plateaus are expected to be  $\rho_{xy} = h/ie^2N$ , where  $N = 172$  is the number of layers. Although  $\rho_{xy}$  stays constant within one part in  $10^4$  through a wide range of magnetic field,  $\rho_{xy}$  is not exactly quantized to the above value;  $\rho_{xy}$  appeared to deviate from the quantized value by 1 part in  $10^3$ . A plausible explanation for this deviation can be found in varying contact resistance to the different layers resulting in slightly different currents. At this point we have not yet reached a detailed understanding of the current and potential distribution in a multiply connected superlattice. Varying contact resistance and closed loop currents passing through several layers complicate the situation considerably. Our data, however, seem to indicate that QHE is not supported by a multilayer sample though each individual layer probed separately might well show quantization to  $\rho_{xy} = h/ie^2$ .

Magnification of  $\rho_{xy}$  by a factor of 100 reveals additional small structure. This originates from the last or the first of the layers, since they are immersed into slightly different surroundings. However, since the deviation in density is small, the dephasing is immaterial for the plateaus at  $B > 5$  T.

In summary, we have measured the deHaas-van Alphen effect in 2D GaAs-(AlGa)As superlattices up to 5T at  $T = 1.5K$ . From the amplitude of the oscillations we can estimate the Landau levels to have a halfwidth of  $\sim 2$  meV. At  $T = 0.4K$  we have measured eddy current relaxation time of  $\sim 300$  s, which implies  $\rho_{xx} \sim 10^{-10} \Omega/\square$  corresponding to a 3D resistivity of  $\sim 10^{-16} \Omega \text{ cm}$ .

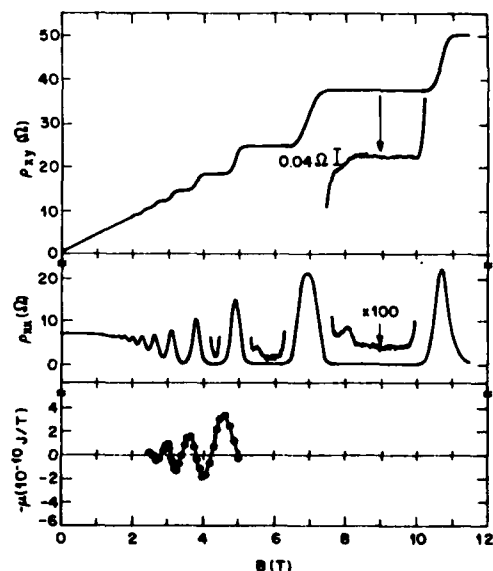
We would like to thank B. Batlogg for a loan of the SQUID magnetometer, D. Shoenberg for enlightening correspondence, A. Savage for carefully preparing the samples, and K. Baldwin for technical support.

#### References

- (1) K. v. Klitzing, G. Dorda and M. Pepper, Phys. Rev. Lett. **45**, 494 (1980).
- (2) D. C. Tsui and A. C. Gossard, Appl. Phys. Lett. **37**, 550 (1981).
- (3) D. C. Tsui, H. L. Stormer and A. C. Gossard, Phys. Rev. **B25**, 1405 (1982).
- (4) H. L. Stormer, T. Haavasoja, V. Narayanamurti, A. C. Gossard and W. Wiegmann, J. Vac. Sci. Technol. **B1**, 423 (1983).
- (5) H. L. Stormer, R. Dingle, A. C. Gossard, W. Wiegmann and M. D. Sturge, Solid State Commun. **29**, 705 (1979).
- (6) T. Haavasoja and D. J. Bishop, to be published.
- (7) D. C. Tsui, H. L. Stormer and A. C. Gossard, Phys. Rev. **B25**, 1405 (1982).

#### Figure Caption

Fig. 1. Magnetic moment  $\mu$  of a GaAs-(AlGa)As superlattice (172 layers, total area =  $33.2 \text{ cm}^2$ ) vs. magnetic field at  $T \sim 1.5K$ . The Hall resistance  $\rho_{xy}$  and Shubnikov-deHaas data  $\rho_{xx}$  are taken at  $T \approx 0.2K$  on a piece of the same sample with all the layers connected at current and voltage probes. Divide  $\rho_{xx}$  values by 3 to get  $\Omega/\square$ .



HYDROSTATIC PRESSURE CONTROL OF THE CARRIER  
DENSITY IN GaAs/GaAlAs HETEROSTRUCTURES  
ROLE OF THE METASTABLE DEEP LEVELS

by  
J.M. MERCY, C. BOUBQUET, J.L. ROBERT, A. RAYMOND,  
Groupe d'Etudes des Semiconducteurs  
Université des Sciences et Techniques du Languedoc  
Place Eugène Bataillon - 34060 MONTPELLIER CEDEX - FRANCE.

G. GREGORY, J. BEERENS, J.C. PORTAL  
Laboratoire de Physique des Solides, I N S A, 31077 TOULOUSE  
S.N.C.I. - CNRS 166 X, 38042 GRENOBLE

P.M. FRIJLINK  
Laboratoire d'Electronique et de Physique Appliquée  
3, Avenue Descartes, B.P. 15 - 95450 LIMEIL BREVANES

P. DELESCLUSE, J. CHEVRIER, T. LINH  
THOMSON-CSF, L.C.R., B.P. 10 - 91401 ORSAY

ABSTRACT

Hydrostatic pressure up to 18 kbar has been used to characterize GaAs/GaAlAs heterostructures manufactured using M.O.C.V.D. and M.B.E. techniques.

The pressure dependence of the carrier concentration  $n_s$  has been deduced from Hall measurements between 4.2 K and 300 K and Shubnikov-de-Haas experiments have been performed at Helium temperature.

The main result we have observed is a linear decrease of the carrier concentration as the pressure increases.

We explain this behaviour taking into account the deep character of the impurity level in GaAlAs connected with the X minimum whose variation is found to be 11 meV/kbar. When the Fermi energy is large enough compared to the difference of affinities  $\Delta E_c$ , a transition between a metallic to an insulating behaviour of the heterojunction is induced. Moreover, the metastable character of this impurity level, clearly pointed out by changing the cooling conditions must be taken into account.

In conclusion, this kind of experiment, in which the carrier concentration may be varied, appears as a powerful tool to investigate the properties of the heterostructures. In the particular case of GaAs/GaAlAs the role of the metastable state is predominant in all the investigations.

I. INTRODUCTION

In order to optimize the fabrication of lattice matched semiconduc-

tor heterojunctions used in semiconductor devices, it is necessary to investigate their electrical properties under various conditions and eventually to relate them to the growth technology used (metal organic chemical vapor deposition : MOCVD, Molecular Beam Epitaxy : MBE). In this paper, we study the electrical behaviour of  $Ga_{1-x}Al_xAs/GaAs$  heterostructures under hydrostatic pressure.

A strong variation of the carrier concentration  $n_s$  is observed in the whole range of temperature, the pressure being applied up to 18 kbar.

A decrease of  $n_s$  is also observed when the temperature decreases and a metastable character of the impurity level is put forward. We propose a model for the heterojunction which takes into account the existence of the spacer layer and the deep character of the impurity level in GaAlAs.

II. EXPERIMENTAL

Two types of heterojunction have been studied. One is obtained by MOCVD techniques (L.E.P.), the other one by MBE (Thomson-CSF). Most of the samples were bridge shaped but some Van der Pauw samples were also studied.

The samples are put in hydrostatic pressure cells (clamps or gaseous cells) where the pressure may be varied between 0 and 18 kbar at room temperature. Lower values of the pressure ( $\sim 12$  kbar) are reached at liquid helium temperature. It is important to note that, in this experiment, the pressure is applied at room temperature in order to avoid the consequences of the metastable behaviour of the donor level in the establishment of the space charge.

In order to measure the carrier density, Hall effect measurements are made as well as Shubnikov-de-Haas experiments which give access to the two-dimensional electron population. Because of the much higher conductivity of two-dimensional electron gas, the bulk conduction can be neglected.

III. RESULTS AND THEORY

On Figs. 1 and 2 we report the variation of the carrier density  $n_s$  when the pressure is applied. A linear dependence of  $n_s$  with  $P$  is obtained, and the heterojunction becomes insulating over a certain pressure which is temperature dependent.

In order to explain this behaviour, we take into account the existence of a deep level associated with the Si impurities in GaAlAs. The activation energy of these donors increases with pressure (1) and the observation of persistent conductivity in bulk GaAlAs (2) suggests that this level is probably associated with the X minimum.

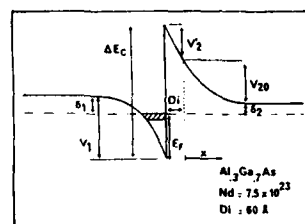
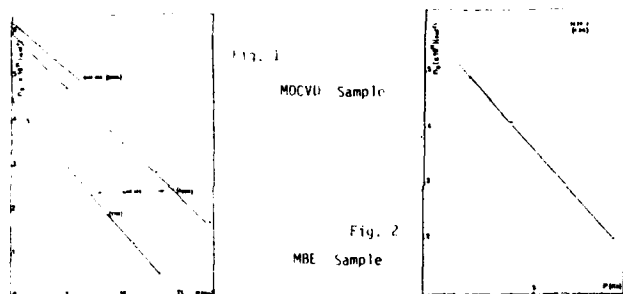


Fig. 3  
Energy Band Diagram  
in the case of MOCVD  
samples

$$n_{s1} = \frac{m^*}{\pi^2} kT \ln \left[ \left( 1 + \exp \left( \frac{E_F - E_0}{kT} \right) \right) \left( 1 + \exp \left( \frac{E_F - E_1}{kT} \right) \right) \right] \quad (2)$$

$$\text{where } E_0 = 7.865 \times 10^{-7} \left( \frac{F_{s1}}{m^*/m_0} \right)^{1/3} \quad (\text{eV})$$

$$\text{and } E_1 = 1.375 \times 10^{-6} \left( \frac{F_{s1}}{m^*/m_0} \right)^{1/3} \quad (\text{eV})$$

The electric field in the GaAlAs side of the interface is found by integrating Poisson equation in the doped region ( $x > 0$ ). We have for the density of charge:  $\rho(x) = (N_d^+ - N_c - n(x))q$

$$N_d^+ = \frac{N_d}{1 + 2 \exp \left( \frac{e_d - \delta_2 - v_2(x)}{kT} \right)} \quad n(x) = \frac{N_c \exp \left( \frac{-\delta_2 - v_2(x)}{kT} \right)}{1 + \frac{1}{4} \exp \left( \frac{-\delta_2 - v_2(x)}{kT} \right)}$$

The acceptor impurities are assumed to be all filled with electrons, and Ehrenberg approximation (5,6) has been used for the calculation of  $n(x)$ .

Poisson equation is integrated to give:

$$\left( \frac{dv_2}{dx} \right)_{x=0} = \frac{2q^2 N_d kT}{\epsilon_2} \ln \frac{a+1}{a + \exp \left( \frac{v_{20}}{kT} \right)} + \frac{N_c v_{20}}{N_d kT} + \frac{4N_c}{N_d} \ln \frac{1 + \frac{1}{4} \exp \left( \frac{-\delta_2}{kT} \right)}{1 + \frac{1}{4} \exp \left( \frac{-(\delta_2 + v_{20})}{kT} \right)}$$

$$= \frac{2q^2 N_d v_{eff}}{\epsilon_2} \quad \text{where } a = 2 \exp \left( \frac{e_d - \delta_2}{kT} \right); v_{20} = v_2(x=0)$$

The carrier density is calculated assuming that the GaAlAs is partially compensated and that the donors are not completely ionized. All the calculations presented here are made in the parabolic band approximation.

The energy band diagram assumed is shown in Fig. 3 where all the parameters are defined. The quantum well is treated in the triangular well approach (3,4) and a solution is found by requiring that the two-dimensional electron population equals the density of electrons depleted from the GaAlAs side. The space layer is considered to be perfectly compensated ( $N_A = N_D$ ) so that the band curvature is negligible in that region. One must however keep in mind that things could be modified if the compensation of the spacer is not complete.

The electron density per unit area in GaAs ( $n_{s1}$ ) and the density of positive charges in GaAlAs ( $n_{s2}$ ) are related to the electric field  $F_s$  at the interface by these relations:

$$n_{s1} = \frac{\epsilon_1 F_{s1}}{q} \quad n_{s2} = \frac{\epsilon_2 F_{s2}}{q} \quad (1)$$

and the continuity of the electric displacement vector ( $\epsilon_1 F_{s1} = \epsilon_2 F_{s2}$ ) at the interface requires that  $n_{s1} = n_{s2}$ .

The population in the GaAs side, considering only the two first quantized levels  $E_0$  and  $E_1$ , is given by (3,4)

An effective value of the band bending,  $v_{eff}$ , is defined in order to obtain the familiar looking relation :

$$n_{s2} = \frac{\epsilon_2}{q} \left( \frac{dv_2}{dx} \right)_{x=0}^{1/2} = \left( \frac{2 \epsilon_2 N_d v_{eff}}{q} \right)^{1/2} \quad (5)$$

The value of  $\delta_2$  is determined from the charge neutrality condition far from the junction in GaAlAs :

$$n_0 + N_a = N_d^+ \quad (6)$$

and  $E_F$  is given by

$$E_F = \Delta E_C - \frac{qn_{s2}d}{\epsilon_2} - v_{20} - \delta_2 \quad (7)$$

where the electric field was considered to be constant in the spacer.

Knowing  $\epsilon_d$ , we can now determine the values of all the quantities by choosing  $v_{20}$  in order to have  $n_{s1} = n_{s2}$ .  $\{ \epsilon_d(0) = 60 \text{ meV } (7) \}$

Other quantities vary with pressure. It is the case of the effective mass in GaAs for which we have (8,9).

$$\frac{m^*}{m_0} = 0.067 + 4 \times 10^{-4} P \quad (P \text{ in kbar})$$

The corresponding dependence of  $m^*$  in GaAlAs is found to have a weak effect. This quantity is only appearing in the calculation of  $n(x)$  (through  $N_d$ ) and this term changes the results by only a few percents even at 300 K for concentration up to  $1 \times 10^{18} \text{ cm}^{-3}$ . As a consequence, the variation of  $m^*$  with  $P$  has been neglected in GaAlAs.

As it can be seen in table 1, a good agreement between theory and experiment is obtained by choosing  $N_a = 0.32$  and  $\beta = 11 \text{ meV/kbar}$ . This concerns the case of an heterojunction grown by MOCVD with a spacer thickness of  $60 \text{ \AA}$  and Si-doped to  $7.5 \times 10^{17} \text{ cm}^{-3}$ . A compensation of 0.32 is considered by the fabricants to be a typical value for this material, and the value of  $\beta$  taken is different from the one proposed by Saxena ( $\beta = 14.1 \text{ meV/kbar}$ ).

$dn_s/dP \text{ (} 10^{11}/\text{kbar)}$	300 K	77 K
Experimental	0.245	0.295
Theoretical	0.240	0.330

TABLE 1 : Theoretical results with SHF 175 sample.

#### IV. DISCUSSION OF THE RESULTS

This model seems to represent adequately the rate of decrease of the two-dimensional electron density with pressure, and the variation of this rate with temperature. It is however unable to explain the variation of  $n_s$  with  $T$  (see Fig. 1 and 2). All the heterojunctions show an increase of  $n_s$  with temperature, when measurements are made in the dark, while calculations give a slight decrease when  $T$  increases.

This behaviour must find its reason in the several points which were not taken into account here, like a possible contribution of the spacer, the presence of interface states, the presence of electrons in higher bands (L and X) at high temperature or the temperature dependence of  $\Delta E_C$ .

The interface states, like the variation of  $\Delta E_C$  with temperature and pressure are however poorly known and their effects are difficult to estimate.

The introduction of the partial compensation of GaAlAs is essential to explain the pressure behaviour (zero compensation leads to a value of  $dn_s/dP$  twice smaller than what is observed). Thus we had to modify the model proposed recently by Lee et al (10), and contrarily to what is said in this reference we find that the free electron population  $n(x)$  in GaAlAs is negligible even at 300 K and high doping level ( $10^{18} \text{ cm}^{-3}$ ).

No attempt was made to fit the calculations to the results at 4.2 K since at this temperature we cannot reach equilibrium because of the relaxation effects. Even at 77 K, we had to wait several minutes to have equilibrium; this can be easily observed by illuminating the sample for a while and looking at the decrease of  $n_s$  toward its equilibrium value.

Coulomb Inelastic Lifetime of a Quasi-Particle  
In a Two Dimensional Electron Gas\*

Gabielle F. Giuliani\*\* and J. J. Quinn  
Brown University, Providence, Rhode Island 02912, USA

We discuss a theory of the coulombic inelastic lifetime  $\tau_i$  of the electronic states of a two dimensional electronic system. Our approach is based on a perturbative diagrammatic analysis of the electron-impurity system. We obtain a general expression for  $1/\tau_i$  which, in contrast to previous work, reduces, in the appropriate limits, to the well known diffusion-dominated and the pure regimes. We show that our results provide a comprehensive picture which can be tested by magnetoconductance experiments in high mobility inversion layer devices. We find that at low temperatures both momentum conserving and diffusive processes contribute to the  $T^2$  term in  $1/\tau_i$ .

The coulomb interaction contribution to the inelastic lifetime  $\tau_i$  of a quasiparticle in a two-dimensional (2D) electron gas has recently received much attention. Such interest is motivated by the relevance of the inelastic mean-free path of a 2D electron in the localization problem [1], [2]. At low temperatures in the pure metal regime  $1/\tau_i$  is found to behave like  $T^2$  [3], whereas in the presence of impurities the diffusive nature of the electron dynamics leads to a much larger value which increases linearly with  $T$  [4]. In Ref. [3] the effect on  $1/\tau_i$  of the low-lying 2D plasma mode has been also investigated.

In previous theoretical work on the impure 2D electron gas [4] the main contributions to  $1/\tau_i$  were evaluated within a diagrammatic approach by making use of expressions for the impurity average of the relevant Green function products. The validity of these expressions is restricted to

the case in which the electron dynamics is purely diffusive. In particular the behaviour of the pure system cannot be recovered by letting the elastic lifetime  $\tau_0$  be infinite. As in a real situation the two regimes are inextricably intermingled [2], there is a need for a unified approach in which the elastic lifetime, or what is the same, the impurity concentration, can be varied at will as an external parameter.

In this paper we provide a simple theory of  $1/\tau_i$  which allows us to bridge the gap between the pure and dirty metal regimes. Our results can be very usefully used in fitting the temperature dependence of  $\tau_i$  as measured in magneto-conductance experiments [2].

The coulomb inelastic lifetime of a quasiparticle of energy  $E=E_F+\Delta$  in the presence of impurities can be defined [4] as

$$\frac{1}{\tau_i(\Delta, T)} = \frac{1}{N_0(E)} \sum_n \delta(E-E_n) \frac{1}{\tau_n} \quad (1)$$

where  $N_0(E)$  is the density of states and  $1/\tau_n$  is the inverse coulomb inelastic lifetime of a quasiparticle in the state  $|n\rangle$  and energy  $E_n$  which is assumed to be an exact eigenstate of the electron Hamiltonian in the presence of the impurity potential. If we assume for  $1/\tau_n$  a Fermi golden rule expression in which the transitions are due to a screened coulomb potential and make use of linear response theory together with the fluctuation-dissipation theorem, we obtain the following general formula [5]

$$\frac{1}{\tau_i(\Delta, T)} = \frac{1}{N_0(E)} \frac{1}{[1+e^{-\Delta/T}]} \sum_q \int_{-\infty}^{\infty} d\omega \, W(\vec{q}, \omega) v_q^2 \ln \frac{1}{c(\vec{q}, \omega)} \times [\coth(\frac{\omega}{2T}) - \tanh(\frac{\omega-\Delta}{2T})] \quad (2)$$

Here  $v_q$  is the fourier transform of the bare coulomb potential and  $c(\vec{q}, \omega)$  is the complex dielectric function of the non-interacting electron gas in the presence of impurities. The function  $W(\vec{q}, \omega)$  contains the wave

#### V. CONCLUSION

We have shown that measurements of electrical properties of GaAlAs/GaAs heterojunction under hydrostatic pressure can lead to several informations concerning the parameters describing the energy band diagram of this structure.

Further experiments on samples with different doping level and spacer thickness are necessary to ameliorate the model, and give a better understanding of the properties of these structures.

The rapid decrease of  $n_s$  with pressure might become very useful in studying localization effects responsible for quantum Hall effect. This kind of work is under way now.

#### ACKNOWLEDGEMENTS

We would like to thank Dr. Damelincourt and Dr. Salom from the Laboratoire de Physique Atomique de Toulouse, who gave us the opportunity to use their computing facilities.

The financial support was provided by Ministère de la Recherche et de l'Industrie.

#### REFERENCES

- (1) A.K. SAXENA, J. Phys. C : Solid St. Phys., 13 (1980) 4323-34.
- (2) R.J. NELSON, Applied Phys. Letters, 31, n°5 (1977) 351-353.
- (3) F. STERN, Phys. Rev. B, 5, 12, (1972), 4891-99.
- (4) D. DELAGEBEAUDEUF, N.T. LINH, IEEE Trans. Electron. Devices ED-29, 955 (1982).
- (5) W. EHRENBERG, Proc. Phys. Soc. A (1950) 63, 75
- (6) R.A. SMITH, Semiconductors, 2nd Edition (Cambridge University, Boston, 1978), p. 83.
- (7) T. ISHIKAWA, J. SAITO, S. SASA, S. MIYAMIZU, Japan J. of Appl. Phys., 21 n° 11 (1982), p. 675-6
- (8) C.N. AHMAD, H.L. TATHAM, A.R. ADAMS, R.J. NICHOLAS, G.D. PITT, Proc. 8th AIRAPT Conference, Uppsala (1981).
- (9) G.D. PITT, J. LEES, R.A. HOULT, R.A. STRADLING, J.Phys.C : Solid State Phys. Vol. 6, 1973, 3282-94.
- (10) K. LEE, M. SHUR, T.J. DRUMMOND and H. MORKOC, J. Appl. Phys. 54 (4), 2093-96, (1983).

function correlations and is defined as

$$\chi(\vec{q}, \omega) = \overline{\sum_{n,m} \langle n | e^{i\vec{q} \cdot \vec{r}} | n \rangle^2 \delta(\omega - E_n + E_m) \delta(E - E_n) \delta_{0n} \delta_{0m}} \quad (3)$$

where the bar denotes the impurity average. In deriving (2) the assumption has been made that the impurity average can be taken independently in evaluating the quantity  $\chi$  and the dielectric function.

Making use of standard methods [6] the quantities  $\chi(\vec{q}, \omega)$  and  $\epsilon(\vec{q}, \omega)$  can be expressed in terms of bilinear forms of the appropriate advanced and retarded Green functions. Perturbation theory can then be used to derive the following results for a two dimensional electron gas [5]

$$\chi(\vec{q}, \omega) = - \frac{1}{\pi\omega} \operatorname{Im} \chi^0(\vec{q}, \omega) \quad (4)$$

and

$$\epsilon(\vec{q}, \omega) = 1 - v_F^2 \chi^0(\vec{q}, \omega) \quad (5)$$

where the response function  $\chi^0(\vec{q}, \omega)$  is given by

$$\chi^0(\vec{q}, \omega) = N_0 \left\{ 1 - \frac{\omega}{\left[ \frac{1}{2} (v_F - Dq^2)^2 - \frac{1}{2} v_F^2 \omega^2 \right]^{1/2} - \frac{1}{2} v_F^2 \omega^2} \right\} \quad (6)$$

In Eq.(6), we have introduced the diffusion constant  $D = v_F^2 \tau_0 / 2$ ,  $v_F$  being the Fermi velocity of the electron gas. This expression for  $\chi^0$  has been derived keeping only ladder diagrams in the perturbation expansion and is valid for small values of  $q$  and  $\omega$ , but it is general enough to

describe the dynamical response of the system as function of  $\tau_0$ . In particular it is readily established that the corresponding well known expressions for the response in the pure and diffusive regimes are recovered as  $\tau_0$  is respectively made to diverge or vanish.

With the use of (3), (4), (5) and (6), Eq.(2) provides a simple and convenient formula for  $1/\epsilon_1$ . For  $\tau_0 \rightarrow \infty$  the integrations can be done analytically in the limit of small  $\Delta/E_F$  and the results of Ref.[3] are recovered. For finite  $\tau_0$  our formula, apart for a factor of  $[1 + \exp(-\Delta/T)]$ , reduces to the one discussed in [4] once the imaginary part of the electronic self-energy is evaluated on the energy shell. In the general case for finite values of the parameters  $\Delta/E_F$  and  $1/\tau_0 E_F$  and  $T$ , Eq.(2) must be evaluated numerically. This involves a two dimensional integral which does not present any particular difficulty.

At high electronic densities the wavevector sum can be safely cut off at the inverse screening length  $k = 2\pi^2 N_0$ . As the actual densities in inversion layers are in general very low, (typically  $n_s = 2 \times 10^{12} \text{ cm}^{-2}$ ), this wavevector may be comparable to or even larger than the Fermi wavevector and an expression for  $\chi^0$  valid also at large  $q$  must be used. We find that a convenient interpolation formula is obtained by adding  $(q^2/2m)^2$  to the argument of the square root appearing in (6). This leads to the correct behaviour for  $\chi^0$  at large  $q$ .

We have studied the behaviour of  $1/\epsilon_1$  as a function of  $\tau_0$  for several values of the relevant parameters. In Figs. 1 and 2 the dependence of  $1/\epsilon_1$  upon  $\Delta/E_F$  for small  $T/\Delta$ , and upon  $T/E_F$  for small  $\Delta/T$  is shown for two different values of  $\tau_0$ . For large  $\tau_0$ ,  $1/\epsilon_1$  is approximately proportional to  $(\Delta/E_F)^2$  and  $(T/E_F)^2$  respectively, whereas for smaller values of  $\tau_0$  this law is replaced, as expected, by an approximately linear dependence. The actual behaviour is more complicated and will be discussed in more detail in a different paper [5].



# REFERENCES

\* Supported in part by the Office of Naval Research.

\*\* On leave from the Scuola Normale Superiore, Pisa, Italy.

1. D. J. Thouless, Phys. Rev. Lett. **39**, 1167 (1977); P. W. Anderson, E. Abrahams, and T. V. Ramakrishnan, Phys. Rev. Lett. **43**, 718 (1979).
2. R. G. Wheeler, Phys. Rev. **B24**, 4645 (1981); M. J. Uren, R. A. Davis, M. Kaveh, and M. Pepper, J. Phys. C: Solid State Phys. **14**, L395.
3. G. F. Giuliani and J. J. Quinn, Phys. Rev. **B26**, 4422 (1982).
4. E. Abrahams, P. W. Anderson, P. A. Lee, and T. V. Ramakrishnan, Phys. Rev. **B24**, 6783 (1981).
5. G. F. Giuliani and J. J. Quinn, to be published.
6. A. A. Abrikosov, L. P. Gorkov, and I. E. Dzyaloshinski, "Methods of Quantum Field Theory in Statistical Physics", (Prentice-Hall, Englewood Cliffs, 1969).

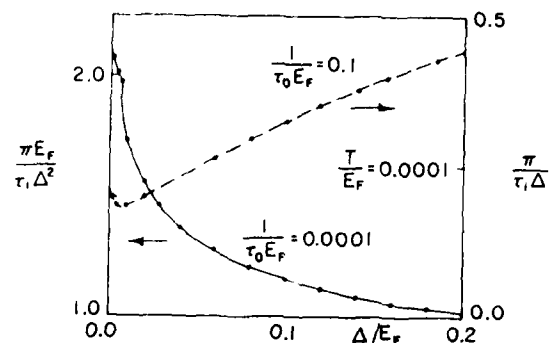


Fig. 1. A plot of  $1/\tau_1$  vs. excitation energy  $\Delta = E - E_F$  at a temperature  $T = 10^{-4} E_F$ . The solid and dashed lines, corresponding to a rather pure and a rather dirty sample respectively, are smooth curves drawn throughout the points obtained numerically. The ordinate for the solid curve appears on the left, that for the dashed curve on the right.

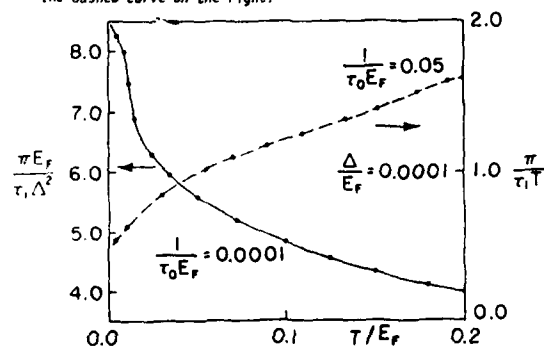


Fig. 2. A plot of  $1/\tau_1$  vs. temperature for an excitation energy  $\Delta = 10^{-4} E_F$ . The solid and dashed curves correspond to pure and dirty samples; the ordinates for each appear on the left and right respectively as in Fig. 1.

TUNNELING SPECTROSCOPY OF LANDAU-LEVELS IN ELECTRON  
INVERSION LAYERS ON (100)-Si SURFACES

U. Kunze and G. Lautz  
Institut für Elektrophysik, Techn. Universität Braunschweig  
and  
Hochmagnetfeldanlage der Techn. Universität Braunschweig  
D-3300 Braunschweig, Fed. Rep. of Germany

**Abstract**

Tunneling studies on metal-SiO<sub>2</sub>-Si-junctions are performed at 4.2 K in high magnetic fields. Oscillations in the differential conductance  $dI/dU$  and its derivative  $d^2I/dU^2$  reflect the Landau-level structure of the lowest subband of the electron inversion layer. In bias-sweep measurements their period gives a direct measure of the effective mass of the surface electrons. The density of states of this subband is deduced from magnetic field sweeps at different biases, varying the effective area in the k-plane. The electron density as a function of applied bias is determined from magneto-oscillations, which are observed in  $d^2I/dU^2$  at high modulation voltages, whenever a Landau-level passes the semiconductor Fermi-level.

Recently the tunneling spectroscopy has been applied to Si accumulation and inversion layers by use of a special technique in preparing planar MOS tunnel devices [1,2]. These experiments proved to be well suited to determine the minimum energies of the quantized 2D-subbands relatively to the semiconductor Fermi-level. We are reporting here first tunneling studies of (100)-electron inversion layers in high magnetic fields.

In tunneling through an oxide barrier between a metal electrode and 2D-subband states the contribution to the differential conductance  $dI/dU$  due to each subband is known to be proportional to the density of states of this subband [3]. When a quantizing magnetic field is present, the subbands split into series of scattering broadened Landau levels, which cause additional oscillations in the tunneling conductance [4,5]. We assume that the contribution of, for instance, the lowest subband to the oscillatory component may be described by [4]

$$\left(\frac{dI}{dU}\right)_{osc} = A \exp\left(-\frac{2\pi^2 k_B T}{\hbar\omega_c}\right) \cdot \cos\left(2\pi \cdot \frac{E_{FS} - E_0(U) - eU}{\hbar\omega_c} + \phi\right) \quad (1)$$

where  $A$  is constant or only weakly dependent on magnetic field,  $T_D$  is the

Dingle temperature,  $\hbar\omega_c$  the Landau splitting,  $E_{FS} - E_0(U)$  the difference between the semiconductor Fermi-level and the bottom of the ground subband,  $U$  the applied bias between metal and semiconductor tunnel electrodes and  $\phi$  a phase angle. These oscillations can be observed for bias values  $U < (E_{FS} - E_0)/e$ , i.e. when the metal Fermi-level  $E_{FM} = E_{FS} - eU$  lies above the subband edge at  $E_0$ .

Our experiments are performed on MOS tunnel junctions with native oxide barriers [2]. The substrates are (100)-oriented p-Si wafers having a net acceptor volume concentration of  $N_A \approx 3.9 \cdot 10^{15}/\text{cm}^3$ . Mg or Ti are used as counter electrodes, whose low work function creates an electron inversion layer of typical  $8 \cdot 10^{12}/\text{cm}^2$  and  $2.5 \cdot 10^{12}/\text{cm}^2$  for Mg and Ti, respectively. The tunnel devices are mounted on a sample holder, which can be rotated (accuracy one degree), and immersed in liquid He. A Bitter magnet is used to provide magnetic fields up to 15.6 Tesla. The tunneling conductance  $dI/dU$  and its derivative  $d^2I/dU^2$  are taken as a function of the applied bias at constant magnetic field, or at constant bias while sweeping the magnetic field, by use of the conventional modulation technique [6].

Fig. 1. shows the conductance vs. bias curves of a Mg-metallized junction with magnetic field directions parallel and perpendicular to the sample surface. The steps in the background conductance are due to the steplike increase of the number of available states in tunneling, when the metal Fermi-level passes the energy minimum of a subband, e.g. at  $U \approx 50$  mV and  $U=0$  for the subbands  $E_0$  and  $E_0'$ , respectively [1]. In case of a perpendicular magnetic field ( $B \perp J$ ), the  $dI/dU$ -curve exhibits weak oscillations, which arise from the Landau-level structure of the ground subband. In the second derivative trace (Fig. 2.) these oscillations are clearly enhanced against the background curve. From eq. (1), their period is given by

$$\Delta(eU) = \hbar\omega_c + \Delta(E_{FS} - E_0(U)). \quad (2)$$

Because in the differential conductance the oscillation amplitude is much smaller than the step height due to the lowest subband, we assume the density of states to have only a small oscillatory component, too. Then the occupation height  $E_{FS} - E_0(U)$  is nearly a linear function of the applied bias even at highest magnetic fields. Indeed, we do not observe any change in the period when either the density-of-states maximum of a Landau-level coincide with the semiconductor Fermi-level or the minimum between two Landau-levels. The dependence  $E_0(U)$  can be obtained from additional measurements, as discussed below, which give us two data points: First at an applied bias  $U_0$ , the metal Fermi-level is aligned with the subband minimum  $E_0$ , i.e.

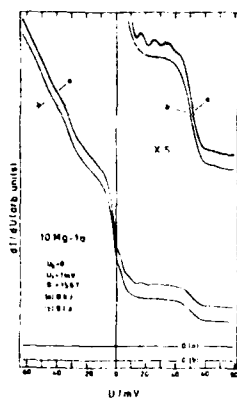


Fig. 1. Tunneling conductance  $dI/dU$  vs. bias  $U$  of a  $Mg/SiO_2/Si$ -junction at  $T = 4.2$  K in a magnetic field applied (a) perpendicular and (b) parallel to the junction surface. The bias sign refers to that of the metal electrode ( $U_0$  denotes the substrate bias,  $U_1$  the modulation voltage).

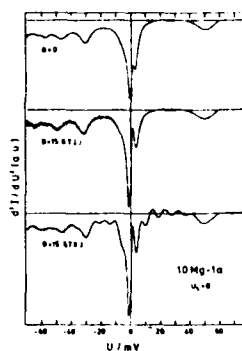


Fig. 2. As in Fig. 1,  $d^2I/dU^2$  vs.  $U$ . For comparison the  $B = U$  curve has also been recorded.

$$eU_0 = E_{FS} - E_0(U_0), \quad (3)$$

second, when the reverse "threshold voltage"  $U_t$  is applied, the occupation height is zero, as the electron density is removed,

$$0 = E_{FS} - E_0(U_t). \quad (4)$$

Using the linear dependence  $E_0(U)$  and eqs. (3) and (4), eq. (2) can be written as

$$\Delta(eU) = \frac{\hbar\omega_c}{e} = \frac{U}{U_t - U_0} \Delta(eU)$$

or

$$\frac{\hbar\omega_c}{e} = \frac{\hbar\omega_c}{e} = \Delta U \frac{U}{U_t - U_0}, \quad (5)$$

thus the period  $\Delta U$  gives directly the cyclotron mass  $m_c/5$ . Typical values of  $U_t/(U_t - U_0)$  are 0.94...0.97. By measurements at different perpendicular components of  $B$ , varying the tilt angle between the directions of  $B$  and the surface normal or the total magnetic field, we get the same cyclotron masses as given in table 1.

When the magnetic field is swept at fixed bias  $U$ , the conductance  $dI/dU$  and its derivative  $d^2I/dU^2$  exhibits de Haas-van Alphen type oscillations periodic in  $(1/B)$ . Their period  $\Delta(1/B)$  is inversely proportional to the effective area in the  $k$ -plane corresponding to a number of states  $N_k(E)$  per unit area of the real space

$$\Delta\left(\frac{1}{B}\right) = \frac{R_V}{\hbar} \cdot \frac{1}{N_k(E)}, \quad (6)$$

where  $R_V = 2$  is the valley degeneracy factor of the ground subband. The enclosing constant-energy contour in the  $k$ -plane is aligned with the metal Fermi-level, therefore  $E = E_{FM} = E_{FS} - eU$ . In Fig. 3,  $N_k$  is plotted as a function of applied bias  $U$  for three different junctions. Obviously, at  $U=0$  where  $E=E_{FS}$ , the  $N_k$  are equal to the densities  $N_s$  of surface electrons with no applied bias (table 1). As expected  $N_k(U)$  are straight lines, and their slopes give the density of states

$$D_0 = \frac{dN_k}{d(E-E_0)} = \frac{dN_k}{dU} \cdot \frac{dU}{d(E-E_0)} = \frac{U_0 - U_t}{eU_t} \cdot \frac{dN_k}{dU} = \frac{R_V m_c}{\hbar^2} \quad (7)$$

Within experimental error, the density-of-states masses  $m_d$  are equal to the cyclotron masses  $m_c$  as determined above (table 1). The extrapolations of the lines to  $N_k = 0$ , marked by arrows, intersect the axis at biases  $U_0$  as introduced in eq. (3). These values agree within a few mV with the bias positions of the dips in  $d^2I/dU^2$  at  $B = 0$  due to the minimum of the 0-subband.

If we assume the validity of eq. (1), we are able to deduce the Dingle temperature  $T_D$  from the magnetic field dependence of the oscillation amplitude.

Table 1. Results.			
junction	10 Mg - 1a	4 Ti - 4c	5 Ti - 4a
$m_c/m_0$	$0.72 \pm 0.01$	$0.21 \pm 0.02$	$0.21 \pm 0.02$
$m_d/m_0$	$0.22 \pm 0.01$	$0.19 \pm 0.02$	$0.22 \pm 0.02$
$N_s(n) \cdot cm^{-2}$	$8.1 \cdot 10^{12}$	$2.6 \cdot 10^{12}$	$2.4 \cdot 10^{12}$
$T_D/K$	19	13	9

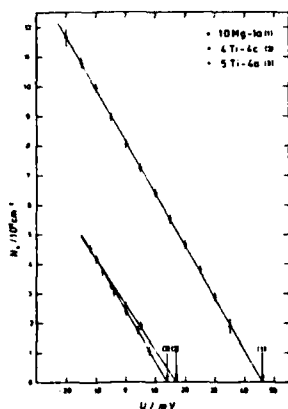


Fig. 3. Number of states  $N_k$  in the lowest subband per unit area of the real space up to an energy  $E$  which lies by  $-eU$  above the Si Fermi-level. Data are taken from three different junctions ( $T = 4.2$  K).

We have plotted the log of the amplitude, normalized by the weakly field dependent preexponential factor ( $X/\sinh X$ ;  $X = 2\pi^2 kT/\hbar\omega_c$ ) vs. reciprocal field and obtained straight lines. From their slopes we evaluated the Dingle temperatures as given in table 1.

At biases  $U \gg U_0$  no Landau-level oscillations appear in the tunneling characteristics. However, if now the modulation voltage is increased by a factor of 10, new oscillations are visible in recordings of  $d^2I/dU^2$  vs.  $B$ . In bias sweeps, these oscillations have periods of about 20 times larger than those of the Landau-oscillations. Long-period oscillations of similar kind were firstly observed by Tsui /5/ in tunneling from a metal electrode through an oxide barrier into an accumulation layer on degenerate InAs. He attributed them to oscillations of the effective barrier height due to changes in the self-consistent surface potential, which occur when in a magnetic field or bias sweep the Landau-levels move discontinuously through the InAs Fermi-level /7/.

We can measure long-periodic oscillations also in the bias region  $U < U_0$ , since the high modulation voltage overmodulates the short-periodic Landau-oscillations. Because of a strong bias dependence of the oscillation amplitude - peak values at negative biases are more than two orders of magnitude higher than those at positive biases - we assume, that the bias (i.e. den-

sity) dependent series resistance of the inversion channel is responsible for the formation of the long-periodic oscillations, since for large reverse biases the tunneling resistance decreases (Fig. 1) and the series resistance of the electron channel increases with diminishing electron density. Accordingly the long-periodic oscillations reflect simply the magneto-oscillations of the channel resistance.

Regardless of the origin of these oscillations, in contrast to the Landau-level oscillations they arise by passing Landau-levels the semiconductor Fermi-level. This enables us to extract the surface electron density  $N_s$  as a function of applied bias from  $B$ -sweep measurements, as depicted in Fig. 4. The arrows indicate extrapolated values of the "threshold voltage", which is needed for evaluating eq. /5/. The zero-bias data  $N_s(0)$  agree well with those deduced from Landau-level oscillations (Fig. 3.).

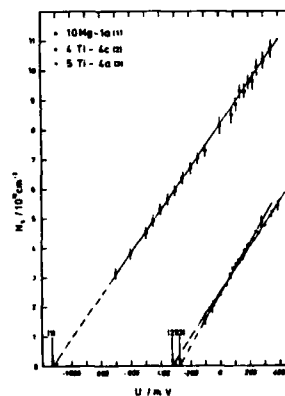


Fig. 4. Surface electron density  $N_s$  as a function of applied bias  $U$  for the junctions used in Fig. 3. ( $T = 4.2$  K).

Acknowledgement - This work was supported by the academy of sciences and literature, Mainz.

#### References

- /1/ U. Kunze, G. Lautz, Surface Sci. 113 (1982) 55
- /2/ U. Kunze, G. Lautz, Solid State Commun. 42 (1982) 27
- /3/ D.J. BenDaniel, C.B. Duke, Phys. Rev. 160 (1967) 679
- /4/ D.C. Tsui, Phys. Rev. B 4 (1971) 4438
- /5/ D.C. Tsui, Phys. Rev. B 8 (1973) 2657
- /6/ M. Altwein, H. Finkenrath, J. Phys. E 6 (1973) 770
- /7/ G.A. Baraff, J.A. Appelbaum, Phys. Rev. B 5 (1972) 475

MULTILAYER SEMICONDUCTOR  
OPTOELECTRONIC DEVICES

F. Capasso

Bell Telephone Laboratories, Murray Hill, N.J.

- An Invited Review -

596

HIGH-SPEED HETEROSTRUCTURE  
DEVICES

T.P. Pearsall

Bell Telephone Laboratories, Murray Hill, N.J.

- An Invited Review -

597

# Dependence of Interface State Density on the Atomic Roughness at the Si-SiO<sub>2</sub> Interface

Peter O. Hahn<sup>a)</sup>, S. Yokohama<sup>b)</sup> and M. Henzler<sup>a)</sup>  
IBM Thomas Watson Research Center  
Yorktown Heights, N.Y. 10598

## Abstract:

Quasi static Capacitance Voltage (C-V) measurements have been performed on Si(111) - metal oxide semiconductor (MOS) structures with different and well known atomic roughness. The atomic roughness was determined on an atomic scale quantitatively with spot profile analysis of low energy electron diffraction pattern (SPA-LEED). The results demonstrate a strong correlation between atomic roughness and interface state density. Even after an additional post metallization annealing (PMA) treatment when surface states should be minimized, the remaining interface state density is strongly correlated to the atomic roughness. A simple model which is associated with each kind of step atom, i.e. edge or kink atoms, suggests the creation of a dangling bond and therefore a surface state can explain the results. The correlation of the fixed charge  $Q_{fix}$  to the atomic roughness can be determined in the same way. Assuming that ionized atoms which are responsible for  $Q_{fix}$  are located preferentially at those steps or kinks which are also correlated to the dangling bonds at the interface we confirm the general opinion that  $Q_{fix}$  and surface states have at least one common physical origin: the atomic roughness.

## I. Introduction

Inversion layers are two-dimensional systems. To understand their electronic properties, it is very important to know the correlation of their structural properties to the interface state density, which is the topic of this paper. With SPA-LEED (spot profile analysis of low energy electron diffraction) (1-8) and special sample handling a method is available (6,9), which for the first time enables us to determine the step density quantitatively at the interface. This method is based on a kinematical approach of LEED-theory (1,2).

In previous studies (6,9) we have shown the influence of the oxidation parameters on the atomic roughness at the Si-SiO<sub>2</sub> interface. The roughness depends on all oxidation parameters (see Table 1 and ref. 6,9). Similar as Revesz et al (26) we proposed a model(6) introducing a roughening and a smoothing factor to explain the results. The random process of the diffusion and the random reaction of oxygen at the interface is the roughening effect, which should increase the roughness with growing oxide thickness. On the other hand, in thermal equilibrium a smooth step-free surface is energetically favored similar to the free surface of silicon. Therefore, diffusion of oxygen and/or silicon smoothens the interface depending on temperature, ambient, and duration of heat treatment. The balance between roughening and smoothing determines the final roughness.

In an earlier study (10) we had reported the influence of the atomic roughness on the mobility in MOS-inversion layers by measuring the Hall effect and conductivity in a temperature range from 4.2 K to room temperature. As a result, it was found that there exists a strong correlation between Hall-mobility and atomic roughness at high inversion ( $9 \times 10^{12} \text{ cm}^{-2}$ ), indicating that the product of mobility and roughness is nearly constant (see Table 1). The aim of this paper is to determine directly and quantitatively the correlation of the atomic roughness on an atomic scale with the interface state density as derived from capacity (C-V) measurements.

## II. Experimental

Similar samples as discussed and described in the previous paper (10) for measurement of mobility and atomic roughness were used for the C-V-measurements. We used 5-100 cm, n-type (phosphorus doped) (111) oriented Si-chips. As explained in our previous study (10), one third of the chips carried only the gate oxide, from this area samples were cut for measuring the atomic roughness with SPA-LEED. Two thirds of the chips were covered with the MOS-transistors as seen in Fig. 1. These MOS-structures were used for the C-V-measurements too. The source, drain and gate-contacts were floating. The values of the interface state density ( $N_{it}$ ) were determined by the quasi static technique (11-13) and measured by a computerized C-V-analysis system. Simultaneously, the 1 MHz C-V curves were measured using the current meter (Keithley 427) and the capacitance meter (Boonton Model 72BD). The ramp voltage was swept ( $\frac{dV}{dt} = 0.4 \sim 0.5 \text{ V/sec}$ ) from -20 to 20 Volts automatically. First the samples have been measured directly after gate oxidation and metallization without any further heat treatment. A second measurement has been performed with the identical samples after a post metallization annealing (PMA) in forming gas (10% H<sub>2</sub>, 90% N<sub>2</sub> at 400°C for 20 min).

## Analysis

Surface state density was obtained by comparing the measured quasi static C-V-curve and the theoretical curve. The thickness of the oxide was obtained from capacitance measurements at 1 MHz for strong accumulation. The gate area was  $7.3 \times 10^{-6} \text{ cm}^2$ .

## III. Results

### A. Atomic Roughness

On the same chips with the MOS structures, the step atom density at the Si-SiO<sub>2</sub> interface has been determined quantitatively, using the evaluation procedure as described in (6,9). The results are shown in Table I. The numerical values of step atom density are derived from many measurements at different positions on the same chip forming an average value and its mean deviation. The table exhibits the correlation of the atomic roughness to the mobility at 4.2 K for high carrier concentration, discussed in (10).

### B. Interface State Density

The interface state density for all four kinds of MOS-structures is shown in Fig. 2. R1 and R2 were processed in the same experimental run, except that the additional annealing in inert atmosphere was carried out only for R2. Comparing R1 and R2, we observe that R1 shows a remarkably higher interface state density than that of R2 throughout the entire gap. The same relationship was found for samples R3 and R4. Fig. 3 shows the influence of the PMA treatment on the density of states for samples R1 and R2. Fig. 4 exhibits the same decrease of the density of states of R3 and R4 due to PMA-treatment. From all these curves the average density of states was determined and added in Table I with and without PMA-treatment.

### C. Fixed Oxide Charge $Q_{fix}$

<sup>a)</sup> Permanent address: Institut f. Festkorperphysik, University Hannover, 3000 Hannover, Appelstr. 2, West Germany

<sup>b)</sup> Permanent address: Dept. of Electrical Engineering, Hiroshima University, Shitami Sojo-cho Higashihiroshima 724, Japan

Finally we calculated the total charge  $Q^*$ . We used the formula

$$Q^* = \frac{C_{ox} V_{FB}^2}{2q} = Q_{FB} + Q_{it}$$

$$\Delta V_{FB} = V_{FB} - V_{FB}^0 \text{ and } Q_{it} > 0$$

with  
 $C_{ox}$  capacity of MOS structure  
 $V_{FB}$  Flatband voltage  
 $V_{FB}^0$  theoretical flat-band voltage  
 $Q_{it}$  area of MOS-structure  
 $q$  electron charge  
 $Q_{FB}$  interface state charge at flat band

We have to assume that most of the interface states are acceptor like, because  $Q^*$  was always smaller than the interface state density. It follows that  $Q_{it}$  is the sum of  $Q_{FB}$  and  $Q^*$  (see Table 1).

#### IV. Discussion

The data shown in Table 1 confirm the general trends of the published dependencies of the processing variables on electronic parameters (15, 21). For the first time, we measured in addition the atomic roughness at the Si/SiO<sub>2</sub> interface quantitatively. Comparing the data we see quite clearly, that there exists strong correlation between the atomic roughness and high interface state density and the fixed charge  $Q_{FB}$ .

Earlier measurements (6,9) have shown, a low-temperature anneal in nitrogen does not change the roughness. Therefore, we can assume that an anneal during PMA does not change the roughness either, because the interface will not be provided with oxygen. Also, SiH<sub>4</sub>, which may be created at the interface, can not evaporate as it can at the free silicon surface during reaction with atomic hydrogen (28). Therefore, we can conclude that a low-temperature anneal in forming gas will not change the roughness. Comparing the roughness with the data of the PMA treated samples, we observe the same strong correlation. The results further confirm a strong correlation to the total fixed charge  $Q_{FB}$  with and without PMA. Considering the whole set of data, it seems that the atomic roughness plays the dominant role controlling the interface properties. But we have to keep in mind that the MOS-structures discussed here were processed to produce a high atomic roughness, to make the influence of the roughness visible and measurable. New measurements with an improved SPA-LEED-system (27) show that the roughness can be decreased further, by choosing the right oxidation condition to a value lower than 1% step atom density (29).

Besides the atomic roughness there exist a couple of other explanations for the discussed behavior such as neutral and charged impurities, (28) mobile ions (11,32), radiation damage (33), point defects, vacancies (34,35) and others. Bruce I. Deal (16) proposed a model and classified all known process dependent effects in four different categories (1)  $Q_{FB}$  fixed positive charge, 2.  $N_{HIT}$  fast interface states, 3.  $N_{HIT}$  traps, 4.  $Q_{FB}$  mobile ions. We can explain our results with an extension of this model. He explained the interface states  $N_{HIT}$  with uncompensated dangling bonds at the interface which can be saturated with hydrogen. Further, an interface state can be created by a missing oxygen atom, which is also responsible for the  $Q_{FB}$  explaining  $Q_{FB} \sim N_{HIT}$ .

We suggest that both effects have the same physical origin. They may be caused by the position of a silicon atom at the interface and the arrangement of the neighboring atoms which can create the dangling bonds and therefore surface states. In our model we suggest now that every atom at the interface has a certain probability to create a dangling bond depending on the position of the atom. The more disturbed the atom position, the greater the probability is (surface atom, edge atom, bulk atom). If for instance the probability is zero for terrace atoms, it is still 0.11% for an edge atom which means that 100,000 edge atoms yield one surface state. Therefore we expect  $1.4 \cdot 10^{11}$  surface states for the sample R1 which is reasonable comparing with the data (Table 1,  $9 \cdot 10^{11}$ ). Further we assume a bulk atom has a higher probability (for instance 1.10%) because the distribution is more accurate. If we consider a probability of  $P=10\%$  for steps, randomly distributed in two directions, then the probability of finding an edge atom, in the first direction is  $\frac{1}{2}$  and also in the second direction. The probability of finding a bulk atom has to be at least  $\frac{1}{2} \cdot \frac{1}{2} = \frac{1}{4}$ .

This means that a reduction by a factor of two or three, reduces the number of surface states caused by links by a factor of 4-9, which may explain the decrease of R1 to R2. PMA-treatment provides the surface states with atomic hydrogen which saturates the surface states to a high degree leading to a further decrease of the state density.

This is also valid for R3 and R4. In the case of the wet oxidation of R3, the interface is already provided with a lot of hydrogen and therefore many dangling bonds are saturated. This explains the relatively high value of R3 at the beginning, which also shows an exceptional mobility (10).

#### V. Comparison With Literature

Since atomic roughness has not yet been measured quantitatively elsewhere, a comparison is not possible in this respect. The extensive literature data on electronic properties of the Si/SiO<sub>2</sub> interface and our previous data (6,9,10) may be used for an indirect comparison.

The data taken from the literature are summarized in Table II. Increasing the oxidation temperature for dry and for a wet oxidation leads in both cases to a decrease in  $Q_{FB}$ ,  $N_{HIT}$  (15,22) and the atomic roughness, too (see Table II). For oxides thicker than 20nm the roughness is independent of the oxide thickness (8,9). The same behavior shows  $Q_{FB}$  and  $N_{HIT}$  (15). Thinner oxides are remarkably rougher (8,9). But due to a lack of (CV) measurements, there is no comparison possible for these oxides (30). Annealing in an inert atmosphere like N<sub>2</sub> at high temperatures significantly decreases the roughness (8,9) and  $Q_{FB}$  (15,23). Johnson et al (23) showed also a decrease for N<sub>2</sub>, but these curves keep their typical V-shape for N<sub>2</sub>-annealing. N<sub>2</sub> and argon annealing results in the same behavior (15). These results are summarized and described by the so called "dry oxygen triangle" introduced by B. Deal (15). We can now easily add the new parameter atomic roughness, which depends on the oxidation temperature. Annealing in dry N<sub>2</sub> always reduces the roughness (9). The lower the temperature the longer the annealing time required to produce the same roughness. The coincidence of the roughness data with all kinds of electronic data is a very striking support of our model, which reveals the edge atoms as source for interface states  $N_{HIT}$  as well as for fixed charge  $Q_{FB}$ . Further we have concluded from our roughness data, that a PMA-treatment will not change the roughness (9). It also should not change  $Q_{FB}$  (15), but it decreases  $N_{HIT}$  dramatically (15,23) which can be explained by saturating the dangling bonds with hydrogen. Johnson et al (23) showed that a high temperature anneal in N<sub>2</sub> decreases the surface state density but keeps the V shape distribution. The number of step atoms is reduced. An additional PMA reduces  $N_{HIT}$  further, but also changes distribution of the density of states. Therefore the best interface is obtained by optimum smoothness of the interface (high temperature N<sub>2</sub> anneal) and by saturation of dangling bonds (PMA). The only wet oxidation is very complex. Water increases the roughness (8,9) due to the high oxidation rate, but it also provides the interface with a lot of hydrogen which saturates the dangling bonds, so that  $N_{HIT}$  will decrease finally.

In the case of  $Q_{FB}$  increments and decrements (15,20) have been observed according to the two competing effects (roughness increase, hydrogen providing). Different kinds of cleaning processes (25) and up with different kinds of contamination or degrees of cleanliness, which can add  $Q_{FB}$  and  $N_{HIT}$  related centers, because the impurities are mostly located at the interface as found with AES-depth-profiling. A strong dependence of state density  $N_{HIT}$  and charge  $Q_{FB}$  on silicon orientation has been observed, with densities nearly a factor of 2-3 higher for the (111) face compared with the (100) face (15,16). Assuming similar quality of the oxides the physical reason for this difference must be the interface. The ratio of the minimum step height of (111) and (100) faces is  $3.1350 \cdot 10^{-3} / 3575$ , i.e. a factor of 2.3. The SPA-LEED data show similar densities of edge atoms for both orientations after identical treatments (9). A higher step constitutes a stronger distortion at the step edge, which might explain the difference.

#### VI. Conclusion

The results demonstrate quite clearly that the atomic roughness, which is now quantitatively measurable with SPA-LEED, has a decisive influence on all kinds of electrical properties of MOS-devices. Obviously edge sites are preferred sites for both surface states and oxide charge. Hydrogen treatment cancels those centers only partially. To obtain low values of  $Q_{FB}$  and  $N_{HIT}$  it is necessary to both smooth the interface (high temperature anneal in inert atmosphere) and saturate the dangling bonds (PMA-treatment).

Therefore it is very important to measure and to control the interface roughness for all new procedures especially with thin oxides in VLSI.

#### Acknowledgments

We are indebted to D.R. Young, F. Stern and G.W. Rubloff for very helpful discussions and reading the manuscript and to M. Fichtel for useful discussions and performing the  $Q_{FB}$  calculations. The silicon samples have been kindly provided by Wacker Chemietronic, Burghausen, F.R. Germany.

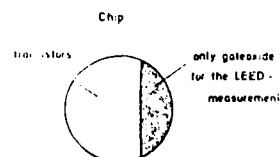


Fig. 1 Schematic diagram showing the location of the gate oxide for the LEED measurements.

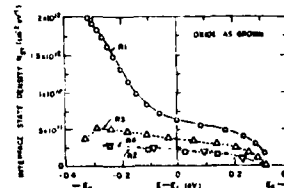


Fig. 2 Interface state density ( $N_{HIT}$ ) strongly decreases for the treatment R1 (17%), R2 (67%) and R3 (21.2%), R4 (10%). Values in brackets in this step mean density, (10% value per unit surface area). R1 and R3 as well as R2 and R4 were prepared in wet oxidation.

# References

- (1) M. Henzler, in *Topics in Current Physics: Electron Spectroscopy for Surface Analysis*, ed. by H. Ibach, Springer, Berlin (1977) Vol. 4, p. 117.
- (2) M. Henzler, in *Advances in Solid State Physics*, ed. by J. Treusch (Heidelberg), Vol. 13, Vieweg, 1979, p. 193.
- (3) P.D. Mahan, J. Clabes and M. Henzler, *J. Appl. Phys.* 51, 2078 (1980).
- (4) M. Henzler and F.W. Walther, *Proceedings of the VIII Conference on the Physics of Semiconductors*, Rome, 1976, p.609 and F.W. Walther, *Diplomarbeit*, T.U. Clausthal, 1976.
- (5) G. Schuler and M. Henzler, *Surf. Sci.* 73, 433 (1978).
- (6) P.D. Mahan and M. Henzler, *J. Appl. Phys.* 52, 4122 (1981).
- (7) M. Henzler, *Appl. Surf. Sci.* 11, 450 (1981).
- (8) M. Henzler, *Surf. Sci.*, in press.
- (9) P.D. Mahan and M. Henzler, in *Springer Series in Electrophysics 7: Insulating Films on Semiconductors*, ed. by M. Schultze and G. Penz (Springer, Berlin, 1981) Vol. 7, p. 26.
- (10) P.D. Mahan and M. Henzler, *J. Appl. Phys.* (Hall-Mobility) in preparation.
- (11) A. Gombert, T. Klammer and M.J. Schulz, *CR. Chim. (Paris)* 1, Jan (1978).
- (12) C.N. Berglund, *IEEE Trans. Electron. Dev.* ED-13, 701 (1966).
- (13) M. Kuhn, *Solid State Electron.* 13, 877 (1970).
- (14) R. Reda, R. Razouk and Bruce L. Deal, *J. Electrochem. Soc.*, *Solid State Science and Technology*, 1979, p. 1573.
- (15) R.E. Deal, *J. Electrochem. Soc.*, *Solid State Science and Technology*, 1979, p. 1573.
- (16) R. Williams, *J. Vac. Sci. Technol.* Vol. 15, 1106 (1977).
- (17) F.H. Noolhan, *J. Vac. Sci. Technol.* Vol. 14, 1112 (1977).
- (18) R.E. Deal, M. Natar, A.S. Grove and E.H. Snow, *J. Electrochem. Soc.*, *Solid State Science*, 1967, p. 266.
- (19) D.J. Boyd and R.P. Kramer, *Solid State Electronics*, 1976, Vol. 19, p. 897.
- (20) F. Morreale and P. Barb, *J. Electrochem. Soc.*, *Solid State Science*, 1977, p. 1464.
- (21) D.K. Lamb and E.R. Ruckenstein, *J. Electrochem. Soc.* 113 (1966).
- (22) N.M. Johnson, D.K. Ruckenstein and M.D. Meyer, *Physics of MOS Insulators*, eds. G. Lucovsky, S.I. Pantelides and E.L. Galkener, (Pergamon, New York, 1980), pp. 311, 315.
- (23) N.M. Johnson, D.J. Bartelink and M. Schulz, in *The Physics of Si<sub>3</sub>N<sub>4</sub> and its Interfaces*, S.I. Pantelides, Editor, p. 421, *Proceedings of the International Topical Conference on the Physics of Si<sub>3</sub>N<sub>4</sub> and its Interfaces*, Pergamon Press, New York (1978).
- (24) J.S. Schwetmann, K.L. Chiang and W.A. Brown, Abstract, 776, p. 688, The Electrochemical Society Extended Abstracts Spring Meeting, Seattle, Washington, May 21-22, 1978.
- (25) A.G. Reves, K.H. Ziemer and R.D. Evans, *J. Phys. Chem. Solids*, 28, 197 (1967).
- (26) F.W. Walther and M. Henzler, to be published.
- (27) G.N. Patz and M. Henzler, *Surf. Sci.* 74, 336 (1983).
- (28) P. Moench and M. Henzler, to be published.
- (29) P.D. Mahan et al., measurements are in progress.
- (30) F.H. Snow, A.S. Grove, B.L. Deal and E.H. Snow, *J. Appl. Phys.* 37, 1664 (1965).
- (31) L. Yen, W.H. Ku and A.R. Kuper, *IEEE Trans. Electron. Devices* ED-13, 276 (1966).
- (32) J.P. Mitchell and K.R. Waldron, *Bell Syst. Techn. J.* 46, 1 (1967).
- (33) F. Herman, R.V. Kasowski, *J. Vac. Sci. Technol.*, in press.
- (34) T. Sugano, K. Hosh, H. Sakaki, T. Iwata, K. Hirai, K. Kuroawa and K. Kakimoto, *Journal of the Faculty of Engineering, University of Tokyo* (B), Vol. XXXII, No. 1, (1973).

TABLE 1. Summary of all results showing the correlation of electrical properties to oxidation, step atom density and oxidation parameters.

TRANSISTOR	Oxidation at 1000°C	Annealing in dry N <sub>2</sub> at 1000°C	Step Atom density (1)	Mobility (cm <sup>2</sup> /V-sec) at high injection (2x10 <sup>17</sup> cm <sup>-3</sup> at 4-2K, ref. 10)	As Grown		After PMA	
					n <sub>ST</sub> (cm <sup>-2</sup> )	Q <sub>12</sub> (cm <sup>-2</sup> )	n <sub>ST</sub> (cm <sup>-2</sup> )	Q <sub>12</sub> (cm <sup>-2</sup> )
R1	dry oxygen 2 1/4 hours	no	17 ± 5	170	9x10 <sup>11</sup>	11.4x10 <sup>11</sup>	4.4x10 <sup>11</sup>	5.6x10 <sup>11</sup>
R2	same as R1	4 hours	8 ± 1	280	2x10 <sup>11</sup>	2x10 <sup>11</sup>	0.4x10 <sup>11</sup>	1x10 <sup>11</sup>
R3	wet oxygen 9 min	no	21.2 ± 2	230	3.8x10 <sup>11</sup>	6.9x10 <sup>11</sup>	2.4 x 10 <sup>11</sup>	4.6x10 <sup>11</sup>
R4	same as R3	4 hours	10 ± 2	330	2.2x10 <sup>11</sup>	6.3x10 <sup>11</sup>	1.7x10 <sup>11</sup>	3 x 10 <sup>11</sup>

TABLE 2. Comparison of Roughness Data (SPA-LEIS) with Fixed Oxide Charge Q<sub>ox</sub>, Interface State Density (N<sub>ST</sub>) and Processing Parameters in Literature.

Process Parameter	Q <sub>ox</sub>	N <sub>ST</sub>	Roughness
Increasing oxidation temp. (dry)	↑	↑	↑
Increasing oxidation temp. (wet)	↑	↑	↑
Increasing oxidation thickness	no change	no change	no change
Dry Anneal (N <sub>2</sub> , Ar, argon) short time (high temp.)	↓	↓	↓
PMA	no change	↓	no change
Water	↑	↑	↑
(cleaning) (clean-contaminated)	↑	↑	↑
Silicon orientation (111)-(100)	↑	↑	↑

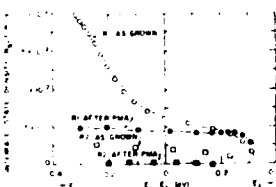


Fig. 3. Surface state density (N<sub>st</sub>) versus energy (E) for R1 and R2.

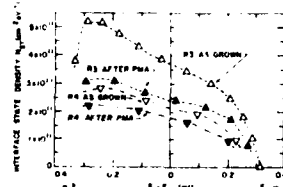


Fig. 4. Surface state density (N<sub>st</sub>) versus energy (E) for R3 and R4.



# OPTICAL PROPERTIES OF STRAINED $\text{In}_{0.13}\text{Ga}_{0.87}\text{As}$ MULTI QUANTUM WELL STRUCTURES.

J.-V. MARIN, M. OUILLET, E. V. V. RAO, G. LEROUX and L. GOLDSTEIN

C.N.E.T 195 rue de Paris, 92220 BAGNEUX

(FRANCE)

## ABSTRACT :

We present photoluminescence and absorption measurements on Molecular Beam Epitaxy grown strained  $\text{In}_{0.13}\text{Ga}_{0.87}\text{As}$ -GaAs multi quantum well structures. The low temperature results are interpreted in terms of excitonic transitions:  $n=1$  and  $n=2$  heavy hole excitons are seen in absorption while the luminescence spectrum exhibits only the  $n=1$  excitonic line.

The possibility of growing thin mismatched layers on a substrate, with elastic accommodation of the mismatch by strain (1), enlarges the choice of the semiconductors used for designing heterostructures. Osbourn et al. first grew GaP-GaAs  $\text{P}_{1-x}\text{As}_x$  superlattices and studied their optical properties (2). The  $\text{In}_{0.13}\text{Ga}_{0.87}\text{As}$ -GaAs system, involving two direct gap semiconductors was the next to be investigated, and the feasibility of Molecular Beam Epitaxy grown  $\text{In}_{0.13}\text{Ga}_{0.87}\text{As}$ -GaAs quantum well heterostructures have been demonstrated (3,4). This system, because of the electronic properties of  $\text{In}_{0.13}\text{Ga}_{0.87}\text{As}$  and of the use of GaAs substrate, is potentially interesting for optoelectronic devices. The object of the present work is to report an experimental study of the photoluminescence and absorption in such a structure. To our knowledge, we observed for the first time clear excitonic transitions in quasi two dimensional layers other than GaAs.

The results presented here were obtained on a sample which structure is shown in the inset of Fig.1. The GaAs buffer layers are 1.6  $\mu\text{m}$  thick and the multi quantum well structure consists in 10 periods of  $\text{In}_{0.13}\text{Ga}_{0.87}\text{As}$ -GaAs. It was grown on (100) GaAs substrate by Molecular Beam Epitaxy. The composition  $x$  of the  $\text{In}_{0.13}\text{Ga}_{0.87}\text{As}$  layers and their width  $L$  have been extrapolated from measurements on thicker layers grown in the same conditions. They are assumed to be  $x=0.13$  and  $L=110 \text{ \AA}$ , and the unstrained  $\text{In}_{0.13}\text{Ga}_{0.87}\text{As}$  layers should thus present a .9% mismatch with GaAs. Transmission Electron Microscope analysis of a thinned bevel showed that a low dislocation density appears in the sample, located only at the interface with the first buffer layer. This was not the case of thicker structures which contained much higher dislocation concentration and showed poor optical properties. Because of these results, we can assume that the range of  $\text{In}$  composition and of thicknesses is such that the  $\text{In}_{0.13}\text{Ga}_{0.87}\text{As}$  layers are strained while the GaAs ones are not. Though it should be necessary for higher  $x$  or thicker structures, we did not need to use graded buffer layers to match the equilibrium parameter of the periodic structure with that of the substrate. Finally, the period of the structure on which the optical data presented here were obtained, was accurately measured, by double crystal X ray diffraction, to be  $297 \pm 2 \text{ \AA}$ .

Photoluminescence was excited by a focused spot of the  $5145 \text{ \AA}$  line of an  $\text{Ar}^+$  ion laser. The emitted light was dispersed by a 1.5m focal length Jobin Yvon grating monochromator and detected either by a dry ice cooled Si cathode photomultiplier or a liquid nitrogen cooled Ge detector. The resulting signal was amplified with the usual lock-in technique. A quartz iodine lamp in combination with a monochromator was employed as a source for the single transmission experiments.

Fig.1 shows the evolution of the 300K luminescence spectrum obtained by

moving the exciting spot along a chemically etched bevel (see inset). The spectrum observed in point A contains three peaks, located at 1.3, 1.35 and 1.42 eV. The latter is the usual near band edge emission of GaAs, and it is also observed in B and C, while the two other lines decrease in intensity and vanish when the spot is moved to point B and C. This proves these peaks are associated with the periodic part of the sample, containing the  $\text{In}_{0.53}\text{Ga}_{0.47}\text{As}$  layers.

Fig. 2a shows the 2K absorption spectrum deduced from single beam transmission experiment. This spectrum contains two peaks at 1.38 and 1.44 eV. As we have verified, those peaks are due to the multi quantum well structure and not to the substrate, and they are likely to be the low temperature equivalent of the 300K luminescence lines. The shape of the absorption peaks are typical of excitonic absorption (see for example ref. 5). We attribute these to the creation of excitons formed respectively from  $n=1$  and  $n=2$  electron and heavy hole quantum levels. The 300K luminescence lines are then interpreted as the corresponding ( $\Delta n=0$ ) band to band transitions. To check the validity of this interpretation, we have calculated the positions of the quantum levels in the  $\text{In}_{0.53}\text{Ga}_{0.47}\text{As}$  wells, taking into account: (1) the variation of the band gap of bulk  $\text{In}_{0.53}\text{Ga}_{0.47}\text{As}$  with  $x$  as in ref. 6, (2) the increase of this band gap and the splitting of the valence band due to the strain, assuming the GaAs barriers are unstrained, (3) an offset between the valence bands of GaAs and  $\text{In}_{0.53}\text{Ga}_{0.47}\text{As}$ , following ref. 7 and interpolating the InAs-GaAs value, (4) the quantification of the electron and heavy hole levels in the growth direction, with a linear interpolation on the electron mass for  $\text{In}_{0.53}\text{Ga}_{0.47}\text{As}$ . We made this calculation using the following values of the parameters: electron mass: 0.067  $m_0$  for GaAs and 0.043  $m_0$  for  $\text{In}_{0.53}\text{Ga}_{0.47}\text{As}$ , heavy hole mass: 0.5  $m_0$ , deformation potentials:  $a=-8$  eV and  $b=-2$  eV (8). For  $x=0.14$

and  $L=120\text{\AA}$ , and assuming a 10 meV exciton binding energy, we find a good agreement between the experimental lines positions and the  $n=1$  and  $n=2$  heavy holes excitons calculated energies. We must note that: (1) the transition corresponding to the exciton formed with the light hole band should be weaker than the transition observed at 1.44 eV mainly because of a lower density of state, (2) we had to take for the composition and thickness of the  $\text{In}_{0.53}\text{Ga}_{0.47}\text{As}$  layer slightly different values compared to those obtained from the growth conditions. This last point is not surprising because these values are not very precise (of the order of 10%), and other parameters are not very well known ( $a, b, \text{offset}$ ).

Fig. 2b shows the 2K luminescence spectrum. The dominant line occurs in the vicinity of the  $n=1$  exciton absorption peak, so we attribute it to excitonic transitions in the wells. This luminescence line, as well as the absorption ones, is rather broad. This broadening can be due to small composition inhomogeneities or fluctuations in the well width, which can also account for the small discrepancy between the absorption and luminescence  $n=1$  line positions.

Let us mention that the great efficiency of the luminescence and the clear observation of excitonic transitions show that this structure is likely to correspond to the same situation as in  $\text{Ga}_{0.47}\text{Al}_{0.53}\text{As}-\text{GaAs}$  heterostructures, where both electrons and holes are confined in the small gap layers. This fact is in agreement with our simple model.

To summarize, we have performed luminescence and absorption experiments on a  $\text{In}_{0.53}\text{Ga}_{0.47}\text{As}$  strained multi quantum well heterostructure. In the low temperature transmission experiment, we have observed two absorption peaks which are interpreted as  $n=1$  and  $n=2$  excitonic transitions. At the same temperature, the luminescence spectrum consists in one line associated with the  $n=1$  excitonic recombination while, at 300K, it includes both  $n=1$  and  $n=2$

subband to subband transitions. Further experiments are required to have a better understanding of the detailed band configuration of those strained multi-quantum well structures. Our results prove however they can exhibit excellent optical behaviour.

#### ACKNOWLEDGMENTS

The authors wish to thank P. Henoc who performed the T.E.M. analysis and G. Bastard, B. Serrage, H. Launois and M. Voos for fruitful comments and discussions.

#### REFERENCES

- 1 -J.M. Matthews and A.E. Blakeslee, *J. of Cryst. Growth* 32,216 (1976), and references therein
- 2 -G.C. Osbourn, *J. Vac. Sci. Technol.* 21,469 (1982), G.C. Osbourn, R.M. Biefeld and P.L. Gourley, *Appl. Phys. Lett.* 41,172 (1982)
- 3 -L. Goldstein, M. Quilic, E.V.K. Rao, J.M. Masson and J.V. Merzin, *International meeting on Epitaxy, Proceedings published by "les Editions de Physique", Perpignan (Sept. 82)*
- 4 -I.J. Fritz, L.R. Dawson, G.C. Osbourn, P.L. Gourley and R.M. Biefeld, 10th International Symposium on GaAs and related compounds, Albuquerque New Mexico (Sept. 82)
- 5 -R. Dingle, M. Wiegmann and C.H. Henry, *Phys. Rev. Lett.* 33,827 (1974)
- 6 -Y.T. Lu, F.A. Thiel, M. Schreiber, J.J. Rubin, B.I. Miller and K.J. Bachmann, *J. Electron. Mater.* 8,663 (1979)
- 7 -M.A. Harrison, *J. Vac. Sci. Technol.* 14,1016 (1977)
- 8 -M. Chandrasekhar and F.H. Pollack, *Phys. Rev. B* 15,2127 (1977)

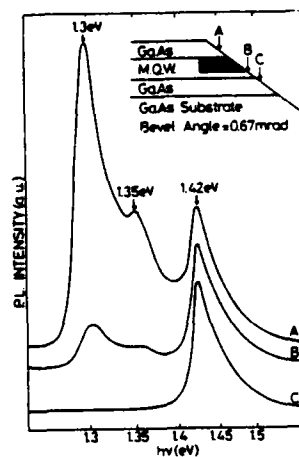


Fig.1

300 K luminescence spectra, obtained for different points along a bevel

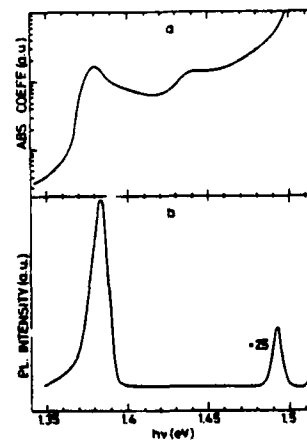


Fig.2

a) Absorption spectrum at 2 K  
b) luminescence spectrum at 2 K (with the same energy scale)

NEW EXPERIMENTAL RESULTS FOR ELECTRON TRANSPORT IN  
WEAK ACCUMULATION LAYERS ON ZnO CRYSTALS

W. Thoren, G. Heiland, D. Kohl, H.v.Löhneysen, W. Platen,  
H.-J. Schink

2. Physikalisches Institut der Rheinisch-Westfälischen Techni-  
schen Hochschule Aachen, D - 5100 Aachen, Germany.

Abstract

Previous Hall measurements on (0001) and  $000\bar{1}$  faces of ZnO have shown a mobility oscillating as a function of surface electron density in the range between  $N_s = 10^6$  and  $10^{11} \text{ cm}^{-2}$  (1). Here we report on new results obtained by a field effect arrangement for free surfaces in UHV. With donors from H exposure or by illumination weak accumulation layers ( $N_s \leq 10^{11} \text{ cm}^{-2}$ ) are established. The field effect shows oscillations in surface conductivity as a function of gate voltage. Also the combination of a field effect with a Hall effect measurement reveals distinct surface electron densities  $N_s$ . Various pretreatments do not change the periodicity of these oscillations. Necessary preconditions are a temperature below 130 K, a surface electron density below  $3 \times 10^{12} \text{ cm}^{-2}$  and a source-drain field in the order of a few V/cm.

A model regarding impurity levels in the space charge layer relates the results of the field effect measurements to the results of the Hall effect measurement.

(1) E. Veuhoff and D. Kohl, J. Phys. C 14 (1980) 2395.

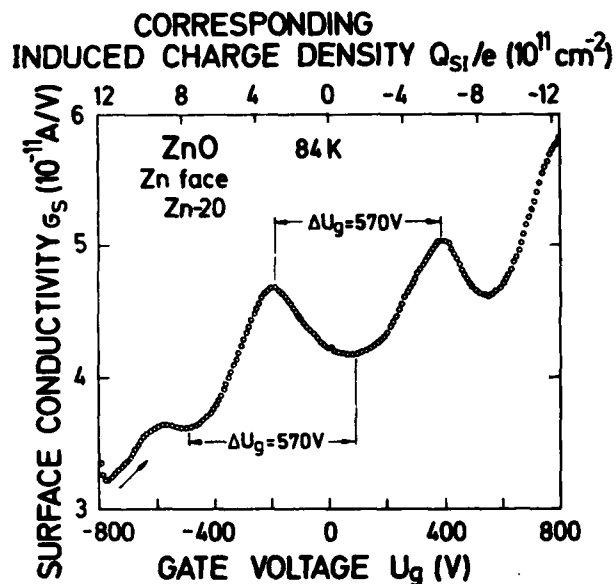


Fig. 1 Surface conductivity  $G_S$  as a function of the gate voltage  $U_g$  increasing from -800 V to +800 V.

Quantum Transport in Semimagnetic HgMnTe Inversion  
Layers-Experiment and Theory

G. Grabecki, T. Dietl, J. Kossut, and W. Zawadzki

Institute of Physics, Polish Academy of Sciences  
02-668 Warsaw, Poland

The first experimental and theoretical study of MIS structures containing localised magnetic moments is reported.  $\text{Hg}_{1-x}\text{Mn}_x\text{Te}$  structures with energy gap ranging from 50 to 200 meV have been investigated.

In contrast to MIS structures not containing localised moments, a pronounced temperature dependence of the positions of SdH maxima has been observed. A theory of two-dimensional, semi-magnetic, narrow-gap structures has been developed, which accounts qualitatively for the observations.

We have investigated experimentally MIS structures which consisted of an aluminum film evaporated on a thin Mylar foil ( $d = 3.5 \mu\text{m}$ ) attached mechanically to the surface of p-type  $\text{Hg}_{1-x}\text{Mn}_x\text{Te}$  ( $N_A - N_D = 2 \times 10^{16} \text{ cm}^{-3}$ ). The semiconductor surface was prepared by mechanical polishing and etching in bromine-methanol solution. Capacitance measurements vs gate voltage  $C(V_g)$  have shown a good stability of the structures. The total electron surface density  $N_s$  is varied by changing the gate voltage  $V_g$  according to relation:  $N_s = C(V_g - V_{th})$ , where  $V_{th}$  is the inversion threshold voltage, corresponding to a crossing of the Fermi level and the conduction band-edge.

The differential conductivity  $d\sigma/dV_g$  vs gate voltage for various magnetic fields is shown in Fig. 1. A standard sharp increase of the field mobility near  $V_g = 0$  corresponds to the inversion threshold. The decrease of the mobility for  $V_g > 150 \text{ V}$  is due to an increase of the surface scattering rate, which occurs when the electrons are driven closer to the surface. In magnetic fields  $B > 2 \text{ T}$  magneto-conductance oscillations are observed, indicating a sufficient mobility of the surface electrons  $\mu > 5 \times 10^4 \text{ cm}^2/\text{Vs}$ . Two periods of oscillations are observed, indicating that electrons occupy at least two electric subbands. From the data we deduce that for  $V_g > 50 \text{ V}$  about 70% of

electrons are in the lowest subband. This is in agreement with calculations for  $\text{Hg}_{1-x}\text{Cd}_x\text{Te}$  possessing similar band parameters [1].

We observe an influence of temperature on the positions of oscillation maxima, as shown in Fig. 2. This is characteristic of the semimagnetic behavior, in which the paramagnetic magnetization of  $\text{Mn}^{2+}$  ions is strongly temperature dependent. It can be seen in Fig. 2 that two separate peaks (indicated by arrows) become one at higher temperatures and then again reappear as two. This is in contrast to the usual SdH behavior, for which the oscillations gradually disappear with increasing temperature. We refer to this observation in the theoretical part.

A theory of the above system must take into account the following essential features: 1/ Energy band structure with a small energy gap  $\epsilon_g$  and a strong spin-orbit interaction  $\Delta$ ; 2/ Quasi two-dimensional character of the electron motion near the interface; 3/ Presence of a magnetic field transverse to the interface; 4/ Semimagnetic properties related to the exchange interaction between the conduction electrons and the  $\text{Mn}^{2+}$  ions. The complete Hamiltonian reads

$$H = H_{el} + V_0 + H_{so} + U(z) + H_{exch} \quad (1)$$

$H_{el} = (1/2m_0)(\vec{p} + e\vec{A}/c)^2$ ,  $V_0$  is the periodic potential of the lattice  $H_{so}$  is the spin-orbit interaction,  $U$  is the potential of the inversion layer:  $U = 0$  for  $z < 0$  and  $U = U(z)$  for  $z > 0$ . The exchange interaction in the mean field approximation is  $H_{exch} = J\langle S_z \rangle s_z$ , where  $J$  is the exchange operator,  $\langle S_z \rangle$  is the thermodynamic mean value of  $\text{Mn}^{2+}$  spins and  $s_z$  is the electron spin operator [2]. The band structure is described using a three-level model of  $\Gamma_6$ ,  $\Gamma_8$ ,  $\Gamma_7$  symmetry levels (8 Luttinger-Kohn functions, cf. [3]). Looking for solutions in the form:  $\Psi = \sum f_i u_{i0}$ , the set of coupled differential equations for the envelopes  $f_i$  is obtained,

$$\sum_l \left[ \frac{\hbar^2}{2m_0} \nabla^2 + H_{exch} + (U + \epsilon_{l0} - \epsilon) \delta_{l1} \right] f_l = 0 \quad (2)$$

where the matrix elements are calculated using the L-K band-edge functions and  $\epsilon_{l0}$  are the band-edge energies (at  $k=0$ ). The explicit form of matrix (1) can be found in [2,3]. In the following we put  $\Delta$  large and the set (1) reduces to 6 equations.

The set can be solved to a good approximation by substitution neglecting commutators  $[p_z, U]$  (cf. [4]), and small off-diagonal terms of the type  $b/\epsilon_g$ . Here we limit our solutions to a parabolic approximation, which gives

$$\epsilon_{rn} = \epsilon_r + \hbar\omega_c \left(n + \frac{1}{2} - \frac{7}{12} \frac{b}{\epsilon_g}\right) \pm \left[a + \frac{1}{2} g^* \mu_B B + \frac{2}{3} \hbar\omega_c \frac{b}{\epsilon_g} \left(n + \frac{1}{2}\right)\right] \quad (3)$$

where  $\epsilon_r$  are the electric subband energies and  $n = 0, 1, \dots$  are the Landau levels.  $\omega_c = eB/m^*$  and  $g^*$  is the spin g-factor resulting from the band structure ( $g^* < 0$ , cf. [3]). The exchange interaction affects the spin-splittings in two ways: it diminishes the splittings of all levels ( $a > 0$ ) and it contributes an increasing term depending on  $n$  ( $b < 0$ ). We denote

$$a = \frac{1}{2} x (S|J|S) \langle S_z \rangle \quad b = \frac{1}{2} x (X|J|X) \langle S_z \rangle \quad (4)$$

where  $x$  is the MnTe mole fraction,  $(S|J|S) = -0.4$  eV,  $(X|J|X) = -0.6$  eV (cf. [5]). The quantity  $\langle S_z \rangle < 0$  is directly related to magnetization. The latter depends strongly on a magnetic field (increasing function) and the temperature (decreasing function) and it has been measured independently for  $\text{Hg}_{0.9}\text{Mn}_{0.1}\text{Te}$  [6].

The electric subband energies are calculated for the triangular potential  $U(z) = eEz$ . They are also modified by the semi-magnetic terms,

$$\epsilon_r^{\pm} = \left[ \frac{\frac{3}{2} \hbar \left(r + \frac{1}{2}\right) eE}{\epsilon_g \mp \frac{b}{3}} \right]^{1/3} \quad (5)$$

In the calculations we took the following values:  $m^* = 0.0089 m_0$ ,  $g^* = -112$ ,  $E = 1.35 \times 10^4$  V/cm.

Fig. 3 shows calculated electron energies for the first two electric subbands at  $T = 4.2$  K. It can be seen that: 1/ The spin splittings exhibit peculiar behavior as functions of a magnetic field, 2/ The splittings increase with the increasing Landau number  $n$ , which may lead to a rearrangement of the levels.

Fig. 4 shows the Landau level energies for the lowest electric subband as functions of the temperature. Due to decreasing magnetization the semi-magnetic terms contribute less at higher

temperatures. As it can be seen, this leads to level crossings for higher  $n$ , as indicated above. We associate the experimental observation indicated in Fig. 2 with the level crossing shown in Fig. 4, both occurring for higher Landau levels.

We have not attempted here a quantitative description of the experiments, since it would require a selfconsistent calculation of electron energies for the nonparabolic band, in which both  $m^*$  and  $g^*$  depend on the absolute positions of the electric subbands.

#### Acknowledgments

One of us (T.D.) is greatly indebted to Prof. F. Koch for giving him the opportunity to initiate studies of inversion layers on  $\text{HgMnTe}$  in the TUM laboratory and for many valuable discussions.

#### References

1. Y. Takada, K. Arai, and Y. Uemura, Lecture Notes in Physics, Vol. 152, ed. E. Gornik et al. (Springer Verlag 1982) p.101
2. R.R. Galazka and J. Kossut, in Lecture Notes in Physics, Vol. 133, ed. W. Zawadzki (Springer Verlag 1980), p.245
3. W. Zawadzki, in Lecture Notes in Physics, ed. W. Zawadzki (Springer Verlag 1980) p.85
4. W. Zawadzki, J. Phys. C: Sol. St. Phys. **16**, 229 (1983)
5. M. Dobrowolska, W. Dobrowolski, M. Otto, T. Dietl and R.R. Galazka, Proc. 15-th Intern. Conf. Phys. Semicond. J. Phys. Soc. Jap. **49**, 815 (1980), Suppl. A
6. W. Dobrowolski, M. von Ortenberg, A.M. Sandauer, R.R. Galazka, A. Mycielski, R. Pauthenet, Lecture Notes in Physics, Vol. 152 (Springer Verlag 1982), Ed. E. Gornik et al., p.302.

# Figure captions

Fig.1. Differential conductivity vs. gate voltage for p -  $\text{Hg}_{0.9}\text{Mn}_{0.1}\text{Te}$  in various magnetic fields at 4.2 K.

Fig.2. Differential magnetoconductivity vs. gate voltage for p -  $\text{Hg}_{0.9}\text{Mn}_{0.1}\text{Te}$  show the peaks which exhibit a strong temperature shift. Note absence of the spin splitting at intermediate temperatures  $T \sim 10$  K.

Fig.3. Calculated magnetic field dependence of the Landau levels in  $\text{Hg}_{0.9}\text{Mn}_{0.1}\text{Te}$ ,  $E_g = 100$  meV at 4.2 K for the two lowest electric subbands ( $r = 0$  solid lines,  $r = 1$  broken lines)

Fig.4. Calculated temperature dependence of the Landau levels associated with the lowest electric subband ( $r = 0$ ) in  $\text{Hg}_{0.9}\text{Mn}_{0.1}\text{Te}$ ,  $E_g = 100$  meV in 5T. The temperature dependence is due to the exchange interaction between conduction electron and localised magnetic moments.

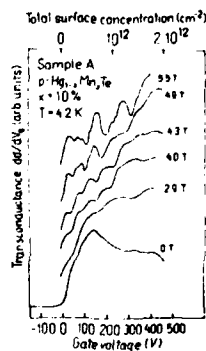


Fig. 1

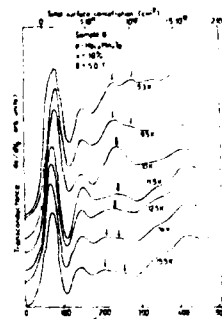


Fig. 2

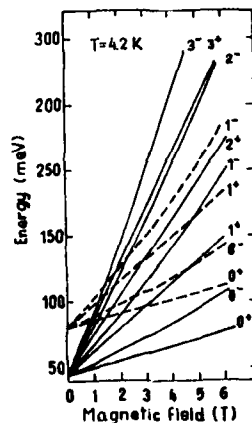


Fig. 3

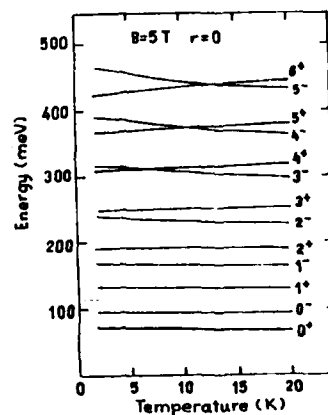


Fig. 4

# MAGNETO-OPTICS IN A II-VI SUPERLATTICE : HgTe-CdTe

Y. Guldner, G. Bastard, J.P. Vieren, M. Voos

Groupe de Physique des Solides de l'Ecole Normale Supérieure  
24 rue Lhomond, 75231 Paris Cedex 05, France

J.P. Faurie\* and A. Million

Laboratoire Infrarouge, LETI/CENG, 85X, 38041  
Grenoble Cedex, France

We report far-infrared magneto-absorption investigations performed in a HgTe-CdTe superlattice. From these studies, we obtain the band structure of the superlattice considered here which is found to be a quasi-zero-energy gap semiconductor. We obtain also the value of the overlap between the HgTe and CdTe valence bands.

We report here far-infrared magneto-absorption studies of a HgTe-CdTe superlattice (SL) grown // by molecular beam epitaxy (MBE). Among other important features, these investigations allow us to obtain the superlattice band structure, demonstrating, in particular, that the system considered in this work is a quasi-zero-energy gap semiconductor. From our results, we determine also the overlap  $\Lambda$  between the HgTe and CdTe valence bands, which is an important parameter whose value was unknown.

The structure under investigation here was grown by MBE on a (111) CdTe substrate, and is constituted of one hundred periods of HgTe and CdTe layers whose thicknesses are  $d_1 = 180$  and  $d_2 = 44$  Å, respectively. In these far-infrared magneto-absorption experiments, which were performed at 1.6 K, the transmission signal was observed at fixed photon energies in the Faraday configuration and detected by a carbon bolometer. Two kinds of infrared sources were used, a molecular laser and carcinotrons, and the magnetic field  $B$ , provi-

ded by a superconducting coil, could be varied continuously between 0 and 10 T.

In Fig.1 are given typical transmission spectra as a function of  $B$  obtained for different infrared wavelengths,  $B$  being perpendicular to the layers ( $\theta = 0$ ). From such data, one can plot, as a function of  $B$ , the energy positions of the transmission minima or absorption maxima as presented in Fig.2. As shown later, the observed optical transitions, labelled 1-0, 2-1 and 3-2 in Fig. 2 are attributed to interband transitions from Landau levels of the ground heavy hole subband ( $HH_1$ ) up to Landau levels of the ground conduction subband ( $E_1$ ) occurring at the center of the SL Brillouin zone. They extrapolate to an energy  $h\nu \sim 0$  at  $B = 0$ , but they cannot be due either to electron cyclotron resonance because our SL is p-type for  $T \lesssim 20$  K, or to hole cyclotron resonance because they would lead to holes masses much too small. In fact, this indicates that our SL is a quasi-zero-gap semiconductor. We have also observed that, for  $B < 0.3$  T, the magnetic field positions of these transitions depend weakly on the angle  $\theta$  between  $B$  and the normal to the layers, which corresponds to a three-dimensional behavior. However, for  $B > 1$  T, their position follows  $(\cos\theta)^{-1}$ , which implies, in a quasi-zero gap semiconductor, a two-dimensional character.

To proceed further, we should now calculate the band structure of the SL considered here and also the resulting Landau levels under magnetic field. The band structure of the host materials is given in Fig.3(a), and that of our SL is obtained from the envelope function approach /2/. A SL state is identified by a subband index ( $E_n, HH_n, h_n, \dots$ ), a SL wavevector  $q$ , with  $-\pi/d < q < \pi/d$ , where  $d$  is the SL period, and a two-dimensional wavevector  $\vec{k}_\perp$  which is perpendicular to the SL axis  $z$ . At  $\vec{k}_\perp = 0$ , the heavy-hole states ( $hh$  in both materials) are fully decoupled from the light particle states ( $\Gamma_6^o, \Gamma_8^{hh}$  in HgTe ;  $\Gamma_6^o, \Gamma_8^{hh}$  in CdTe). As obtained later from the data  $\Lambda \sim 40$  meV, and the CdTe layers are potential barriers for heavy-holes. The calculated SL band structure /3/ is presented in Fig.3(b) with the energy origin taken at the top of the  $\Gamma_6$  CdTe valence band. The ground heavy-hole subband  $HH_1$  is almost flat along  $q$  and lies



at  $\sim 2$  meV below the  $\Gamma_1$  HgTe band edge. The ground conduction subband  $E_1$  has a mixed electron (HgTe) and light hole (CdTe) character, which explains its energy position and the quasi-zero-gap nature of the SL band structure. In addition, the upper light hole subband  $h_1$  is found to lie here in the energy gap (0,A). Fig.4 gives for HgTe-CdTe SL's, the position and width of different subbands as a function of  $d_1$  for  $d_1/d_2 = 4$ , as obtained from such calculations. It shows that the cross-over of  $E_1$  and  $HH_1$  at  $q=0$  occurs for  $d_1 \sim 50 \text{ \AA}$ . For finite  $\vec{k}_\perp$  or finite  $B$ , the situation is much more complicated due to the intricate  $\Gamma_1$  bands kinematics. In fact, to calculate the  $E_1$  Landau levels, we have used approximate SL dispersion relations described in Ref.2 for finite  $\vec{k}_\perp$ . We have neglected spin effects, and we have replaced  $\vec{k}_\perp^2$  by  $(2n+1)eB/\hbar$ , where  $n = 0, 1, \dots$  is the Landau level index. For the  $HH_1$  Landau levels, we have considered that they are flat along  $q$ , so that their energy is  $HH_1(n) = HH_1 - (n+1/2)\hbar eB/m_{hh}$ , where  $m_{hh}$  is the heavy-hole effective mass in bulk HgTe. This model depends only on  $A$ , the other parameters being well-known bulk parameters. Theoretical fits to the data using this model are shown in Fig.2. For the electron (hole) effective mass and the band gap of bulk HgTe, we took  $4.5/0.03 m_0$  ( $0.3 m_0$ ) and  $0.3025 \text{ eV}$ , respectively, and, for the band gap of bulk CdTe,  $1.6 \text{ eV}$ . We consider also that the Fermi level  $E_F$  is close to  $HH_1$  due to the large heavy-hole mass. The curve labelled 1-0 corresponds to transitions from the  $n = 1$   $HH_1$  Landau level to the  $n = 0$   $E_1$  Landau level at  $q = 0$ . The other curves are analogous transitions with hole and electron Landau indices  $n$  equal to 2, 3 and 1, 2, respectively. A good agreement is obtained between experiment and theory for  $A \sim (40 \pm 10) \text{ meV}$ . The transition energies are remarkably non-linear as a function of  $B$  (in contrast to bulk HgTe), the in-plane apparent electron mass increasing from  $0.008 m_0$  to  $0.03 m_0$  between  $0.15$  and  $8 \text{ T}$  as a consequence of the  $\vec{k}_\perp \cdot \vec{p}$  interaction between the  $E_1$ ,  $HH_1$  and  $h_1$  subbands. We have also calculated the width  $\Delta E_1$  of  $E_1$  as a function of  $B$  for  $n = 0$ , and  $\Delta E_1$  is found to decrease from  $12$  to  $2 \text{ meV}$  between  $B = 0$  and  $B = 10 \text{ T}$ , explaining the observed change from three to two dimensional behavior. The variation of  $\Delta E_1$  with  $B$  can also be under-

stood from the  $\vec{k}_\perp \cdot \vec{p}$  interaction between  $E_1$ ,  $HH_1$  and  $h_1$ . Furthermore, the deviation from the theoretical fit of the experimental data (Fig.2) for the 1-0 transition around  $2.5 \text{ T}$  is thought to be due to an interband polaron effect, the LO-phonon energy being  $16 \text{ meV}$  in bulk HgTe.

We have also performed similar experiments at higher photon energy ( $300\text{--}400 \text{ meV}$ ), and the energy of the observed transitions converge to  $340 \text{ meV}$  at  $B = 0$ . They are attributed to interband transitions from Landau levels of  $LH_1$  (derived from the  $\Gamma_6^{th}$  HgTe states) up to Landau levels of  $E_1$  (Fig.3(b)) since the  $LH_1$ - $E_1$  band gap at  $q = 0$  is  $325 \text{ meV}$  from our calculations. The slope of the energy of the observed transitions is also well accounted for by our model. Finally, we wish to point out that one can deduce from these investigations that interdiffusion between HgTe and CdTe layers is certainly weak in the superlattice studied here.

This work has been partly supported by the Direction des Recherches et Etudes Techniques.

#### References

- \* Laboratoire associé au C.N.R.S.
- \* Present address : University of Illinois, Chicago, Illinois 60680, U.S.A.
- /1/ J.P. Faurie, A. Million and J. Piegnot, Appl. Phys. Lett. **41**, 713 (1982).
- /2/ G. Bastard, Phys. Rev. B **25**, 7584 (1982).
- /3/ Detailed calculations will be published elsewhere.
- /4/ J. Tuchendler, M. Grynberg, Y. Couder, H. Thomé and R. Le Toullec, Phys. Rev. B **8**, 3884 (1973).
- /5/ Y. Guldner, C. Rigaux, M. Grynberg and A. Mycielski, Phys. Rev. B **8**, 3875 (1973).

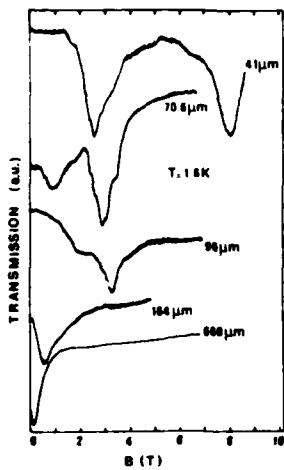


Figure 1

Typical transmission spectra obtained as a function of the magnetic field  $B$  for several infrared wavelengths.

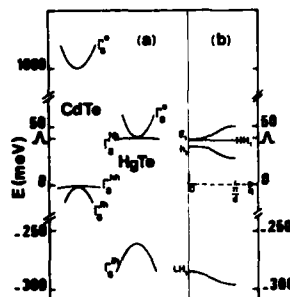


Figure 3

(a) Band structure of bulk HgTe and CdTe  
(b) Calculated band structure in the  $q$  direction of the superlattice studied here.

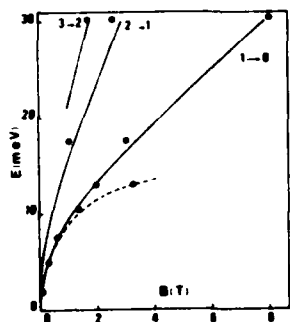


Figure 2

Energy position of the transmission minima as a function of  $B$  ( ). The solid lines are theoretical fits as described in the text. The dashed line is only an eyeguide evidencing the deviation between experiment and theory around 2.5 T.

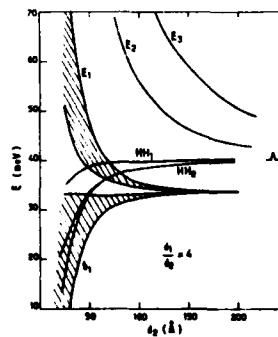


Figure 4

Energy and width of different subbands in HgTe-CdTe superlattices

### Quantum Wells of InAs Between AlSb\*

C. A. Chang, E. E. Mendez,† L. L. Chang,† and L. Esaki

IBM Thomas J. Watson Research Center  
P. O. Box 218, Yorktown Heights, N.Y. 10598

**ABSTRACT** Quantum wells consisting of a single InAs layer confined between two AlSb layers were made, and they exhibited characteristic two-dimensional electron behavior from magneto-transport measurements. Unexpectedly, the electrons appeared to be predominantly extrinsic in nature, unlike the situation in the InAs-GaSb system.

In our efforts to realize the polytype heterostructures of InAs, GaSb and AlSb,<sup>1</sup> we have investigated different combinations of two of the three materials. The InAs-GaSb structure has been studied for some time from both magneto-transport and magneto-optical experiments.<sup>2,3</sup> It is characterized by a semiconductor-semimetal transition with an increase in the InAs layer thickness, a consequence of the energy positions of the conduction bandedge of InAs lying below the valence bandedge of GaSb. The GaSb-AlSb structure has recently been successfully fabricated. Energy quantization in GaSb was demonstrated from luminescence and absorption measurements,<sup>4,6</sup> although the bandedge relationship could not be accurately determined. In this work, we report preliminary results on our first attempt for the InAs-AlSb system. We concentrate on single well structures<sup>7</sup> of InAs sandwiched between two AlSb layers, and compare them with those between two GaSb. It turns out that, while there are similarities in the formation of

two-dimensional quantum states in InAs, the predominant source of the electrons appears to be different in these two systems.

The samples were grown on semi-insulating (100)GaAs substrates by molecular beam epitaxy,<sup>8</sup> starting with a thin homoepitaxial growth of 500Å GaAs to smooth out the initial surface and a thick growth of 4000Å AlSb to accommodate the misfit stress from lattice mismatch. This was followed by a single layer of InAs with variable thickness, and then another AlSb of 200Å thick. An overlayer of 100Å GaSb was finally deposited to serve as protection for the underlying AlSb which reacts strongly with moisture.<sup>8</sup> The InAs-GaSb structures used for comparison were prepared in a similar sequence with the AlSb replaced by GaSb. In all cases, with the exception of the initial GaAs, the growths were carried out at 500°C, which was higher than that used previously.<sup>8</sup> The layers were all undoped which, by themselves, had an electron concentration of  $10^{16}\text{cm}^{-3}$  for InAs, and a hole concentration of  $10^{16}\text{cm}^{-3}$  and  $10^{15}\text{cm}^{-3}$  for GaSb and AlSb, respectively. For the latter materials, the carriers tend to freeze out with decreasing temperatures.

Figures 1 and 2 show the carrier densities and mobilities, obtained from Hall measurements at 77K, as a function of the InAs layer thickness. The range of interest of this parameter is between 50Å and 200Å where the electron density is expected to change significantly as a result of charge transfer, the origin of the semimetallic behavior in the InAs-GaSb structure.<sup>2</sup> The spread in the data points represent multiple samples measured from both the van der Pauw and the "spider" geometry which show some discrepancies.

In the case of GaSb-InAs-GaSb, both the electron density and the mobility increase with the InAs layer thickness as expected. With a widening layer, the electron state in InAs is quantized at a lower energy, allowing a larger number of electrons to be transferred from GaSb to maintain a higher Fermi level for charge neutrality. The increase in mobility may arise from two contributing factors: an enhancement in the carrier screening effect and a reduction in relative interface scattering. In comparison with results reported earlier,<sup>2</sup> both the electron density and the mobility are higher. The slight increase in density calls for a somewhat larger value of the energy difference between the valence band edge of GaSb and the conduction band edge of InAs, which was previously determined to be around 150 meV. The strong increase in mobility, by nearly an order of magnitude to  $10^5 \text{ cm}^2/\text{V}\cdot\text{sec}$  in thicker layers where it tends to saturate, represents a significant improvement in film quality, probably as a result of the higher deposition temperature.

In the case of AlSb-InAs-AlSb, as can be seen in Fig. 2, the mobility increases similarly with the InAs layer thickness, although it reaches a saturating value about a factor of 10 lower than that with GaSb confining layers. One would be tempted to infer, from these data alone, that the same charge transfer mechanism as in the case of GaSb-InAs-GaSb might be operative. However, as shown in Fig. 1, the electron density itself, scattering around  $1-2 \times 10^{12} \text{ cm}^{-2}$ , is unreasonably large and independent of the layer thickness. Extrinsic effect is probably dominant in this case. For example, a large number of positive charge or donor-like states either in AlSb in the vicinity of

the interface or at the interface itself could conceivably give rise to the high electron density in InAs. Among the different combinations of the three polytype materials of our interest, the InAs-AlSb heterostructure is likely to be the most difficult to achieve in perfection. It has a relatively large lattice mismatch, 1.3% which is twice as large as in the other two cases, and it contains the highly reactive Al component (absent in InAs-GaSb) without sharing a common element (present in GaSb-AlSb). The relatively low electron mobility is indicative of the existence of additional scattering imperfections. At present, little is known about such imperfections or the defects in general which contribute to the electrons. The possibility that the properties of AlSb may have been inadvertently affected during chemical processing because of its hygroscopic nature can not be completely excluded.

Nonetheless, magneto-transport measurements have clearly demonstrated the presence of two-dimensional electrons in this new type of single well structures of AlSb-InAs-AlSb. Figure 3 shows the magneto- and Hall-resistance at 4.2K and fields up to 22T. The sample has an InAs layer of 120 Å, an electron density of  $1.1 \times 10^{12} \text{ cm}^{-2}$ , and a mobility greater than  $10^4 \text{ cm}^2/\text{V}\cdot\text{sec}$ . Pronounced oscillations are observed in Fig. 3(b): The oscillatory period confirms the electron density; and the spin splitting, which becomes well resolved at the Landau level  $n = 1$ , gives an effective g-value of 22, consistent with that reported earlier in the InAs-GaSb superlattice.<sup>9</sup> The Hall resistance in Fig. 3(a) exhibits well-defined plateaus<sup>10,11</sup> with magnitudes given by  $h/ie^2$ ,  $i$  being the occupation number of the magnetic levels.

The drop after each plateau is believed to arise from incomplete overlap of the Hall contacts with the longitudinal current path, which affects the value of the Hall resistance corresponding to  $i = 5$ . The quantum limit can not be reached with available fields, however, because of the high electron density in all these samples.

In summary, the single well structure of InAs with two-dimensional electrons confined between AlSb layers has been fabricated. It represents a different type of structure in which, apparently, the carriers are induced primarily from external sources, in contrast to the situation in the InAs-GaSb system. What remains to be seen is whether or not the large electron densities can be reduced to reach the intrinsic limit.

The authors would like to thank L. F. Alexander and M. S. Christie for their technical help in film preparation and sample fabrication.

#### REFERENCES

- \* Sponsored in part by the US Army Research Office
- † Visiting scientist at the National Magnet Laboratory, Cambridge, MA.
1. E. E. Mendez, L. L. Chang and L. Esaki, *Surf. Sci.* **113**, 474 (1982).
2. L. L. Chang, in *Proc. 15th Int'l. Conf. Phys. Semicond.*, ed. by S. Tanaka and Y. Toyozawa, Kyoto, 1980 (*J. Phys. Soc. Jpn. Suppl. A*) **49**, 997 (1980).
3. M. Voos, *Surf. Sci.* **113**, 94 (1982).
4. M. Naganuma, Y. Suzuki and H. Okamoto, in *Proc. Int'l. Symp. GaAs and Related Compounds*, ed. by T. Sugano (Inst. Phys., Univ. of Reading, Berkshire, 1981) P. 125.
5. E. E. Mendez, C. A. Chang, H. Takaoka, L. L. Chang and L. Esaki, *J. Vac. Sci. Technol.* **B1**, 152 (1983).
6. P. Voisin, G. Bastard, M. Voos, E. E. Mendez, C. A. Chang, L. L. Chang and L. Esaki, *J. Vac. Sci. Technol.* **B1**, 409 (1983).
7. G. Bastard, E. E. Mendez, L. L. Chang and L. Esaki, *J. Vac. Sci. Technol.* **21**, 531 (1982).

8. C. A. Chang, H. Takaoka, L. L. Chang and L. Esaki, *Appl. Phys. Lett.* **40**, 983 (1982).
9. L. L. Chang, E. E. Mendez, N. J. Kawai and L. Esaki, *Surf. Sci.* **113**, 306 (1982).
10. K. von Klitzing, G. Dorda and M. Pepper, *Phys. Rev. Lett.* **45**, 494 (1980).
11. D. C. Tsui and A. C. Gossard, *Appl. Phys. Lett.* **38**, 550 (1981).

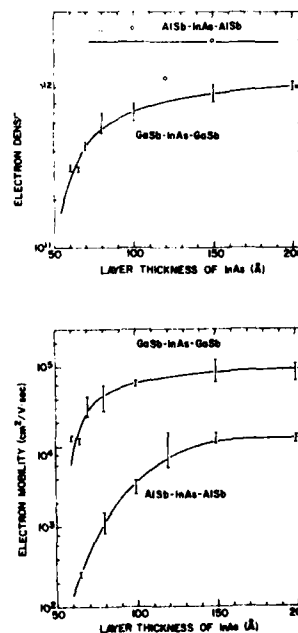


Fig. 2. Electron mobility vs. InAs layer thickness at 77K in AlSb-InAs-AlSb and GaSb-InAs-GaSb single-well structures.

Fig. 1. Electron density vs. InAs layer thickness at 77K in AlSb-InAs-AlSb and GaSb-InAs-GaSb single-well structures.

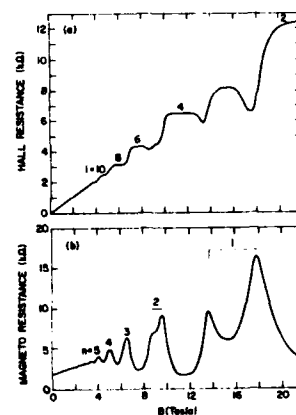


Fig. 3. Hall-resistance (a) and magneto-resistance (b) vs. magnetic field at 1.5K in a single-well structure of AlSb-InAs-AlSb with an InAs well thickness of 120Å. Indicated are numbers of magnetic-level occupation (i) and Landau indices (n). Distance ratio of Hall to magneto-resistance is 1/10.

## Experiments on Literally Two-Dimensional Magnets

Melvin Pomerantz

IBM T. J. Watson Research Center, Yorktown Heights, N. Y. 10598, U. S. A.

**Abstract** - A review is given of experiments on a magnetic material that is a single layer of magnetic ions, Mn stearate deposited by the Langmuir-Blodgett technique. Magnetic monolayers produced by condensation of magnetic gases are briefly surveyed. Some comparisons with the theory of 2-d magnetism are made.

**1. Introduction** - Previous Conferences on the Electronic Properties of Two-Dimensional Systems have not emphasized the magnetic properties of such systems. The interest has rather centered on electrical properties or at most the response of the electrical parameters to applied magnetic fields. This has happened despite the fact that the first suggestions that physical properties might be strongly influenced by dimensionality actually arose in the study of magnetism [ 1 ]. There still continues to be an abundance of theoretical work on model magnetic systems of low dimensionality, often with fruitful analogies to other properties. An example of this is the theory by Kosterlitz and Thouless [ 2 ] which started as an attack on the problem of the x-y model of a magnet in 2-d, but was first applied to experiments on superfluidity, the melting of 2-d solids and to the resistive transition of 2-d superconductors, before it finally was shown to be relevant to a magnetic material [ 3 ]. Thus magnetism has influenced much of the theory of 2-d physics. On the experimental side, magnetism seems to offer the best possibility of physically constructing a clearly 2-d system. An ideal 2-d system would be a single layer of atoms (here used in the original Greek meaning of indivisible units without structure), suspended in space for our study. No one has yet constructed such an object; the nearest has been liquid crystal films drawn over an aperture [ 4 ]. We usually have some kind of supporting structure. In the cases of adsorbed gases on solid surfaces, or even of electrons near a semiconductor or liquid He surface, one must make arguments why the system of gas or electrons may be regarded as distinct from its support despite the fact that it is of the same nature as the support and is bound to it with the same kind of forces with which it interacts within itself. We can avoid that awkward state by making the 2-d system of interest entirely different in nature from the supporting structure. In this

sense it is obvious that insofar as its magnetic properties are concerned, a layer of magnetic atoms can be totally distinguished from a non-magnetic support.

It is thus not surprising that there has been a great amount of study of the effects of dimensionality in magnetic materials. Many experiments [ 5 ] were done on "quasi 2-d" magnets, i.e., crystals in which the magnetic ions occupied layers that were relatively widely spaced compared to their spacing within the layers. Much interesting information was obtained, but there was a major prediction of theory that remained elusive. This is the well known result, sometimes referred to as the Mermin-Wagner Theorem [ 6 ], that for continuous symmetric interactions between the magnetic ions, there could be no long ranged magnetic order in two- or one dimensional structures. This seemed beyond testing in quasi 2-d materials because there were always residual interactions that were three-dimensional. As the temperature was lowered the magnetic correlations built up until three-dimensional interactions were large, and 3-d magnetic ordering always set in before 2-d ordering was observed [ 7 ].

The direct solution to the problem of 3-d interactions was to create a literally 2-d magnetic material. This was finally accomplished in two ways: the adsorption of a monolayer of gaseous magnetic atoms or molecules, and the deposition of monolayers of organic molecules to which magnetic ions had been chemically bonded. The organic molecule used was manganese stearate (abbr.  $\text{MnSt}_2$ ), which was deposited by the Langmuir-Blodgett technique. This paper will review the methods and results obtained thus far by these two methods. I shall emphasize my own work on  $\text{MnSt}_2$ , naturally, but that does not imply that the condensed film studies are less interesting.

Section 2 will review some of the theoretical predictions of the importance of dimensionality effects in magnetism. Then I shall describe the condensed film techniques and results in Section 3. In Section 4 I summarize the Langmuir-Blodgett method for the deposition of organic monolayers, the preparation of the magnetic molecule  $\text{MnSt}_2$ , and the results of our experiments. In the final section I compare the two methods, and indicate some future directions for the experimental study of 2-d magnetism.

2. *Some Results of Theory of the Effects of Dimensionality on Magnetism*—The modern theory of magnetic phase transitions hypothesizes that the are only two parameters that determine the nature of the transition [ 8 ] . These are the dimensionality of the spatial structure and the symmetry of the interaction between the elementary magnets. It is also assumed that the interaction is short ranged. Such a Universality Hypothesis is the reason that a theory of the  $s$ - $y$  model in 2-d by Kosterlitz and Thouless referred to above, could be applied to such a wide range of materials: they may differ in other ways but they have in common a 2-d structure and a two component order parameter with cylindrical symmetry. The assumption of short range forces is true for the exchange interaction, but as we shall see, the dipolar interaction is long-ranged, which has important consequences. The effect of dimensionality was pointed out by Bloch [ 1 ] in a calculation of the effect of temperature on the magnetization of a ferromagnet. He assumed highly symmetric Heisenberg coupling between spins,  $S$ , such that the energy,  $E = JS S$ , where  $J$  is the exchange constant. He found that the number of thermally excited spin waves increased as  $T^{1/3}$  in 3-d, but that in 2-d or 1-d the number of spin waves diverged at any finite temperature. Since each spin wave represents a decrease in the magnetization of the ferromagnet, an infinite number of spin waves meant that the magnet was disordered in 2-d or 1-d. The prediction of the absence of order was extended to the  $s$ - $y$  interactions, and to antiferromagnetism, by Mermin and Wagner [ 6 ] .

The predicted instabilities of ordered structures in low dimensions is so well known that the restrictions on the theory are sometimes overlooked. The result applies only to highly symmetrical interactions. It does not apply if there is uniaxial directionality of either anisotropy or exchange. Bloch expressed his result that order was absent only as the limit as any uniaxial anisotropy went to zero. The case of uniaxial exchange is the Ising model, interactions of the form  $E = JS_z S_z$ . For this case there is the celebrated analytic solution by Onsager [ 9 ] which showed that there is a second order transition to an ordered state in 2-d. Both the Ising interaction and anisotropy introduce an energy gap in the spin wave spectrum, so that a thermal energy comparable to this gap is needed to excite spin waves. This is the physical difference between such models and the Heisenberg and  $s$ - $y$  interactions which have continuous symmetry. In the case of continuous symmetry the spins can execute small deviations from each other, which cost an energy which vanishes as the wavelength goes

to infinity. It is the high density in low dimensions of the very low energy spin waves that washes out the ordered state.

Even in the cases of symmetric interactions there is a question whether the excitation energy can vanish, because the wavevector cannot go to zero since samples are always of finite size. There has been progress in taking finite size effects into account but very high resolution measurements are needed to distinguish short range from true long-range order.

In addition, there are questions about the effects of randomness in low-dimensional systems. Since randomness tends to oppose an ordered state, one might wonder whether randomness would be sufficient to prevent order in the Ising model, the one case in which it is permitted by theory. This problem is currently being actively studied. Theory distinguishes two cases: random exchange and random fields. Random exchange could arise because of random introduction of non magnetic spins, or of strains. This is likely for 2-d materials since roughness is present. An analysis, due to Harris [ 10 ] , suggests that in 2-d the only effect of random exchange will be a shift of the transition temperature; the nature of the transition, the critical exponents, will not change. It would be interesting to test this prediction. The case of random fields is more difficult and is still controversial. It can be realized in a dilute antiferromagnet in an external magnetic field [ 11 ] . Theory predicts that random fields will destroy the transition of an Ising system in 2-d [ 12 ] ; the disagreement is whether it will also prevent order in the 3-d Ising model. It is obviously important to establish the 2-d result experimentally.

3. *Condensed Gas 2-d Magnets*—The most obvious way to prepare a 2-d magnet is to evaporate a thin film of magnetic metal. Such films are questionable because of the problems of formation of islands, diffusion, roughness of the substrate, and impurity effects. Efforts in this field have emphasized surface magnetism and "dead layers", i.e., whether some outer layers of a magnet possess an ordered moment, or any moment at all. Early work, involving epitaxial films grown in ultra-high vacuum, could achieve films of a few atomic layers [ 13 ] . More recently experiments involving sub-monolayer amounts of Ni and Fe condensed at about 10 K and maintained at  $10^{-11}$  Torr have been reported [ 14 ] . These show that Ni does not develop long-range magnetic order until about 3 monolayer coverage. With only 1/6 of a monolayer of Fe, however, there was already magnetic

ordering. The differences between Ni and Fe, and Ni on various substrates, can be understood on the basis of electronic interaction (hybridization) with the substrate [ 15 ] .

In order to produce better single crystals of condensed magnetic films, Prinz and Krebs [ 16 ] have grown Fe on GaAs using molecular beam epitaxy. They describe samples as thin as 20 Å which have good crystal structure, albeit with strain due to lattice mismatch, but with well-defined magnetic anisotropy. Their ferromagnetic resonance data can be explained by including a surface magnetic mode introduced by Rado.

A rather different approach was used by Mc Tague and Nielson to obtain a sample that had monolayer coverage, but a macroscopic amount of sample. Their substrate [ 17 ] was grafoil, which is graphite that has been exfoliated, like puff pastry, to expose about 100 m<sup>2</sup> /gm. of interior surfaces of the graphite. This was permeated by known amounts of O<sub>2</sub> gas, such that when it was cooled the O<sub>2</sub> condensed with the desired coverage. The O<sub>2</sub> molecule is magnetic, so that they could search for magnetic ordering. They observed neutron diffraction peaks due to antiferromagnetic order below 10 K. Again because of the large quantity of sample available in this method (about 0.1 gm of O<sub>2</sub> per gram of substrate), a range of properties have been measured: magnetic susceptibility [ 18 ] , x-ray crystal structures [ 19 ] , specific heat [ 20 ] , and effects of substrates [ 21 ] and dilution by other gases [ 22 ] .

4. 2-d Magnets of Manganese Stearate- The technique that I have used to prepare literally 2-d magnets was developed by Langmuir and Blodgett [ 23, 24 ] . It is based on the tendency for oils and water to repel each other, and separate when mixed. The molecules used in the Langmuir-Blodgett method are "fatty" or "carboxylic" acids. These are dominantly fats, i.e., long-chain hydrocarbons that are solid at room temperature, but which have at one end an acidic group. That group is attracted to the water, and would dissolve except that the fatty end is repelled from the water. The result is that the molecule floats at the water surface, as a balance between the opposing tendencies of its fatty and acid parts. We used the fatty acid C<sub>17</sub>H<sub>35</sub>COOH, octadecanoic acid, commonly known as stearic acid. Its structure is illustrated in Fig 1a and a dilute layer of such molecules on the surface of water is shown in b. The Langmuir-Blodgett method consists of compressing the dilute layer with a movable surface piston (c) until a relatively incompressible solid film is

formed. This film is transferred from the water surface by inserting and removing a suitable substrate through the surface (d and e). When all goes well, the film adheres to the substrate and is pushed onto the substrate by the continual application of the surface pressure. Thus a single monolayer may be deposited, as in e. If the substrate is reinserted another layer attaches, as indicated in (f), and another upon exiting as in (g). The way in which the layers attach to each other and to the substrate is that the fatty surfaces attach to each other and the hydrophilic surfaces attach to each other.

To make the monolayers magnetic we bonded magnetic ions to the acidic end of the molecule. Following some results in the literature [ 25 ] , and our experiments [ 26 ] , we determined that Mn<sup>2+</sup> ions would replace the H<sup>+</sup> when the concentration of MnCl<sub>2</sub> was 10<sup>-3</sup> molar and the pH = 7. As illustrated in Fig. 1 b and c, under these conditions a monolayer of Mn stearate (Mn(C<sub>18</sub>H<sub>35</sub>OO)<sub>2</sub>, abbr. MnSt<sub>2</sub>) is formed at the surface. We have made literally 2-d magnets in two ways. The first is as shown in Fig. 1e: simply by depositing a single monolayer of MnSt<sub>2</sub>. In the second method, a non-magnetic layer of Cd stearate was deposited and then two layers of MnSt<sub>2</sub>. The Mn ions in this structure are in a more symmetrical situation, and also are more dense. Henceforth when I refer to 2-d MnSt<sub>2</sub>, I shall be speaking only of the Mn layers formed by the second method. The first did not show magnetic ordering down to T = 1.5 K and so are not of as great interest.

Before discussing magnetic ordering further, I shall describe briefly some of the chemical, structural and magnetic studies that confirmed the proposed method for producing the 2-d magnet structure by the Langmuir-Blodgett technique. A monolayer is only about 1 μm / cm<sup>2</sup>, so that one needs quite sensitive methods to study the monolayers. Sometimes we used bulk powders because the measurement required large quantities of sample. Sometimes a useful sample could be made by skimming the entire film off the bath, like crumpling a sheet of newspaper, and collecting this on to a substrate. Of course we preferred to study monolayers themselves, in as small number as possible. In many cases it was surprising that one could indeed study a monolayer. A case in point is x-ray diffraction. Normally x rays are very penetrating and one would not expect to observe a diffraction effect from a single molecular layer. The Langmuir-Blodgett film has special advantages: its thickness of about 25 Å, and a unit cell of two molecules (hence 50 Å), results in a Bragg angle of about 1° from the grazing angle. This is close to the angle for total internal reflection of x rays and the



intensity of the interfering beams is enhanced. As shown in Fig. 2, one can observe [ 27 ] the diffraction from a single layer, on a  $4 \text{ cm}^2$  substrate. This required a diffractometer with excellent collimation and monochromaticity, and long counting times. The structure is sufficiently simple that it can be modeled as laminae of the known chemical constituents of the molecule [ 28 ]. The resulting calculated diffraction pattern, shown by the solid lines in Fig. 2, is in excellent quantitative agreement with the data.

A simple way to study the reaction of the Mn in the water with the stearic acid on the surface was to skim a film on to a Si substrate. The infra-red spectra were measured on a Beckman spectrograph. We could observe the bonding of the Mn to the molecule by the reduction in the COOH carbonyl peak at  $6 \mu\text{m}$  and the growth of an absorption at  $6.5 \mu\text{m}$ , characteristic of bonded metal ions [ 29 ]. Using a surface wave technique it was possible to observe  $\pi$  absorption on as few as one monolayer [ 30 ]. The  $\pi$  absorption showed that Mn was bonded to the stearate molecule, but we had to ensure that there was no other Mn in the samples. This is an unwanted possibility that could occur if precipitates from the bath, or water containing Mn, were trapped in the films. Precautions were taken to avoid this by washing the films with pure water to purge soluble or lodged impurities, and was checked by two means. Chemical analyses on samples of some tens of layers were performed using electron microprobe and Rutherford backscattering. The chemical analyses showed that the Mn concentration corresponded with that expected for  $\text{MnSt}_2$  with no excess Mn. Since  $\pi$  showed that Mn was located at the ionic ends of the molecules, this indicated that Mn was being picked up only in the desired way.

Further confirmation that Mn was located in 2-d arrays and not elsewhere was found in the electron spin resonance (ESR) in the paramagnetic state. It had been shown [ 31 ] that the ESR should possess anisotropy in both the line width,  $\Delta H$ , and line position,  $H_0$ , as a function of the angle of the external magnetic field with respect to the film normal. The line width effect arises because the dipolar broadening depends on spin diffusion, and diffusion depends on dimensionality. In 2-d there are long correlation times which lead to enhancement of the term in the dipole interaction that is at zero frequency, namely the term proportional to  $(3\cos^2\theta - 1)$ . In Fig. 3 are measured linewidths vs the angle  $\theta$  between the resonance field and the film normal. They fit well to the

prediction of a form  $\Delta H = A + B(3\cos^2\theta - 1)^2$ . The dipolar interaction also contributes an average magnetic field that is anisotropic in 2-d. This results in a shift in  $H_0$  to higher values in the normal direction (to overcome the opposing dipole fields), and to lower fields in the in-plane orientation. This is a small effect but was observed in a multilayer film in the highest field available to us (See Fig. 4). The significance of these ESR results in the paramagnetic phase is that they demonstrate the anisotropic magnetic characteristics expected for 2-d arrays; there is not a significant amount of Mn in 3-d environments.

ESR was also the method used to search for spontaneous magnetic ordering. If ordering occurs it drastically changes the resonance spectrum: the resonance field, the lineshape or the intensity may all be affected. ESR also has quite high sensitivity, although it proved helpful to improve the signal by stacking 50 plates each coated on both sides with a magnetic monolayer. This served to increase the area of the sample, but did not introduce 3-d interactions since the monolayers were separated by macroscopic distances in a partial vacuum. The behavior of the ESR as the temperature was lowered is indicated in Figs. 5 and 6. The line width was observed to broaden and become independent of orientation. This behavior had been observed in quasi 2-d magnets as they approached a transition to an antiferromagnetic state [ 31 ]. The resonance fields for all orientations shifted to lower fields, but the  $H_0$  at normal showed the greatest shift. Its temperature dependence is shown in Fig. 6, and is seen to be very abrupt below about 2 K. This shift of the resonance indicates the rapid development of large internal magnetic fields, which is characteristic of an ordered magnetic state. The anisotropy of  $H_0$  is large and also indicative of an ordered state; I know of no Mn compound that has a remotely similar anisotropy in a paramagnetic phase.

The observation of rapid temperature variation of  $H_0$  to a state with large anisotropy are the bases for the conclusion that an exactly 2-d magnet of  $\text{MnSt}_2$  undergoes magnetic ordering. However the nature of the magnetic state is not certain. We have given arguments that it may be a "weak ferromagnet" [ 32 ]. This is dominantly antiferromagnetic, which accounts for the behaviour of the line width, and the susceptibility [ 26 ]. The opposing magnetic sublattices do not cancel exactly, resulting in a small ferromagnetic moment. This explains why the resonance does not disappear entirely, as happens with an antiferromagnet. This model can give a semiquantitative fit to the

unusual anisotropy of  $H_0$ , as shown in Fig. 7. The solid curve is a three parameter fit of the theory [ 33 ] of a uniaxial weak-ferromagnet to our data. One of the fitting parameters is the temperature. If the transition is taken as 2 K, the computed  $T = 1.3$  K is found to be in agreement with the measurement  $T$  of 1.4 K. There is some difficulty in reconciling one of the parameters with an independent estimate of the exchange field, derived [ 34 ] from the room temperature line widths. We have suggested, alternatively, that the ordered state may be antiferromagnetic, but that there are missing Mn ions which leads to a residual magnetic moment, as suggested by Neel [ 35 ]. This idea has some support because antiferromagnetic  $MnSi_2$  has been achieved in a very careful synthesis as a bulk powder [ 36 ]. We have not yet modified the deposition of Langmuir-Blodgett films to verify whether films can be made pure antiferromagnets. We also lack a theory of the ESR of a defect antiferromagnet.

5. Discussion- I shall conclude with a discussion of the relative advantages of the several methods of producing 2-d magnets, and some prospects. As for the evaporated metal films, perhaps the reason they have not been prominent in studies of statistical mechanics is that magnetism even in bulk metals is not well understood. It may be more comfortable to apply the theories to insulating materials in which we think we know where the spins are, and have some idea of their interaction. There may be an exception to this in the case of spin-glasses the major experimental effort is on metals, and the goal is to understand the nature of the magnetic transition. Here the origin of the interaction may not be calculable but it is believed that its spatial variation is of the Ruderman-Kittel-Kasuya-Yosida type, which gives rise to the important feature of the problem (the random antiferromagnetic and ferromagnetic exchange). Another factor is the small quantity in each sample, which limits the number of properties that can be measured. Roughness of the substrate seems to be a limiting factor; most experimenters do not have much confidence in the quality of films as thin as a monolayer.

The principal limitation of the technique employing the adsorption of gases on grafoil is that it requires gases that are magnetic.  $O_2$  may be a unique case, unless someone has the courage to try to diffuse a vapor of iron into grafoil (the grafoil would have to be heated). A problem with grafoil has been the lack of orientation and the small sizes of the flakes, about 3000 Å, which limits the ability to

do angular variations and the possible range of magnetic order. This difficulty has been largely overcome lately by the development of grafoil with relatively large and well-oriented surfaces [ 37 ].

The Langmuir-Blodgett technique offers a wider range of possible magnetic materials. The most studied case,  $MnSi_2$  described above, should be the best example of a Heisenberg interaction among the transition metal ions. We have examined the other transition metal stearates, and other carboxylates [ 38 ], to search for others that might undergo magnetic order. The only one that showed clear signs of ordering was ferric stearate [ 39 ]. The ordering temperature seemed to be greater than 50 K, much higher than for  $MnSi_2$ , which clearly is convenient from an experimental viewpoint. It is also encouraging if one harbors hopes of applying these materials to practical devices. Another class of materials that might have interesting properties are rare-earths, deposited by the Langmuir-Blodgett method. There might be some complications due to the trivalency of these ions. One supposes that the ions should be close together to get strong interaction, and thus the minimum amount of hydrocarbon chains seems desirable. If we are fortunate, the trivalent rare-earths will not bind to three carboxyl chains, but two, as has been found for some trivalent transition metals [ 39 ]. Each compound has its peculiarities, so it is difficult to predict which will be interesting and feasible. It should be remarked that the Langmuir-Blodgett method is less sensitive to surface roughness than are the methods of condensed gases. The Langmuir-Blodgett layers have some lateral strength, and can suspend between the peaks of the roughness, thereby becoming smoother than the original surface [ 28 ].

I have touched on some of the unsolved problems of 2-d magnetism, but let me collect them here. There still remains to do a definitive experiment to put the Mermin-Wagner Theorem in perspective. Despite at least three different experiments that indicate that a 2-d magnet does show magnetic order, most solid-state physicists will say that order is forbidden, except for the Ising model. Ordering of a Heisenberg magnet can be induced not only by uniaxial anisotropies, as mentioned above, but also by dipolar interactions [ 40 ], which are inherent in magnets. The fact to be remembered is that stability is delicate in low-dimensional systems and small perturbations may have profound consequences. Thus it would be desirable to study the transition of  $MnSi_2$  in zero magnetic field, unlike my experiment which needed a field for resonance. Other types of experiments, such as SQUID magnetometry, optical absorption, or Mössbauer effect are in progress, or should be.

I mentioned that randomness was an actively studied problem, having ramifications in electrical conduction (localization), spin glasses, as well as phase transitions. The effect of random exchange is predicted to be minimal, but random fields are thought to have important effects that depend on the dimensionality. It may be important to use exactly 2-d samples in order to avoid confusing the effects of randomness with the effects of the third dimension.

There are a number of predictions of the effects of variable dimensionality, i.e., the cross-over from 2-d to 3-d. With the ever increasing control of materials these theories may be testable.

**Acknowledgments:** My work has benefitted from the contributions of many colleagues including A. Aviram, J. Aze, P. Brosius, Ch. Chen, F. Dacol, F. Ferrieu, G. Grinstein, H. Lillenthal, R. Linn, F. Mehran, R. Pelcovits, T. D. Schultz, B. D. Silverman, J. Slonczewski, K. W. H. Stevens, A. R. Taranko. Early work was partially supported by the Defense Advanced Research Projects Agency of the Department of Defense and was monitored by the U. S. Army Research Office under contract No. DAH CO4-75-C-0010.

#### References

1. F. Bloch, *Z. Phys.* **61** (1930), 206.
2. J. M. Kosterlitz and D. J. Thouless, in *Prog. in Low Temp. Phys.* VIIB, Ed. D. F. Brewer, (North-Holland, Amsterdam 1978) p. 371.
3. H. Hasegawa, *J. of App. Physics*, **53**(1982)1893.
4. C. Y. Young, R. Pindak, N. A. Clark, and R. B. Meyer, *Phys. Rev. Lett.* **40**(1978)773.
5. Reviewed by I. J. de Jongh and A. R. Miedema, *Adv. Phys.* **23** (1974), 1.
6. N. D. Mermin and H. Wagner, *Phys. Rev. Lett.* **17**(1966)1133.
7. An exception is H. Ikeda, M. T. Hutchings and M. Suzuki, *J. Phys. C*, **11** (1978), L359.
8. M. E. Fisher in *Essays in Physics* Vol. 4, Academic Press N. Y., (1972) p. 43.
9. L. Onsager, *Phys. Rev.* **65** (1944), 117.
10. A. B. Harris, *J. of Phys. C*, **7**(1974)1671.
11. S. Fishman and A. Aharony, *J. Phys. C* **12**(1979)L729.
12. J. F. Fernandez, G. Grinstein, Y. Imry, S. Kirkpatrick, *Phys. Rev. Lett.* **51**(1983)203.
13. U. Gradmann, *Appl. Phys.* **3**(1974)161.
14. G. Bergmann, *J. Appl. Phys.* **50**(1979)7790.
15. J. Tersoff and L. M. Falikoff, *Phys. Rev. B*, **26**(1982)6186.
16. Reviewed by G. A. Prinz, G. T. Rado, and J. J. Krebs, *J. App. Phys.* **53**(1982)2087.
17. J. P. McTague and M. Nielson, *Phys. Rev. Lett.* **37**(1976)596.
18. S. Gregory, *ibid.* **40**(1978)723.
19. P. W. Stephens, P. A. Heiney, R. J. Birgenau, P. M. Horn, J. Stoltenberg, O. E. Vilches, *ibid.* **45**(1980)1959.
20. J. Stoltenberg and O. E. Vilches, *Phys. Rev. B*, **22**(1980)2920.
21. S. Gregory, *Phys. Rev. Lett.* **39**(1977)1035.
22. G. N. Lewis, D. D. Awschalom, and S. Gregory, in press.
23. K. B. Blodgett, *J. Am. Chem. Soc.* **57** (1935), 1007.
24. Reviewed by G. L. Gaines, *Insoluble Monolayer at Liquid-Gas Interfaces* (Interscience, New York, 1966).
25. G. A. Wolstenholme and J. H. Schulman, *Proc. Farad. Soc.* **46** (1950)475.
26. Reviewed by M. Pomerantz in *Phase Transitions in Surface Films* Eds. J. G. Dash and J. Ruvalds, Plenum Press, N. Y. 1980) p. 317.
27. M. Pomerantz, F. Dacol and A. Segmüller, *Phys. Rev. Lett.* **40**(1978)246.
28. M. Pomerantz and A. Segmüller, *Thin Solid Films* **68**, (1980), 38.
29. B. Ellis and H. Pyszora, *Nature* **181** (1958), 181.
30. A. Hjortsberg, W. P. Chen, E. Burstein and M. Pomerantz, *Optics Comm.* **25**(1978) 65.
31. ESR in quasi 2-d is reviewed by P. M. Richards, in *Proceedings of the International School of Physics "Enrico Fermi"*, Course LIX, Eds. K. A. Müller and A. Rigamonti (North Holland, Amsterdam, 1976) p. 539.
32. M. Pomerantz, *Solid State Comm.*, **27**(1978)1413.
33. H. Yoshioka and K. Sakai, *J. Phys. Soc. Japan* **33**(1972)1566.
34. F. Ferrieu and M. Pomerantz, *Sol. State Comm.* **39** (1981), 707.
35. L. Néel, *Ann. Phys. Ser. 12* (1949), 249.
36. A. Aviram and M. Pomerantz, *Sol. State Comm.*, **41**(1982)297.
37. T. Rosenbaum, S. E. Nagler, P. M. Horn, and R. Clarke, *Phys. Rev. Lett.*, **50**(1983)1791.

- 38 M Pomerantz, A. R. Taranko, and R. J. Begum, *Bull. Am. Phys. Soc.* 28(1983)p. 366  
 39 M Pomerantz, A. Aviram, A. R. Taranko, N. D. Heiman, *J. App. Phys.* 53(1982)7960  
 40 S. V. Mal'nev, *Sov. Phys. J. E. T. P.* 43(1976)1240

#### Figure Captions

Fig. 1(a) Structure of stearic acid. (b) - (g), the steps in producing 2-d magnets by the Langmuir-Blodgett technique. In (b), stearic acid is spread on the water containing  $Mn^{+2}$  ions. The ionized acid reacts with  $Mn^{+2}$  to produce  $MnSi_2$ . (c) The monolayer is compacted. (d) A hydrophilic substrate (e.g. glass) is inserted. No film is removed from the water. The barrier is stationary. If the substrate were hydrophobic (e.g. graphite) a layer would deposit, tail toward the substrate. (e) Lifting the substrate, film is deposited. The barrier moves forward. This produces a literally 2-d magnet. (f) Second layer is deposited by reinserting the substrate. Layers attach tail-to-tail. The meniscus turns downward and barrier moves forward. (g) Third layer is deposited on lifting the substrate. Many layers can be built up by repeating.

Fig. 2 X-ray diffraction pattern from 1 layer of  $MnSi_2$  on a Si substrate. The dots are experimental points, the solid curve is calculated from a model structure described in ref. 28.

Fig. 3 The measured ESR linewidth, (peak to peak of the derivative) vs.  $\theta$ , the angle between  $H_0$  and the film normal, of 2-d  $MnSi_2$ . The solid curve is the form  $A + B(3 \cos^2 \theta - 1)^2$  fitted to the data.  $T = 80$  K.  $f = 9.3$  GHz.

Fig. 4 The ESR field,  $H_0$ , vs.  $\theta$ , of 35 multilayers of  $MnSi_2$ . The dashed curve is a fit to theory of dipolar shifted lines. See ref. 26.  $T = 80$  K.  $f = 34.8$  GHz.

Fig. 5 ESR linewidth (full width at half max. of absorption), of 2-d  $MnSi_2$  vs. temperature.  $\perp$  and  $\parallel$  refer to the direction of the external field with respect to the film plane.  $f = 9.3$  GHz.

Fig. 6 Temperature dependence of the down-field shift of  $H_{0\perp}$ , the peak of ESR absorption in perpendicular orientation, for 2-d  $MnSi_2$ .  $f = 9.3$  GHz.

Fig. 7 Angular dependence of resonance fields of 2-d  $MnSi_2$ , at  $T = 1.4$  K. The solid curve is a best fit to the theory of resonance in a uniaxial weak-ferromagnet [32].

Fig. 1

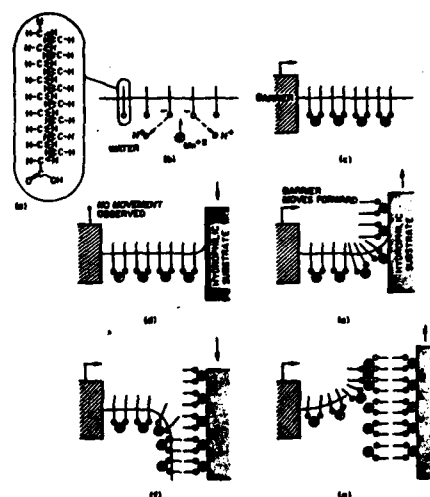


Fig. 2

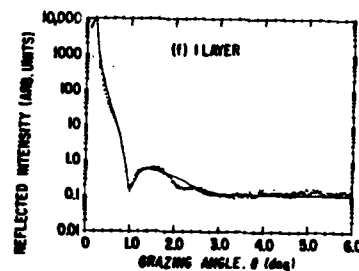


Fig. 3

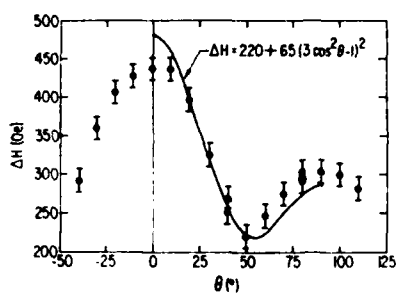


Fig. 4

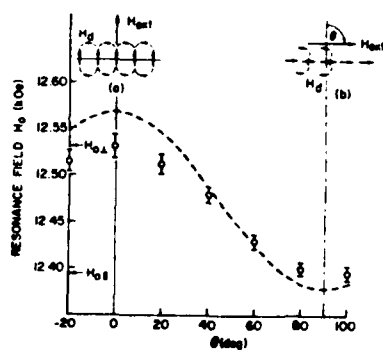
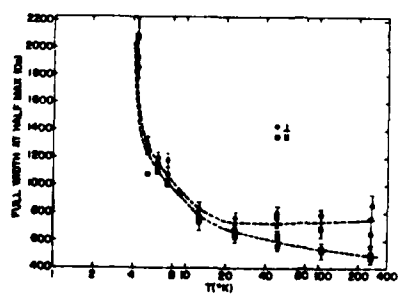


Fig. 5



644

Fig. 6

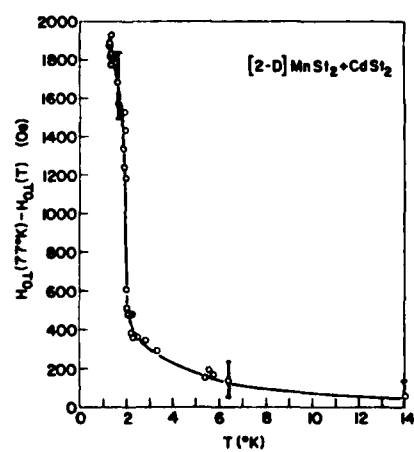
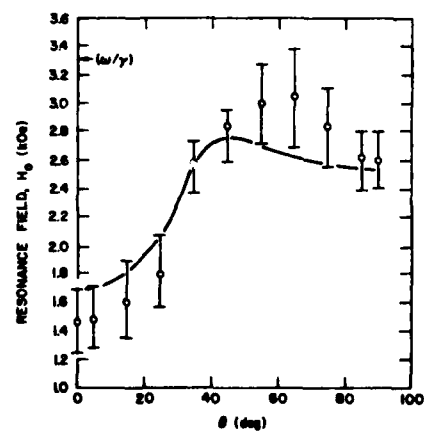


Fig. 7



645

## TWO-DIMENSIONAL ELECTRONIC SYSTEMS FOR HIGH-SPEED DEVICE APPLICATIONS (Invited Paper)

Thomas P. Pearsall  
Bell Laboratories  
Murray Hill, New Jersey 07974

### ABSTRACT

The use of a two-dimensional electron gas in electronic devices leads to improved performance through reductions in scattering, confinement of the electron current to a well-defined sheet, and from tailor-made adjustments of the electronic bandstructure. These new structures have resulted in dramatic reductions in room temperature device switching time and power consumption compared to classic designs. We will review the physics of the operation of this new class of devices and compare results obtained in AlInAs/GaInAs heterostructures which have the highest 2-dimensional electron velocity and 300K mobility, with AlGaAs/GaAs heterostructures which have been the subject of more extensive fundamental and applied investigations.

## TWO-DIMENSIONAL ELECTRONIC SYSTEMS FOR HIGH-SPEED DEVICE APPLICATIONS (Invited Paper)

Thomas P. Pearsall  
Bell Laboratories  
Murray Hill, New Jersey 07974

### 1. Introduction

The effect of two-dimensional electrons has been used to achieve special effects in semiconductor devices for nearly 10 years since the synthesis of the first semiconductor super-lattices.<sup>1,2</sup> More recently, the presence of a two-dimensional electron gas, confined to the interface between a high band gap and low band gap semiconductor have been observed in three systems of III-V compound semiconductors: InP/Ga<sub>0.47</sub>In<sub>0.53</sub>As, Al<sub>0.48</sub>In<sub>0.52</sub>As/Ga<sub>0.47</sub>In<sub>0.53</sub>As and of course Al<sub>x</sub>Ga<sub>1-x</sub>As/GaAs.<sup>3-5</sup>

One of the striking features of the two-dimensional electron gas seen in all of these systems is the enhanced mobility of the carriers at low electric fields and temperatures, see Fig. 1. This effect has stimulated much work in laboratories world-wide to realize a new class of ultra high speed devices based on this effect. Of the three systems mentioned above, the majority of this device effort has involved the AlGaAs/GaAs system, because of the relatively advanced state of both the crystal growth and device technologies compared to the other two. This work has established that the properties of the two-dimensional transport do indeed lead to improved device performance, but not necessarily in terms of speed alone. Indeed nearly equivalent speed of performance has been demonstrated using conventional GaAs MESFET devices.

If the art of crystal growth and device fabrication of the AlInAs/GaInAs, or the InP/GaInAs systems could be brought to the same level as that currently enjoyed by GaAs, we could expect to see an 50% improvement in speed and a factor of two reduction in power consumption at 300K. If this were not enough, the GaInAs material is in addition compatible with many processing applications in lightwave communications, while the GaAs devices are fundamentally incompatible. Hence, there is considerable motivation to develop the GaInAs two-dimensional electron system for device applications.

Two aspects in particular of the two-dimensional behavior are of interest for device applications.

One mentioned above, is the enhanced mobility of conduction electrons. The second is the actual confinement of the electrons themselves. This latter feature can be used in several ways: One is the obvious possibility to perform different device functions in different layers of the semiconductor wafer. It has been exploited to combine both photodetection and amplification in the same structure. A consequence of confinement is the modification of the band structure through the formation of sub-bands. The quantum well structure has been used in lasers<sup>7</sup> and light-emitting diodes<sup>8</sup> to tune the emission to the desired wavelength. The multi-quantum-well device structure is shown schematically in Fig. 2. The confinement of the quantum wells shifts the wavelength of emission by more than 1000Å toward the visible. The multi-quantum-well effect is particularly useful in the AlInAs/GaInAs system because the small effective mass (see Table 1) of electrons in GaInAs permits twice the tuning range possible using AlGaAs/GaAs. A 1000Å shift in wavelength moves the emission line of these devices from 1.67µm where the absorption of light by optical fibers is high to 1.57µm where absorption is at its minimum. This effect is shown in Fig. 3. In the sections which follow, we will describe our work on AlInAs/GaInAs and AlGaAs/GaAs devices, showing how the two-dimensional electrons lead to new horizons in semiconductor device design.

## 2 Two Dimensional Effects in $\text{Ga}_{1-x}\text{In}_x\text{As}$ Heterostructures

$\text{Ga}_{1-x}\text{In}_x\text{As}$  (GaInAs) is a ternary alloy with a 300K bandgap of 0.75 eV. The electronic structure<sup>9</sup> of this semiconductor has been extensively studied because of its important position in lightwave telecommunications applications.<sup>10</sup>  $\text{Al}_{1-x}\text{In}_x\text{As}$  (AlInAs) is indirect-gap at 300K, with a bandgap of 1.46 eV.<sup>11</sup> Both GaInAs and AlInAs are grown lattice-matched on InP substrates.<sup>12</sup> The basic structure of the AlInAs/GaInAs interface is shown in Fig. 4. Measurements of the conduction band discontinuity show the AlInAs conduction band to be about 0.5 eV above that of GaInAs.<sup>13</sup> The accumulation well is 40 meV deep and contains two sub-bands separated by 26 meV.<sup>14</sup> Electrons in these sub-bands show properties which clearly reflect the two-dimensional nature of the electronic states which dominate the transport. The electronic g-factor shows substantial enhancement from its bulk value of -3.7, and values as high as -9.2 have been measured at magnetic fields sufficiently large ( $> 3\text{T}$ ) to induce spin splitting of these levels.<sup>15</sup> These measurements show

the presence of substantial correlation and exchange effects in this two-dimensional system. Enhancement of the electron effective mass of about 20% above its bulk value<sup>16</sup> of 0.041 is also measured as a result of the two-dimensional confinement and the non-parabolicity of the energy bands.<sup>4</sup>

Two dimensional quantum transport has also been observed at the InP/GaInAs heterojunction interface.<sup>3</sup> The quantum well supports only one sub-band with no enhancement of the electronic g-factor<sup>17,18</sup> in distinct contrast to the AlInAs/GaInAs system. The persistence of quantum effects associated with the two-dimensional electron gas at temperatures close to 300K indicates the high degree of confinement and absence of significant interfacial scattering at the heterojunction.<sup>19</sup> It is remarkable that this two-dimensional system is so different from AlInAs/GaInAs, even though in both cases the current is carried in the GaInAs ternary alloy. That such a difference could exist is an indication of the richness of the information contained in the results of the two-dimensional transport experiments. An explanation of the larger differences in electron behavior between these two systems will require improvements in the quality and purity of the materials growth as well as additional experimental measurements.

The 300K electron mobility of bulk GaInAs is 50% larger than that of GaAs, and 20% larger than the best enhanced mobility obtained in AlGaAs/GaAs selectively-doped heterostructures.<sup>20</sup> In Fig. 5a we show the mobility of n-type GaInAs as a function of carrier concentration at 300K and at 77K. Note that while the room temperature mobility is greater than  $10,000\text{ cm}^2\text{-V}^{-1}\text{sec}^{-1}$ , the 77K mobility, even for the most pure material is considerably less than that of bulk GaAs. The fundamental presence of alloy disorder scattering in GaInAs significantly reduces the low temperature mobility.<sup>21</sup> In Fig. 5b, the Hall mobility of a AlInAs/GaInAs selectively-doped heterostructure displays a similar low temperature enhancement from two-dimensional effects<sup>4</sup> as that shown in Fig. 1. While the highest mobility obtained ( $\mu_H > 90,000\text{ cm}^2\text{-V}^{-1}\text{sec}^{-1}$ ) exceeds the best bulk results by 20%, it is still one order of magnitude less than the best comparable figures for AlGaAs/GaAs structures.<sup>6</sup> For this reason, GaInAs may not be the preferred material for low temperature studies of two-dimensional effects, however its higher room temperature mobility makes

it very attractive for device applications.

In high speed electronic or optical device applications, additional physical features of the two-dimensional semiconductor system need to be taken into account in order to optimize device performance. In comparing the AlGaAs/GaAs system to the AlInAs/GaInAs system, both technological and fundamental properties came into play. In the preceding paragraph we have discussed the relative mobilities of these two systems. The speed of a high-field majority carrier device, such as an FET, is determined not by the low field mobility, but rather by the drift velocity. While the two-dimensional electron gas in GaAs may have a higher Hall mobility at 77K, the drift velocity does not appear to be significantly different  $\sim 1.5 \times 10^7$  cm/sec.

In GaInAs, the high field drift velocity is 50% higher  $\sim 2.1 \times 10^7$  cm/sec, and again does not increase in a two-dimensional structure.<sup>22-24</sup> However, another important device property, the power dissipation does depend inversely on the mobility. Electrons in all III-V materials can gain only a few tens of millivolts of energy at high velocity before they scatter into a low velocity sink at the L minimum. The L-L splitting is an essential parameter in determining FET performance.<sup>25</sup> For GaInAs this splitting is 0.55 eV, 60% larger than in GaAs, indicating a considerable advantage in maintaining higher current and higher drift velocity in the ternary alloy.<sup>26</sup> In every instance, the electronic structure favors GaInAs over GaAs as a high-speed, low-noise material for two-dimensional device applications.

Two features of the device technology which are desirable for high speed device fabrication are a high quality Schottky barrier, essential for obtaining short gate length, and good confinement of the 2d electron gas even at high current levels. GaAs has both of these features, while the technology of AlInAs/GaInAs can produce only mediocre Schottky barriers and confinement. Hence, the choice between these two materials is essentially a trade-off between ease of fabrication versus potential performance.<sup>22,24</sup> A summary of some relevant properties for two-dimensional electron device materials is given in table 1. It seems certain that continued research work will produce a satisfactory Schottky gate technology. It is less clear that development of the materials growth techniques will produce the lightly doped p-type layer which is needed to obtain good carrier

confinement at the heterostructure.

### 3. Design and Performance of Some 2-Dimensional Electron Devices

#### a. High electron mobility transistors

The announcement by Minura, Hiyanizu, and co-workers at Fujitsu in 1980 of selectively-doped AlGaAs/GaAs field-effect transistor (FET) provided the first demonstration of the beneficial effects of the 2-dimensional electron transport in the channel region.<sup>27,28</sup> The basic FET configuration employing a 2-dimensional electron gas in the channel is shown in Fig. 6. The band width of the transistor is characterized by the ratio of the transconductance  $g_m$  to the input capacitance of the gate,  $C_i$

$$F_T \approx \frac{g_m}{2\pi C_i} = \frac{V_D}{L_G} \quad (1)$$

where  $V_D$  is the electron drift velocity and  $L_G$  is the length of the gate. The transconductance is the differential increase in source-to-drain current for an incremental change in gate voltage. While the transconductance can be raised by increasing the carrier concentration in the channel, this gain is offset by an increase in capacitance.  $F_T$  is ultimately limited by the transit-time under the gate which is a function of the drift velocity and some geometric factors.

The enhanced mobility of the 2-dimensional electron gas obtains only when the electric field is low, that is: at the source and drain regions. The effect of the high mobility is to lower the parasitic resistances associated with the distances between the source and drain contact and the gate region as indicated in Fig. 6. These resistances reduce the measured transconductance from its intrinsic value:

$$g_m(\text{meas}) = g_m(\text{intr}) / (1 + R_s g_m(\text{intr})) \quad (2)$$

Parasitic resistance effects can be reduced obviously by shortening the spacing between the ohmic contacts and the gate. However, a reduction below 2  $\mu\text{m}$  leads to avalanche breakdown between the gate and drain and operating voltages too small to make the device useful. The increase in mobility gained by using 2-dimensional electrons in the channel also serves to reduce



parasitic resistances, and is an alternative to shortening the source-gate-drain spacings which have practical limits as discussed above. Using Eqn. 2, it can be shown that for GaAs, a channel mobility of  $15,000 \text{ cm}^2/\text{V} \cdot \text{sec}$  is sufficient to reduce parasitic effects to negligible levels. Thus, an increase in carrier mobility from  $4,000 \text{ cm}^2/\text{V} \cdot \text{sec}$  to  $6000 \text{ cm}^2/\text{V} \cdot \text{sec}$ , achieved by using a 2-dimensional electron gas, significantly improves the measured  $g_m$ , without any accompanying increase in capacitance. The direct effect of the 2-dimensional electron gas is thus to increase the amount of current in the transistor without any degradation in switching time.

In Fig. 7 we show the d.c. characteristics taken at 77K for an AlGaAs/GaAs transistor (7a) and a AlInAs/GaInAs transistor (7b).<sup>4,24</sup> The effect of the 2-d gas on the characteristic is immediately evident in the sharp rise in the drain current leading to saturation at less than 1V. The slope of this line is a measure of the parasitic resistances. These two transistors show nearly identical characteristics with transconductance of about 300 mS/mm.

#### b. High Speed Integrated Circuits

The switching speed of 2-dimensional electron gas transistors falls commonly in the range of 10-30 psec. Delay times this short are most conveniently measured using a ring oscillator integrated circuit with a large enough number of stages to give an easily measurable round-trip transit time.

The time delay is composed of the transit time of the charge under the gate and the time required to charge the gate and parasitic capacitances,  $C_p$ .

$$\tau = \frac{2L_g}{V_D} + \frac{C_p V}{I_{DS}} \quad (3)$$

In Eqn. 5,  $V$  is the logic swing which is determined by system specifications, and  $I_{DS}$  is the channel current from the previous stage which charges the gate and inter-connection wires.

The power consumption may be expressed:

$$P = \frac{1}{2} I_{DS} V_{DS} = \frac{1}{4} qQW V_D V_{DS} \quad (4)$$

where  $Q$  is the sheet charge of the 2-dimensional electrons  $W$  is the width of the gate and  $V_{DS}$  is the

source-drain bias voltage. In Eqns. 3 and 4, the presence of parasitic resistance results in a lower value of  $I_{DS}$ . The power-time delay product may be expressed:

$$P \cdot T = \frac{1}{2} V_{DS} qQW \left[ L_g + \frac{1}{2} \frac{C_p V V_D}{I_{DS}} \right] \quad (5)$$

The power-time delay product consists of two terms, the first depending on intrinsic transport properties and the second on parasitic effects. By introducing a 2-dimensional electron gas in the channel region, the power-time delay product is reduced because the channel current may be increased without increasing the supply voltage. In addition this allows the number of gates to be driven by the transistor, or the fan-out, to be increased. If the fan-out is not increased, then the required source-drain voltage can be reduced. In this way the power consumption is dramatically reduced and a small sacrifice in speed, as can be seen in Eqns. 3-5 because the parasitic effects are small.

In Fig. 8 we show power-time delay product for several types of high-speed devices including Josephson junction switches. It can be seen in Fig. 8 that FET circuits using 2-dimensional electrons in the channel show the best P.T product of any semiconductor device currently under study. In table 2 we show a summary of some current results for these kinds of devices.

Because of the need to develop an integrated circuit technology in order to test high speed FET devices, the momentum exists to pursue other, more complicated circuits. Kiehl and co-workers<sup>21</sup> from Bell Labs have announced results on a divide by two circuit which operates at 2.5 GHz at room temperature. Fujitsu has announced a major effort to use the high electron mobility transistor in a 1000-gate device for a new micro-processor. The natural advantage of 2-dimensional electron devices in integrated circuits is clear: The lower power dissipation through reduction of parasitic resistance allows a higher packing density, which implies shorter interconnect distances and improved switching times.

The future of high-speed 2-dimensional electron FETs is best summarized in Fig. 8, reproduced here from the work of Abe, et al.<sup>22</sup> The total allowed power dissipation per chip, which is fixed,

requires that increases in circuit complexity, or packing density be accompanied by a reduction in FET gate width. This reduction in size limits the driving power or fan-out of the FET, and cannot be continued indefinitely. The GaAs MESFET, operating with the same power dissipation and fan-out as a 2-dimensional electron HEMT, must run more slowly. The difference between these two devices becomes significant when the complexity increases above 10K gates per chip. In large scale integration, typical of that planned for computers of the near future, the 2-dimensional electron device can offer a factor of 2 reduction in switching speed compared to that obtainable with GaAs, because of the restrictions of allowable power dissipation.

#### Acknowledgments

The author wishes to acknowledge the collaboration of A. Y. Cho, K. Alavi, R. Hendel, and P. O'Connor in this work. Thanks are also due to S. H. Wemple, R. Kiehl, M. D. Feuer, and R. Dingle for many helpful discussions.

#### REFERENCES

- [1] L. L. Cheng, L. Esaki, and R. Tsu, *Appl. Phys. Lett.*, **22**, (1974) 593-595.
- [2] R. Dingle, W. Wiegmann, and C. H. Henry, *Phys. Rev. Lett.*, **33**, (1974) 827-829.
- [3] M. Razeghi, M. A. Pissin, J. P. Larivain, B. deCremoux, J. P. Duchemin, and M. Voos, *Electron Lett.*, **18**, (1982) 339-340.
- [4] A. Kastalsky, R. Dingle, K. Y. Cheng, and A. Y. Cho, *Appl. Phys. Lett.*, **41**, (1982) 274-277.
- [5] H. L. Stormer, A. L. Gossard, W. Wiegmann, and K. Baldwin, *Appl. Phys. Lett.*, **39**, (1981) 912-914.
- [6] J. V. DiLorenzo, R. Dingle, M. Feuer, A. C. Gossard, R. Hendel, J. C. M. Hwang, A. Kastalsky, V. E. Keramidas, R. Kiehl, and P. O'Connor, *Tech. Digest of IEDM*, paper 25.1, (1982) pp. 578-581.
- [7] K. Alavi, T. P. Pearsall, S. R. Forrest, and A. Y. Cho, *Electronics Lett.*, **19**, (1983) 227-229.
- [8] H. Temkin, K. Alavi, W. R. Wagner, T. P. Pearsall, and A. Y. Cho, *Appl. Phys. Lett.*, **42**, (1983) 845-847.
- [9] T. P. Pearsall, *GaInAsP Alloy Semiconductors*, ed. T. P. Pearsall (Chichester, John Wiley & Sons, Ltd, 1982) pp. 295-312.
- [10] T. P. Pearsall, *IEEE J. Quant. Electron.*, **QE-16**, (1980) 709-720.
- [11] H. Ohno, C.E.C. Wood, L. Rathbun, D. V. Morgan, G. W. Wicks, and L. F. Eastman, *J. Appl. Phys.*, (1981) 4033-4037.
- [12] K. Y. Cheng, A. Y. Cho, and W. R. Wagner, *Appl. Phys. Lett.*, **39**, (1981) 607-609.
- [13] R. People, K. W. Wehr, K. Alavi, and A. Y. Cho, *Appl. Phys. Lett.*, **43**, (1983) 118-120.
- [14] J. C. Portal, R. J. Nicholas, M. A. Brummel, A. Y. Cho, K. Y. Cheng, and T. P. Pearsall, *Sol. St. Comm.*, **43** (1982) 907-911.

- [15] R. J. Nicholas, M. A. Brummel, J. C. Portal, K. Y. Cheng, A. Y. Cho and T. P. Pearsall, *Sol. St. Comm.* **45**, (1983) 911-914.
- [16] R. J. Nicholas, J. C. Portal, C. Houlbert, P. Porner and T. P. Pearsall, *Appl. Phys. Lett.*, **34**, (1979) 491-493.
- [17] R. J. Nicholas, M. A. Brummel, J. C. Portal, M. Razeghi and M. A. Poisson, *Sol. St. Comm.* **43**, (1982) 825-828.
- [18] Y. Guldner, J. P. Vieren, P. Voisin, M. Voss, M. Razeghi, and M. A. Poisson, *Appl. Phys. Lett.* **40**, (1982) 877-879.
- [19] M. A. Brummel, R. J. Nicholas, J. C. Portal, M. Razeghi, and M. A. Poisson, *Physica 118B* (1983) 753-755.
- [20] T. P. Pearsall, G. Beuchet, J. P. Hirtz, N. Vincent, M. Bonnet, and A. Raizes, *GaAs and Related Compounds Vienna 1980*, (Bristol Inst. of Physics, 1981) 639-649.
- [21] Y. Takeda, *GaInAsP Alloy Semiconductors*, ed. T. P. Pearsall (Chichester, John Wiley & Sons, Ltd. 1982) 213-241.
- [22] P. O'Connor, T. P. Pearsall, K. Y. Cheng, A. Y. Cho, J. M. Hwang, and K. Alavi, *IEEE Electron Dev. Lett.*, *EDL-3*, (1982) 64-65.
- [23] M. A. Littlejohn, T. H. Glisson, and J. R. Hauser, *GaInAsP Alloy Semiconductors*, ed. T. P. Pearsall (Chichester, John Wiley & Sons, Ltd, 1982) 243-274.
- [24] T. P. Pearsall, R. Hendel, P. O'Connor, K. Alavi and A. Y. Cho, *IEEE Electron Dev. Lett.* *EDL-4*, 5-8 (1983).
- [25] A. Cappy, B. Carrez, R. Fauquembergues, G. Salmer, and E. Constant, *IEEE Trans. Electron Dev.* *ED-27*, (1980) 2158-2159.
- [26] K. Y. Cheng, A. Y. Cho, S. B. Christman, T. P. Pearsall, and J. E. Rowe, *Appl. Phys. Lett.* **40**1, (1982) 429-431.

- [27] A. Hiyamazu, T. Mimura, T. Fuji, and N. Kanbu, *Appl. Phys. Lett.* **37**, (1980) 805-807.
- [28] T. Mimura, S. Hiyamazu, T. Fuji, and K. Nanbu, *Japan J. Appl. Phys.* **19** (1980) 1225-1227.
- [29] P. N. Tung, D. Delagebeaudeuf, M. Laviron, P. Delescluse, J. Chapiart, N. T. Linh, *Electron Lett.* **18**, (1982) 109-110.
- [30] C. P. Lee, D. L. Miller, D. Hou, R. J. Anderson, *Program of the Dev. Res. Conf.* **41** (1983), paper IIA-7.
- [31] R. A. Kiehl, M. D. Feuer, R. H. Hendel, J. C. M. Hwang, V. G. Keramidis, C. I. Allyn, and R. Dingle, *Program of the Dev. Res. Conf.* **41** (1983) paper IVA-3.
- [32] R. A. Kiehl, P. G. Flahive, S. H. Wemple, and H. M. Cox, *IEEE Electron Dev. Lett.* *EDL-3* (1982) 325-326.
- [33] M. Abe, T. Mimura, N. Yokoyama, and H. Ishikawa, *IEEE Trans. Electron Dev.* *ED-29*, (1982), 1068-1093.

#### TABLE CAPTIONS

Table I. Some physical parameters for some III-V semiconductor materials suitable for 2-dimensional electron devices. The saturated drift velocity, ( $V_D$ ), the electron effective mass, and electron mobility are among the most important parameters affecting device performance.

Table II. Some performance results obtained in III-V FETs and circuits employing a 2-dimensional electron gas in the channel. For reference, some results for conventional GaAs MESFETs are included. Direct comparison of ring oscillator results should not be made because the power dissipation is proportional to device size.

TABLE I

2D CHANNEL MATERIALS	$E_g$ eV	$\mu$ $\text{cm}^2 \text{V}^{-1} \text{sec}^{-1}$	$V_D$ $\text{cm} \text{ sec}^{-1}$	$\Delta E_{1,2}$ eV	$m_e^*$	Schottky Barrier	High Purity p-Confinement
GaInAs	0.75	11,000	$2.2 \times 10^7$	0.55	0.041		
GaAs	1.43	8,000	$1.5 \times 10^7$	0.34	0.067		yes
HIGH BANDGAP CONFINEMENT MATERIALS							
AlGaAs	1.45					YES	
InP	1.35					NO	
AlGaAs	1.90					YES	

TABLE II

TRANSISTOR STRUCTURE	$\mu_n$ , T=300K ( $\text{mS} \cdot \text{mm}$ )	$\mu_n$ , T=77K ( $\text{mS} \cdot \text{mm}$ )	Ref.
(a) AlInAs/GaInAs (HEMT)	190	300	24
AlGaAs/GaAs (HEMT)	191	405	33
GaAs (MESFET)	135	190	32

Ring Oscillator Circuit FET Type	Switching Time (ps) and Power Dissipation (mW)	Power-Time Delay Product (fJ)	Ref.
(b) AlGaAs/GaAs (HEMT)	19.1 ps/6.6 mW, T=300K	126 fJ	29
AlGaAs/GaAs (HEMT)	29 ps/2 mW, T=300K	58 fJ	6
GaAs (MESFET)	17.8 ps/12.7 mW, T=300K	226 fJ	32
AlGaAs/GaAs (HEMT)	56.5 ps/0.46 mW, T=300K	26 fJ	33

HEMT Integrated Circuit	Temp	Frequency of Operation	Power Diss. Per Gate	Ref.
(c) Type D Flip-Flop Divider Circuit	300	2.6 GHz	2.4 mW	31
	300	3.7 GHz	0.5 mW	31
	77	6.0 GHz	3.75 mW	31

FIGURE CAPTIONS

Figure 1. Electron mobility of the 2-dimensional electron gas at the AlGaAs/GaAs interface. The best samples show a mobility greater than  $10^6 \text{cm}^2 \text{V}^{-1} \text{sec}^{-1}$  at 4K. (After DiIorenzo, et al.\* Reproduced with the permission of the authors and the IEEE.)

Figure 2. The structure of the AlGaAs/GaInAs multiquantum-well laser. The shift of the light emission toward higher energies can easily be made quite large because of the low electron effective mass of GaInAs.

Figure 3. The output spectrum of a multiquantum-well laser. The output wavelength has been shifted from 1.7  $\mu\text{m}$  to 1.55  $\mu\text{m}$  by virtue of the quantum confinement of the 2-dimensional electrons.

Figure 4. The electron structure of the AlInAs/GaInAs hetero interface. Two electronic subbands are seen in the quantum transport properties.

Figure 5. The electron mobility of GaInAs is affected by alloy scattering. (a) In bulk samples the presence of alloy scattering lowers the 77K mobility to  $\sim 5 \times 10^4 \text{cm}^2 \text{V}^{-1} \text{sec}^{-1}$  for a background doping of  $1 \times 10^{15} \text{cm}^{-3}$ . (b) In a 2-dimensional electron gas, some of this scattering is avoided and mobilities as high as  $9 \times 10^4 \text{cm}^2 \text{V}^{-1} \text{sec}^{-1}$  have been reached at the same impurity level. (Fig. 5b after Kasatsky et al.\* Reproduced with the permission of the authors and the AIP.)

Figure 6. The structure of a 2-dimensional, selectively-doped AlInAs/GaInAs FET. The contribution of the mobility, enhanced by the 2-dimensional confinement of electrons from impurities, is seen chiefly in lower parasitic resistances. The device speed is limited by the electron drift velocity.

Figure 7. Current-voltage characteristics for some 2-dimensional FETs at 77K. (a) AlGaAs/GaAs and (b) AlInAs/GaInAs. These devices are built from different 2-dimensional materials, but share a common structure, and geometry. The measured

transconductance in both cases is  $\sim 300 \text{ mS/mm}$ . (Fig 7a after DiLorenzo et al<sup>8</sup> reproduced with the permission of the authors and the IEEE).

Figure 8 The power consumption-switching time delay (P.T) for an assortment of electronic devices. Josephson junctions show the best P.T product. III-V semiconductors show a significant improvement in both speed and power over Si devices. The 2-dimensional electron devices discussed in this paper show a similar improvement over 3d devices made from III-V compounds. While FETs have been measured with switching speeds shorter than those obtained using Josephson junctions, the power consumption of Josephson junction devices is still two orders of magnitude less.

Figure 9 The system delay as a function of circuit complexity projected for 3-dimensional (MESFET) and 2-dimensional (HEMT) GaAs transistors. The major advantage in power time delay product for HEMT devices becomes apparent only after circuit complexity becomes significantly larger than  $10^4$  devices. (After Abe, et al<sup>11</sup> Reproduced with the permission of the authors and the IEEE.)

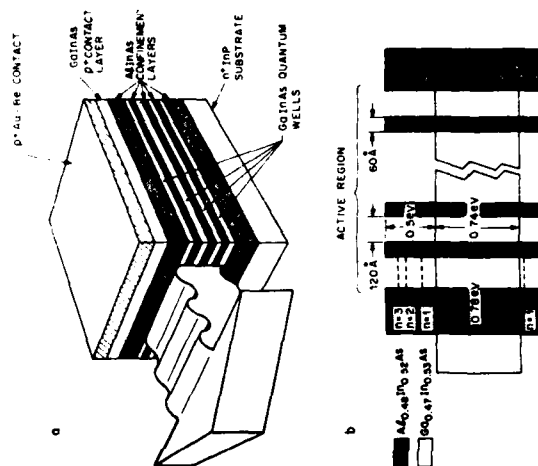


Figure 2

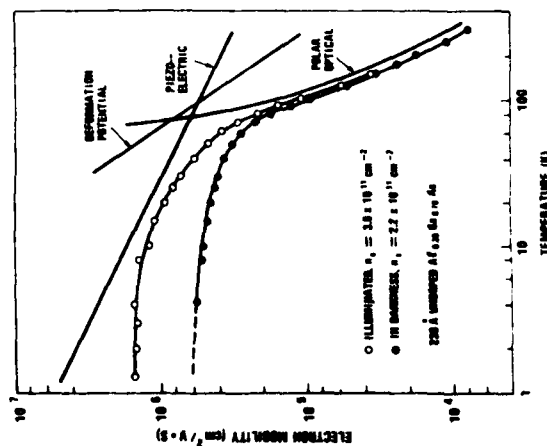


Figure 1

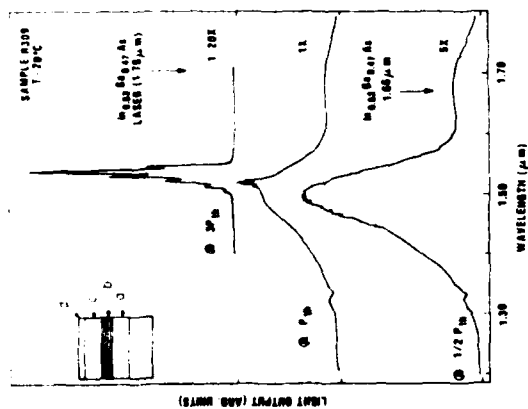


Figure 3

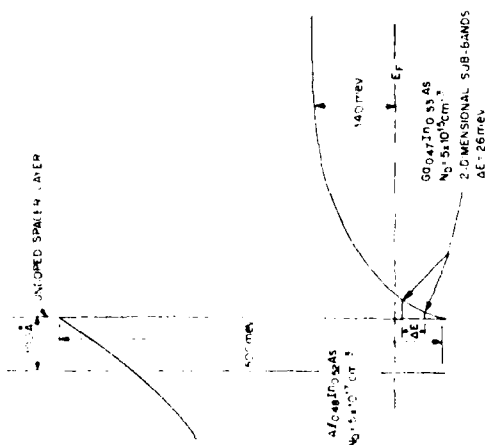


Figure 4

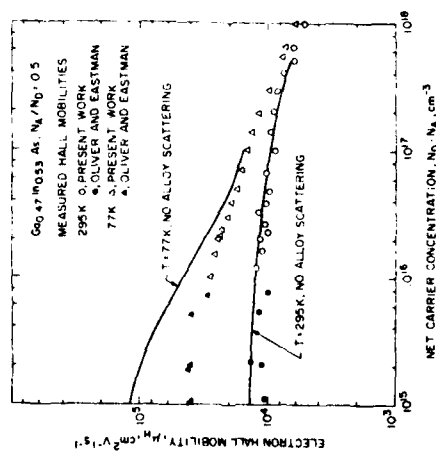


Figure 5(a)

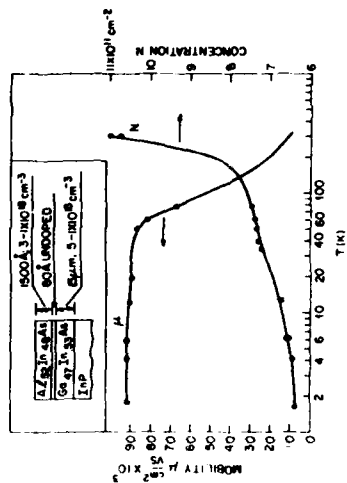
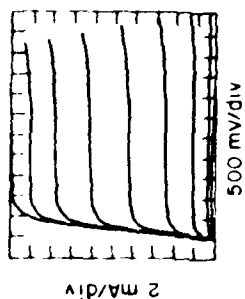


Figure 5(b)



T = 77K  
GATE DIMENSION: 15 μm x 125 μm

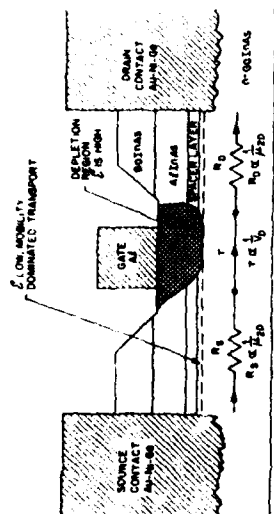


Figure 6

62 24

# SPEED/POWER PERFORMANCE OF VARIOUS TECHNOLOGIES

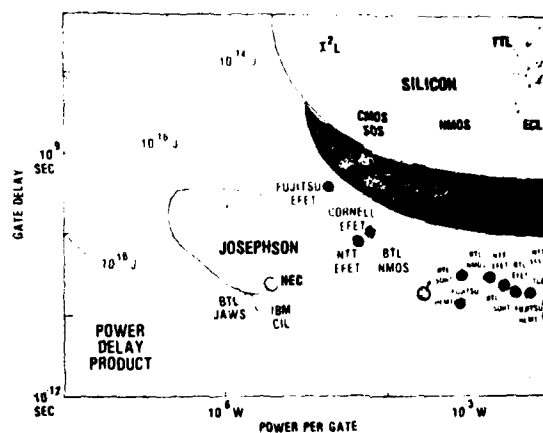


Figure 8

5/82

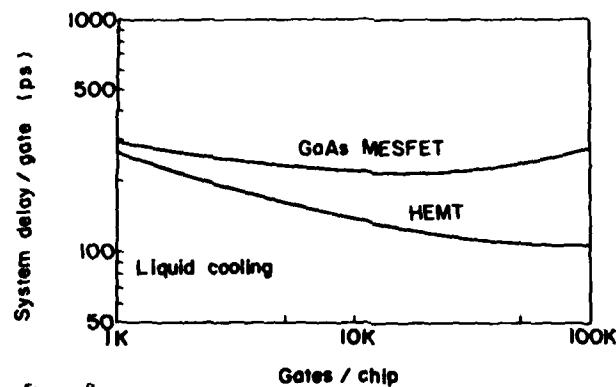


Figure 9

Gates / chip

665

Effects of Electron Heating on the Two-Dimensional Magnetotransport  
in AlGaAs/GaAs Heterostructures

H. Sakaki, K. Hirakawa, J. Yoshino, S. P. Svensson<sup>†</sup>  
Y. Sekiguchi, T. Hotta, S. Nishi and N. Miura<sup>\*</sup>

<sup>\*</sup>Institute of Industrial Science, University of Tokyo  
<sup>\*</sup>Institute for Solid State Physics, University of Tokyo  
4-22-1 Roppongi, Minato-ku, Tokyo 106, Japan

<sup>†</sup>Dept. of Physics, Chalmers Univ. of Tech., S-402 21, Göteborg, Sweden

**Abstract:** Effects of electron heating on Shubnikov-de Haas oscillations are studied at 4.2K in N-AlGaAs/GaAs heterostructures. Electron temperatures  $T_e$  are determined and found to depend only on the input power  $P_e$  per electron, suggesting the dominant energy relaxation process in low temperatures is independent of sample mobilities and carrier concentrations. When  $P_e > 10^{13}$  W and  $T_e > 4$  K, extra peaks are observed for the first time in SDH oscillations, which can be attributed to the resonant emission of optical phonons. The electron heating is found to reduce the plateau width of quantized Hall resistivities, probably because such a heating causes the delocalization of electrons.

## 1. Introduction

The study of two-dimensional (2D) electron transport along the layer planes of AlGaAs/GaAs superlattices and heterojunctions was initiated in 1977<sup>(1)</sup> and has become an extremely important subject. One of the main reasons of this importance is that electrons in this system can be well isolated from their parent donor impurities in AlGaAs and exhibit extremely high mobilities at low temperatures.<sup>(2)</sup>

Advantages of using such a high mobility system are well recognized and are already applied to such devices as high-speed field-effect transistors<sup>(3,4)</sup> and a standard resistor based on the quantized Hall effect<sup>(5)</sup>. It is because a higher electron mobility leads to a higher switching speed in the former application and the formation of well-defined Landau levels ( $\hbar\omega_c/\mu_B \gg 1$ ) in the latter. One should note, however, that such a benefit of the high-mobility system is not always effective, but could be invalidated in many cases, especially when electrons are heated appreciably by an applied

electric field and undergo extra scattering mechanisms. Hence, we attempt in this paper to evaluate the electron heating process in N-AlGaAs/GaAs

heterojunctions by measuring the electric field dependence of Shubnikov-de Haas (SDH) oscillations in the low and medium magnetic field range ( $B < 6$  T).

Furthermore, we study the effect of electron heating on SDH oscillations at 4.2K in high magnetic field range ( $6 \text{ T} < B < 15 \text{ T}$ ) and present, for the first time, the direct evidence of the resonant emission of optical phonons by hot electrons. We investigate also the electron heating effect on quantized Hall resistance and show that the use of excessive current level results in the rise of electron temperature and leads to the reduction of the Hall plateau width, even though the power consumption is essentially zero in the plateau regions because of  $\rho_{xx}$  being zero.

## 2. Experimental Methods and Results

### (1) Sample Preparations

Samples used in the present study are modulation-doped n-AlGaAs/GaAs single heterostructures grown by molecular beam epitaxy. They were fabricated by growing onto semi-insulating substrates a 0.5–1.0  $\mu\text{m}$  thick undoped GaAs layer, an undoped AlGaAs spacer layer and a 0.1  $\mu\text{m}$  thick Si-doped AlGaAs layer successively. Table I summarizes the sample specifications; namely, the alloy composition  $x$ , the thickness of undoped AlGaAs spacer layers  $w_{sp}$ , the electron concentrations  $N_s$  and the mobilities  $\mu$  at 4.2K. Note that they cover a wide range of  $N_s$  and  $\mu$ . Each sample was shaped into a standard Hall bar geometry, 50  $\mu\text{m}$  wide and 600  $\mu\text{m}$  long by mesa etching technique. Potential probes on this Hall bar were placed at two positions which were 200  $\mu\text{m}$  away from the end electrodes. All the measurements were done by flowing constant current  $I_x$  and measuring the fields  $E_x$ ,  $E_y$ , parallel and perpendicular to the current, respectively.



## (2) Electric Field Dependence of SdH Oscillations and Electron Temperatures

When the two-dimensional electron gas (2DEG) is heated appreciably by an applied electric field, the thermal equilibrium between the electron system and the phonon system collapses: the result of such heating can be approximately described by one parameter, "electron temperature  $T_e$ ". Since the increase in electron temperature leads to the damping of SdH oscillations, one can determine  $T_e$  from the electric field dependence of the SdH oscillations. Figures 1 and 2 show a typical results of SdH measurement at 4.2K and clearly indicates the damping of SdH oscillations. We estimated the electron temperature  $T_e$  on various samples, from at relatively low magnetic field range ( $B < 3T$ ) under the assumption of constant Dingle temperature. (This assumption is relevant because the 2DEG mobilities scarcely change at low temperatures ( $T < 30K$ )). On the other hand, the simple relation of power balance is described by the following equation:

$$k(T_e - T_L)/\tau_e = (Ex \cdot J_x / N_s) = P_e \quad (1)$$

where  $T_L$  is the lattice temperature,  $\tau_e$  is the energy relaxation time,  $Ex$  is the electric field,  $J_x$  is the current density and  $P_e$  is the input power per electron. Equation 1 suggests that the rise ( $T_e - T_L$ ) in electron temperature is uniquely determined by the power-relaxation-time product  $P_e \tau_e$ . Hence, we have plotted in Fig.3 the measured values of  $T_e$  as a function of  $P_e$ . Note that the experimental data (circles, triangles and squares) for three different samples fall on a single curve, although the electron concentrations  $N_s$  and the mobilities  $\mu$  differ widely from sample to sample. This indicates that a dominant cooling process of heated electrons is independent of  $N_s$  and  $\mu$  and that  $\tau_e$  is determined by a rather universal mechanism.

A similar attempt to obtain a  $T_e$  vs  $P_e$  curve was recently done by J. Shah et al.<sup>(3)</sup> by using the photoluminescence measurement on modulation-doped GaAs/AlGaAs superlattice structures. Their results are plotted by a solid line in Fig.3. Although their work covers the range of higher temperatures

( $20K < T_e < 90K$ ) and ours the lower temperature range ( $4.2 < T_e < 25K$ ), these two measurements can be connected smoothly, suggesting again the universality of energy loss mechanisms.

When we estimate  $\tau_e$  from the data point of Fig.3 in the range of  $T_e < 20K$ , we find  $\tau_e = 9.4$  nsec at  $T_e = 5K$ , 5.4 nsec at  $T_e = 10K$ , and 4.7 nsec at  $T_e = 20K$ . Such large values of  $\tau_e$  indicate that the energy loss mechanism in this range is not so efficient and lead to the rapid rise of  $T_e$  with  $P_e$ . As suggested by G. Bauer and H. Kahlert for bulk  $InAs$ ,<sup>(4)</sup> the main loss mechanism in this region is likely to be the emission of acoustic phonons, since  $T_e$  is a little too low to emit optical phonons efficiently. We discuss in the next section the dominant energy loss mechanisms in higher temperature range.

## (3) Effects of Electron Heating on $\rho_{xx}$ at High Magnetic Fields and Magnetophonon Resonance

When the input power  $P_e$  to heat electrons is raised above  $10^{-6}W$ , then  $T_e$  is expected to exceed 25K and the amplitudes of SdH oscillations in the range of weak magnetic fields ( $B < 3T$ ) become vanishingly small. Hence, it is no longer possible to determine  $T_e$  simply from the SdH data in the low field range.

In the range of high magnetic field, however, an oscillatory nature of resistivity  $\rho_{xx}$  is still preserved as shown in Fig.1 and 2. If one examines the oscillations in Fig.2 closely, then one notices the appearance of two extra peaks at 8T and 12T, as the current level is raised up to 4-mA/cm. To clarify the origin of such peaks, we have performed similar measurements on various samples, and found out that these peaks at 8-12T and 6T appear in all the samples, irrespective of the carrier concentrations  $N_s$  (and the Fermi levels), as shown by the arrows in Figs.1, 2 and 4, although the amplitudes of peaks are somewhat different from sample to sample. This suggests that these

peaks are not SDH oscillations but are likely to result from the magnetophonon resonance (MPR) process, which is independent of  $N_s$ . In fact, the cyclotron energies ( $\hbar\omega_c = \hbar eB/m$ ) for  $B=12T$  and  $6T$  are exactly equal to  $(1/2)$  and  $(1/4)$  of the optical phonon energy  $\hbar\omega_{LO}$  ( $\approx 36meV$ ), and satisfies the condition of the magnetophonon resonance ( $\hbar\omega_c = \hbar\omega_{LO}$ ).

To confirm this interpretation, further we have carried out magnetoresistance measurement both at  $4.2K$  and at  $17K$  on a same sample by using a pulsed magnet as shown in Fig.4. The high temperature data, shown by the broken line, exhibit clearly the presence of three MPR peaks at  $B=24T, 12T$  and  $6T$ , whereas the low temperature data shown by the solid lines exhibit the corresponding peaks at  $B=12T$  when the current level is raised above a certain value. Hence, it can be concluded that extra peaks which appear in SDH oscillations at high current levels are the first direct evidence of the MPR process.

Note that the MPR observed in low temperature regions is caused by the resonant emission of optical phonons, whereas the usual MPR observed at high (or intermediate) temperatures are due to both the emission and the absorption of optical phonons. Hence, the appearance of the MPR peaks in the low temperature data can be viewed as an evidence that  $T_e$  is high enough to emit appreciable number of optical phonons.

To estimate  $T_e$  in these regions where MPR peaks are observed, we calculate first the input electrical power per electron  $P_e$ . Because the resistivity  $\rho_{xx}$  is high in such high magnetic field,  $P_e (= \rho_{xx} J^2 / N_s)$  is found to be as high as  $10^{-10}W$ . If one puts this value into Fig.3, then  $T_e$  for the onset of optical phonon emission is estimated to be approximately  $40-50K$ . Such values are quite reasonable in view of the fact that a photoluminescence study of Shah et al. has established that the dominant energy loss mechanism of two dimensional electrons for  $T_e > 40K$  is due to optical phonon emission, as illustrated by the upper portion of the solid curve in Fig.3.

#### (4) Effects of Electron Heating on Quantized Hall Resistance $R_H$

One expects that the heating of electrons may affect the quantized Hall effect (QHE). We measured, therefore, the Hall resistance  $R_H$  at  $4.2K$  at different current levels  $J$ , as shown in Fig.5. One notices that the width  $\Delta B$  of plateau regions is reduced as  $J$  is increased. Fig.6 shows the measured plateau width  $\Delta B$  as a function of current density  $J$ . Also plotted in Fig.6 are the two magnetic fields, corresponding to the two edges of the plateau region. We also plot the electron temperature  $T_e$ , which is estimated from the SDH oscillations in the low magnetic field region.

Figs.5 and 6 suggest that the electron heating with a current above a certain threshold reduces the plateau width considerably. Such a tendency is probably due to the fact that the electron localization mechanism responsible for the plateau formation is disturbed by the high current density.

One should be aware, however, that the input electrical power  $P_e (= \rho_{xx} J^2 / N_s)$  dissipated in this system becomes almost zero, once the system is in the plateau region, where the resistivity  $\rho_{xx}$  is vanishingly small, as shown in Fig.1. Hence, the electron system at the edge of plateaus is expected to experience a kind of phase transition between a non-dissipative state and a dissipative state, as the magnetic field is swept. This transition is probably the main reason for the appearance rather sharp structures on the two edges of Hall plateaus in Fig.5 and the two edges of zero resistance states in Fig.1.

To clarify the reason for the observed shrinkage of the plateau width  $\Delta B$ , we measured  $\Delta B$  at lower temperatures ( $1.3K \sim 4.2K$ ), as shown by the squares in Fig.7. Note that  $\Delta B$  determined at a low current level decreases monotonically when the lattice temperature  $T_L$  is raised. This indicates that the localization of electrons, which is responsible for the plateau formation, is less prominent at higher temperatures. It also suggests that the shrinkage of  $\Delta B$  observed at  $4.2K$  for higher current levels (Fig.6) could be ascribed to the rise of electron temperatures  $T_e$  by the electric field. To check such an

interpretation, we picked up the electron temperature data  $T_e(J)$  of Fig.3 and also the plateau width data  $\Delta B(J)$  of Fig.6 and eliminated the common variable  $J$ . The results are shown in Fig.7, where  $\Delta B$  is replotted as a function of  $T_e$ . Note that the  $\Delta B$  vs  $T_e$  curve connects smoothly with the  $\Delta B$  vs  $T_L$  curve. Such a smooth connection suggests that the temperature of the electron system is the dominant factor, which determines the electron localization process and the plateau width in the present system.

In summary, effects of electron heating on Shubnikov-de Haas oscillations are studied to evaluate electron temperatures. We have shown that the rise in electron temperature ( $\Delta T_e = T_e - T_L$ ) in the low temperature range is described by the power-relaxation-time product ( $T_e = P_e \tau_e / k$ ) with  $\tau_e \sim 5$  nsec and that the energy relaxation time  $\tau_e$  is independent of sample parameters. The electron heating with the power  $P_e$  in excess of  $10^{-13}$  W per electron is shown to generate extra peaks in magnetoresistivities, which can be ascribed to the resonant emission of optical phonons. Finally, electron heating is shown to lead to the electron delocalization and result in the shrinkage of plateau width in the quantized Hall effect.

#### Acknowledgements

The authors wish to acknowledge with gratitude valuable discussions with Professors S. Kawaji and T. Ando and collaborations of Dr. G. Kido and Mr. I. Oguro in performing magnetotransport experiments. This work is partly supported by the Grant-in-Aid for Special Promotion Research from the Ministry of Education, Science, and Culture and by the Joint Research Program of Institute for Solid State Physics, University of Tokyo.

#### References

- (1) L. L. Chang, H. Sakaki, C. A. Chang and L. Esaki: Phys. Rev. Lett. **38**, 148 (1977).
- (2) R. Dingle, H. L. Störmer, A. C. Gossard and W. Wiegmann: Appl. Phys. Lett. **32**, 665 (1978).
- (3) T. Mimura, S. Hiyanizu, T. Fujii and K. Nanbu: Jpn. J. Appl. Phys. **19**, L225 (1980).
- (4) T. Motta, H. Sakaki and H. Ohno: Jpn. J. Appl. Phys. **21**, L122 (1982).
- (5) D. C. Tsui and A. C. Gossard: Appl. Phys. Lett. **38**, 550 (1981).
- (6) J. Shah, A. Pinczuk, H. L. Störmer, A. C. Gossard and W. Wiegmann: Appl. Phys. Lett. **42**, 55 (1983).
- (7) G. Bauer and H. Kahlert: Phys. Rev. **85**, 566 (1972).

Table I. Structural parameters and characteristics of the samples.

Sample	alloy composition $x$	undoped AlGaAs layer thickness $w_{ep}$ (Å)	carrier concentration $N_d \times 10^{17}$ (1/cm <sup>2</sup> )	mobility $\mu \times 10^4$ (cm <sup>2</sup> /Vs)
R-6	0.30	150	4.6	28.5
ON-52	0.30	60	5.7	23.0
S-101	0.30	60	6.0	15.4
U-119	0.33	0	8.1	3.0
U-133	0.30	60	3.5	7.0

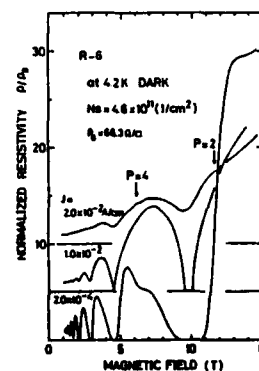


Fig. 1 Shubnikov-de Haas oscillations of sample R-6.

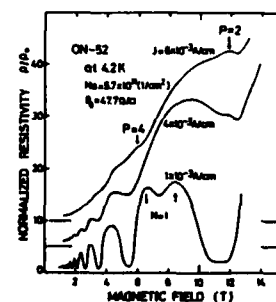


Fig. 2 Shubnikov-de Haas oscillations of sample ON-52.

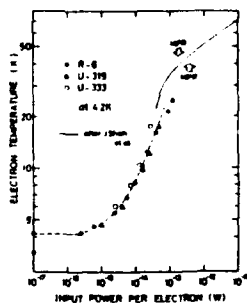


Fig. 3 Electron temperature determined for three different samples from the damping of SDH oscillations. Also shown by the solid line is  $T_e$  determined by J. Shah et al. using photoluminescence data.

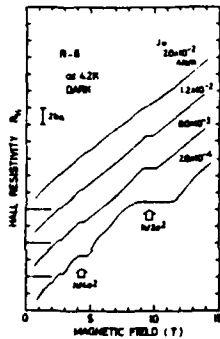


Fig. 5 Quantized Hall resistivity  $R_H$  vs  $B$  measured on sample R-6.

Fig. 7 The location and the width of Hall plateaus as a function of lattice temperatures (squares) and electron temperatures (circles).

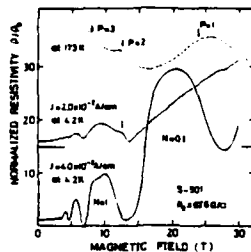


Fig. 4 Oscillatory magnetoresistance at 4.2K and 173K. (Peak positions at 173K are determined by taking account of the damping factor of NPR).

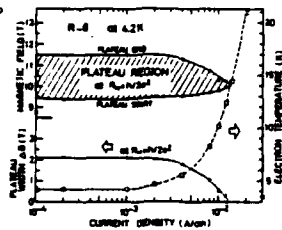
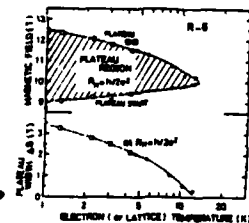


Fig. 6 The location and the width of plateau region vs current density  $J$ . Plotted by a broken line is the electron temperature  $T_e$ .



# Dimensionality Crossover of Spin-orbit Scattering Observed via Localization Effects

Effects

R.S. Markiewicz,<sup>\*,†</sup> C.L. Rollins,<sup>\*\*</sup> and J.S. Brooks<sup>\*\*</sup>

<sup>\*</sup>Northeastern University, Boston, Mass., USA, <sup>†</sup>Boston University, Boston, Mass., USA, and <sup>\*\*</sup>Francis Bitter National Magnet Lab., Cambridge, Mass., USA<sup>\*\*</sup>

In the temperature range 1-50K, ultrathin films of Pd/Pd<sub>2</sub>Si (6-55Å) show a positive, anisotropic magnetoresistance which is logarithmic in field at high magnetic fields, characteristic of two-dimensional localization with strong (three-dimensional) spin-orbit scattering. At lower temperatures, the magnetoresistance saturates to a field-independent value. We interpret this change as due to a crossover of spin-orbit scattering from its bulk value to a form characteristic of a 2-d film. The resulting magnetoresistance is consistent with the theoretical results of Hikami, Larkin and Nagaoka.

Below 4.2K, our analysis is complicated by superconducting effects in the Pd<sub>2</sub>Si.

## 1. Introduction

In a recent analysis of low temperature (T=1.3-50K) magnetoresistance (mr) of ultrathin Pd films (6-55Å) on Si substrates (1), we found a general overall agreement with localization theory. However, the data displayed an anomalous temperature-dependence of the amplitude of the mr, which decreased with decreasing T. To study this behavior further, we have measured mr of similar films at still lower T (0.075-1K) in a dilution refrigerator. These experiments reveal a new anomaly--the mr saturates to a field-independent value at high fields. We believe that both anomalies can be interpreted as indicative of a changeover of the spin-orbit scattering from a 3-d (at high T) to 2-d behavior. This same mechanism can also explain unusual structure observed in the zero-field resistivity of some films.

<sup>\*\*</sup> Supported at MIT by the National Science Foundation

## 2. Magnetoresistance of the films.

Localization theory predicts (2) a magnetoconductance given by (for H|| the film):

$$\Delta\sigma = B(\psi_1 - \psi_2 + \frac{1}{2}(\psi_3 - \psi_4)) \quad (1)$$

where  $B = e^2/2\pi h$  and  $\psi_j = \psi(\frac{1}{2} + X_j) - \ln(X_j)$ ,  $\psi$  is the digamma function,  $X_j = k_H^2/2k_e k_j$ ,  $k_H^2 = \hbar c/eH$ , and the  $k_j$ 's are various combinations of scattering lengths:  $k_e$  (elastic),  $k_i$  (inelastic),  $k_g$  (magnetic impurity), and  $k_{so}$  (spin-orbit scattering). If spin-dependent scattering is negligible, only  $\psi_1$  contributes, with  $k_1 = k_i = T^{-P}$ , with the exponent P being characteristic of the inelastic scattering mechanism. In the Pd films, electron-electron scattering is dominant, with P=2. However, in Pd spin-orbit scattering is very strong. If  $k_{so}$  is isotropic, only  $\psi_4$  contributes to  $\Delta\sigma$ , and  $k_4^{-1} = (2k_g^{-1} + k_i^{-1})$ . Since the spin-orbit scattering is proportional to the angular momentum  $\vec{r} \times \vec{p}$ , in a sufficiently thin film only the z-component of the scattering will remain finite ( $\propto \perp$  to the film plane). In this case (2d spin-orbit scattering), both  $\psi_3$  and  $\psi_4$  are comparable, and at high fields ( $\psi_j + \ln H$ ) the mr saturates.

The films are prepared by sputtering Pd onto a single crystal Si substrate. The Pd and Si interact at room temperature, forming a layer of ~30Å of Pd<sub>2</sub>Si, with the remaining Pd above this layer. (The 6Å film may represent a different phase)(1). In the initial study (T > 1.3K), the mr was found to be positive and very anisotropic, as expected for localization effects in the presence of strong 3d spin-orbit scattering. A detailed comparison with theory yielded scattering lengths similar to those found in the present study, Table I. Most films have similar values of all parameters except  $k_g$ . This variation could be due to impurities introduced in the sputtering process (we estimate that the smallest  $k_g$  would correspond to only about 400ppm of Fe); alternatively, it may be that the films with very large  $k_g$  were essentially pure silicide, for which magnetic impurity scattering may be weak (d-bands filled). This variation in  $k_g$  is responsible

the appearance of the  $\psi_3$  term, as shown in Fig. 1 and 2.

Two pronounced anomalies were observed in the data. (1) In the low- $\ell_B$  films, the amplitude of the  $\psi_3$  is not monotonically increasing, but begins to decrease as  $T$  is lowered below 4K (Fig. 2). (2) The high- $\ell_B$  films show an anomalous flat curve of zero-field resistivity vs  $T$ , sometimes having an s-shaped structure (Fig. 3).

The most varied low  $T$  displays yet a third anomaly. In high fields the  $\psi_3$  is expected to increase logarithmically with  $H$ , as observed at higher  $T$  (Fig. 1). In low  $T$ ,  $\psi_3$  saturates to a field-independent value above a  $T$ -dependent field which is only 21 at  $T = .075K$ . (Fig. 4). (The 6A film again appears anomalous). This saturation is just what would be expected for 2-d spin-orbit scattering. However, the earlier fits using constant

$\xi = \ell_B^2 / \ell_{SO}^2$  found  $\xi = 1$  in the low  $\ell_B$ -films ( $\xi = 10$  in the high  $\ell_B$ -films).

4) three anomalies can be understood with a  $T$ -dependent  $\xi$ .

### 3. $T$ -dependent spin-orbit anisotropy.

A crossover of  $\xi$  from 3-d ( $\xi = 1$ ) to 2d ( $\xi = 0$ ) as  $T$  is lowered would immediately explain the observed change of high field  $\psi_3$  from  $\ln H$  to constant. It would also account for the  $T$ -dependence of the  $\psi_3$  amplitude: as the  $\psi_3$  term in Eq. 1 grows, it cancels part of  $\psi_4$ . Finally, the same mechanism can account for the s-shaped curve of zero-field resistivity (Fig. 3). In the strong-3d-spin-orbit-scattering limit, the zero-field resistivity is

$$\rho(T) = \frac{1}{\rho_0} - B[(1-F)\ln T - \frac{1}{2} \ln(\ell_B/\ell_A)] \quad (2)$$

where  $\rho_0$  is the residual resistance, the term with  $(1-F)$  is due to electron interaction (3), and the last term to localization. If  $\ell_A = \ell_1 \propto T^{-P}$ , the coefficient of  $\ln T$  is  $1 - F - \frac{P}{2}$ . For our films  $F \approx 0$ ,  $P = 2$ , so this coefficient is approximately zero. The fit in Fig. 3 includes a Bloch-function contribution to  $\rho_0$  (4) at high  $T$ , but at lower  $T$  it becomes very flat. Below about 4K, the decrease in  $\rho$  can be understood as due to a new logarithmic

term, corresponding to  $\psi_3$  of Eq. 1, which appears when  $\xi$  becomes two-dimensional.

The solid curves in Figs. 1-4 represent the theory (1) with parameters from Table I.  $\xi(T)$  was found to be approximately linear in  $T$ ,  $\xi(T) = \xi_0 T$  at low temperatures, levelling off to  $\xi = 1$ , at high  $T$ .

### 4. Superconductivity

We have observed a superconducting transition in our thicker films at  $T_c \approx .25-.5K$  (Fig. 5). The transition appears to be complete in the 30A film, while the 50A film shows a residual resistivity below  $T_c$ . The superconductivity probably occurs in the  $Pd_2Si$  layer, and the proximity effect from the pure Pd in the thicker film drives part of the  $Pd_2Si$  normal.

Acknowledgements: This research was supported in part by the Research Corporation and Northeastern's Research and Scholarship Development Fund (RSH and CSR) and by NSF Grant-Low Temperature Physics-DMR811-3456(JSB).

### References

- (1) R.S. Markiewicz and C.J. Rollins, to be published.
- (2) S. Hikami, A.I. Larkin, and Y. Nagaoka, Prog. Theor. Phys. **63** (1980) 707.
- (3) P.A. Lee and T.V. Ramakrishnan, Phys. Rev. **B26** (1982) 4009.
- (4) M. Wittner, D.L. Smith, P.W. Lew, and M.-A. Nicolet, Sol. St. Elect. **21** (1978) 573.
- (5) W.J. Skocpol and M. Tinkham, Repts. Prog. Phys. **38** (1975) 1049.

Table 1. Scattering Lengths

Energy (eV)	$\ell_p$ (Å)	$\ell_{ph}$ (Å)	$\ell_s$ (Å)	$\ell_{so}$ (Å)	$\epsilon_0^{-1}$	$B=B/(e^2/2\pi^2\hbar)$
15	7	61	3	1100	1.8	1.0
30	9.5	50	40	900	3.6	1.7
45	15	31	0.2	(10)*	120	1.1
55	22	31	0.9	(20)*	150	2.8

\* Not sensitive

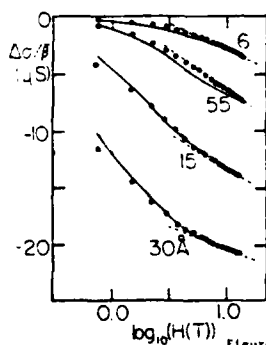


Figure 1

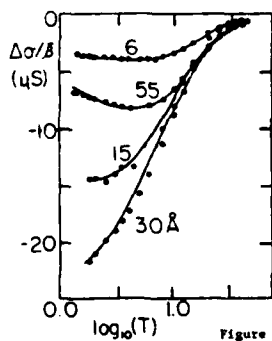


Figure 2

Figure 1. Magnetoresistance of Pd films at 2K, showing approximate  $\log H$  behavior at high fields (dashed line). Solid lines = theory.

Figure 2. Magnetoresistance  $\Delta\sigma = \sigma(H = 13.5T) - \sigma(H = 0)$  vs  $T$  for Pd films. Solid lines = theory.

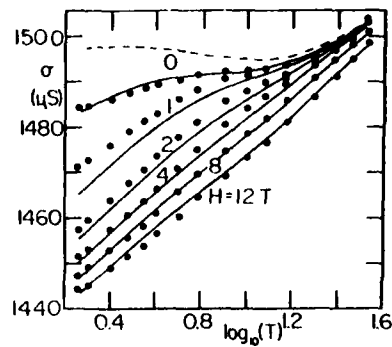


Figure 3

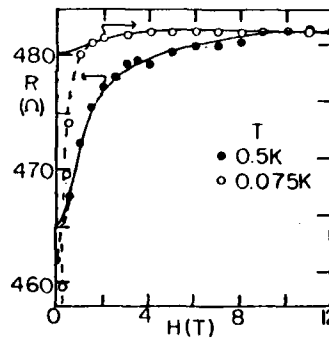


Figure 4

Figure 3. Total conductance vs  $T$  at various fields for 30 Å film. Solid curves = theory with variable  $\xi(T)$ ; dashed curve:  $\xi(T) = \xi_\infty$ .

Figure 4. Magnetoresistance of 30 Å Pd film at low  $T$ . Solid line = theory, with  $\xi = .035(0.5K), .00066(0.075K)$ . Dashed line = guide to the eye.

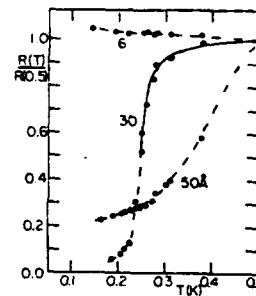


Figure 5

Figure 5. Resistance vs  $T$  for Pd films. Dashed lines = guide to the eye; solid line = theory of 2-d superconducting fluctuations [Ref. 5].

UCRL  
PREPRINT

Primitive and Composite Ground States in the  
Fractional Quantum Hall Effect

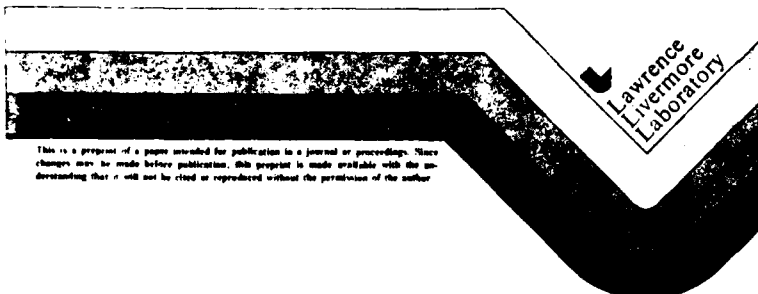
R.B. Laughlin  
University of California, Lawrence Livermore National Laboratory  
P.O. Box 808, Livermore, California 94550

PRIMITIVE AND COMPOSITE GROUND STATES  
IN THE FRACTIONAL QUANTUM HALL EFFECT

R. B. Laughlin  
University of California, Lawrence Livermore National Laboratory  
Livermore, California 94550

This paper was prepared for submittal to:  
*Fifth International Conference on  
Electronic Properties of Two-Dimensional Systems*  
Oxford, England  
September 5-9, 1983

August 17, 1983



ABSTRACT

Our theory of the Fractional Quantum Hall Effect is reviewed. Arguments are presented that the fractionally charged quasiparticles associated with the effect are fermions. Wavefunctions for the 2/7 and 2/5 states are proposed, and estimates for the cohesive energies and gaps of these states are given.

I. INTRODUCTION

This paper has two functions. The first is to review our theory (1) of the Fractional Quantum Hall Effect and supplement it with some computational details we feel make the theory more complete. The second is to introduce approximate ground state and excited state wavefunctions for the 2/7 and 2/5 states recently discovered by Störmer, et. al. (2), and from them to estimate the cohesive energies and gaps of these states. We describe the states as charge 1/3 quasiparticles of either sign themselves forming the 1/3 state, or equivalently as a product of Jastrow-type wavefunctions, one in electrons and one in holes. Central to our new theory is the idea that the quasiparticles are fermions.

II. THE 1/3 STATE

We consider a two-dimensional metal in the x-y plane subject to a magnetic field  $H_0$  in the z direction. The many-body Hamiltonian is

$$H = \sum_j \left[ \frac{1}{2m} \left| \frac{\hbar}{i} \nabla - \frac{e}{c} \vec{A} \right|^2 + V(z_j) \right] + \sum_{j < k} \frac{e^2}{|z_j - z_k|} \quad (1)$$

where  $z_j = x_j - iy_j$  is a complex number locating the  $j^{\text{th}}$  electron,  $V(z_j)$  is the potential generated by a uniform neutralizing background of appropriate charge density  $\sigma$ :

$$V(z) = -\sigma e^2 \int \frac{dx' dy'}{|z - z'|} \quad (2)$$

and  $\vec{A} = \frac{H_0}{2} (x\hat{y} - y\hat{x})$  is the symmetric gauge vector potential. We restrict our



attention to the lowest Landau level, for which the single-body wavefunctions are

$$|n\rangle = \frac{1}{\sqrt{2^{n+1}n!}} z^n e^{-\frac{1}{4}|z|^2} \quad (3)$$

with the magnetic length  $a_0 = (\hbar/m\omega_c)^{1/2} = (\hbar c/eH_0)^{1/2}$  set to 1. These states are degenerate:

$$\frac{1}{2m} \left| \frac{\hbar}{c} \nabla^2 - \frac{e}{c} \vec{A} \right|^2 |n\rangle = \frac{1}{2} m\omega_c |n\rangle \quad (4)$$

Many-body wavefunctions comprised of such states take the form

$$\psi(z_1, \dots, z_N) = P(z_1, \dots, z_N) e^{-\frac{1}{4} \sum_{j=1}^N |z_j|^2} \quad (5)$$

where  $P$  is any antisymmetric polynomial. Such polynomials may always be written

$$P(z_1, \dots, z_N) = S(z_1, \dots, z_N) \prod_{j < k} (z_j - z_k)^m \quad (6)$$

where  $S$  is a symmetric polynomial.

Our approximation to the  $1/3$  state is one of a sequence of variational wavefunctions of the form

$$\psi_m(z_1, \dots, z_N) = \prod_{j < k} (z_j - z_k)^m e^{-\frac{1}{4} \sum_{j=1}^N |z_j|^2} \quad (7)$$

with  $m$  odd. This form is predicated by the conditions a.) that the polynomial prefactor be a product of Jastrow functions, b.) that the state be an eigenfunction of angular momentum  $m$ , and c.) that the Pauli principle be obeyed. The nature of this state is understood by interpreting its square as the probability distribution function of a classical plasma. We let

$$|\psi|^2 = e^{-\beta\phi} \quad (8)$$

where  $\beta = 1/m$  and  $\phi$ , the classical potential energy, takes the form

$$\phi(z_1, \dots, z_N) = -2m^2 \sum_{j < k} \ln|z_j - z_k| + \frac{m}{2} \sum_{j=1}^N |z_j|^2 \quad (9)$$

$\phi$  describes particles of "charge"  $m$  repelling one another logarithmically and being attracted logarithmically by a uniform background of "charge" density  $\sigma_1 = (2\pi)^{-1}$ . Local neutrality of this "charge" requires that the electrons be spread out uniformly to a density  $\sigma_m = (2\pi m)^{-1}$ . The Fractional Quantum Hall Effect occurs when  $\sigma_m = \sigma$ , with  $\sigma$  defined per Eqn (2).

We calculate the cohesive energy of  $\psi_m$  using the hypernetted chain

approximation for the radial distribution function  $g(r)$  of the plasma, which is equivalent to the density-density correlation function of  $\psi_m$ . If we let  $x = r/R$ , where  $R = \sqrt{2m}$  is the ion disc radius, and if we define Fourier transforms in the manner

$$\hat{h}(k) = \int_0^\infty h(x) J_0(kx) x dx \quad (10)$$

where  $J_0$  is an ordinary Bessel function of the first kind, then we have

$$g(x) = \exp(-\beta v(x) + h(x) - c(x) + B(x)) \quad (11)$$

and

$$\hat{h}(k) = \hat{c}(k) + 2\hat{c}(k)\hat{h}(k) \quad (12)$$

with  $h(x) = g(x) - 1$ . In Eqn (11) we set  $\exp(-\beta v(x)) = x^{2m}$ .  $B(x)$  is the model bridge function described by Caillol et. al. (3). It provides a small correction and may for the present purposes be considered zero. Eqns (11) and (12) are solved iteratively, with the long-range "coulomb" divergences handled in the manner

$$g(x) = \exp(h(x) - c_s(x) - 2mK_0(Qx)) \quad (13)$$

where  $K_0$  is a modified Bessel function of the second kind and where

$$\hat{c}_s(k) = \hat{c}(k) + \frac{2mQ^2}{k^2(k^2 + Q^2)} \quad (14)$$

$g(x)$  is independent of the cutoff parameter  $Q$ . In terms of  $g(x)$ , the total energy per electron is

$$U_{\text{total}} = \frac{\langle \psi_m | H | \psi_m \rangle}{\langle \psi_m | \psi_m \rangle} / N = \left( \frac{1}{\sqrt{2m}} \int_0^\infty (g(x) - 1) dx \right) \frac{e^2}{a_0} \quad (15)$$

Solving these equations, we arrive at the semiempirical formula

$$U_{\text{total}}(m) = \frac{0.814}{\sqrt{m}} \left( \frac{0.230}{m^{0.64}} - 1 \right) \frac{e^2}{a_0} \quad (16)$$

We note that  $\psi_m$  as written describes a circular liquid drop. To describe a drop of a different shape, we write

$$\psi'_m = \psi_m e^{-\frac{1}{2} f(z_L)} \quad (17)$$

where  $f$  is any analytic function.

The elementary excitations of  $\Psi_m$  are particles of charge  $1/m$ . We make them with a thought experiment in which the liquid is pierced at  $z_0$  with an infinitely thin solenoid through which is passed adiabatically a flux quantum  $\Lambda\Phi = hc/e$ . By gauge invariance, this operation maps the ground state uniquely onto an excited eigenstate of  $H$ . We have argued that these excitations may be written approximately

$$\Psi_m^{+z_0} = A_{z_0} \Psi_m = \prod_i (z_i - z_0) \Psi_m \quad (18)$$

and

$$\Psi_m^{-z_0} = A_{z_0}^\dagger \Psi_m = \prod_i (2 \frac{\partial}{\partial z_i} - z_0^*) \Psi_m \quad (19)$$

for the quasihole and quasielectron, respectively, with the understanding in Eqn (19) that differentiation be performed only on the polynomial part of  $\Psi_m$ .  $A_{z_0}$  and  $A_{z_0}^\dagger$  are adjoint under the inner product

$$\langle \Psi_1 | \Psi_2 \rangle = \int \dots \int \Psi_1^*(z_1, \dots, z_N) \Psi_2(z_1, \dots, z_N) dx_1 dy_1 \dots dx_N dy_N. \quad (20)$$

That is,

$$\langle \Psi_1 | A_{z_0} \Psi_2 \rangle = \langle A_{z_0}^\dagger \Psi_1 | \Psi_2 \rangle. \quad (21)$$

It is somewhat cleaner to write  $A_{z_0}$  and  $A_{z_0}^\dagger$  in terms of ladder operators (4):

$$A_{z_0} = \prod_i (a_i^\dagger - z_0) \quad (22)$$

$$A_{z_0}^\dagger = \prod_i (a_i - z_0^*) \quad (23)$$

with

$$a_j = \left[ \frac{x_j + iy_j}{2} + i \left( \frac{\partial}{\partial x_j} + i \frac{\partial}{\partial y_j} \right) \right] \quad (24)$$

and

$$a_j^\dagger = \left[ \frac{x_j - iy_j}{2} - i \left( \frac{\partial}{\partial x_j} - i \frac{\partial}{\partial y_j} \right) \right]. \quad (25)$$

The derivatives in  $a_j$  and  $a_j^\dagger$  have the ordinary meaning.

To show that  $\Psi_m^{+z_0}$  describes a quasihole of charge  $-1/m$  electrons, we write

$$|\Psi_m^{+z_0}|^2 = e^{-\Phi\phi'} \quad (26)$$

with  $\Phi = 1/m$  and

$$\phi'(z_1, \dots, z_N) = -2m^2 \sum_{j < k}^N \ln|z_j - z_k| + \frac{m}{2} \sum_i |z_i|^2 - 2m \sum_i \ln|z_i - z_0|. \quad (27)$$

Eqn (27) describes the same plasma as Eqn (9) except for an additional phantom particle of "charge" 1 located at  $z_0$ . In screening this phantom, the plasma accumulates "charge" -1, which is equivalent to a real charge of  $-1/m$  electrons.

We calculate the energy to make the quasihole using the two-component hypernetted chain (5):

$$g_{ij}(x) = \exp(-\beta v_{ij}(x) + h_{ij}(x) - c_{ij}(x)) \quad (28)$$

$$\hat{h}_{ij}(k) = \hat{c}_{ij}(k) + 2 \sum_l \hat{h}_{il}(k) \rho_l \hat{c}_{lj}(k). \quad (29)$$

The indices in Eqns (28) and (29) run over two kinds of particles: 1.) electrons and 2.) phantoms.  $\rho_l$  is the density of each component. With  $x$  defined as before we have  $\rho_1 = 1$  and  $\rho_2 = 1/N$ . We perform perturbation theory in  $\rho_2$ : To zeroth order, the 1-1 equations decouple and revert to Eqns (11) and (12). Thus we consider  $g_{11}(x) = g(x)$  to be given. For  $g_{12}(x)$  we have

$$\hat{h}_{12}(k) = (1 + 2\hat{h}_{11}(k)) \hat{c}_{12}(k) \quad (30)$$

and

$$g_{12}(x) = \exp(-\beta v_{12}(x) + h_{12}(x) - c_{12}(x)) \quad (31)$$

with  $\exp(-\beta v_{12}(x)) = x^2$ . Using  $g_{11}(x)$  obtained from Eqns (30) and (31) we construct the change to  $g_{11}(x)$  resulting from the presence of the phantom. We have

$$\delta \hat{h}_{11}(k) = (1 + 2\hat{h}_{11}(k))^2 \delta \hat{c}_{11}(k) + \frac{2}{N} \hat{h}_{12}^2(k) \quad (32)$$

and

$$\delta c_{11}(x) = \left\{ \frac{h_{11}(x)}{1 + h_{11}(x)} \right\} \delta h_{11}(x) . \quad (33)$$

The energy to make a quasihole is then given by

$$\Delta_{\text{Quasihole}} = \left\{ \frac{N}{2m} \int_0^\infty \delta h_{11}(x) dx \right\} \frac{e^2}{a_0} . \quad (34)$$

Solving these equations, we obtain  $0.026 e^2/a_0$  for  $m=3$  and  $0.008 e^2/a_0$  for  $m=5$ . The 16% discrepancy between these energies and those quoted in Reference (1) is due to the discovery of a computer error.

We remark that the above formalism goes correctly to the Debye-Hückel limit when the plasma is weakly coupled. In that limit, the size of the quasiparticle is the Debye length  $a_0/\sqrt{2}$  and its energy is  $\pi/(4\sqrt{2} m^2) e^2/a_0$ . We remark also that the degeneracy of the quasiparticle band, as measured by the number of linearly independent places a quasiparticle can be created, can be seen from expansion of Eqn (22) in powers of  $z_0$  to be  $N$ , or  $N-1$  if center of mass motion is disallowed.

We can make a similar argument for the quasidelectron. The electron density in its presence is given by

$$\frac{\rho(z_1)}{N} = \frac{\int \dots \int |\Psi_m^{-20}(z_1, \dots, z_N)|^2 dx_2 dy_2 \dots dx_N dy_N}{\int \dots \int |\Psi_m^{-20}(z_1, \dots, z_N)|^2 dx_1 dy_1 \dots dx_N dy_N} . \quad (35)$$

Since for any polynomial  $P(z)$  we have

$$|2 \frac{\partial P}{\partial z} - z_0|^2 = |\vec{q} - \vec{r}_0|^2 |P|^2 . \quad (36)$$

Eqn (35) may be rewritten

$$\frac{\rho(\vec{r})}{N} = e^{-\frac{1}{2} r^2} |\vec{q} - \vec{r}|^2 \left\{ \frac{e^{\frac{1}{2} r^2}}{|\vec{r} - \vec{r}_0|^2 - 2} \frac{\tilde{\rho}(\vec{r})}{N} \right\} . \quad (37)$$

with

$$\frac{\tilde{\rho}(\vec{r})}{N} = \frac{\int \dots \int e^{-\frac{1}{2} \sum_k |z_k|^2} \prod_{j=1}^N (|z_j - z_0|^2 - 2) \prod_{j,k} |z_j - z_k|^{2m} dx_2 dy_2 \dots dx_N dy_N}{\int \dots \int e^{-\frac{1}{2} \sum_k |z_k|^2} \prod_{j=1}^N (|z_j - z_0|^2 - 2) \prod_{j,k} |z_j - z_k|^{2m} dx_1 dy_1 \dots dx_N dy_N} . \quad (38)$$

This is again a two-component plasma problem. We have  $\tilde{\rho}(\vec{r} - \vec{r}_0) = \tilde{\rho} g_{12}(x)$  with  $\tilde{\rho} = (2\pi m)^{-1}$  and  $g_{12}(x)$  given by Eqns (30) and (31) with  $\exp(-8v_{12}(x)) = x^2 - 1/n$ . Because the charge accumulated around the phantom is determined by the long-range behavior of  $v_{12}(x)$ , we have, as with the quasihole,

$$\int (\tilde{\rho}(\vec{r}) - \tilde{\rho}) d\vec{r} = -1/n . \quad (39)$$

Placing the phantom at the origin and rewriting Eqn (37), we obtain

$$\rho(\vec{r}) = (v^2 + 2 \vec{r} \cdot \vec{q} + r^2 + 2) \left\{ \frac{\tilde{\rho}(\vec{r})}{r^2 - 2} \right\} . \quad (40)$$

Thus  $\rho(\vec{r})$  also goes asymptotically to  $\tilde{\rho}$ , and we have

$$\begin{aligned} \int (\rho(\vec{r}) - \tilde{\rho}) d\vec{r} &= \int (\tilde{\rho}(\vec{r}) - \tilde{\rho}) d\vec{r} \\ &+ \int (v^2 + 2 \vec{r} \cdot \vec{q} + 4) \left\{ \frac{\tilde{\rho}(\vec{r})}{r^2 - 2} \right\} \\ &= -\frac{1}{n} + 2 \int_{\text{Boundary}} \frac{\tilde{\rho}(\vec{r})}{r^2 - 2} \vec{r} \cdot d\vec{S} \\ &= +\frac{1}{n} \text{ electrons} . \end{aligned} \quad (41)$$

To calculate  $\Delta_{\text{Quasielectrons}}$ , we introduce a "pseudopotential"  $v_{ps}(x)$ , defined to be that potential which, when substituted for  $v_{12}(x)$  in Eqns (30) and (31), leads to  $g_{12}(\vec{r}) = \rho(\vec{r})/\tilde{\rho}$  as defined by Eqn (40). Justification for this step comes from the empirical observation that classical liquid behavior can always be modeled with a sum of pair potentials. With  $v_{ps}(x)$  defined in this way, we calculate  $\Delta_{\text{Quasielectrons}}$  using Eqns (32) - (34). We obtain  $0.030 e^2/a_0$  for  $m=3$  and  $0.006 e^2/a_0$  for  $m=5$ .

### III. QUASIPARTICLE STATISTICS

We consider a liquid drop described by  $\Psi_m$  to be placed beneath and parallel to a similar drop described by  $\Psi_1$ , so that an infinitely thin solenoid passing through one passes through the other in the same place. Since the adiabatic mapping from the ground state onto an excited state induced by adding a flux quantum through this solenoid is nominally unitary, the excitations

generated in this manner in the two systems are in one-to-one correspondence. In the drop described by  $\psi_1$  these excitations are ordinary holes in a full Landau level, and are thus fermions. We argue that excitations in one-to-one correspondence with these must be fermions too. The following example illustrates this one-to-one correspondence and shows how it leads to compatibility between the commutivity of the operators  $A_{z_0}$  and fermi statistics. Let solenoids be brought to  $z_a$  and  $z_b$  and let  $\phi$  be added simultaneously and adiabatically through each. We obtain approximately

$$A_{z_a} A_{z_b} \psi_m = \prod_i (z_i - z_a)(z_i - z_b) \prod_{j < k} (z_j - z_k)^m e^{-\frac{1}{4} \sum_k |z_k|^2} \quad (42)$$

From analysis of the form of Eqn (27) it is clear that this wavefunction, when  $z_a$  and  $z_b$  are far apart, correctly describes the presence of two quasiparticles, one at  $z_a$  and one at  $z_b$ , even if  $m=1$  is substituted. If  $z_a$  and  $z_b$  are now allowed to coalesce at the origin, we have in the  $\psi_1$  drop

$$A_0^2 \psi_1 = \prod_i z_i^2 \prod_{j < k} (z_j - z_k) e^{-\frac{1}{4} \sum_k |z_k|^2} \\ = \sum_{\sigma} \text{sgn}(\sigma) z_{\sigma(1)}^2 \dots z_{\sigma(n)}^{n+1} e^{-\frac{1}{4} \sum_k |z_k|^2} \quad (43)$$

where  $\sigma$  is a permutation and  $\text{sgn}(\sigma)$  its sign. This is a state with two adjacent holes, one in  $\langle 0|$  and one in  $\langle 1|$  (cf. Eqn (3)). We shall henceforth consider a symmetric polynomial  $S$  to be an approximate representation of the unitary transformation generated, for example, by passing flux quanta through an array of solenoids, and that  $S\psi_m$  "means" the same thing  $S\psi_1$  means: a ground state plus fermion quasiholes. Since the transformation is unitary, we consider  $S^\dagger \psi_m$  to be the approximate image of  $\psi_m$  under the inverse transformation: a ground state plus fermion quasielectrons.

We remark that care must be taken in discussing how many "locations" are available for putting quasiparticles into  $\psi_m$  because their presence changes its nature. An example of this is  $A_0^N \psi_m$ , which is the drop described by  $\psi_m$  with a large hole in its center. To "count" such states is unphysical, and thus we propose to count only the states of lowest energy, those with a minimal number of zeros near singularities of the potential. We do this by means of a functional  $F$  which annihilates excessively energetic excitations. If a symmetric polynomial is expanded in the manner

$$S(z_1, \dots, z_N) = \sum_{i_1, \dots, i_N} b_{i_1, \dots, i_N} z_1^{i_1} \dots z_N^{i_N} \quad (44)$$

then we let

$$FS(z_1, \dots, z_N) = \sum_{i_1, \dots, i_N} b_{i_1, \dots, i_N} \left\{ \frac{z_1^{i_1}}{(N-1)!} \left( \frac{\partial}{\partial z_1} \right)^{N-1-i_1} \prod_{j \neq 1} (z_j - z_1) \right\} \\ \times \dots \times \left\{ \frac{z_N^{i_N}}{(N-1)!} \left( \frac{\partial}{\partial z_N} \right)^{N-1-i_N} \prod_{j \neq N} (z_j - z_N) \right\} \quad (45)$$

If the degree of  $S$  is small,  $F$  merely removes its center of mass motion. For example, we have

$$F \prod_i z_i = \left( \frac{N-1}{N} \right) \prod_i (z_i - \bar{z}) \quad (46)$$

where  $\bar{z} = \frac{1}{N} \sum z_j$ . As the degree of  $S$  increases, the action of  $F$  becomes increasingly severe, and in the limit that any  $z_j$  exceeds  $N-1$ , annihilation occurs. By this reckoning the number of low energy quasiholes which can be put into  $\psi_m$  is  $N-1$ , since  $F A_0^N = 0$ . Also, we have

$$F A_0^{N-1} = (-1)^{N(N-1)/2} \prod_{j < k} (z_j - z_k)^2 \quad (47)$$

so that  $\psi_m$  "full" of quasiholes equals  $\psi_{m+2}$ . Likewise,  $\psi_m$  "full" of quasi-electrons equals  $\psi_{m-2}$ . It is important that while the number of allowed quasiparticle states in this picture always equals the number of electrons, the quasiparticle density depends on context. For example, when  $n$  is small,  $FA_0^N \psi_m$  describes a state of  $n$  quasiholes of charge  $1/m$  packed to a density  $\frac{1}{2n}$  at the origin. As  $n$  increases toward  $N-1$ , however, the total electron density at the origin goes continuously to  $\frac{1}{2(N-1)}$ , so that the density of quasiparticles, to the extent it makes sense, must go to  $\frac{1}{2(N-1)}$ .

#### IV. THE 2/5 AND 2/7 STATES

The 2/3 state is the electron-hole conjugate of the 1/3 state. Denoting it by  $\psi_{3/2}$ , we have

$$\Psi_{3/2}(z_1, \dots, z_N) = \int \dots \int \Psi_1(z_1, \dots, z_{3N/2}) \Psi_3^*(z_{N+1}, \dots, z_{3N/2})$$

$$dx_{N+1} dy_{N+1} \dots dx_{3N/2} dy_{3N/2} \quad (48)$$

$\Psi_{3/2}(z_1, \dots, z_N)$  is divisible by  $\Psi_1(z_1, \dots, z_N)$ , the quotient being a symmetric polynomial  $S_{3/2}(z_1, \dots, z_N)$ . Per the foregoing discussion,  $S_{3/2}$  is a representation of a unitary transformation generating the 1/3 state in holes from  $\Psi_1$ . Accordingly,  $S_{3/2}\Psi_3$  must be an approximate image of the same transformation acting on  $\Psi_3$ : the 1/3 state in quasiholes. We shall argue that  $S_{3/2}\Psi_3$  is the 2/7 state  $\Psi_{7/2}$  and that  $S_{3/2}^\dagger\Psi_3$  is the 2/5 state  $\Psi_{5/2}$ .

We first observe that  $\Psi_{3/2}$ , being the particle-hole conjugate of  $\Psi_3$ , is a variational wavefunction with a minimal expectation value across  $\mathcal{H}$ . It does this by being small when any two electrons are close. We model this behavior by approximating the magnitude of  $\Psi_{3/2}$  in the manner

$$|\Psi_{3/2}(z_1, \dots, z_N)|^2 = \alpha \prod_{j < k} |z_j - z_k|^{-3} e^{-\frac{1}{2} \sum_k |z_k|^2} \quad (49)$$

when it is large.  $\alpha$  is a normalization constant. We justify this approximation on three grounds: a.) It properly describes the electrons uniformly spread out to a density  $(3\pi)^{-1}$ . b.) Classical liquids can always be described by pair potentials. c.) It gives the correct cohesive energy. From Eqn (16) we obtain a total energy per particle for  $\Psi_3$  of  $-0.115 e^2/a_0$ . The cohesive energy per particle, defined by

$$U_{\text{coh}} = U_{\text{tot}} + \frac{1}{N} \sum \frac{e^2}{|z_j - z_k|} \quad (50)$$

is  $-0.207 e^2/a_0$ . The correct cohesive energy per particle for  $\Psi_{3/2}$  must be 1/2 this value, or  $-0.1035 e^2/a_0$ . Substituting 3/2 for  $m$  in Eqn (50), we obtain  $-0.521 e^2/a_0$  for the correct total energy per particle of  $\Psi_{3/2}$ . The value generated from Eqn (49) by substituting 3/2 for  $m$  in Eqn (16) is  $-0.547 e^2/a_0$ . The error is 5% in the total energies and 23% in the cohesive energies. It is possible to remove this disparity with a more judicious choice of pair potential. For simplicity, we elect not to do so.

Eqn (49) enables us to evaluate the properties of  $\Psi_{7/2} = S_{3/2}\Psi_3$ . We have

$$|\Psi_{7/2}(z_1, \dots, z_N)|^2 = \alpha \prod_{j < k} |z_j - z_k|^{-7} e^{-\frac{1}{2} \sum_k |z_k|^2} \quad (51)$$

when it is large. Thus  $\Psi_{7/2}$  describes electrons uniformly spread out to a density  $(7\pi)^{-1}$  with a total energy per electron, given by Eqn (16), of  $-0.399 e^2/a_0$ . For the 2/5 state, we write

$$|\Psi_{5/2}(z_1, \dots, z_N)|^2 = \frac{1}{\alpha} \prod_{j < k} |z_j - z_k|^{-5} e^{-\frac{1}{2} \sum_k |z_k|^2} \quad (52)$$

and thus estimate a total energy per electron of  $-0.449 e^2/a_0$ . The connection between  $S_{3/2}^\dagger\Psi_3$  and Eqn (52) is ad hoc. We make only the nebulous argument that  $S_{3/2}^\dagger$  represents the inverse of the unitary operator represented by  $S_{3/2}$  and thus should be approximated by  $S_{3/2}^{-1}$  when the latter is defined.

If the liquid drop described by  $\Psi_{7/2}$  or  $\Psi_{5/2}$  is pierced at  $z_0$  with a solenoid through which is passed a flux quantum, a particle of charge 2/7 or 2/5 is generated. However, lower energy particles also exist, those corresponding to an excitation within the layer of quasiparticles added to  $\Psi_3$ . In constructing these excitations we must first observe that  $\Psi_3$  has charge 2/3 excitations which are not simply two charge 1/3 excitations. These are generated by the three-step process a.) Particle-hole conjugate the wavefunction. b.) Insert a solenoid at  $z_0$  and pass through it a flux quantum. c.) Particle-hole conjugate again. If we abbreviate particle-hole conjugation by  $C$ , then we have

$$B_{z_0} = C A_{z_0}^\dagger C \quad (53)$$

and

$$B_{z_0}^\dagger = C A_{z_0} C \quad (54)$$

for the operators creating a quasihole and quasielectron, respectively, of charge  $1-1/m$  in  $\Psi_m$ . Similarly, these operators create quasiparticles of charge 1/3 in  $\Psi_{3/2}$  which have a lower energy than do the excitations of charge 2/3. These charge 1/3 excitations give rise to symmetric polynomials in the manner

$$S_{3/2}^{z_0} \Psi_1 = A_{z_0} \Psi_{3/2} \quad (55)$$

and these, in turn, give rise to excited states of the form  $S_{3/2}^{+2} \psi_3$  and  $(S_{3/2}^{+2})^2 \psi_3$ , which are particles of charge 1/7 and 1/5, respectively. To show this, we make an approximate representation of the magnitude of  $B_{z_0} \psi_{3/2}$  of the form

$$|B_{z_0} \psi_{3/2}(z_1, \dots, z_N)|^2 = a' \prod_i |z_i - z_0| \prod_{j < k} |z_j - z_k|^3 e^{-\frac{1}{2} \sum_i |z_i|^2}. \quad (56)$$

This is correctly a particle of charge 1/3. Calculating the particle creation energy using Eqs (13), (14) and (30)-(34), we obtain  $0.034 e^2/a_0$ , which compares well with the value  $0.026 e^2/a_0$  known from particle-hole symmetry. Using this approximate representation, we then obtain for the elementary excitation of  $\psi_{7/2}$

$$|S_{3/2}^{+2} \psi_3(z_1, \dots, z_N)|^2 = a' \prod_i |z_i - z_0| \prod_{j < k} |z_j - z_k|^7 e^{-\frac{1}{2} \sum_i |z_i|^2}. \quad (57)$$

This is a particle of charge 1/7 with a creation energy of  $0.005 e^2/a_0$ . We obtain similarly for the 7/5 state

$$|(S_{3/2}^{+2})^2 \psi_3(z_1, \dots, z_N)|^2 = \frac{1}{a'} \prod_i |z_i - z_0| \prod_{j < k} |z_j - z_k|^5 e^{-\frac{1}{2} \sum_i |z_i|^2}. \quad (58)$$

This describes a particle of charge 1/5 with a creation energy of  $0.011 e^2/a_0$ .

We remark finally that our wavefunctions, while complex, are similar to ones recently proposed by Halperin (7), though on different grounds.  $\psi_{7/2}$ , for example, written out explicitly in his notation, is

$$\begin{aligned} \psi_{7/2}(z_1, \dots, z_N) = & \int d^2 n_1 \dots d^2 n_N \left( \prod_{i < j} (z_i - z_j)^3 \right) \\ & \times \left( \prod_{k < m} (\eta_k^* - \eta_m^*)^3 (\eta_k - \eta_m) \right) \left( \prod_{i, k} (z_i - \eta_k) \right) \\ & \times \left( \prod_i e^{-|z_i|^2/4} \right) \left( \prod_k e^{-|\eta_k|^2/2} \right). \quad (59) \end{aligned}$$

#### V. ACKNOWLEDGEMENTS

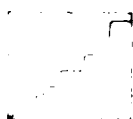
I am especially grateful to P.A. Lee for pointing out to me the significance of zeros in the wavefunction. I am also grateful to B.I. Halperin, S.H. Girvin, F.D.M. Haldane and P.M. Platzman for helpful discussions. This work was performed under the auspices of the U.S. Department of Energy under Contract No. W-7405-Eng-48.

#### VI. REFERENCES

- (1) R.B. Laughlin, Phys. Rev. Lett. 50 (1983) 1395.
- (2) H.L. Störmer, A.M. Chang, D.C. Tsui, J.C.M. Huang, A.C. Gossard, and W. Wiegmann, Phys. Rev. Lett. 50 (1983) 1953.
- (3) J.M. Caillol, D. Levesque, J.J. Weis and J.P. Hansen, J. Stat. Phys. 23 (1982) 325.
- (4) The use of ladder operators is also discussed in S.H. Girvin, Phys. Rev. B (in press).
- (5) F.J. Rogers, J. Chem Phys. 73 (1980) 272.
- (6) B.I. Halperin, Conference of the Condensed Matter Division of the European Physical Society, Lausanne, 28-30 March 1983. Proceedings to appear in Helvetica Physica Acta.

#### DISCLAIMER

This document was prepared as an account of work sponsored by an agency of the United States Government. Neither the United States Government nor the University of California nor any of their employees, makes any warranty, express or implied, or assumes any legal liability or responsibility for the accuracy, completeness, or usefulness of any information, apparatus, product, or process disclosed, or represents that its use would not infringe privately owned rights. References herein to any specific commercial products, process, or service by trade name, trademark, manufacturer, or otherwise, does not necessarily constitute or imply its endorsement, recommendation, or favoring by the United States Government or the University of California. The views and opinions of authors expressed herein do not necessarily state or reflect those of the United States Government thereof, and shall not be used for advertising or product endorsement purposes.



Fifth International Conference on

## **ELECTRONIC PROPERTIES OF TWO-DIMENSIONAL SYSTEMS**

Oxford, England, U.K. 5-9 September 1983

### **EP2DS V**

#### **LIST OF PARTICIPANTS**

Dr. G. Abstreiter  
Physik Department E16  
TU Munchen  
8046 Garching  
FEDERAL REPUBLIC OF GERMANY

Dr. A.R. Adams  
Physics Dept.  
University of Surrey  
Guildford  
Surrey GU2 5XH  
ENGLAND

Dr. M. Altarelli  
Max-Planck-Institut  
HML - BP 166X  
F-38042 Grenoble  
FRANCE

Dr. K.-E. Ambrosch  
University of Leoben  
Institute of Physics  
A8700 Leoben  
AUSTRIA

Dr. D. Anderson  
R.S.R.E.  
St. Andrews Road  
Malvern  
Worcs.  
ENGLAND

Dr. D.A. Andrews  
Dept. R.3.11  
British Telecom Research Labs.  
Martlesham Heath  
Ipswich IP5 7RE  
ENGLAND

Dr. G. Bastard  
Ecole Normale Supérieure  
24 rue Lhomond  
75231 Paris Cedex 05  
FRANCE

Dr. P.K. Basu  
CAS in Radio Physics and  
Electronics  
92 Acharya Prafulla Chandra Road  
Calcutta 700009  
INDIA

Dr. E. Bathe  
Universität Hamburg  
Institut für Angewandte Physik  
2 Hamburg 36  
Jungiusstrasse 11  
FEDERAL REPUBLIC OF GERMANY

Dr. G. Bauer  
Institut für Physik  
Montanuniversität Leoben  
A-8700 Leoben  
FEDERAL REPUBLIC OF GERMANY

Prof. J.L. Beeby  
Physics Dept.  
Leicester Univ.  
Leicester LE1 7RH  
ENGLAND

Dr. J. Beerens  
Dept. de Physique  
INSA  
Av de Rangueil  
31077 Toulouse CEDEX  
FRANCE

Dr. R. Bharat  
Rockwell International Science Centre  
3370 Miraloma Ave  
Anaheim CA 92803  
U.S.A.

Dr. P. Blood  
Phillips Res. Labs.  
Redhill  
Surrey  
ENGLAND

Dr. W.L. Bloss  
GTE Labs.  
40 Sylvan Road  
Waltham MA 01776  
U.S.A.

Dr. C. Bousquet  
Lab. Prof. J.L. Robert  
U.S.T.L.  
34060 Montpellier  
FRANCE

Dr. S. Brand  
Dept. of Applied Physics  
& Electronics  
Science Laboratories  
South Road  
Durham DM1 3LE  
ENGLAND

Mr. M.A. Brummell  
Clarendon Laboratory  
Parks Road  
Oxford OX1 3PU  
ENGLAND

Dr. L.C. Brunel  
S.N.C.I. C.N.R.S.  
Avenue des Martyrs  
B.P. 166X  
38042 Grenoble Cedex  
FRANCE

Dr. M.G. Burt  
BTRL  
Martlesham Heath  
Ipswich  
Suffolk IP5 7RE  
ENGLAND

Prof. P.N. Butcher  
University of Warwick  
Coventry CV4 7AL  
ENGLAND

Dr. M.E. Cage  
Elec. Measurements & Standards Div.  
Bldg. 220 Rm B258  
National Bureau of Standards  
Washington DC 20234  
U.S.A.

Dr. F. Capasso  
Bell Laboratories  
600 Mountain Ave  
Murray Hill  
NJ 07974  
U.S.A.

Dr. B.C. Cavenett  
Dept. of Physics  
Univ. of Hull  
Hull  
Nth Humberside  
ENGLAND

Dr. J.T. Chalker  
Institut für Theoretische Physik  
Philosophenweg 19  
D.6900 Heidelberg  
FEDERAL REPUBLIC OF GERMANY

Prof. L.J. Challis  
Physics Dept  
Nottingham University  
Nottingham  
ENGLAND

Dr. J.M. Chamberlain  
Physics Dept.  
Nottingham Univ.  
Nottingham NG7 2RD  
ENGLAND

Dr. A.M. Chang  
Dept. of EECS  
Princeton University  
Princeton NJ 08544  
U.S.A.

Dr. L.L. Chang  
IBM Watson Research Center  
P.O. Box 218  
Yorktown Heights NY 10598  
U.S.A.



Dr. R. Claridge  
Physics Dept.  
University of Essex  
Wivenhoe Park  
Colchester  
Essex  
ENGLAND

Dr. A.A. Cottey  
School of Mathematics & Physics  
University of East Anglia  
Norwich NR4 7TJ.  
ENGLAND

Dr. N. Couch  
G.E.C.  
Hirst Research Centre  
East Lane  
Wembley  
Middx HA9 9QU  
ENGLAND

Dr. M. D'lorio  
National Research Council of Canada  
Division of Physics M36  
Ottawa Ont. K1A 0R6  
CANADA

Dr. I.C. Da Cunha Lima  
Dept. of Physics  
Brown University  
Providence  
RI 02912  
U.S.A.

Prof. A.J. Dahm  
Physics Dept.  
Case Western Reserve U.  
Cleveland OH 44106  
U.S.A.

Dr. S. Das Sarma  
Dept. of Physics  
University of Maryland  
College Park MD 20742  
U.S.A.

Dr. R.A. Davies  
GEC Research Labs.  
Hirst Research Centre  
East Lane  
Wembley  
Middx HA9 7PP.  
ENGLAND

Dr. P.J. Dean  
RSRE  
St. Andrews Road  
Great Malvern  
Worcestershire.  
ENGLAND

Dr. C. Delalande  
Ecole Normale Supérieure  
24 rue Lhomond  
75231 Paris Cedex 05  
FRANCE

Dr. M.H. Dickens  
Crogenic Consultants Ltd.  
Metrostore Building  
231 The Vale  
London W3 7QS  
ENGLAND

Dr. T. Dietl  
Institute of Physics  
Polish Academy of Sciences  
Al Lotnikow 32/46  
02-668 Warsaw  
POLAND

Prof. G. Dohler  
Max Planck Institut für  
Festkörperforschung  
Heisenberg Strasse 1  
D-7000 Stuttgart 80  
FEDERAL REPUBLIC OF GERMANY

Dr. G. Dorda  
Siemens AG  
Otto-Hahn Ring 6  
8000 München 83  
FEDERAL REPUBLIC OF GERMANY

Dr. L. Eaves  
Dept. of Physics  
Univ. of Nottingham  
Nottingham NG7 2RD  
ENGLAND

Dr. G. Ebert  
Techn. Univ. Munchen E16  
Physik Dept.  
James Frankh Strasse  
8046 Garching  
FEDERAL REPUBLIC OF GERMANY

Dr. M. Elliott  
Universitat Hamburg  
Institut fur Angewandte Physik  
Junglusstrasse 11  
2000 Hamburg  
FEDERAL REPUBLIC OF GERMANY

Dr. T. Englert  
Max-Planck-Institut  
fur Festkorperforschung  
hochfeld-Magnetlabor Grenoble  
F - 38042 Grenoble  
166 X Grenoble Cedex  
Avenue des Martyrs (C.N.R.S.)  
FRANCE

Dr. L. Esaki  
IBM Watson Research Ctr.  
P.O. Box 218  
Yorktown Heights  
N.Y. 10598  
U.S.A.

Dr. F.F. Fang  
IBM Research Center  
Yorktown Heights  
NY 10598  
U.S.A.

Prof. G. Fano  
Istituto di Fisica  
della Universita di Bologna  
46 Via Irnerio  
40126 Bologna  
ITALY

Dr. A. Fasolino  
Max-Planck-Institut  
fur Festkorperforschung  
Hochfeld-Magnetlabor  
166X  
F38042 Grenoble  
FRANCE

Dr. G. Fishman  
Route du Platre  
Haute-Jarrie  
38506-Jarrie  
FRANCE

Dr. K.W.H. Foulds  
Physics Dept.  
University of Surrey  
Guildford  
Surrey GU2 5XH  
ENGLAND

Dr. A. Fowler  
IBM Res. Ctr.  
Yorktown Hts NY 10598  
U.S.A.

Dr. L. Friedman  
GTE Laboratories  
40 Sylvan Road  
Waltham MA 02254  
U.S.A.

Dr. H. Fujiyasu  
Faculty of Engineering  
Shizuoka University  
Hamamatsu 432  
JAPAN

Dr. J.E. Furneaux  
Code 6873  
Naval Research Laboratory  
Washington DC 20375  
U.S.A.

Dr. G.F. Giuliani  
Department of Physics  
Brown University  
Providence  
RI 02912  
U.S.A.

Dr. D. Glattli  
Service du Physique du Solide  
Institut de Recherche Fondamental  
C.E.N. Saclay  
91191 Gif-sur-Yvette Cedex  
FRANCE

Dr. R. Goodfellow  
Plessey Research (Caswell) Ltd.  
Optoelectronics Division  
Towcester  
ENGLAND

Prof. E. Gornik  
Inst. für Experimental Physik  
Schopfstrasse 41  
A6020 Innsbruck  
AUSTRIA

Dr. G. Grabecki  
Institute of Physics  
Polish Academy of Sciences  
Al. Lotnikow 32/46  
02-668 Warsaw  
POLAND

Dr. F. Green  
School of Physics  
U.N.S.W.  
P.O. Box 1  
Kensington  
N.S.W. 2033  
AUSTRALIA

Dr. G. Gregoris  
I.N.S.A.  
dept. de Physique  
avenue de Rangueil  
31077 Toulouse Cedex  
FRANCE

Dr. Y. Guldner  
Ecole Normale Supérieure  
24 rue Lhomond  
75231 Paris Cedex 05  
FRANCE

Dr. U. Gummich  
Institut für Theor. Physik  
der Universität zu Köln  
Zulpichertr. 77  
D-5000 Köln 41  
FEDERAL REPUBLIC OF GERMANY

Dr. P.O. Hahn  
IBM  
T.J. Watson Res. Center  
Yorktown Heights  
New York 10598  
U.S.A.

Dr. J. Hajdu  
Institut für Theoretische Physik  
der Universität zu Köln  
5 Köln 41  
Zolpicher Str. 77  
FEDERAL REPUBLIC OF GERMANY

Dr. W. Hansen  
Universität Hamburg  
Institut für Angewandte Physik  
Jungiusstrasse 11  
2000 Hamburg 36  
FEDERAL REPUBLIC OF GERMANY

Dr. A. Hartland  
National Physical Laboratory  
Teddington  
Middlesex  
ENGLAND

Dr. A. Hartstein  
IBM  
T.J. Watson Research Center  
Box 218  
Yorktown Heights  
NY 10598  
U.S.A.

Dr. R. Haydock  
TCM  
Cavendish Laboratory  
Madingley Road  
Cambridge CB3 0HE  
ENGLAND

Dr. K. Heift  
Institut für Theoretische Physik  
Universität zu Köln  
Zulpicher Str. 77  
5000 Köln 41  
FEDERAL REPUBLIC OF GERMANY

Dr. J.P. Hirtz  
Thomson CSF  
Domaine de Carbeville  
91401 Orsay  
FRANCE

Dr. D. Heitmann  
Inst. f. Angewandte Physik  
Jungiusstr. 11  
D-2000 Hamburg 36  
FEDERAL REPUBLIC OF GERMANY

Dr. A.J. Holden  
Plessey Research (Caswell) Ltd.  
Allen Clark Research Centre  
Caswell  
Towcester  
Northants  
ENGLAND

Dr. J.C. Hensel  
Bell Laboratories IC-421  
600 Mountain Ave.  
Murray Hill  
New Jersey 07974  
U.S.A.

Dr. W. Honlein  
Physikalisches Institut  
Röntgenring 8  
D-8700 Würzburg  
FEDERAL REPUBLIC OF GERMANY

Dr. F. Herman K32/281  
IBM Research Lab.  
5600 Cottle Road  
San Jose CA 95193  
U.S.A.

Dr. R.A. Hopfel  
Institut für Experimentale Physik  
Schopfstrasse 41  
A-6020 Innsbruck  
AUSTRIA

Dr. W.G. Herrenden Harker  
H.H. Wills Physics Lab.  
University of Bristol  
Royal Fort  
Tyndall Avenue  
Bristol BS8 1TL  
ENGLAND

Dr. R.E. Horstman  
Philips Research Lab.  
P.O. Box 80.000  
5600 JA Eindhoven  
THE NETHERLANDS

Prof. R.J. Higgins  
Dept. of Physics  
Univ. of Oregon  
Eugene  
Oregon 97403  
U.S.A.

Dr. S. Huant  
S.N.C.I. C.N.R.S.  
Avenue des Martyrs  
B.P. 166X  
38042 Grenoble Cedex  
FRANCE

Dr. O. Hipolito  
Depto. Física  
C.P. 369  
13560 Sao Carlos  
BRAZIL

Dr. H.P. Hughes  
Cavendish Laboratory  
Madingley Road  
Cambridge CB3 0HE  
ENGLAND

Dr. C.J. Humphreys  
Dept. of Metallurgy & Science of Materials  
University of Oxford  
Parks Road  
Oxford  
ENGLAND

Dr. K. Kajita  
Department of Physics  
Tohu University  
Miyama 2-2-1 Funabashi  
Chiba 274  
JAPAN

Dr. R.G. Humphreys  
RSRE  
St. Andrews Road  
Malvern  
Worcs.  
ENGLAND

Ms. C. Kallin  
Jefferson Lab. of Physics  
Harvard University  
Cambridge MA 02138  
U.S.A.

Dr. S.A. Jackson  
Bell Laboratories  
1D-337  
600 Mountain Ave.  
Murray Hill NJ 07974  
U.S.A.

Dr. Y. Kawaguchi  
Yale University  
Applied Physics  
Becton Center  
P.O. Box 2157  
New Haven CT 06520  
U.S.A.

Dr. M. Jaros  
Department of Theoretical Physics  
The University  
Newcastle upon Tyne.  
ENGLAND

Dr. M.J. Kelly  
The General Electric Co. Ltd.  
Hirst Research Centre  
East Lane  
Wembley  
Middx HA9 7PP

Dr. N.C. Jarosik  
SUNY at Buffalo  
239 Franczak Hall  
Buffalo  
NY 14260  
U.S.A.

Dr. M. Khalkin  
Inst. for Phys. Problems  
Academy SCI USSR  
Kosygin Street 2  
Moscow 117334  
USSR

Dr. H. Jung  
Max-Planck-Institut  
für Festkörperforschung  
Heisenbergstrasse 1  
D-7000 Stuttgart 80  
FEDERAL REPUBLIC OF GERMANY

Dr. R. Kishore  
INPE CP515  
12.200 S.J. Campos  
S.P.  
BRAZIL

Dr. E. Kaczmarck  
Institute of Physics  
Polish Academy of Sciences  
Al. Lotnikow 32146  
02-668 Warszawa  
POLAND

Prof. T. Kobayashi  
Physics Dept.  
University of Surrey  
Guildford  
Surrey GU2 5XH  
ENGLAND

Prof. Dr. F. Koch  
Physik-Department  
der Technischen Universität München  
D-8046 Garching  
FEDERAL REPUBLIC OF GERMANY

Prof. G. Landwehr  
MPI für Festkörperforschung  
HML (CNRS) 166X  
F 38042 Grenoble  
FRANCE

Dr. F. Komori  
Dept. of Physics  
Univ. of Tokyo  
7-3-1 Hongo  
Bunkyo-ku  
Tokyo 113  
JAPAN

Dr. R. Lassnig  
Institut für Experimental-  
Physik  
Schopfstrasse 41  
A-6020 Innsbruck  
AUSTRIA

Dr. J. Kossut  
Instytut Polskiej Akademii Nauk  
Al. Lotników 32/46  
02-668 Warsaw  
POLAND

Dr. R.B. Laughlin  
Lawrence Livermore Nat'l Lab.  
P.O. Box 808  
Livermore  
California 94550  
U.S.A.

Prof. Dr. J.P. Kotthaus  
Universität Hamburg  
Institut für Angewandte Physik  
Jungiusstrasse 11  
2000 Hamburg 36  
FEDERAL REPUBLIC OF GERMANY

Dr. J. Lee  
Box 1843 Physics  
Brown Univ.  
Providence RI 02912  
U.S.A.

Dr. F. Kuchar  
Physics Dept.  
St. Andrews University  
North Haugh  
St. Andrews KY16 9SS  
SCOTLAND

Dr. J. Leotin  
Service des Champs Magnétiques Intenses  
I.N.S.A.  
Avenue de Rangueil  
31077 Toulouse Cedex  
FRANCE

Dr. U. Kunze  
Institut für Elektrophysik  
Techn. Universität Braunschweig  
Postfach 3329  
3300 Braunschweig  
FEDERAL REPUBLIC OF GERMANY

Dr. P.E. Lindelof  
Physics Laboratory  
University of Copenhagen  
H.C. Ørsted Institute  
Universitetsparken 5  
DK-2100 Copenhagen Ø  
DENMARK

Prof. P.T. Landsberg  
Univ. of Southampton SO9 5NH  
ENGLAND

Dr. Y.E. Lozovik  
Institute of Spectroscopy  
142092 Moscow Obl  
Troitsk  
RUSSIA

Dr. S. Mori  
Osaka University  
Faculty of Engineering Science  
Toyonaka  
Osaka 560  
JAPAN

Dr. Z. Ovadyahu  
Phys. Dept.  
Ben-Gurion Univ.  
Beer-Sheeva 84105  
ISRAEL

Dr. K. Muro  
Osaka University  
Faculty of Engineering Science  
Toyonaka  
Osaka 560  
JAPAN

Dr. T.P. Pearsall  
Bell Laboratories  
600 Mountain Ave  
Murray Hill  
NJ 07974  
U.S.A.

Dr. Shin-ichiro Narita  
Osaka University  
Faculty of Engineering Science  
Toyonaka  
Osaka 560  
JAPAN

Prof. J.B. Pendry  
The Blackett Lab.  
Imperial College  
Prince Consort Road  
London SW7 2BZ  
ENGLAND

Dr. R.J. Nicholas  
Clarendon Laboratory  
Parks Road  
Oxford OX1 3PJ  
ENGLAND

Dr. M. Pepper  
Cavendish Laboratory  
Madingley Road  
Cambridge  
ENGLAND

Dr. S. Nishi  
Research Laboratory  
OKI Electric Industry Co. Ltd.  
550-5 Higashiasakawa-cho  
Hachioji-shi  
Tokyo 193  
JAPAN

Dr. C.H. Perry  
Physics Department  
Northeastern Univ.  
360 Huntingdon Ave  
Boston Mass. 02115  
U.S.A.

Ms. J. Nunn-Price  
S.E.R.C.  
Polaris House  
North Star Ave.  
Swindon  
Wilts SN2 1ET  
ENGLAND

Dr. A. Pinczuk  
Rm 4B-437  
Bell Labs.  
Holmdel NJ 07733  
U.S.A.

Dr. H. Obloh  
Technische Universitaet  
Muenchen  
Phys Dep. E 6  
8058 Garching  
James-Franck-Str.  
FEDERAL REPUBLIC OF GERMANY

Dr. M. Pomerantz  
I.B.M. T.J. Watson Research Center  
Yorktown Heights  
NY 10598  
U.S.A.

Dr. J.C. Moan  
Max-Planck-Institut  
HML - BP 166X  
F-38042 Grenoble  
FRANCE

Mr. D.A.H. Mace  
Physics Department  
University of Exeter  
Exeter  
Devon EX4 4QL  
ENGLAND

Dr. U. Mackens  
Inst. für Angewandte Physik  
Jungiusstrasse 11  
2000 Hamburg 36  
FEDERAL REPUBLIC OF GERMANY

Dr. A. MacKinnon  
Blackett Laboratory  
Imperial College  
Prince Consort Road  
London SW7 2BZ  
ENGLAND

Dr. R.S. Markiewicz  
Physics Dept.  
Northeastern Univ.  
360 Huntingdon Ave  
Boston  
Mass 02115  
U.S.A.

Dr. J.-Y. Marzin  
Centre National d'Etudes  
des Telecommunications  
196 rue de Paris  
92220 Bagneux  
FRANCE

Dr. C. Mazure  
Physik Dept. E16  
Technische Universität  
D-8056 Garching  
FEDERAL REPUBLIC OF GERMANY

Dr. B.D. McCombe  
Dept. of Physics  
Franczak Hall  
SUNY at Buffalo  
Buffalo NY 14260  
U.S.A.

Dr. Mehmet Rona  
Arthur D. Little, Inc.  
Acorn Park  
Cambridge MA 02140  
U.S.A.

Dr. E.E. Mendez  
IBM Watson Research Center  
P.O. Box 218  
Yorktown Heights  
New York 10598  
U.S.A.

Dr. J.M. Mercy  
Lab. Prof. J.L. Robert  
USTL  
34060 Montpellier  
FRANCE

Dr. U. Merkt  
Universität Hamburg  
Institut für Angewandte Physik  
2 Hamburg 36  
Jungiusstrasse 11  
FEDERAL REPUBLIC OF GERMANY

Dr. R. Merlin  
Dept. of Physics  
Univ. of Michigan  
Ann Arbor MI 48103  
U.S.A.

Dr. J.E. Mooij  
Dept. Applied Physics  
Delft University of Technology  
Delft  
THE NETHERLANDS



Prof. J.C. Portal  
I.N.S.A.  
Dept. de Physique  
Ave de Ranguell  
FRANCE

Prof. J.J. Quinn  
Brown University  
Providence  
Rhode Island 02912  
U.S.A.

Prof. H. Raether  
Universitat Hamburg  
Institut fur Angewandte Physik  
Jungiusstrasse 11  
2 Hamburg 36  
FEDERAL REPUBLIC OF GERMANY

Dr. H.J. Ralph  
Philips Res. Labs.  
Redhill  
Surrey  
ENGLAND

Dr. G.J. Rees  
Plessey Research (Caswell) Ltd.  
Allen Clark Research Centre  
Caswell  
Towcester  
Northants  
ENGLAND

Dr. T.L. Reinecke  
Code 6877  
Naval Research Laboratory  
Washington DC 20375  
U.S.A.

Dr. G. Remenyi  
Max Planck Institut fur  
Festkorper Forschung  
Ave. des Martyrs  
B.P. 38042 Grenoble  
FRANCE

Dr. F.A. Riddoch  
Department of Physics  
University of Essex  
Wivenhoe Park  
Colchester CO4 3SQ  
ENGLAND

Dr. B.K. Ridley  
Dept. of Physics  
Univ. of Essex  
Colchester.  
ENGLAND

Dr. D.J. Robbins  
Plessey Research (Caswell) Ltd.  
Allen Clark Research Centre  
Caswell  
Towcester  
Northants  
ENGLAND

Prof. J.L. Robert  
U.S.T.L.  
34060 Montpellier  
FRANCE

Prof. G.G. Roberts  
Dept. of Applied Physics  
& Electronics  
Univ. of Durham  
Science Laboratories  
South Road  
Durham DH1 3LE  
ENGLAND

Mr. D.C. Rogers  
Clarendon Laboratory  
Parks Road, Oxford OX1 3PU  
ENGLAND

Dr. M. Saitoh  
Department of Physics  
University of Cambridge  
Cavendish Laboratory  
Madingley Road  
Cambridge CB3 0HE  
ENGLAND

Dr. C.K. Sarkar  
Clarendon Laboratory  
Parks Road,  
Oxford OX1 3PU  
ENGLAND

Mr. J. Singleton  
Clarendon Laboratory  
Parks Road  
Oxford OX1 3PU  
ENGLAND

Dr. Z. Schlesinger  
IC302  
Bell Laboratories  
Murray Hill  
New Jersey 07974  
U.S.A.

Dr. W.J. Skocpol  
Room 4D-327,  
Bell Laboratories  
Holmdel NJ 07733  
U.S.A.

Dr. J.T. Schriempf  
N.R.L.  
Code 6600  
Washington  
D.C. 20375  
U.S.A.

Dr. M.S. Skolnick  
RSRE  
St. Andrews Road  
Great Malvern  
Worcestershire.  
ENGLAND

Dr. J.N. Schulman  
University of Hawaii  
2505 Correa Road  
Honolulu Hi 96822  
U.S.A.

Dr. R.P. Smith  
Box 1843  
Physics Dept.  
Brown University  
Providence RI 02912  
U.S.A.

Dr. W. Seidenbusch  
Institut für Experimental Physik  
Schopfstrasse 41  
A-6020 Innsbruck  
AUSTRIA

Dr. H.H. Soanpaa  
Dept. of Physics  
Univ. of North Dakota  
Grand Forks ND 58202  
U.S.A.

Dr. B.E. Sernelius  
Linköping University  
Dept. of Physics and Measurement Technology  
S-581 83 Linköping  
SWEDEN

Dr. J.W. Steeds  
Physics Dept.  
University of Bristol  
Bristol BS8 1TL  
ENGLAND

Dr. B.V. Shanabrook  
Code 6873  
Naval Research Lab.  
Washington D.C.  
U.S.A.

Prof. P.J. Stiles  
Physics Dept.  
Brown University  
Providence RI 02912  
U.S.A.

Dr. V.B. Shikin  
Solid State Physics Inst.  
Academy of Sciences  
142432 Chernogolovka Moscow  
USSR

Dr. H.L. Stormer (ID.458)  
Bell Labs.  
600 Mountain Ave.  
Murray Hill NJ 07974  
U.S.A.

Prof. R.A. Stradling  
Department of Physics  
University of St. Andrews  
North Haugh  
St. Andrews KY16 9SS  
SCOTLAND

Prof. D.J. Thouless  
Dept. of Physics FM-15  
Univ. of Washington  
Seattle WA 98195  
U.S.A.

Dr. N. Studart  
Departamento de Fisica  
Univ. Fed. de Sao Carlos  
Caixa Postal 676  
13560 Sao Carlos SP  
BRAZIL

Dr. J.C. Thuillier  
Faculte des Sciences  
Universite de Dijon  
BP 138  
21004 Dijon Cedex  
FRANCE

Dr. J. Sutton  
Oxford Instruments Ltd.  
Osney Mead  
Oxford OX2 ODX  
ENGLAND

Prof. E. Tosatti  
Int. School for  
Advanced Studies  
Strada Costiera 11  
Miramare  
34100 Trieste  
ITALY

Dr. D.A. Syphers  
Box 1843  
Brown University  
Providence RI 02912  
U.S.A.

Dr. A. Tselis  
Department of Physics  
Purdue University  
West Lafayette  
Indiana 47907  
U.S.A.

Dr. Tausendfreund  
Physik Dept. E16  
TU Munchen  
D-8046 Garching  
FEDERAL REPUBLIC OF GERMANY

Dr. D.C. Tsui  
EECS  
Princeton Univ.  
Princeton  
NJ 08544  
U.S.A.

Dr. T.N. Theis  
I.B.M. T.J. Watson Research Center  
Yorktown Heights  
NY 10598  
U.S.A.

Dr. J.T. Vallin  
Physics Dept. CTH  
S-41296 Gothenburg  
SWEDEN

Dr. W. Thoren  
2 Physikalisches Institut der RWTH Aachen  
Templergraben 55  
D-5100 AACHEN  
FEDERAL REPUBLIC OF GERMANY

Dr. P. Vashishta  
Argonne Natl Lab.  
Argonne  
Illinois 60439  
U.S.A.

Dr. J.P. Vieren  
Ecole Normale Supérieure  
24 rue Lhomond  
75231 Paris Cedex 05  
FRANCE

Dr. R.G. Wheeler  
Becton Center  
Yale University  
New Haven Conn 06520  
U.S.A.

Dr. B. Vinter  
Thomson-CSF  
Domaine de Corbeville  
B.P.10  
F-91401 Orsay  
FRANCE

Dr. A.D. Wieck  
Universität Hamburg  
Institut für Angewandte Physik  
2 Hamburg 36  
Jungiusstrasse 11  
FEDERAL REPUBLIC OF GERMANY

Dr. P. Voisin  
Groupe de Physique des  
Solides de l'ENS  
24 rue Lhomond  
75005 Paris  
FRANCE

Dr. F.I.B. Williams  
DPH-SPSRM  
Cen-Saclay  
91191 Gif-sur-Yvette  
FRANCE

Dr. K. von Klitzing  
Physik-Department E16  
der Tu München  
D-8076 Garching  
FEDERAL REPUBLIC OF GERMANY

Dr. R. Wisniewski  
Becton Centre  
Yale Univ.  
15 Prospect Street  
New Haven CT 06520  
U.S.A.

Dr. M. Voos  
Groupe de Physique  
des Solides de l'ENS  
24 rue Lhomond  
75005 Paris  
FRANCE

Dr. P.H. Woerlee  
Philips Research Labs (WP-7)  
P.O. Box 80.000  
5600 JA Eindhoven  
THE NETHERLANDS

Ms. T.H.H. Vuong  
Clarendon Laboratory  
Parks Road  
Oxford OX1 3PU  
ENGLAND

Dr. J.M. Worlock  
Room 4B-427  
Bell Labs.  
Holmdel NJ 07733  
U.S.A.

Prof. R.F. Wallis  
Physics Dept.  
Univ. of California  
Irvine CA 92717  
U.S.A.

Dr. M. Wynne Jones  
Plessey Research (Caswell) Ltd.  
Optoelectronics Division  
Towcester  
ENGLAND

Dr. J. Yoshino  
Inst. of Indust. Science  
Univ. of Tokyo  
7-22-1 Roppongi  
Minato-ku Tokyo 106  
JAPAN

Dr. D. Yoshioka  
Institute for Solid State Phys.  
Tokyo University  
Roppongi  
Minato-ku  
Tokyo 106  
JAPAN

Prof. W. Zawadski  
Instytut Polskiej Akademii Nauk  
Al. Lotnikow 32/46  
02-668 Warsaw  
POLAND

Dr. C. Zeller  
Physikdept E16  
Technische Universität München  
8046 Garching  
FEDERAL REPUBLIC OF GERMANY

Dr. R.T. Zeller  
Physics Dept.  
Brown Univ.  
P.O. Box 1843  
Providence RI 02912  
U.S.A.

Dr. Wen-qin Zhao  
Physik-Department E16  
Technische Universität München  
8046 Garching b. München  
FEDERAL REPUBLIC OF GERMANY

Dr. V.O. Ziemelis  
Ecole Normale Supérieure  
24 rue Lhomond  
75231 Paris Cedex 05  
FRANCE